The Synthesis and Reactivity of Group 4 metal Hydrazides

Daniel Schofield MChem AMRSC

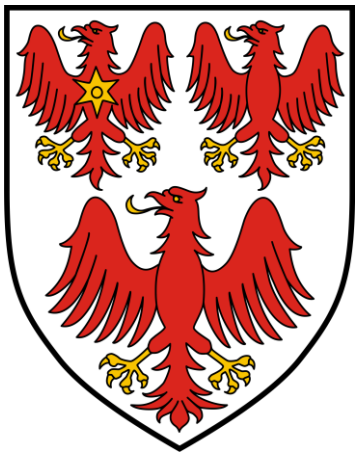

Thesis submitted to the University of Oxford for the degree of
Doctor of Philosophy, July 2012.

The work described in this Thesis was carried out in the Chemistry Research Laboratory, University of Oxford from October 2008 to June 2012 under the supervision of Professor Philip Mountford. All work is my own unless stated to the contrary, and has not previously been submitted for any degree at this or any other university.

Alfred Daniel Huntley Schofield

June 2012

Abstract

Daniel Schofield Trinity 2012

The Queen's College D.Phil. Thesis

This Thesis describes the synthesis, characterisation and reactivity of diamide-amine and bis(cyclopentadienyl) supported Group 4 hydrazido(2-) compounds towards unsaturated molecules. The mechanisms of these transformations are probed using a range of structural, kinetic and computational methods.

Chapter 1 provides an introduction to the current chemistry of Group 4 metal hydrazides in the context of dinitrogen fixation using mid/late transition metal hydrazide compounds. Comparisons are also made with the well established Group 4 imide chemistry.

Chapter 2 describes a detailed experimental and computational study of the previously reported, unique N_α-N_β bond insertion reactivity observed between $Ti(N_2N^{Me})(NNPh_2)(py)$ (**1.93**) and a range of alkynes.

Chapter 3 presents experimental and computational studies of the reactions of $Ti(N_2N^{Me})(NNPh_2)(py)$ (**1.93**) with a range of unsaturated substrates including nitriles, isocyanides and isochalcocyanates.

Chapter 4 describes a new route to the synthesis of the previously reported hydrazide $Cp_2Zr(NNPh_2)(DMAP)$ (**1.151**), which is then applied in the synthesis of related compounds. The mechanism of the combined N_α-N_β cleavage, C-H activation reactivity seen between **1.151** and alkynes is studied in depth using structural, kinetic and computational studies. This is compared with a recently published mechanism.

Chapter 5 presents full experimental procedures and characterising data for the new complexes reported.

CD Appendix contains .cif files for all new crystallographically characterised complexes, details of all kinetic data presented and nOe NMR spectra.

Contents

Acknowledgements

It has been an honour and a privilege to have had the opportunity to work in Prof. Philip Mountford's research group for both my Part II and DPhil. I found the subject of this Thesis both challenging and stimulating and I wish to thank Phil for the extensive work he has put into it and me. Without his foresight, knowledge and patience it would not have yielded the results it did. I would also like to express my gratitude for the way in which I have been treated throughout my time here, I think few people in his position share as much concern for others as he does.

Of course, without all the other members of the group, past and present, my project and time here could have turned out very differently. In particular I would like to thank Dr. John Selby for his help during the initial stages of my research, showing me his own unique style of chemistry and sharing his many and, sometimes barely believable, anecdotes. I would like to thank Dr. Andrew Schwarz for his extensive advice in the world of crystallography and always bringing a good vibe, a laugh and a lot of noise to the lab. I would also like to mention Junjuda Unruangsri (Guun to her friends) for being an excellent Part II student. They really helped S2 remain the dominant force that it was.

Despite never working in the same lab, Lawrence Clark has been an ever-present feature of my time in the group. While he is often a man of few words, over the last couple of years I have got to know him both as a colleague and friend. His sense of humour is first class, especially when accompanied by his wry smile, I feel lucky to have had him as my contemporary and look forward to staying in touch.

In addition to those I have already mentioned I would like to pay my respects to all the people who help make my project into the Thesis of which I am so proud. Dr. Eric Clot and Dr. Ainara Nova's computational expertise and mechanistic insight led to significant breakthroughs on many occasions. Dr Nick Rees and Dr. Amber Thompson for giving up their time to teach me in using the NMR and X-ray diffraction equipment and always being there to help when a more experienced hand was required. Also to Matt Blake for giving up the time to proof read what is quite a lengthy document and everyone else who has taken time out of their day to provide assistance.

There are also several very important people from outside the department whom I would like to thank. My parents, without all the help, advice and sacrifices they have

made for me over the years I would not be sitting here writing this. I would also like to say thank you to Polly and Tessa for having me as your older brother. I hope we can make time to see each other as our lives progress. Finally I want to thank my fiancée Diana. Since coming into my life nearly seven years ago she has transformed it, I never realised one person could make me this happy. She has given me the confidence to believe in myself and be the best that I can be. She is always on hand with a smile, a hug and the right thing to say. For all this and so much more, thank you.

Notes

Literature compounds described in this Thesis are numbered **1.x**, **2.x**, **3.x**, **4.x** according to the Chapter in which they first occur. The new compounds described in this Thesis are numbered **1** – **xx**. Model systems used in calculations are denoted by **#Q**. Density functional theory (DFT) calculated compounds are given letters for hypothetical/non-experimentally observed species.

X-ray crystallography data was collected, solved and refined by the author with help and guidance from Prof. Philip Mountford and Dr. A. Thompson.

DFT calculations were performed in collaboration with Dr Ainara Nova and Dr Eric Clot of Université Montpellier, France.

Abbreviations

General

Å	Ångstrom
atm	atmosphere(s)
avg.	average
ca.	*circa*, about
calcd.	calculated
cf.	*confer*, compared to
Cp_{cent}	computed cyclopentadienyl ring carbon centroid
CSD	Cambridge Structural Database
°C	degrees Celsius
°	degrees
d	day(s)
DFT	Density Functional Theory
equiv(s).	equivalents
fac	facially coordinating
g	grams
mg	milligram(s)
μg	microgram(s)
h	hour(s)
K	Kelvin
k	rate constant
kcal mol^{-1}	kilocalorie(s) per mole
mbar	millibar(s)
min	minute(s)
mL	millilitre(s)
μL	microlitre(s)
mmol	millimole(s)
μmol	micromole(s)
RT	room temperature
s	second(s)
T	temperature
vs.	versus

Chemical

acac	acetylacetonate
Ad	adamantyl
Ar	aryl group
Ar′	2,6- $C_6H_3{}^iPr_2$
^{n}Bu	*n*-butyl
^{t}Bu	*tert*-butyl
^{t}Bu-bipy	4,4′-di-*tert*-butyl-2,2′-bipyridine
bipy	2,2′-bipyridine
Cp	C_5H_5
Cp′	C_5H_4Me
Cp^{Me_4}	C_5Me_4H
Cp*	C_5Me_5
dap	α-(dimethylaminomethyl)pyrrole)
DMAP	4-dimethylaminopyridine
dme	1,2-dimethoxyethane
dppe	$Ph_2PCH_2CH_2PPh_2$
E	generic chalcogen atom
Et	ethyl
H_2enp	N,N'-dimethylethylenediamine-N,N'-bis(2-methylpyrrole)
$H_2N_2N^{Me}$	$MeN(CH_2CH_2N(H)SiMe_3)_2$
$H_2N_2N^{SiMe_3}$	$Me_3SiN(CH_2CH_2N(H)SiMe_3)_2$
$H_2N_2N^{Me}$	$MeN(CH_2CH_2CH_2N(H)SiMe_3)_2$
$H_2N_2N^{py}$	$MeC(2\text{-}C_5H_4N)(CH_2N(H)SiMe_3)_2$
$H_2N^*{}_2N^{py}$	$MeC(2\text{-}C_5H_4N)(CH_2N(H)Si(^tBu)Me_2)_2)$
$H_2N_2{}^{Xyl}N^{py}$	$MeC(2\text{-}C_5H_4N)(CH_2N(H)\text{-}2,6\text{-}C_6H_3Me_2)_2)$
$H_2N_2{}^{Mes}N^{py}$	$MeC(2\text{-}C_5H_4N)(CH_2N(H)\text{-}2,4,6\text{-}C_6H_2Me_3)_2)$
H_2Me_4taa	tetramethyl dibenzotetraaza[14]annulene
H_2TTP	*meso*-tetra-*p*-tolylporphyrine
HIPT	$3,5\text{-}(2,4,6\text{-}C_6H_2{}^iPr_3)_2C_6H_3$
L	a supporting ligand (set)
M	metal or mol L^{-1}
Me	methyl
Me_2Calix	dianion of 1,3-dimethyl ether of *tert*-butyl calix[4]arene

Me_3[6]ane	1,3,5-trimethyltriazacyclohexane
Me_3[9]ane	1,4,7-trimethyltriazacyclononane
Me_2pz	3,5-dimethylpyrazolyl
Mes	2,4,6-$C_6H_2Me_3$
NS_3	$N(CH_2CH_2S)_3$
$N^{Xyl}NH$	N-(3,5-dimethylphenyl)-4,5-dihydro-3H-pyrrol-2-amine
OTf	$CF_3SO_3^-$
P	generic phosphine ligand
Ph	phenyl
^{i}Pr	*iso*-propyl
^{n}Pr	*n*-propyl
py	pyridine
pz	pyrazolyl
R	generic aryl or alkyl
THF	tetrahydrofuran
Tol	4-C_6H_4Me
X	Generic halide
Xyl	2,6-$C_6H_3Me_2$

Calculations

BDEs	bond dissociation energies
DFT	density functional theory
EHMO	extended Hückel molecular orbital
HOMO	highest occupied molecular orbital
LP	lone pair
LUMO	lowest unoccupied molecular orbital
MO	molecular orbital
NBO	natural bond orbital
TS	transition state(s)

Mass Spectrometry

EI	electron impact
ES	electrospay
FI	field ionisation
m/z	mass to charge ratio

MS	mass spectrometry

Nuclear Magnetic Resonance Spectroscopy

$^{13}C\{^{1}H\}$	proton-decoupled ^{13}C
$^{19}F\{^{13}C\}$	carbon-decoupled ^{19}F
app.	apparent
br.	broad
COSY	correlation spectrocopy
d	doublet
HMBC	heteronuclear multiple bond correlation
HMQC	heteronuclear single quantum correlation
Hz	Hertz
i	*ipso*
J	coupling constant
m	*meta*
m	multiplet
MHz	Megahertz
NMR	nuclear magnetic resonance
nOe	nuclear Overhauser effect
o	*ortho*
p	*para*
ppm	parts per million
q	quartet
ROESY	rotating-frame nuclear Overhauser Effect spectroscopy
s	singlet
sept	septet
t	triplet
VT	variable temperature
δ	chemical shift in ppm

Infrared Spectroscopy

br.	broad
FT-IR	fourier transform infrared red
IR	infrared red
cm^{-1}	wavenumber

m	medium
s	strong
w	weak
ν	frequency

Chapter One

Introduction

1.1 General Introduction

Nitrogen-containing molecules are not only essential for all aspects of life, but also a significant number of industrial processes.[1-6] Their production, both in nature and industry, however, is hindered by the high strength of bonds between nitrogen atoms. As a result syntheses often require multiple steps and large amounts of energy (not least in the formation of ammonia from dinitrogen). It is therefore of great interest to develop processes which allow atom-efficient syntheses of nitrogen-containing molecules under more benign conditions.

Group 6 hydrazido(2-) compounds of the type (L)M=NNR_2 (L = an ancillary ligand or ligand set, R = H, alkyl or aryl) have been the subject of detailed study for over 30 years[7,8] with a view to understanding the catalytic process by which ammonia is formed from dinitrogen.[9-12] With the knowledge that these catalysts are unlikely to supersede the currently used Haber-Bosch process, focus shifted to the direct synthesis of more complicated organo-nitrogen products. To this end, the reactivity of mid-transition metal hydrazides[11,13-15] and a wide range of transition metal imido(2-) compounds, of the type (L)M=NR (L = an ancillary ligand or ligand set, R = alkyl or aryl), was investigated.[16-28] The latter were found to be successful catalysts for a range of reactions including the hydroamination of alkynes, formally N–H addition across a C≡C bond.[22,29-33] Despite the successes of these related areas, early-transition metal hydrazido(2-) chemistry has, until several recent advances, remained remarkably understudied.[34-58]

This Thesis investigates the large scope of reactivity accessible to the hydrazido(2-) moiety when bound to a Group 4 metal centre, involving novel transformations at both the M=N_α and N_α–N_β bonds. These are explored using a range of computational and crystallographic methods. Particular focus is given to the previously reported reactivity between certain diamide-amine and bis(cyclopentadienyl) supported Group 4 terminal hydrazides and alkynes.[51,57] The mechanisms are probed using a wide range of computational, spectroscopic and crystallographic work. During the course of this, the synthesis of several new heavy Group 4 metal hydrazides was carried out and these are also reported. Parts of this work have been published.[59-61]

This Chapter places the chemistry of Group 4 and transition-metal hydrazido(2-) complexes in general, in the context of ammonia and organo-nitrogen compound

formation *via* N_α–N_β bond cleavage. The bonding of the hydrazido(2-) ligand in both early and late transition metals is introduced, compared to each other and to that of the related imido(2-) ligand. The synthesis and reported reactivity of transition metal terminal hydrazido(2-) complexes, focusing on Group 4 in particular, is discussed and their evolution compared with that of their imido(2-) counterparts.

1.2 Metal hydrazido chemistry

1.2.1 Metal hydrazido(2-) compounds in nitrogen fixation

For many years mankind has understood the importance of nitrogen-containing compounds.[1-6] Yet despite nitrogen being the major constituent of the atmosphere, human bodies are unable to utilise it directly due to the extreme inertness of the triple bond in dinitrogen. Several industrial processes, most notably the Haber-Bosch process for converting dinitrogen into ammonia and, to a lesser extent, the Frank-Caro cyanamide process have been developed to utilise atmospheric dinitrogen (Equations 1.1 and 1.2).[62,63]

$$N_{2\,(g)} + 3\,H_{2\,(g)} \xrightarrow[200\ \text{atm.},\ 400\ ^\circ\text{C}]{\text{metal catalyst}} 2\,NH_{3\,(g)}$$

Equation 1.1

$$CaC_{2\,(s)} + N_{2\,(g)} \xrightarrow{1000\ ^\circ\text{C}} CaNCN_{\,(s)} + C_{\,(s)}$$

Equation 1.2

Whilst both are excellent routes for the production of small nitrogen-containing molecules from dinitrogen on a large scale, they require highly forcing conditions and the range of molecules which can be directly synthesised is severely limited.[9,13,64,65] The elevated temperatures and pressures required in these commercial processes differ from those used in the fixation of dinitrogen by organisms containing nitrogenase enzymes (Equation 1.3).

$$N_{2\,(g)} + 8\,H^+ + 8\,e^- + 16\,\text{MgATP} \xrightarrow{\text{nitrogenase}} 2\,NH_{3\,(g)} + H_2 + 16\,\text{MgADP}$$

Equation 1.3

This occurs at ambient temperature and pressure, although a significant amount of energy (16 MgATP) and an electron source are still required. The discovery of this

biological process has led to a large amount of research aimed at fixating dinitrogen utilising milder conditions than those currently employed in industry.[9,10,13] There are three known types of nitrogenase enzyme, the most common contains an iron-molybdenum-sulfur cluster in the active site.[66,67] The other types, FeV[68,69] and Fe,[70,71] have the molybdenum replaced by vanadium and iron atoms, respectively, however, these are found to be less active. For this reason much work in the field has utilised Fe and Mo complexes (Figure 1.1).[72,73]

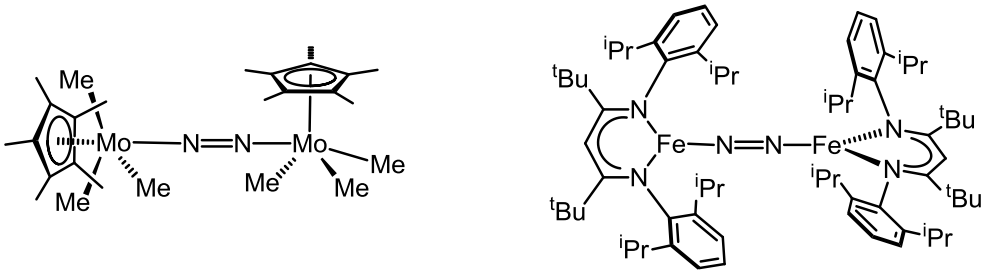

1.1 **1.2**

Figure 1.1. Early examples of N_2 activating complexes. N–N = 1.235 Å (**1.1**), 1.182 Å (**1.2**), N_2 = 1.097(5) Å.

Following the publication of the molecular structure of the Fe–Mo nitrogenase enzyme derived from Azotobacter vinelandii in 1992 (Figure 1.2),[74] much effort was spent attempting to understand the processes by which nitrogenase enzymes convert dinitrogen to ammonia. However, to date no consensus concerning the binding of dinitrogen in the active site or the mechanism by which it is reduced has been reached.[75]

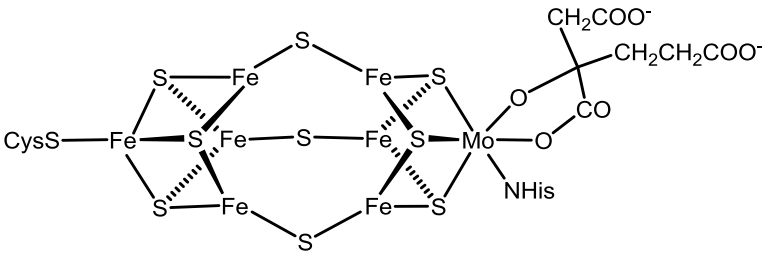

Figure 1.2. FeMo cofactor of FeMo nitrogenase.

In trying to understand the biological fixation of dinitrogen many compounds have been synthesised which bind and reduce dinitrogen. However, very few have been able to fully cleave the N≡N bond. Those that do typically contain a Group 6 metal centre, supported by phosphine ancillary ligands of the type $(P)_4M(N_2)L$ (M = Mo or W, P = phosphine ligand, L = a monodentate ligand including N_2).[14,76-78] The first

examples were developed by Chatt and have been shown to convert dinitrogen into ammonia *via* the stepwise, but non-catalytic, ′Chatt cycle′ (Scheme 1.1).

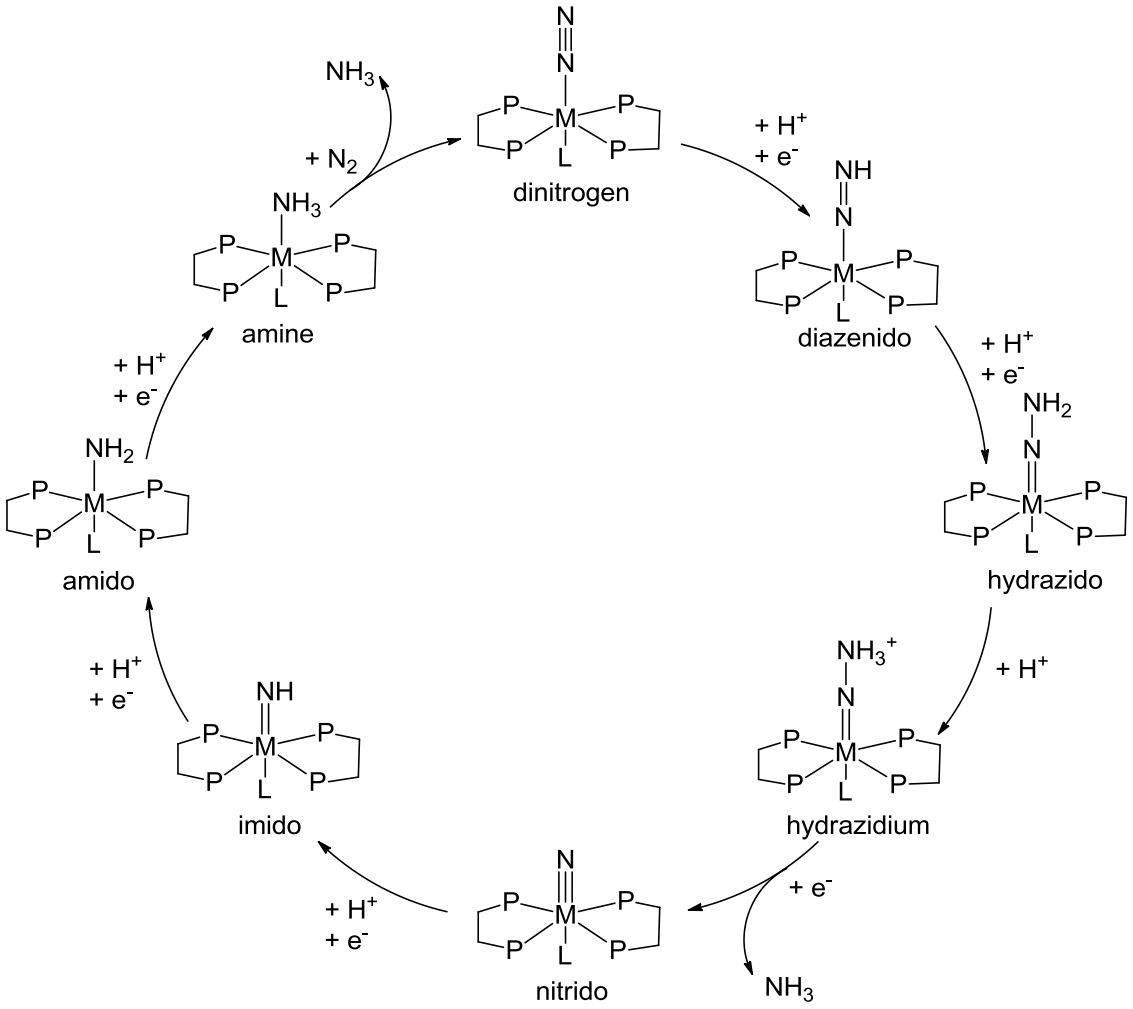

Scheme 1.1. The Chatt cycle (M = Mo or W, L = monodentate ligand including N_2).

A fully catalytic cycle for the conversion of dinitrogen to ammonia, albeit with a low turnover number, was developed by Schrock using Mo(HIPTN$_3$N) (**1.3**, HIPT = 3,5-(2,4,6-$C_6H_2{}^iPr_3)_2C_6H_3$, Figure 1.3).[79-82] Again this utilised a Group 6 metal centre but with bulky amido ancillary ligands in place of the phosphines used by Chatt. These ligands suppress the formation of inert, dimeric species of the type M–N=N–M, a major problem in this class of compound. The mechanism, for which eight intermediates have been isolated, proceeds *via* the ′Schrock cycle′. The individual steps are similar to those of the ′Chatt cycle′, the main difference being that the metal centre oscillates between the +VI and +III oxidation states not +III and 0.

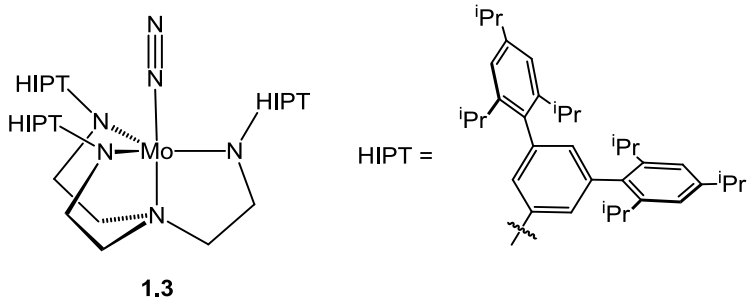

Figure 1.3. Molybdenum complex, containing the (tris)amido-amine ligand which enables catalytic conversion of dinitrogen to ammonia.

Later work by Coucouvanis attempted to combine FeS clusters with Mo, but was only able to catalyse the disproportionation of hydrazine to ammonia and dinitrogen.[83-85] Recently several other examples of molybdenum based catalysts have been discovered which convert dinitrogen to ammonia with greater turnover numbers.[86-89]

The presence of hydrazido(2-) and imido intermediates in both the Chatt and Schrock cycles highlights the potential for these compounds to be used in the atom-efficient synthesis of organo-nitrogen compounds.

1.2.2 The hydrazido ligand

The hydrazido ligand can exhibit several different coordination modes.[16,55] This is caused by variations of the ligand charge, hapticity with respect to the metal centre and whether the ligand is terminally bound or bridging between two metal centres. The favoured coordination mode for a given compound is influenced by a range of factors including the N_α and/or N_β substituents, metal centre and the ancillary ligand set. Figure 1.4 illustrates several possible binding modes for a 1,1 disubstituted hydrazide. This Thesis concentrates on the chemistry of terminal hydrazido(2-) complexes of the type (L)M=NNR$_2$ (M = Group 4 metal, L = an ancillary ligand or ligand set, R = alkyl or aryl). Where other binding modes are reported they are clearly labelled, in all cases the nitrogen atoms are described as M=$N_\alpha N_\beta R_2$.

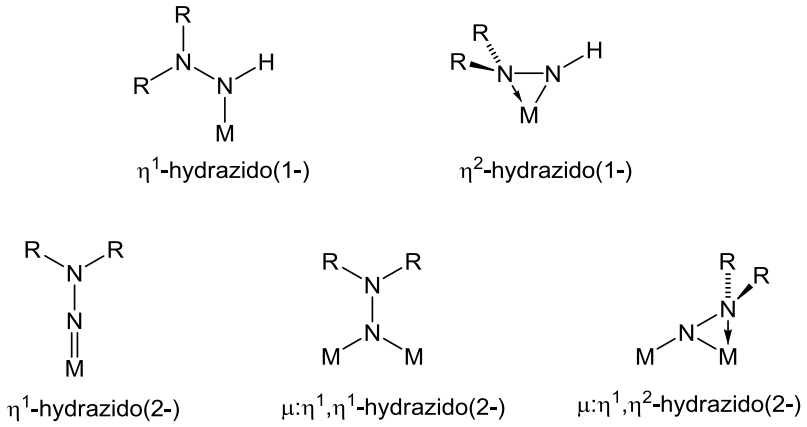

Figure 1.4. Selected coordination modes of the 1,1 disubstituted hydrazido(2-) ligand.

1.2.3 Group 6 and later transition metal hydrazido(2-) compounds

Following the successes of Chatt and Schrock in converting dinitrogen into ammonia *via* a hydrazido(2-) intermediate using Mo and W complexes, much of the work in this field initially concentrated on Group 6, before progressing to more electropositive metal centres.

Following the extensive structural studies performed in the course of understanding the mechanisms of the aforementioned Chatt and Schrock cycles, which indicated an essentially linear M–N_α–N_β fragment with an N_α–N_β bond order between 1 and 2 and an M–N_α distance indicative of multiple bond character,[80] research shifted towards exploring the reactivity of these novel metallated hydrazido(2-) compounds. The bonding has also been extensively studied and is discussed in Section 1.4.

A significant proportion of this work was carried out by Hidai using complexes such as *trans*-[M(NNH_2)F($dppe)_2$][BF_4] (M = Mo (**1.4**) or W (**1.5**), dppe = 1,2-bis(diphenylphosphino)ethane) and *cis,mer*-[M(NNH_2)X_2($PMe_2Ph)_3$] (M = Mo (**1.6**) or W (**1.7**), X = Cl, Br or I).[90-93] He found that N_β, being a strong nucleophile, reacted with a large range of compounds containing a carbonyl group, forming a diverse range of organo-dinitrogen ligands (Scheme 1.2).[13,14,94] One of the most interesting reactions is the condensation with ketones and aldehydes, forming diazoalkane compounds (e.g. [M(NNCHPh)F($dppe)_2$][BF_4] (**1.8**)).[90,91,95,96] These are related to the parent hydrazido(2-) compounds studied in this Thesis, and have also been widely studied due to their relevance to dinitrogen fixation.[13,97-99]

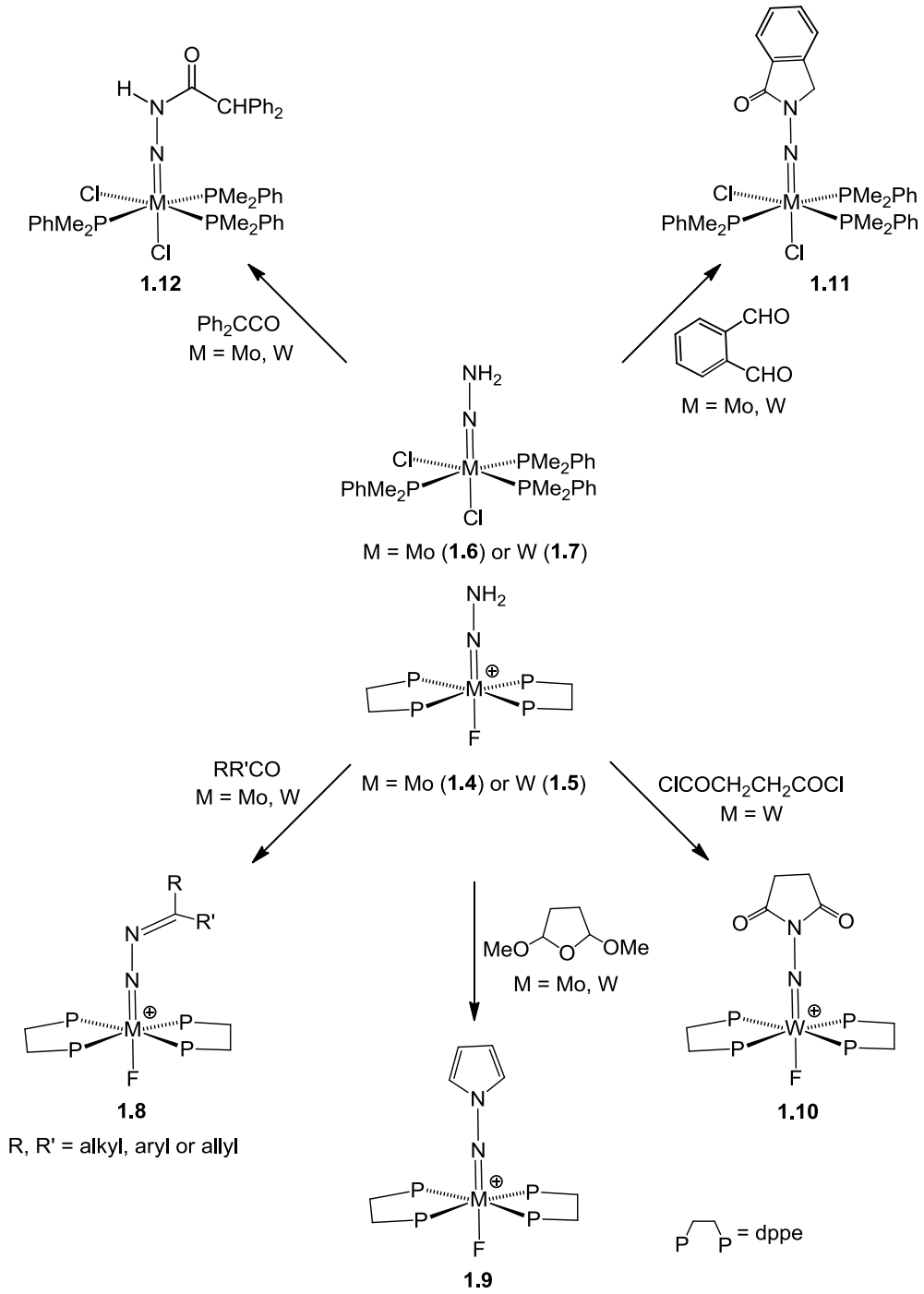

Scheme 1.2. Reactivity of phosphine supported Group 6 hydrazido(2-) complexes.[13,14]

In addition to the reactivity outlined in Scheme 1.2, the pyrrole ring in *trans*-$[W(NNC_4H_4)F(dppe)_2][BF_4]$ (**1.9**) undergoes *β*-regioselective electrophilic substitution (unlike in free pyrrole where substitution occurs preferentially at the *α*-position), further increasing the scope of ligands accessible from these compounds (Equation 1.4).[13,14,100]

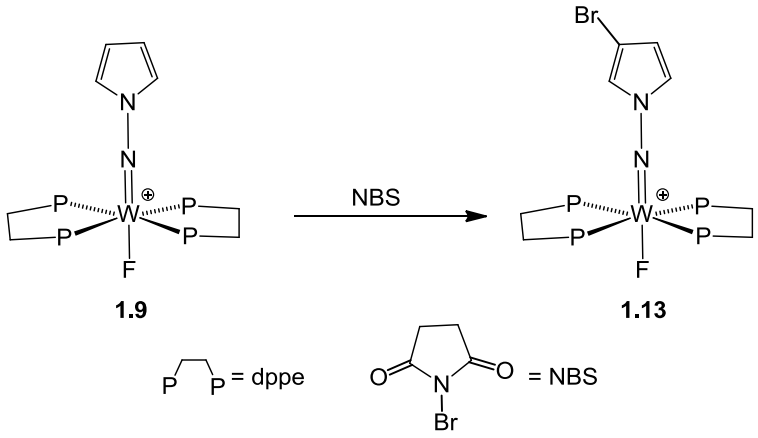

Equation 1.4

It is immediately clear that the reactivity of Group 6 hydrazido(2-) compounds is generally limited to substitution at N_β. Indeed, N_α–N_β cleavage only occurs under forcing conditions, typically involving $LiAlH_4$, Cp_2Co or Zn/Hg, as in the formation of ammonia and pyrrole from N_2 and 2,5-dimethoxytetrahydrofuran, using $M(dppe)_2(N_2)_2$ (M = Mo (**1.14**) or W (**1.15**)) as catalysts.[100-102]

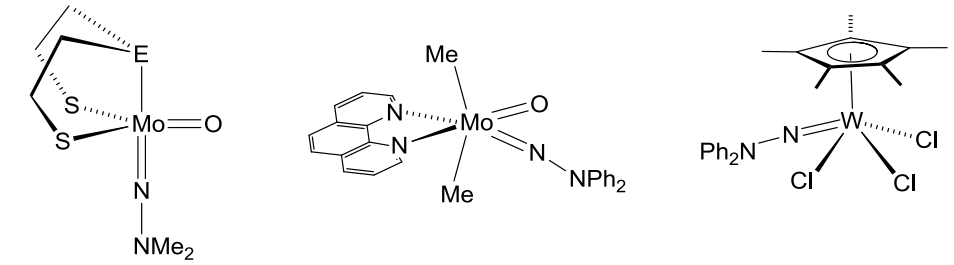

Figure 1.5. Selected examples of Group 6 terminal hydrazido(2-) complexes.

Some selected examples of structurally characterised Group 6 metal hydrazido(2-) complexes are presented in Figure 1.5. $Mo\{E(CH_2CH_2S)_2\}(NNMe_2)O$ (E = O (**1.16**) or S (**1.17**)) were synthesised by Sobota.[103] He found that protonation occurred at the metal centre, in contrast to the ligand protonation observed by Chatt, Schrock and others with phosphine ancillary ligands.[77-79,81,82,101,104,105] This demonstrates the importance of the ancillary ligand set on the reactivity of the hydrazide moiety.

Carrillo reported the molecular structure of $Mo(NNPh_2)(O)Me_2(1,10\text{-phen})$ (**1.18**).[106,107] It contains a short Mo=N_α but slightly lengthened N_α–N_β distance when compared to other Group 6 hydrazides (1.770(3) and 1.330(4) Å, respectively). This implies that there is a significant contribution from the hydrazido(2-) description of

the bonding. Changing the methyl groups for chlorides causes an increase in the Mo=N_α distance to 1.791(4) Å and a slight decrease in the N_α–N_β bond length to 1.276(5) Å, implying a greater contribution from the isodiazene canonic. This point is elaborated on in a discussion of the bonding in Section 1.4. Cp*W($NNPh_2$)Cl_3 (**1.19**) contains both short W=N_α (1.769(2) Å) and N_α–N_β bonds (1.296(3) Å),[108] indicating significant delocalisation of the electron density along the hydrazide fragment.

A number of other heavy Group 6 metal hydrazides have been structurally characterised.[104,109-114] However, there are no examples using a chromium centre, despite dimeric [CpCr($NNSiMe_3$)$_2$]$_2$ (**1.20**) being synthesised by Wiberg in 1978.[115] A limited number of diazoalkane complexes have been prepared,[116-119] with three structurally characterised. These include Cr($NNCPh_2$)$_2$(^{t}Bu$_3$SiO)$_2$ (**1.21**, Figure 1.6) which contains a bent hydrazide linkage (avg. Cr–N_α–N_β = 150.3(3) º).[120] Crystallographically-characterised examples of bent hydrazido ligands are rare, as are later transition metal examples in general.[121-131] CpRe{NNMe(*p*-C_6H_4OMe)}$(CO)_2$ (**1.22**, Figure 1.6) is a very unusual compound, containing a strongly bent hydrazido(2-) ligand (Re–N_α–N_β = 138.1(6) º) bound to a Group 7 metal centre.[132]

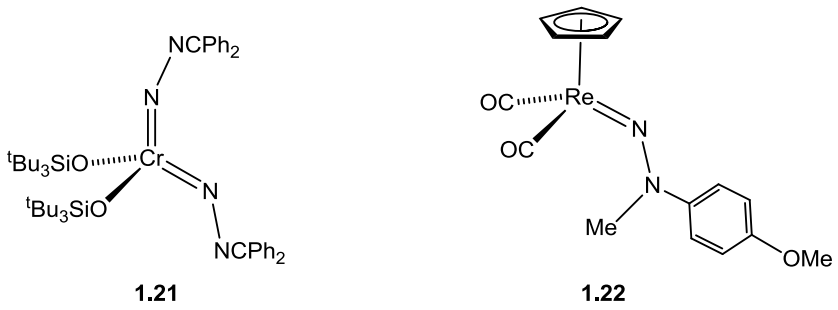

1.21 **1.22**

Figure 1.6. Cr($NNCPh_2$)$_2$(^{t}Bu$_3$SiO)$_2$ (**1.21**) and CpRe{NNMe(*p*-C_6H_4OMe)}$(CO)_2$ (**1.22**).

While the majority of work concentrated on the formation of hydrazido(2-) complexes several groups also synthesised hydrazido(1-) compounds. McCleverty reported Mo{HB(Me_2pz)$_3$}(NHNRR′)(NO)I (R = R′ = Me (**1.23**) or R = Me, R′ = Ph (**1.24**), Figure 1.7) with the molecular structure of **1.23** indicating multiple bonding character between both the Mo–N_α and N_α–N_β bonds.[133,134] Unlike the hydrazido(2-) compounds synthesised by Chatt, protonolysis yielded only free hydrazine with no N_α–N_β bond cleavage occurring.[78,135]

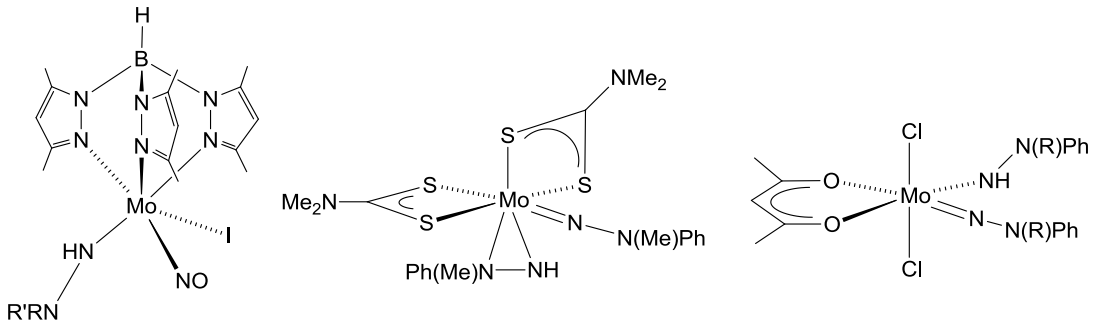

Figure 1.7. Selected Group 6 hydrazido(1-) complexes.

The synthesis of the unusual mixed η^2-hydrazido(1-)/η^1-hydrazido(2-) Mo{NN(Me)Ph}{N(H)N(Me)Ph}$(Me_2NCS_2)_2$ (**1.25**, Figure 1.7)[136] by Dilworth allowed comparison between a terminal hydrazido(2-) and bent hydrazido(1-) ligand. The η^1-hydrazido(2-) ligand contains a short Mo=N_α bond length (1.752(1) Å) and linear Mo=N_α–N_β group (169.6(7) º) indicating considerable multiple bond character, while the short N_α–N_β distance (1.285(14) Å) suggests that there is a significant degree of delocalisation within the hydrazide moiety. This can be attributed to a discernible contribution from the isodiazene canonic. In the η^2-hydrazido(1-) fragment both the Mo–N_α and N_α–N_β are indicative of single bonds (2.069(8) and 1.388(12) Å, respectively).

In contrast to **1.25**, the mixed hydrazido(1-)/hydrazido(2-) compounds Mo{NN(R)Ph}{N(H)N(R)Ph}Cl_2(acac) (R = Me (**1.26**) or Ph (**1.27**), acac = acetylacetonate)[137] contain both hydrazido ligands bound in an η^1- fashion (Figure 1.7). Again the hydrazido(2-) ligands exhibit significant delocalisation throughout the fragments, (Mo=N_α = 1.752(4) and 1.750(2) Å, N_α–N_β = 1.313(6) and 1.301(3) Å, Mo=N_α–N_β = 171.9(4) and 173.8(2) º for **1.26** and **1.27**, respectively). The η^1-hydrazido(1-) moieties, meanwhile, have Mo–N_α and N_α–N_β distances in-between those of single and double bonds (Mo–N_α = 1.948(5) and 1.948(2) Å, N_α–N_β = 1.359(6) and 1.339(3) Å for **1.26** and **1.27**, respectively), indicative of π-donation from N_α to Mo and N_β to N_α.

1.2.4 Group 5 metal hydrazido(2-) complexes

With the knowledge that Mo can be replaced by Fe and V in nitrogenase, and following the successes with Group 6, it was inevitable that the study of hydrazides would be extended to Group 5 metals.[69,138]

The first, $Cp_2V\{NN(SiMe_3)_2\}$ (**1.28**, Figure 1.8), was reported by Wiberg in 1976,[115] with the molecular structure solved by Veith.[139] The synthesis, analogous to that of $Cp_2Ti\{NN(SiMe_3)_2\}$ (**1.29**, *vide infra*), is performed by reacting Cp_2V with 1,2-bis(trimethylsilyl)diazene and is proposed to proceed *via* a silyl-transfer mechanism. The $V{=}N_\alpha$ distance is 1.666(6) Å and $N_\alpha{-}N_\beta$ is 1.369(9) Å, slightly longer than in the majority of Group 6 cases, consistent with a more reduced NNR_2 fragment.

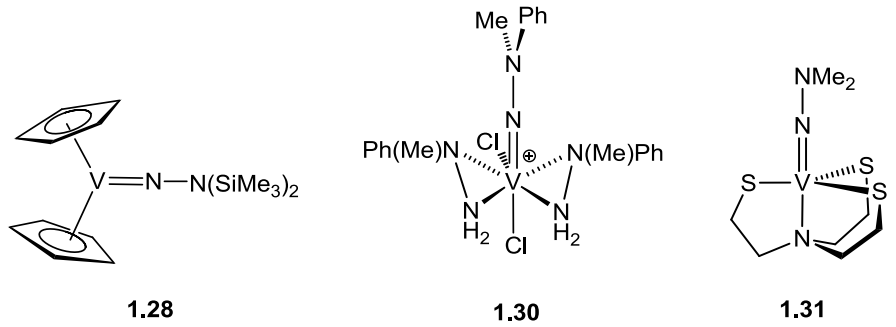

1.28 **1.30** **1.31**

Figure 1.8. Selected examples of vanadium hydrazido(2-) complexes.

The next vanadium hydrazido compound to be structurally characterised was $[V\{NN(Me)Ph\}C1_2\{NH_2N(Me)Ph\}_2]Cl$ (**1.30**, Figure 1.8) containing a cationic vanadium fragment surrounded by two neutral hydrazine ligands and two chlorides, in addition to the hydrazido(2-) group.[140] The $V{=}N_\alpha$ distance is slightly longer than in **1.28** (1.696(24) Å) with the $N_\alpha{-}N_\beta$ slightly shorter (1.295(17) Å) indicating a greater contribution from the isodiazene canonical form of the NN(Me)Ph moiety.

Sobota synthesised a family of alkyl and aryl substituted vanadium hydrazides of the type $V(NS_3)(NNRR')$ (NS_3 = $N(CH_2CH_2S)_3$) from the reaction of $V(NS_3)O$ with substituted hydrazines. $V(NS_3)(NNMe_2)$ (**1.31**), shown in Figure 1.8, could also be synthesised from $V(NNMe_2)(OAr')_3$ (**1.32**, Ar′ = 2,6-$C_6H_3{}^iPr_2$), itself made from treatment of the dianion $[(VCl)_3(\mu\text{-}NNMe_2)_3]^{2-}$ with LiOAr′.[141-143] Other vanadium hydrazide compounds have been made by Odom and Banerjee.[138]

In 1997, Green published the first niobium hydrazides formed by reaction of $CpNbCl_4$ with 1,1 disubstituted hydrazines. For dimethylhydrazine this led to formation of the unusual dimer $Cp_2Nb_2(\mu{:}\eta^1,\eta^2\text{-}NNMe_2)(\eta^1\text{-}NNMe_2)Cl_4$ (**1.33**), the two hydrazide ligands exhibiting different coordination modes. This could be cleaved to form monomeric $CpNb(NNMe_2)\{P(OMe)_3\}Cl_2$ (**1.34**) by addition of trimethyl phosphite (Figure 1.9). Compound **1.34** contains an sp^3 hybridised N_β, indicative of hydrazido(2-) bonding, despite having a reasonably long $Nb{=}N_\alpha$ distance (1.789(2) Å) and short $N_\alpha{-}N_\beta$ bond length (1.338(2) Å).[144] These characteristics are mirrored in the niobocene hydrazide $Cp'_2Nb(NNMe_2)Cl$ (**1.35**, Figure 1.9, $Cp' = C_5H_4Me$).[145]

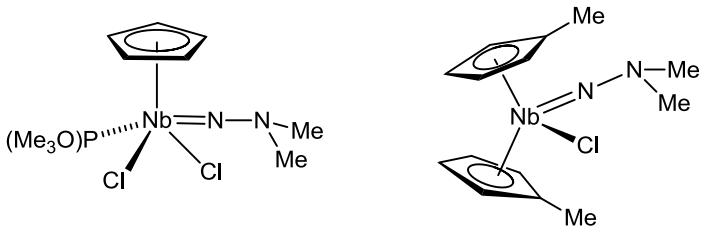

1.34 **1.35**

Figure 1.9. Cyclopentadienyl supported terminal hydrazido(2-) complexes of niobium.

Winter reported the cationic niobium mixed hydrazine/hydrazido(2-) complex $[Nb(NNMe_2)Cl_2(NH_2NMe_2)(TMEDA)]Cl$ (**1.36**, TMEDA = tetramethylethylenediamine) and extended it to a tantalum metal centre (**1.37**, Figure 1.10).[146] Compound **1.36** has slightly shorter $Nb{=}N_\alpha$ and $N_\alpha{-}N_\beta$ distances than those seen in **1.34** and **1.35** (1.776(3) Å and 1.317(4) Å, respectively). The tantalum analogue, **1.37**, possesses $Ta{=}N_\alpha$ and $N_\alpha{-}N_\beta$ lengths of 1.773(3) and 1.328(5) Å, respectively.

Very recently Bercaw published the synthons $M(NNPh_2)Cl_3(DME)$ (M = Nb (**1.38**) or Ta (**1.39**), DME = 1,2-dimethoxyethane)[147,148] reminiscent of $Ti(NNPh_2)Cl_2(py)_3$ (**1.40**) published by Mountford (*vide infra*).[56] Compound **1.39** allows a wide range of anionic ancillary ligand supported hydrazides to be accessed, including $Cp_2Ta(NNPh_2)Cl$ (**1.41**) and $Ta(N_2N^{Me})(NNPh_2)(Cl)$ (**1.42**, $H_2N_2N^{Me} = MeN(CH_2CH_2N(H)SiMe_3)_2$, Figure 1.10) *via* salt metathesis. The pertinent distances for **1.41** and **1.42** are 1.8153(16) and 1.7988(1) Å ($Ta{=}N_\alpha$) and 1.3358(22) and 1.363(1) Å ($N_\alpha{-}N_\beta$), respectively. Reactions between **1.38** and anionic ligands have not, to date, been studied.

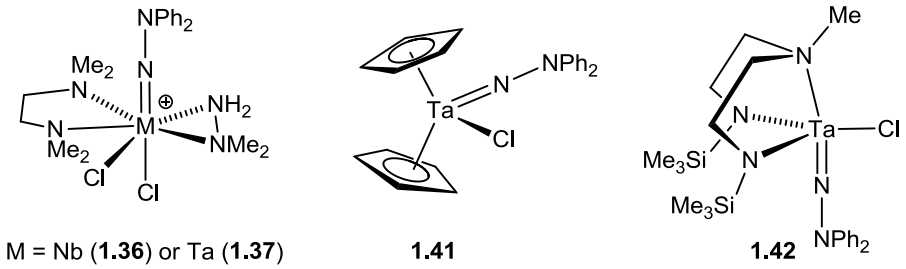

Figure 1.10. Selected heavy Group 5 metal hydrazido(2-) complexes.

1.3 Group 4 metal-nitrogen multiple bond chemistry

1.3.1 Group 4 metal imido chemistry

The chemistry of Group 4 metal hydrazide compounds has evolved in a very similar way to their imido cousins, in many cases utilising the same synthetic techniques. A short review of Group 4 imido(2-) complexes is presented here, to enable a comparison with that of the hydrazido(2-) ligand. The use of imido(2-) complexes in catalysis and reactivity has been extensively studied.[8,16,18,19,21-23,29-33,149-157]

Bergman reported the first Group 4 imido complex *via* thermolysis of $Cp_2Zr(NH^tBu)(Me)$ (**1.43**, Scheme 1.3). This formed the transient species $Cp_2Zr(N^tBu)$ (**1.44**) which could be isolated as the THF adduct $Cp_2Zr(N^tBu)(THF)$ (**1.45**).[17,20] Concurrent with this report was the synthesis of $Zr\{N(Si^tBu_3)\}\{(N(H)(Si^tBu_3)\}_2(THF)$ (**1.46**) by Wolczanski also using thermolysis of an alkyl/amido complex.[158]

Bergman went on to investigate the bonding and reactivity of **1.45** and its aryl analogous $Cp_2Zr(NAr)(L)$ (Ar = 2,6-$C_6H_3Me_2$ (**1.47**, Xyl) and 2,6-$C_6H_3{}^iPr_2$ (**1.48**), L = THF, $OPPh_3$ or $NC_5H_4{}^tBu$) in detail.[20,21,159,160] They showed a rich reaction chemistry towards unsaturated reagents dominated by [2+2] or [2+3] cycloaddition (and subsequent elimination) at the Zr=N bond[17,159-165] and C–H activation reactions[160,166] (Scheme 1.3). In addition to the synthesis of a large range of organo-nitrogen ligands *via* novel methods, these studies indicated that elimination of the carbodiimide (or related) fragment was significantly more favourable for the alkyl imide. This observation has been mirrored in hydrazide chemistry.[46]

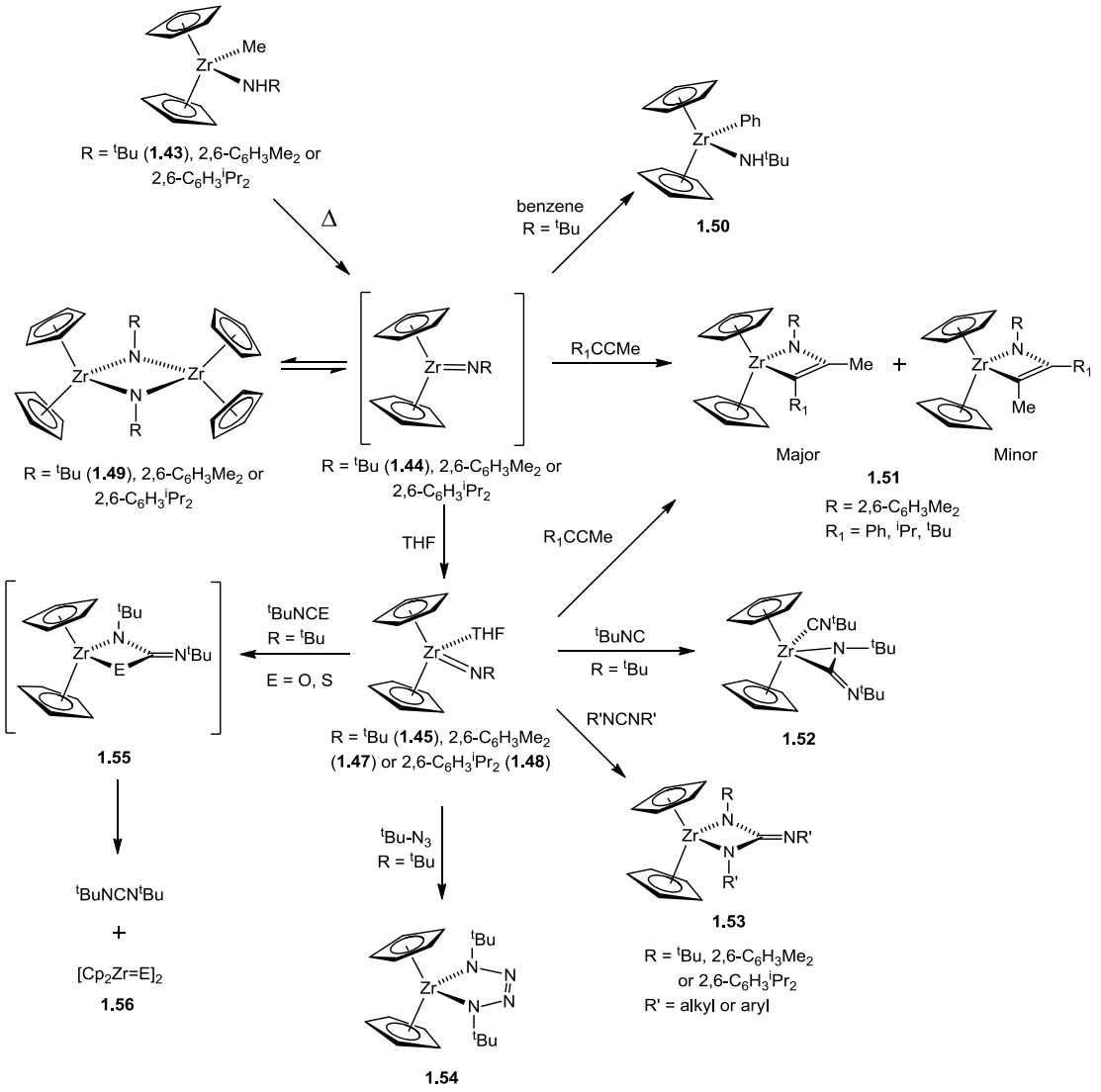

Scheme 1.3. Selected reactions of zirconocene imido complexes.[20]

$Cp_2Zr(NXyl)(THF)$ (**1.47**) was also shown to be an efficient catalyst for the hydroamination of alkynes, formally N–H addition across a C≡C bond (Scheme 1.4). Detailed mechanistic work on this reaction and the reversible [2+2] cycloaddition with alkynes were presented.[161,162,167] Recently the catalytic hydroamination reaction (and related hydrohydrazination reaction in hydrazide chemistry, *vide infra*) has attracted significant interest as an atom-efficient way of synthesising small, nitrogen containing molecules. Some examples of other successful catalysts are presented in Figure 1.11.[168-170]

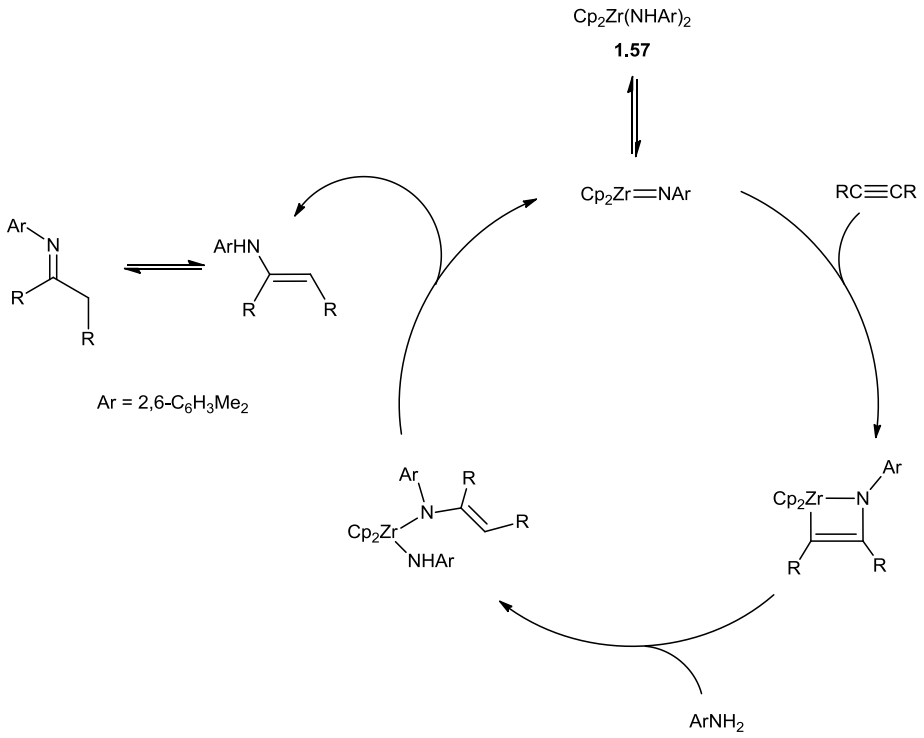

Scheme 1.4. Hydroamination catalytic cycle using $Cp_2Zr(NHXyl)_2$ (**1.57**) as a pre-catalyst.

1.58 **1.59**

Figure 1.11. Titanium based catalysts for the hydroamination of alkynes.

Rothwell[24] and Roesky[25] reported the first titanium imido(2-) complexes, with the former using a protonolysis method which has been successfully employed in the synthesis of a large range of imido(2-) compounds. In 1997 Mountford reported formation of the synthon $Ti(NR)Cl_2(py)_3$ (R = alkyl (**1.60**) or aryl (**1.61**)), building upon initial work performed by Winter in 1992 who synthesised $Ti(N^tBu)Cl_2(OPPh_3)_2$ (**1.62**) from $TiCl_4$, H_2N^tBu and $OPPh_3$.[154,155] Compounds **1.60** and **1.61** have allowed access to a wide range of neutral and anionic ligand supported alkyl and aryl imides *via* salt metathesis and/or pyridine displacement (Scheme 1.5).[18,19,156,171-187] The compounds made in this fashion have demonstrated diverse reactivity with the imido ligand acting both as a spectator (as in the polymerisation of ethylene by **1.67** - **1.70**) and participating ligand in reactivity studies.[19,171,179,181,183,188-200]

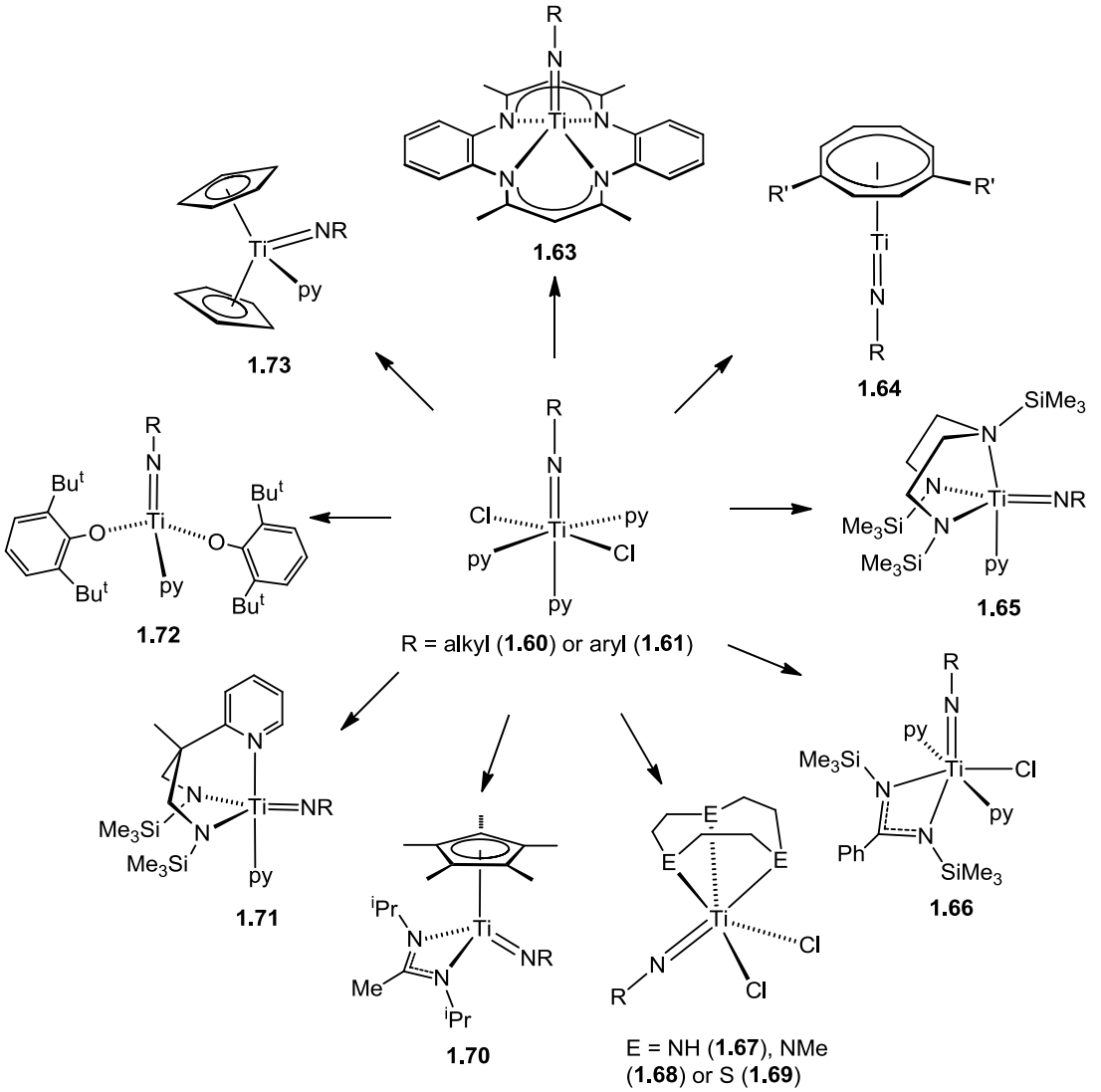

Scheme 1.5. Synthesis of titanium imido(2-) complexes from $TiCl_2(NR)(py)_3$.

The reactivity displayed by the imido group of the diamide-amine supported imido complex $Ti(N_2N^{py})(N^tBu)(py)$ (**1.71**, $H_2N_2N^{py}$ = $MeC(2\text{-}C_5H_4N)(CH_2N(H)SiMe_3)_2$) is particularly rich and selected transformations are outlined in Scheme 1.6.[19,156,201-207] Reaction of **1.71** with terminal alkynes proceeded *via* anti-Markovnikov addition to yield the azatitanacyclobutenes $Ti(N_2N^{py})\{N(^tBu)C(H)C(Ar)\}$ (Ar = Ph (**1.74**) or Tol (**1.75**)). Allenes and internal alkynes (RCCMe, R = Me or Ph) led to the formation of titanaazetidines (**1.76**). The mechanism for the transformation with alkynes is proposed to proceed *via* initial C–H activation of the methyl group across the $Ti{=}N_\alpha$ bond. This is followed by H atom transfer forming a π-bonded allene with a final [2+2] cycloaddition yielding the observed products. Isocyanates were found to insert into a metal-amide bond of the ancillary ligand (**1.77**).

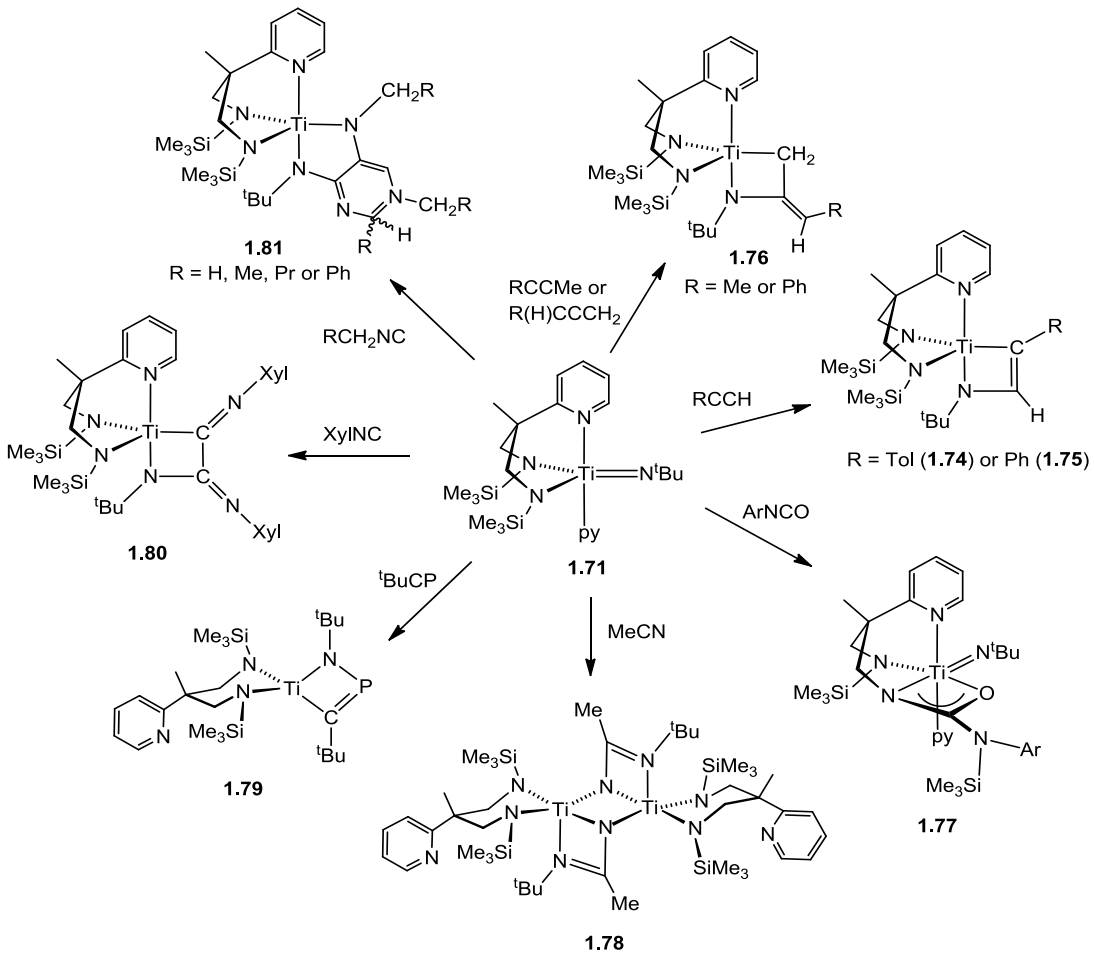

Scheme 1.6. Selected reactions of Ti(N_2N^{py})(N^tBu)(py) (**1.71**).

Acetonitrile and *tert*-butyl phosphaalkyne react with **1.71** in similar ways, both proceeding through a [2+2] cycloaddition intermediate before the ancillary ligand changes to a κ^2-bound conformation. In the case of MeCN, this is followed by dimerisation to form **1.78**, but in the case of ^{t}BuCP, where the *N,C*-bound metallacycle is formed in preference to the *N,P*-bound, the product remains a monomer (**1.79**). When reacted with two or three equivalents of isocyanides **1.71** underwent highly selective coupling of the imido linkage to form **1.80** and **1.81**. Schemes 1.3 and 1.6 indicate the large scope of reactivity accessible to Group 4 imido complexes supported by bis(cyclopentadienyl) and diamide-amine ancillary ligands. These successes have, in part, contributed to the rapid surge in interest of Group 4 hydrazides over the last few years.

1.3.2 Titanium hydrazido compounds

The first titanium hydrazido compound, $Cp_2Ti\{NN(SiMe_3)_2\}$ (**1.29**), was synthesised in 1978 by Wiberg[115] through a silyl-transfer reaction between $CpTiCl_2$ and two equivalents of $Me_3SiN{=}NSiMe_3$ (Equation 1.5). Further study and full characterisation were not carried out, possibly due to the thermal instability of $Me_3SiN{=}NSiMe_3$ which decomposes above -30 ºC.[208]

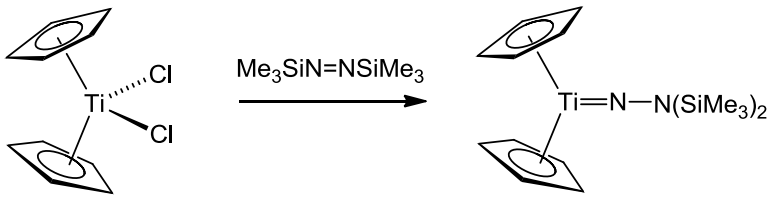

1.29

Equation 1.5

In 1999 the first fully characterised titanium hydrazido(2-) complex, $Ti(NNPh_2)(Me_4taa)$ (**1.82**, H_2Me_4taa = tetramethyl dibenzotetraaza[14]annulene, Equation 1.6) was published.[171] The synthesis, *via* imido/hydrazine exchange from the *tert*-butyl imido compound $Ti(N^tBu)(Me_4taa)$ (**1.63**), is significantly more simple than that of **1.29** and has been successfully applied in the synthesis of other titanium hydrazides.[39,46,47] The reactions with CO_2 and TolNCO were investigated, forming [2+2] cycloaddition products (exclusively *N*,*N*′-bound in the case of TolNCO (**1.83**), Equation 1.6).

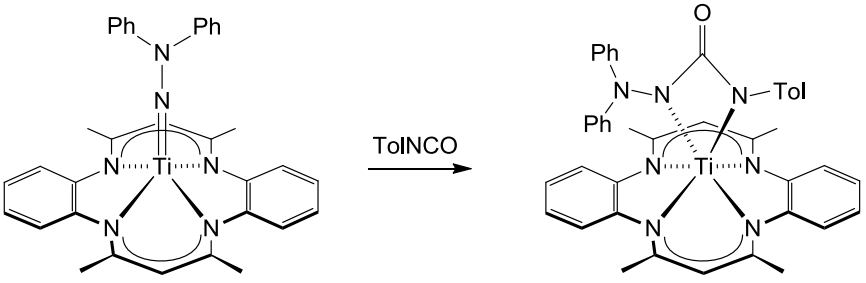

1.82 **1.83**

Equation 1.6

The following year Woo reported two macrocycle supported titanium hydrazides, $Ti(NNR_2)(TTP)$ (R = Me (**1.84**) or Ph (**1.85**), TTP = *meso*-tetra-*p*-tolyporphyrinato dianion). These were found to react with *p*-chlorobenzaldehyde to form the corresponding hydrazone, $(4\text{-}C_6H_4Cl)C(NNR_2)H$, and oxo compound, Ti(TTP)O.[209] It

was not until 2004 that the first structurally characterised terminal titanium hydrazide, Ti(NNMe$_2$)(^{t}Bu-bipy)(dap) (**1.86**, dap = α-(dimethylaminomethyl)pyrrole, ^{t}Bu-bipy = 4,4′-di-*tert*-butyl-2,2′-bipyridine), was reported by Odom.[55]

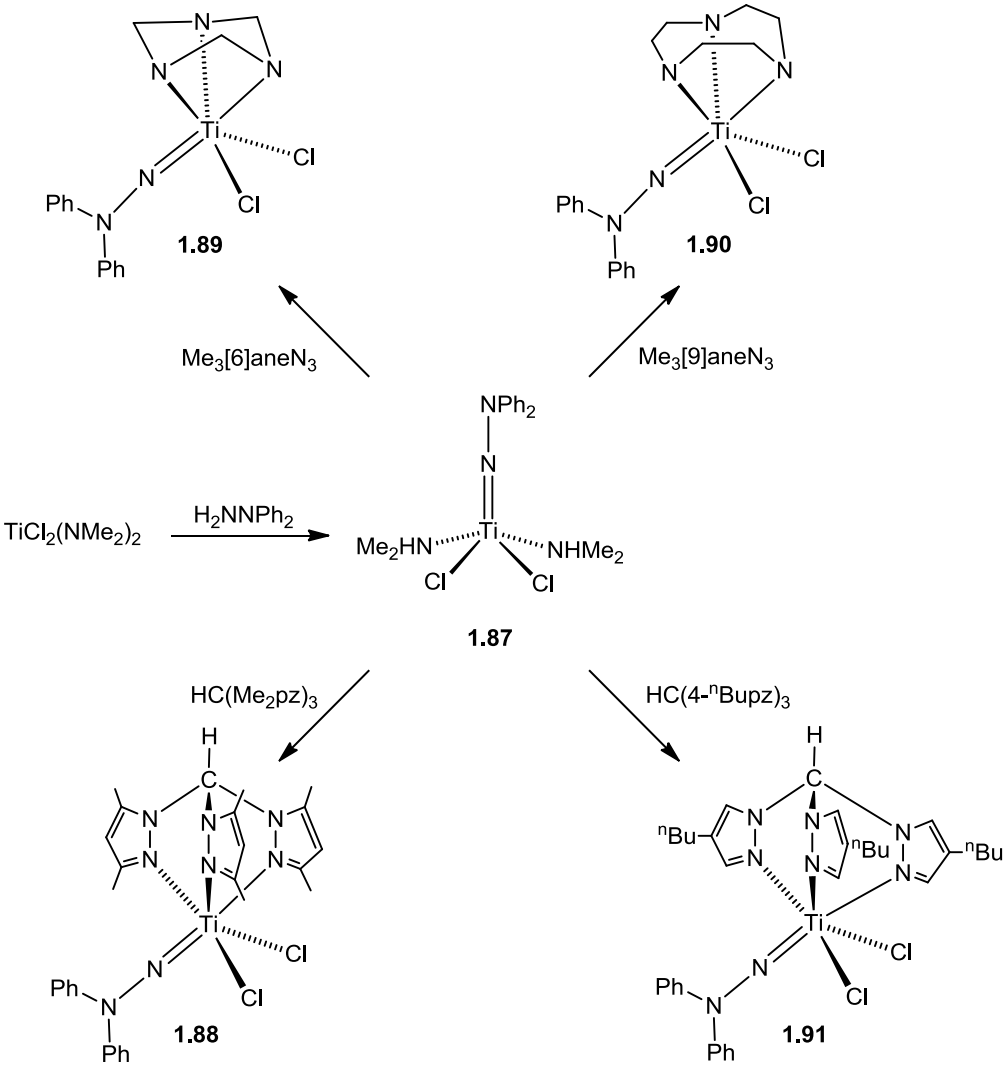

Scheme 1.7. Examples of titanium hydrazido(2-) complexes supported by neutral face-capping ligands.

Building on the successes of the imido synthons Ti(NR)Cl$_2$(py)$_3$ (R = alkyl (**1.60**) or aryl (**1.61**)),[19] Mountford and co-workers found that the related hydrazido synthons, Ti(NNPh$_2$)Cl$_2$(L)$_3$ (L = NHMe$_2$ (**1.87**) or py (**1.40**)), could be easily made by protonolysis of TiCl$_2$(NMe$_2$)$_2$ (for **1.87**) or Ti(N^{t}Bu)Cl$_2$(py)$_3$ (for **1.40**) with H$_2$NNPh$_2$.[56] As in the case of the imido synthons, **1.87** reacted with a range of neutral tridentate ligands (including Me$_3$[6]ane, Me$_3$[9]ane, HC(3,5-Me$_2$pz)$_3$ and HC(4-^{n}Bupz)$_3$) to yield *fac*-N$_3$ donor ligand supported complexes (**1.88** – **1.91**, Scheme 1.7). The solid state structure of Ti(HC(Me$_2$pz)$_3$)(NNPh$_2$)Cl$_2$ (**1.88**) was

solved and DFT calculations used to probe the nature of the bonding of the hydrazido(2-) ligand, these are discussed later.[56]

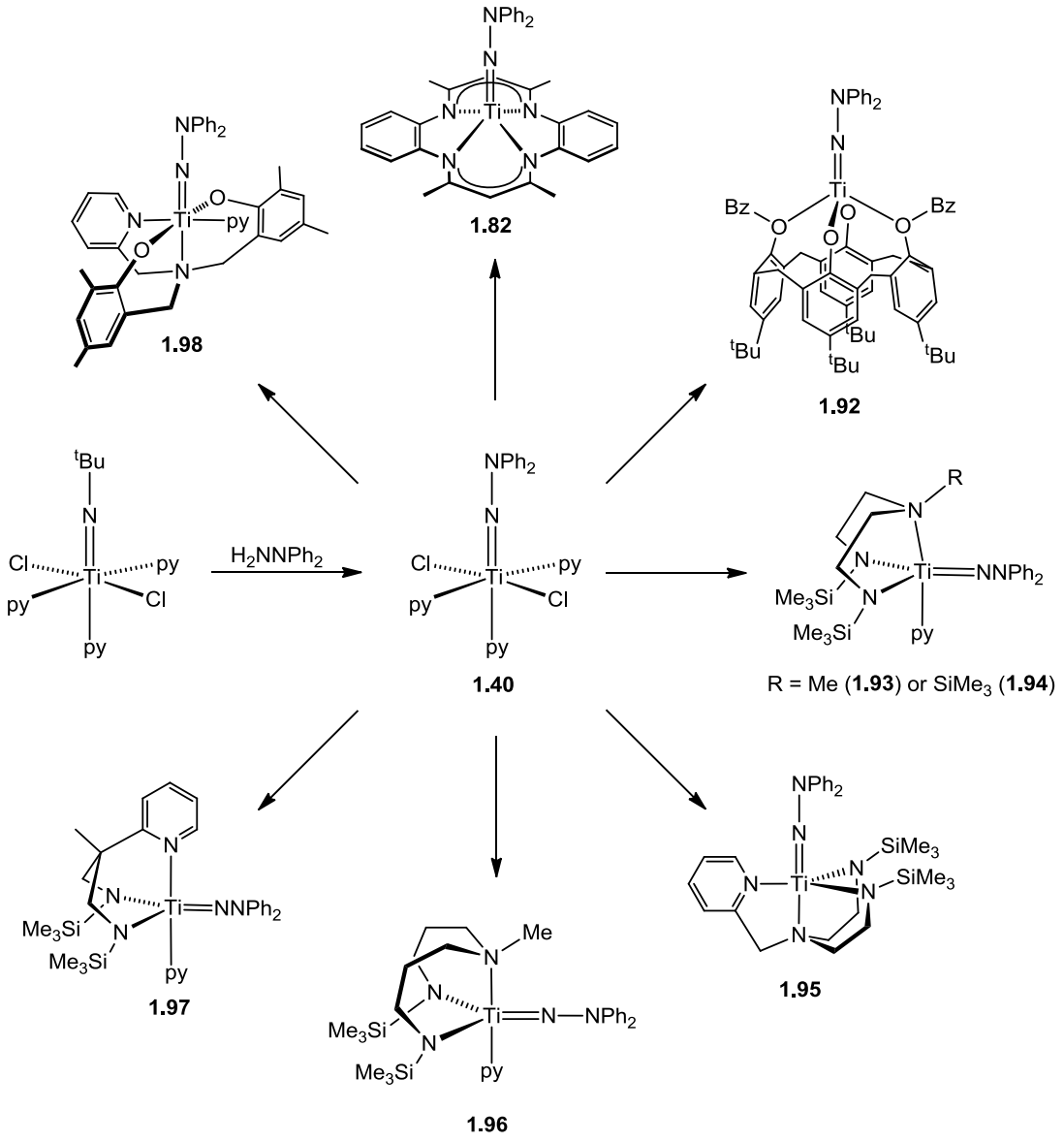

Scheme 1.8. Examples of titanium hydrazido(2-) complexes supported by dianionic ancillary ligands.

With anionic ligands, the acidic nature of $HNMe_2$ led to multiple side reactions. Syntheses using **1.40**, however, were much more successful and allowed isolation of a range of terminal titanium hydrazido(2-) compounds supported by anionic ancillary ligands (**1.82** and **1.92 - 1.98**, Scheme 1.8).[48,51] Attempts to make dimethyl analogues of **1.87** and **1.40** were unsuccessful due to dimerisation, yielding the bridged dimers $Ti_2(\mu{:}\eta^2,\eta^1\text{-}NNMe_2)_2Cl_4(L)_2$ (L = $NHMe_2$ (**1.99**) or py (**1.100**)).[56] These were found to

be inert to protonolysis or salt metathesis indicating that μ:η^2,η^1-$NNMe_2$ bridges are not readily cleaved.

N_β coordination to the metal centre occurs in a wide range of Group 4 hydrazido compounds, particularly with dimethyl substituted N_β, where the lone pair is more nucleophilic than in the corresponding aryl substituted cases. Dimeric hydrazido(2-) complexes with N_β coordination were first reported by Leigh[210] and there are now a significant number of structurally authenticated examples.[211,212] The dimers formed are often unsymmetrical containing bridging N_α atoms but coordination of only one N_β lone pair to a metal centre, such as in **1.101** (Figure 1.12).[213]

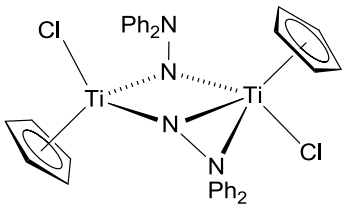

1.101

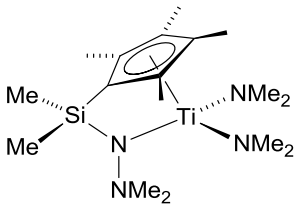

1.102

Figure 1.12. Examples of titanium hydrazido complexes.

Further studies on the ability of the N_β lone pair to donate to the metal centre were performed by Park who synthesised the *ansa*-cyclopentadienyl hydrazido(1-) complex **1.102** (Figure 1.12, shown as η^1-coordinated). The hydrazido ligand could be switched between η^1 and η^2-coordination by making the metal centre more or less electron rich, with η^2 favoured by electron deficiency.[214,215]

Since the synthesis of $Ti(NNPh_2)(Me_4taa)$ (**1.82**), a significant number of titanium hydrazides have been reported utilising *tert*-butyl imido/hydrazine exchange. These include $Cp_2Ti(NNPh_2)(py)$ (**1.103**)[47,51] and Cp*Ti{MeC(N^iPr)$_2$}(NNRR′) (R = R′ = Ph (**1.104**), R = Me, R′ = Ph (**1.105**) and R = R′ = Me (**1.106**)),[46,51] reported by Mountford, and Gade's Cp*Ti(N^{Xyl}N)(NNRR′)(L) (R = R′ = Ph (**1.107**), R = Me, R′ = Ph (**1.108**), R = R′ = Me (**1.109**), N^{Xyl}NH = N-(3,5-dimethylphenyl)-4,5-dihydro-3H-pyrrol-2-amine, Figure 1.13).[39] The Ti=N_α and N_α–N_β distances range from 1.723(2) to 1.757(2) Å and 1.351(3) to 1.386(2) Å, respectively, indicative of metal-nitrogen multiple bonds and N_α–N_β single bonds. These distances are typical for Group 4 hydrazides, clearly indicating hydrazido(2-) character with minimal contributions from the isodiazene canonical form (*vide infra*).

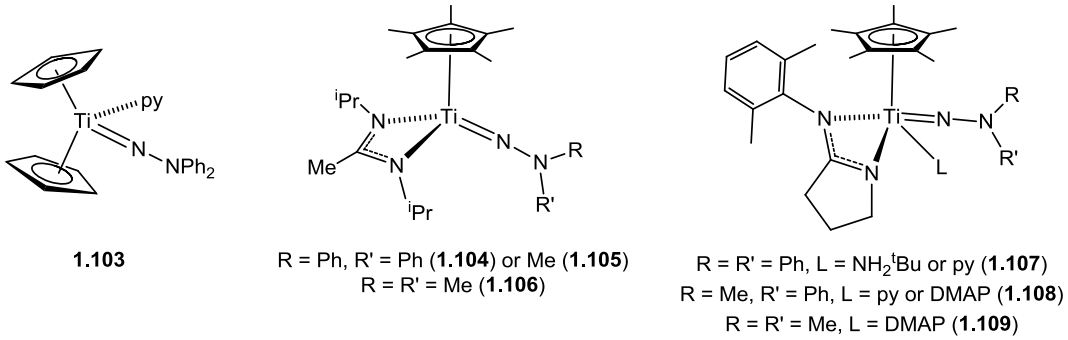

1.103

R = Ph, R' = Ph (**1.104**) or Me (**1.105**)
R = R' = Me (**1.106**)

R = R' = Ph, L = $NH_2{}^tBu$ or py (**1.107**)
R = Me, R' = Ph, L = py or DMAP (**1.108**)
R = R' = Me, L = DMAP (**1.109**)

Figure 1.13. Selected titanium hydrazido(2-) complexes synthesised *via* imido/hydrazine exchange.

$Cp_2Ti(NNPh_2)(py)$ (**1.103**) is a rare example of a formally 20 electron compound. For this reason computational studies have been performed on the bonding which indicate that the ′excess′ electrons occupy a ligand based non-bonding orbital possessing Cp and N_α character.[47] This is manifested in weaker and longer Ti–Cp and Ti–N_α interactions and has been demonstrated by a comparison of the ligand redistribution between $Cp_2Ti(NNPh_2)(py)$ (**1.103**) and $Ti(NNPh_2)Cl_2(py)_3$ (**1.40**), which proceeds at 60 ºC, while that of Cp_2TiCl_2 and $TiCl_4$ requires 120 ºC and extended reaction times. Compound **1.103** has been shown to form a *C,N*-bound cycloaddition with ^{t}BuCP, $Cp_2Ti\{N(NPh_2)PC(^tBu)\}$ (**1.110**, similar to **1.79** formed by the reaction of ^{t}BuCP with **1.71)** and an azatitanacyclobutene with PhCCPh, $Cp_2Ti\{N(NPh_2)C(Ph)C(Ph)\}$ (**1.111**).[49]

As for the related imido compounds,[216] the chemistry of $Cp^*Ti\{MeC(N^iPr)_2\}(NNR_2)$ (**1.104** and **1.106**) has been systematically studied.[45,46,60,99,217] A summary of this reactivity is shown in Schemes 1.9 and 1.10. With CE_2 (E = O or S) the expected cycloaddition/Ti=N_α insertion chemistry was observed forming compounds **1.112** and **1.113**. $Cp^*Ti\{MeC(N^iPr)_2\}(NNPh_2)$ (**1.104**) also reacted with RNCE (R = alkyl or aryl, E = O or S) to form [2+2] cycloadditions (**1.114**). However, with $Cp^*Ti\{MeC(N^iPr)_2\}(NNMe_2)$ (**1.106**) elimination of the carbodiimide (or related) fragment occurred more readily yielding the oxo-bridged dimer $[Cp^*Ti\{MeC(N^iPr)_2\}(\mu\text{-}O)]_2$ (**1.116**, Scheme 1.9). The higher propensity of alkyl substituents to eliminate organic fragments mirrors the trend seen in imido chemistry.

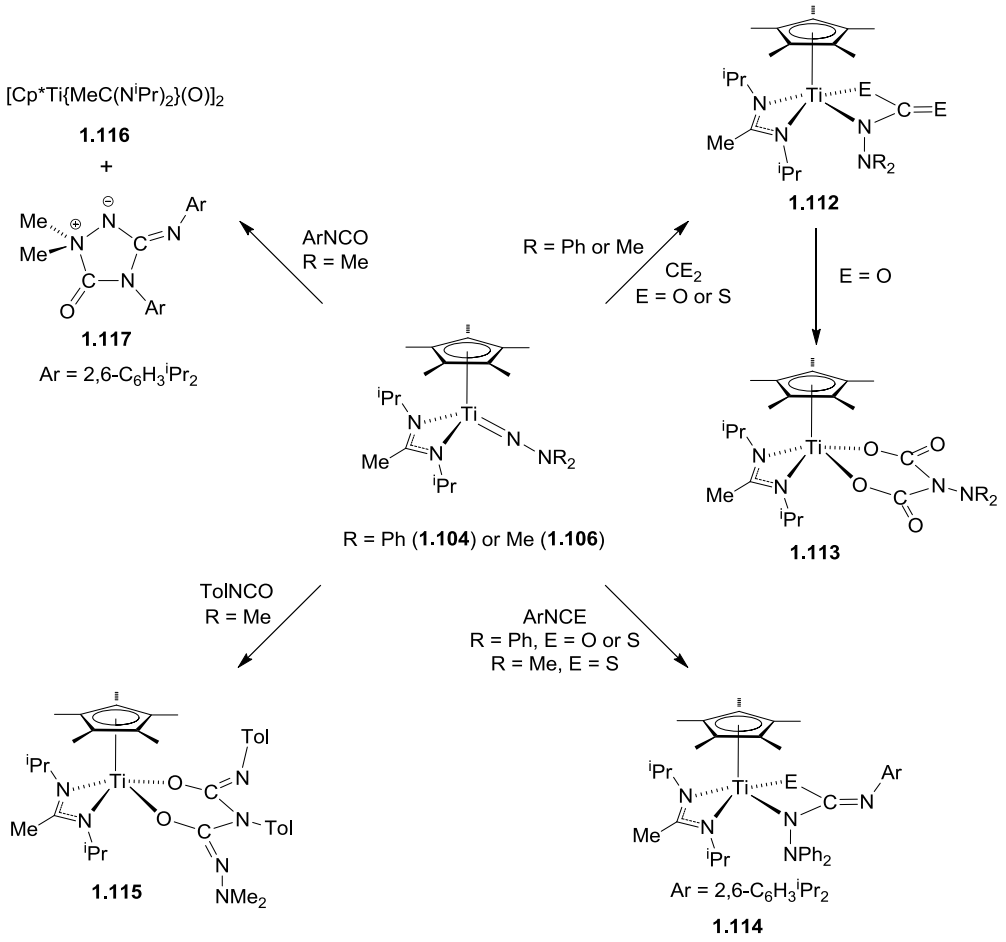

Scheme 1.9. Cycloaddition, insertion and elimination reactivity of Cp*Ti{MeC(N^{i}Pr)$_2$}(NNR$_2$) (R = Ph (**1.104**) and Me (**1.106**)).[46,60]

The most interesting reactivity of Cp*Ti{MeC(N^{i}Pr)$_2$}(NNR$_2$) (**1.104** and **1.106**) is that seen with various silanes and chlorosilanes (Scheme 1.10). For Cp*Ti{MeC(N^{i}Pr)$_2$}(NNMe$_2$) (**1.106**) these cause protonation or chlorination at the metal centre, while the silyl group binds to N$_\alpha$ and the hydrazide group becomes η^2-coordinated (**1.118**). The mechanism for the silane addition is reported as proceeding *via* an initial coupling of the Si–H bond across Ti=N$_\alpha$ followed by N$_\beta$ coordination. However, for chlorosilanes, N$_\beta$ coordination occurs before the coupling step.[45] Different reactivity is observed between chlorosilanes and Cp*Ti{MeC(N^{i}Pr)$_2$}(NNPh$_2$) (**1.104**) yielding compounds **1.119** and **1.120** where ligand transfer to a silicon has occurred.[45]

Alkylation of **1.106** is found to occur exclusively at N$_\beta$, the reaction with MeI forming **1.121**, in contrast to protonation, which occurs at N$_\alpha$ forming an η^2-bound hydrazido(1-) fragment (**1.122**).

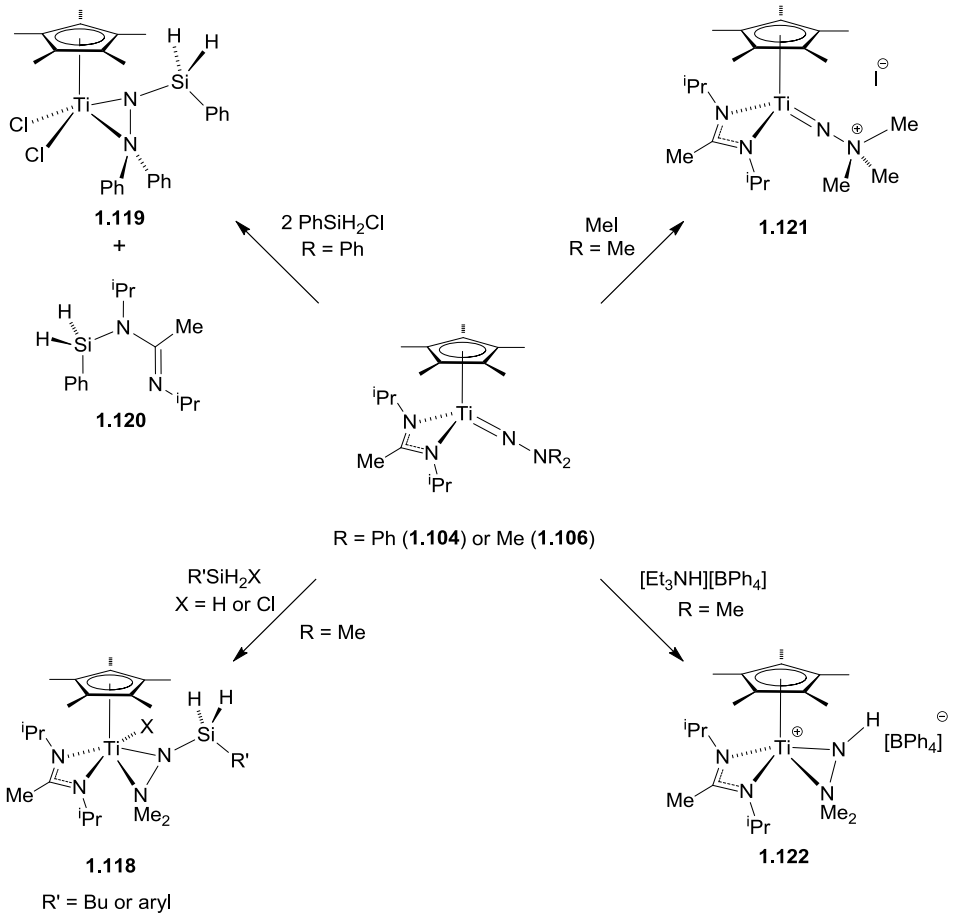

Scheme 1.10. Alkylation, protonation and Si–X reactivity of Cp*Ti{MeC(N^{i}Pr)$_2$}(NNR$_2$) (R = Ph (**1.104**) and Me (**1.106**)).[45,217]

Ancillary ligand reactivity has also been seen in the series of titanium hydrazido(2-) complexes Ti(Me$_2$calix)(NNR$_2$) (**1.123** - **1.125**, Me$_2$calix = dianion of 1,3-dimethyl ether of *tert*-butyl calix[4]arene, Figure 1.14). These were formed from Ti(Me$_2$calix)Cl$_2$ and two equivalents of the relevant lithiated hydrazine.[50]

Reaction of Ti(Me$_2$calix)(NNMe$_2$) (**1.125**) with methyl iodide, instead of yielding the expected [Ti(Me$_2$calix)(NNMe$_3$)]I, led to formation of the zwitterionic product **1.126** (Figure 1.14). It was proposed that initial methylation at N$_\beta$ was followed by demethylation of the non-innocent supporting ligand by the iodide anion. This is supported by labelling studies with MeI-d_3 and the observation that the reaction proved to be catalytic with respect to MeI. Similar reactivity was observed with ^{t}BuNCO, initial cycloaddition bringing N$_\beta$ within close proximity of one of the ligand ether groups, enabling methyl migration. This was followed by a rearrangement to yield the *N*,*O*-bound zwitterionic metallacycle **1.127**, the first reported cleavage of the Ti=N$_\alpha$ bond in a hydrazido(2-) complex.

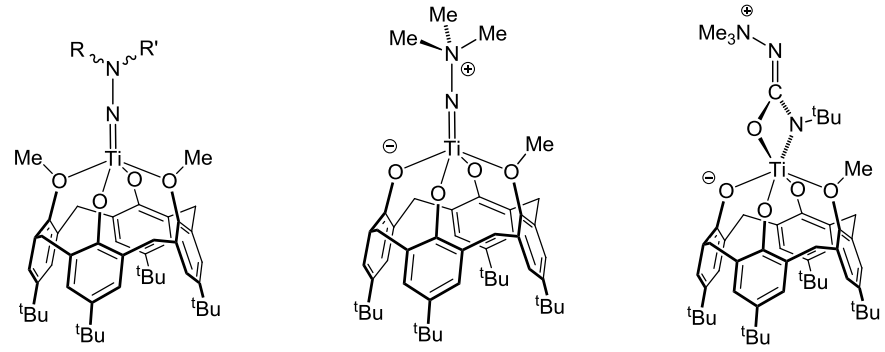

Figure 1.14. Calix[4]arene supported Titanium hydrazides and products formed by the reactions with MeI and ^{t}BuNCO.

Cycloadditions between Cp*Ti(N^{Xyl}N)(NNR$_2$)(L) (**1.107** - **1.109**, Figure 1.13) and PhNCE (E = O or S) have also been observed by Gade.[38] In contrast to the chemistry of Cp*Ti{MeC(N^{i}Pr)$_2$}(NNPh$_2$) (**1.104**), where cycloadditions with isocyanates were solely formed as the *N*,*O*-bound product, complexes **1.128** - **1.131** are present as both *N*,*E*- and *N*,*N′*-bound isomers (Scheme 1.11). The reaction with phenyl allene gave a mixture of diastereotopic [2+2] cycloaddition products (**1.132** and **1.133**, Scheme 1.11).

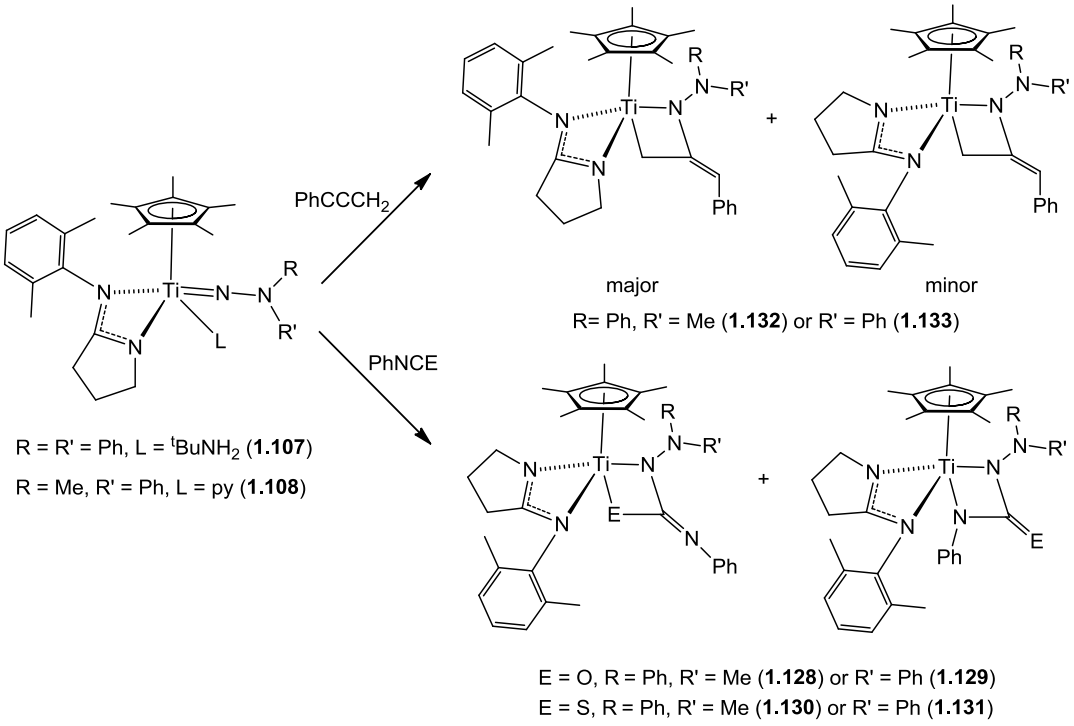

Scheme 1.11. Reaction between Cp*Ti(N^{Xyl}N)(NNR$_2$)(L) (**1.107** or **1.108**) and PhCCCH$_2$ (**1.132** and **1.133**, top) or PhNCE (E = O or S (**1.128** - **1.131**), bottom).[38]

In addition to the reactivity described above, Cp*Ti($N^{Xyl}N$)(NNR_2)(L) (**1.107** - **1.109**) were found to catalytically produce hydrazones *via* the hydrohydrazination reaction (a modification of the hydroamination reaction described earlier).[39] The reactions were quantitative over 1 h with a catalyst loading of 5 mol% and exhibited Markovnikov regioselectivities of > 99 % at ambient temperature. Interestingly, this regioselectivity is opposite to that seen between alkynes and the diamide-amine supported titanium hydrazide Ti(N_2N^{py})($NNPh_2$)(py) (**1.97**, *vide infra*).[51,61]

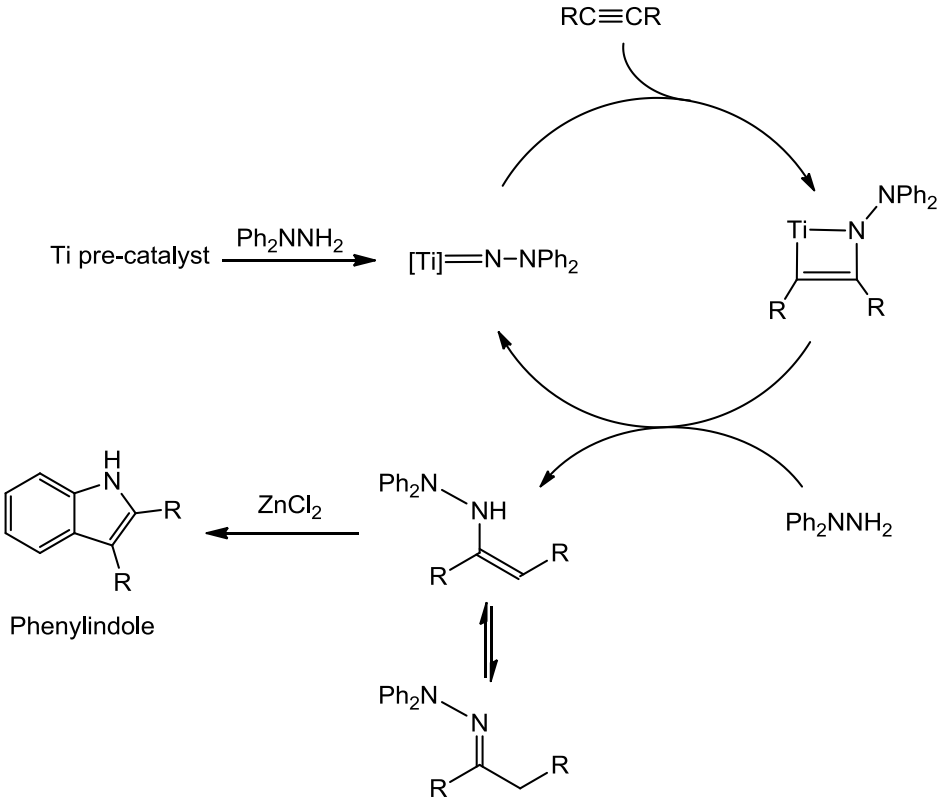

Scheme 1.12. Schematic of titanium catalysed hydrohydrazination using 1,1-diphenylhydrazine and a generic alkyne, followed by Fischer indole cyclisation.

While Gade did not study the mechanism of hydrazone formation, work undertaken by Odom and comparison with the hydroamination cycle indicate that it is likely to proceed *via* an initial [2+2] cycloaddition at Ti=N_α of a terminal hydrazido(2-) complex, followed by protonation (Scheme 1.12).[53,55,218] Odom has investigated the activity of various catalysts, including Ti(dap)$_2$(NMe_2)$_2$ (**1.134**), Ti(NMe_2)$_2$(SC_6F_5)$_2$($NHMe_2$) (**1.135**), Ti(enp)(NMe_2)$_2$ (**1.136**, H_2enp = *N*,*N*′-dimethylethylenediamine-*N*,*N*′bis(2-methylpyrrole)) and Ti(pypyr)$_2$(NMe_2)$_2$ (**1.137**, Hpypyr = 2-(2′-pyridyl)-3,5-dimethylpyrrole, Figure 1.15). Hydrazone formation is typically combined with Fischer-indole cyclisation using $ZnCl_2$ in a one-pot

method.[22,218,219] More recently Odom has begun to study the coupling between alkynes, hydrazines and isocyanides in the iminohydrazination reaction, where the active species is a mixed hydrazide(1-)/hydrazide(2-). One molecule of ^{t}BuNC was found to insert into the Ti–C bond of the initially formed cycloaddition between Ti(NNMe$_2$)(NHNMe$_2$)(dap) (**1.138**) and ^{n}BuCCH, before proton exchange with the hydrazide(1-) group yielded the intermediate Ti(NNMe$_2$){N(^{t}Bu)CHCHC(^{n}Bu)N(NMe$_2$)}(dap) (**1.139**). The catalytic cycle is completed by protonation of the chelating ligand with H_2NNMe_2, forming the corresponding 1,3-iminohydrazone.[54,220]

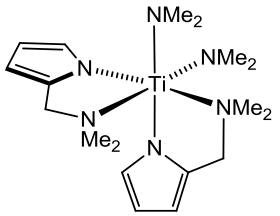

1.134

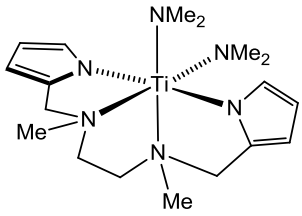

1.136

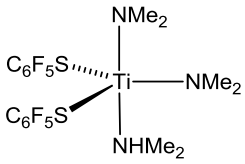

1.135

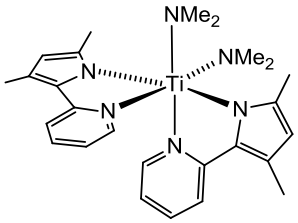

1.137

Figure 1.15. Titanium based precatalysts for the hydrohydrazination of alkynes.

Compounds **1.134** - **1.137** are moderately successful hydrohydrazination catalysts forming hydrazones (and the related indoles) in yields of up to 87 %, however elevated temperatures are required, 80 – 100 ºC depending on the catalyst used, combined with long reaction times. The yields in the iminohydrazination reaction are slightly lower. All reactions were carried out with a 10 mol% catalyst loading. Beller has also investigated the catalytic activity of a range of Group 4 metal salts.[221-225]

Concurrent with the work in this Thesis, a detailed study on the reactivity of Ti(N_2N^{py})(NNPh$_2$)(py) (**1.97**) was carried out and is summarised in Scheme 1.13.[59] The reaction with MeCN formed the dimeric compound **1.140**, analogous to **1.78** (formed from **1.71**). With electron withdrawing nitriles, instead of cycloadditions, Ti=N$_\alpha$ insertion occurred forming Ti(N_2N^{py}){NC(Ar^F)NNPh$_2$}(py) (Ar^F = C_6F_5

(**1.141**) or 2,6-$C_6H_3F_2$ (**1.142**)). In contrast to the coupling reactions of Ti(N_2N^{py})(N^tBu)(py) (**1.71**) with several equivalents of isocyanides, **1.97** reacts with just one equivalent forming the N_α–N_β bond cleaved products Ti(N_2N^{py})(NCNR)(NPh_2) (R = ^{t}Bu (**1.143**) or Xyl (**1.144**)) as a mixture of *cis* and *trans* isomers. Reactivity was also seen with $B(Ar^F)_3$ (Ar^F = C_6F_5) forming **1.145**.

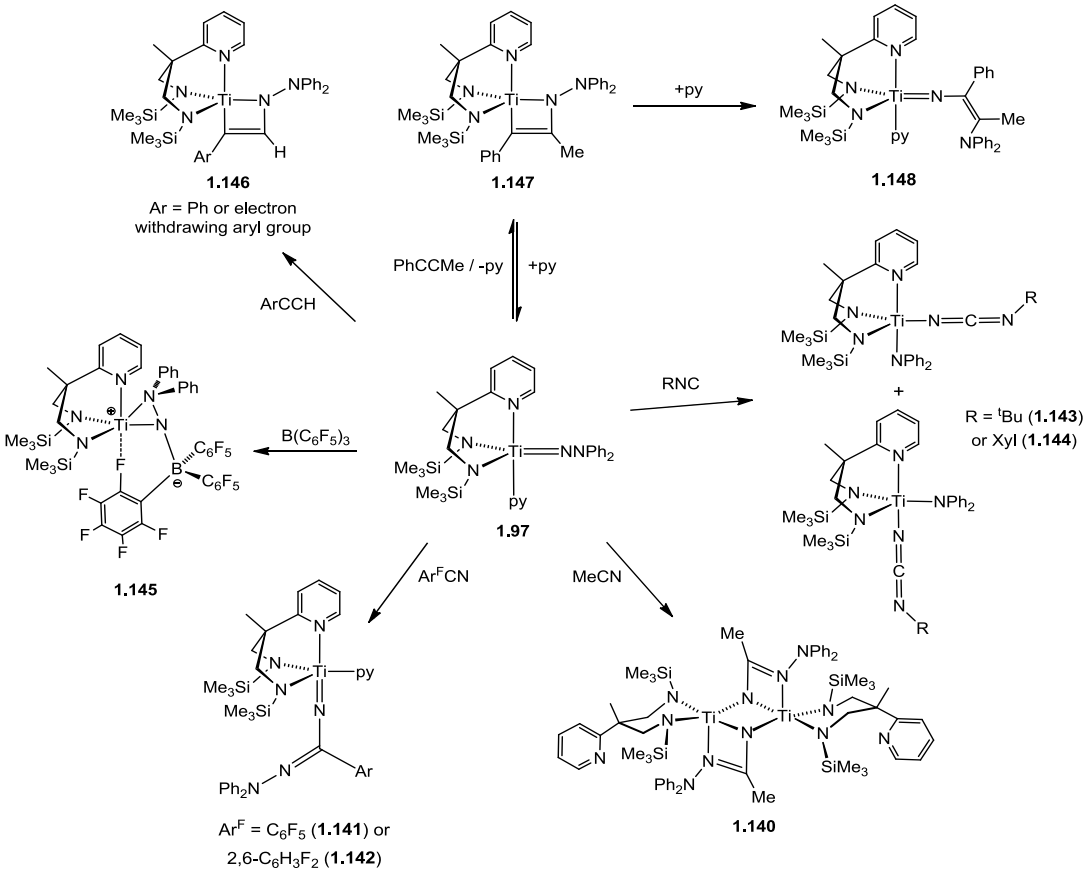

Scheme 1.13. Reactivity of Ti(N_2N^{py})($NNPh_2$)(py) (**1.97**) with a range of small, unsaturated molecules.[59,61]

The most interesting reactivity of Ti(N_2N^{py})($NNPh_2$)(py) (**1.97**) was seen with alkynes.[61] Terminal alkynes of the type ArCCH (Ar = Ph or electron withdrawing aryl) form azatitanacyclobutenes with the aryl substituted carbon bound to the metal centre (**1.146**, anti-Markovnikov selectivity). The stability of the products was found to increase with decreasing electron density of the alkyne. With PhCCMe, an equilibrium between **1.97**, PhCCMe and Ti(N_2N^{py}){$N(NPh_2)C(Me)C(Ph)$} (**1.147**) was initially formed. In the presence of pyridine this reacted slowly to form Ti(N_2N^{py}){$NC(Ph)C(Me)NPh_2$}(py) (**1.148**) containing a vinyl imido fragment, the alkyne molecule having inserted into the N_α–N_β bond.

When the similar compound Ti(N_2N^{Me})($NNPh_2$)(py) (**1.93**) was taken with PhCCMe, there was no evidence of a cycloaddition, but rapid formation of Ti(N_2N^{Me}){NC(Ph)C(Me)NPh_2}(py) (**1.149**) ensued. Furthermore, the vinyl imido fragment in **1.149** could be protonated by a molecule of H_2NNPh_2 reforming **1.93** and releasing $H_2NC(Ph)C(Me)NPh_2$. The reaction was found to be catalytic with loadings of 10 mol% making **1.93** the first 1,2-diamination catalyst derived from a Group 4 hydrazido(2-) compound (Figure 1.16). Analogous reactivity was found with 2-butyne.[51]

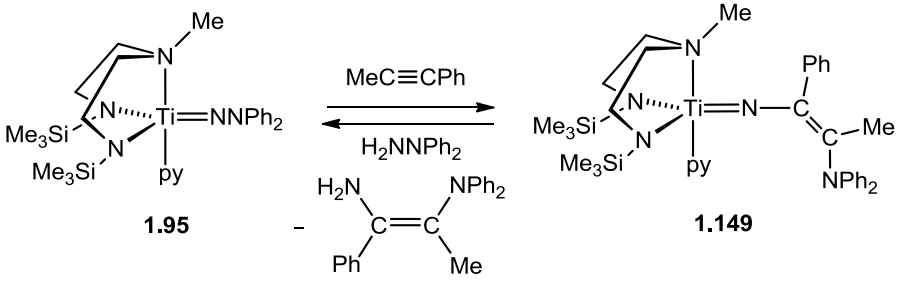

Figure 1.16. 1,2-diamination reaction of Ti(N_2N^{Me})($NNPh_2$)(py) (**1.93**) with alkynes.

Mindiola proposed a mechanism for this transformation proceeding *via* pyridine loss, N_β-coordination, then [2+1] coupling of the alkyne molecule to N_α to form an N-metallated azirine. Nucleophilic attack by N_β then occurs forming the vinyl imide product (Scheme 1.14).[52] This mechanism is examined in detail in this Thesis.

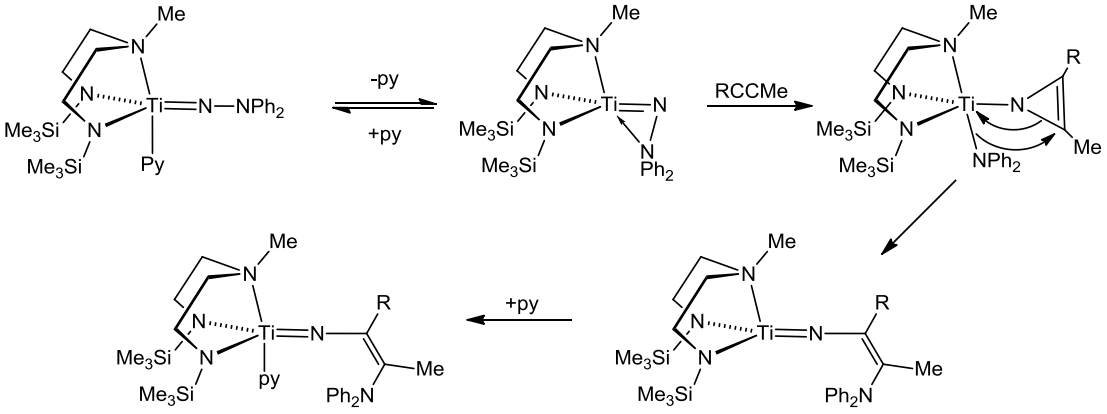

Scheme 1.14. Proposed mechanism for the 1,2-diamination reaction between Ti(N_2N^{Me})($NNPh_2$)(py) (**1.93**) and RCCMe.[52]

Following the work presented in this Thesis several hydrazido(2-) complexes using ancillary ligands based on N_2N^{Me} have been synthesised. These include Ti(N_2O)($NNPh_2$)$(py)_2$ (**1.150**, H_2N_2O = $O(CH_2CH_2N(H)SiMe_3)_2$),[226,227] which showed reactivity with Ar′NCE (E = O, S or Se, Ar′ = 2,6-$C_6H_3{}^iPr_2$). For E = O, insertion into

a metal amide bond (reminiscent of **1.77**) was followed by [2+2] cycloaddition of a further equivalent at Ti=N_α forming the *N*,*N*′-bound isomer. For E = S or Se only one equivalent was required with the expected products from [2+2] cycloaddition at Ti=N_α being formed. However, for E = Se this was followed by rapid elimination of the carbodiimide fragment to yield a seleno-bridged dimer. Reactivity with nitriles and isocyanides mirrored that of Ti(N_2N^{py})($NNPh_2$)(py) (**1.97**).

1.3.3 Zirconium and Hafnium hydrazide chemistry

While the chemistry of titanium hydrazides has undergone rapid development over the last decade, with a range of structural, reactivity and catalytic studies being published, those of zirconium, and to a greater extent hafnium, have remained relatively underdeveloped. This is in spite of the fact that the first structurally characterised terminal zirconium hydrazido(2-) complex was reported as long ago as 1991 by Bergman.[57] The bis(cyclopentadienyl) 1,1-diphenylhydrazide $Cp_2Zr(NNPh_2)$(DMAP) (**1.151**, DMAP = 4-dimethylaminopyridine) was formed by thermolysis of the mixed alkyl/hydrazido(1-) compound $Cp_2Zr(NHNPh_2)(CH_2CH_2{}^tBu)$ (**1.152**, Scheme 1.15). Compound **1.151** is the hydrazide analogue of the imido complexes **1.45**, **1.47** and **1.48** presented in Section 1.3.1.

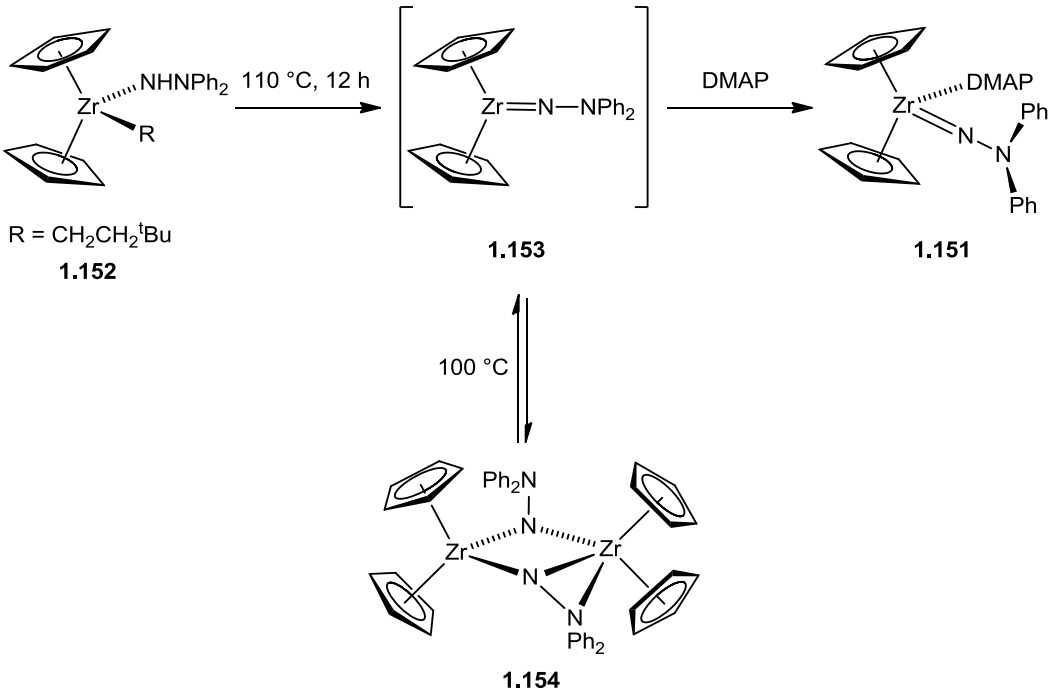

Scheme 1.15. Monomeric and dimeric terminal zirconocene hydrazido(2-) complexes.[57]

Thermolysis of **1.152** at 110 ºC for twelve hours formed the transient intermediate $Cp_2Zr(NNPh_2)$ (**1.153**) with concomitant loss of 2,2-dimethylbutane. In the presence DMAP, the monomeric species **1.151** was formed. However, in the absence of a strongly donating ligand the unsymmetrical dimer **1.154** was formed (Scheme 1.15). Unlike the titanium dimers discussed above, when **1.154** was heated with excess DMAP it could be cleaved to produce **1.151**. $Cp_2Zr(NNPh_2)(DMAP)$ (**1.151**) contains a short $Zr=N_\alpha$ bond (1.873(7) Å), similar to that found in the related aryl imido complex $Cp_2Zr(NAr)(THF)$ (**1.48**, $Zr=N_\alpha$ = 1.888(2) Å)[20] and consistent with the hydrazide group acting as a four electron donor to the metal centre. The N_α–N_β distance of 1.364(10) Å is indicative of a single bond, again implying the hydrazide ligand is behaving as a dianionic ligand, as in related titanium examples.

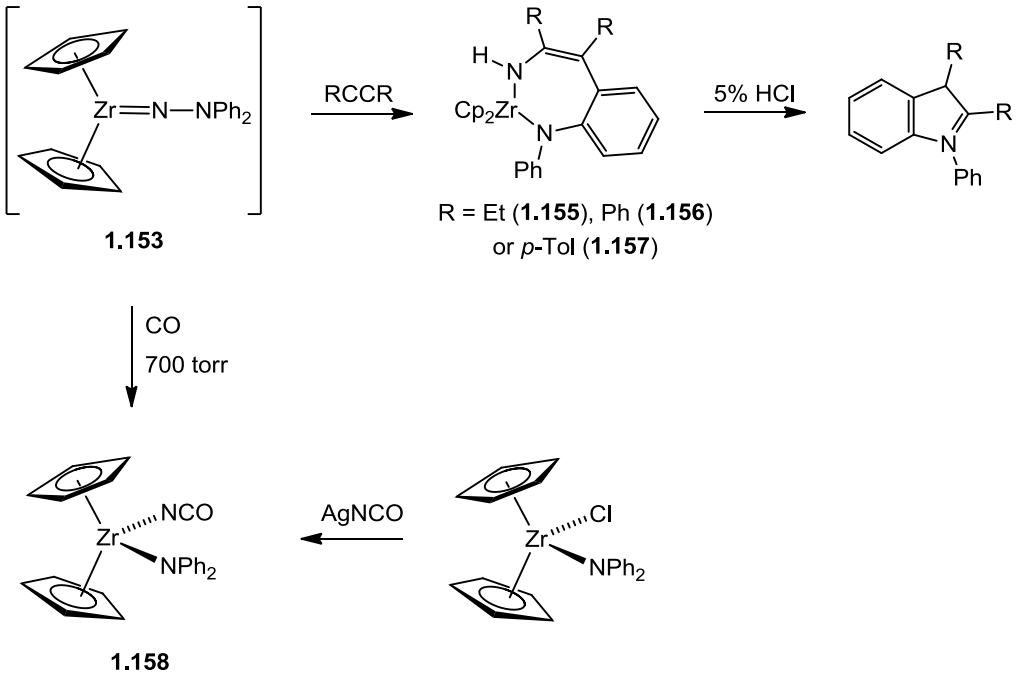

Scheme 1.16. Reactions of $Cp_2Zr(NNPh_2)$ (**1.153**) with CO and alkynes.[57]

When $Cp_2Zr(NHNPh_2)(CH_2CH_2{}^tBu)$ (**1.152**) was heated to 110 ºC in the presence of the symmetrical alkynes RCCR (R = Et, Ph or Tol), N_α–N_β bond cleavage occurred, followed by C–H activation to yield the 7-membered ring complexes $Cp_2Zr\{N(H)C(R)C(R)\text{-}1,2\text{-}C_6H_4N(Ph)\}$ (**1.155** - **1.157**, Scheme 1.16). Upon treatment with aqueous HCl, the corresponding N-phenylindoles were formed. The reaction with carbon monoxide also led to N_α–N_β bond cleavage forming the mixed

amide/metallated isocyanate $Cp_2Zr(NCO)(NPh_2)$ (**1.158**). This could be prepared independently by treatment of $Cp_2Zr(NPh_2)Cl$ with AgNCO.

Compounds **1.155 - 1.157** were the first examples of this type of reactivity between alkynes and hydrazides. However, recent work by Gade, concurrent with that presented in this Thesis, has observed similar reactivity between $Zr(N_2{}^{R}N^{py})(NN(Ph)R')(L)$ (R = *, R′ = Ph (**1.159**), $H_2N_2{*}N^{py}$ = $MeC(2\text{-}C_5H_4N)(CH_2N(H)Si(^tBu)Me_2)_2$; R = Xyl, R′ = Ph (**1.160**), $H_2N_2{}^{Xyl}N^{py}$ = $MeC(2\text{-}C_5H_4N)(CH_2N(H)\text{-}2,6\text{-}C_6H_3Me_2)_2$; R = Xyl, R′ = Me (**1.161**); R = Mes, R′ = Ph (**1.162**), $H_2N_2{}^{Mes}N^{py}$ = $MeC(2\text{-}C_5H_4N)(CH_2N(H)\text{-}2,4,6\text{-}C_6H_2Me_3)_2$) and a range of internal and terminal alkynes.[34,35] These reactions were found to be catalytic, forming N-phenylindoles from a mixture of hydrazine, alkyne and 10 mol% of the bis(amide) pre-catalyst. Note that it is not possible to isolate **1.162** from the reaction of $Zr(N_2{}^{Mes}N^{py})(NMe_2)_2$ and H_2NNPh_2, with only mixed amide/hydrazide(1-) or bis(hydrazido(1-)) complexes being formed. The catalytic activity, however, implies that **1.162** is formed under the conditions used. Compounds **1.160** and **1.161** can be formed directly from $Zr(N_2{}^{Xyl}N^{py})(NMe_2)_2$ and H_2NNPh_2 in the presence of DMAP.

The reaction of $Zr(N_2{*}N^{py})(NNPh_2)(py)$ (**1.159**) with 2-butyne formed an equal mixture of the 7-membered ring product $Zr(N_2{*}N^{py})\{N(H)C(Me)C(Me)\text{-}1,2\text{-}C_6H_4N(Ph)\}$ (**1.163**) and the vinyl imide $Zr(N_2{*}N^{py})\{NC(Me)C(Me)NPh_2\}(py)$ (**1.164**). DFT studies on the formation of these products were carried out and an N-metallated azirine (**1.166**) was identified as the key intermediate following N_α–N_β cleavage *via* a [2+2] cycloaddition (Scheme 1.17).[34,35]

The syntheses of $Zr(N_2{*}N^{py})(NNPh_2)(py)$ (**1.159**) and its hafnium congener $Hf(N_2{*}N^{py})(NNPh_2)(py)$ (**1.167**) were performed using a synthetic methodology which combines salt metathesis and dehydrohalogenation to form the desired complex (Scheme 1.18).[41,228] The mixed hydrazide(1-)/chlorides were formed by treatment of $M(N_2{*}N^{py})Cl_2$ with $LiNHNPh_2$, subsequent addition of $LiN(SiMe_3)_2$ and pyridine yielding the desired products. Compound **1.159** was structurally characterised and contains a $Zr{=}N_\alpha$ bond length which is slightly longer than that of **1.151** (1.899(2) Å), but still indicative of multiple bonding between N_α and the metal centre. The N_α–N_β distance was 1.398(3) Å, indicative of a single bond.[229]

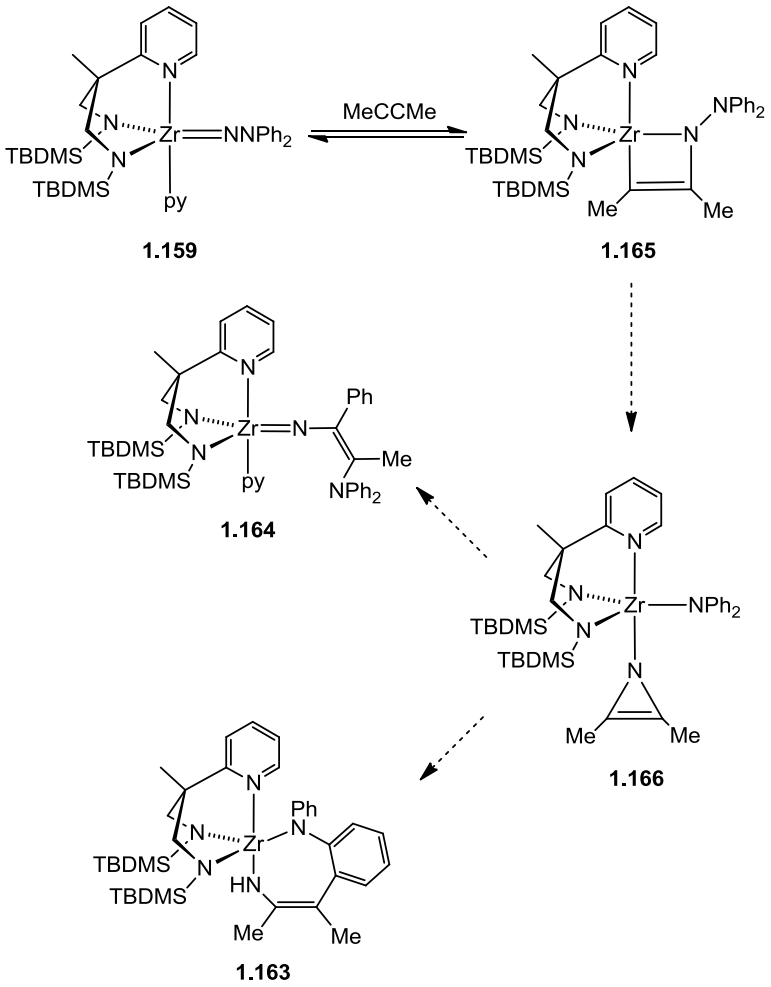

Scheme 1.17. Proposed mechanism for the formation of $Zr(N_2{*}N^{py})\{N(H)C(Me)C(Me)\text{-}1,2\text{-}C_6H_4N(Ph)\}$ (**1.163**) and $Zr(N_2{*}N^{py})\{NC(Me)C(Me)NPh_2\}(py)$ (**1.164**) from $Zr(N_2{*}N^{py})(NNPh_2)(py)$ (**1.159**) and 2-butyne.

A methyl phenyl analogue of **1.159**, $Zr(N_2{*}N^{py})\{NN(Me)Ph\}(py)$ (**1.168**), was also synthesised by the same method. However, DMAP was required to ensure it remained a monomer, pyridine leading to aggregation. Attempts to make a dimethyl analogue were unsuccessful yielding only $Zr(N_2{*}N^{py})(\eta^2\text{-}NHNMe_2)Cl$ (**1.169**).[40] As described above, recent variations on the ancillary ligand have allowed access to the hydrazido(2-) compound $Zr(N_2^{Xyl}N^{py})(NNPh_2)(DMAP)_2$ (**1.160**) by protonolysis from the corresponding bis(amide) complex.[34]

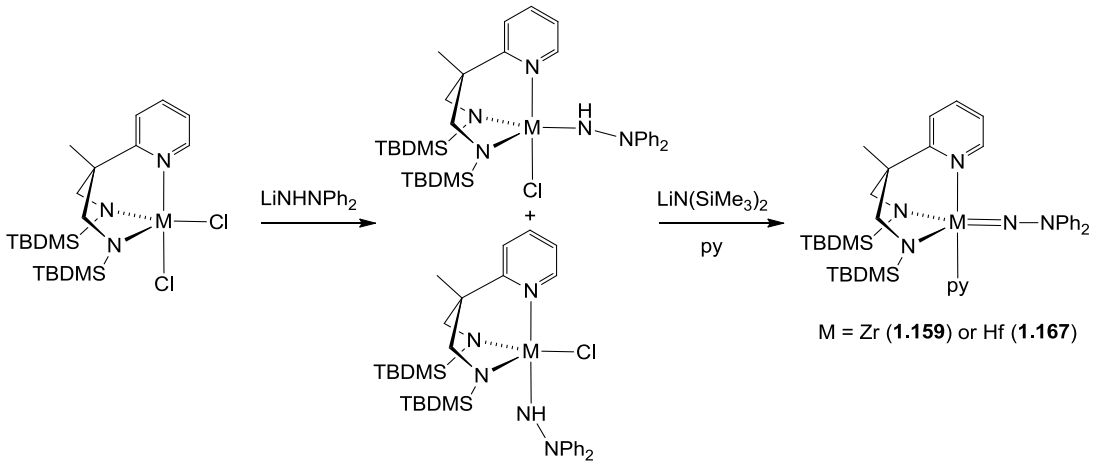

Scheme 1.18. Formation of heavy Group 4 hydrazides *via* a metathesis/dehydrohalogenation pathway.

In addition to the reactivity with alkynes outlined above, the reactivity of $Zr(N_2{*}N^{py})(NNPh_2)(py)$ (**1.159**) with other unsaturated molecules has been investigated (Scheme 1.19).[36,37,41,58,228] Some of these have also been performed with $Hf(N_2{*}N^{py})(NNPh_2)(py)$ (**1.167**). With $B(Ar^F)_3$, N_α acts as a nucleophile and the hydrazide moiety changes to an η^2-coordination mode, forming **1.170**, analogous to **1.145**. [2+2] cycloaddition reactions are observed with metal carbonyl compounds, isothiocyanates and allenes, producing complexes **1.171** and **1.172** and [2+3] cycloaddition products are seen with organic azides leading to **1.173**. Upon heating, **1.173** liberated dinitrogen and underwent N_α–N_β bond cleavage to yield a side on bound diazenido ligand, with NPh_2 occupying an equatorial site (**1.174**).

N_α–N_β bond cleavage could be achieved by the reactions with *tert*-butyl isocyanide, forming exclusively *cis*-$Zr(N_2{*}N^{py})(NCN^tBu)(NPh_2)$ (**1.175**), and the chalcogen transfer agents propylene sulphide and Ph_3Se, forming the chalcogen bridged species **1.176** and **1.177**, respectively.

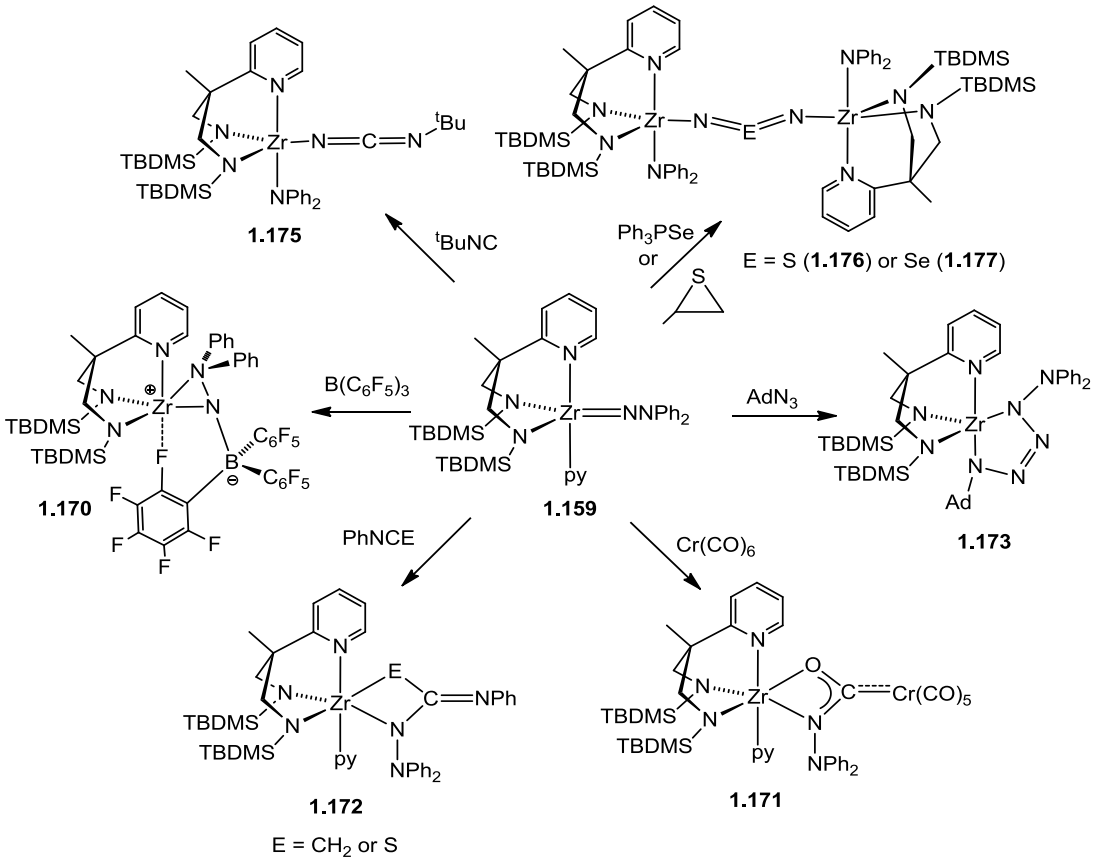

Scheme 1.19. Reactivity of Zr(N_2*N^{py})($NNPh_2$)(py) (**1.159**) with small, unsaturated molecules.

The only other examples of heavy Group 4 hydrazido(2-) compounds are M(N_2*N^{py})(NNC_5H_5)(OTf)(py) (M = Zr (**1.178**) or Hf (**1.179**), Figure 1.17) formed by the reaction of the relevant bis(amide) compound with 1-aminopyridinium triflate in the presence of pyridine.[42,43] Compound **1.179** is the only structurally characterised Hf hydrazido(2-) complex and contains a Hf=N_α distance of 1.933(5) [1.940(5)] Å and an N_α–N_β bond length of 1.331(7) [1.318(6)] Å. N_α–N_β bond cleavage of **1.178** and **1.179** proved to be facile, occurring with ^{t}BuNC or CO and concomitant pyridine elimination, to yield M(N_2*N^{py})(NCN^tBu)(OTf)(py) (M = Zr (**1.180**) or Hf (**1.181**)) and M(N_2*N^{py})(NCO)(OTf)(py) (M = Zr (**1.182**) or Hf (**1.183**)), respectively (Figure 1.17). In addition the triflate ligand could be substituted with anionic ligands such as PhCCLi.

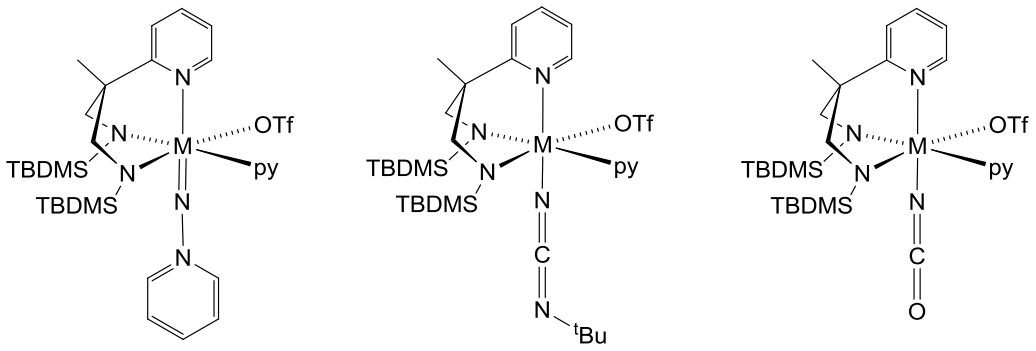

M = Zr (**1.178**) or Hf (**1.179**) M = Zr (**1.180**) or Hf (**1.181**) M = Zr (**1.182**) or Hf (**1.183**)

Figure 1.17. (1-pyridinio)imido complexes of zirconium and hafnium and their reaction products with ^{t}BuNC and CO.

Part of the reason why zirconium hydrazido(2-) chemistry has remained underdeveloped compared to that of titanium is due to preferential formation of bis(hydrazido(1-)) complexes at the larger metal centre. This has been observed by Mountford in the attempted synthesis of Zr(Me_2calix)(NNR_2), direct analogues of **1.123** - **1.125**, where addition of two equivalents of LiNHNRR′ yielded only Zr(Me_2calix)($NHNRR'_2$ (R = R′ = Me (**1.184**) or Ph (**1.185**); R = Me, R′ = Ph (**1.186**)).[50] Similar reactivity was seen by Martins with Zr(Bn_2cyclam)Cl_2 (Bn_2cyclam = 1,8-dibenzyl-1,4,8,11-tetraazacyclotetradecane) and $LiNHNPh_2$.[230]

1.3.4 Heteroatom substituted imido complexes of Group 4 metals.

In addition to the imido(2-) and hydrazido(2-) complexes described above, there are isolated reports of heteroatom substituted imido(2-) compounds bound exclusively to a titanium metal centre (**1.187**, **1.188** and **1.190**, Figure 1.18).[231-236] Studies on these compounds are limited to a comparison of the bonding in Ti(NOMe)Cl_2($NHMe_2$)$_2$ (**1.189Q**, a model for Ti(NO^{t}Bu)Cl_2($NHMe_2$) (**1.189**)) with the analogous imido(2-) and hydrazido(2-) complexes, and the reactivity of Ti(N_2N^{Me})(NO^{t}Bu)(py) (**1.190**) with PhCCMe, leading to the formation of Ti{MeN($CH_2CH_2NSiMe_3$)(CH_2CH_2NC(Me)C(Ph)$NSiMe_3$)}(O^{t}Bu) (**1.191**).

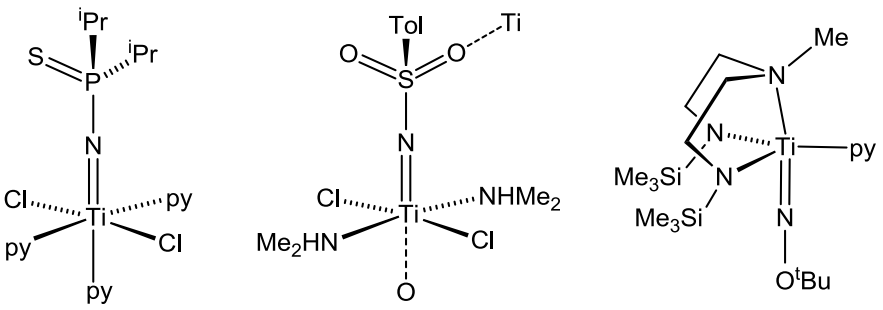

Figure 1.18. Heteroatom substituted imido(2-) complexes.

1.4 Bonding in hydrazido complexes

1.4.1 Hydrazido(2-) *versus* isodiazene

In the same way that the chemistry of carbenes and alkylidenes differ dramatically (and that of nitrenes and imidos), it is clear from the examples presented earlier in this Chapter that the chemistry of Group 4 and Group 6 hydrazido(2-) compounds are markedly different.

The NNR_2 ligand can be thought of as either a neutral isodiazene fragment or dianionic hydrazido(2-) fragment (Figure 1.19). In the former, the N_α–N_β π^* molecular orbital is unoccupied and the nitrogens are therefore joined by a double bond. Reducing the fragment with two electrons populates this N_α–N_β π^* molecular orbital, causing the bond order to decrease to one, and the N_α–N_β distance to increase.[55] In addition to a shorter N_α–N_β distance, a compound with an isodiazene ligand would be expected to contain a planar N_β atom, the double bond between N_α–N_β requiring it to be sp^2 hybridised, while in the dianionic form N_β would be formally sp^3 hybridised and pyramidal.

Figure 1.19. Hydrazido(2-) and isodiazene(0) canonical representations of the hydrazide ligand.

The difference in bonding between these canonical forms is demonstrated by a comparison between the $NNMe_2$ fragments of $[Mo_3S_8(NNMe_2)_2]^{2-}$ (**1.192**)[113] and $Mo(NNMe_2)(S_2CN^iBu_2)_2O$ (**1.193**, Figure 1.20).[237] Compound **1.192** is a rare example

of a compound containing ′pure′ isodiazene NNR_2 ligands, the MoS_4 groups preventing π donation between the metal and N_α. The Mo–N_α distance in **1.192** is markedly longer than that of **1.193** (2.13(1) *vs*. 1.841(18) Å), while the N_α–N_β bond length is significantly shorter (1.16(2) *vs*. 1.390(18) Å).

The presence of a planar N_β in both compounds indicates contribution from the isodiazene canonical form in each instance. However, the above observations clearly show the difference between a ′pure′ isodiazene complex (**1.192**) and **1.193**, which, although still retaining a contribution from the isodiazene form, has significant hydrazido(2-) character.

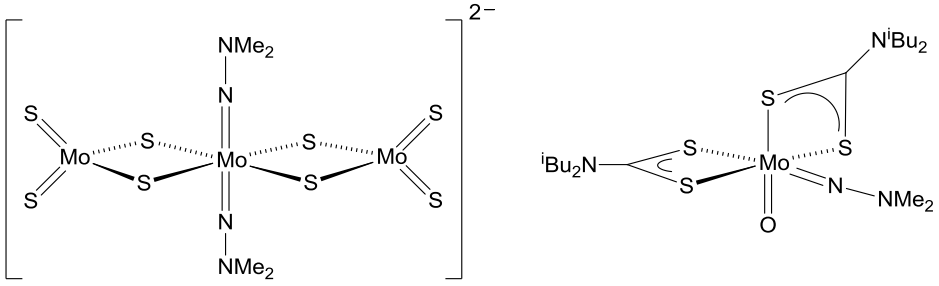

1.192 **1.193**

Figure 1.20. $[Mo_3S_8(NNMe_2)_2]^{2-}$ (**1.192**) and $Mo(NNMe_2)O(S_2CN^iBu_2)_2$ (**1.193**).

In keeping with the observations discussed above, Carillo, in his computational study on the binding of NNR_2 to Mo, suggests that for mid/later transition metals the hydrazido ligand generally contains a mixture of both isodiazene and hydrazido(2-) contributions (with a formal charge between 0 and -1).[238] Density functional theory (DFT) calculations investigating the mechanism of the Chatt cycle support this conclusion.[76,239]

Changing to more electropositive metal centres should cause an increase in the hydrazido(2-) character, embodied by an increase in the N_α–N_β distance, as the electron density in the π* molecular orbital grows, and a changing of the hybridisation of N_β to sp^3 as discussed above. This can be seen in the comparative structural data for Group 4 – 6 hydrazido complexes illustrated in Table 1.1, with Group 4 hydrazide compounds exhibiting markedly lengthened N_α–N_β distances compared to their Group 6 analogues and therefore a more reduced NNR_2 fragment. Note that the geometry at N_β only takes alkyl substituted hydrazides into account. Aryl substituted examples exhibit significant delocalisation of the N_β lone pair into the aryl group, causing a planar geometry in the majority of compounds.[229]

Table 1.1. Comparative structural data for Group 4 – 6 hydrazido complexes.

	N_α–N_β range (Å)	N_α–N_β avg. (Å)	Geometry at N_β (alkyl)
Group 4	1.344(2) − 1.398(3)	1.363	Pyramidal
Group 5	1.244(3) – 1.402(4)	1.318	Planar or pyramidal
Group 6	1.16(2) − 1.415(5)	1.318	Planar

As mentioned earlier, the isodiazene/hydrazido(2-) relationship can be compared to that of Fischer carbenes and Schrock alkylidenes (Figure 1.21).[48,56,240] Indeed, the pure isodiazene fragment can even be considered a substituted Fischer nitrene.[111] Fischer carbenes are generally found for mid/late transition metals and are stabilised by heteroatom substituents. The bonding is donor-acceptor in nature with σ-electron donation of the lone pair on carbon into an empty metal d-orbital and π-back donation from the metal into the empty carbon p-orbital. It is formally a neutral carbene and the reactivity is typified by nucleophilic attack at carbon or electrophilic attack at the metal centre.[241,242] Schrock alkylidenes meanwhile are found for high oxidation state early transition metals with H or alkyl substituents. The alkylidene unit behaves as a dianionic 4 electron donor ligand. Alkylidenes are generally more reactive than Fischer carbenes due to the highly polarised M=CR bond, with electrophilic attack typically occurring at the carbon and nucleophilic attack at the metal centre.[242,243]

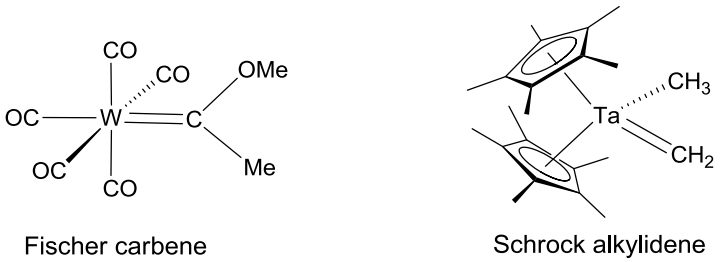

Fischer carbene Schrock alkylidene

Figure 1.21. Examples of a Fischer carbene and Schrock alkylidene.[244-247]

This comparison satisfactorily accounts for the difference in reactivity seen for isodiazene (typically Group 6) and hydrazido(2-) (typically Group 4) complexes. The former are generally less reactive, the dative $M{=}N_\alpha$ and partial double bond character of N_α–N_β, limiting reactivity to N_β functionalisation except under forcing conditions.

The latter, however, show diverse reactivity (*vide supra*), a consequence of the unsaturated M=N_α and weakened N_α–N_β bonds.

1.4.2 Comparison of the bonding in Group 4 hydrazido(2-) and imido complexes

Several investigations into the similarities in bonding between hydrazido(2-) and imido ligands have been reported, which show the isolobal relationship between the two.[48,51,56]

Both groups have the capability to bind to the metal centre with a formal triple bond through one σ and two π interactions. The difference between the two groups stems from the presence of the N_β π* lone pair in the hydrazido(2-) moiety. This destabilises a π interaction, breaking the degeneracy seen in imido compounds (although interactions with aryl π* systems also raise the energy of one π interaction in aryl imido systems).

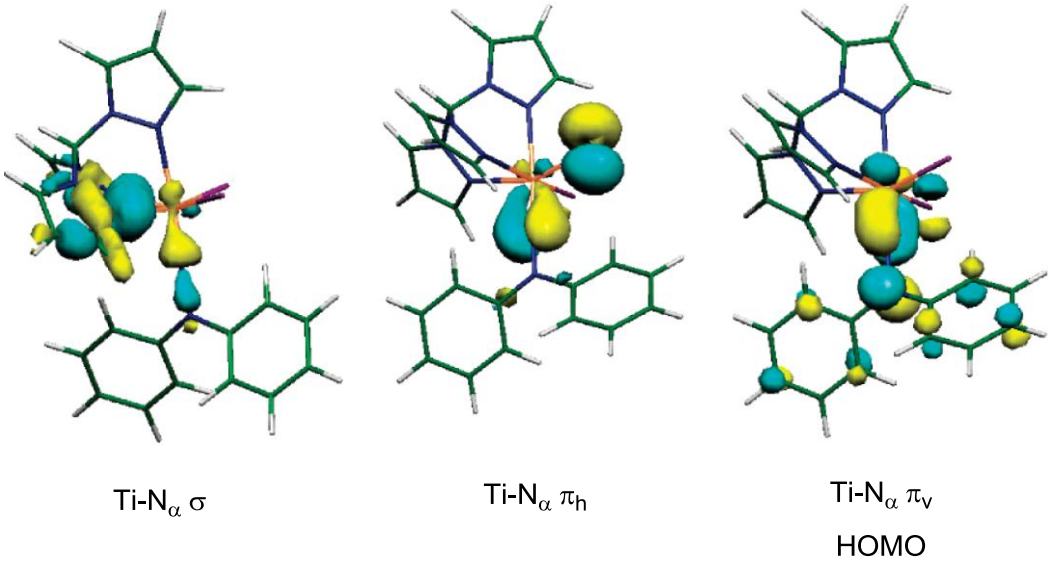

Figure 1.22. Frontier MOs of the model system Ti{$HC(pz)_3$}$(NNPh_2)Cl_2$ (**1.88Q**).[56]

Mountford reported a DFT computational study on the bonding using Ti{$HC(pz)_3$}$(NNPh_2)Cl_2$ (**1.88Q**), as a model for Ti{$HC(Me_2pz)_3$}$(NNPh_2)Cl_2$ (**1.88**), and the three frontier MOs are illustrated in Figure 1.22.[56] As stated above, while the two π interactions are degenerate in Ti{$HC(pz)_3$}$(NMe)Cl_2$ (**1.194Q**), a model for the alkyl imido complex Ti{$HC(pz)_3$}$(N^tBu)Cl_2$ (**1.194**), the Ti–N_α π_v bond (HOMO) in **1.88Q** is destabilised by 1.38 eV relative to Ti–N_α π_h. This manifests itself as a lengthening of the Ti=N_α distance when changing from the imide to hydrazide (1.718(2) Å (**1.88**) *vs.* 1.703(2) Å (**1.194**)). This increase in bond length is typical for

a wide range of imido and hydrazido complexes with identical ancillary ligands, such as the increase in Ti=N_α distance from 1.724(2) Å in Ti(N_2N^{py})(N^tBu)(py) (**1.71**) to 1.759(2) Å in Ti(N_2N^{py})($NNPh_2$)(py) (**1.97**).

Calculations by Gade[41] and Odom[53] also found similar increases in the energy of one π bond relative to the other. As the chemistry of Group 4 hydrazides has become more established, early suggestions that this destabilisation might affect the reactivity of the hydrazido(2-) functional group have been shown to be correct.[19,41]

1.5 Summary and Objectives

This Chapter has mapped the evolution of Group 6 hydrazido(2-) compounds, from their origins as intermediates in the Chatt and Schrock cycles of dinitrogen reduction to ammonia, to their multiple uses in the novel syntheses of organo-dinitrogen ligands. The subsequent expansion of the field into Groups 4 and 5 has been discussed. Particular attention has been paid to the synthetic methods employed in the formation of Group 4 hydrazido(2-) complexes and their stoichiometric and catalytic reactivity towards small, unsaturated molecules. This reactivity has been compared with that seen for related Group 4 imido(2-) compounds. A brief description of the bonding in early and mid/late transition metal hydrazides was presented in order to rationalise the difference in reactivity of the M=NNR_2 fragment observed. While several unique transformations of the M=$NNPh_2$ ligand have been reported, their mechanistic pathways are still poorly understood. The aim of this Thesis is to demonstrate the scope of reactivity of the M=$NNPh_2$ moiety and to probe the mechanisms of these transformations.

1.6 References

1. Maxwell, G.; Editor; *Synthetic Nitrogen Products: A Practical Guide to the products and Processes*; Kluwer Academic, 2004.
2. Kirkby, E. A.; Le, B. J.; Adamowicz, S.; Romheld, V.; *Proc. - Int. Fert. Soc.* **2009**, *653*, 1.
3. Krapp, A.; Saliba-Colombani, V.; Daniel-Vedele, F.; *Photosynth. Res.* **2005**, *83*, 251.
4. Higashio, Y.; Shoji, T.; *Appl. Catal., A* **2004**, *260*, 251.
5. Munro, H. N.; Allison, J. B.; *Mammalian Protein Metabolism. Vol. II*; Academic Press, 1964.

6. Munro, H. N.; Allison, J. B.; *Mammalian Protein Metabolism. Vol. I*; Academic Press., 1964.
7. Johnson, B. F. G.; Haymore, B. L.; Dilworth, J. D.: Comprehensive Coordination Chemistry. Wilkinson, G., Gillard, R. D., McCleverty, J. A., Eds.; Pergamon Press: Oxford, 1987; Vol. 2; pp 100.
8. Nugent, W. A.; Mayer, J. M.; *Metal-Ligand Multiple Bonds*; Wiley-Interscience: New York, 1988.
9. Fryzuk, M. D.; Johnson, S. A.; *Coord. Chem. Rev.* **2000**, *200-202*, 379.
10. MacKay, B. A.; Fryzuk, M. D.; *Chem. Rev.* **2004**, *104*, 385.
11. Fryzuk, M. D.; *Chem. Rec.* **2003**, *3*, 2.
12. Chatt, J.; Dilworth, J. R.; Richards, R. L.; *Chem. Rev.* **1978**, *78*, 589.
13. Hidai, M.; *Chem. Rev.* **1995**, *95*, 1115.
14. Hidai, M.; *Coord. Chem. Rev.* **1999**, *185-186*, 99.
15. Shaver, M. P.; Fryzuk, M. D.; *Adv. Synth. Catal.* **2003**, *345*, 1061.
16. Nugent, W. A.; Haymore, B. L.; *Coord. Chem. Rev.* **1980**, *31*, 123.
17. Walsh, P. J.; Hollander, F. J.; Bergman, R. G.; *J. Am. Chem. Soc.* **1988**, *110*, 8729.
18. Mountford, P.; *Chem. Commun.* **1997**, 2127.
19. Hazari, N.; Mountford, P.; *Acc. Chem. Res.* **2005**, *38*, 839.
20. Duncan, A. P.; Bergman, R. G.; *Chem. Rec.* **2002**, *2*, 431.
21. Wigley, D. E.; *Prog. Inorg. Chem.* **1994**, *42*, 239.
22. Odom, A. L.; *Dalton Trans.* **2005**, 225.
23. Bolton, P. D.; Mountford, P.; *Adv. Synth. Catal.* **2005**, *347*, 355.
24. Hill, J. E.; Profilet, R. D.; Fanwick, P. E.; Rothwell, I. P.; *Angew. Chem. Int. Ed. Engl.* **1990**, *29*, 664.
25. Roesky, H. W.; Voelker, H.; Witt, M.; Noltemeyer, M.; *Angew. Chem. Int. Ed. Engl.* **1990**, *29*, 669.
26. Cummins, C. C.; Schaller, C. P.; Van Duyne, G. D.; Wolczanski, P. T.; Chan, A. W. E.; Hoffmann, R.; *J. Am. Chem. Soc.* **1991**, *113*, 2985.
27. McGrane, P. L.; Jensen, M.; Livinghouse, T.; *J. Am. Chem. Soc.* **1992**, *114*, 5459.
28. Milas, N. A.; Iliopulos, M. I.; *J. Am. Chem. Soc.* **1959**, *81*, 6089.
29. Janssen, T.; Severin, R.; Diekmann, M.; Friedemann, M.; Haase, D.; Saak, W.; Doye, S.; Beckhaus, R.; *Organometallics* **2010**, *29*, 1806.

30. Doye, S.; *Synlett* **2004**, 1653.
31. Bytschkov, I.; Doye, S.; *Eur. J. Org. Chem.* **2003**, 935.
32. Pohlki, F.; Doye, S.; *Chem. Soc. Revs.* **2003**, *32*, 104.
33. Müller, T. E.; Hultzsch, K. C.; Yus, M.; Foubelo, F.; Tada, M.; *Chem. Rev.* **2008**, *108*, 3795.
34. Gehrmann, T.; Scholl, S. A.; Fillol, J. L.; Wadepohl, H.; Gade, L. H.; *Chem. Eur. J.* **2012**, *18*, 3925.
35. Gehrmann, T.; Fillol, J. L.; Scholl, S. A.; Wadepohl, H.; Gade, L. H.; *Angew. Chem. Int. Ed.* **2011**, *50*, 5757.
36. Gehrmann, T.; Fillol, J. L.; Wadepohl, H.; Gade, L. H.; *Organometallics* **2010**, *29*, 28.
37. Gehrmann, T.; Fillol, J. L.; Wadepohl, H.; Gade, L. H.; *Angew. Chem. Int. Ed.* **2009**, *48*, 2152.
38. Weitershaus, K.; Fillol, J. L.; Wadepohl, H.; Gade, L. H.; *Organometallics* **2009**, *28*, 4747.
39. Weitershaus, K.; Wadepohl, H.; Gade, L. H.; *Organometallics* **2009**, *28*, 3381.
40. Herrmann, H.; Wadepohl, H.; Gade, L. H.; *Dalton Trans.* **2008**, 2111.
41. Herrmann, H.; Fillol, J. L.; Gehrmann, T.; Enders, M.; Wadepohl, H.; Gade, L. H.; *Chem. Eur. J.* **2008**, *14*, 8131.
42. Herrmann, H.; Fillol, J. L.; Wadepohl, H.; Gade, L. H.; *Organometallics* **2008**, *27*, 172.
43. Herrmann, H.; Gehrmann, T.; Wadepohl, H.; Gade, L. H.; *Dalton Trans.* **2008**, 6231.
44. Herrmann, H.; Fillol, J. L.; Wadepohl, H.; Gade, L. H.; *Angew. Chem. Int. Ed.* **2007**, *46*, 8426.
45. Tiong, P. J.; Nova, A.; Schwarz, A. D.; Selby, J. D.; Clot, E.; Mountford, P.; *Dalton Trans.* **2012**, *41*, 2277.
46. Tiong, P. J.; Nova, A.; Groom, L. R.; Schwarz, A. D.; Selby, J. D.; Schofield, A. D.; Clot, E.; Mountford, P.; *Organometallics* **2011**, *30*, 1182.
47. Selby, J. D.; Feliz, M.; Schwarz, A. D.; Clot, E.; Mountford, P.; *Organometallics* **2011**, *30*, 2295.
48. Selby, J. D.; Manley, C. D.; Schwarz, A. D.; Clot, E.; Mountford, P.; *Organometallics* **2008**, *27*, 6479.

49. Selby, J. D.; Schulten, C.; Schwarz, A. D.; Stasch, A.; Clot, E.; Jones, C.; Mountford, P.; *Chem.Commun.* **2008**, 5101.
50. Clulow, A. J.; Selby, J. D.; Cushion, M. G.; Schwarz, A. D.; Mountford, P.; *Inorg. Chem.* **2008**, *47*, 12049.
51. Selby, J. D.; Manley, C. D.; Feliz, M.; Schwarz, A. D.; Clot, E.; Mountford, P.; *Chem. Commun.* **2007**, 4937.
52. Mindiola, D. J.; *Angew. Chem. Int. Ed.* **2008**, *47*, 1557.
53. Patel, S.; Li, Y.; Odom, A. L.; *Inorg. Chem.* **2007**, *46*, 6373.
54. Banerjee, S.; Odom, A. L.; *Organometallics* **2006**, *25*, 3099.
55. Li, Y.; Shi, Y.; Odom, A. L.; *J. Am. Chem. Soc.* **2004**, *126*, 1794.
56. Parsons, T. B.; Hazari, N.; Cowley, A. R.; Green, J. C.; Mountford, P.; *Inorg. Chem.* **2005**, *44*, 8442.
57. Walsh, P. J.; Carney, M. J.; Bergman, R. G.; *J. Am. Chem. Soc.* **1991**, *113*, 6343.
58. Gehrmann, T.; Plundrich, G. T.; Wadepohl, H.; Gade, L. H.; *Organometallics* **2012**.
59. Schofield, A. D.; Nova, A.; Selby, J. D.; Schwarz, A. D.; Clot, E.; Mountford, P.; *Chem. Eur. J.* **2011**, *17*, 265.
60. Tiong, P. J.; Schofield, A. D.; Selby, J. D.; Nova, A.; Clot, E.; Mountford, P.; *Chem. Commun.* **2010**, *46*, 85.
61. Schofield, A. D.; Nova, A.; Selby, J. D.; Manley, C. D.; Schwarz, A. D.; Clot, E.; Mountford, P.; *J. Am. Chem. Soc.* **2010**, *132*, 10484.
62. Jennings, J. R.; Editor; *Catalytic Ammonia Synthesis. Fundamentals and Practice*; Plenum, 1991.
63. Ertl, G.; *Angew. Chem., Int. Ed.* **2008**, *47*, 3524.
64. Cotton, F. A.; Wilkinson, G.; Murillo, C. A.; Bochmann, M.; *Advanced Inorganic Chemistry*; 6th ed.; Wiley-Interscience: New York, 1999.
65. Finlay, M. R.; *British J. Hist. Sci.* **2002**, *35*, 97.
66. Burgess, B. K.; Lowe, D. J.; *Chem. Rev.* **1996**, *96*, 2983.
67. Coughlan, M. P.; Editor; *Molybdenum and Molybdenum-Containing Enzymes*; Pergamon Press, 1980.
68. Rehder, D.; *Coord. Chem. Rev.* **1999**, *182*, 297.
69. Eady, R. R.; *Coord. Chem. Rev.* **2003**, *237*, 23.

70. Siemann, S.; Schneider, K.; Drottboom, M.; Muller, A.; *Eur. J. Biochem.* **2002**, *269*, 1650.
71. Krahn, E.; Weiss, B. J. R.; Krockel, M.; Groppe, J.; Henkel, G.; Cramer, S. P.; Trautwein, A. X.; Schneider, K.; Muller, A.; *J. Biol. Inorg. Chem.* **2002**, *7*, 37.
72. Schrock, R. R.; Kolodziej, R. M.; Liu, A. H.; Davis, W. M.; Vale, M. G.; *J. Am. Chem. Soc.* **1990**, *112*, 4338.
73. Smith, J. M.; Lachicotte, R. J.; Pittard, K. A.; Cundari, T. R.; Lukat-Rodgers, G.; Rodgers, K. R.; Holland, P. L.; *J. Am. Chem. Soc.* **2001**, *123*, 9222.
74. Kim, J.; Rees, D. C.; *Science* **1992**, *257*, 1677.
75. Seefeldt, L. C.; Dance, I. G.; Dean, D. R.; *Biochemistry* **2004**, *43*, 1401.
76. Stephan, G. C.; Sivasankar, C.; Studt, F.; Tuczek, F.; *Chem. Eur. J.* **2008**, *14*, 644.
77. Chatt, J.; Pearman, A. J.; Richards, R. L.; *Nature* **1975**, *253*, 39.
78. Chatt, J.; Pearman, A. J.; Richards, R. L.; *J. Chem. Soc., Dalton Trans.* **1977**, 1852.
79. Schrock, R. R.; *Acc. Chem. Res.* **2005**, *38*, 955.
80. Schrock, R. R.; *Angew. Chem. Int. Ed.* **2008**, *47*, 5512.
81. Yandulov, D. V.; Schrock, R. R.; *Inorg. Chem.* **2005**, *44*, 1103.
82. Weare, W. W.; Dai, X.; Byrnes, M. J.; Chin, J. M.; Schrock, R. R.; Mueller, P.; *Proc. Natl. Acad. Sci. U. S. A.* **2006**, *103*, 17099.
83. Coucouvanis, D.; Mosier, P. E.; Demadis, K. D.; Patton, S.; Malinak, S. M.; Kim, C. G.; Tyson, M. A.; *J. Am. Chem. Soc.* **1993**, *115*, 12193.
84. Mosier, P. E.; Kim, C. G.; Coucouvanis, D.; *Inorg. Chem.* **1993**, *32*, 2620.
85. Palermo, R. E.; Singh, R.; Bashkin, J. K.; Holm, R. H.; *J. Am. Chem. Soc.* **1984**, *106*, 2600.
86. Nishibayashi, Y.; *Dalton Trans* **2012**.
87. Arashiba, K.; Miyake, Y.; Nishibayashi, Y.; *Nature. Chem.* **2011**, *3*, 120.
88. Tanaka, H.; Sasada, A.; Kouno, T.; Yuki, M.; Miyake, Y.; Nakanishi, H.; Nishibayashi, Y.; Yoshizawa, K.; *J. Am. Chem. Soc.* **2011**, *133*, 3498.
89. Schrock, R. R.; *Nat. Chem.* **2011**, *3*, 95.
90. Hidai, M.; Mizobe, Y.; Sato, M.; Kodama, T.; Uchida, Y.; *J. Am. Chem. Soc.* **1978**, *100*, 5740.
91. Hidai, M.; Kodama, T.; Sato, M.; Harakawa, M.; Uchida, Y.; *Inorg. Chem.* **1976**, *15*, 2694.

92. Iwanami, K.; Mizobe, Y.; Takahashi, T.; Kodama, T.; Uchida, Y.; Hidai, M.; *Bull. Chem. Soc. Jpn.* **1981**, *54*, 1773.
93. Chatt, J.; Pearman, A. J.; Richards, R. L.; *J. Chem. Soc., Dalton Trans.* **1978**, 1766.
94. Aoshima, T.; Mizobe, Y.; Hidai, H.; Tsuchiya, J.; *J. Organomet. Chem.* **1992**, *423*, 39.
95. Mizobe, Y.; Ono, R.; Uchida, Y.; Hidai, M.; Tezuka, M.; Moue, S.; Tsuchiya, A.; *J. Organomet. Chem.* **1980**, *204*, 377.
96. Mizobe, Y.; Uchida, Y.; Hidai, M.; *Bull. Chem. Soc. Jpn.* **1980**, *53*, 1781.
97. Bai, G.; Roesky, H. W.; Hao, H.; Noltemeyer, M.; Schmidt, H.-G.; *Inorg. Chem.* **2001**, *40*, 2424.
98. Dartiguenave, M.; Menu, J. M.; Dyedier, E.; Dartiguenave, Y.; Siebald, H.; *Coord. Chem. Rev.* **1998**, *178-180*, 623.
99. Tiong, P. J.: D.Phil Thesis. University of Oxford, 2012.
100. Seino, H.; Ishii, Y.; Hidai, M.; *J. Am. Chem. Soc.* **1994**, *116*, 7433.
101. Bevan, P. C.; Chatt, J.; Leigh, G. J.; Leelamani, E. G.; *J. Organomet. Chem.* **1977**, *139*, C59.
102. Schrock, R. R.; Glassman, T. E.; Vale, M. G.; Kol, M.; *J. Am. Chem. Soc.* **1993**, *115*, 1760.
103. Janas, Z.; Jerzykiewicz, L. B.; Richards, R. L.; Sobota, P.; *Inorg. Chim. Acta* **2003**, *350*, 379.
104. Niemoth-Anderson, J. D.; Debord, J. R. D.; George, T. A.; Ross, C. R., II; Stezowski, J. J.; *Polyhedron* **1996**, *15*, 4031.
105. Yandulov, D. V.; Schrock, R. R.; *Science* **2003**, 76.
106. Galindo, A. M.; Mardones, M.; Manzur, C.; Boys, D.; Hamon, J.-R.; Carrillo, D.; *Eur. J. Inorg. Chem.* **1999**, 387.
107. Manzur, C.; Bustos, C.; Carrillo, D.; Boys, D.; Hamon, J.-R.; *Inorg. Chim. Acta* **1997**, *255*, 73.
108. Redshaw, C.; Gibson, V. C.; Clegg, W.; Edwards, A. J.; Miles, B.; *J. Chem. Soc., Dalton Trans.* **1997**, 3343.
109. DeBord, J. R. D.; George, T. A.; Chang, Y.; Chen, Q.; Zubieta, J.; *Inorg. Chem.* **1993**, *32*, 785.
110. Shaikh, S. N.; Zubieta, J.; *Inorg. Chim. Acta* **1986**, *115*, L19.

111. Arndtsen, B. A.; Schoch, T. K.; McElwee-White, L.; *J. Am. Chem. Soc.* **1992**, *114*, 7041.

112. Dahlstrom, P. L.; Dilworth, J. R.; Shulman, P.; Zubieta, J.; *Inorg. Chem.* **1982**, *21*, 933.

113. Dilworth, J. R.; Zubieta, J.; Hyde, J. R.; *J. Am. Chem. Soc.* **1982**, *104*, 365.

114. Redshaw, C.; Elsegood, M. R.; *Inorg. Chem.* **2000**, *39*, 5164.

115. Wiberg, N.; Haring, H.-W.; Huttner, G.; Friedrich, P.; *Chem. Ber.* **1978**, *111*, 2708.

116. Connelly, N. G.; Demidowicz, Z.; *J. Organomet. Chem.* **1974**, *73*, C31.

117. Chew, K. C.; Clegg, W.; Coles, M. P.; Elsegood, M. R. J.; Gibson, V. C.; White, A. J. P.; Williams, D. J.; *J. Chem. Soc., Dalton Trans.* **1999**, 2633.

118. Menu, M. J.; Crocco, G.; Dartiguenave, M.; Dartiguenave, Y.; Bertrand, G.; *J. Chem. Soc., Chem. Commun.* **1988**, 1598.

119. Herberhold, M.; Bernhagen, W.; *Z. Naturforsch., Teil B* **1974**, *29*, 801.

120. Sydora, O. L.; Kuiper, D. S.; Wolczanski, P. T.; Lobkovsky, E. B.; Dinescu, A.; Cundari, T. R.; *Inorg. Chem.* **2006**, *45*, 2008.

121. Mason, R.; Thomas, K. M.; Zubieta, J. A.; Douglas, P. G.; Galbraith, A. R.; Shaw, B. L.; *J. Amer. Chem. Soc.* **1974**, *96*, 260.

122. Nicholson, T.; Kramer, D. J.; Davison, A.; Jones, A. G.; *Inorg. Chim. Acta* **2003**, *353*, 269.

123. Abrams, M. J.; Chen, Q.; Shaikh, S. N.; Zubieta, J.; *Inorg. Chim. Acta* **1990**, *176*, 11.

124. Nicholson, T.; Hirsch-Kuchma, M.; Davison, A.; Jones, A. G.; *Inorg. Chim. Acta* **1998**, *271*, 191.

125. Paulat, F.; Lehnert, N.; Ishikawa, Y.; Okamoto, K.-I.; Fujisawa, K.; *Inorg. Chim. Acta* **2008**, *361*, 901.

126. Gernert, M. B.; Kooijman, H.; Hiller, W. P.; Dilworth, J. R.; Parrott, S. J.; *Acta Crystallogr., Sect. C: Cryst. Struct. Commun.* **1996**, *C52*, 545.

127. Coia, G. M.; White, P. S.; Meyer, T. J.; Wink, D. A.; Keefer, L. K.; Davis, W. M.; *J. Am. Chem. Soc.* **1994**, *116*, 3649.

128. Huynh, M. H. V.; Meyer, T. J.; White, P. S.; *J. Am. Chem. Soc.* **1999**, *121*, 4530.

129. Coia, G. M.; Devenney, M.; White, P. S.; Meyer, T. J.; Wink, D. A.; *Inorg. Chem.* **1997**, *36*, 2341.

130. Dilworth, J. R.; Harrison, S. A.; Walton, D. R. M.; Schweda, E.; *Inorg. Chem.* **1985**, *24*, 2594.
131. Dilworth, J. R.; Jobanputra, P.; Miller, J. R.; Parrott, S. J.; Chen, Q.; Zubieta, J.; *Polyhedron* **1993**, *12*, 513.
132. Barrientos-Penna, C. F.; Einstein, F. W. B.; Jones, T.; Sutton, D.; *Inorg. Chem.* **1982**, *21*, 2578.
133. McCleverty, J. A.; Rae, A. E.; Woochowicz, I.; Bailey, N. A.; Smith, J. M. A.; *J. Chem. Soc., Dalton Trans.* **1983**, 71.
134. McCleverty, J. A.; Rae, A. E.; Wolochowicz, I.; Bailey, N. A.; Smith, J. M. A.; *J. Organomet. Chem.* **1979**, *168*, C1.
135. Chatt, J.; *J. Organomet. Chem.* **1975**, *100*, 17.
136. Chatt, J.; Dilworth, J. R.; Dahlstrom, P. L.; Zubieta, J.; *J. Chem. Soc., Chem. Commun.* **1980**, 786.
137. Bustos, C.; Manzur, C.; Carrillo, D.; Robert, F.; Gouzerh, P.; *Inorg. Chem.* **1994**, *33*, 1427.
138. Banerjee, S.; Odom, A. L.; *Dalton Trans.* **2008**, 2005.
139. Veith, M.; *Angew. Chem. Int. Ed.* **1976**, *15*, 387.
140. Bultitude, J.; Larkworthy, L. F.; Povey, D. C.; Smith, G. W.; Dilworth, J. R.; Leigh, G. J.; *J. Chem. Soc., Chem. Commun.* **1986**, 1748.
141. Davies, S. C.; Hughes, D. L.; Janas, Z.; Jerzykiewicz, L.; Richards, R. L.; Sanders, J. R.; Sobota, P.; *Chem. Commun.* **1997**, 1261.
142. Davies, S. C.; Hughes, D. L.; Janas, Z.; Jerzykiewicz, L. B.; Richards, R. L.; Sanders, J. R.; Silverston, J. E.; Sobota, P.; *Inorg. Chem.* **2000**, *39*, 3485.
143. Henderson, R. A.; Janas, Z.; Jerzykiewicz, L. B.; Richards, R. L.; Sobota, P.; *Inorg. Chim. Acta* **1999**, *285*, 178.
144. Green, M. L. H.; James, J. T.; Saunders, J. F.; Souter, J.; *J. Chem. Soc., Dalton Trans.* **1997**, 1281.
145. Green, M. L. H.; James, J. T.; Chernega, A. N.; *J. Chem. Soc., Dalton Trans.* **1997**, 1719.
146. Sebe, E.; Heeg, M. J.; Winter, C. H.; *Polyhedron* **2006**, *25*, 2109.
147. Tonks, I. A.; Bercaw, J. E.; *Inorg. Chem.* **2010**, *49*, 4648.
148. Tonks, I. A.; Durrell, A. C.; Gray, H. B.; Bercaw, J. E.; *J. Am. Chem. Soc.* **2012**.
149. Schrock, R. R.; *Acc. Chem. Res.* **1990**, *23*, 158.

150. Gibson, V. C.; *Adv. Materials* **1994**, *6*, 37.
151. Wilson, P. J.; Cooke, P. A.; Blake, A. J.; Mountford, P.; Schröder, M.; *New J. Chem.* **1999**, *23*, 271.
152. Coles, M. P.; Dalby, C. I.; Gibson, V. C.; Clegg, W.; Elsegood, M. R. J.; *J. Chem. Soc., Chem. Commun.* **1995**, 1709.
153. Scheuer, S.; Fischer, J.; Kress, J.; *Organometallics* **1995**, *14*, 2627.
154. Winter, C. H.; Sheridan, P. H.; Lewkebandara, T. S.; Heeg, M. J.; Proscia, J. W.; *J. Am. Chem. Soc.* **1992**, *114*, 1095.
155. Lewkebandra, T. S.; Sheridan, P. H.; Heeg, M. J.; Rheingold, A. L.; Winter, C. H.; *Inorg. Chem.* **1994**, *33*, 5879.
156. Gade, L. H.; Mountford, P.; *Coord. Chem. Rev.* **2001**, *216-217*, 65.
157. Chisholm, M. H.; Rothwell, I. P.: Amido and Imido metal complexes. In *Comprehensive Coordination Chemistry*; Pergamon Press: Oxford, 1987; Vol. 2; pp 162.
158. Cummins, C. C.; Baxter, S. M.; Wolczanski, P. T.; *J. Am. Chem. Soc.* **1988**, *110*, 8731.
159. Zuckerman, R. L.; Bergman, R. G.; *Organometallics* **2000**, *19*, 4795.
160. Walsh, P. J.; Hollander, F. J.; Bergman, R. G.; *Organometallics* **1993**, *12*, 3705.
161. Baranger, A. M.; Walsh, P. J.; Bergman, R. G.; *J. Am. Chem. Soc.* **1993**, *115*, 2753.
162. Lee, S. Y.; Bergman, R. G.; *Tetrahedron* **1995**, *51*, 4255.
163. Lee, S. Y.; Bergman, R. G.; *J. Am. Chem. Soc.* **1996**, *118*, 6396.
164. Meyer, K. E.; Walsh, P. J.; Bergman, R. G.; *J. Am. Chem. Soc.* **1995**, *117*, 974.
165. Zuckerman, R. L.; Bergman, R. G.; *Organometallics* **2001**, *20*, 1792.
166. Lee, S. Y.; Bergman, R. G.; *J. Am. Chem. Soc.* **1995**, *117*, 5877.
167. Walsh, P. J.; Baranger, A. M.; Bergman, R. G.; *J. Am. Chem. Soc.* **1992**, *114*, 1708.
168. Majumder, S.; Gipson, K. R.; Staples, R. J.; Odom, A. L.; *Adv. Synth. Catal.* **2009**, *351*, 2013.
169. Majumder, S.; Gipson, K. R.; Odom, A. L.; *Org. Lett.* **2009**, *11*, 4720.
170. Cao, C.; Ciszewski, J. T.; Odom, A. L.; *Organometallics* **2001**, *20*, 5011.
171. Blake, A. J.; McInnes, J. M.; Mountford, P.; Nikonov, G. I.; Swallow, D.; Watkin, D. J.; *J. Chem. Soc., Dalton Trans.* **1999**, 379.

172. Blake, A. J.; Collier, P. E.; Dunn, S. C.; Li, W.-S.; Mountford, P.; Shishkin., O. V.; *J. Chem. Soc., Dalton Trans.* **1997**, 1549.

173. Dunn, S. C.; Mountford, P.; Robson, D. A.; *J. Chem. Soc., Dalton Trans.* **1997**, 293.

174. Stewart, P. J.; Blake, A. J.; Mountford, P.; *J. Organomet. Chem.* **1998**, *564*, 209.

175. Stewart, P. J.; Blake, A. J.; Mountford, P.; *Organometallics* **1998**, *17*, 3271.

176. Cloke, F. G. N.; Hitchcock, P. B.; Nixon, J. F.; Wilson, D. J.; Mountford, P.; *Chem. Commun.* **1999**, 661.

177. Skinner, M. E. G.; Toupance, T.; Cowhig, D. A.; Tyrrell, B. R.; Mountford, P.; *Organometallics* **2005**, *24*, 5586.

178. Blake, A. J.; Collier, P. E.; Gade, L. H.; Mountford, P.; Lloyd, J.; Pugh, S. M.; Schubart, M.; Skinner, M. E. G.; Trösch, J. M.; *Inorg. Chem.* **2001**, *40*, 870.

179. Dubberley, S. R.; Friedrich, A.; Willman, D. A.; Mountford, P.; Radius, U.; *Chem. Eur. J.* **2003**, *9*, 3634.

180. Dunn, S. C.; Hazari, N.; Jones, N. M.; Moody, A. G.; Blake, A. J.; Cowley, A. R.; Green, J. C.; Mountford, P.; *Chem. Eur. J.* **2005**, *11*, 2111.

181. Dunn, S. C.; Hazari, N.; Cowley, A. R.; Green, J. C.; Mountford, P.; *Organometallics* **2006**, *25*, 1755.

182. Adams, N.; Arts, H. J.; Bolton, P. D.; Cowell, D.; Dubberley, S. R.; Friederichs, N.; Grant, C.; Kranenburg, M.; Sealey, A. J.; Wang, B.; Wilson, P. J.; Cowley, A. R.; Mountford, P.; Schröder, M.; *Chem. Commun.* **2004**, 434.

183. Guiducci, A. E.; Cowley, A. R.; Skinner, M. E. G.; Mountford, P.; *J. Chem. Soc., Dalton Trans.* **2001**, 1392.

184. Lloyd, J.; Vatsadze, S. Z.; Robson, D. A.; Blake, A. J.; Mountford, P.; *J. Organomet. Chem.* **1999**, *591*, 114.

185. Gardner, J. D.; Robson, D. A.; Rees, L. H.; Mountford, P.; *Inorg. Chem.* **2001**, *40*, 820.

186. Male, N. A. H.; Skinner, M. E. G.; Bylikin, S. Y.; Wilson, P. J.; Mountford, P.; Schröder, M.; *Inorg. Chem.* **2000**, *39*, 5483.

187. Fletcher, J. S.; Male, N. A. H.; Wilson, P. J.; Rees, L. H.; Mountford, P.; Schröder, M.; *Dalton Trans.* **2000**, 4130.

188. Hayday, G. J.; Wang, C.; Rees, N. H.; Mountford, P.; *Dalton Trans.* **2008**, 3301.

189. Swallow, D.; McInnes, J. M.; Mountford, P.; *J. Chem. Soc., Dalton Trans.* **1998**, 2253.

190. McInnes, J. M.; Mountford, P.; *Chem. Commun.* **1998**, 1669.

191. Boyd, C. L.; Clot, E.; Guiducci, A. E.; Mountford, P.; *Organometallics* **2005**, *24*, 2347.

192. Bolton, P. D.; Clot, E.; Adams, N.; Dubberley, S. R.; Cowley, A. R.; Mountford, P.; *Organometallics* **2006**, *25*, 2806.

193. Adams, N.; Arts, H. J.; Bolton, P. D.; Cowell, D.; Dubberley, S. R.; Friederichs, N.; Grant, C. M.; Kranenburg, M.; Sealey, A. J.; Wang, B.; Wilson, P. J.; Zuideveld, M. A.; Blake, A. J.; Schröder, M.; Mountford, P.; *Organometallics* **2006**, *25*, 3888.

194. Bolton, P. D.; Adams, N.; Clot, E.; Cowley, A. R.; Wilson, P. J.; Schröder, M.; Mountford, P.; *Organometallics* **2006**, *25*, 5549.

195. Owen, C. T.; Bolton, P. D.; Cowley, A. R.; Mountford, P.; *Organometallics* **2007**, *26*, 83.

196. Bolton, P. D.; Clot, E.; Cowley, A. R.; Mountford, P.; *J. Am. Chem. Soc.* **2006**, *128*, 15005.

197. Bolton, P. D.; Feliz, M.; Cowley, A. H.; Clot, E.; Mountford, P.; *Organometallics* **2008**, *27*, 6096.

198. Feliz, M.; Bolton, P. D.; Clot, E.; Mountford, P.; *Organometallics* **2008**, *27*, 6111.

199. Guiducci, A. E.; Boyd, C. L.; Clot, E.; Mountford, P.; *Dalton Trans.* **2009**, 5960.

200. Protchenko, A. V.; Saleh, L. M. A.; Vidovic, D.; Dange, D.; Jones, C.; Mountford, P.; Aldridge, S.; *Chem. Commun.* **2010**, *46*, 8546.

201. Trösch, D. J. M.; Collier, P. E.; Bashall, A.; Gade, L. H.; McPartlin, M.; Mountford, P.; Radojevic, S.; *Organometallics* **2001**, *20*, 3308.

202. Ward, B. D.; Maisse-Francois, A.; Mountford, P.; Gade, L. H.; *Chem. Commun.* **2004**, 704.

203. Vujkovic, N.; Fillol, J. L.; Ward, B. D.; Wadepohl, H.; Mountford, P.; Gade, L. H.; *Organometallics* **2008**, *27*, 2518.

204. Bashall, A.; Collier, P. E.; Gade, L. H.; McPartlin, M.; Mountford, P.; Trösch, D. T.; *Chem. Commun.* **1998**, 2555.

205. Bashall, A.; Collier, P. E.; Gade, L. H.; McPartlin, M.; Mountford, P.; Pugh, S. M.; Radojevic, S.; Schubart, M.; Scowen, I. J.; Trösch, D. J. M.; *Organometallics* **2000**, *19*, 4784.

206. Pugh, S. M.; Trösch, D. J. M.; Wilson, D. J.; Bashall, A.; Cloke, F. G. N.; Gade, L. H.; Hitchcock, P. B.; McPartlin, M.; Nixon, J. F.; Mountford, P.; *Organometallics* **2000**, *19*, 3205.

207. Ward, B. D.; Orde, G.; Clot, E.; Cowley, A. R.; Gade, L. H.; Mountford, P.; *Organometallics* **2005**, *24*, 2368.

208. Wiberg, N.; Joo, W. C.; Uhlenbrock, W.; *Angew. Chem., Int. Ed. Engl.* **1968**, *7*, 640.

209. Thorman, J. L.; Woo, L. K.; *Inorg. Chem.* **2000**, *39*, 1301.

210. Dilworth, J. R.; Latham, I. A.; Leigh, G. J.; Huttner, G.; Jibril, I.; *J. Chem. Soc., Chem. Commun.* **1983**, 1368.

211. Latham, I. A.; Leigh, G. J.; Huttner, G.; Jibril, I.; *J. Chem. Soc., Dalton Trans.* **1986**, 377.

212. Hughes, D. L.; Jimenez-Tenorio, M.; Leigh, G. J.; Walker, D. G.; *J. Chem. Soc., Dalton Trans.* **1989**, 2389.

213. Hughes, D. L.; Latham, I. A.; Leigh, G. J.; *J. Chem. Soc., Dalton Trans.* **1986**, 393.

214. Park, J. T.; Yoon, S. C.; Bae, B.-J.; Seo, W. S.; Suh, I.-H.; Han, T. K.; Park, J. R.; *Organometallics* **2000**, *19*, 1269.

215. Yoon, S. C.; Bae, B.-J.; Suh, I.-H.; Park, J. T.; *Organometallics* **1999**, *18*, 2049.

216. Guiducci, A. E.; Boyd, C. L.; Mountford, P.; *Organometallics* **2006**, *25*, 1167.

217. Tiong, P. J.; Nova, A.; Clot, E.; Mountford, P.; *Chem. Commun.* **2011**, *47*, 3147.

218. Banerjee, S.; Barnea, E.; Odom, A. L.; *Organometallics* **2008**, *27*, 1005.

219. Cao, C.; Shi, Y.; Odom, A. L.; *Org. Lett.* **2002**, *4*, 2853.

220. Dissanayake, A. A.; Odom, A. L.; *Chem. Commun.* **2012**, *48*, *440*.

221. Alex, K.; Tillack, A.; Schwarz, N.; Beller, M.; *Angew. Chem. Int. Ed.* **2008**, *47*, 2304.

222. Krüger, K.; Tillack, A.; Beller, M.; *Adv. Synth. Catal.* **2008**, *350*, 2153.

223. Sayyed, I. A.; Alex, K.; Tillack, A.; Schwarz, N.; Michalik, D.; Beller, M.; *Eur. J. Org. Chem.* **2007**, 4525.

224. Schwarz, N.; Alex, K.; Sayyed, I. A.; Khedkar, V.; Tillack, A.; Beller, M.; *Synlett* **2007**, 1091.
225. Alex, K.; Tillack, A.; Schwarz, N.; Beller, M.; *Org. Lett.* **2008**, *10*, 2377.
226. Morgan, H. E., Master's Thesis, University of Oxford, 2011.
227. Unruangsri, J., Master's Thesis, University of Oxford, 2010.
228. Herrmann, H.; Fillol, J. L.; Wadepohl, H.; Gade, L. H.; *Angew. Chem. Int. Ed.* **2007**, *46*, 8426.
229. Fletcher, D. A.; McMeeking, R. F.; Parkin, D.; *J. Chem. Inf. Comput. Sci.* **1996**, *36*, 746 (The UK Chemical Database Service: CSD version 5.33 updated February 2012).
230. Munha, R. F.; Veiros, L. F.; Duarte, M. T.; Fryzuk, M. D.; Martins, A. M.; *Dalton Trans.* **2009**, 7494.
231. Basuli, F.; Watson, L. A.; Huffman, J. C.; Mindiola, D. J.; *Dalton Trans.* **2003**, 4228.
232. Olms, P.; Roesky, H. W.; Keller, K.; Noltemeyer, M.; *Z. Naturforsch., B: Chem. Sci.* **1992**, *47*, 1609.
233. Roesky, H. W.; Raubold, T.; Witt, M.; Bohra, R.; Noltemeyer, M.; *Chem. Ber.* **1991**, *124*, 1521.
234. Lorber, C.; Choukroun, R.; Vendier, L.; *Inorg. Chem.* **2007**, *46*, 3192.
235. Schwarz, A. D.; Nova, A.; Clot, E.; Mountford, P.; *Chem. Commun.* **2011**, *47*, 4926.
236. Schwarz, A. D.; Nova, A.; Clot, E.; Mountford, P.; *Inorg. Chem.* **2011**, *50*, 12155.
237. Stergiou, A. C.; Bladenopoulou, S.; Tsiamis, C.; *Inorg. Chim. Acta* **1994**, *217*, 61.
238. Kahlal, S.; Saillard, J.-Y.; Hamon, J.-R.; Manzur, C.; Carrillo, D.; *New J. Chem.* **2001**, *25*, 231.
239. Studt, F.; Tuczek, F.; *Angew. Chem. Int. Ed.* **2005**, *44*, 5639.
240. Kahlal, S.; Saillard, J.-Y.; Hamon, J.-R.; Manzur, C.; Carrillo, D.; *J. Chem. Soc., Dalton Trans.* **1998**, 1229.
241. Bernasconi, C. F.; *Chem. Soc. Rev.* **1997**, *26*, 299.
242. de, F. P.; Marion, N.; Nolan, S. P.; *Coord. Chem. Rev.* **2009**, *253*, 862.
243. Hartley, R. C.; McKiernan, G. J.; *J. Chem. Soc., Perkin Trans. 1* **2002**, 2763.
244. Schrock, R. R.; Sharp, P. R.; *J. Am. Chem. Soc.* **1978**, *100*, 2389.

245. Guggenberger, L. J.; Schrock, R. R.; *J. Am. Chem. Soc.* **1975**, *97*, 6578.

246. Dötz, K. H.; Fischer, E. O.; *Chem. Ber.* **1972**, *105*, 1356.

247. Fischer, E. O.; Maasböl, A.; *Angew. Chem. Int. Ed. Engl.* **1964**, *3*, 580.

Chapter Two

$Ti=N_{\alpha}$ cycloaddition and N_{α}-N_{β} insertion reactions between titanium hydrazides and alkynes

2.1 Overview

Terminal transition metal hydrazide(2-) or isodiazene(0) compounds (L)M=NNR_2 (R = H, alkyl or aryl) have been of ongoing interest for over 30 years.[1-3] Initial studies focused on molybdenum and tungsten derivatives in the context of the biological conversion of dinitrogen to ammonia.[4-6] Both the stoichiometric Chatt (using low oxidation state phosphine compounds[7-10]) and catalytic Schrock (using bulky tris(amido)-amine-supported molybdenum compounds[11,12]) model systems involve (L)M=NNH_2 intermediates immediately prior to the key N_α–N_β bond cleavage step, in agreement with computational studies.[13-17] Considerable effort has also been spent on trying to use mid-transition metal complexes of the type (L)M=NNR_2 as reagents or intermediates for the synthesis of organo-nitrogen products.[4,18,19] However, M=NNR_2 functional group reactivity is minimal for these metals, being characterised only by transformations involving the N_β atom (protonation or reactions involving N_β–H).[18,20,21] In particular, reactions at the M=N_α bond are not seen and N_α–N_β bond cleavage only occurs under forcing conditions using external reductants (e.g. $LiAlH_4$).

This is in stark contrast to early transition metal hydrazides, which show very rich and diverse reactivity comprising *either* reaction at the M=N_α[22-29] bond (cycloaddition or insertion), *or* cleavage or insertion reactions at the N_α–N_β bond[24,25,30-32] and is studied in detail in Chapter Three. The difference in reactivity between early and late transition metal hydrazides can be seen as analogous to the way early and later metal alkylidene/carbene systems differ.[2,33] The reasons for this difference in structure and reactivity are outlined in Chapter One.

While synthetic routes to isolable Group 4 hydrazides have steadily become established,[22,23,27,30-32,34-42] their stoichiometric and catalytic reaction chemistry has only begun to develop during the last few years, and is still very much in its infancy. The metal-catalysed reactions of alkynes with hydrazines in general, are important and topical from an organic synthesis point of view, as variations of the well-established hydroamination reaction with amines RNH_2 (R = alkyl or aryl).[43-46] Bergman,[47] Odom[36,48-50] and others[27,51-53] have found that a range of titanium compounds catalyse the hydrohydrazination of allenes or alkynes with hydrazines (N–H bond addition across C≡C). It is proposed[46] that the key step in these 100 % atom efficient reactions (and in the related iminohydrazination reaction[38,54]) involves [2+2] cycloaddition to a transient hydrazido intermediate forming azametallacycles, but as yet little is known

about their electronic and molecular structures, and they have only been characterised spectroscopically in the last few years.[24,27]

This absence of detailed mechanistic studies is in contrast to the position for Group 4 imides, themselves pivotal in the development of metal-heteroatom multiple bonds in general, and which have been extensively studied in terms of reactions, applications, mechanisms and bonding.[46,55-61]

Given the emerging richness and significance of early transition metal hydrazide chemistry, it is clearly now important to understand the relationship between $M{=}N_\alpha$ cycloaddition and $N_\alpha{-}N_\beta$ cleavage/insertion, and in particular the mechanism(s) of the latter. Although there has been some speculation regarding the mechanism of the $N_\alpha{-}N_\beta$ bond cleavage/insertion reactions of Group 4 hydrazido[3,25,31] and related[62] compounds, only a couple of detailed studies have emerged, all either concurrent with or subsequent to this work.[25,63] In these regards, the chemistry of these highly reduced hydrazides is poorly understood, both in comparison to their later metal isodiazene-like analogues and early metal imido counterparts.

This Chapter describes a detailed experimental and computational study on the scope and mechanism of the unique reaction involving insertion of a single alkyne molecule into the $N_\alpha{-}N_\beta$ bond of either $Ti(N_2N^{Me})(NNPh_2)(py)$ (**1.93**) or $Ti(N_2N^{py})(NNPh_2)(py)$ (**1.97**), to form the corresponding vinyl imide compounds. This involves the isolation of intermediates, a range of mechanistic studies and detailed DFT calculations. The conclusions drawn regarding these specific compounds and substrates can be extrapolated to early transition metal hydrazide reactivity in general. The reaction between **1.93** and a mixture of H_2NNPh_2/PhCCMe was also found to catalytically produce $H_2NC(Ph)C(Me)NPh_2$, making it the only current example of a diamination catalyst derived from an early transition metal hydrazide. The diamination reaction and catalytic activity of **1.93** was discovered previously in the group and has been communicated.[32,42] The work in this Chapter has been published in full.[64]

2.2 Alkyne cycloaddition to $Ti{=}N_\alpha$

Previous work within the Mountford group discovered that $Ti(N_2N^{py})(NNPh_2)(py)$ (**1.97**) reacted with a range of terminal and internal alkynes forming the [2+2] cycloaddition products $Ti(N_2N^{py})\{N(NPh_2)C(R)C(Ar)\}$ (R = H, Ar = Ph, Tol, 3-C_6H_4F, 4-$C_6H_4CF_3$ or C_6F_5 (**2.1**), R = Me, Ar = Ph (**1.147**) or 4-$C_6H_4CF_3$, Equation

2.1). The regioisomer shown in Equation 2.1 (i.e. with ArC bound to Ti and MeC bound to N_α) was the only isomer observed.[24,64] The results also demonstrated that electron-releasing Ar substituents on the alkynes, ArCCR, destabilise the azatitanacyclobutene products whereas electron deficient Ar groups or terminal alkynes tend to give more stable species.

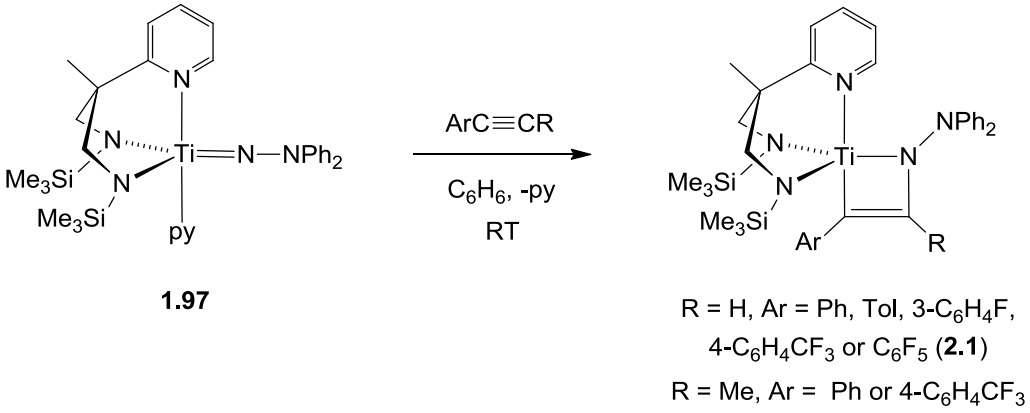

1.97

R = H, Ar = Ph, Tol, 3-C_6H_4F, 4-$C_6H_4CF_3$ or C_6F_5 (**2.1**)
R = Me, Ar = Ph or 4-$C_6H_4CF_3$

Equation 2.1

Although [2+2] cycloaddition reactions of Group 4 imido compounds with terminal and internal alkynes forming metallacycles are well-established,[46,55-59,65-71] and hydrazide-derived metallacycles of the type Ti(L){N(NR_2)C(R′)C(Ar)} have been implicated as intermediates in the catalytic hydrohydrazination of alkynes[46] (and in one instance spectroscopically observed[27]), only Ti(N_2N^{py}){N(NPh_2)C(H)C(3-C_6H_4F)} has been structurally characterised. The solution was of poor quality but nonetheless confirmed the connectivity and orientation of the regioisomer. As yet, no azatitanacyclobutenes formed between Group 4 hydrazides and internal alkynes have been structurally authenticated.

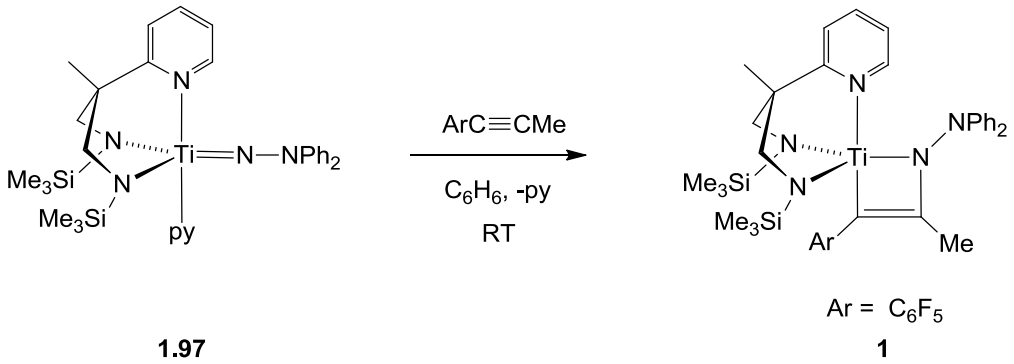

1.97

Ar = C_6F_5

1

Equation 2.2

Based on the above observations the reaction between Ti(N_2N^{py})($NNPh_2$)(py) (**1.97**) and C_6F_5CCMe was carried out. As expected this formed the corresponding [2+2] cycloaddition product Ti(N_2N^{py}){N(NPh_2)C(Me)C(C_6F_5)} (**1**, Equation 2.2) as a dark red microcrystalline powder which was stable in solution for up to one week. Diffraction-quality crystals were grown by slow cooling of a concentrated hexanes solution from 60 ºC to room temperature. The ^1H and $^{13}C\{^1H\}$ NMR spectra are presented in Figure 2.1, with the solid state structure shown in Figure 2.2. Selected bond lengths and angles are given in Table 2.1.

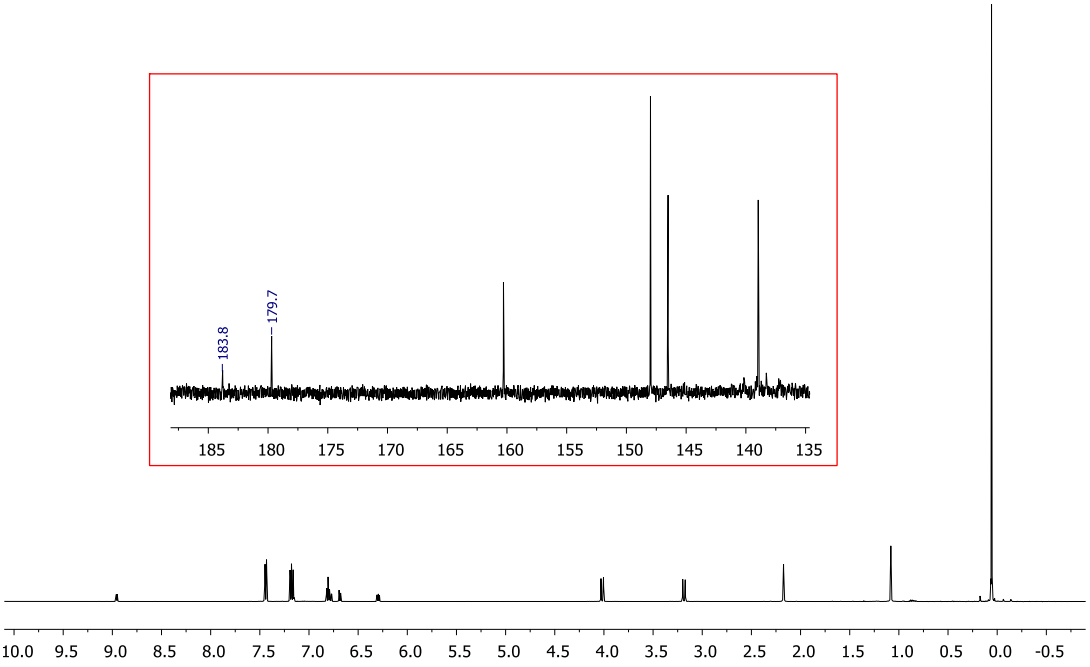

Figure 2.1. ^1H NMR spectrum (499.9 MHz, 293 K) of the isolated product Ti(N_2N^{py}){N(NPh_2)C(Me)C(C_6F_5)} (**1**) in C_6D_6. The inset illustrates the $^{13}C\{^1H\}$ spectrum (125.7 MHz) between 135 and 190 ppm. The labelled resonances correspond to the Ar<u>C</u>=CMe and ArC=<u>C</u>Me ^{13}C resonances, respectively.

The ^1H NMR spectrum and an expansion of the $^{13}C\{^1H\}$ NMR spectrum of Ti(N_2N^{py}){N(NPh_2)C(Me)C(C_6F_5)} (**1**) are presented in Figure 2.1. They clearly show that the pyridine present in the starting material has been lost, the remaining pyridyl resonance being attributable to the N_2N^{py} ligand. The hydrazide and N_2N^{py} ligand resonances are typical of other azametallacycles formed between **1.97** and alkynes.[24,64] The $^{13}C\{^1H\}$ NMR spectrum shows resonances at 183.8 and 179.7 ppm corresponding

to the ArC=CMe and ArC=CMe resonances, respectively, similar to those found in the related cycloaddition product Ti(N_2N^{py}){N(NPh_2)C(H)C(C_6F_5)} (**2.1**, *vida infra*).

It is important to note that the ^{13}C NMR shifts for the ArC=CR (R = Me or H) carbons of the previously mentioned azatitanacyclobutenes, Ti(N_2N^{py}){N(NPh_2)C(R)CAr}, are particularly characteristic, being similar to those previously reported for metallacycles formed between titanium imides (L)Ti=NR and alkynes.[65-69] With the exception of Ar = C_6F_5, the ArC–Ti resonances are in the range *ca.* 207 – 216 ppm, whereas the N_α–bound carbons CR, for all examples, have shifts between 175 and 180 (R = Me) or 160 and 168 (R = H) ppm. In the case of Ar = C_6F_5 (compounds **1** and **2.1**) the ArC–Ti carbons appeared at 183.8 and 181.2 ppm, respectively, as illustrated in Figure 2.1 for **1**.

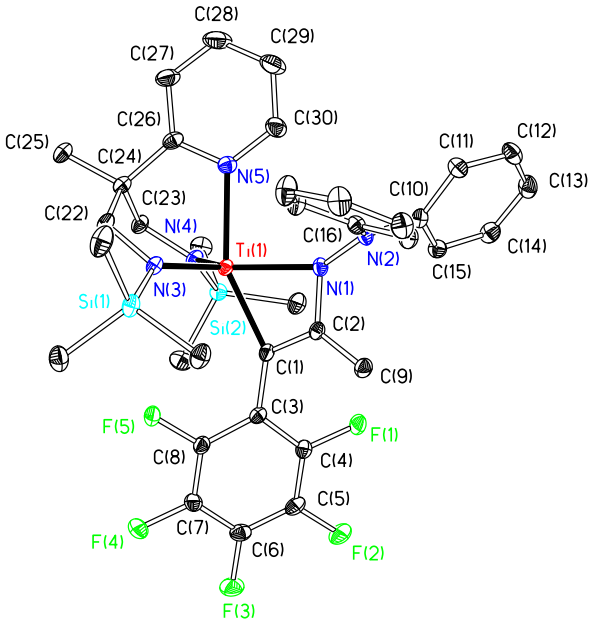

Figure 2.2. Displacement ellipsoid plot (25% probability) of Ti(N_2N^{py}){N(NPh_2)C(Me)C(C_6F_5)} (**1**). H atoms omitted for clarity.

The molecular structure of Ti(N_2N^{py}){N(NPh_2)C(Me)C(C_6F_5)} (**1**, Figure 2.2) unambiguously confirms the formation of a [2+2] cycloaddition product. Selected distances and angles are listed in Table 2.1. The coordination geometry at Ti(1) is approximately trigonal bipyramidal. As in the starting compound **1.97** itself, the N_{amide} and N_α atoms lie in the equatorial plane. The Ti–N_{amide} bonds in **1** (avg. 1.899(2) Å) are considerably shorter compared to those in **1.97** (avg. 1.974(2) Å). This is due to the lengthening of Ti–N_α from 1.759(2) Å in **1.97** to 2.119(2) Å in **1** and concomitant

reduction in Ti–N_α bond order on formation of the metallacycle core containing Ti(1), N(1), C(1) and C(2). The C(1)–C(2) distance of 1.378(3) Å is consistent with a formal double bond and is comparable to those found in azametallacyclobutenes derived from Group 4 imides and alkynes (7 structurally authenticated examples, range 1.326 – 1.399 Å, avg. 1.367 Å).[65-67,69-71] The distances and angles around Ti(1) and within the metallacyclic ring are very similar to those in Ti(N_2N^{py}){N(Ar)C(H)CTol}(py) (Ar = 2,6-$C_6H_3{}^iPr_2$) formed from the aryl imido analogue of **1.97**, Ti(N_2N^{py})(NAr)(py), and TolCCH (Ti–NAr = 2.087(3), C=C = 1.362(4), avg. Ti–N_{amide} = 1.904(3) Å). [66]

Table 2.1. Selected distances (Å) and angles (^{o}) for Ti(N_2N^{py}){N(NPh_2)C(Me)C(C_6F_5)} (**1**).

Ti(1)–N(1)	2.119(2)	N(1)–Ti(1)–N(3)	126.91(7)
Ti(1)–N(3)	1.895(2)	N(1)–Ti(1)–N(4)	127.79(7)
Ti(1)–N(4)	1.902(2)	N(5)–Ti(1)–C(1)	153.50(7)
Ti(1)–N(5)	2.232(2)	Ti(1)–N(1)–N(2)	141.61(12)
Ti(1)–C(1)	2.065(2)	Ti(1)–N(1)–C(2)	88.27(11)
N(1)–N(2)	1.418(2)	Ti(1)–C(1)–C(2)	90.62(12)
N(1)–C(2)	1.382(3)	N(2)–N(1)–C(2)	116.78(16)
N(2)–C(10)	1.398(2)	N(1)–C(2)–C(9)	121.48(17)
N(2)–C(16)	1.416(2)		
C(1)–C(2)	1.378(3)		
C(1)–C(3)	1.448(3)		

2.3 Alkyne insertion into N_α–N_β

Work carried out prior to this Thesis showed that when the equilibrium mixture formed between Ti(N_2N^{py})($NNPh_2$)(py) (**1.97**) and PhCCMe in C_6D_6 was allowed to stand for three days at room temperature, the new complex Ti(N_2N^{py}){NC(Ph)C(Me)NPh_2}(py) (**1.148**) was formed as the sole product (Equation 2.3). Heating a mixture of **1.97** and PhCCMe at 60 ^{o}C accelerated the reaction forming **1.148** within 3 hours. Compound **1.148** is a vinyl imido species formally formed by

insertion of PhCCMe into the N_α–N_β bond of **1.97**. The solid state structure has been determined and, consistent with the spectroscopic data, shows that only the isomer with the alkyne substituents *cis* to each other is formed.[24,64] The insertion did not occur with any other alkynes.

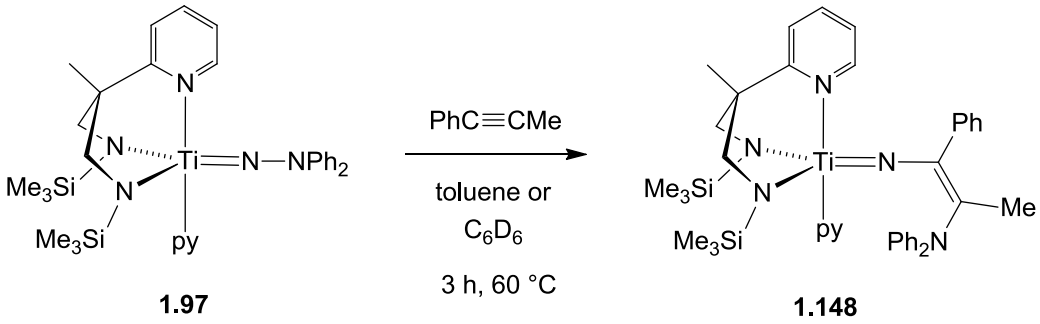

1.97 **1.148**

Equation 2.3

The work also involved the screening of a range of other diamide-amine supported titanium hydrazides (Figure 2.3),[42] varying the chelating ring size, apical N substituent and coordination number, in order to better understand the effects of the diamide-amine ligand on the reactivity of the hydrazide group with terminal and internal alkynes. The most promising candidate appeared to be $Ti(N_2N^{Me})(NNPh_2)(py)$ (**1.93**), possessing the least sterically demanding apical donor (NMe) and smallest chelating ring size. It was found to readily form the well-defined N_α–N_β insertion products $Ti(N_2N^{Me})\{NC(R)C(Me)NPh_2\}(py)$ (R = Me (**2.2**), Ph (**1.149**)) when reacted with MeCCMe and PhCCMe, respectively. Compound **1.149** has been structurally characterised.[32,42] In addition it was found that the vinyl imido ligand in **1.149** could be protonated by 1,1-diphenylhydrazine to reform **1.93** and the corresponding 1,2-diaminoalkene. This reaction was also discovered to be catalytic with up to 20 equivalents of alkyne and hydrazine per metal centre. A greater number of equivalents led to decomposition, possibly *via* ancillary ligand protonation.[32]

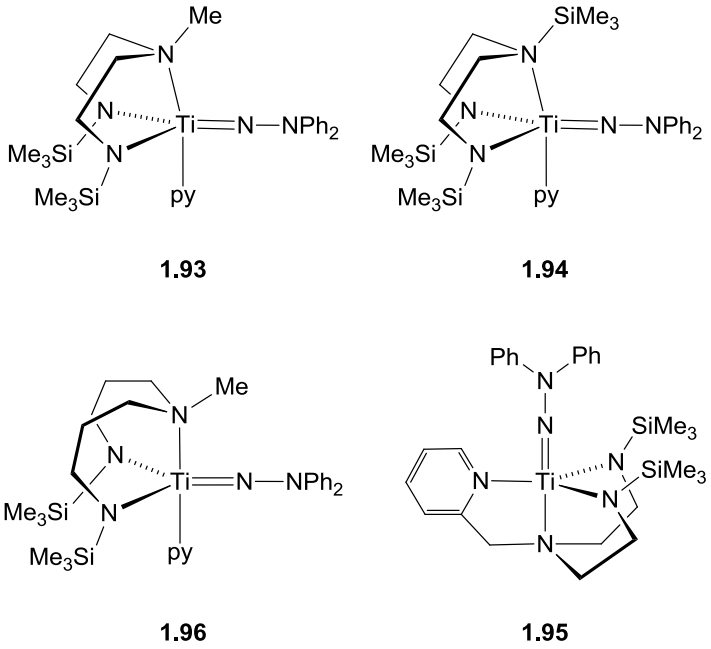

Figure 2.3. Examples of diamide-amine supported terminal titanium hydrazides.

Following these initial results, it was of interest to investigate the scope of alkynes for which this reaction would proceed and to probe the mechanism of this novel transformation. To this end Ti(N_2N^{Me})($NNPh_2$)(py) (**1.93**) was reacted with a range of alkynes, varying both the steric and electronic factors. Compound **1.93** reacted with a large range of aryl substituted alkynes of the type ArCCMe (Ar = 4-C_6H_4X or C_6F_5, X = MeO, ^{t}Bu, Me, F, Cl or CF_3) to form the series of compounds Ti(N_2N^{Me}){NC(R)C(Me)NPh_2}(py) (R = Me, Ph or aryl, Equation 2.4). All of the reactions proceeded readily at room temperature and were quantitative when followed by ^{1}H NMR spectroscopy in C_6D_6. In general, the more electron-rich alkynes ArCCMe (Ar = 4-C_6H_4OMe or 4-$C_6H_4{}^t$Bu) gave the fastest insertion reactions. Low yields were obtained on scale up in some instances due to the high solubility of many of the products. In contrast to the corresponding reactions of **1.97** (Equation 2.1), no cycloaddition products were observed at room temperature. A detailed experimental and DFT mechanistic study is presented later in this Thesis.

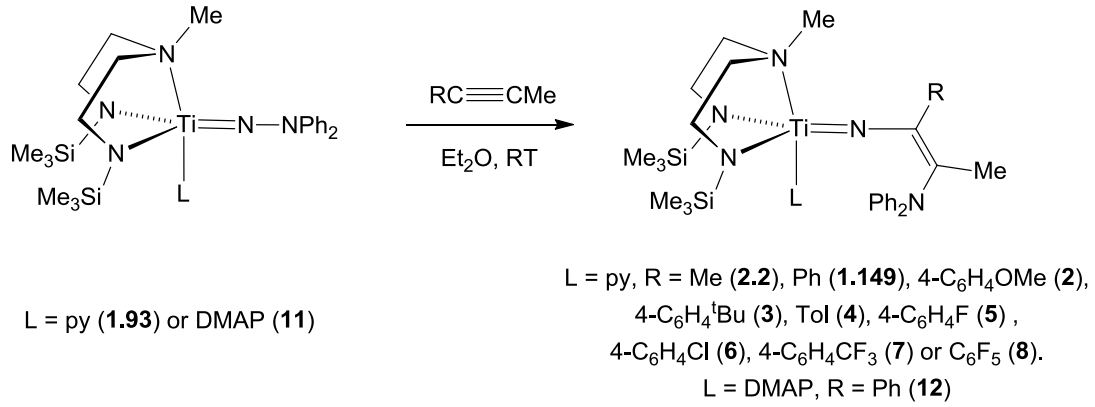

Equation 2.4

It is important to note that the ^{13}C chemical shifts for the internal quaternary carbons of the *cis*-$N_\alpha\underline{C}(R)=\underline{C}(Me)NPh_2$ ligand appear between *ca.* 142 and 158 ppm for the N_α-bound carbons, and between *ca.* 112 and 118 ppm for the carbons bearing NPh_2. The ^1H and $^{13}C\{^1H\}$ NMR spectra of $Ti(N_2N^{Me})\{NC(4\text{-}C_6H_4Cl)C(Me)NPh_2\}(py)$ (**6**, Figure 2.4), representative for the entire series of compounds **2** - **8**, illustrates this clearly. The marked ^{13}C resonances correspond to $N_\alpha\underline{C}(4\text{-}C_6H_4Cl)=C(Me)NPh_2$ and $N_\alpha C(4\text{-}C_6H_4Cl)=\underline{C}(Me)NPh_2$, respectively. These chemical shifts are significantly different to the ranges found for the corresponding metallacycles (*vide supra*).[24,64]

Extending the reactions of **1.93** to the dialkyne $MeCC(2,3,5,6\text{-}C_6F_4)CCMe$ (**9**) in a 2:1 (**1.93**:**9**) ratio gave the dinuclear N_α–N_β insertion product $[Ti(N_2N^{Me})\{NCC(Me)NPh_2\}(py)]_2(\mu\text{-}2,3,5,6\text{-}C_6F_4)$ (**10**, Equation 5) in 36% isolated yield.[72] Reaction of **1.93** with **9** in a 1:1 ratio gave a mixture of species containing both **1.93** and **10**.

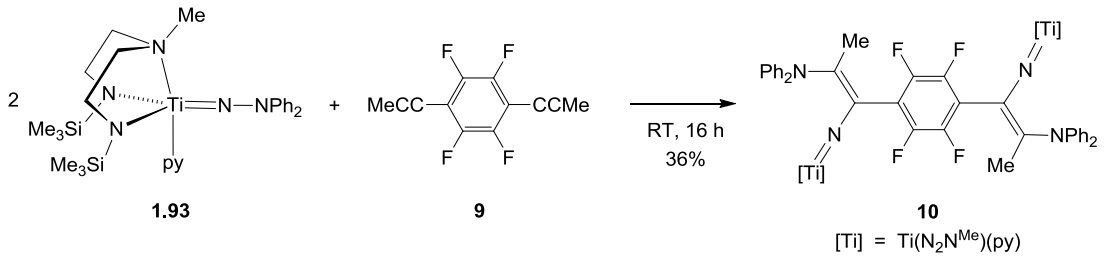

Equation 2.5

Reactions between **1.93** and a range of terminal alkynes (RCCH, R = Ph, $SiMe_3$, $4\text{-}C_6H_4CF_3$) yielded unidentified mixtures. The same was true for the reactions with 1- and 3-hexyne. No reaction occurred with $Me_3SiCCMe$, $Me_3SiCCPh$ or ^tBuCCMe

either at room temperature or upon prolonged heating. When reacted with FcCCMe (Fc = $CpFeC_5H_4$) and a range of bisaryl alkynes of the type ArCCAr (Ar = Ph, 4-C_6H_4OMe or 4-$C_6H_4CF_3$), Ti(N_2N^{Me})($NNPh_2$)(py) (**1.93**) showed promising reactivity, with either one or two well-defined products being formed. These were found to be mixtures of vinyl imides, of the type shown in Equation 2.4, and 7-membered ring products as reported by Bergman and Gade.[30,63] These observations are addressed in Chapter Four.

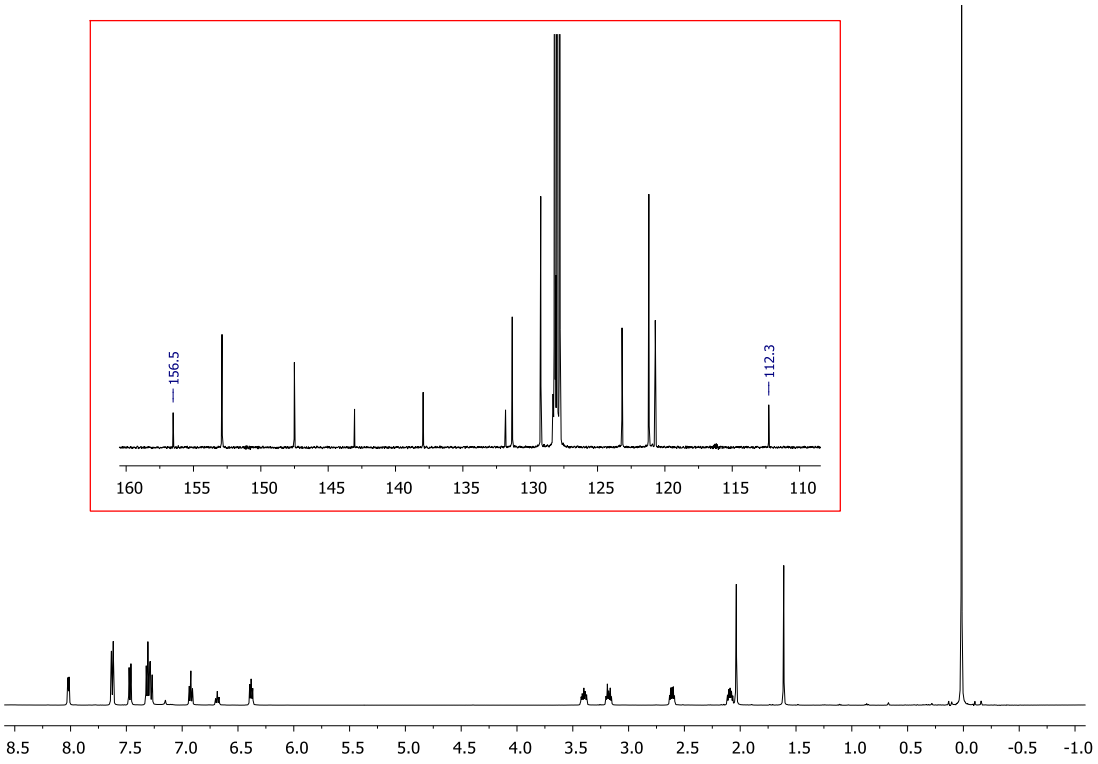

Figure 2.4. ^{1}H NMR spectrum (499.9 MHz, 293 K) of the isolated product Ti(N_2N^{Me}){NC(4-C_6H_4Cl)C(Me)NPh_2}(py) (**6**) in C_6D_6. The inset illustrates the $^{13}C\{^1H\}$ spectrum (125.7 MHz) between 110 and 160 ppm. The marked resonances correspond to the R<u>C</u>=CMe and RC=<u>C</u>Me ^{13}C resonances.

Diffraction quality crystals of [Ti(N_2N^{Me}){NCC(Me)NPh_2}(py)]$_2$(μ-2,3,5,6-C_6F_4) (**10**) were grown by slow diffusion of pentane into a toluene solution and the structure is presented in Figure 2.5. Selected distances and angles are listed in Table 2.2. The solution ^{1}H and $^{13}C\{^1H\}$ NMR spectra are in full agreement with the solid state structure of **10**. Single crystals of Ti(N_2N^{Me}){NC(4-C_6H_4F)C(Me)NPh_2}(py) (**5**) and Ti(N_2N^{Me}){NC(C_6F_5)C(Me)NPh_2}(py) (**8**) were also analysed but found to be poor diffractors. Nevertheless, the connectivity of each could be confidently established

(see Appendix A) and were found to be consistent with the structures proposed in Equation 2.4.

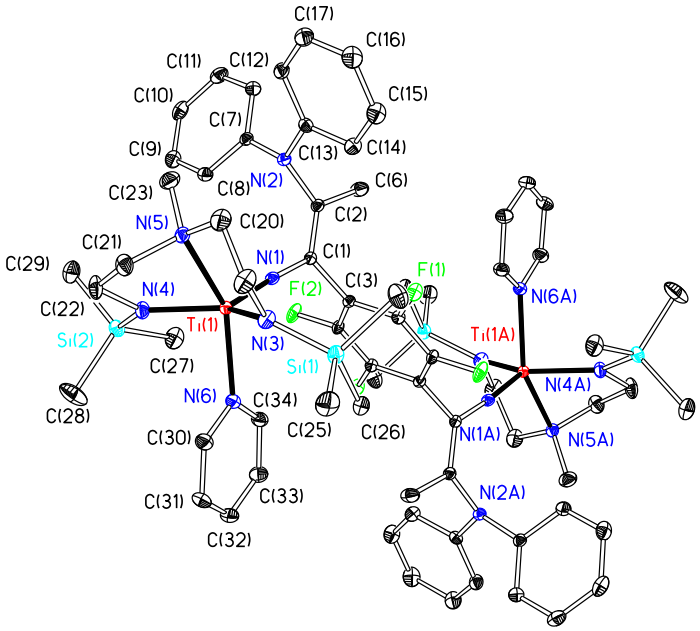

Figure 2.5. Displacement ellipsoid plot (20 % probability) of $[Ti(N_2N^{Me})\{NCC(Me)NPh_2\}(py)]_2(\mu\text{-}2,3,5,6\text{-}C_6F_4)$ (**10**). Atoms carrying the suffix 'A' are related to their counterparts by the symmetry operator 2-*x*,1-*y*,1-*z*. H atoms are omitted for clarity.

$[Ti(N_2N^{Me})\{NCC(Me)NPh_2\}(py)]_2(\mu\text{-}2,3,5,6\text{-}C_6F_4)$ (**10**) possesses a trigonal bipyramidal Ti atom with the N_{amide} atoms and N_α of the new vinyl imido ligand occupying the equatorial coordination sites. The Ti=N_α bond distance (1.758(2) Å) is slightly longer than that found in $Ti(N_2N^{Me})\{NC(Ph)C(Me)NPh_2\}(py)$ (**1.149**, Ti=N_α = 1.733(5) Å), consistent with a formal triple bond, as previously established for compounds of the general type $Ti(N_2N^{R})(NR')(py)$ (R′ = alkyl, aryl, $NNPh_2$; R = Me, $SiMe_3$ and py).[42,69,73,7475] The C(1)–C(2) distance within the vinyl imido ligand (1.346(3) Å) is consistent with a C=C double bond. The Ti=N_α and NPh_2 moieties are mutually *cis* to each other, the aryl group is bound to the same carbon as Ti=N_α (i.e. C(1)) and the methyl group of the original alkyne (C(6)) is bound to C(2). The Ti–N_{amide} distances in **10** (avg. 2.003 Å) are similar to those found in **1.149** but significantly longer than those in **1.148** (avg. 2.014 (**1.149**) and 1.961 Å (**1.148**)). The Ti–N_{amine} distance is also similar to **1.149** and longer than **1.148** (Ti–N_{amine} = 2.230(2) (**10**), 2.232(3) (**1.149**) and 2.192(2) (**1.148**) Å) while the Ti–N_{py} distances of **10** and

1.149 are shorter than that found in **1.148** (Ti–N_{py} = 2.219(2) (**10**), 2.199(3) (**1.149**) and 2.268(2) (**1.148**) Å). These structural features parallel those found in a comparison of the starting hydrazides **1.97** (for **1.148**) and **1.93** which have been discussed in detail elsewhere.[42] Overall, **10** has a very similar structure to **1.148** and **1.149**, and the key distances and angles around titanium are comparable to the starting hydrazide.

Table 2.2. Selected bond distances (Å) and angles (^{o}) for $[Ti(N_2N^{Me})\{NCC(Me)NPh_2\}(py)]_2(\mu\text{-}2,3,5,6\text{-}C_6F_4)$ (**10**).

Ti(1)–N(1)	1.758(2)	N(1)–Ti(1)–N(3)	112.6(1)
Ti(1)–N(3)	2.001(2)	N(1)–Ti(1)–N(4)	112.8(1)
Ti(1)–N(4)	2.006(2)	N(1)–Ti(1)–N(5)	110.4(1)
Ti(1)–N(5)	2.230(2)	N(1)–Ti(1)–N(6)	100.5(1)
Ti(1)–N(6)	2.219(2)	N(5)–Ti(1)–N(6)	148.9(1)
N(1)–C(1)	1.360(2)	N(3)–Ti(1)–N(4)	133.6(1)
C(1)–C(2)	1.346(3)	Ti(1)–N(1)–C(1)	174.7(1)
C(1)–C(3)	1.506(2)	N(1)–C(1)–C(2)	128.24(2)
C(2)–N(2)	1.440(2)	N(1)–C(1)–C(3)	114.9(2)
C(2)–C(6)	1.501(3)	C(1)–C(2)–N(2)	121.3(2)
		C(1)–C(2)–C(6)	124.4(2)

Titanium vinyl imido compounds have previously been prepared by reaction of sources of alkylidene compounds such as $Cp_2Ti{=}CH_2$ with organic nitriles.[76,77] These vinyl imides can have a rich reaction chemistry with other unsaturated substrates *via* [4+2] cycloaddition reactions. Although cleavage reactions of the N_α–N_β bond of terminal Group 4 hydrazide and related ligands with a number of unsaturated substrates (including alkynes) have been previously reported (see Chapter One), the reactions in Equations 2.3 – 2.5 are unique examples of net substrate insertion into the N_α–N_β bond of a terminal hydrazide ligand.

The rarity, selectivity and high yield of the reaction meant that it was of interest to study the mechanism leading to the formation of the vinyl imide products, in an effort to further understand this remarkable transformation and to aid in the development of superior catalysts. It was probed using a variety of experimental and computational methods as outlined below.

2.4 Mechanistic investigations of the N_α–N_β insertion reaction

The reaction between Ti(N_2N^{Me})($NNPh_2$)(py) (**1.93**) and PhCCMe in toluene-d_8 was monitored by ^{1}H NMR spectroscopy between -50 and 0 °C in the presence of 1,4-dimethoxybenzene as an internal standard. Between -50 and -40 ^{o}C there was no reaction between **1.93** and the alkyne. Above -40 to -35 ^{o}C, the starting materials were quantitatively converted to the N_α–N_β insertion product Ti(N_2N^{Me}){NC(Ph)C(Me)NPh_2}(py) (**1.149**). No intermediates or other product regioisomers were observed, and the reaction was complete within two hours at 0 ^{o}C.

When the reaction between **1.93** and an excess of PhCCMe (10 – 50 equivalents) was followed at -26 °C in toluene-d_8 the decay of hydrazide starting material (and evolution of **1.149**) followed well-behaved pseudo first order kinetics as illustrated in Figure 2.6. It would have been preferable to add an excess amount of pyridine to the reaction mixture. Unfortunately this could not be done, due to the formation of a 'bis(pyridine)' compound of **1.93** in the presence of excess pyridine at low temperatures (**13**, *vide infra*). However, as there were no intermediates observed during the reaction and there is no net release of pyridine in proceeding from the reactants to the products, it can be assumed that the concentration of free pyridine is minimal and will not have any effect on the kinetics of the reaction.

As shown in Figure 2.7 (top), the observed rate constants (k_{obs}) obtained from the linear ln plots do not scale linearly with the equivalents of PhCCMe used. At high values of [PhCCMe]:[**1.93**] the onset of saturation kinetics is very evident. In contrast, the corresponding double-reciprocal plot (Figure 2.7, bottom) is linear over the range of PhCCMe equivalents used.

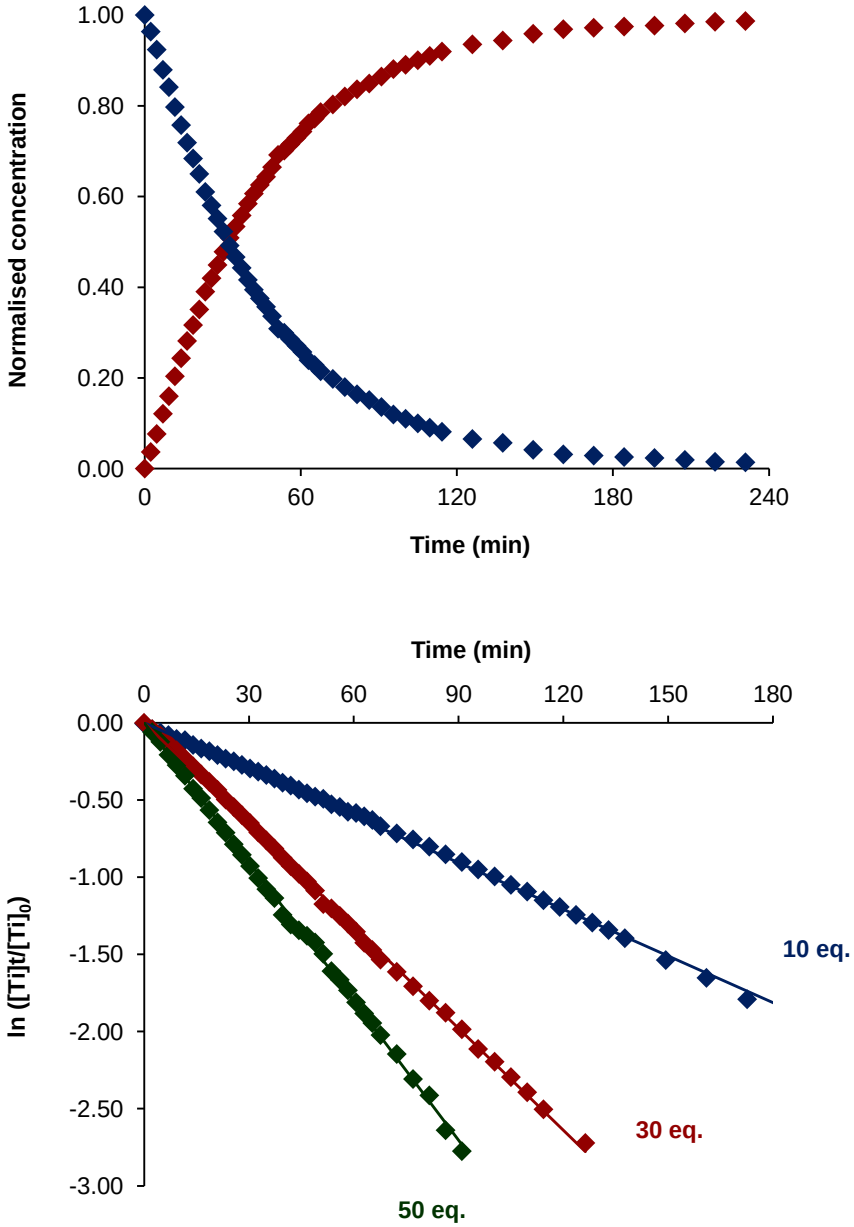

Figure 2.6. Top: decay of Ti(N_2N^{Me})($NNPh_2$)(py) (**1.93**, blue) and growth of Ti(N_2N^{Me}){NC(Ph)C(Me)NPh_2} (**1.149**, red) with time for the reaction between **1.93** and PhCCMe (30 equivalents) at -26 ^{o}C. Bottom: pseudo first order ln plots for the reaction of Ti(N_2N^{Me})($NNPh_2$)(py) (**1.93**) with PhCCMe (10, 30, 50 equivalents) at -26 ^{o}C. The best-fit lines shown had r^2 = 0.999 in all cases.

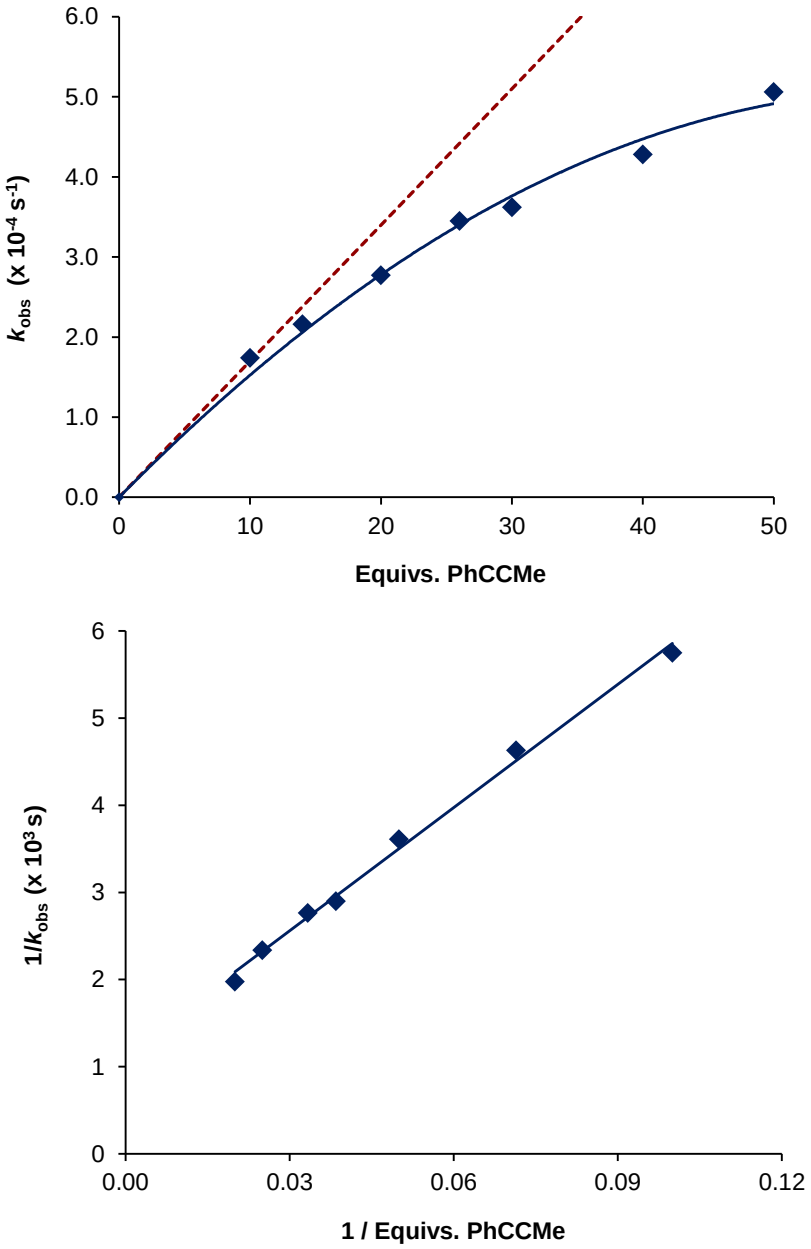

Figure 2.7. Top: plot of k_{obs} *vs.* equivalents of alkyne for the reaction of $Ti(N_2N^{Me})(NNPh_2)(py)$ (**1.93**) with PhCCMe; the dotted line is that expected for a linear relationship between k_{obs} and equivalents based on extrapolation from the first data point (10 equivalents). Bottom: the corresponding double-reciprocal plot. The linear fit ($r^2 = 0.995$) gives an intercept of $1/k_{obs} = 1.15(8) \times 10^3$ s.

At first sight, the data in Figures 2.6 and 2.7 are consistent with the general process outlined in Scheme 2.1 in which dissociation of py from **1.93** forms a reactive pyridine-free intermediate **1.93′** prior to the rate limiting step (or steps), the rate constant for which is denoted as "k_2". Scheme 2.1 is analogous to mechanisms

previously established[69,78] for the cycloaddition reactions of the base-stabilised imides $Cp_2Zr(NXyl)(L)$ (**1.47**, L = THF or $OPPh_3$) or $Ti(N_2N^R)(N^tBu)(py)$ (N_2N^R = N_2N^{py} (**1.71**) or $N_2{}^{Xyl}N^{py}$) with alkynes. Scheme 2.1 predicts that, in the presence of an excess of alkyne, the rates of reaction should follow pseudo first order kinetics according to Equation 2.6 where k_{obs} is given by Equation 2.7. The linear double-reciprocal plot is consistent with Equation 2.8 and is found to give a value for k_1 of 8.7(12) x 10^{-4} s^{-1}.

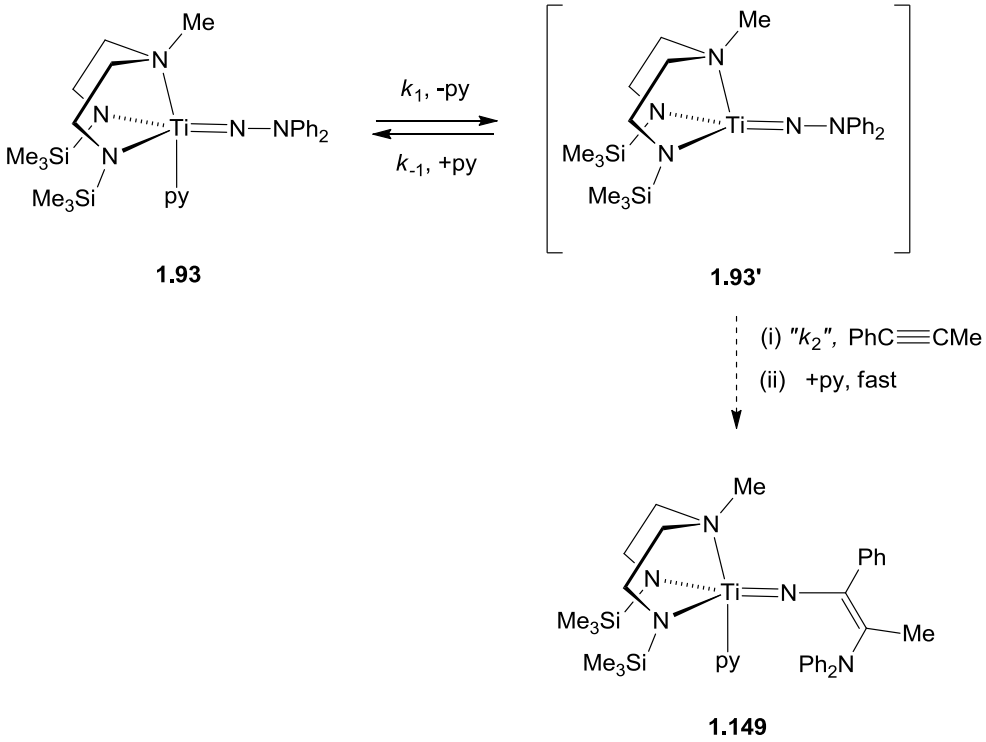

Scheme 2.1. Experimentally implicated steps in the formation of **1.149** from **1.93** and PhCCMe.

$$\text{Rate} = k_{obs}[\mathbf{1.93}] \qquad \text{(Equation 2.6)}$$

$$k_{obs} = \frac{k_1 k_2[\text{PhCCMe}]}{k_2[\text{PhCCMe}] + k_{-1}[\text{py}]} \qquad \text{(Equation 2.7)}$$

$$\frac{1}{k_{obs}} = \frac{1}{k_1} + \frac{k_{-1}[\text{py}]}{k_1 k_2} \times \frac{1}{[\text{PhCCMe}]} \qquad \text{(Equation 2.8)}$$

As a test of Equation 2.7 the DMAP analogue of **1.93**, namely $Ti(N_2N^{Me})(NNPh_2)(DMAP)$ (**11**) was prepared. DMAP is a stronger donor than pyridine and, in agreement with Scheme 2.1 and Equation 2.7, compound **11** reacted

with PhCCMe significantly more slowly than **1.93** to form the corresponding insertion product Ti(N_2N^{Me}){NC(Ph)C(Me)NPh_2}(DMAP) (**12**, Equation 2.4). When followed by ^{1}H NMR spectroscopy in toluene-d_8, the reaction between **11** and PhCCMe (20 equivalents) had $t_{1/2}$ = 3 h at 0 ^{o}C whereas for **1.93** $t_{1/2}$ = 41 min at -26 ^{o}C under otherwise identical conditions.

Addition of one or two equivalents of pyridine to a mixture of **1.93** and PhCCMe in toluene-d_8 also significantly decreased the rate of the insertion reaction, consistent with Scheme 2.1 and Equation 2.7. However, a control experiment in toluene-d_8 showed that **1.93** on its own reacts with the additional pyridine to form a fluxional new species (**13**) with apparent C_s symmetry, the amount of which increases with decreasing temperature.

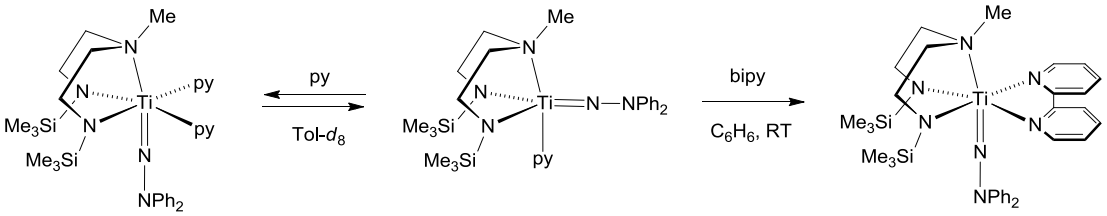

Scheme 2.2. Reactions of **1.93** with pyridine and bipy.

Compound **13** is probably the bis(pyridine) adduct Ti(N_2N^{Me})($NNPh_2$)$(py)_2$ (Scheme 2.2). Although the decreased rate of reaction of **1.93** with PhCCMe in the presence of added pyridine is consistent with a reciprocal dependence on k_{-1}[py] (Equations 2.6 and 2.7), it is also consistent with partial trapping (to some unknown extent) of **1.93** to form unreactive **13** which exists in a rapid dynamic equilibrium with **1.93** at -30 ^{o}C (separate resonances for **1.93**, **13** and the added pyridine are only observed below -50 ^{o}C).

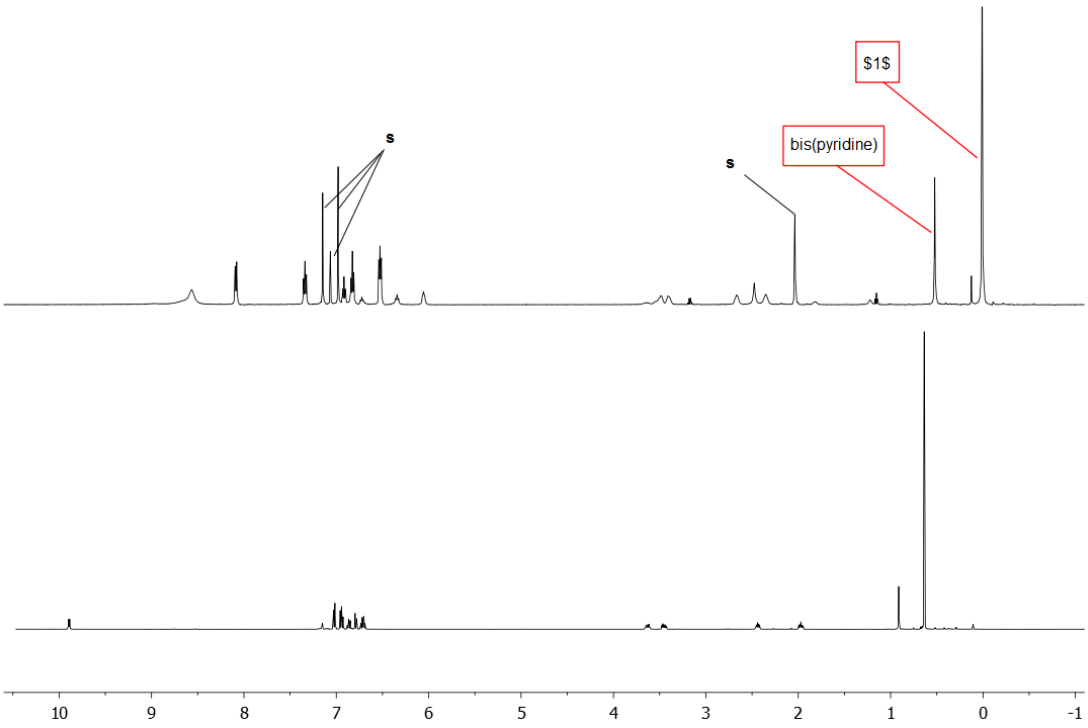

Figure 2.8. Bottom: ^{1}H NMR spectrum (499.9 MHz) of Ti(N_2N^{Me})($NNPh_2$)(bipy) (**14**) in C_6D_6 at 293 K. Top: ^{1}H NMR spectrum of Ti(N_2N^{Me})($NNPh_2$)(py) (**1.93**) with 1 equivalent of pyridine added, in toluene-d_8 at 193 K. ('s' denotes residual protio solvent).

Although **13** is labile and cannot be isolated, the 2,2′-bipyridyl analogue Ti(N_2N^{Me})($NNPh_2$)(bipy) (**14**, bipy = 2,2′-bipyridine) was readily prepared (Scheme 2.2). The ^{1}H NMR spectra of Ti(N_2N^{Me})($NNPh_2$)$(py)_2$ (**13**, at -80 ºC) and Ti(N_2N^{Me})($NNPh_2$)(bipy) (**14**) are presented in Figure 2.8. They clearly show the similarities between the $SiMe_3$ resonances of the two compounds which are shifted significantly (~ 0.5 ppm) from that found in the mono(pyridine) hydrazide Ti(N_2N^{Me})($NNPh_2$)(py) (**1.93**). This indicates the probable reorientation of the hydrazide group in **13** to an axial position, with the two pyridine molecules equatorially placed, consistent with **14** and the structure proposed in Scheme 2.2.

Diffraction-quality crystals of Ti(N_2N^{Me})($NNPh_2$)(bipy) (**14**) were grown from a saturated C_6H_6 solution at room temperature. The solid state structure is presented in Figure 2.9, with selected bond lengths and angles given in Table 2.3.

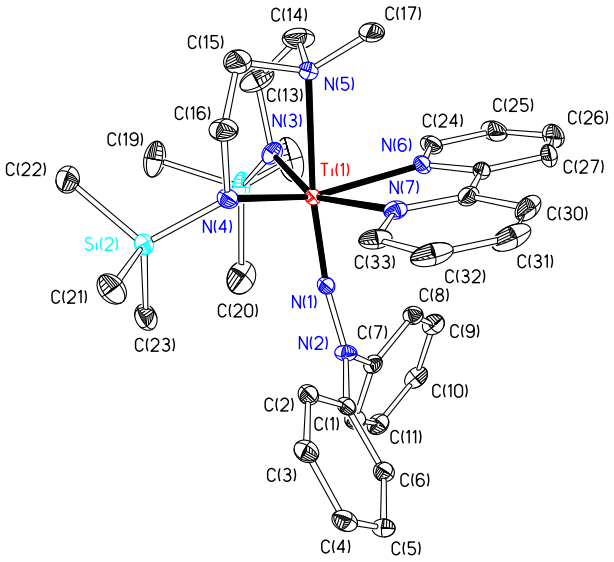

Figure 2.9. Displacement ellipsoid plot (20% probability) of Ti(N_2N^{Me})($NNPh_2$)(bipy) (**14**). H atoms omitted for clarity.

The geometry at Ti(1) is approximately octahedral with the $NNPh_2$ positioned *trans* to the NMe donor. This is the first example of a diamide-amine supported titanium hydrazide with the hydrazide group in an axial position. All previous examples of titanium imide/hydrazide compounds of the type M(L)(NR)(py) (L = N_2N^{py}, $N_2{}^*N^{py}$, N_2N^{Me} and related; M = Ti, Zr or Hf; R = ^{t}Bu, aryl, NPh_2 or N(Me)Ph) have the M=NR bond equatorially positioned.[40-42,69,73,74] However, the related titanium *tert*-butoxyimide compound, Ti(N_2N^{Me})(NO^tBu)(py) (**1.190**) made subsequent to this work, exists as a mixture with the NO^tBu ligand in either the equatorial or axial position.[79] It is also worth noting that the products from the reactions between Ti(N_2N^{Me})($NNPh_2$)(py) (**1.93**) and electron-deficient nitriles (see Chapter Three) have the resulting hydrazonamide fragments axially positioned, as do various 5-coordinate compounds of this general type with different metal centres.[80-83]

The Ti=N_α bond in **14** (1.754(2) Å) is somewhat longer than in **1.93** (1.733(5) Å) but the N_α–N_β distance remains the same within error (1.368(3) Å *vs.* 1.359(7) Å), as do the Ti-N_{amide} distances (avg. 2.032(2) *vs.* 2.028(4) Å in **14** and **1.93**, respectively). Compound **14** did not react at all with PhCCMe or C_6F_5CCMe at room temperature over the course of several days.

These initial observations provide strong evidence that the reaction proceeds *via* a pyridine free intermediate, however it does not provide information about the subsequent steps ("k_2" in Scheme 2.1). In order to gain further insight into the nature of the highest energy transition state, an Eyring analysis was therefore carried out.

Table 2.3. Selected bond distances (Å) and angles (^{o}) for Ti(N_2N^{Me})($NNPh_2$)(bipy) (**14**).

Ti(1)–N(1)	1.754(2)	Ti(1)–N(1)–N(2)	170.4(2)
Ti(1)–N(3)	2.013(2)	N(1)–Ti(1)–N(5)	173.5(1)
Ti(1)–N(4)	2.054(2)	N(3)–Ti(1)–N(4)	105.5(1)
Ti(1)–N(5)	2.387(2)	N(6)–Ti(1)–N(7)	70.2(1)
Ti(1)–N(6)	2.259(2)		
Ti(1)–N(7)	2.293(2)		
N(1)–N(2)	1.368(3)		

The reaction between **1.93** and PhCCMe (20 equivalents) was followed at five different temperatures between -16 and -35 ^{o}C. The linear pseudo first order ln plots and corresponding Eyring analysis (ln(k_{obs}/T) *vs.* 1/T) are shown in Figure 2.10. The derived activation enthalpy and entropy values for the rate-limiting barrier on the reaction coordinate **1.93** + PhCCMe → **1.149** are $\Delta H^{\ddagger}$ = 18.8(4) kcal mol^{-1} and $\Delta S^{\ddagger}$ = 1(1) cal mol^{-1} K^{-1}. The negligible $\Delta S^{\ddagger}$ term implies that the rate limiting step involves neither ligand loss (e.g. **1.93** → **1.93′** + py (k_1, Scheme 2.1)) nor ligand gain.[84] The highest activation barrier within the "k_2" process in Scheme 2.1 is therefore likely to be an intramolecular rearrangement.

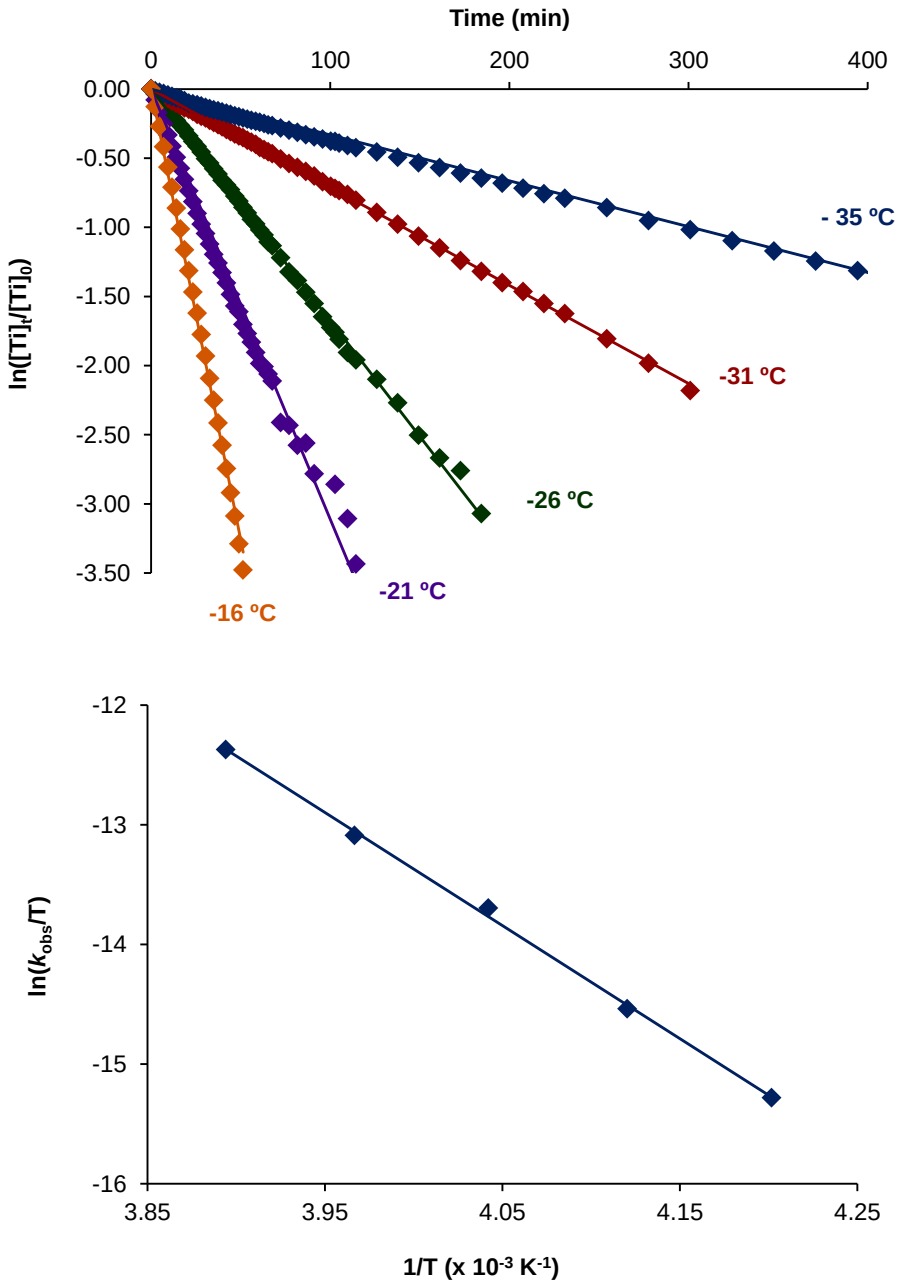

Figure 2.10. Top: pseudo first order ln plots for the reaction of $Ti(N_2N^{Me})(NNPh_2)(py)$ (**1.93**) with PhCCMe (20 equivalents) at the temperatures indicated (avg. r^2 = 0.990, range 0.975 – 0.999). Bottom: corresponding plot of $\ln(k_{obs}/T)$ *vs.* 1/T. Activation parameters derived from linear regression analysis (r^2 = 0.999): $\Delta H^{\ddagger}$ = 18.8(4) kcal mol^{-1}, $\Delta S^{\ddagger}$ = 1(1) cal mol^{-1} K^{-1}; $\Delta G_{298}^{\ddagger}$ = 18.5(7) kcal mol^{-1}.

As shown in Equation 2.4, compound **1.93** also reacted with a series of *p*-substituted alkynes (4-C_6H_4X)CCMe (X = Me, ^{t}Bu, OMe, F, Cl, CF_3) to form the corresponding N_α–N_β insertion products **2** – **7**. To gain insight into the rate-limiting "k_2" step, all six

reactions were followed at -26 ^{o}C in toluene-d_8 with 20 equivalents of alkyne. The reactions for X = Me, ^{t}Bu, and OMe showed the same behaviour as for PhCCMe (i.e., X = H, Figure 2.6, top), whereas for X = F, Cl or CF_3 a different kinetic regime was entered which is discussed below. The pseudo first order rate constants (k_{obs}) for X = H, Me, ^{t}Bu, OMe are listed in Table 2.4 along with the corresponding Hammett substituent constants, σ_p.[85] Table 2.4 also gives the Gibbs free energy ($\Delta G^{\ddagger}$, kcal mol^{-1}) of the DFT calculated transition state for N_α–N_β cleavage which will be discussed in the Computational Studies section below.

Table 2.4. Rate constants (k_{obs}) for the N_α–N_β insertion reactions of Ti(N_2N^{Me})($NNPh_2$)(py) (**1.93**) with (4-C_6H_4X)CCMe (20 equivalents, X = H, Me, ^{t}Bu or OMe) at -26 ^{o}C in toluene-d_8. σ_p is the substituent constant. $\Delta G^{\ddagger}$ is the Gibbs free energy (kcal mol^{-1}) of the transition state for N_α–N_β cleavage according to DFT using the model hydrazide **A1** (see the Computational Studies section for further details).

X	k_{obs} ($\times 10^{-4}$ s^{-1})	σ_p	$\Delta G^{\ddagger}$ (kcal mol^{-1})
H	2.79(1)	0.00	20.7
Me	3.85(2)	-0.17	20.4
^{t}Bu	3.90(4)	-0.20	20.0
OMe	4.42(2)	-0.27	19.6

The k_{obs} data clearly show that the rate of reaction increases as the *para*-X substituent becomes more electron-releasing. The Hammett plot of log(k_{obs}/k_H) *vs.* σ_p (Figure 2.11) gave a good agreement and yielded a reaction constant, ρ, of –0.74(5). A plot of log(k_{obs}/k_H) *vs.* σ_p^{+} gave a poorer fit (r^2 = 0.778). The negative value of ρ is indicative of the development of positive charge (or disappearance of negative charge) at the Ar<u>C</u> alkyne carbon in the transition state for alkyne insertion into N_α–N_β. This point is elaborated on in the Computational Studies section.

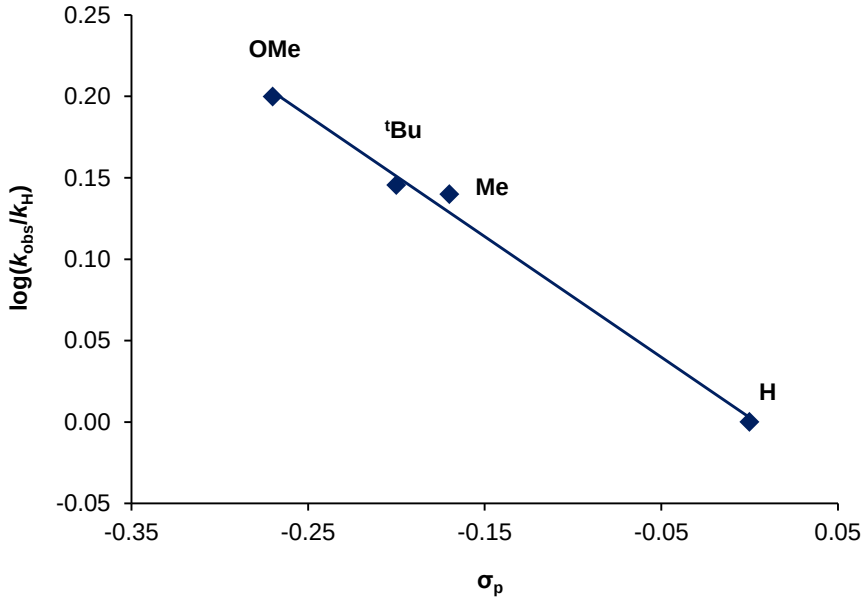

Figure 2.11. Plot of $\log(k_{obs}/k_H)$ *vs.* σ_p for the reactions of $Ti(N_2N^{Me})(NNPh_2)(py)$ (**1.93**) with $(4\text{-}C_6H_4X)CCMe$ (20 equivalents, X = H, Me, ^{t}Bu, OMe) at -26 ^{o}C in toluene-d_8. The best-fit line shown had $r^2 = 0.992$ giving $\rho = -0.74(5)$. k_H is k_{obs} for X = H.

As mentioned above, the more electron-deficient alkynes ArCCMe (Ar = $4\text{-}C_6H_4F$, $4\text{-}C_6H_4Cl$, $4\text{-}C_6H_4CF_3$ or C_6F_5) also undergo N_α–N_β insertion reactions with **1.93** forming **5 - 8** (Equation 2.4). However, when these reactions were monitored in toluene-d_8 at low temperature, a different kinetic regime was observed. In each instance, at temperatures between -40 and -30 ^{o}C, equilibrium mixtures were formed (Scheme 2.3) consisting of **1.93** (and/or its bis(pyridine) homologue, **13**), ArCCMe, free pyridine and a new species. For ArCCMe (Ar = $4\text{-}C_6H_4F$ and $4\text{-}C_6H_4Cl$) the concentration of the new species was too small to allow characterisation therefore these were not investigated further.

For ArCCMe (Ar = $4\text{-}C_6H_4CF_3$ or C_6F_5) the concentrations of the intermediate were larger and they were subsequently characterised as the cycloaddition products $Ti(N_2N^{Me})\{N(NPh_2)C(Me)C(Ar^F)\}$ (Ar^F = $4\text{-}C_6H_4CF_3$ (**15**) or C_6F_5 (**16**)) on the basis of the similarity of their NMR data to those of the isolated and fully authenticated metallacycles $Ti(N_2N^{py})\{N(NPh_2)C(Me)C(Ar^F)\}$ (Ar^F = $4\text{-}C_6H_4CF_3$ or C_6F_5 (**1**)). On warming to -26 ^{o}C, these first-formed equilibrium mixtures quantitatively converted to the final insertion products **7** and **8** (Scheme 2.3). Single crystals of **5** and **8** were

grown but found to be of poor quality. They did however allow the connectivity to be established (see Appendix A), confirming that shown in Equation 2.4.

Due to the experimental uncertainties concerning the extent to which **1.93** (or indeed the vinyl imide products) trap (or are trapped by) the free pyridine generated from the formation of the cycloaddition intermediates (whose relative concentration varies throughout the reaction), the new kinetic regime has not been quantitatively modelled. However, it is qualitatively clear from the rate of evolution of **7** (Figure 2.12) that the overall reaction of **1.93** with (4-$C_6H_4CF_3$)CCMe takes significantly longer than with (4-C_6H_4X)CCMe (X = H, Me, ^{t}Bu, OMe; $t_{1/2}$ = *ca* 26 – 41 mins, X = CF_3; $t_{1/2}$ = 65 min) under otherwise identical conditions.

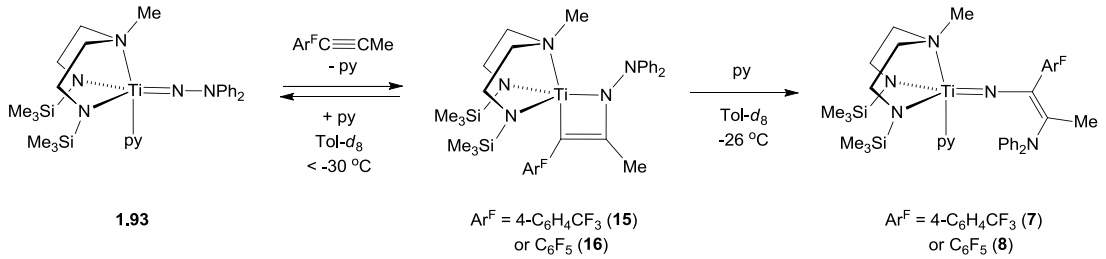

Scheme 2.3. Reaction of Ti(N_2N^{Me})($NNPh_2$)(py) (**1.93**) with Ar^FCCMe (Ar^F = 4-$C_6H_4CF_3$ or C_6F_5).

The reactions of **1.93** with Ar^FCCMe are reminiscent of that between Ti(N_2N^{py})($NNPh_2$)(py) (**1.97**) and PhCCMe. In each case a first-formed equilibrium mixture of starting hydrazide and [2+2] cycloaddition product goes on to form an N_α–N_β insertion product. For both **1.93** and **1.97**, it appears that the electron-withdrawing aryl ring substituents in Ar^FCCMe stabilise the resultant metallacycles, whereas electron-donating groups (*cf.* Figure 2.11) promote N_α–N_β bond insertion. Although Figure 2.12 suggests that metallacycles might lie on the reaction coordinate from **1.93** and **1.97** to the insertion products, such species are not observed in the majority of instances (*cf.* Figure 2.6 and the reactions of **1.93** with (4-C_6H_4X)CCMe (X = H, Me, ^{t}Bu, OMe)). To gain further insight into this chemistry a comprehensive series of DFT studies was carried out by Dr E. Clot and Dr A. Nova and is described below.

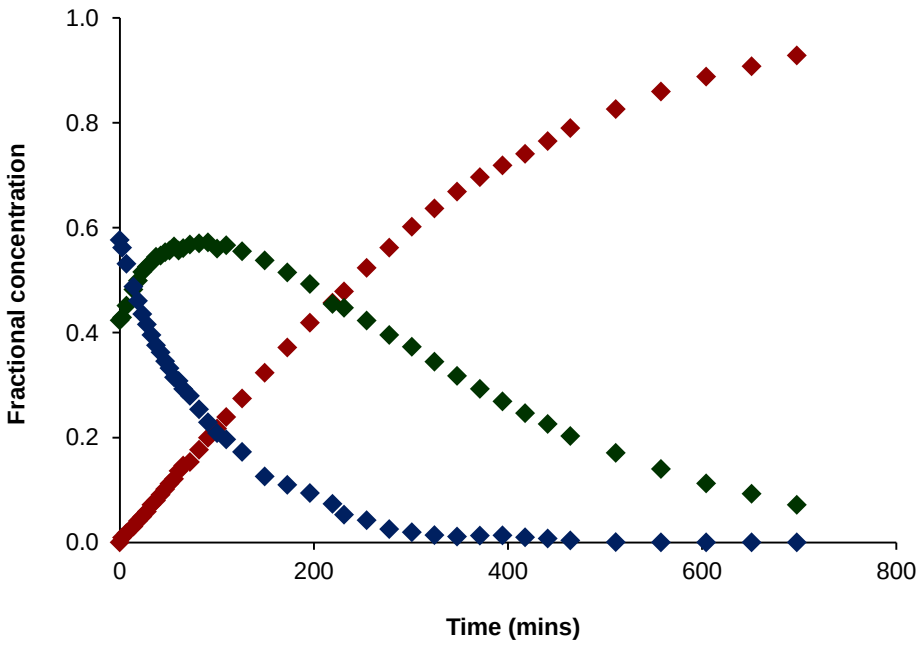

Figure 2.12. Decay and/or evolution with time of titanium species involved in the reaction of Ti(N_2N^{Me})($NNPh_2$)(py) (**1.93**, blue) with (4-$C_6H_4CF_3$)CCMe (20 equivalents) at -26 ºC in toluene-d_8. Other species are: Ti(N_2N^{Me}){NC(4-$C_6H_4CF_3$)C(Me)NPh_2}(py) (**7**, red) and Ti(N_2N^{Me}){N(NPh_2)C(Me)C(4-$C_6H_4CF_3$)} (**15**, green).

2.5 Computational Studies

2.5.1 Mechanism of alkyne insertion into N_α–N_β

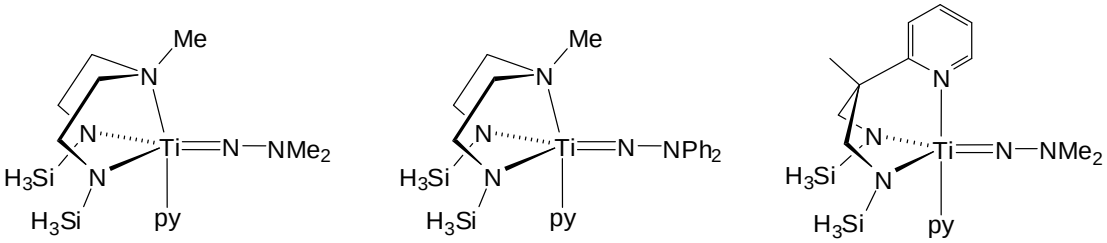

Figure 2.13. DFT models for Ti(N_2N^{Me})($NNPh_2$)(py) (**1.93**) and Ti(N_2N^{py})($NNPh_2$)(py) (**1.97**).

Calculations were carried out using Ti($N_2{}^{SiH_3}N^{Me}$)(NNR_2)(py) (R = Me (**A1**) or Ph (**B1**)) as models for **1.93**, and Ti($N_2{}^{SiH_3}N^{py}$)($NNMe_2$)(py) (**C1**) as a model for **1.97**. In all three the $SiMe_3$ groups of N_2N^R (R = Me or py) have been replaced by SiH_3, and in **A1** and **C1** Ti=$NNPh_2$ is modelled by Ti=$NNMe_2$ for computational efficiency

(Figure 2.13). To establish the basic electronic features of the mechanism, MeCCMe (2-butyne) was considered as the reacting alkyne.

Scheme 2.4 shows the two mechanisms (designated Pathways A and B) which have been investigated for the N_α–N_β insertion reactions of **1.93** and **1.97**. Pathway A has been proposed by Mindiola following the initial communication on the insertion reaction of **1.93** with PhCCMe.[3] In this mechanism, loss of pyridine from **I** forms an η^2-hydrazide **III** *via* base-free **II**. This intermediate was proposed to then undergo [2+1] cycloaddition at N_α with RCCR′ forming an N-metallated azirine intermediate (**IV**) with concomitant N_α–N_β bond breaking. Ring-opening of the azirine *via* NPh_2 group transfer from Ti back to CR′ affords the four-coordinate insertion product **V** which is then trapped by pyridine giving **VI**. Gade has also proposed a similar η^2-hydrazido intermediate in the N_α–N_β cleavage reaction of $Zr(N_2{*}N^{py})(NNPh_2)(py)$ (**1.159**) with isocyanides.[31]

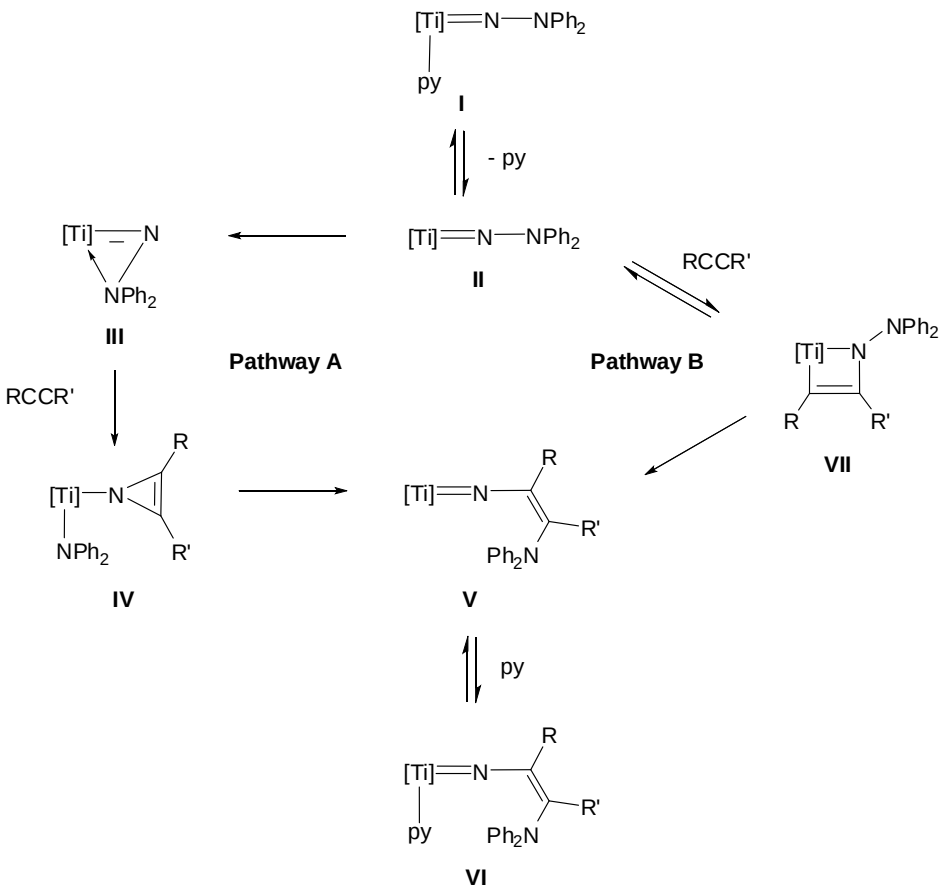

Scheme 2.4. Two potential mechanisms for alkyne insertion into the N_α–N_β bond of the hydrazide ligand in **1.93** or **1.97**. [Ti] = $Ti(N_2N^{py})$ or $Ti(N_2N^{Me})$.

Mindiola's mechanism is consistent with the experimental evidence of a pyridine-free intermediate being formed before reaction with the alkyne. Furthermore, if the intramolecular transformation **IV** → **V** were the rate limiting step, then the experimental near-zero entropy of activation (Figure 2.10) could likewise be consistent with Pathway A. Finally, Prof. P. Mountford and Dr J. Selby have described how a version of **III** derived from Ti(N_2N^{py})($NNPh_2$)(py) (**1.97**) can be trapped by electrophilic addition of $B(C_6F_5)_3$ to N_α.[86] Therefore, DFT calculations were used to determine the details of the mechanism along Pathway A and the nature of the rate-limiting step.

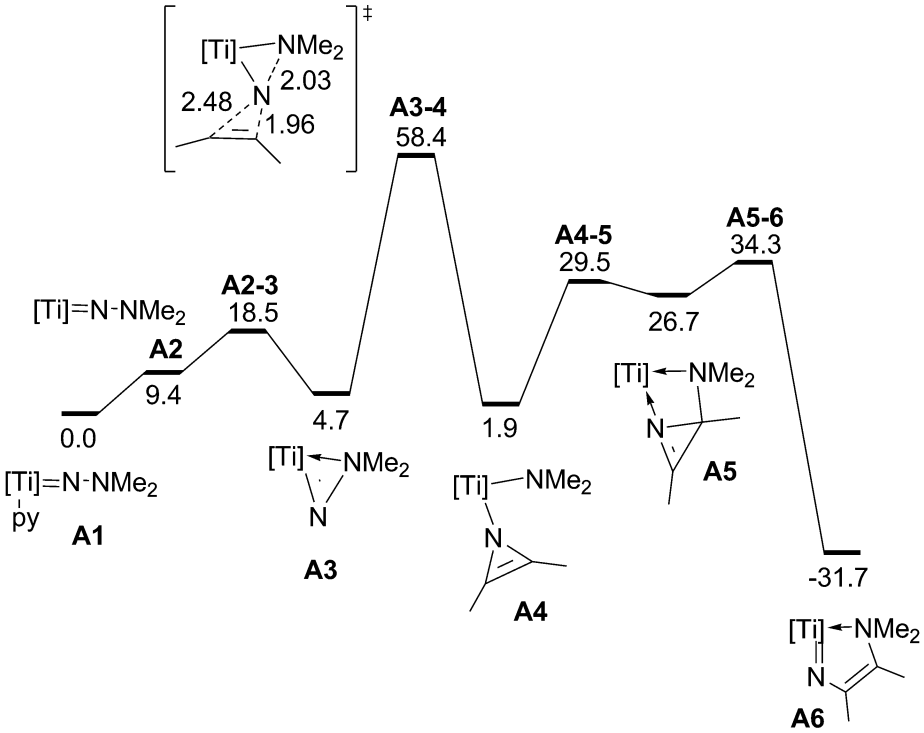

Scheme 2.5. Gibbs free energy (kcal mol^{-1}) profile for MeCCMe insertion into the N_α–N_β bond of Ti($N_2^{SiH_3}N^{Me}$)($NNMe_2$)(py) (**A1**) along Pathway A.
[Ti] = Ti($N_2^{SiH_3}N^{Me}$).

The DFT Gibbs free energy profile along Pathway A for **A1** reacting with MeCCMe is shown in Scheme 2.5. Formation of a vacant site (in **A2**) by pyridine dissociation is unfavourable by ΔG = 9.4 kcal mol^{-1}. Dissociation of DMAP was calculated to be even more difficult (ΔG = 11.8 kcal mol^{-1}), as expected. The calculated ΔG value for pyridine loss from **A1** compares well with those measured experimentally for some imidotitanium complexes.[87] The activation barrier for dissociation of a ligand is not very easy to estimate computationally as often no transition state (TS) can be located

for such a process. However, on the assumption[88] that the activation barrier $\Delta G^{\ddagger}$ is essentially the enthalpy cost of breaking the metal–ligand bond (i.e. $\Delta G^{\ddagger} \approx \Delta H$), the barriers for pyridine and DMAP dissociation are 21.9 and 24.6 kcal mol^{-1}, respectively. These values constitute an upper estimate of the actual activation barriers. The larger value for DMAP is in agreement with the lower rate of reaction observed with **11** compared to **1.93**. Experimentally-determined $\Delta G^{\ddagger}$ values for pyridine loss from certain 5- and 6-coordinate imidotitanium complexes (including a homologue of **1.97**) have been reported to be *ca.* 15 kcal mol^{-1},[69,87] very similar to that obtained from the double reciprocal plot and k_1, found to be 17.8 kcal mol^{-1} (Figure 2.7, *vide supra*).

From **A2** (Scheme 2.5) coordination of N_β yields two potential intermediates: **A3**, where N_α shifts to the vacant site and N_β coordinates in the equatorial plane (Scheme 2.5), and **A3b**, where N_β coordinates directly to the vacant site as indicated for species **III** in Scheme 2.4. **A3** is 8.7 kcal mol^{-1} more stable than **A3b**, and only for the former could a TS for N_α–N_β bond breaking be located. Formation of **A3** from **A2** is exergonic (-4.7 kcal mol^{-1}) and proceeds with a low activation barrier (9.1 kcal mol^{-1} relative to **A2**).

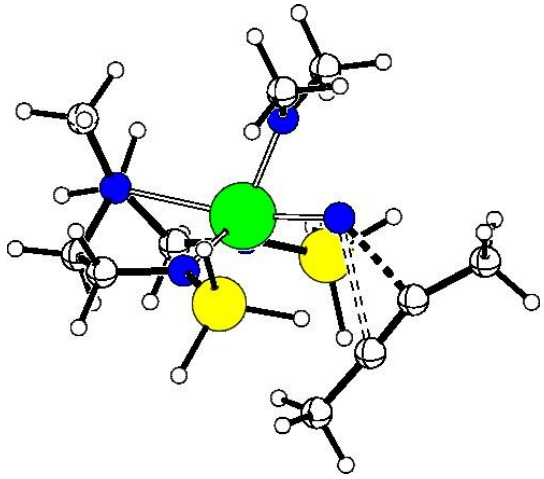

Figure 2.14. Optimised geometry for the transition state **A3-4** for N_α–N_β bond breaking along Pathway A (see Scheme 2.5).

The crucial step in Pathway A is the formation of the N-metallated azirine **IV**. This is modelled as **A4** in Scheme 2.5, formed by reaction of **A3** with MeCCMe. As proposed by Mindiola, this reaction is a [2+1] cycloaddition between the alkyne and N_α of a bent hydrazido ligand. The cycloaddition occurs with concomitant N_α–N_β bond

cleavage as illustrated by the lengthening of the N_α–N_β bond from 1.41 Å in **A3** to 2.03 Å in the transition state **A3-4** (illustrated in Figure 2.14). However, even though the transformation from **A3** to **A4** is slightly exergonic (-2.8 kcal mol^{-1}), the associated activation barrier is prohibitively high (53.7 kcal mol^{-1} at 298 K). Frontier orbital analysis shows that this is because N_α in this type of η^2-hydrazide species is nucleophilic in nature, not electrophilic.

A3-4 is a late transition state for N_α–N_β cleavage *with little C–N_α bond forming character* (C–N_α = 1.96 and 2.48 Å in **A3-4**), thus explaining the high activation barrier (Scheme 2.5). The DFT activation barrier is also far too high when compared with the experimental $\Delta G_{298}^{\ddagger}$ of 18.5(7) kcal mol^{-1} for the reaction of **1.93** with PhCCMe. Moreover, both the alkyne and the bent-hydrazido complex **A3** are implicated in the bimolecular TS **A3-4**, and this is not in agreement with the low value for the experimental near-zero entropy of activation (*cf.* Figure 2.10). Indeed $\Delta S^{\ddagger}$ for the transformation **A3** + MeCCMe → **A3-4** at 298 K is calculated to be substantially negative (-41.3 cal mol^{-1} K^{-1}).

From **A4**, nucleophilic transfer of the Ti-bound NMe_2 group to an azirine ring carbon atom affords **A5**, and subsequent ring opening leads to the *Z* aza-allyl intermediate **A6** in an energetically favourable process. Upon decoordination of the chelating NMe_2 group, the vinyl imido shifts to the equatorial position and coordination of pyridine finally yields the insertion product (not shown in Scheme 2.5).

The high computed barrier **A3-4** for Pathway A and the bimolecular nature of the rate-determining step suggest that the N_α–N_β insertion reactions of **1.93** and **1.97** follow another mechanism. This is designated Pathway B in Scheme 2.4 and assumes that azatitanacyclobutenes of the type **VII** play an *active role* in the formation of **V** and **VI**, rather than being separate species unconnected with N_α–N_β insertion. While they are not always observed, metallacycles (e.g. **1** (Equation 2.2) and **15** and **16** (Scheme 2.3)) have sometimes been seen in reaction mixtures that also give rise to N_α–N_β insertion. DFT calculations of Pathway B were therefore also carried out on the model system **A1** (Scheme 2.6). This pathway would constitute a way to insert an alkyne into the N_α–N_β bond after pyridine dissociation and so could be in agreement with the experimental kinetic studies, providing the rate-determining step occurs *after* the [2+2] cycloaddition of the alkyne. A pathway starting by coordination of the alkyne

before pyridine dissociates was searched for but no stable intermediate could be located on the potential energy surface. Therefore, only Pathway B, initiated by pyridine dissociation, will be described.

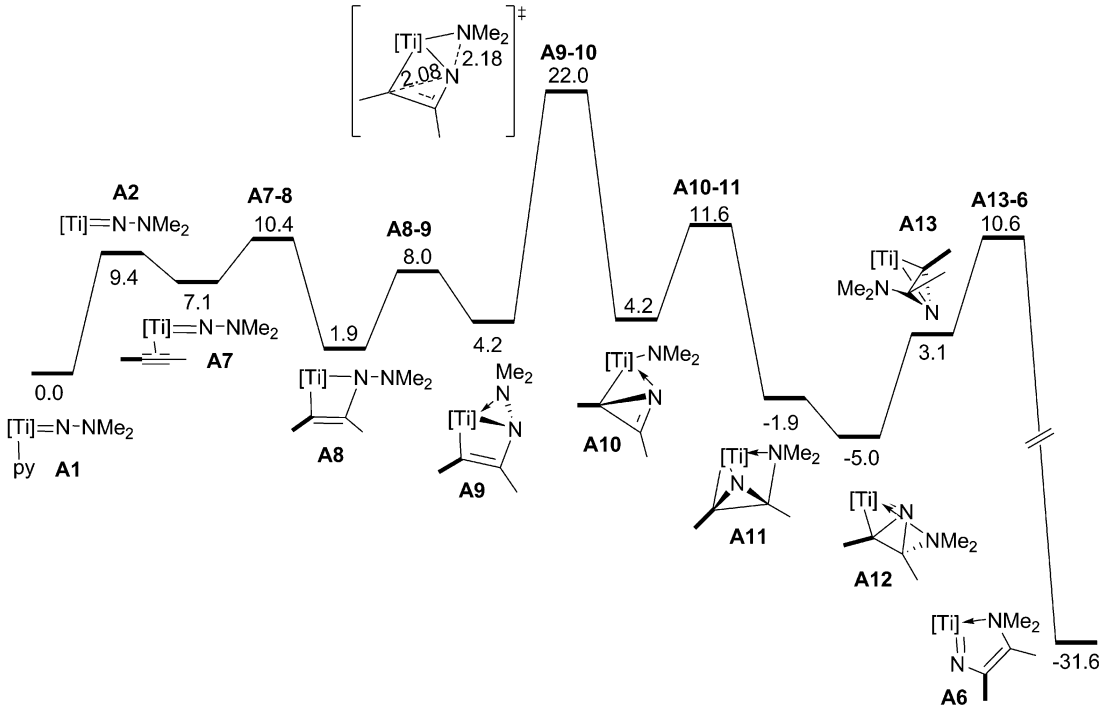

Scheme 2.6. Gibbs free energy (kcal mol^{-1}) profile for MeCCMe insertion into the N_α–N_β bond of Ti($N_2^{SiH_3}N^{Me}$)($NNMe_2$)(py) (**A1**) along Pathway B. The bond shown in bold for the alkyne is to help the reader trace the fate of the Ti-bound CMe group in **A8**. [Ti] = Ti($N_2^{SiH_3}N^{Me}$).

The vacant site in **A2**, created by pyridine decoordination, is a potential site for alkyne coordination. Coordination of MeCCMe (forming **A7**) is less favourable than formation of the η^2-hydrazide **A3** (Scheme 2.5), partly due to the loss of translational entropy in the former case. Nonetheless, [2+2] cycloaddition from **A7** to form the azatitanacyclobutene **A8** occurs readily with a low barrier (3.3 kcal mol^{-1}) and is thermodynamically competitive with **A1** (ΔG = 1.9 kcal mol^{-1}). From **A8**, intramolecular coordination of $N_\beta Me_2$ is facile and proceeds with a low barrier (6.1 kcal mol^{-1}) to yield the key intermediate **A9**, lying only 4.2 kcal mol^{-1} above the separated reactants **A1** and MeCCMe. The N_α–N_β bond breaking step proceeds through **A9-10** yielding the C,N-metallated azirine **A10** in a thermoneutral reaction. The activation barrier is only 17.8 kcal mol^{-1} above **A9**, and is 36.4 kcal mol^{-1} less than the N_α–N_β bond cleavage through **A3-4** (Scheme 2.5). This is because N_α–N_β

bond breaking in **A9-10** is coupled with C–N_α bond formation, thus lowering the activation barrier of the process. A detailed discussion of the sequence **A8** → **A9** → **A9-10** and the electronic structures of these species is given later on.

From **A10** the reaction proceeds *via* exergonic nucleophilic attack of the Ti-bound NMe_2 group on the azirine ring to form **A11** with a low activation barrier. Two other isomers (**A12** and **A13**), differing in the relative orientations of N_α and N_β with respect to the $N_2^{SiH_3}N^{Me}$ ligand, have been located on the potential energy surface. The activation barrier for the isomerisation of **A11** to **A12** (through **A11-12**, not shown in Scheme 2.6) is only 5.5 kcal mol^{-1}. Each of these three intermediates can lead to the cleavage of the C–N_α bond to form **A6**. However, the TS with the lowest energy is **A13-6** originating from **A13**, and the corresponding activation barrier is 7.5 kcal mol^{-1}. Overall, the net *N_α–N_β insertion* reaction is mechanistically a *Ti=N_α cycloaddition* followed by an *N_α atom migration* process.

Comparison of DFT computed Pathways A and B (Schemes 2.5 and 2.6) shows clearly that the latter is preferred. From **A1**, the activation barrier to overcome along Pathway A (**A3-4**) is 58.4 kcal mol^{-1}, whereas the highest point along Pathway B (**A9-10**) is only 22.0 kcal mol^{-1}. The latter value is in much better agreement with the experimental activation barrier determined for PhCCMe reacting with **1.93** ($\Delta G_{298}^{\ddagger}$ = 18.5(7) kcal mol^{-1}). Moreover, whereas in Pathway A the rate-determining step is bimolecular, in Pathway B it is intramolecular. The experimental low value for $\Delta S^{\ddagger}$ (1(1) cal mol^{-1} K^{-1}) is in better agreement with an intramolecular rate-determining step, lending further support to Pathway B as the most likely reaction mechanism. The relevant calculated $\Delta S^{\ddagger}$ values are -41.3 cal mol^{-1} K^{-1} (**A3-4**) and 4 cal mol^{-1} K^{-1} (**A9-10**), the latter being consistent with experimental measurement.

2.5.2 $NNMe_2$ vs. $NNPh_2$ - Influence of the hydrazide N_β substituents

Although the hydrazide ligand in the real compound $Ti(N_2N^{Me})(NNPh_2)(py)$ (**1.93**) is $NNPh_2$, it has so far been modeled by $NNMe_2$ in the calculations carried out with $Ti(N_2^{SiH_3}N^{Me})(NNMe_2)(py)$ (**A1**). However, since the lone pair on N_β is intimately involved in the mechanism shown in both Schemes 2.5 and 2.6, it is important to determine whether the conjugation of this lone pair with the phenyl rings[23,42] has a significant effect on the various intermediates and transition states. Therefore, the two

reaction profiles and/or key transition states have also been computed with the model system Ti($N_2^{SiH_3}N^{Me}$)($NNPh_2$)(py) (**B1**), which differs from **A1** by the substitution of $NNMe_2$ with $NNPh_2$. The model **B1** is very close to the experimental system with only the $SiMe_3$ groups being simplified.

Pathway A, through a bent hydrazide **III**, is also unambiguously ruled out with $NNPh_2$ since the rate limiting activation barrier through **B3-4** is computed to be prohibitively large (49 kcal mol^{-1}).

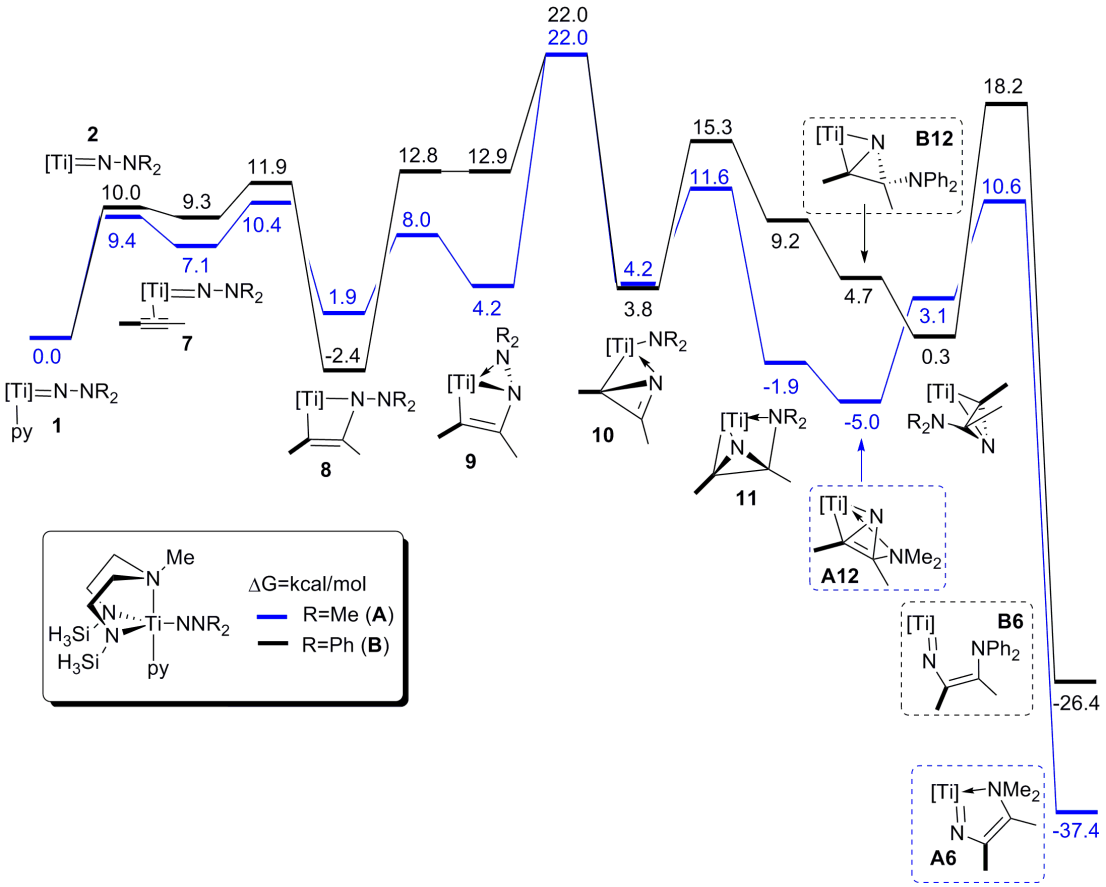

Scheme 2.7. Gibbs free energy (kcal mol^{-1}) profiles for MeCCMe insertion into the N_α–N_β bond of Ti($N_2^{SiH_3}N^{Me}$)($NNMe_2$)(py) (**A1**) and Ti($N_2^{SiH_3}N^{Me}$)($NNPh_2$)(py) (**B1**) along Pathway B. The bond showed in bold for the alkyne is to help the reader trace the fate of the Ti-bound CMe group in **A/B8**. The geometries that are different with system **A** and **B** are depicted inside squares.

For Pathway B, the sequence of steps starting from **B1** is again similar to that obtained for **A1** (Scheme 2.7). The activation energy for pyridine dissociation from **B1** (20.8 kcal mol^{-1}) is similar to that obtained with **A1** (21.9 kcal mol^{-1}), and the relative energy of the unsaturated fragment **B2** is ΔG = 10 kcal mol^{-1}. The main differences

between the pathways starting from **B1** and **A1** concern all the steps involving coordination of N_β. These are destabilised because the N_β lone pair is less available in the **B1**-derived systems due to conjugation with the Ph rings. For example, the cycloaddition adduct **B9** (intramolecular coordination of NPh_2) is less favoured (12.9 kcal mol^{-1}) than **A9** (4.2 kcal mol^{-1}, coordination of NMe_2). The intermediates **B11** and **B12** are also significantly destabilised (9.2 kcal mol^{-1}, **B11**; 4.7 kcal mol^{-1}, **B12**). Despite these differences, the rate-determining step is still N_α–N_β bond cleavage through the TS **B9-10**, and its energy, relative to separated reactants **B1** and MeCCMe, is 22.0 kcal mol^{-1}, coincidentally the same value as that obtained for **A9-10**. Overall, there is no substantial difference between the rates of N_α–N_β bond insertion on changing from $NNMe_2$ to $NNPh_2$.

2.5.3 Electronic structure of the Ti=N_α cycloaddition products: origins of regioselectivity for N_α–N_β insertion

When **1.93** and **1.97** undergo N_α–N_β insertion with unsymmetrical alkynes ArCCMe, the products always have CAr bound to Ti=N_α of the originating hydrazide and CMe bound to $N_\beta Ph_2$ (Equations 2.3 and 2.4). In the corresponding metallacycles, however, it is always CMe which is bound to N_α (Equations 2.1 and 2.2). This is fully consistent with Pathway B. As illustrated by a bold bond for one of the alkyne C–Me groups in Scheme 2.6, it is the regiochemistry of the *cycloaddition product* which determines that of the insertion product. I.e., the alkyne carbon initially bonded to Ti in the metallacycle **A8** ends up bonded to N_α in the insertion product **A6**, and the alkyne substituents are mutually *cis* as found exclusively by experiment.

To fully understand the origins of this critical regiochemical preference, the electronic structure of the azatitanacyclobutene **A8** has been analysed. The HOMO of this complex (Figure 2.15(a)) results from the stabilisation of the 4-electron repulsion between the lone pair on N_α and the filled π_{cc} MO by the vacant π^*_{cc} MO (Figure 2.15(b)). As a consequence of the mixing between these three orbitals, the HOMO is essentially based on N_α and the carbon atom bonded to Ti (denoted C_{Ti}). An NBO (natural bond orbital) analysis of **A8** yielded a Lewis structure (Figure 2.15(c)) with the C=C π bond polarised toward C_{Ti} (π_{cc} = 0.7278 C_{Ti} + 0.6858 C_N), in agreement with Figures 2.15(a) and 2.15(b).

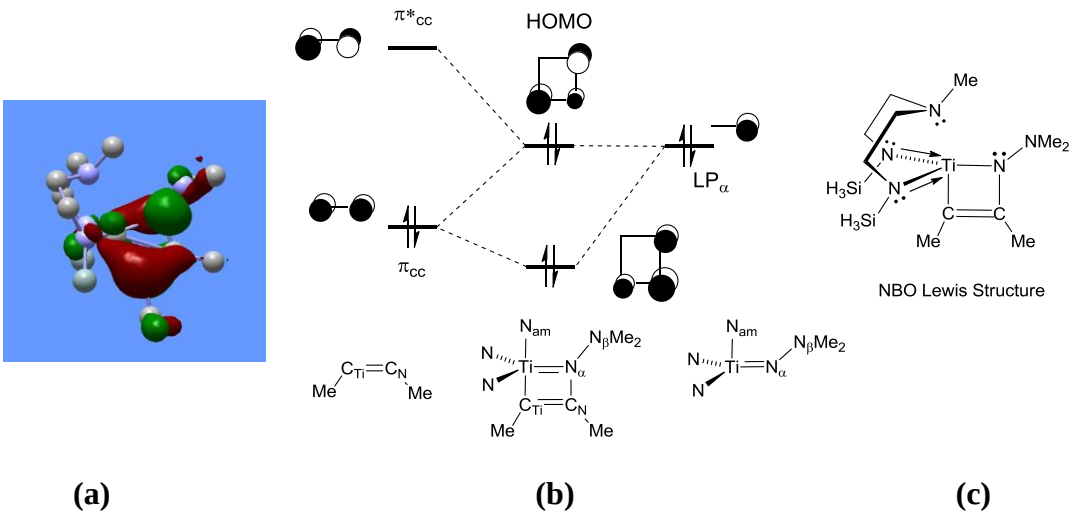

Figure 2.15. (a) HOMO of **A8**. (b) Schematic MO diagram for the π interactions within the 4-membered metallacycle. (c) Lewis structure as deduced from a NBO analysis.

With regard to regiochemical preferences, substitution of a methyl group in **A8** by any group "X" that would strengthen the aforementioned contributions would result in a more stable metallacycle. For example, an electron-withdrawing group X would increase the effective electronegativity of the carbon to which it is attached. This would in turn result in a stabilisation of both π_{cc} and π^*_{cc} and also in a polarisation of π_{cc} toward the X-substituted carbon atom. The schematic MO diagram in Figure 2.15(b) indicates that the best situation corresponds to the regioisomer with the electron-withdrawing X bonded to C_{Ti}. In that case, the destabilising overlap between LP_α and π_{cc} would be reduced and the favourable overlap between LP_α and π^*_{cc} would be increased; both factors combine to lower the energy of the HOMO.

These arguments, based on the effective electronegativity of the alkyne carbon atoms, essentially involve the σ-acceptor properties of the X group. However, π-effects must also be considered. For example, it is well known[89] that the HOMO of an alkene moiety $XC(R)=CR_2$ is more strongly developed on the $\underline{C}R_2$ carbon when X is a π-donor. In the case of an azatitanacyclobutene of the type **A8**, the best arrangement to minimise repulsion between π_{cc} and LP_α would be the regioisomer with X bonded to C_N. For σ-accepting but π-donating groups the preferred product will come from a balance of the two effects as each favours a different regioisomer. For X groups which

are both σ- and π-accepting, the two contributions favour the same regioisomer, with X bonded to C_{Ti}.

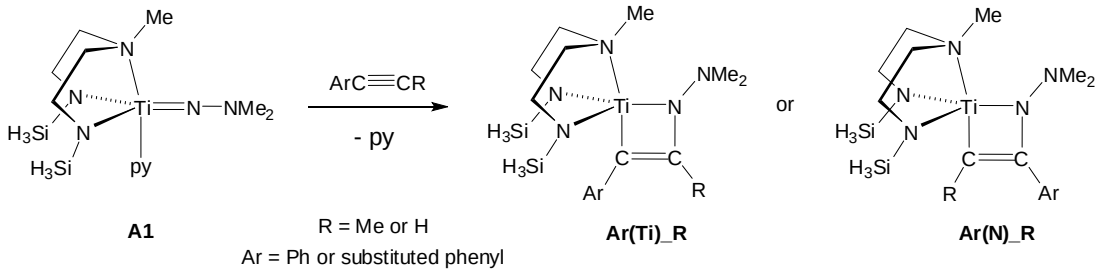

A1 **Ar(Ti)_R** **Ar(N)_R**

Equation 2.9

Equation 2.9 shows the possible products **Ar(Ti)_R** and **Ar(N)_R** that can be formed between **A1** and ArCCR (Ar = Ph or substituted phenyl; R = Me or H). These are homologues of **A8**, formed from **A1** and MeCCMe for which ΔG = 1.9 kcal mol^{-1} (Scheme 2.6). Changing from MeCCMe to PhCCMe gives two possible regioisomers, **Ph(Ti)_Me** and **Ph(N)_Me** for which ΔG = 1.3 kcal mol^{-1} and 6.7 kcal mol^{-1}, respectively. The increased stability of **Ph(Ti)_Me** compared to **A8** (ΔΔG = -0.6 kcal mol^{-1}) is in agreement with a larger effective electronegativity at an sp^2 hybridised carbon atom (*ipso*-Ph) compared to an sp^3 hybridised one (Me). The decreased stability of **Ph(N)_Me** with respect to both **A8** (ΔΔG = +4.8 kcal mol^{-1}) and **Ph(Ti)_Me** (ΔΔG = +5.4 kcal mol^{-1}) indicates that Ph behaves as a π-accepting group in the azametallacycles. Consistent with this, the C–Ph bond in **Ph(Ti)_Me** (1.459 Å) is shorter than that in **Ph(N)_Me** (1.495 Å) as a result of better π conjugation. Shorter $C–N_\alpha$ and longer C=C bonds in **Ph(Ti)_Me** compared to **Ph(N)_Me** are also consistent with this model.

Changing from PhCCMe to the terminal alkyne PhCCH stabilises both regioisomers relative to PhCCMe and MeCCMe. For **Ph(Ti)_H** ΔG = -7.5 kcal mol^{-1} and for **Ph(N)_H** ΔG = -1.9 kcal mol^{-1}. This is because H is less electron-releasing than Me, but Ph is more electron-accepting. Again the regioisomer with Ph bonded to C_{Ti} is very strongly favored by *ca.* 10^4 in terms of an equilibrium between the two. Focusing on this regioisomer, the ΔG for forming **Ar(Ti)_Me** from **A1** and experimentally relevant *para*-substituted alkynes, namely ArCCMe (Ar = C_6F_5 or 4-C_6H_4X with X = ^{t}Bu, OMe or CF_3) were also calculated. The results are given in Table 2.5 together with those for the other alkynes and are globally consistent with the bonding model

introduced above. Strongly σ-accepting groups (Ar = 4-$C_6H_4CF_3$ (ΔG = -0.7 kcal mol^{-1}) or C_6F_5 (ΔG = -1.6 kcal mol^{-1})) stabilise **Ar(Ti)_Me** compared to the compounds where Ar = Ph or 4-$C_6H_4{}^tBu$ (ΔG = 1.3 kcal mol^{-1}). Interestingly, although the strongly π-donating *para* substituent OMe should in principle destabilise **Ar(Ti)_Me** (see above), the competing inductive and mesomeric influences of σ acceptor (-I) and π donor (+M) effects, respectively, lead to a product of only slightly lower stability (ΔG = 1.4 kcal mol^{-1}) than when Ar = Ph or 4-$C_6H_4{}^tBu$.

The DFT results and explanations for the model azatitanacyclobutenes are fully consistent with the experimental data. The metallacycles are more stable with electron-withdrawing Ar groups for both **1.93** and **1.97**; the only regioisomers observed are with Ar bound to C_{Ti}. Furthermore, when Ar is bound to C_{Ti} in Ar(Ti)_Me (i.e. at the bold bond in **A8** in Scheme 2.6) the product of the insertion reaction has precisely the geometry of the compounds observed experimentally.

Table 2.5. Gibbs free energies (ΔG, kcal mol^{-1}) for the cycloaddition products **Ar(Ti)_R** (see Equation 2.9) expressed relative to separated **A1** and ArCCR. The cycloaddition product formed with MeCCMe (**A8**) has ΔG = 1.9 kcal mol^{-1}.

Ar	R	ΔG
Ph	H	-7.5
Ph	Me	1.3
C_6F_5	Me	-1.6
4-$C_6H_4CF_3$	Me	-0.7
4-$C_6H_4{}^tBu$	Me	1.3
4-C_6H_4OMe	Me	1.4

2.5.4 Understanding the N_α–N_β bond cleavage step

The ground state electronic preference of the azatitanacyclobutenes, which ultimately control the *regiochemistry* of the N_α–N_β insertion reaction, is for *electron-withdrawing* alkyne substituents, ideally attached to C_{Ti}. However, the experimental

kinetic data (Table 2.4, Figure 2.11) suggest that *overall rates* of the insertion reaction are favored by *electron-releasing* alkyne substituents. At first sight, the factors that control the stability of the metallacycle are not necessarily the same as those governing the transition state for N_α–N_β cleavage. The rate-determining N_α–N_β breaking process for RCCMe (R = Me or Ar) was therefore examined in further detail.

In the reaction of **A1** with MeCCMe (Scheme 2.6), cleavage of the N_α–N_β bond is effective in two steps from the azatitanacyclobutene **A8**. Firstly coordination of $N_\beta Me_2$ to Ti forms **A9**, and then N_α–N_β cleavage occurs through the transition state **A9-10** to form **A10**. This last step constitutes the rate-determining step of the entire alkyne insertion reaction. The geometries of the three critical extrema (**A8**, **A9**, and **A9-10**) are shown in Figure 2.16.

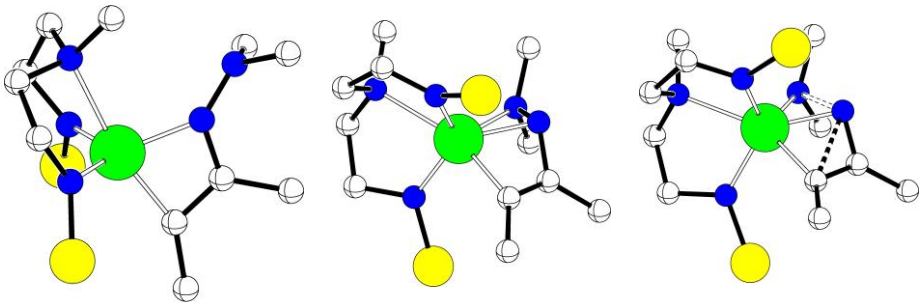

A8 **A9** **A9-10**

Figure 2.16. Optimised geometries for the azatitanacyclobutene **A8**, the $N_\beta Me_2$-chelated intermediate **A9** and the TS for N_α–N_β cleavage (**A9-10**). H atoms have been omitted for clarity.

The coordination of $N_\beta Me_2$ induces a deformation of the 4-membered ring in the metallacycle **A8**. In **A9**, N_β is coplanar with Ti and the two carbon atoms (N_β–Ti–C_{Ti}–C_N = 1.3 °), while N_α is situated above that plane. Ti–N_β is longer than Ti–C_{Ti} (2.193 Å *vs*. 2.068 Å). The N_β–Ti–C_{Ti} angle is 101 ° and N_α is situated between C_N and N_β (N_α–C_N = 1.444 Å, N_α–N_β = 1.454 Å). The coordination of $N_\beta Me_2$ results in a slight activation of the N_α–N_β bond (1.401 Å in **A8**, 1.454 Å in **A9**), and has positioned the N_α–N_β axis above the plane containing the C=C π bond.

The geometry of **A9** is perfectly adapted for nucleophilic attack from the π density polarised towards C_{Ti} into the σ*(N_α–N_β) antibonding MO. Indeed, the geometry of

the transition state **A9-10** confirms the description of the N_α–N_β cleavage as effectively nucleophilic attack of C_{Ti} on N_α. The $C_{Ti}\cdots N_\alpha$ distance decreases by *ca*. 0.2 Å (from 2.268 Å in **A9** to 2.077 Å in **A9-10**) while the $N_\alpha\cdots N_\beta$ distance increases by *ca*. 0.7 Å (from 1.454 Å in **A9** to 2.185 Å in **A9-10**). These variations are accompanied by an increase of the N_β–Ti–C_{Ti} angle to 117 °, a lengthening of Ti–C_{Ti} to 2.127 Å, and a shortening of Ti–N_β to 2.068 Å. To increase the nucleophilic character at C_{Ti}, the C=C π bond is partially lost. This is illustrated by the increase in the Me–C_{Ti}–C_N–Me dihedral angle from 4.1 ° in **A9** to 33.2 ° in **A9-10** and lengthening of C_{Ti}–C_N from 1.355 Å in **A9** to 1.383 Å in **A9-10**. The twist around the C_{Ti}–C_N axis allows the formation of a N_α=C_N π bond, while preserving some lone pair character at C_{Ti}. The N_α–C_N bond distance shortens significantly in the transition state **A9-10** (1.444 Å in **A9**, 1.348 Å in **A9-10**). The relative low energy of **A9-10**, and hence the facile N_α–N_β bond cleavage, is the result of several stabilising effects working cooperatively. The nucleophilic substitution at N_α of N_β by C_{Ti} is facilitated by the formation of stabilising Ti–NMe_2 and N_α=C_N interactions. Any factor increasing the nucleophilicity at C_{Ti} is likely to lower the energy of the transition state.

The TS Gibbs free energies ($\Delta G^\ddagger$) for the N_α–N_β cleavage step (analogous to **A9-10** with MeCCMe) for the alkynes (4-C_6H_4X)CCMe (X = H, Me, ^{t}Bu, OMe) used in the Hammett study are listed in Table 2.4 alongside the experimental rate constants. The $\Delta G^\ddagger$ values for ArCCMe are all less than for MeCCMe itself (22.0 kcal mol^{-1}), in keeping with experimental observations that the reaction of **1.93** with MeCCMe is much slower than with PhCCMe. The $\Delta G^\ddagger$ values decrease in the order *para*-X = H > Me > ^{t}Bu > OMe, which is consistent with the ordering of the experimental rate constants (k_{obs} for *para*-X = H < Me < ^{t}Bu < OMe) and nucleophilic attack of C_{Ti} on N_α in the N_α–N_β breaking TS being promoted by electron-releasing *para*-substituents. $\Delta G^\ddagger$ for the reaction of (4-$C_6H_4CF_3$)CCMe with **A1** was calculated to be 21.7 kcal mol^{-1}, higher than for PhCCMe (20.7 kcal mol^{-1}) because the electron-withdrawing *para*-CF_3 group diminished the nucleophilicity of C_{Ti}. Note that $\Delta G^\ddagger$ for N_α–N_β cleavage starting from the less stable, alternative cycloaddition regioisomer **Ph(N)_Me** was 24.1 kcal mol^{-1}.

Consistent with the *para* substituent effects, we find that the NPA charge of C_{Ti} in **A8**, **A9** and **A9-10** becomes more positive along the reaction coordinate (-0.473, -0.363,

-0.187, respectively). An analogous trend was found for the corresponding species formed with PhCCMe (-0.506, -0.387, -0.232, respectively) but with the Ph group stabilising a more negative charge at C_{Ti} at each stage as expected. The overall NPA charge of the Ph group also becomes more positive on going from the metallacycle **Ph(Ti)_Me** (-0.060) to the N_α–N_β breaking TS (+0.030), again consistent with the effects of electron-releasing ring substituents.

Taken together, the trends in the computed $\Delta G^{\ddagger}$ and experimental k_{obs} values, and the negative Hammett reaction constant ρ are consistent with N_α–N_β bond cleavage being caused by intramolecular nucleophilic attack of C_{Ti} on N_α. The form of the conversion *vs.* time plot in Figure 2.12 is a consequence of enhanced ground state stabilisation of the metallacycle (*cf.* Table 2.5) and concomitant destabilisation of the N_α–N_β cleavage TS by the electron-withdrawing 4-$C_6H_4CF_3$ group. The observed product regiochemistry with ArCCMe comes from both the relative stability of the precursor metallacycles and the associated transition states.

2.5.5 N_2N^{py} vs. N_2N^{Me}: influence of the diamide-amine ligand sets

Experimentally, there is a significant difference between the rates of the N_α–N_β insertion reaction for Ti(N_2N^{py})($NNPh_2$)(py) (**1.97**) and Ti(N_2N^{Me})($NNPh_2$)(py) (**1.93**). While the latter leads to PhCCMe insertion within *ca.* 5-10 minutes at room temperature, the former requires *ca.* 3 days (or heating at 60 ^oC for 3 hours). In addition, alkyne cycloaddition products are readily isolated with **1.97**, whereas these were barely observable with **1.93**, and only at -30 ^oC or below (Scheme 2.3).

To probe these differences, the Gibbs free energy profile for the N_α–N_β insertion reaction along Pathway B (Scheme 2.4) for the model system Ti($N_2^{SiH_3}N^{py}$)($NNMe_2$)(py) (**C1**) has been calculated. It is described in detail elsewhere.[64] However, the energies of the various intermediates and transition states are illustrated in Scheme 2.8.[64]

The greater *trans* influence of the pyridyl donor and larger chelating ring size (6-membered *vs.* 5-membered) of the less compact $N_2^{SiH_3}N^{py}$ ligand in **C1** (and **1.97**) compared to $N_2^{SiH_3}N^{Me}$ in **A1** (and **1.93**), allows a better relative orientation of the various N_{amide} and N_α π-donors in **C2** leading to an overall effective stabilisation of

the unsaturation at Ti.[42] As a result, the metal centre is less electrophilic in **C2** compared to **A2**, making the intramolecular coordination of NMe_2 less effective. This results in an overall higher energy for both **C9** (6.4 kcal mol^{-1}) and the crucial transition state **C9-10** (25.5 kcal mol^{-1}) compared to **A9** (4.2 kcal mol^{-1}) and **A9-10** (22.0 kcal mol^{-1}), allowing the experimentally observed, isolation of azametallacyclobutenes.

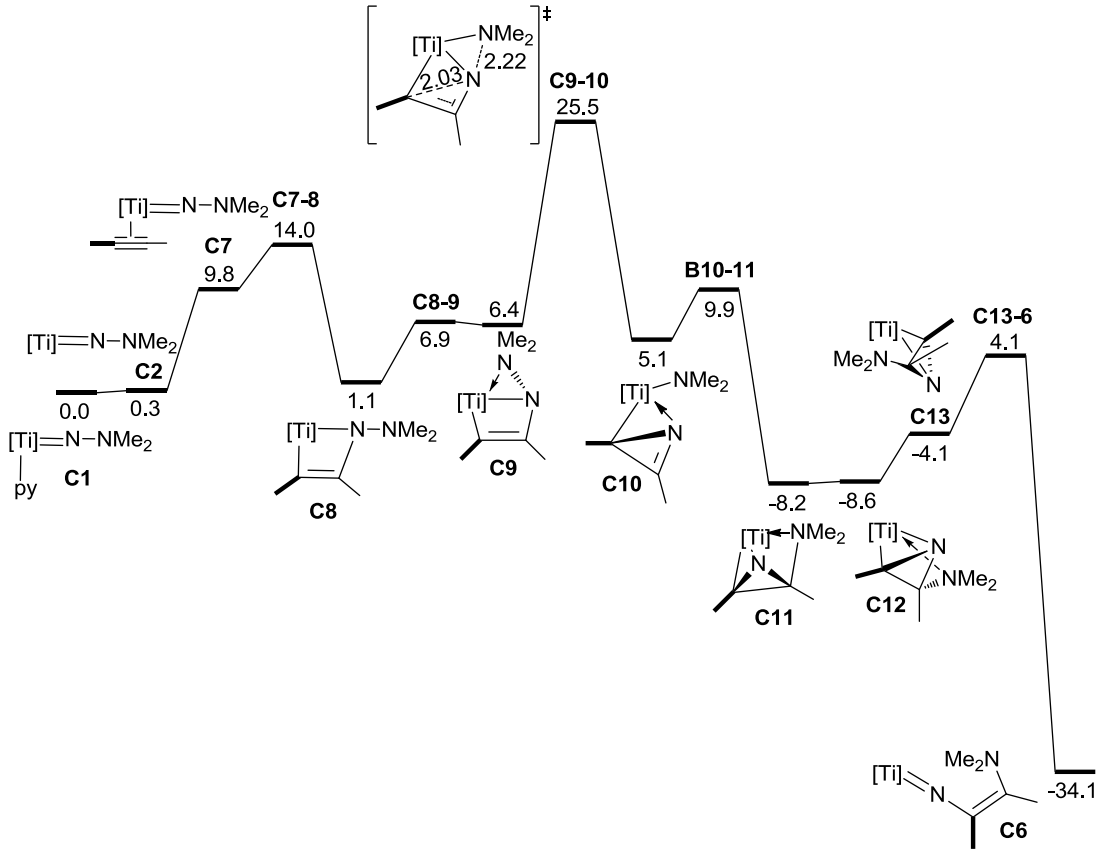

Scheme 2.8. Gibbs free energy (kcal mol^{-1}) profile for MeCCMe insertion into the N_α–N_β bond of Ti($N_2^{SiH_3}N^{py}$)($NNMe_2$)(py) (**C1**) along Pathway B. The bond shown in bold for the alkyne is to help the reader trace the fate of the Ti-bound CMe group in **C8**. [Ti] = Ti($N_2^{SiH_3}N^{py}$).

Taking the Gibbs free energy of **A9-10** or **C9-10** with respect to separated reactants (**A1** or **C1** and MeCCMe) as an estimate of the activation energy, then the $\Delta\Delta G^{\ddagger}$ value of 3.5 kcal mol^{-1} between the two model systems translates into a ratio between the rate constants of between 2 and 3 orders of magnitude at room temperature, with system **A** being the faster. Qualitatively, this is in good agreement with the relative rates of the real N_α–N_β insertion reactions **1.93** and **1.97** with PhCCMe (*ca.* 5–10 minutes and 3 days, respectively).

2.6 Summary

This Chapter has described a detailed synthetic, mechanistic and computational investigation into the unique transformation, outlined in Equations 2.3 and 2.4, where a single alkyne molecule inserts into the N_α–N_β bond of a reduced hydrazide(2-) ligand forming a vinyl imide product of the type $Ti(N_2N^R)\{NC(R)C(Me)NPh_2\}(py)$.

Previous work showed $Ti(N_2N^{py})(NNPh_2)(py)$ (**1.97**) to react with terminal and internal aryl alkynes, ArCCR (Ar = Ph or substituted phenyl, R = Me or H) at room temperature. These formed isolable $Ti{=}N_\alpha$ [2+2] cycloaddition products of the kind $Ti(N_2N^{py})\{N(NPh_2)C(R)CAr\}$ with a specific regiochemistry (Ar<u>C</u> bound to Ti). This Chapter built on this work by reporting the first structurally authenticated azametallacyclobutene made from the reaction of a Group 4 hydrazide and an internal alkyne $Ti(N_2N^{py})\{N(NPh_2)C(Me)C(C_6F_5)\}$ (**1**). This result, when combined with previous work and DFT calculations, has shown that electron-withdrawing aryl groups stabilise the metallacycles in the observed regiochemistry by decreasing the destabilising overlap between the N_α lone pair and filled π_{cc} of the azametallacyclobutene ring and increasing overlap between the N_α lone pair and the vacant π^*_{cc} orbital. $Ti{=}N_\alpha$ [2+2] cycloaddition products were also observed for $Ti(N_2N^{Me})(NNPh_2)(py)$ (**1.93**) but were only stable below *ca.* -30 ^oC and with electron-deficient alkynes Ar^FCCMe (Ar^F= 4-$C_6H_4CF_3$ or C_6F_5).

Compound **1.97** only undergoes N_α–N_β bond cleavage with PhCCMe. Even then prolonged reaction time or gentle heating is required. This is in contrast to **1.93**, which shows the same reactivity with a range of alkynes of the type ArCCMe (Ar = electron donating or withdrawing aryl group) cleanly and at temperatures as low as -35 ^oC. The reaction follows pseudo first order kinetics with respect to **1.93**. DFT studies showed that the previously proposed mechanism[3] involving attack of the alkyne at N_β of an η^2-bound NNR_2 ligand is highly unfavorable due to the nucleophilic nature of N_β and the late nature of the C–N bond forming transition state. Instead, a low energy pathway involving initial alkyne cycloaddition to $Ti{=}N_\alpha$ followed by intramolecular coordination of NPh_2 precedes the actual N_α–N_β bond breaking event. The calculated activation parameters for this process (modest $\Delta G_{298}^{\ddagger}$ and near-zero $\Delta S^{\ddagger}$) for realistic model systems were also fully consistent with mechanistic experiments. The rate limiting step in the N_α–N_β insertion process, nucleophilic attack of C_{Ti} at N_α

(displacing NPh_2), is supported by a Hammett analysis of the rate constants and NPA charge analyses.

It is generally accepted that Group 4 hydrohydrazination catalysis proceeds *via* azatitanacyclobutenes.[43,44,46] The results presented in this Chapter have shown that such metallacycles can also be intermediates *en route* to N_α–N_β insertion, and hence can lead to alkyne diamination rather than hydrohydrazination.

Given the rich chemistry of Group 4 metal-ligand multiple bonds in general, it seems possible that all examples of N_α–N_β cleavage may proceed *via* initial addition to Ti=N_α. This postulation, which encompasses N_α–N_β cleavage reactions with carbon monoxide or isocyanides and the N_α–N_β cleavage (as opposed to insertion) and C–H activation reactivity with alkynes, observed by Bergman and Gade, is further demonstrated in Chapters Three and Four of this Thesis. This explicit connection, between M=N_α bond ("imide-like") and N_α–N_β bond reactivity, along the same reaction coordinate, will hopefully aid the understanding of early metal hydrazide reactivity, an area still very much in its infancy.

2.7 References

1. Johnson, B. F. G.; Haymore, B. L.; Dilworth, J. D.: Comprehensive Coordination Chemistry. Wilkinson, G., Gillard, R. D., McCleverty, J. A., Eds.; Pergamon Press: Oxford, 1987; Vol. 2; pp 100.
2. Nugent, W. A.; Mayer, J. M.; *Metal-Ligand Multiple Bonds*; Wiley-Interscience: New York, 1988.
3. Mindiola, D. J.; *Angew. Chem. Int. Ed.* **2008**, *47*, 1557.
4. Fryzuk, M. D.; *Chem. Rec.* **2003**, *3*, 2.
5. MacKay, B. A.; Fryzuk, M. D.; *Chem. Rev.* **2004**, *104*, 385.
6. Kozak, C. M.; Mountford, P.; *Angew. Chem. Int. Ed.* **2004**, *43*, 1186
7. Chatt, J.; Pearman, A. J.; Richards, R. L.; *Nature* **1975**, *253*, 39.
8. Pickett, C. J.; Leigh, G. J.; *J. Chem. Soc., Chem. Commun.* **1981**, 1033.
9. Hussain, W.; Leigh, G. J.; Pickett, C. J.; *J. Chem. Soc., Chem. Commun.* **1982**, 747.
10. Pickett, C. J.; Talamarin, J.; *Nature* **1985**, *317*, 652.
11. Yandulov, D. V.; Schrock, R. R.; *Science* **2003**, 76.
12. Schrock, R. R.; *Acc. Chem. Res.* **2005**, *38*, 955.

13. Stephan, G. C.; Sivasankar, C.; Studt, F.; Tuczek, F.; *Chem. Eur. J.* **2008**, *14*, 644.
14. Studt, F.; Tuczek, F.; *Angew. Chem. Int. Ed.* **2005**, *44*, 5639.
15. Schrock, R. R.; *Angew. Chem. Int. Ed.* **2008**, *47*, 5512.
16. Schenk, S.; Kirchner, B.; Reiher, M.; *Chem. Eur. J.* **2009**, *15*, 5073.
17. Schenk, S.; Le Guennic, B.; Kirchner, B.; Reiher, M.; *Inorg. Chem.* **2008**, *47*, 3634.
18. Hidai, M.; *Coord. Chem. Rev.* **1999**, *185-186*, 99.
19. Ohki, Y.; Fryzuk, M. D.; *Angew. Chem. Int. Ed.* **2007**, *46*, 3180.
20. Fryzuk, M. D.; Johnson, S. A.; *Coord. Chem. Rev.* **2000**, *200-202*, 379.
21. Hidai, M.; *Chem. Rev.* **1995**, *95*, 1115.
22. Blake, A. J.; McInnes, J. M.; Mountford, P.; Nikonov, G. I.; Swallow, D.; Watkin, D. J.; *J. Chem. Soc., Dalton Trans.* **1999**, 379.
23. Clulow, A. J.; Selby, J. D.; Cushion, M. G.; Schwarz, A. D.; Mountford, P.; *Inorg. Chem.* **2008**, *47*, 12049.
24. Selby, J. D.; Schulten, C.; Schwarz, A. D.; Stasch, A.; Clot, E.; Jones, C.; Mountford, P.; *Chem.Commun.* **2008**, 5101.
25. Gehrmann, T.; Fillol, J. L.; Wadepohl, H.; Gade, L. H.; *Angew. Chem. Int. Ed.* **2009**, *48*, 2152.
26. Weitershaus, K.; Fillol, J. L.; Wadepohl, H.; Gade, L. H.; *Organometallics* **2009**, *28*, 4747.
27. Weitershaus, K.; Wadepohl, H.; Gade, L. H.; *Organometallics* **2009**, *28*, 3381.
28. Gehrmann, T.; Fillol, J. L.; Wadepohl, H.; Gade, L. H.; *Organometallics* **2010**, *29*, 28.
29. Tiong, P. J.; Schofield, A. D.; Selby, J. D.; Nova, A.; Clot, E.; Mountford, P.; *Chem. Commun.* **2010**, *46*, 85.
30. Walsh, P. J.; Carney, M. J.; Bergman, R. G.; *J. Am. Chem. Soc.* **1991**, *113*, 6343.
31. Herrmann, H.; Fillol, J. L.; Wadepohl, H.; Gade, L. H.; *Angew. Chem. Int. Ed.* **2007**, *46*, 8426.
32. Selby, J. D.; Manley, C. D.; Feliz, M.; Schwarz, A. D.; Clot, E.; Mountford, P.; *Chem. Commun.* **2007**, 4937.
33. Schrock, R. R.; *J. Chem. Soc., Dalton Trans.* **2001**, 2541.

34. Wiberg, N.; Haring, H.-W.; Huttner, G.; Friedrich, P.; *Chem. Ber.* **1978**, *111*, 2708.
35. Thorman, J. L.; Woo, L. K.; *Inorg. Chem.* **2000**, *39*, 1301.
36. Li, Y.; Shi, Y.; Odom, A. L.; *J. Am. Chem. Soc.* **2004**, *126*, 1794.
37. Parsons, T. B.; Hazari, N.; Cowley, A. R.; Green, J. C.; Mountford, P.; *Inorg. Chem.* **2005**, *44*, 8442.
38. Banerjee, S.; Odom, A. L.; *Organometallics* **2006**, *25*, 3099.
39. Patel, S.; Li, Y.; Odom, A. L.; *Inorg. Chem.* **2007**, *46*, 6373.
40. Herrmann, H.; Fillol, J. L.; Gehrmann, T.; Enders, M.; Wadepohl, H.; Gade, L. H.; *Chem. Eur. J.* **2008**, *14*, 8131.
41. Herrmann, H.; Wadepohl, H.; Gade, L. H.; *Dalton Trans.* **2008**, 2111.
42. Selby, J. D.; Manley, C. D.; Schwarz, A. D.; Clot, E.; Mountford, P.; *Organometallics* **2008**, *27*, 6479.
43. Bytschkov, I.; Doye, S.; *Eur. J. Org. Chem.* **2003**, 935.
44. Doye, S.; *Synlett* **2004**, 1653.
45. Hultzsch, K. C.; *Adv. Synth. Catal.* **2005**, *347*, 367.
46. Odom, A. L.; *Dalton Trans.* **2005**, 225.
47. Johnson, J. S.; Bergman, R. G.; *J. Am. Chem. Soc.* **2001**, *123*, 2923.
48. Cao, C.; Shi, Y.; Odom, A. L.; *Org. Lett.* **2002**, *4*, 2853.
49. Banerjee, S.; Barnea, E.; Odom, A. L.; *Organometallics* **2008**, *27*, 1005.
50. Dissanayake, A. A.; Odom, A. L.; *Chem. Commun.* **2012**, *48*, *440*.
51. Ackermann, L.; Born, R.; *Tet. Letts.* **2004**, *45*, 9541.
52. Khedkar, V.; Tillack, A.; Michalik, M.; Beller, M.; *Tet. Letts.* **2004**, *45*, 3123.
53. Tillack, A.; Jiao, H.; Garcia Castro, I.; Hartung, C. G.; Beller, M.; *Chem. Eur. J.* **2004**, *10*, 2409.
54. Banerjee, S.; Shi, Y.; Cao, C.; Odom, A. L.; *J. Organomet. Chem.* **2005**, *690*, 5066.
55. Wigley, D. E.; *Prog. Inorg. Chem.* **1994**, *42*, 239.
56. Mountford, P.; *Chem. Commun.* **1997**, 2127.
57. Gade, L. H.; Mountford, P.; *Coord. Chem. Rev.* **2001**, *216-217*, 65.
58. Duncan, A. P.; Bergman, R. G.; *Chem. Rec.* **2002**, *2*, 431.
59. Hazari, N.; Mountford, P.; *Acc. Chem. Res.* **2005**, *38*, 839.
60. Bolton, P. D.; Mountford, P.; *Adv. Synth. Catal.* **2005**, *347*, 355.
61. Fout, A. R.; Kilgore, U. J.; Mindiola, D. J.; *Chem. Eur. J.* **2007**, *13*, 9428.

62. Kaplan, A. W.; Polse, J. L.; Ball, G. E.; Andersen, R. A.; Bergman, R. G.; *J. Am. Chem. Soc.* **1998**, *120*, 11649.
63. Gehrmann, T.; Fillol, J. L.; Scholl, S. A.; Wadepohl, H.; Gade, L. H.; *Angew. Chem. Int. Ed.* **2011**, *50*, 5757.
64. Schofield, A. D.; Nova, A.; Selby, J. D.; Manley, C. D.; Schwarz, A. D.; Clot, E.; Mountford, P.; *J. Am. Chem. Soc.* **2010**, *132*, 10484.
65. Polse, J. L.; Andersen, R. A.; Bergman, R. G.; *J. Am. Chem. Soc.* **1998**, *120*, 13405.
66. Ward, B. D.; Maisse-Francois, A.; Mountford, P.; Gade, L. H.; *Chem. Commun.* **2004**, 704.
67. Wang, H.; Chan, H.; Xie, Z.; *Organometallics* **2005**, *24*, 3772.
68. Bolton, P. D.; Feliz, M.; Cowley, A. H.; Clot, E.; Mountford, P.; *Organometallics* **2008**, *27*, 6096.
69. Vujkovic, N.; Ward, B. D.; Maisse-Francois, A.; Wadepohl, H.; Mountford, P.; Gade, L. H.; *Organometallics* **2007**, *26*, 5522.
70. Walsh, P. J.; Baranger, A. M.; Bergman, R. G.; *J. Am. Chem. Soc.* **1992**, *114*, 1708.
71. Basuli, F.; Aneetha, H.; Huffman, J. C.; Mindiola, D. J.; *J. Am. Chem. Soc.* **2005**, *127*, 17992.
72. Compound **9** was structurally characterised and details can be found in Appendix A.
73. Collier, P. E.; Pugh, S. M.; Clark, H. S. C.; Love, J. B.; Blake, A. J.; Cloke, F. G. N.; Mountford, P.; *Inorg. Chem.* **2000**, *39*, 2001.
74. Blake, A. J.; Collier, P. E.; Gade, L. H.; Mountford, P.; Lloyd, J.; Pugh, S. M.; Schubart, M.; Skinner, M. E. G.; Trösch, J. M.; *Inorg. Chem.* **2001**, *40*, 870.
75. The synthesis and solid state structure of $Ti(N_2N^{Me})(N^tBu)(py)$ (**47**) are presented in Appendix B of this Thesis.
76. Doxsee, K. M.; Farahi, J. B.; Hope, H.; *J. Am. Chem. Soc.* **1991**, *113*, 8889.
77. Bailey, B. C.; Fout, A. R.; Fan, H.; Tomaszewski, J.; Huffman, J. C.; Gary, J. B.; Johnson, M. J. A.; Mindiola, D. J.; *J. Am. Chem. Soc.* **2007**, *129*, 2234.
78. Lee, S. Y.; Bergman, R. G.; *Tetrahedron* **1995**, *51*, 4255.
79. Schwarz, A. D.; Nova, A.; Clot, E.; Mountford, P.; *Chem. Commun.* **2011**, *47*, 4926.

80. Pugh, S. M.; Blake, A. J.; Gade, L. H.; Mountford, P.; *Inorg. Chem.* **2001**, *40*, 3992.
81. Ward, B. D.; Orde, G.; Clot, E.; Cowley, A. R.; Gade, L. H.; Mountford, P.; *Organometallics* **2004**, *23*, 4444.
82. Pugh, S. M.; Trösch, D. J. M.; Skinner, M. E. G.; Gade, L. H.; Mountford, P.; *Organometallics* **2001**, *20*, 3531.
83. Tonks, I. A.; Bercaw, J. E.; *Inorg. Chem.* **2010**, *49*, 4648.
84. Jordan, R. B.; *Reaction Mechanisms of Inorganic and Organometallic Systems*; Oxford University Press: Oxford, 1998.
85. Hansch, C.; Leo, A.; Taft, R. W.; *Chem. Rev.* **1991**, *91*, 165.
86. Schofield, A. D.; Nova, A.; Selby, J. D.; Schwarz, A. D.; Clot, E.; Mountford, P.; *Chem. Eur. J.* **2011**, *17*, 265.
87. Stewart, P. J.; Blake, A. J.; Mountford, P.; *Inorg. Chem.* **1997**, *36*, 3616.
88. Hartwig, J. F.; Cook, K. S.; Hapke, M.; Incarvito, C. D.; Fan, Y.; Webster, C. E.; Hall, M. B.; *J. Am. Chem. Soc.* **2005**, *127*, 2538.
89. Nguyen, T., A.; *Frontier Orbitals, a Practical Manual*; John Wiley & Sons: Chichester, 2007.

Chapter Three

$Ti{=}N_{\alpha}$ and N_{α}-N_{β} reactions of $Ti(N_2N^{Me})(NNPh_2)(py)$ (1.93) with nitriles, isocyanides and isocyanates

3.1 Overview

Until fairly recently, few examples of terminal Group 4 hydrazido complexes (L)M=NNR_2 were known, and the chemistry of the early transition metal M=NNR_2 functional group was virtually unexplored. This position is in considerable contrast to the situation for the related Group 4 imido complexes (L)M=NR (R = alkyl or aryl) which have been a focus of ongoing activity for nearly 20 years.[1-8]

Several structural and computational investigations into the bonding of terminal early transition metal hydrazides have been described, mostly within the last five years.[9-16] These have established the presence of polar metal-nitrogen triple bonds and shown that in these early metal complexes the NNR_2 groups are best viewed formally as reduced hydrazide(2-) moieties (consistent with the short M=N_α and somewhat lengthened N_α–N_β bonds found). This is in contrast to the situation for their Group 6 analogues, widely studied in the context of understanding and modelling biological N_2 fixation.[17-26] Here the NNR_2 ligands are more like neutral isodiazenes with significant N_α–N_β multiple bond character and a M–N_α bond that is more dative (donor-acceptor) in nature.[27-30] The bonding in isodiazene and hydrazide complexes is discussed in detail in Chapter One.

Alongside these synthetic and computational advances, a body of distinctive reaction chemistry of the Group 4 M=NNR_2 functional group has started to emerge. This involves both reactions at the M=N_α[31-39] bond (cycloaddition or insertion) and cleavage or insertion reactions at the N_α–N_β bond and is described in detail in Chapter One.[16,33,34,40-42] These patterns of reactivity appear to originate from the combination of an unsaturated, polar M=N_α bond (as in the related imido systems) and a lengthened and reduced N_α–N_β bond. This reactivity is very different from the later metal hydrazide/isodiazene compounds where reactions at the M=N_α bond are not seen and direct N_α–N_β bond cleavage only occurs under forcing conditions using external reductants (e.g. $LiAlH_4$).[25]

This Chapter describes the reactivity of the well-defined titanium hydrazido(2-) species Ti(N_2N^{Me})($NNPh_2$)(py) (**1.93**) towards a range of small, polar, unsaturated molecules, demonstrating the breadth of reactivity accessible to the hydrazide group. In addition, DFT studies on the products and mechanisms of formation are presented.

Both this work and the concurrent study of the reactivity of the titanium hydrazido(2-) species $Ti(N_2N^{py})(NNPh_2)(py)$ (**1.97**) have been published.[43]

3.2 Reactions with organic nitriles

The reactions of nitriles with transition metal imides and hydrazides are almost unknown, in contrast to the situation with metal nitrides[44,45] and, in particular, metal alkylidenes[46-50] and alkylidynes.[51-56] Previous work in the Group involved the reaction between $Ti(N_2N^{py})(NNPh_2)(py)$ (**1.97**) and MeCN leading to the formation of the dimeric compound $Ti_2(N_2N^{py})_2\{\mu\text{-}NC(Me)(NNPh_2)\}_2$ (**1.140**, Equation 3.1).

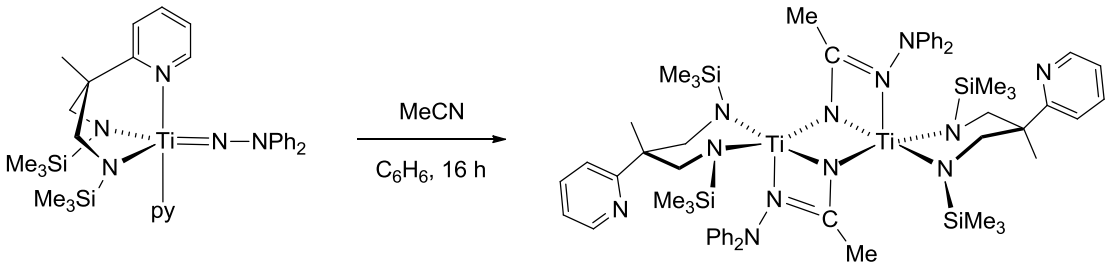

1.97 **1.140**

Equation 3.1

Encouraged by this result and the observation, from the reactions between **1.93**, **1.97** and a range of alkynes, that electron withdrawing aryl groups (e.g Ar = C_6F_5) stabilised metallacycles of the type $Ti(N_2N^{R})\{N(NPh_2)C(Me)C(Ar)\}$ (R = Me, py) relative to Ar = Ph (as discussed in Chapter Two), the reactivity between $Ti(N_2N^{Me})(NNPh_2)(py)$ (**1.93**) and a range of organic nitriles was investigated.

When **1.93** was reacted with the electron deficient arylnitriles $Ar^{F_2}CN$ (Ar^{F_2} = 2,6-$C_6H_3F_2$) and $Ar^{F_5}CN$ (Ar^{F_5} = C_6F_5) the novel reactivity summarised in Equation 3.2 was observed, leading to the formation of the doubly deprotonated hydrazonamido compounds $Ti(N_2N^{Me})\{NC(Ar^{F_2})NNPh_2\}(py)$ (**17**) and $Ti(N_2N^{Me})\{NC(Ar^{F_5})NNPh_2\}(py)$ (**18**). Work concurrent with this Thesis indicated analogous reactivity between **1.97** and the same nitriles.[43]

These are the first examples of a terminal hydrazonamide ligand in transition metal chemistry, although polynuclear clusters of mono- and di-metallated hydrazonamides have been reported by the sequential reaction of $AlMe_3$ or dialkyl zincs with Me_2NNH_2 and MeCN.[57,58] They are also related to the vinyl imides formed from alkylidenes and organic nitriles.[46-50]

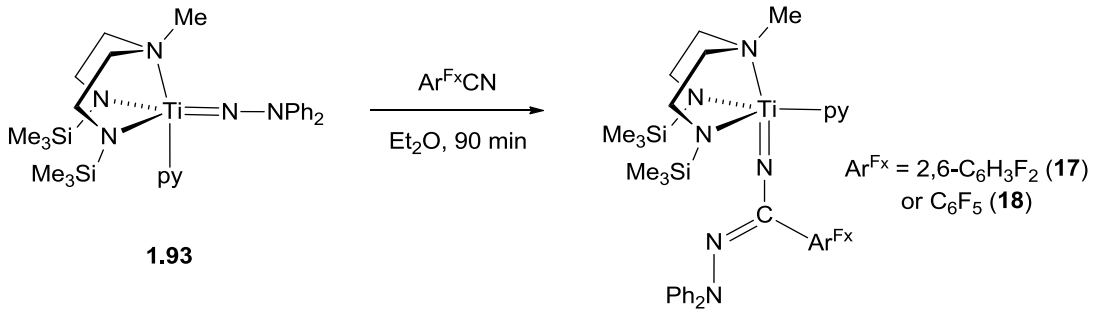

Equation 3.2

In the case of $Ar^{F_2}CN$, 3 equivalents of the nitrile were needed to achieve complete conversion to $Ti(N_2N^{Me})\{NC(Ar^{F_2})NNPh_2\}(py)$ (**17**), whereas with $Ar^{F_5}CN$ only a stoichiometric amount was required to form $Ti(N_2N^{Me})\{NC(Ar^{F_5})NNPh_2\}(py)$ (**18**). No reaction occurred with 5 to 10 equivalents of PhCN or MeCN when followed by ^1H NMR spectroscopy in C_6D_6. Use of PhCN as the solvent gave an unknown mixture after 16 h, using MeCN however, led to the formation of two distinct products.

It was possible to purify one of these compounds, in 58 % yield, by recrystallisation from a concentrated MeCN solution at -30 ºC. The ^1H NMR spectrum is presented in Figure 3.1. The resonances attributed to the ligand and hydrazide groups are similar to those of **17** and **18**. However, there are no resonances corresponding to pyridine. Instead, two singlets arising or derived from MeCN molecules at 2.05 and 2.03 ppm are observed. This is confirmed by the presence of two resonances at 178.5 and 173.0 ppm in the $^{13}C\{^1H\}$ NMR spectrum, attributable to the quaternary carbons of MeCN.

These observations point towards similar reactivity to that of **1.93** with electron withdrawing nitriles, although it is not possible to conclusively say whether the final product is the initially formed metallacycle (**19a**, Figure 3.2) or if it undergoes a retrocycloaddition, as in **17** and **18**, to give the terminal hydrazonamide **19b** (*vide infra*). They also indicate that, due to the large excess of MeCN, the bound pyridine found in **17** and **18** has been replaced by a molecule of MeCN. Elemental analysis and the presence of a peak at *m/z* = 530 in the mass spectrometry trace, corresponding to $[M\text{-MeCN}]^+$, agree with the structures illustrated in Figure 3.2, which should easily undergo MeCN loss upon fragmentation. The isolated, pure compound does not, however, react with MeCN-d_3, but does revert to the original mixture of products over the course of several days.

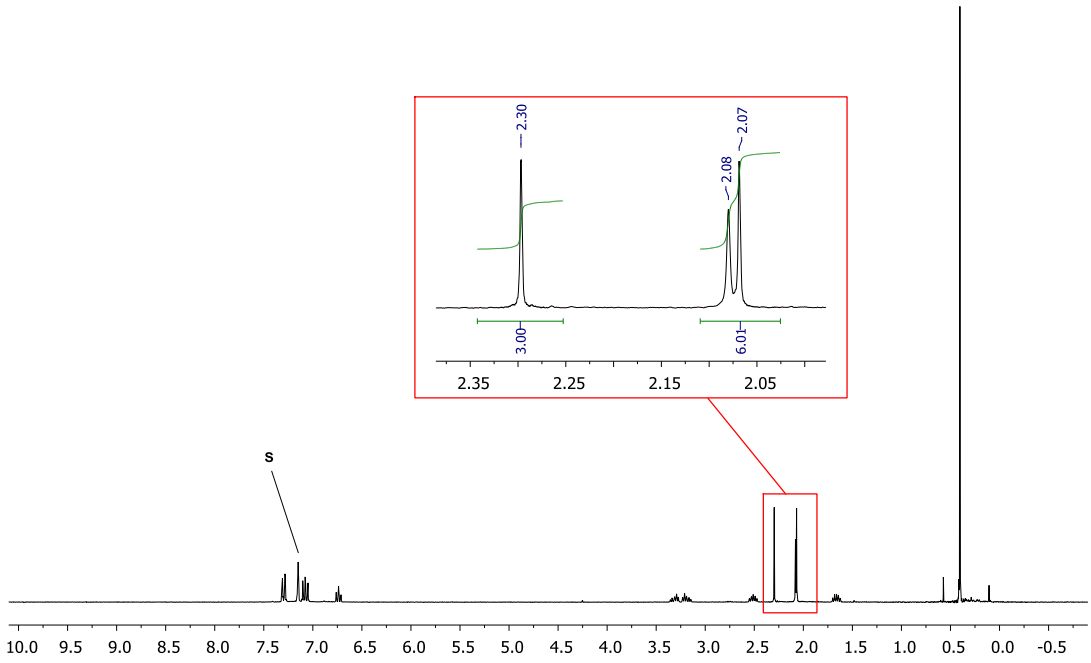

Figure 3.1. ^{1}H NMR spectrum (499.9 MHz, 293 K) of the isolated product Ti(N_2N^{Me}){NC(Me)NNPh$_2$}(MeCN) (**19**) in C_6D_6. The expansion illustrates the three methyl resonances, one relating to the ligand apical donor (2.30 ppm), the others deriving from MeCN molecules. ('s' denotes residual protio solvent).

It is interesting to note that recent work has indicated the ability of further equivalents of nitriles to undergo further, reversible, cycloaddition at the Ti=N_α bond of the hydrazonamide group. This cannot be ruled out, although the presence of the peak corresponding to [*M*-MeCN]$^+$ in the mass spectrometry trace implies that this has not occurred.[59]

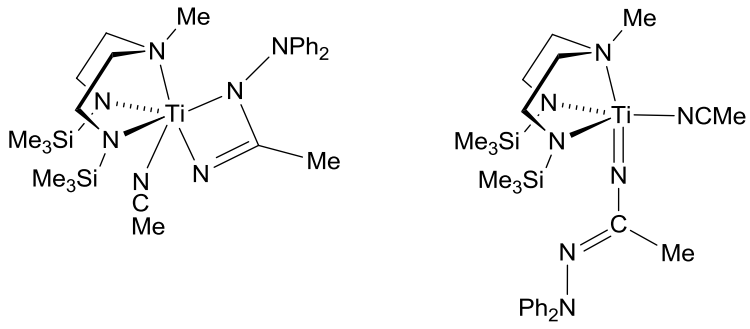

19a **19b**

Figure 3.2. Possible products formed from the reaction of Ti(N_2N^{Me})(NNPh$_2$)(py) (**1.93**) with excess MeCN.

Purification of the second product was unsuccessful and the nature of the species is unclear, although it is possibly a dimer of **19** with the apical N_2N^{Me} amine decoordinated, analogous to **1.140** (Equation 3.1). In this instance, however, one MeCN molecule per metal centre would have to remain coordinated to be consistent with the NMR data. Despite repeated attempts, diffraction-quality crystals could not be obtained due to the instability of the products in solvents other than MeCN. ROESY, nOe, $^{13}C\{^1H\}$ NMR and IR spectra were unable to satisfactorily distinguish between **19a** and **19b** or elucidate the nature of the second species. Addition of one equivalent of H_2NNPh_2 to solutions of **17**, **18** or **19** in C_6D_6, in an attempt to protonate the hydrazonamide fragment and reform the starting hydrazide **1.93**, gave complicated mixtures of products.

The milder conditions required for the reactions involving electron-deficient nitriles clearly illustrate the importance of the fluorine substituents in stabilising the hydrazonamide products. DFT studies of these reactions are discussed below. The molecular structures of **17** and **18** as determined by X-ray crystallography are shown in Figure 3.3 and selected distances and angles are given in Table 3.1.

Compounds **17** and **18** are 5-coordinate monomeric hydrazonamide complexes in the solid state, consistent with the structures proposed in Equation 3.2. The geometry at titanium is approximately trigonal bipyramidal with the N_2N^{Me} ligands *fac*-coordinated in a κ^3*N* manner. The amide donors occupy equatorial coordination sites and the hydrazonamide ligand lies *cis* to these in one of the axial positions. The remaining coordination sites are occupied by the amine donor of N_2N^{Me} and a pyridine ligand. The axial coordination of the hydrazonamide ligand is unexpected based on related Group 4 imido and hydrazido compounds of the type M(L)(NR)(py) (L = N_2N^{py}, $N_2{}^*N^{py}$, N_2N^{Me} and related; M = Ti, Zr or Hf; R = ^{t}Bu, aryl, NPh_2 or N(Me)Ph) which all have the M=NR bond equatorially positioned.[14,15,60-63, 64] However, the 2,2′-bipyridine analogue of **1.93**, Ti(N_2N^{Me})($NNPh_2$)(bipy) (**14**, Chapter Two) does have the hydrazide group in an axial position. In addition, the related titanium *tert*-butoxyimide compound, Ti(N_2N^{Me})(NO^tBu)(py) (**1.190**), exists as an equilibrium mixture with the NO^tBu ligand in either the equatorial or axial position.[65]

More generally it has been found that 5-coordinate compounds of this general type can exist with the NR ligand in either an equatorial position (e.g., Nb(N_2N^{py})(N^tBu)Cl and Ta(N_2N^{py})(N^tBu)Me)[66,67] or an axial one (e.g., Ta(N_2N^{Me})($NNPh_2$)Cl) and

$[W(N_2N^{py})(NPh)Me]^+$).[67-69] The electronic and steric origins of these coordination site preferences have been described elsewhere.[67]

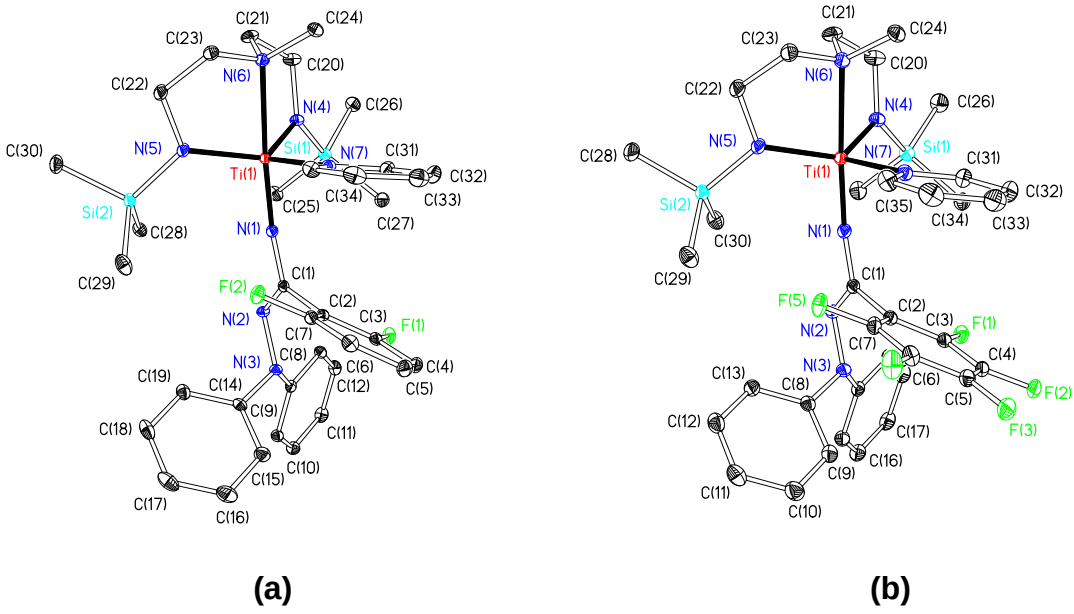

Figure 3.3. Displacement ellipsoid plots (20 % probability) of (a) $Ti(N_2N^{Me})\{NC(Ar^{F_2})NNPh_2\}(py)$ (**17**) and (b) $Ti(N_2N^{Me})\{NC(Ar^{F_5})NNPh_2)\}(py)$ (**18**). H atoms omitted for clarity.

In addition to the different positions of the $NNPh_2$ and $NC(Ar^{F_x})NNPh_2$ ligands in **1.93** and **17**/**18**, there are significant differences between the Ti–N distances for the N_2N^{Me} and NR groups. The Ti(1)–N(1) bond lengths in **17** and **18** (1.7759(12) and 1.7808(11) Å respectively) are significantly longer than in **1.93** ($Ti{=}N_\alpha$ = 1.733(5) Å) suggesting diminished Ti=N multiple bond character. However, the Ti(1)–N(1) bond lengths and the angles subtended at N(1) in **17** and **18** (168.62(10) and 168.03(10) ^{o}) are still consistent with *sp* hybridisation of N(1) and a formal Ti≡N triple bond. The $Ti–N_{amide}$ distances in **1.93** (avg. 2.027(4) Å) are longer than their counterparts in **17** and **18** (avg. 1.969(1) and 1.964(1) Å, respectively) indicating better $N_{2p(\pi)}\rightarrow Ti_{3d(\pi)}$ in the latter. This would follow from the longer Ti=NR bonds and also the axial positioning of the hydrazonamide ligand.[67] There appears to be some small but self-consistent effects on changing from an Ar^{F_2} to an Ar^{F_5} hydrazonamide C(1) substituent. In particular, the Ti(1)–N(1) distance in **18** is marginally longer and the Ti–N distances to the N_2N^{Me} amide and amine nitrogens are marginally shorter. While the pairwise differences between the individual bond distances is small, the apparent

trend suggests that increasing the extent of fluorination in the Ar^{Fx} rings draws electron density away from N(1).

Table 3.1. Selected distances (Å) and angles (°) for Ti(N_2N^{Me}){NC(Ar^{F2})$NNPh_2$}(py) (**17**) and Ti(N_2N^{Me}){NC(Ar^{F5})$NNPh_2$)}(py) (**18**).

Parameter	**17**	**18**
Ti(1)–N(1)	1.7759(12)	1.7808(11)
Ti(1)–N(4)	1.9673(12)	1.9644(12)
Ti(1)–N(5)	1.9712(12)	1.9644(11)
Ti(1)–N(6)	2.3318(12)	2.3259(11)
Ti(1)–N(7)	2.1828(12)	2.1944(11)
N(1)–C(1)	1.3446(18)	1.3375(17)
N(2)–C(1)	1.3098(18)	1.3075(17)
N(2)–N(3)	1.4438(16)	1.4410(15)
N(1)–Ti(1)–N(4)	102.60(5)	102.78(5)
N(1)–Ti(1)–N(5)	104.61(5)	104.19(5)
Ti(1)–N(1)–C(1)	168.62(10)	168.03(10)
N(3)–N(2)–C(1)	112.48(11)	111.92(11)
N(1)–C(1)–N(2)	122.78(13)	122.50(12)

The distances within the NC(Ar^{Fx})$NNPh_2$ ligands are consistent with the valence bond representations in Equation 3.2. The N(1)–C(1) (avg. 1.341(1) Å) and N(2)–C(1) (avg. 1.309(1) Å) distances are consistent with C–N single and C=N double bonds, respectively.[70] In keeping with an increased electron-withdrawing effect of Ar^{F5} compared with Ar^{F2}, the N(1)–C(1) and N(2)–C(1) distances in **18** appear slightly shorter. Interestingly, there are some relatively close contacts between certain ring carbons of the Ar^{Fx} groups, the adjacent pyridine and one of the NN$\underline{Ph}_2$ rings (e.g., for **17**: C(7)···C(35) = 3.465(1), C(2)···C(14) = 3.160 Å; corresponding distances for **18**: C(7)···C(35) = 3.423(1), C(2)···C(8) = 3.043(1) Å). Such π-stacking type interactions

are well known in general for fluorinated aryl rings,[71-75] including between the N-substituents of titanium imido compounds.[76-78]

It is not immediately clear whether the nitrile molecule has inserted into the Ti=N_α or N_α–N_β bond. To help identify which bond was cleaved a DFT study was carried out by Dr E. Clot and Dr. A. Nova to elucidate the mechanism of formation of **17** and **18**. Calculations were performed using the model compound Ti($N_2^{SiH_3}N^{Me}$)($NNMe_2$)(py) (**A1**, Figure 3.4) which has also been used in the studies of the Ti=N_α cycloaddition and N_α–N_β bond insertion reactions of **1.93** with alkynes, as described in Chapter Two.[16] Scheme 3.1 shows the computed mechanisms for the reactions of **A1** with PhCN and $Ar^{F5}CN$. Calculations were also performed with $Ar^{F2}CN$, MeCN and CF_3CN as discussed below.

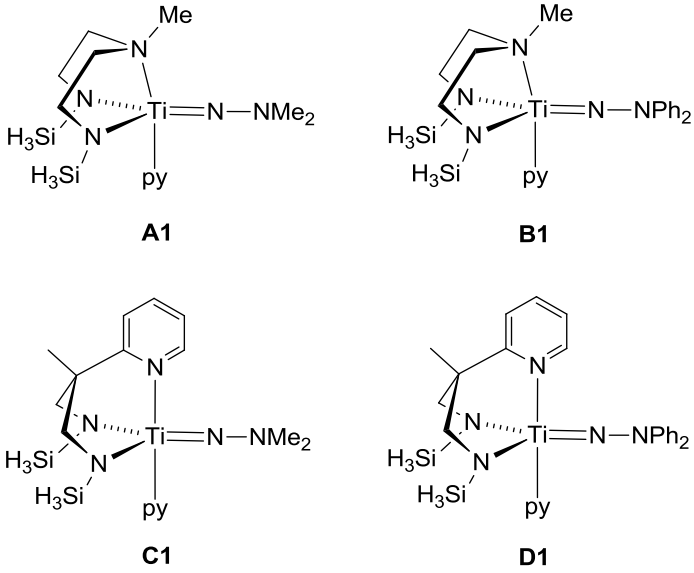

Figure 3.4. Models used to describe complexes **1.93** (**A1** and **B1**) and **1.97** (**C1** and **D1**).

As for the reactions with alkynes, the mechanism begins with loss of py to form **A2** which has a vacant coordination site for nitrile binding. From **A2**, an initial adduct **A3_R** is formed in an exergonic process relative to **A2**. However, both **A3_Ph** and **A3_Ar^{F5}** are unstable relative to **A1** and the respective nitriles. From **A3_R** another exergonic [2+2] cycloaddition reaction occurs *via* the TSs **A3-4_R** to form the diazametallacyclobutene complexes **A4_R**. These TSs are the highest points on the reaction profile and so [2+2] cycloaddition is considered to be the rate determining step. For both nitriles this is kinetically accessible ($\Delta G^{\ddagger}$ = 16.0 and 12.0 kcal mol^{-1} for

PhCN and $Ar^{F5}CN$, respectively). The most favourable regioisomer of **A4_R** (as illustrated in Scheme 3.1) has the ArC carbon of ArCN bound to N_α. The alternative isomers, with the nitrile N bound to N_α, were calculated to be *ca* 7 kcal mol^{-1} less stable and were not considered further. The higher stability of **A4_Ar^{F5}** relative to **A4_Ph** (-5.0 kcal mol^{-1} in favour of **A4_Ar^{F5}**) is reminiscent of the corresponding reactions of **1.93** with ArCCMe (Ar = Ph or Ar^{F5}) for which only the cycloaddition product with $Ar^{F5}CCMe$ was experimentally observed (see Chapter Two). The computed energy difference (ΔΔG) between the [2+2] metallacycles formed between **A2** and ArCCMe was -2.9 kcal mol^{-1} in favour of Ar = Ar^{F5}.[16]

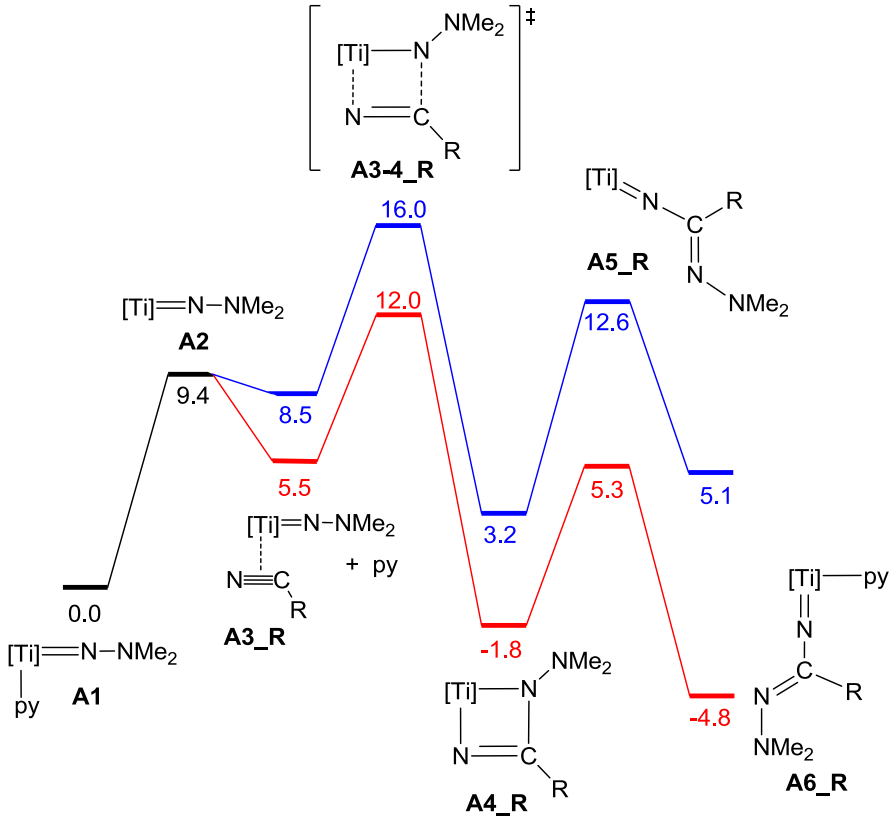

Scheme 3.1. Gibbs free energy (kcal mol^{-1}) profile for RCN insertion into the Ti=N_α bond of Ti($N_2^{SiH_3}N^{Me}$)($NNMe_2$)(py) (**A1**). [Ti] = Ti($N_2^{SiH_3}N^{Me}$); R = Ph (blue lines after common intermediate **A2**) or Ar^{F5} (red lines after **A2**). Note that **A5_R** is not a transition state.

Although **A4_Ar^{F5}** is stable relative to **A1** and $Ar^{F5}CN$, it is not predicted to be the final outcome of the reaction. Ring-opening *via* dissociation of the original Ti–N_α bond of **A1** to form the four-coordinate terminal hydrazonamide intermediate **A5_Ar^{F5}** (lying 7.1 kcal mol^{-1} above **A4_Ar^{F5}**) is thermally accessible. This is then

trapped by pyridine in an exoergic step (-10.1 kcal mol^{-1} relative to **A5_Ar^{F5}**; -4.8 kcal mol^{-1} relative to **A1**) to give **A6_Ar^{F5}**, a model for the real compound **18**. In contrast, the corresponding process for Ar = Ph is predicted to be unfavourable, with **A6_Ph** being 1.9 kcal mol^{-1} less stable than the diazametallacycle **A4_Ph**, and 5.1 kcal mol^{-1} less stable than **A1** and PhCN.

This mechanism is reminiscent of a classical Chauvin-type metathesis reaction in that it proceeds *via* [2+2] cycloaddition (**A4_R**) and retrocycloaddition steps.[79] In alkyne or alkene metathesis, however, separation of the bond-exchanged partners can occur, whereas if it were to occur in this instance the radical species Ti(N_2N^{Me})(py)(=N$^{\bullet}$) and $Me_2NN{=}C^{\bullet}Ar^{Fx}$ would be formed. These are clearly not stable relative to the observed products **A6_R**, thus this can be thought of as an 'arrested' Ti=N/C≡N metathesis reaction.

As mentioned, calculations were also carried out for other nitriles. With $Ar^{F2}CN$, the energy of the insertion product **A6_Ar^{F2}** (a model for the real compound **17**) was between that of **A6_Ph** and **A6_Ar^{F5}** as expected (ΔG = 0.2 kcal mol^{-1} with respect to **1.93** and $Ar^{F2}CN$). With MeCN, the reaction to form **A6_Me** was significantly endoergic (ΔG = 3.1 kcal mol^{-1} with respect to **1.93** and MeCN), whereas the intermediate metallacycle **A4_Me** (+ py) was approximately isoenergetic with respect to **A1** and MeCN (ΔG = 0.2 kcal mol^{-1}). This indicates that the likely product of the reaction between **1.93** and MeCN is **19a** as opposed to **19b** (vide supra). Use of CF_3CN in place of MeCN gave the substantially more stable **A6_CF$_3$** (ΔG = -11.6 kcal mol^{-1} with respect to **A1** and the free nitrile).

The DFT computed mechanism satisfactorily accounts for the experimental results found with **1.93** (directly modelled by **A1**). Only terminal hydrazonamides **A6_R** with electron-withdrawing R-groups are sufficiently stabilised with regard to **A1** and/or **A4_R** to be formed using approximately stoichiometric amounts of the nitrile. This R-group effect is predominantly inductive in nature as shown by the relative stabilities of **A6_Me** and **A6_CF$_3$**. Although the X-ray structures of **17** and **18** (Figure 3.3) suggest that some intramolecular π-stacking may additionally stabilise them; these dispersive effects are not taken into account in the DFT calculations. An NBO (natural bond orbital) analysis[80] of the three **A6_Ar** systems showed that increasing the electron-withdrawing nature of Ar leads to a stabilisation of the C=N(NMe_2) π*

orbital. This, in turn, is then better able to stabilise the Ti=N π system which is polarised towards N. Experimental structural evidence for this effect was described above for **17** and **18** (shortening of the N(1)–C(1) and avg. Ti–N_{amide} distances from **17** to **18**; lengthening of the Ti(1)–N(1) distance). These features are reproduced in the DFT structures of **A6_Ar**. For Ar = Ph, $Ar^{F_2}CN$ or $Ar^{F_5}CN$: N–C(Ar)$NNMe_2$ = 1.361, 1.352 or 1.349 Å; Ti=N = 1.732, 1.735 or 1.739 Å; avg. Ti–N_{amide} = 1.953, 1.949 or 1.946 Å, respectively.

The [2+2] cycloaddition intermediates **A4_R** in Scheme 3.1 are analogous to the metallacycles formed *en route* to alkyne N_α–N_β bond insertion products of the type described in Chapter Two. Therefore it was also of interest to calculate the mechanism for MeCN inserting into the N_α–N_β bond of **A1** starting from **A4_R**. The principal steps are summarised in Equation 3.3. The first intermediate (**A7**, intramolecular NMe_2 chelation) lies only 11.2 kcal mol^{-1} above **A4_Me** and is expected to be thermally accessible. The energies of the corresponding intermediates in the reaction of **A1** with MeCCMe are not dissimilar (1.9 and 4.2 kcal mol^{-1} for the analogues of **A4_Me** and **A7**, respectively).[16] However, the next intermediate, **A8**, is much less stable than in the corresponding reaction with MeCCMe (27.1 *vs* 4.2 kcal mol^{-1}), as is the final insertion product **A9** (4.2 *vs* -30.0 kcal mol^{-1}). Furthermore, **A9** is thermodynamically unstable relative to **A1** and MeCN. The TS (not illustrated) from **A7** to **A8** is also very high in energy (41.4 kcal mol^{-1}) in contrast to the corresponding TS with MeCCMe (22.0 kcal mol^{-1}). Overall the N_α–N_β insertion reaction of **A1** with MeCN is both kinetically and thermodynamically unfavourable.

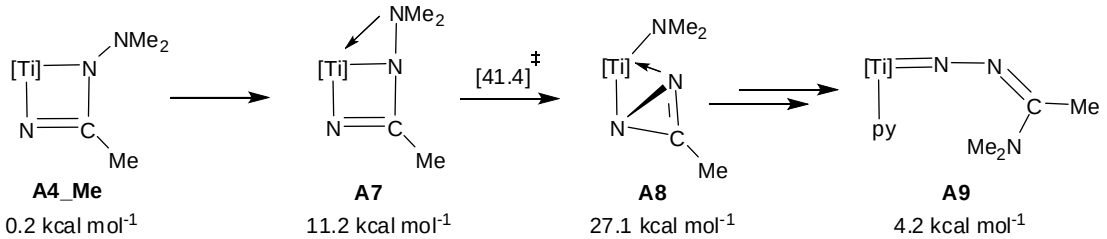

Equation 3.3

3.3 Reactions with isocyanides

In Chapter One, it was described that the reaction of $Cp_2Zr(NNPh_2)$ (**1.153**) with CO led to N_α–N_β bond cleavage, forming the mixed diphenylamide-isocyanate complex $Cp_2Zr(NCO)(NPh_2)$ (**1.158**).[40] More recently Gade reported the apparently related

reaction of $Zr(N_2{}^*N^{py})(NNPh_2)(py)$ (**1.159**) with ^{t}BuNC forming a mixed diphenylamide-metallated carbodiimide **1.175** (Scheme 3.2).[41] Work parallel with that presented in this Thesis, involving the reaction between $Ti(N_2N^{py})(NNPh_2)(py)$ (**1.97**) and RNC (R = ^{t}Bu and Xyl), also formed the corresponding carbodiimide compounds, $Ti(N_2N^{py})(NCNR)(NPh_2)$ (R = ^{t}Bu (**1.143**) and Xyl (**1.144**), Scheme 3.2). In these instances they were formed as a mixture of *cis* and *trans* isomers, in contrast to the exclusive *cis* isomer observed by Gade.[81,43]

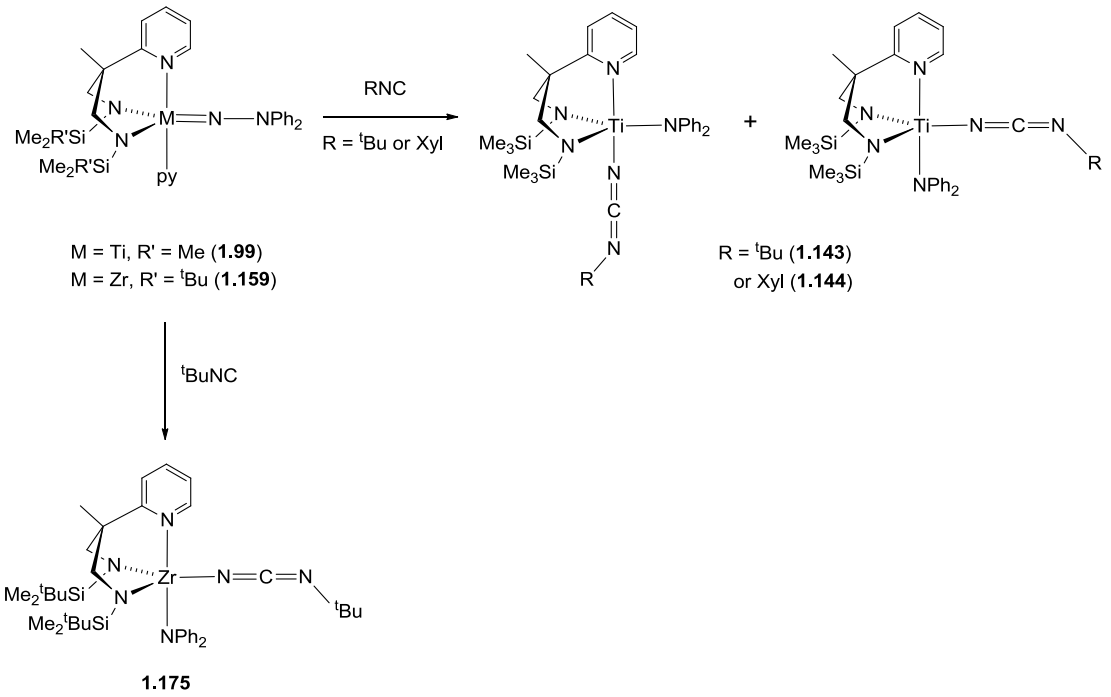

Scheme 3.2. Reaction of diamide-pyridyl supported Group 4 hydrazido complexes with isocyanides.

Prior to compounds **1.143**, **1.144** and the example below, reactions of titanium hydrazides with CO or organic isocyanides had not been reported. It is of interest, however, that Andersen and Bergman found CO-induced N_α–N_β bond cleavage in the titanocene diazoalkane complex $Cp^*_2Ti\{\eta^2$-NNC(H)Tol$\}$, giving a mixed ketimide-isocyanate product reminiscent of **1.158**.[82] Several papers have reported the reactions of alkyl or aryl imido compounds with isocyanides. While N_α–N_β bond cleavage is clearly not an option in these systems, several different product types based on C–C and C–N bond forming processes have been described.[83-87] Noting these literature precedents and also the N_α–N_β bond insertion reactions of $Ti(N_2N^{Me})(NNPh_2)(py)$

(**1.93**) with internal alkynes, it seemed prudent to study the reactivity towards isocyanides and CO.

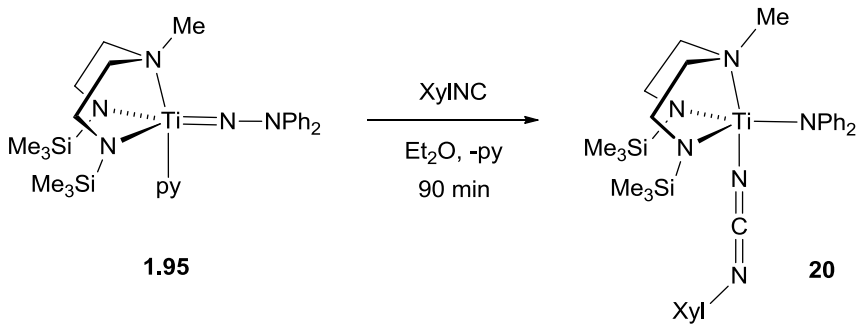

1.95 **20**

Equation 3.4

While the reaction between Ti(N_2N^{Me})($NNPh_2$)(py) (**1.93**) and ^{t}BuNC formed a complex mixture of products, changing to XylNC gave Ti(N_2N^{Me})(NCNXyl)(NPh_2) (**20**, Equation 3.4) in 59 % isolated yield as a single isomer. Mindful of Bergman's reaction of $Cp_2Zr(NNPh_2)$ (**1.153**) with CO,[40] the corresponding reaction of **1.93** was also carried out (1.1 atm., room temperature). Unfortunately this led to a complex mixture of products, possibly as a result of competitive insertion into the Ti–N_{amide} bonds.[88,89]

Isocyanide adducts of d^0 imido complexes have been reported previously.[90,91] This and the calculated stability of the adducts using **B2** (*vide infra*), gave rise to the possibility that mixing the reagents cold (~ -30 °C) and following the reaction at low temperature might allow observation of the isocyanide adduct in this system. However, at low temperatures (< -10 °C), the starting materials were unchanged and, upon warming to -10 °C, they transformed cleanly into **20** and free pyridine, with no intermediates observable by ^{1}H NMR spectroscopy.

Diffraction-quality crystals of Ti(N_2N^{Me})(NCNXyl)(NPh_2) (**20**) were grown from a saturated Et_2O solution at -30 °C. The solid state structure is presented in Figure 3.5 and selected distances and angles are given in Table 3.2. The coordination geometry at Ti(1) is trigonal bipyramidal. The *fac*-coordinated N_2N^{Me} ligand occupies one axial and two equatorial sites as expected, and the associated Ti–N distances are in the usual ranges. The main point of interest is the formation of the diphenylamide and metallated carbodiimide (NCNXyl) ligands, derived *via* N_α–N_β bond cleavage of the Ti=$NNPh_2$ group of **1.93**. The Ti(1)–N(1) bond length is within the usual ranges for titanium amide complexes.

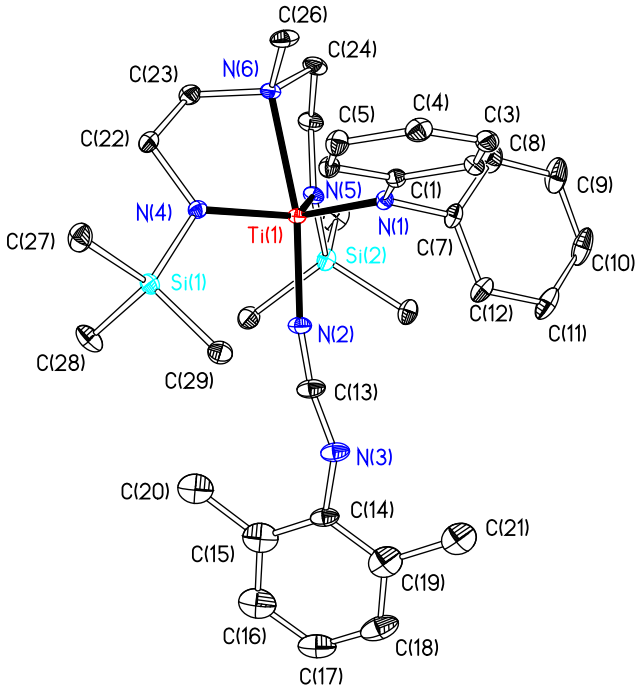

Figure 3.5. Displacement ellipsoid plot (20% probability) of *trans*-Ti(N_2N^{Me})(NCNXyl)(NPh_2) (**20**). H atoms omitted for clarity.

Metallated carbodiimides and related compounds of the type (L)M–NCNR (R = alkyl, aryl, CN, etc.) are well known and a large number have been structurally authenticated.[92] The distances for N(2)–C(13) (1.173(5) Å) and N(3)–C(13) (1.222(7) Å) are within the known ranges (1.01 – 1.28, mean 1.16(3) Å; 1.14 – 1.41, mean 1.29(4) Å, respectively, for 84 examples). The C(13)–N(3)–C(14) angle of 138.9(7) ^{o} is likewise within known ranges (literature range 109 – 141, mean 121(4) ^{o}), although at the longer end. This possibly reflects the bulky nature of the xylyl substituent.

Five Group 4 compounds of the type (L)M–NCNR have been structurally characterised previously. For M = Ti these are Ti(N_2N^{py})(NCN^{t}Bu)(NPh_2) (**1.143**), Cp_2Ti(NCNPh)$_2$ (**3.1**) and [Cp_2Ti(NCNCN)]$_2$(μ–O) (**3.2**);[93,94] for M = Zr they are Gade's Zr($N_2^{*}N^{py}$)(NCN^{t}Bu)(NPh_2) (**1.175**) and Zr($N_2^{*}N^{py}$)(NCN^{t}Bu)(OTf)(py) (**1.180**).[41,95,96] For **1.143**, the Ti–N_{Ph} distance and those within the carbodiimide are very similar to those found in **20** (Ti–N_{Ph} = 1.973(6), N=CN^{t}Bu = 1.172(8), NC=N^{t}Bu = 1.234(10) Å). However, the Ti–N_{CN} distance is slightly longer (2.022(5) Å) due to the nature and position of the pyridyl donor of the ancillary ligand. The Ti–N distances in the titanocene examples are slightly longer (avg. 2.045 Å), as are the C=NR bonds furthest from Ti (avg. 1.272 Å). The C=N distances within the NCN^{t}Bu ligands for the zirconium examples are similar to those in **20** and **1.143**.

Table 3.2. Selected distances (Å) and angles (°) for *trans*-Ti(N_2N^{Me})(NCNXyl)(NPh_2) (**20**).

Ti(1)–N(1)	1.969(3)	N(1)–Ti(1)–N(2)	101.31(15)
Ti(1)–N(2)	1.970(3)	N(1)–Ti(1)–N(4)	113.76(13)
Ti(1)–N(4)	1.926(3)	N(1)–Ti(1)–N(5)	117.25(14)
Ti(1)–N(5)	1.964(3)	N(1)–Ti(1)–N(6)	93.28(13)
Ti(1)–N(6)	2.271(3)	N(4)–Ti(1)–N(5)	123.65(15)
N(2)–C(13)	1.173(5)	Ti(1)–N(1)–C(1)	135.6(3)
N(3)–C(13)	1.222(7)	Ti(1)–N(1)–C(7)	110.1(2)
N(3)–C(14)	1.407(7)	C(1)–N(1)–C(7)	114.3(3)
		Ti(1)–N(2)–C(13)	171.6(4)
		N(2)–C(13)–N(3)	164.7(7)
		C(13)–N(3)–C(14)	138.9(7)

Interestingly, the NCN^{t}Bu ligand in **1.175** is reported to lie exclusively *cis* to the pyridyl of $N_2{}^*N^{py}$, whereas in **1.143** and **1.144** two isomers exist, and in **20** only the isomer with NCNXyl *trans* to the apical donor is observed (Scheme 3.2 and Equation 3.4). It is also worthy of note that the 6-coordinate compound Zr($N_2{}^*N^{py}$)(NCN^{t}Bu)(OTf)(py) (**1.180**) has the NCN^{t}Bu ligand *trans* to pyridyl. The reasons for these coordination site preferences in **1.143**, **1.144** and **20** are addressed in a DFT study of the mechanism of this reaction (*vide infra*).

To understand the mechanism involved in the reductive N_α–N_β cleavage reaction outlined above a DFT study was carried out. The same mechanism as that obtained for the insertion of alkynes into the N_α–N_β bond of **1.93** was considered, with the model isocyanide MeNC replacing the alkyne MeCCMe. All the steps were first computed using the models **A1** and **C1** for complexes **1.93** and **1.97**, respectively (Figure 3.4). However, these smaller models were not able to adequately reproduce the experimental results. Therefore, the more realistic models **B1** and **D1** where the $NNPh_2$ group has been explicitly included in the calculations were used. The

mechanism corresponding to **1.97** is described elsewhere,[43] but a profile illustrating the energies of the various intermediates and transition states is provided (Scheme 3.4) to allow a comparison with the mechanism relating to **1.93** (Scheme 3.3).

With **B1**, the model of **1.93**, both the *cis* and the *trans* pathways for the isocyanide-induced N_α–N_β bond cleavage were considered, even though only the *trans*-carbodiimide isomer of **20** was observed experimentally (Equation 3.4). The energy profiles are shown in Scheme 3.3.

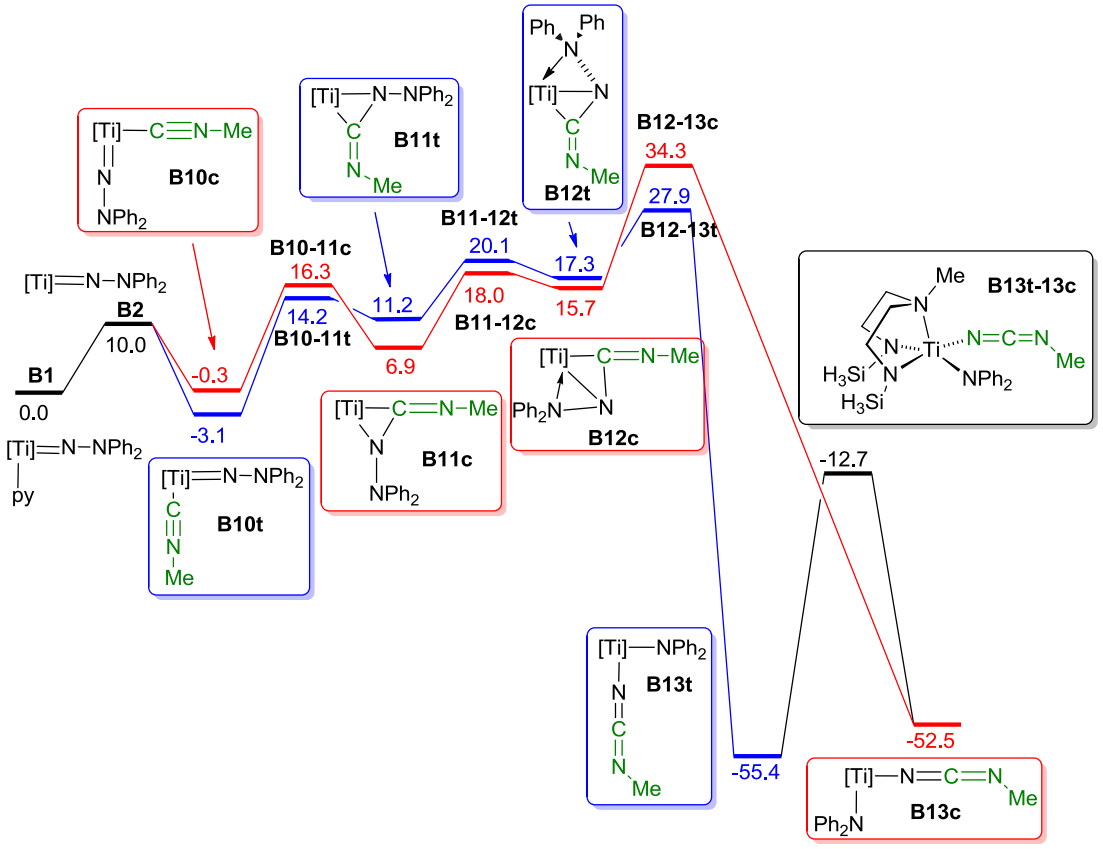

Scheme 3.3. Gibbs free energy (kcal mol^{-1}) profile for MeNC insertion into the N_α–N_β bond of $Ti(N_2^{SiH3}N^{Me})(NNPh_2)(py)$ (**B1**) along *cis* (red) and *trans* (blue) pathways.

Decoordination of pyridine to form **B2** is endergonic with a ΔG value of 10.0 kcal mol^{-1}. The formation of a vacant site on Ti allows coordination of MeNC either *trans* to the apical amine donor (**B10t**) or, after isomerisation of the hydrazide ligand, in the *cis* position (**B10c**). In each case the isocyanide is κ^1-C coordinated to the metal centre. Formation of the MeNC adduct is exergonic for the *trans* isomer ((ΔG = -3.1

kcal mol^{-1}, **B10t**) and almost thermoneutral for the *cis* isomer (ΔG = -0.3 kcal mol^{-1}, **B10c**) compared to **B1** and free isocyanide.

The subsequent step is the nucleophilic addition of N_α to the isocyanide carbon, effectively a [2+1] coupling of MeNC across the Ti=N_α double bond of **B2**, leading to intermediates **B11t** and **B11c**. This is endergonic for both *cis* and *trans* isomers (ΔG = +14.3 from **B10t** and +7.2 kcal mol^{-1} from **B10c**) proceeding through similar free energy barriers (**B10-11t**, $\Delta G^{\#}$ = 17.3 kcal mol^{-1}; **B10-11c**, $\Delta G^{\#}$ = 16.6 kcal mol^{-1}). This is analogous to the [2+2] cycloaddition reactions between **1.93**, **1.97** and alkynes.

The key step facilitating N_α–N_β bond cleavage, as seen in the insertion mechanism of **1.93** and **1.97** with alkynes,[16] is N_β chelation. Unlike in the related model compound **D1** (Scheme 3.4), where $N_\beta Ph_2$ chelation and therefore N_α–N_β bond cleavage is only possible for the *cis* isomer, with **B1** it is possible from both orientations through transition states **B11-12t** and **B11-12c** forming the intermediates **B12t** and **B12c**. The processes are endergonic by +6.1 and +8.8 kcal mol^{-1} respectively. Consequently, N_α–N_β cleavage can then occur *via* the TSs **B12-13t** and **B12-13c**, in which the N_α–N_β bond is broken and a new C–N_α π bond is formed in a concerted way (e.g. for **B12-13t**; N_α–N_β = 1.77 Å and C–N_α = 1.34 Å). This step is strongly exergonic for both isomers making the overall process thermodynamically favourable by 55.4 kcal mol^{-1} for **B13t** and 52.5 kcal mol^{-1} for **B13c**. Hydrazides with the N_β atom donating to the metal centre, in an analogous way to intermediates **B13t** and **B13c**, have been seen from the reactions of Ti(N_2N^{py})($NNPh_2$)(py) (**1.97**) with B(Ar^{F5})$_3$ and Cp*Ti{MeC(N^iPr)$_2$}(NNR_2) (R = Ph (**1.104**) or Me (**1.106**)) with a range of silanes.[43,97]

Note that the highest point (namely TS **B12-13t**) on the reaction pathway required to form **B13t**, which has the carbodiimide *trans* to the NMe donor, is 6.4 kcal mol^{-1} lower than that for the *cis* isomer (TS **B12-13c**) making **B13t** the kinetic as well as thermodynamic product.

Although the *trans* isomer **B13t** is both thermodynamically and kinetically preferred according to DFT, the *cis* isomer **B13c** is only 2.9 kcal mol^{-1} higher in energy. This difference in energy is effectively the same as that between **D13t** and **D13c** (2.5 kcal mol^{-1}, Scheme 3.4) for which the experimental systems exist as both *cis* and *trans* isomers. However, whereas the TS for interconverting **D13t** and **D13c** lies only 24.1

kcal mol^{-1} above the former, the corresponding square-based pyramidal TS (**B13t-13c**) connecting **B13t** and **B13c** is 42.7 kcal mol^{-1} above **B13t**. This is clearly kinetically inaccessible and so the observation of only the single (*trans*) isomer of **20** in Equation 3.4 is attributed to kinetic control both in terms of its initial formation and inability to equilibrate with the corresponding *cis* isomer.

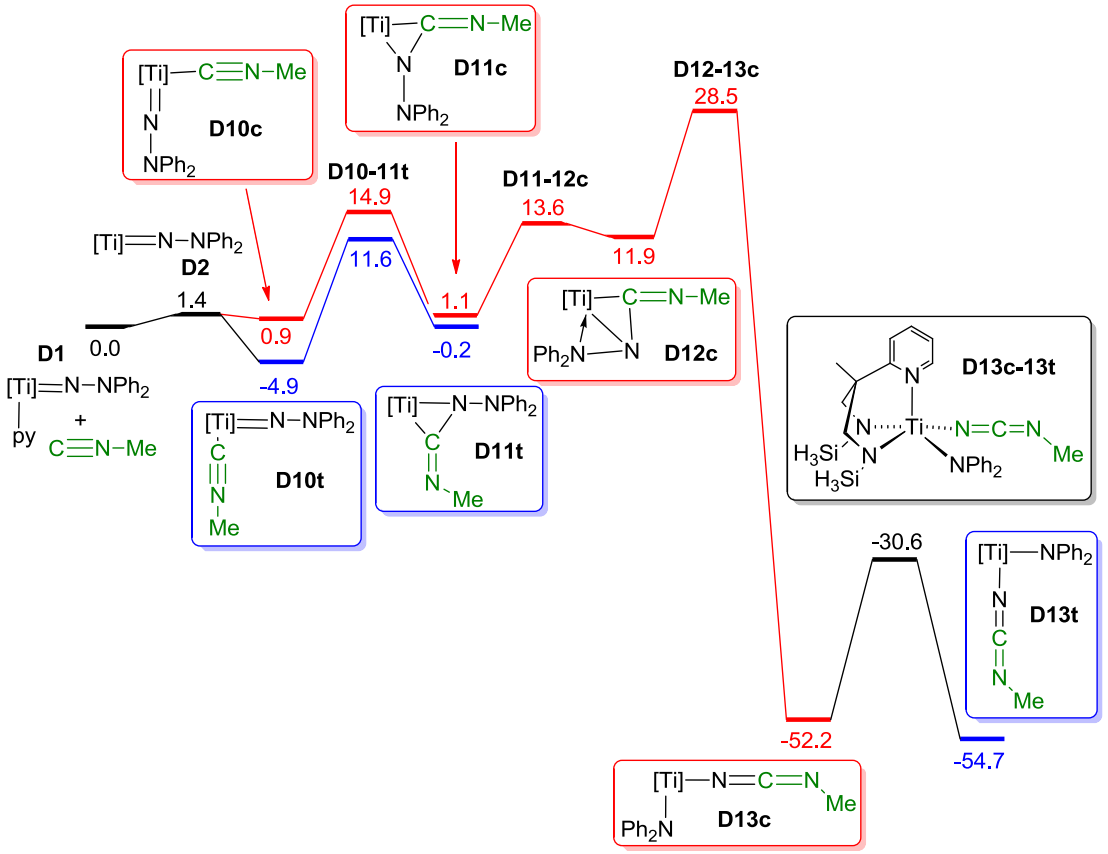

Scheme 3.4. Gibbs free energy (kcal mol^{-1}) profile for MeNC insertion into the N_α–N_β bond of Ti($N_2^{SiH_3}N^{py}$)($NNPh_2$)(py) (**D1**) along *cis* (red) and *trans* (blue) pathways.

The high energy of **B13t-13c** relative to **B13t** is due to the greater required extent of distortion of the Ti($N_2^{SiH_3}N^{Me}$) moiety in this TS compared to that of Ti($N_2^{SiH_3}N^{py}$) in **D13c-13t**. Whereas the N_{amide}–Ti–N_{amide} angle decreases by only 8 º from **D13c** to **D13c-13t**, in the case of **B13t-13c** this angle is required to compress by 23 º from 117 º in **B13t** to 94 º in the TS. This preference of the N_2N^{Me}-supported systems (chain-like diamide-amine topology) for more open N_{amide}–Ti–N_{amide} angles compared to their N_2N^{py}-supported analogues (podand-like topology) can be seen experimentally in *trans*-Ti(N_2N^{py})(NCN^{t}Bu)(NPh_2) (**1.143**) and *trans*-Ti(N_2N^{Me})(NCNXyl)(NPh_2) (**20**) (N(4)–Ti(1)–N(5) = 104.3(2) and 123.65(15) º, respectively) and also the

corresponding hydrazide compounds themselves (Ti(N_2N^{py})($NNPh_2$)(py) (**1.97**), N_{amide}–Ti–N_{amide} = 106.64(7) º; Ti(N_2N^{Me})($NNPh_2$)(py) (**1.93**), N_{amide}–Ti–N_{amide} = 130.5(2) º).[15]

Finally, calculations have also been performed on Gade's system, Zr($N_2{}^*N^{py}$)(NCN^tBu)(NPh_2) (**1.175**) which is reported to exist only as the *cis* isomer (Scheme 3.2). As with the titanium compounds, the energies of the model systems *trans*- and *cis*-Zr($N_2{}^{SiH_3}N^{py}$)(NPh_2)(NCNMe) (**D13t_Zr** and **D13c_Zr**) differ by only 3.1 kcal mol^{-1}. Again the *trans* isomer is more thermodynamically stable, however, by analogy with Scheme 3.4, it is clear that it must be formed *via* the kinetically favoured *cis* isomer, the only one for which $N_\beta Ph_2$ chelation is possible. The relative energy of the square-based pyramidal TS (**D13c-13t_Zr**) linking **D13c_Zr** and **D13t_Zr** is comparable to that of the titanium system, with a N_{amide}–Zr–N_{amide} angle of 91.4 º. However, although the full experimental system has not been modelled explicitly with the bulky $N_2{}^*N^{py}$ and NCN^tBu groups, it seems very likely that the presence of the considerably bulkier –$SiMe_2{}^tBu$ amide substituents in **1.175** (as opposed to the $SiMe_3$ moieties in **1.143** and **1.144**) leads to significantly higher steric repulsions in the real TS. Thus **1.175** appears to be a kinetic product which is unable to equilibrate with the more favoured *trans* isomer.

3.4 Reactions with CO_2, isocyanates and related substrates

The reactions of Group 4 imides with CO_2, isocyanates and other heterocumulenes are well established.[2,4,6] The corresponding hydrazide chemistry has not yet been explored to any significant extent. The first such reactions were for Ti($NNPh_2$)(Me_4taa) (**1.82**) giving the [2+2] cycloaddition products Ti(Me_4taa){$N(NPh_2)C(O)O$} and Ti(Me_4taa){$N(NPh_2)C(O)NTol$} (**1.83**) with CO_2 and TolNCO, respectively.[31] The ureate-type (i.e. semicarbazide) ligand formed with TolNCO was *N,N′*-coordinated to Ti. A similar compound was proposed as an intermediate in the reactions of Ti(Me_2Calix)($NNMe_2$) (**1.123**) with ^tBuNCO.[32] Reactions of Cp*Ti{$MeC(N^iPr)_2$}(NNR_2) (R = Ph (**1.104**) or Me (**1.106**)) with CO_2 and TolNCO also gave [2+2] cycloaddition products. Further equivalents of CO_2 could insert giving Ti=N_α bond cleavage (Scheme 1.9, Chapter One).[38,39] The reaction with TolNCO formed an {$N(NPh_2)C(NTol)O$} moiety which was *N,O*-bound to Ti. Gade recently reported the cycloaddition reactions of other half-sandwich titanium hydrazides with PhNCE (E = O or S).[35] In these products a mixture of both *N,N′*- and

N,*E*- bound ureate and thioureate products were formed (Scheme 1.11, Chapter One). Work carried out in the Group on the related system $Ti(N_2O)(NNPh_2)(py)_2$ (**1.150**), subsequent to that described in this Thesis, also formed cycloaddition products with Ar′NCE (Ar′ = 2,6-$C_6H_4{}^iPr_2$, E = O, S) forming an *N*,*N′*-bound ureate and *N*,*E*-thioureate respectively. To gain further insight into this aspect of hydrazide chemistry, the reactivity of $Ti(N_2N^{Me})(NNPh_2)(py)$ (**1.93**) was investigated with CO_2 and certain isocyanates and related substrates.

Unfortunately $Ti(N_2N^{Me})(NNPh_2)(py)$ (**1.93**) gave complicated mixtures of products with CO_2 and a range of isocyanates, RNCO (R = Et, Ph, ^{t}Bu), possibly due to competition with Ti–N_{amide} bond insertion reactions of the supporting ligands, as has been noted elsewhere.[88] However, the reaction of **1.93** with the bulky 2,6-di*iso*propylphenyl isochalcocyanates Ar′NCO, Ar′NCS, and Ar′NCSe [98] in Et_2O at room temperature gave the [2+2] cycloaddition products $Ti(N_2N^{Me})\{N(NPh_2)C(NAr')O\}(py)$ (**21**), $Ti(N_2N^{Me})\{N(NPh_2)C(NAr')S\}$ (**22**) and $Ti(N_2N^{Me})\{N(NPh_2)C(NAr')Se\}$ (**23**), respectively, in 51 – 65 % isolated yield (Scheme 3.5; Ar′ = 2,6-$C_6H_3{}^iPr_2$).

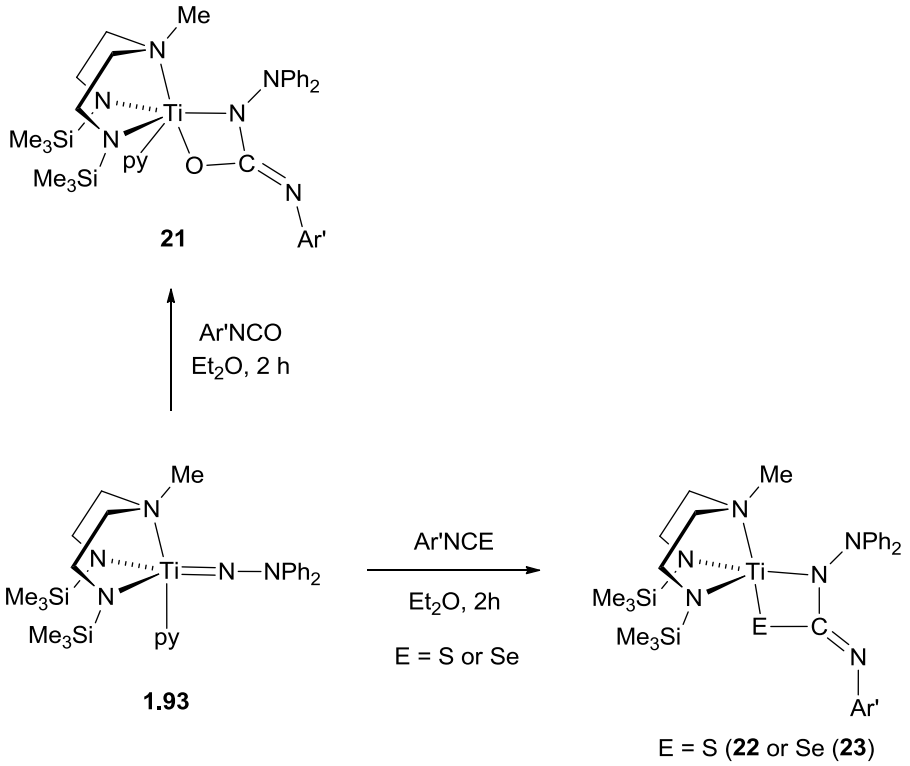

Scheme 3.5. Reactions of $Ti(N_2N^{Me})(NNPh_2)(py)$ (**1.93**) with Ar′NCE (E = O, S or Se).

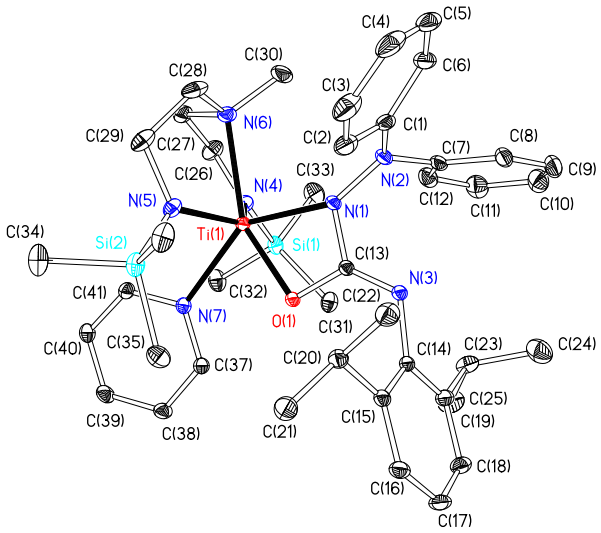

Figure 3.6. Displacement ellipsoid plot (20 % probability) of Ti(N_2N^{Me}){N(NPh_2)C(NAr′)O}(py) (**21**). H atoms omitted for clarity.

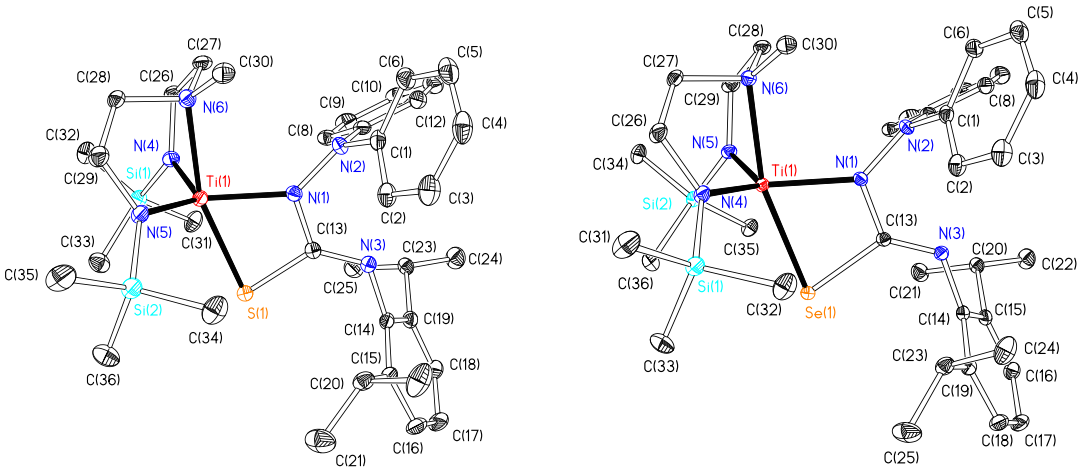

(a) **(b)**

Figure 3.7. Displacement ellipsoid plots (25% probability) of (a) Ti(N_2N^{Me}){N(NPh_2)C(NAr′)S} (**22**) and (b) Ti(N_2N^{Me}){N(NPh_2)C(NAr′)Se} (**23**). H atoms omitted for clarity.

All three compounds in this homologous series have been crystallographically characterised. The molecular structure of **21** is shown in Figure 3.6 and those of **22** and **23** are given in Figure 3.7. Selected distances and angles are compared in Table 3.3. NMR spectroscopy and other data are fully consistent with the solid state

structures. When the reactions were followed by ^{1}H NMR spectroscopy in C_6D_6, only a single isomer was observed in each case. Compounds **21** and **22** are stable in solution for several days, whereas **23** degrades quickly with $t_{1/2}$ ~ 2 h at room temperature. Compounds **21**, **22** and **23** constitute the first such series for any transition metal imido or hydrazido compound.

Table 3.3. Selected distances (Å) and angles (^{o}) for Ti(N_2N^{Me}){N(NPh_2)C(NAr′)O}(py) (**21**), Ti(N_2N^{Me}){N(NPh_2)C(NAr′)S} (**22**) and Ti(N_2N^{Me}){N(NPh_2)C(NAr′)Se} (**23**).

Parameter	**21**	**22**	**23**
Ti(1)–N(1)	2.0719(15)	2.023(3)	2.0258(15)
Ti(1)–N(4)	1.9542(17)	1.902(3)	1.9221(16)
Ti(1)–N(5)	1.9609(17)	1.923(3)	1.9124(16)
Ti(1)–N(6)	2.3023(16)	2.227(3)	2.2268(16)
Ti(1)–N(7)	2.2670(16)	–	–
Ti(1)–E(1)[a]	1.9637(13)	2.3858(10)	2.4974(3)
N(1)–C(13)	1.371(2)	1.391(4)	1.389(2)
E(1)–C(13)[a]	1.351(2)	1.794(3)	1.9569(17)
C(13)–N(3)	1.277(2)	1.274(4)	1.262(2)
N(1)–Ti(1)–N(4)	109.38(7)	114.37(11)	123.58(7)
N(1)–Ti(1)–N(5)	109.12(7)	123.35(11)	114.47(6)
N(1)–Ti(1)–E(1)[a]	64.28(5)	70.54(8)	71.97(4)
N(6)–Ti(1)–E(1)[a]	150.46(6)	162.23(7)	164.57(4)
Ti(1)–N(1)–C(13)	92.93(11)	103.38(19)	106.70(11)
Ti(1)–E(1)–C(13)[a]	98.46(10)	79.35(11)	75.68(5)
N(1)–C(13)–E(1)	128.50(16)	106.5(2)	105.49(12)

[a] E = O, S or Se for **21**, **22** or **23**, respectively.

All three compounds contain a κ^3N coordinated N_2N^{Me} and a κ^2N,E bound {N(NPh_2)C(NAr′)E} ligand (E = O, S or Se) formed by the [2+2] cycloaddition of

Ar′NCE to the Ti=NNPh$_2$ functional group of **1.93**. Compound **21** also contains an additional pyridine ligand from the starting hydrazide which is absent in **22** and **23**, both in the isolated products and in the NMR tube scale experiments. The presence of pyridine only in **21** is attributed to the higher electronegativity and smaller radius of O compared to those of S and Se. Although the room temperature NMR data for **21** were consistent with the pyridine remaining coordinated in solution, on warming the sample to *ca* 60 ^{o}C the pyridine resonances moved close to those of free pyridine in toluene-d_8 (Figure 3.8). This suggests that **21** is close in free energy to its base-free analogue Ti(N$_2$N^{Me}){N(NPh$_2$)C(NAr′)O}, which appears to exist in a dynamic equilibrium with **21** under entropically favoured conditions.

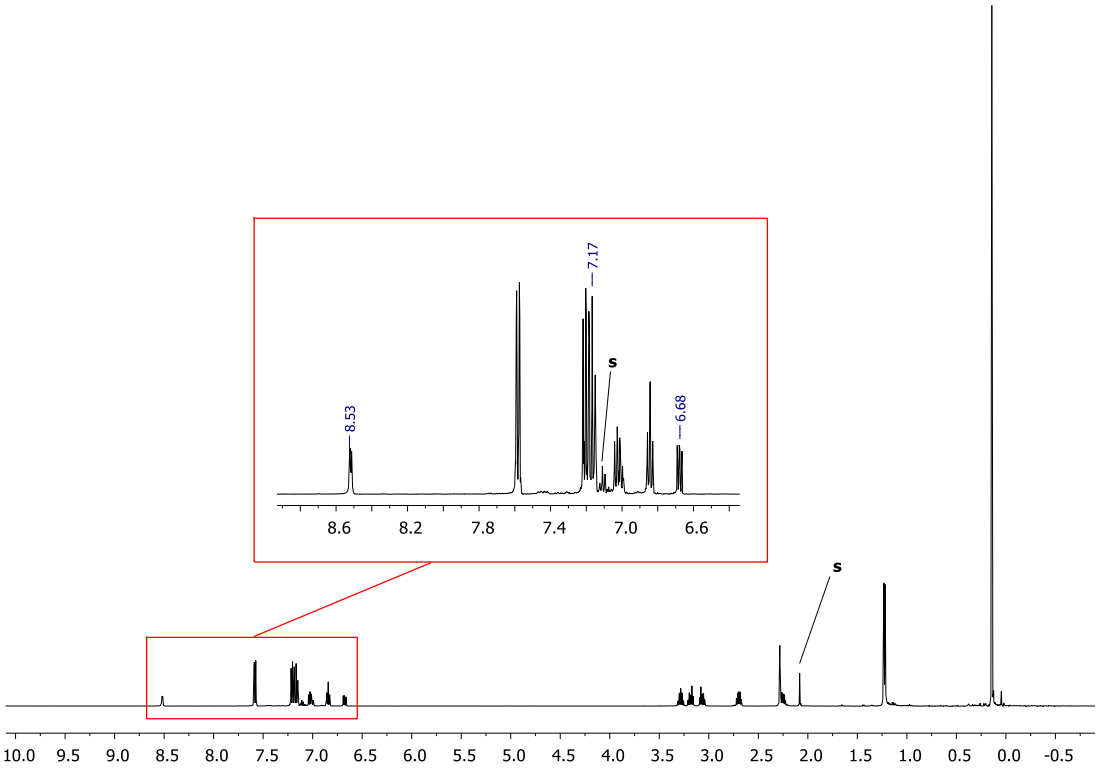

Figure 3.8. ^{1}H NMR spectrum (499.9 MHz, 333 K) of Ti(N$_2$N^{Me}){N(NPh$_2$)C(NAr′)O}(py) (**21**), in toluene-d_8, with an expansion of the aromatic region. Labelled resonances correspond to pyridine. (‘s’ denotes residual protio solvent).

The coordination geometry at Ti(1) for **22** and **23** is distorted trigonal bipyramidal, with the N(6)–Ti(1)–E(1) angles (162.23(7) and 164.57(4) ^{o} for **22** and **23**, respectively) being constrained by the 4-membered ring formed by Ti(1), N(1), C(13) and E(1). The equatorial nitrogens N(1), N(4) and N(5) are effectively coplanar (sums

of angles subtended at Ti(1) = 356.1(3) and 356.4(3) ^{o} for **22** and **23**, respectively). The geometry at Ti(1) in **21** is distorted octahedral due to the additional pyridine. For all three compounds the Ti–N bond lengths to the N_2N^{Me} ligand are within the known ranges, with those for **21** being systematically longer due to the higher coordination number. The Ti(1)–N(1) bond lengths are within the range so far found for other [2+2] cycloaddition products of $Ti{=}NNPh_2$ (4 examples, 1.974(2) – 2.119(2) Å),[16,33,35] with that for **21** being significantly longer.

The main point of interest in **21** – **23** are the four-membered titanium-ureate moieties $Ti\{N(NPh_2)C(NAr')E\}$ which form a unique series in metal-nitrogen multiple bond chemistry. Structurally characterised Group 4 ureates (E = O) derived from imido complexes are fairly well-established.[2,4,6,92] As stated, both *N,N′*- and *N,O*-bound systems derived from titanium hydrazides have been reported.[31,35,38,39,99] Structurally authenticated thioureates are in general much less common for the earlier transition metals with only two examples to date for Group 4, one being the afore-mentioned Gade compound, the other made subsequently in this research group by reacting the related hydrazide $Ti(N_2O)(NNPh_2)(py)_2$ (**1.150**) with Ar′NCS (Ar′ = 2,6-$C_6H_3{}^{i}Pr_2$) forming $Ti(N_2O)\{N(NPh_2)C(NAr')S\}(py)$ (**3.3**, Figure 3.9).[99]

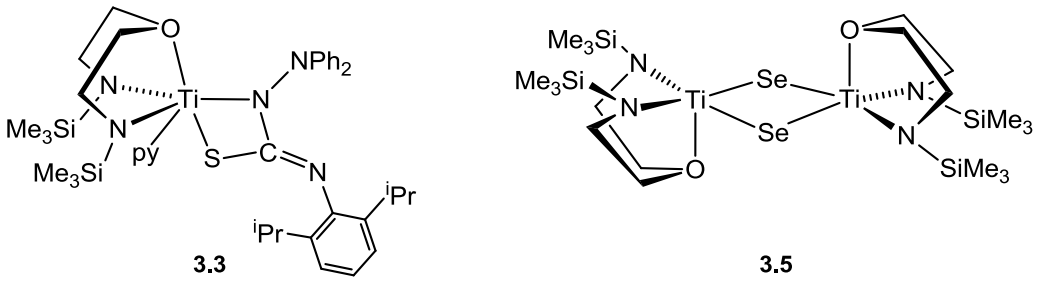

Figure 3.9. $Ti(N_2O)\{N(NPh_2)C(NAr')S\}(py)$ (**3.3**) and $[Ti(N_2O)Se]_2$ (**3.5**).

The stability of these compounds (and of **22**) is interesting because in the related titanium imido chemistry, thioureate ligands (and their thiocarbamate analogues) have a pronounced tendency to eliminate the carbodiimide (or isothiocyanate) to form sulphido dimers.[100,101] No selenoureate complex has been structurally characterised for the early transition metals. Henderson's $Pt\{N(Ph)C(NPh)Se\}(PPh_3)_2$ (**3.4**, formed from PhNHC(Se)NHPh and *cis*-$PtCl_2(PPh)_2$) is the only such example to date for any transition metal.[102] However, considering the absence of carbodiimide elimination from compounds **21** - **23**, it is interesting to note that when **1.150**, which forms a

stable cycloaddition product with Ar′NCS, is reacted with Ar′NCSe it does eliminate the carbodiimide fragment leaving a selenium bridged dimer (**3.5**, Figure 3.9).

The increase in Ti(1)–E(1) and C(13)–E(1) (E = O, S, Se) bond distances from **21** to **23** follows the expected trend with increasing atomic radius.[103] Along this series the Ti(1)–E(1)–C(13) angle becomes progressively more acute and the Ti(1)–N(1)–C(13) more obtuse. The distances within the Ti{N(NPh$_2$)C(NAr′)E} (E = O, S) metallacycles are similar to the previous examples mentioned above. For **23** the Se(1)–C(13) distance is identical within error to that in **3.4**. The Ti(1)–Se(1) distance of 2.4974(3) Å is within the expected range for Ti–Se single bonds (mean 2.57(10) Å; range 2.369 – 2.796 Å).[92] Overall, the structural trends within this series of compounds follow the expected pattern. As mentioned, the stabilities of these species appear to be slightly unusual compared to the imido-derived analogues described elsewhere. Further examples will be required, however, before firm conclusions can be drawn.

In principle, the {N(NPh$_2$)C(NAr′)E} ligands in **21** – **23** could be bound in either an *N,E*- (as found experimentally) or *N,N′*- fashion. Consistent with this, Gade reported that mixtures of isomeric metallacycles are formed in the reactions of PhNCO or PhNCS and certain half-sandwich titanium hydrazides (Scheme 1.11, Chapter One).[35] Prior to this Mountford *et al*. have shown that the [2+2] cycloaddition product formed between Cp$_2$Ti(NNPh$_2$)(py) (**1.103**) and ^{t}BuCP was in fact not the isomer favoured on electronic grounds.[33] Related results have been found in imido chemistry where steric effects have overcome electronic preferences.[31,100]

To test the basic electronic preferences of **1.93** in the reactions with isocyanates the two isomeric products for the reaction of Ti(N$_2^{SiH_3}$N^{Me})(NNMe$_2$)(py) (**A1**) with MeNCO were calculated (Figure 3.10). These are Ti(N$_2^{SiH_3}$N^{Me}){N(NMe$_2$)C(NMe)O} (**A14_O**; *N,O*-bound) and Ti(N$_2^{SiH_3}$N^{Me}){N(NMe$_2$)C(O)NMe)} (**A15_O**; *N,N′*-bound). The formation of **A14_O** from **A1** and MeNCO was significantly exoergic with ΔG = -10.4 kcal mol^{-1}. However, **A15_O** was -4.0 kcal mol^{-1} more stable than **A14_O** indicating that the former is the electronically preferred base-free isomer. Interestingly, while the ΔE of formation of Ti(N$_2^{SiH_3}$N^{Me}){N(NMe$_2$)C(NMe)O}(py) (**A16**, a model for the real system **21**) from **A14_O** is -9.5 kcal mol^{-1}, the corresponding ΔG is +4.3 kcal mol^{-1}. These results are

consistent with the experimental observation that pyridine is readily dissociated from **21** in solution. Note that entropy changes (ΔS) in the gas phase are overestimated with respect to those expected in solution,[104] and therefore the associated ΔGs always disfavour the association of molecules.

To probe for steric effects in the base-free cycloaddition products calculations of the corresponding products between **A1** and XylNCO, namely **14_O_Xyl** and **A15_O_Xyl** were performed. Here the xylyl groups better model the 2,6-$C_6H_3{}^iPr_2$ substituents used in the experimental systems. With these models the steric repulsion between the xylyl groups and the amide SiH_3 substituents made isomer **A15_O_Xyl** 5.3 kcal mol^{-1} less stable than **A14_O_Xyl**.

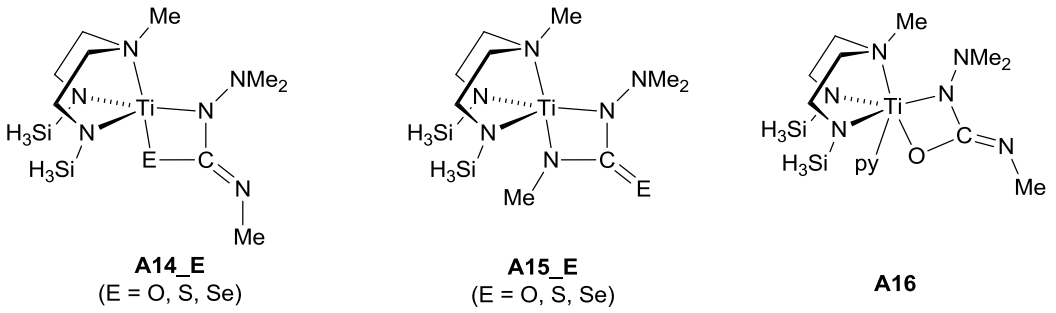

Figure 3.10. Computational models for the products formed by the reaction between $Ti(N_2N^{Me})(NNPh_2)(py)$ (**1.93**) and Ar′NCE (E = O, S or Se).

Using MeNCE (E = S or Se) in the calculations in place of MeNCO leads to the corresponding products **A14_S**, **A15_S**, **A14_Se** and **A15_Se** (Figure 3.10). The calculations gave similar results to those with X = O. In both cases the *N*,*N*′-bound isomer is the most stable (E = S, ΔΔG = -1.7 kcal mol^{-1}; E = Se, ΔΔG = -1.3 kcal mol^{-1}) with the electronic preference for **A15_E** decreasing in the sequence E = O > S > Se. Therefore, in the experimental sulfur and selenium systems **22** and **23** the formation of the *N*,*E*-bound isomers is due to both steric preferences for this isomer and a decreasing electronic preference for the *N*,*N*′-bound alternative. The results are consistent with recent experimental and computational results reported by Gade *et al.*[35]

Experimentally, the [2+2] cycloaddition products **21** – **23** do not undergo $Ti{=}N_\alpha$ or $N_\alpha{-}N_\beta$ cleavage/insertion processes. DFT studies showed that formation of the NMe_2 chelated species **A17** (Scheme 3.6), analogous to the key intermediates in the $N_\alpha{-}N_\beta$ cleavage reactions with alkynes[16] and isocyanides, is thermodynamically accessible

with respect to **A14_O** (ΔG = 8.2 kcal mol^{-1}). However, subsequent N_α–N_β cleavage to form **A18** is thermodynamically unfavourable (ΔG = 47.5 kcal mol^{-1} with respect to **A14_O** and 43.2 kcal mol^{-1} with respect to **A16**) and no TSs between **A17** and **A18** could be found. Likewise, a reverse cyclisation reaction (*cf.* **A4_R** → **A5_R** in Scheme 3.1) to form zwitterionic **A19** is also mechanistically and thermodynamically forbidden.

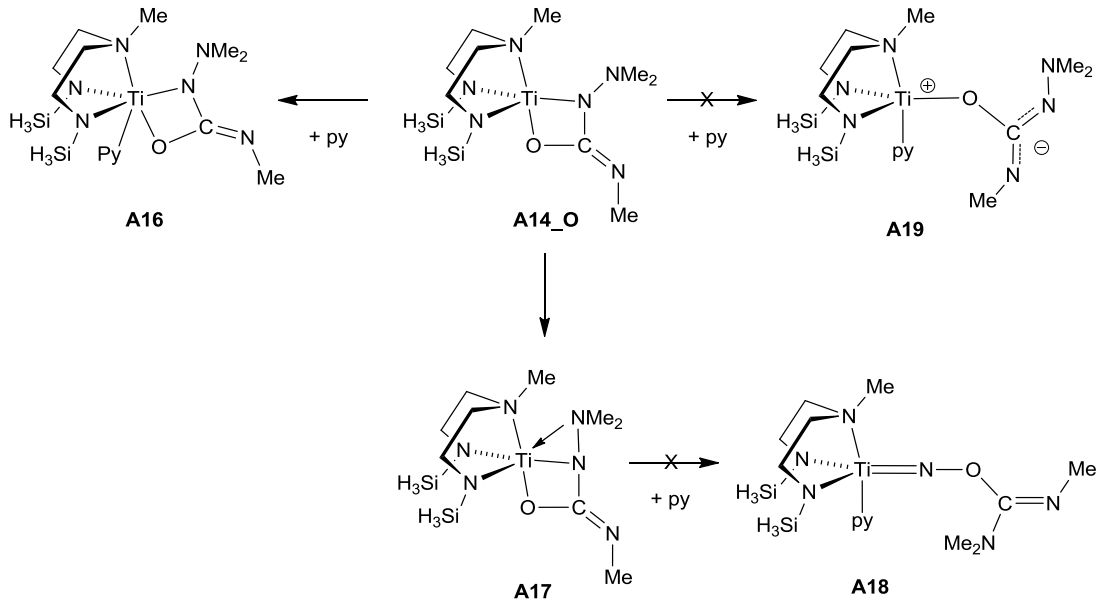

Scheme 3.6. Reaction of **A14_O** with py and DFT attempts to find Ti–N_α and N_α–N_β insertion reactions with MeNCO.

3.5 Summary

This Chapter has demonstrated the wide scope of titanium hydrazido(2-) reactivity; namely Ti=N_α insertion with organic nitriles, N_α–N_β bond cleavage with isocyanides and cycloaddition at Ti=N_α with isochalcocyanates. These reaction types complement those described in Chapter Two with alkynes. The isocyanide cleavage reaction was previously reported by Gade for zirconium[41] and is related to the CO-induced N_α–N_β bond cleavage reactions first described by Bergman.[40] Scheme 3.7 compares the key features of these three types of reaction, along with that for alkyne insertion into the N_α–N_β bond, starting from a generic terminal hydrazide depicted as [Ti]=NNR_2 (**I**).

As described previously, alkyne insertion into N_α–N_β to give a vinyl imide (**I** → **IV**) begins with [2+2] addition for form a metallacycle (**II**, sometimes isolated and/or

observed). A key step is N_β atom coordination (**III**) which facilitates simultaneous Ti–NR_2 and C–N_α bond formation. Isocyanide-induced N_α–N_β bond cleavage can be seen as another facet of this cycloaddition - N_β coordination - C–N_α bond formation sequence (**I** → **VII** → **VIII** → **IX**). Although N_β coordinated intermediates of the type **III** and **VIII** have not been observed experimentally, six-coordinate structurally related species have been formed by the reaction of Ti(N_2N^{py})($NNPh_2$)(py) (**1.97**) or Zr($N_2{}^*N^{py}$)($NNPh_2$)(py) (**1.159**) with B(Ar^{F5})$_3$.[14,43]

Nitrile insertion into Ti=N_α to form a hydrazonamide (**I** → **VI**) is also related to the alkyne and isocyanide chemistry, beginning again with a cycloaddition reaction (*via* **V**). However, although N_β coordination is energetically accessible from **V**, this species cannot proceed further (i.e. it cannot mimic the **III** → **IV** N_α migration step) because of the stronger Ti–N bond formed to the nitrile N and the unfavourable N–N_α bond that would need to form. Thus **V** is unable to cleave N_α–N_β but is nonetheless unstable, undergoing a retrocycloaddition to form terminal hydrazonamides. The ring-opened species **VI** is favoured by electron-withdrawing groups which stabilise the negative charge at Ti=N–C. With isocyanates (and related R′CNE substrates), cycloaddition to Ti=NNR_2 also readily occurs (**I** → **X**). However, neither N_α migration nor reverse cycloaddition (ring-opening) pathways are now able to operate, and compounds of the type **X** could be isolated for E = O, S or Se. Stable cycloaddition products of titanium hydrazides with isocyanates and other heterocumulenes have been reported previously.[31,35,38]

Overall, Scheme 3.7 exemplifies the principle reactivity paradigms of terminal Group 4 hydrazides. Thus all M=N_α and N_α–N_β bond insertion or cleavage processes, including so-called "metallanitrene equivalent" reactivity,[41] probably begin by initial coupling of a substrate with M=N_α (or N_α itself) of an intact M=N–NR_2 linkage. The reactions that follow from this initial step are then governed by the balance of affinities of the N_α atom for the metal or the substrate. The N_α–N_β bond cleavage/insertion processes are all likely to be facilitated by M–N_β bond formation leading up to and during the key bond-making/breaking steps.

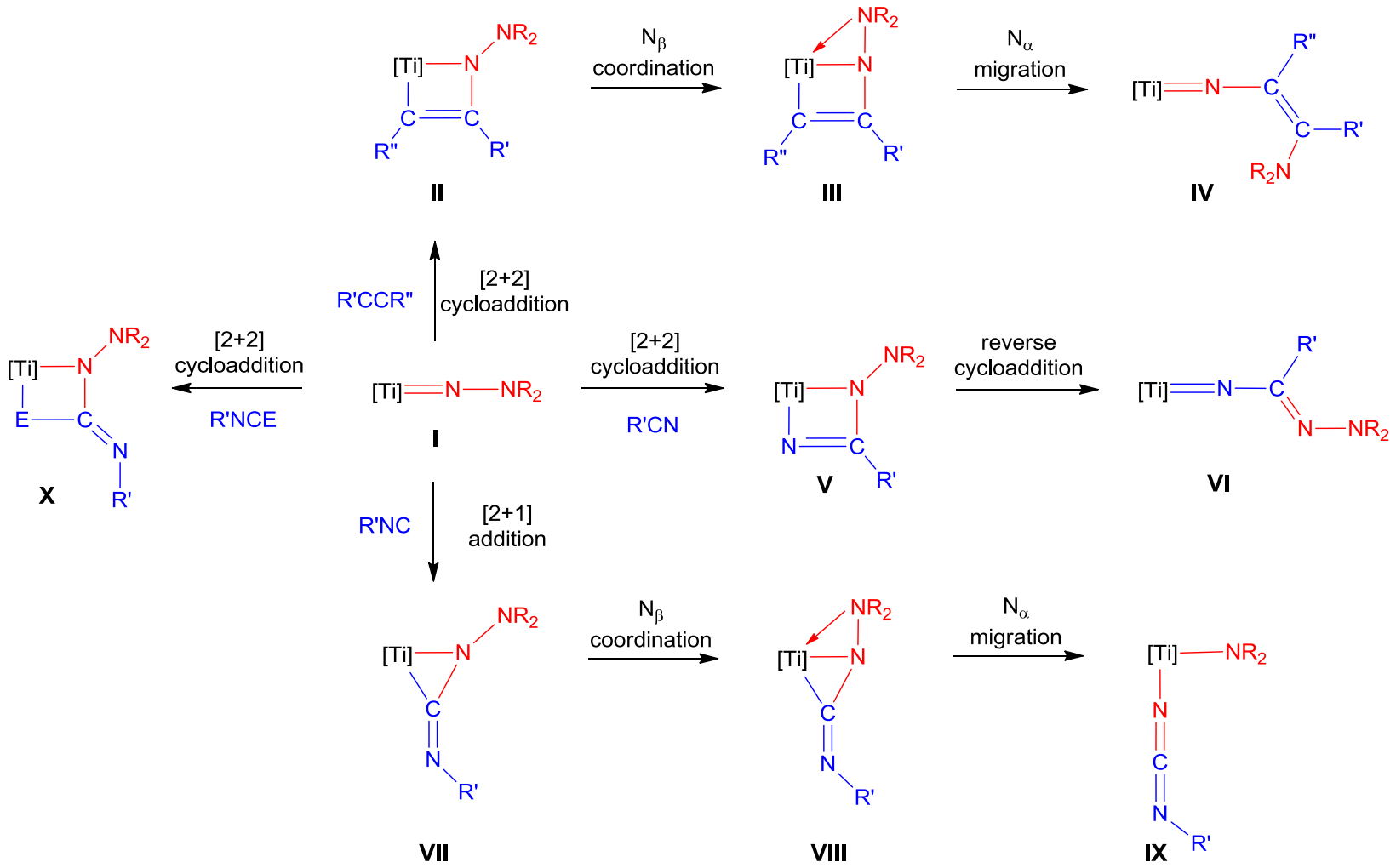

Scheme 3.7. Unifying summary of the reactions of Ti=NNR$_2$ functional groups with alkynes, nitriles, isocyanides and isocyanates.

3.6 References

1. Wigley, D. E.; *Prog. Inorg. Chem.* **1994**, *42*, 239.
2. Mountford, P.; *Chem. Commun.* **1997**, 2127.
3. Gade, L. H.; Mountford, P.; *Coord. Chem. Rev.* **2001**, *216-217*, 65.
4. Duncan, A. P.; Bergman, R. G.; *Chem. Rec.* **2002**, *2*, 431.
5. Odom, A. L.; *Dalton Trans.* **2005**, 225.
6. Hazari, N.; Mountford, P.; *Acc. Chem. Res.* **2005**, *38*, 839.
7. Bolton, P. D.; Mountford, P.; *Adv. Synth. Catal.* **2005**, *347*, 355.
8. Fout, A. R.; Kilgore, U. J.; Mindiola, D. J.; *Chem. Eur. J.* **2007**, *13*, 9428.
9. Banerjee, S.; Odom, A. L.; *Organometallics* **2006**, *25*, 3099.
10. Thorman, J. L.; Woo, L. K.; *Inorg. Chem.* **2000**, *39*, 1301.
11. Kahlal, S.; Saillard, J.-Y.; Hamon, J.-R.; Manzur, C.; Carrillo, D.; *J. Chem. Soc., Dalton Trans.* **1998**, 1229.
12. Parsons, T. B.; Hazari, N.; Cowley, A. R.; Green, J. C.; Mountford, P.; *Inorg. Chem.* **2005**, *44*, 8442.
13. Patel, S.; Li, Y.; Odom, A. L.; *Inorg. Chem.* **2007**, *46*, 6373.
14. Herrmann, H.; Fillol, J. L.; Gehrmann, T.; Enders, M.; Wadepohl, H.; Gade, L. H.; *Chem. Eur. J.* **2008**, *14*, 8131.
15. Selby, J. D.; Manley, C. D.; Schwarz, A. D.; Clot, E.; Mountford, P.; *Organometallics* **2008**, *27*, 6479.
16. Schofield, A. D.; Nova, A.; Selby, J. D.; Manley, C. D.; Schwarz, A. D.; Clot, E.; Mountford, P.; *J. Am. Chem. Soc.* **2010**, *132*, 10484.
17. Johnson, B. F. G.; Haymore, B. L.; Dilworth, J. D.: Comprehensive Coordination Chemistry. Wilkinson, G., Gillard, R. D., McCleverty, J. A., Eds.; Pergamon Press: Oxford, 1987; Vol. 2; pp 100.
18. Nugent, W. A.; Mayer, J. M.; *Metal-Ligand Multiple Bonds*; Wiley-Interscience: New York, 1988.
19. Mindiola, D. J.; *Angew. Chem. Int. Ed.* **2008**, *47*, 1557.
20. Fryzuk, M. D.; *Chem. Rec.* **2003**, *3*, 2.
21. MacKay, B. A.; Fryzuk, M. D.; *Chem. Rev.* **2004**, *104*, 385.
22. Kozak, C. M.; Mountford, P.; *Angew. Chem. Int. Ed.* **2004**, *43*, 1186
23. Yandulov, D. V.; Schrock, R. R.; *Science* **2003**, 76.
24. Schrock, R. R.; *Acc. Chem. Res.* **2005**, *38*, 955.

25. Hidai, M.; *Coord. Chem. Rev.* **1999**, *185-186*, 99.
26. Ohki, Y.; Fryzuk, M. D.; *Angew. Chem. Int. Ed.* **2007**, *46*, 3180.
27. Stephan, G. C.; Sivasankar, C.; Studt, F.; Tuczek, F.; *Chem. Eur. J.* **2008**, *14*, 644.
28. Studt, F.; Tuczek, F.; *Angew. Chem. Int. Ed.* **2005**, *44*, 5639.
29. Mersmann, K.; Horn, K. H.; Bores, N.; Lehnert, N.; Studt, F.; Paulat, F.; Peters, G.; Ivanovic-Burmazovic, I.; van Eldik, R.; Tuczek, F.; *Inorg. Chem.* **2005**, *44*, 3031.
30. Lehnert, N.; Tuczek, F.; *Inorg. Chem.* **1999**, *38*, 1671.
31. Blake, A. J.; McInnes, J. M.; Mountford, P.; Nikonov, G. I.; Swallow, D.; Watkin, D. J.; *J. Chem. Soc., Dalton Trans.* **1999**, 379.
32. Clulow, A. J.; Selby, J. D.; Cushion, M. G.; Schwarz, A. D.; Mountford, P.; *Inorg. Chem.* **2008**, *47*, 12049.
33. Selby, J. D.; Schulten, C.; Schwarz, A. D.; Stasch, A.; Clot, E.; Jones, C.; Mountford, P.; *Chem.Commun.* **2008**, 5101.
34. Gehrmann, T.; Fillol, J. L.; Wadepohl, H.; Gade, L. H.; *Angew. Chem. Int. Ed.* **2009**, *48*, 2152.
35. Weitershaus, K.; Fillol, J. L.; Wadepohl, H.; Gade, L. H.; *Organometallics* **2009**, *28*, 4747.
36. Weitershaus, K.; Wadepohl, H.; Gade, L. H.; *Organometallics* **2009**, *28*, 3381.
37. Gehrmann, T.; Fillol, J. L.; Wadepohl, H.; Gade, L. H.; *Organometallics* **2010**, *29*, 28.
38. Tiong, P. J.; Schofield, A. D.; Selby, J. D.; Nova, A.; Clot, E.; Mountford, P.; *Chem. Commun.* **2010**, *46*, 85.
39. Tiong, P. J.; Nova, A.; Groom, L. R.; Schwarz, A. D.; Selby, J. D.; Schofield, A. D.; Clot, E.; Mountford, P.; *Organometallics* **2011**, *30*, 1182.
40. Walsh, P. J.; Carney, M. J.; Bergman, R. G.; *J. Am. Chem. Soc.* **1991**, *113*, 6343.
41. Herrmann, H.; Fillol, J. L.; Wadepohl, H.; Gade, L. H.; *Angew. Chem. Int. Ed.* **2007**, *46*, 8426.
42. Selby, J. D.; Manley, C. D.; Feliz, M.; Schwarz, A. D.; Clot, E.; Mountford, P.; *Chem. Commun.* **2007**, 4937.
43. Schofield, A. D.; Nova, A.; Selby, J. D.; Schwarz, A. D.; Clot, E.; Mountford, P.; *Chem. Eur. J.* **2011**, *17*, 265.

44. Chisholm, M. H.; Delbridge, E. E.; Kidwell, A. R.; Quinlan, K. B.; *Chem. Commun.* **2003**, 126.
45. Gdula, R. L.; Johnson, M. J. A.; Ockwig, N. W.; *Inorg. Chem.* **2005**, *44*, 9140.
46. Wood, C. D.; McLain, S. J.; Schrock, R. R.; *J. Am. Chem. Soc.* **1979**, *101*, 3210.
47. Schrock, R. R.; Fellmann, J. D.; *J. Am. Chem. Soc.* **1978**, *100*, 3359.
48. Doxsee, K. M.; Farahi, J. B.; Hope, H.; *J. Am. Chem. Soc.* **1991**, *113*, 8889.
49. Hessen, B.; Buijink, J.-K. F.; Meetsma, A.; Teuben, J.; Helgesson, G.; Hakansson, M.; Jagner, S.; Spek, A. L.; *Organometallics* **1993**, *12*, 2268.
50. Basuli, F.; Aneetha, H.; Huffman, J. C.; Mindiola, D. J.; *J. Am. Chem. Soc.* **2005**, *127*, 17992.
51. Listemann, M. L.; Schrock, R. R.; *Organometallics* **1985**, *4*, 74.
52. Freudenberger, J. H.; Schrock, R. R.; *Organometallics* **1986**, *5*, 398.
53. Chisholm, M. H.; Folting, K.; Lynn, M. L.; Tiedtke, D. B.; Lemoigno, F.; Eisenstein, O.; *Chem. Eur. J.* **1999**, *5*, 2318.
54. Geyer, A. M.; Gdula, R. L.; Wiedner, E. S.; Johnson, M. J. A.; *J. Am. Chem. Soc.* **2007**, *129*, 3800.
55. Bailey, B. C.; Fout, A. R.; Fan, H.; Tomaszewski, J.; Huffman, J. C.; Gary, J. B.; Johnson, M. J. A.; Mindiola, D. J.; *J. Am. Chem. Soc.* **2007**, *129*, 2234.
56. Geyer, A. M.; Wiedner, E. S.; Gary, J. B.; Gdula, R. L.; Kuhlmann, N. C.; Johnson, M. J. A.; Dunietz, B. D.; Kampf, J. W.; *J. Am. Chem. Soc.* **2008**, *130*, 8984.
57. Gibson, V. C.; Redshaw, C.; White, A. J. P.; Williams, D. J.; *Angew. Chem. Int. Ed.* **1999**, *38*, 961.
58. Elsegood, M. R.; Redshaw, C.; *Chem. Eur. J.* **2008**, *14*, 3530.
59. Groom, L. R. M., P; Unpublished Results.
60. Collier, P. E.; Pugh, S. M.; Clark, H. S. C.; Love, J. B.; Blake, A. J.; Cloke, F. G. N.; Mountford, P.; *Inorg. Chem.* **2000**, *39*, 2001.
61. Blake, A. J.; Collier, P. E.; Gade, L. H.; Mountford, P.; Lloyd, J.; Pugh, S. M.; Schubart, M.; Skinner, M. E. G.; Trösch, J. M.; *Inorg. Chem.* **2001**, *40*, 870.
62. Vujkovic, N.; Ward, B. D.; Maisse-Francois, A.; Wadepohl, H.; Mountford, P.; Gade, L. H.; *Organometallics* **2007**, *26*, 5522.
63. Herrmann, H.; Wadepohl, H.; Gade, L. H.; *Dalton Trans.* **2008**, 2111.

64. Details, including the molecular structure, of Ti(N_2N^{Me})(N^tBu)(py) (**47**) can be found in Appendix B. Reactivity studies have not been performed on this compound.
65. Schwarz, A. D.; Nova, A.; Clot, E.; Mountford, P.; *Chem. Commun.* **2011**, *47*, 4926.
66. Pugh, S. M.; Blake, A. J.; Gade, L. H.; Mountford, P.; *Inorg. Chem.* **2001**, *40*, 3992.
67. Ward, B. D.; Orde, G.; Clot, E.; Cowley, A. R.; Gade, L. H.; Mountford, P.; *Organometallics* **2004**, *23*, 4444.
68. Pugh, S. M.; Trösch, D. J. M.; Skinner, M. E. G.; Gade, L. H.; Mountford, P.; *Organometallics* **2001**, *20*, 3531.
69. Tonks, I. A.; Bercaw, J. E.; *Inorg. Chem.* **2010**, *49*, 4648.
70. Allen, F. H.; Kennard, O.; Watson, D. G.; Brammer, L.; Orpen, A. G.; Taylor, R.; *J. Chem. Soc., Perkin Trans. 2* **1987**, S1.
71. Blanchard, M. D.; Hughes, R. P.; Concolino, T. E.; Rheingold, A. L.; *Chem. Mater.* **2000**, *12*, 1604.
72. Lorenzo, S.; Lewis, G. R.; Dance, I.; *New J. Chem.* **2000**, *24*, 295.
73. Deck, P. A.; Kroll, C. E.; Hollis, W. G.; Fronczek, F. R.; *J. Organomet. Chem.* **2001**, *637-639*, 107.
74. Deck, P. A.; Lane, M. J.; Montgomery, J. L.; Slebodnick, C.; Fronczek, F. R.; *Organometallics* **2000**, *19*, 1013.
75. Hair, G. S.; Cowley, A. H.; Gorden, J. D.; Jones, J. N.; Jones, R. A.; Macdonald, C. L. B.; *Chem. Commun.* **2003**, 424.
76. Adams, N.; Cowley, A. R.; Dubberley, S. R.; Sealey, A. J.; Skinner, M. E. G.; Mountford, P.; *Chem. Commun.* **2001**, 2738.
77. Adams, N.; Bigmore, H. R.; Blundell, T. L.; Boyd, C. L.; Dubberley, S. R.; Sealey, A. J.; Cowley, A. R.; Skinner, M. E. G.; Mountford, P.; *Inorg. Chem.* **2005**, *44*, 2882.
78. Adams, N.; Arts, H. J.; Bolton, P. D.; Cowell, D.; Dubberley, S. R.; Friederichs, N.; Grant, C. M.; Kranenburg, M.; Sealey, A. J.; Wang, B.; Wilson, P. J.; Zuideveld, M. A.; Blake, A. J.; Schröder, M.; Mountford, P.; *Organometallics* **2006**, *25*, 3888.
79. Chauvin, Y.; *Angew. Chem. Int. Ed* **2006**, *45*, 3740.

80. Weinhold, F.; Landis, C. R.; *Valency and Bonding: A Natural Bond Orbital Donor-Acceptor Perspective*; Cambridge University Press: Cambridge, 2005.
81. *trans* refers to the relative position of the carbodiimide and the amine/pyridyl donor.
82. Kaplan, A. W.; Polse, J. L.; Ball, G. E.; Andersen, R. A.; Bergman, R. G.; *J. Am. Chem. Soc.* **1998**, *120*, 11649.
83. Glueck, D. S.; Wu, J.; Hollander, F. J.; Bergman, R. G.; *J. Am. Chem. Soc.* **1991**, *113*, 2041.
84. Walsh, P. J.; Hollander, F. J.; Bergman, R. G.; *Organometallics* **1993**, *12*, 3705.
85. Danopoulos, A. D.; Wilkinson, G.; Sweet, T. K. N.; Hursthouse, M. B.; *J. Chem. Soc., Dalton Trans.* **1996**, 271.
86. Blake, A. J.; Collier, P. E.; Gade, L. H.; McPartlin, M.; Mountford, P.; Schubart, M.; Scowen, I. J.; *Chem. Commun.* **1997**, 1555.
87. Bashall, A.; Collier, P. E.; Gade, L. H.; McPartlin, M.; Mountford, P.; Pugh, S. M.; Radojevic, S.; Schubart, M.; Scowen, I. J.; Trösch, D. J. M.; *Organometallics* **2000**, *19*, 4784.
88. Ward, B. D.; Orde, G.; Clot, E.; Cowley, A. R.; Gade, L. H.; Mountford, P.; *Organometallics* **2005**, *24*, 2368.
89. Compound **1.93** was also reacted with H_2 and $SiMe_3N_3$, however, no reaction occurred even upon heating.
90. Dunn, S. C.; Hazari, N.; Cowley, A. R.; Green, J. C.; Mountford, P.; *Organometallics* **2006**, *25*, 1755.
91. Royo, P.; Sánchez-Nieves, J.; *J. Organomet. Chem.* **2000**, *597*, 61.
92. Fletcher, D. A.; McMeeking, R. F.; Parkin, D.; *J. Chem. Inf. Comput. Sci.* **1996**, *36*, 746 (The UK Chemical Database Service: CSD version 5.33 updated February 2012).
93. Veneziani, G.; Shimada, S.; Tanaka, M.; *Organometallics* **1998**, *17*, 2926.
94. Honzicek, J.; Erben, M.; Cisarova, I.; Vinklarek, J.; *Inorg. Chim. Acta* **2005**, *358*, 814.
95. Herrmann, H.; Fillol, J. L.; Wadepohl, H.; Gade, L. H.; *Organometallics* **2008**, *27*, 172.
96. Herrmann, H.; Gehrmann, T.; Wadepohl, H.; Gade, L. H.; *Dalton Trans.* **2008**, 6231.

97. Tiong, P. J.; Nova, A.; Schwarz, A. D.; Selby, J. D.; Clot, E.; Mountford, P.; *Dalton Trans.* **2012**, *41*, 2277.

98. Ar'NCSe was synthesised by the author. Full details can be found in the experimental section

99. Morgan, H. E., Master's Thesis, University of Oxford, 2011.

100. Guiducci, A. E.; Boyd, C. L.; Mountford, P.; *Organometallics* **2006**, *25*, 1167.

101. Dubberley, S. R.; Friedrich, A.; Willman, D. A.; Mountford, P.; Radius, U.; *Chem. Eur. J.* **2003**, *9*, 3634.

102. Henderson, W.; Nicholson, B. K.; Dinger, M. B.; *Inorg. Chim. Acta* **2003**, *355*, 428.

103. Bondi, A.; *J. Phys. Chem.* **1964**, *68*, 441.

104. Braga, A. A.; Ujaque, G.; Maseras, F.; *Organometallics* **2006**, *25*, 3647.

Chapter Four

Synthesis and reactions of bis(cyclopentadienyl) supported Group 4 hydrazides with alkynes

4.1. Overview

For over 30 years, research based upon terminal hydrazide(2-) or isodiazene(0) complexes, (L)M=NNR_2 (R = H, alkyl, aryl), has concentrated on the heavier Group 6 transition metals following their implication as intermediates in the stepwise and catalytic conversion of dinitrogen to ammonia.[1-17] Other mid-transition metal compounds have also been widely studied in roles leading to the synthesis of organo-nitrogen products.[4,18,19] This differs from the chemistry of early transition metal hydrazides currently at a much earlier stage in its development.

The majority of Group 4 hydrazides to date have been based on a titanium metal centre and a range of synthetic routes to these target compounds have steadily become established.[20-35] However, translating these to the heavier Group 4 congeners has proved problematic, dimerisation or formation of bis(hydrazido(1-)) complexes often precluding formation of the terminal hydrazide.[20] This relative paucity of rational syntheses means that to date only eight isolated (five structurally characterised) terminal zirconium hydrazide(2-) compounds[24,29,30,36-38] and two examples on hafnium (one structurally authenticated) have been reported.[30,37] Despite this, the reactivity of the heavier Group 4 hydrazides has been shown to be equally, if not more, diverse than that of the related titanium systems.[24,25,36-41]

The metal-catalysed reactions of Group 4 hydrazides is a little understood but, given the success with related imide systems,[33,42-48] potentially fruitful area. Examples using titanium have so far been limited to the catalytic hydrohydrazination reaction of allenes or alkynes with hydrazines forming hydrazones. These are then either reacted with $ZnCl_2$[23,47,49-57] to promote cyclisation and indole formation or, more recently, other unsaturated substrates.[32,58-62] The only other type of catalytic activity seen is the diamination of alkynes outlined in Chapter Two.[21,27,63]

To date, only one example of a zirconium hydrazide catalyst has been reported, concurrent with the work in this Thesis.[36,39] In this system, $Zr(N_2{}^{R}N^{py})(NMe_2)_2(py)$ (R = *, Xyl or Mes) has been shown to catalytically produce indoles from 1,1-diphenylhydrazine and a range of alkynes with a loading of 10 mol % *via* terminal hydrazido(2-) active species. This one-pot synthesis proceeds through identical reactivity to that seen by Bergman with $Cp_2Zr(NNPh_2)(DMAP)$ (**1.151**).[25] A mechanistic and computational study of the mechanism was also presented in the

work. Similar reactivity has not been observed with a titanium hydrazide making a strong case for further reactivity studies utilising heavy Group 4 hydrazides.

Interestingly, given its historical successes in the related imido chemistry and use as a supporting ligand platform for the first examples of transition metal hydrazides,[25,26,64-66] the bis(cyclopentadienyl) ligand set has rarely been used.[67] Since Bergman's initial communication,[25] no further structural or reactivity studies have been performed using $Cp_2Zr(NNPh_2)(DMAP)$ (**1.151**) or its derivatives. Recently Mountford has presented an investigation into the bonding of $Cp_2Ti(NNPh_2)(py)$ (**1.103**) and its reactivity with PhCCPh and ^{t}BuCP,[68,69] while Beckhaus has reported the synthesis of $Cp^{Ad}{}_2Ti(NNPh_2)(py)$ (**4.1**, $Cp^{Ad} = C_5H_4Ad$, Ad = adamantyl).[70] Examples of transition metal hydrazides supported by mono(cyclopentadienyl) derived ligand sets are more common.[21,23,71-79] However, these typically concentrate on the mid/late transition metals, Group 4 complexes being limited to a few examples on titanium. The chemistry of bis(cyclopentadienyl), and related, early transition metal hydrazides and heavier Group 4 examples in general, remain greatly understudied areas when compared to their imido analogues.[2,22,64,80-117]

This Chapter begins by describing the first example of combined N_α–N_β bond cleavage, C–H activation reactivity with a titanium hydrazide. It then introduces a new synthesis of $Cp_2Zr(NNPh_2)(DMAP)$ (**1.151**) which is extended for use in forming the hafnium and bis(monomethylcyclopentadienyl) derivatives. In addition, the attempted syntheses of permethylated-bis(cyclopentadienyl) zirconium hydrazides is discussed. The mechanism of the N_α–N_β bond cleavage, C–H activation reaction, first discovered by Bergman, is probed using a range of experimental, mechanistic and computational methods. This is then compared to that proposed by Gade in his recent study of the corresponding reactivity of $Zr(N_2{}^{R}N^{py})(NNPh_2)(py)$ (**1.159** – **1.162**).[25,36]

4.2. Competition between alkyne insertion into N_α–N_β and combined N_α–N_β cleavage, C–H activation reactions

As discussed in Chapter Two, when $Ti(N_2N^{Me})(NNPh_2)(py)$ (**1.93**) is mixed with 2-butyne or a range of alkynes of the type RCCMe (R = Me, electron-donating or -withdrawing aryl subsituent), one alkyne molecule inserts into the N_α–N_β bond in a regiospecific manner to form vinyl imide compounds of the type shown in Equation 4.1.[21,63]

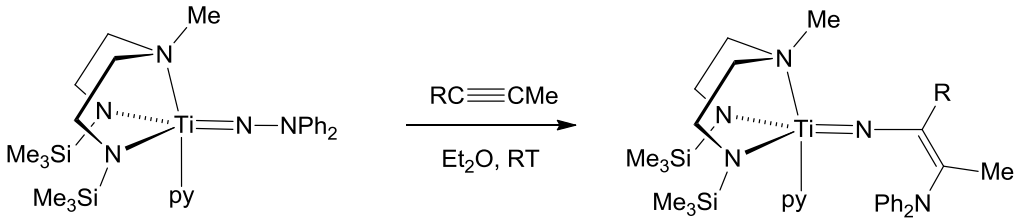

1.93

2.2, **1.149, 2 - 8**

R = Me, Ph or Aryl

Equation 4.1

However, when 1-ferrocenyl-1-propyne (FcCCMe) was reacted with $Ti(N_2N^{Me})(NNPh_2)(py)$ (**1.93**), instead of the expected vinyl imide, $Ti(HN_2N^{Me})\{N(SiMe_3)C(Me)C(Fc)\text{-}1,2\text{-}C_6H_4N(Ph)\}$ (**24**, HN_2N^{Me} = $HNCH_2CH_2N(Me)CH_2CH_2NSiMe_3$) was recrystallised in modest yield (30 %) from a mixture of other, unidentifiable products (Equation 4.2). In this case N_α–N_β cleavage has occurred, as in the previous examples, but is accompanied by C–H activation at the *ortho* position of one of the phenyl rings bound to N_β. The final step involves $SiMe_3$ migration from the ligand to the nitrogen derived from N_α in **1.93**. This reaction appears to be regiospecific with only the isomer illustrated in Equation 4.2 formed.

The NMR data are consistent with the structure drawn in Equation 4.2 and compounds **25b** and **26b** (*vide infra*). The most notable characteristics of the ^1H NMR spectrum are the presence of two $SiMe_3$ resonances, both downfield with respect to the starting hydrazide **1.93** and the vinyl imide products seen previously (Equation 4.1), the absence of bound pyridine and a singlet at 6.68 ppm arising from an NH resonance. In addition, due to the $SiMe_3$ migration there are eight inequivalent diamide-amine ligand backbone protons, as opposed to the four seen in C_s symmetric **1.93** and the vinyl imides. The $^{13}C\{^1H\}$ NMR spectrum contains six quaternary carbons with the resonances arising from the alkyne, $N(SiMe_3)\underline{C}(Me)C(Fc)$ and $N(SiMe_3)C(Me)\underline{C}(Fc)$, at 139.6 and 89.1 ppm, respectively.

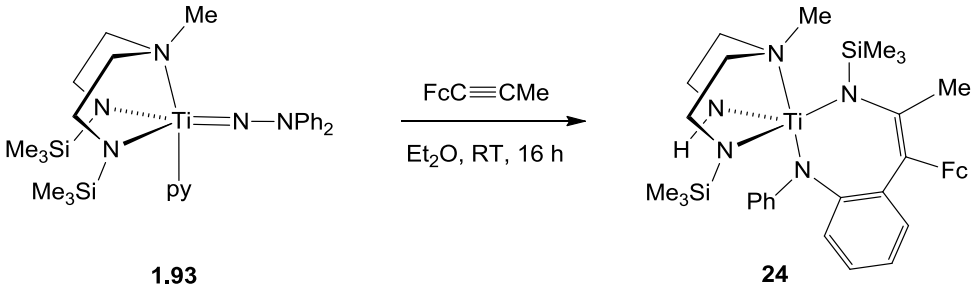

Equation 4.2

As mentioned earlier (Scheme 1.16, Chapter One), this reactivity has been seen previously by Bergman with $Cp_2Zr(NNPh_2)(DMAP)$ (**1.151**)[25] and also, more recently, by Gade using similar diamide-amine ligands supporting a zirconium hydrazide.[36,39] In spite of these results, this is the first example of this type of reactivity for titanium and demonstrates not just the breadth of reactivity accessible to diamide-amine supported terminal hydrazides but also the sensitive nature of hydrazide reactivity to both the electronic and steric characteristics of the alkyne.

Diffraction-quality crystals of $Ti(HN_2N^{Me})\{N(SiMe_3)C(Me)C(Fc)\text{-}1,2\text{-}C_6H_4N(Ph)\}$ (**24**) were grown by slow cooling of a saturated hexanes solution from 50 ºC to room temperature, and the solid state structure is presented in Figure 4.1. Selected bond lengths and angles are given in Table 4.1.

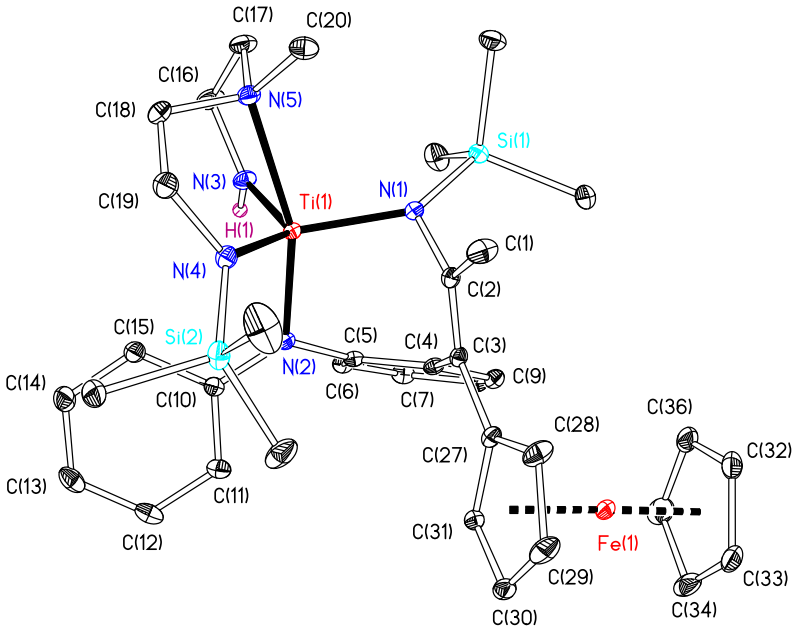

Figure 4.1. Displacement ellipsoid plot (20 % probability) of $Ti(HN_2N^{Me})\{N(SiMe_3)C(Me)C(Fc)\text{-}1,2\text{-}C_6H_4N(Ph)\}$ (**24**). C bound H atoms omitted for clarity. H(1) is drawn as a sphere of arbitrary radius.

Table 4.1. Selected distances (Å) and angles (°) for Ti(HN_2N^{Me}){N($SiMe_3$)C(Me)C(Fc)-1,2-C_6H_4N(Ph)} (**24**).

Ti(1)−N(1)	1.9501(11)	N(1)−Ti(1)−N(2)	102.12(4)
Ti(1)−N(2)	1.9826(10)	N(1)−Ti(1)−N(3)	109.81(5)
Ti(1)−N(3)	1.9275(11)	N(1)−Ti(1)−N(4)	120.59(5)
Ti(1)−N(4)	1.9891(11)	N(2)−Ti(1)−N(5)	158.54(4)
Ti(1)−N(5)	2.2988(11)	Ti(1)−N(1)−C(2)	104.19(8)
N(1)−C(2)	1.4253(16)	Ti(1)−N(2)−C(5)	114.59(8)
N(2)−C(5)	1.4177(16)	N(1)−C(2)−C(3)	120.09(11)
C(1)−C(2)	1.5105(18)	C(2)−C(3)−C(4)	118.85(11)
C(2)−C(3)	1.3631(17)	C(3)−C(4)−C(5)	123.48(11)
C(3)−C(4)	1.4962(17)	N(2)−C(5)−C(4)	121.64(11)
C(4)−C(5)	1.4115(18)		

The solid state structure of Ti(HN_2N^{Me}){N($SiMe_3$)C(Me)C(Fc)-1,2-C_6H_4N(Ph)} (**24**) is fully consistent with the solution NMR data and the structure drawn in Equation 4.2. The 7-membered metallacycle, formed from N_α–N_β cleavage and C–H activation is clearly visible, as is the $SiMe_3$ group bound to N(1) (derived from N_α), presumably having migrated from the diamide-amine ligand. The metal centre is in a distorted trigonal bipyramidal geometry, with the ligand κ^3-N bound in a *fac* manner. The two amide nitrogens occupy the remaining sites, with N(2) (derived from N_β) axially placed and N(1) in the equatorial plane.

The Ti(1)–N(1) and Ti(1)–N(2) distances (1.9501(11) Å and 1.9826(10) Å, respectively) are within the range expected for similar titanium amide bonds (lit. range for Ti(1)–N(1), 1.838 – 2.185 Å, 154 examples; for Ti(1)–N(2), 1.920 – 2.243 Å, 73 examples).[118] The C(2)–C(3) bond length (1.3631(17) Å) is typical of a C=C double bond. The Ti–N_{amide} ligand distances (Ti(1)–N(3) = 1.9275(11) Å, Ti(1)–N(4) = 1.9891(11) Å) are substantially less than those of the starting material Ti(N_2N^{Me})($NNPh_2$)(py) (**1.93**),[27] the related imide Ti(N_2N^{Me})(N^tBu)(py) (**47**) and the

vinyl imide product Ti(N_2N^{Me}){NC(Ph)C(Me)NPh_2}(py) (**1.149**, avg. Ti–N_{amide} = 2.024 Å). This is due to reduced competition between the equatorial nitrogen (N(1)) and the ligand-amide lone pairs. Not only is N(1) an amide donor as opposed to an imide, but the steric constraints and electronic delocalisation of the 7-membered ring limit the ability of the lone pair to donate to the metal centre. As expected, Ti(1)–N(3) is significantly shorter than Ti(1)–N(4) which can be attributed to the lower steric bulk of a hydrogen compared to a $SiMe_3$ group.

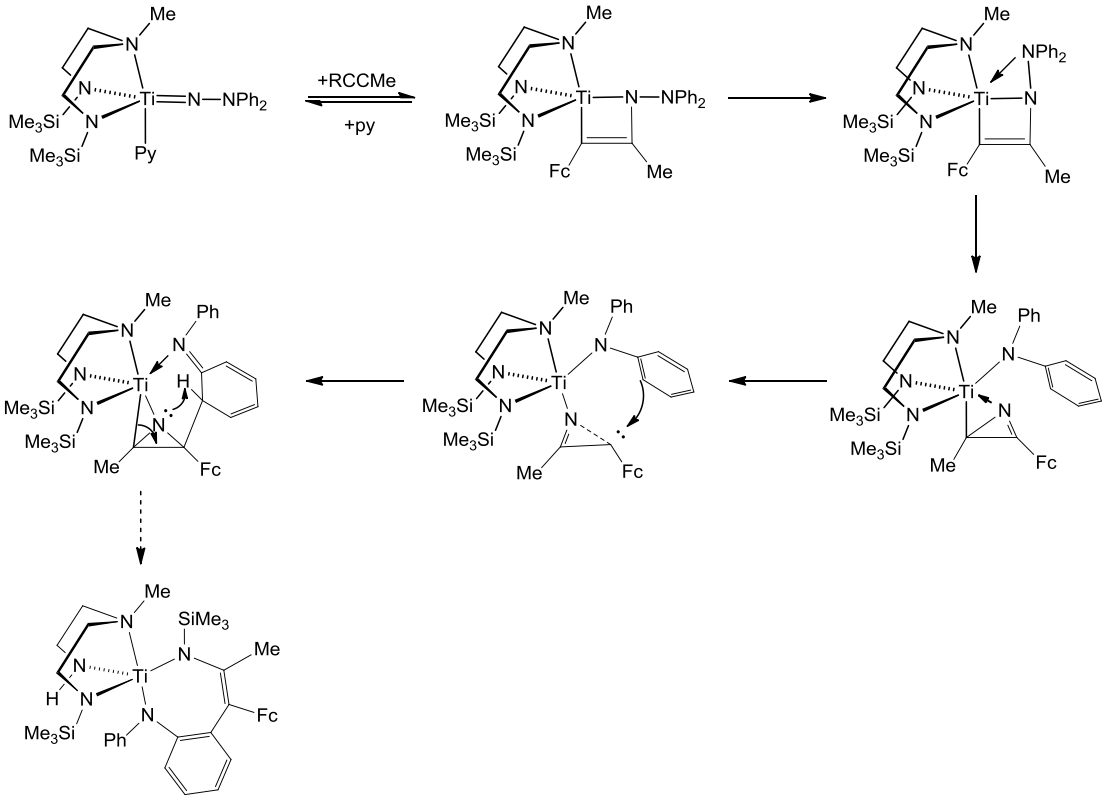

Scheme 4.1. Mechanism of the combined N_α-N_β, C-H activation reaction between Ti(N_2N^{Me})($NNPh_2$)(py) (**1.93**) and FcCCMe, as proposed by experimental and computational results presented later in the Chapter using bis(cyclopentadienyl) zirconium and hafnium systems.

The apical-amine donor in **24** (N(5)) is less tightly bound than in **1.93**, **47** and **1.149** due to the stronger donating properties of the *trans* amide (N(5)) in **24** compared to the *trans* pyridine donor in the other comounds (**24**, Ti(1)–N(5) = 2.2988(11) Å; avg. Ti–N^{Me} for **1.93**, **47** and **1.149** = 2.244(4) Å). The difference in steric bulk of the N(3) and N(4) substituents also causes the N(1)–Ti(1)–N(3) angle to be significantly more acute than N(1)–Ti(1)–N(4) (109.81(5) º *vs*. 120.59(5) º). In **1.93**, **47** and **1.149**, where both amide nitrogens have $SiMe_3$ substituents, the angles are nearly equal (avg.

113.9(3) º and 112.8(5) º). The angle between the axial nitrogens is similar to those in the other examples (**24**, N(2)–Ti(1)–N(5) = 158.54(4) º; **1.93**, **47** and **1.149**, avg. = 154.0(3) º).

While the mechanism for the reaction between Ti(N_2N^{Me})($NNPh_2$)(py) (**1.93**) and FcCCMe has not been explicitly studied, Scheme 4.1 provides a schematic representation for the combined N_α-N_β, C-H activation mechanism for the reaction based on that elucidated from the reactions between bis(cyclopentadienyl) zirconium and hafnium hydrazides and various alkynes, which is presented later in the Chapter.

Intrigued by this novel reactivity, the reactions between Ti(N_2N^{Me})($NNPh_2$)(py) (**1.93**) and other alkynes was explored in more depth. As mentioned in Chapter Two, sterically bulky alkynes possessing a $SiMe_3$ or ^tBu group (such as ^tBuCCMe, $Me_3SiCCPh$ or $Me_3SiCCMe$) did not react with **1.93** even upon heating to 110 ºC for 48 h. In contrast, the reactions with ArCCAr (Ar = 4-C_6H_4X, X = H, OMe or CF_3) at room temperature, gave either one or two distinct products (**25** – **27**, Equation 4.3, Table 4.2).

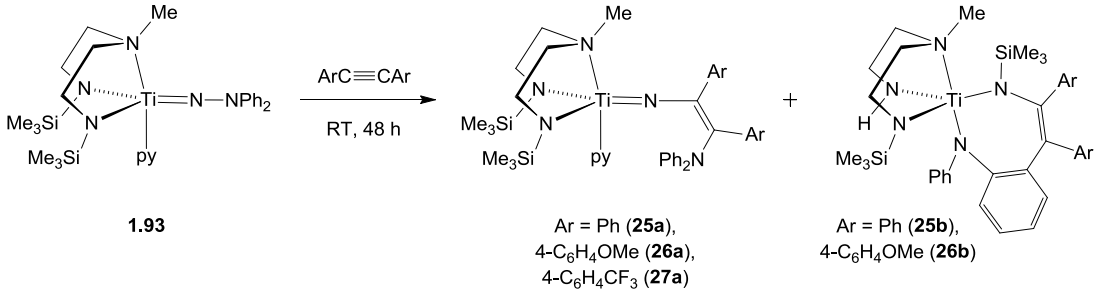

Equation 4.3

Table 4.2. Ratios of the insertion (**a**) and 7-membered ring (**b**) products formed from the reactions between Ti(N_2N^{Me})($NNPh_2$)(py) (**1.93**) and ArCCAr.

Ar	**a**	**b**
Ph	44	56
4-C_6H_4OMe	32	68
4-$C_6H_4CF_3$	100	0

In the case of the less electron-deficient alkynes (X = H, OMe) a mixture of three compounds was initially formed. Two of these, **25a**/**26a** and **25b**/**26b**, remained unchanged while the other converted over time into **25b**/**26b** leading to the observed product ratios. Using a range of NMR spectroscopy techniques and comparison with similar compounds, these were characterised as the vinyl imides $Ti(N_2N^{Me})\{NC(Ar)C(Ar)NPh_2\}(py)$ (Ar = Ph (**25a**), 4-C_6H_4OMe (**26a**)), analogous to those formed with ArCCMe (Equation 4.1) and the 7-membered ring products $Ti(HN_2N^{Me})\{N(SiMe_3)C(Ar)C(Ar)$-1,2-$C_6H_4N(Ph)\}$ (Ar = Ph (**25b**), 4-C_6H_4OMe (**26b**)) related to **24**.[119] The intermediates are proposed to be $Ti(N_2N^{Me})\{N(H)C(Ar)C(Ar)$-1,2-$C_6H_4N(Ph)\}$, the 7-membered ring compounds prior to N–H/N–$SiMe_3$ exchange.

Compounds **25** – **27** were isolated and fully characterised, in the case of **25** and **26** as a mixture of the two isomers. The ^{1}H NMR spectrum of **25a** and **25b** is shown in Figure 4.2 and is very similar to that of **26a** and **26b**. It clearly shows the presence of two distinct products, one with two $SiMe_3$ resonances (**25b**, analogous to **24**), the other with only one (**25a**, analogous to the vinyl imide products shown in Equation 4.1). In addition each has one methyl resonance and only one of the products (**25a**) has bound pyridine (the broad *ortho*-pyridine resonance at 8.50 ppm corresponds to free pyridine). Although there is no clear NH resonance in either the ^{1}H NMR or IR spectra, these are not always observed. The $^{13}C\{^1H\}$ NMR spectrum (not shown) has resonances at 147.9 and 117.9 ppm, corresponding to N<u>C</u>(Ph)C(Ph) and NC(Ph)<u>C</u>(Ph) in **25a**, respectively. This agrees with shifts seen in related compounds (N<u>C</u>CMe, range 142 – 159 ppm; NC<u>C</u>Me, range 112 – 119 ppm, see Chapter Two). Resonances at 147.9 and 124.3 ppm, corresponding to $N(SiMe_3)$<u>C</u>(Ph)C(Ph) and $N(SiMe_3)$C(Ph)<u>C</u>(Ph) in **25b**, show strong agreement with other 7-membered metallacycles formed from Group 4 hydrazides and bis(aryl)-substituted alkynes (typical values are *ca*. 150 and 120 ppm, respectively, *vide infra*). Precendence for the formation of both vinyl imide and 7-membered metallacycle products from the reaction between a Group 4 hydrazide and an alkyne has been shown by Gade.[36]

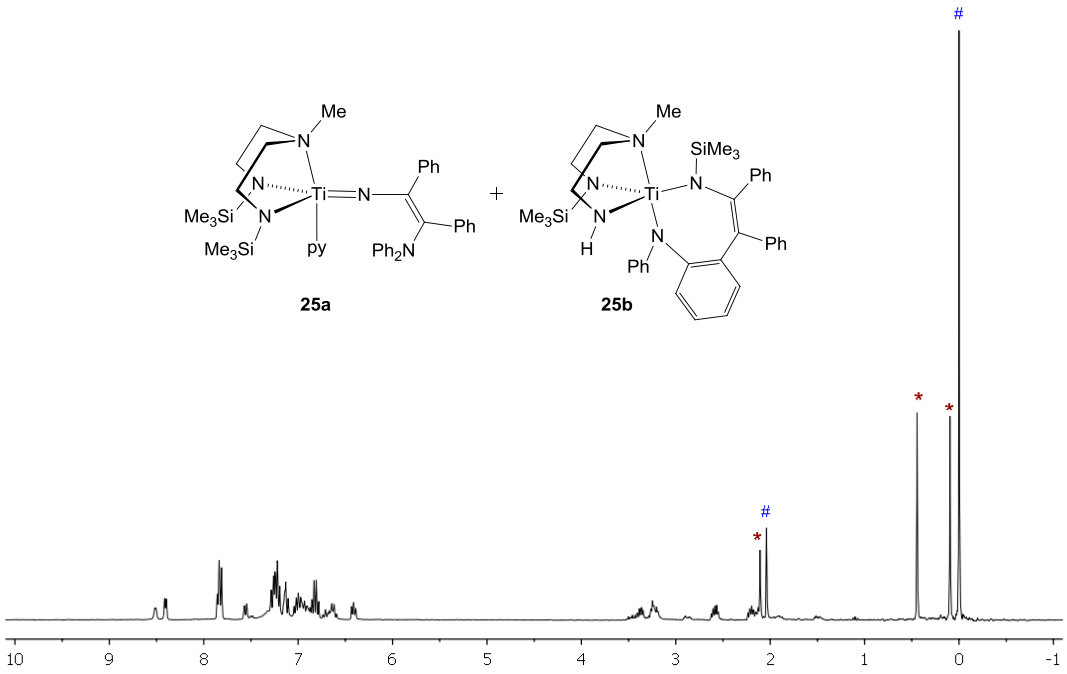

Figure 4.2. ^{1}H NMR spectrum (299.9 MHz, 293 K) of Ti(N_2N^{Me}){NC(Ph)C(Ph)NPh_2}(py) (**25a**) and Ti(HN_2N^{Me}){N($SiMe_3$)C(Ph)C(Ph)-1,2-C_6H_4N(Ph)} (**25b**) in C_6D_6. Resonances marked with # and * correspond to the NMe and $SiMe_3$ resonances of **25a** and **25b**, respectively.

The ratio of **a**:**b** was found to decrease slightly from 44:56 for **25** to 32:68 for **26** as the alkyne was changed from Ph to 4-C_6H_4OMe. In keeping with this observation the reaction between Ti(N_2N^{Me})($NNPh_2$)(py) (**1.93**) and ArCCAr (Ar = 4-$C_6H_4CF_3$) exclusively formed Ti(N_2N^{Me}){NC(Ar)C(Ar)NPh_2}(py) (**27a**, Equation 4.3) when followed in C_6D_6 and was isolated in 77 % yield. Addition of H_2NNPh_2 to a mixture of **25a** and **25b** did not lead to formation of the corresponding 1,2-diaminoalkene or phenyl indole. However following addition of an aqueous HCl solution, H_2NC(Ph)C(Ph)NPh_2 was observed by mass spectrometry.

The reasons behind the subtle differences in reactivity leading to the formation of either a vinyl imide, 7-membered ring product, or a mixture of both, are unclear. Nonetheless, following the work presented in Chapter Two, probing the formation of the vinyl imide type products, it was of interest to study the mechanism leading to the 7-membered ring products **24**, **25b** and **26b**. However, instead of performing mechanistic studies on the reactions involving Ti(N_2N^{Me})($NNPh_2$)(py) (**1.93**), which led to the formation of multiple products, it seemed sensible to return to Bergman's

bis(cyclopentadienyl) system which undergoes analogous reactivity with a larger range of alkynes, exclusively forming the 7-membered ring products.

4.3. Synthesis of bis(cyclopentadienyl) supported Group 4 hydrazides

Bergman synthesised $Cp_2Zr(NNPh_2)(DMAP)$ (**1.151**) *via* Schwartz's reagent as illustrated in Scheme 4.2.[120-122] The reactivity with alkynes was probed from both the isolated, base stabilised terminal hydrazide(2-) (**1.151**) and more generally the mixed alkyl-hydrazide(1-) compound (**1.152**) at high temperatures (110 ºC).[25]

To enable a mechanistic investigation into the combined N_α–N_β cleavage, C–H activation reaction, it was necessary to study the reactivity of $Cp_2Zr(NNPh_2)(DMAP)$ (**1.151**) at lower temperatures. Although each stage of the synthesis of **1.151** proceeds in a good yield, due to the number of steps involved the overall yield is only 30 - 42 % (based on literature values). In addition, the final stage, alkane elimination and trapping of the base-free hydrazide(2-) by DMAP proved to be problematic when attempted on scales larger than 200 mg.

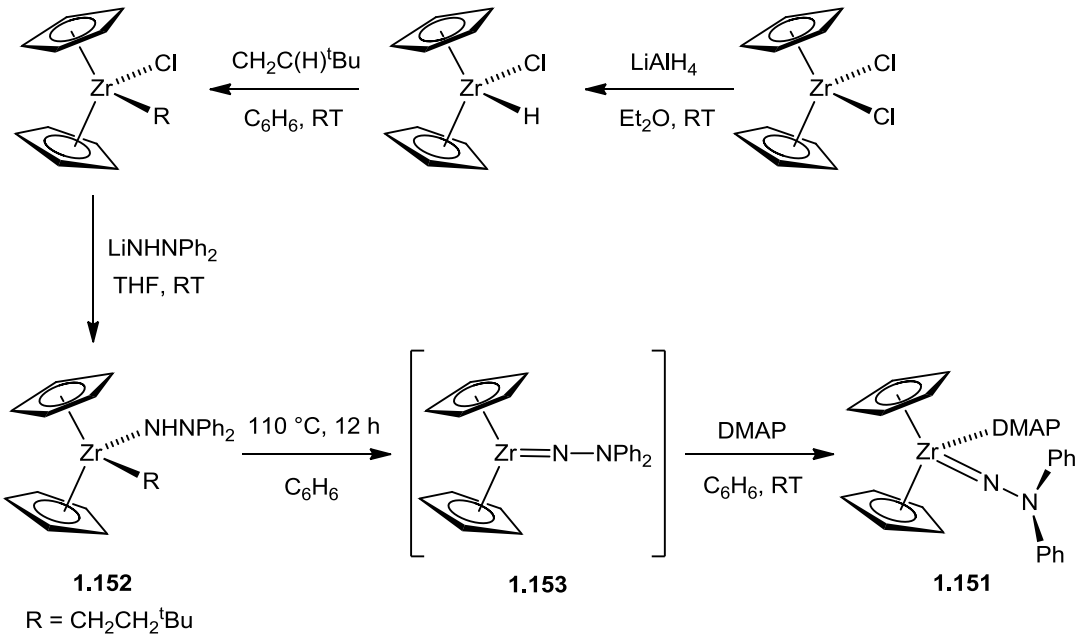

Scheme 4.2. Synthesis of $Cp_2Zr(NNPh_2)(DMAP)$ (**1.151**) *via* Schwartz's reagent.

A new method of synthesising $Cp_2Zr(NNPh_2)(DMAP)$ (**1.151**) was developed, proceeding in one step from readily available Cp_2ZrCl_2 (Equation 4.4). Although the yield is only modest (54 %), it is still superior to the overall yield of the literature synthesis and considerably more convenient. This novel route also enabled the

synthesis of the hafnium and zirconium methylcyclopentadienyl analogues $Cp_2Hf(NNPh_2)(DMAP)$ (**28**) and $Cp'_2Zr(NNPh_2)(DMAP)$ (**29**) in similar yields (58 and 52 %, respectively, Equation 4.4).

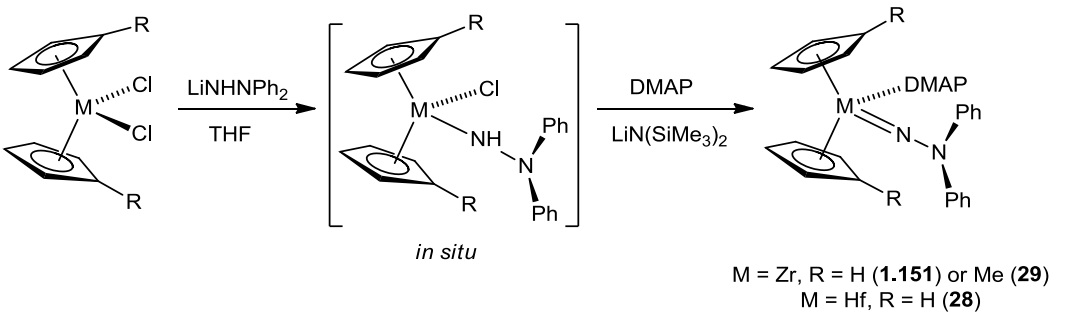

Equation 4.4

The ^{1}H NMR spectrum of $Cp_2Hf(NNPh_2)(DMAP)$ (**28**) is nearly identical to that of **1.151**. There is one cyclopentadienyl environment and the phenyl resonance shifts are highly indicative of a terminal hydrazido(2-) ligand with resonances at 7.56, 7.31 and 6.88 ppm. The $^{13}C\{^1H\}$ NMR spectrum is also fully consistent with the structure drawn in Equation 4.4 and that of **1.151**. $Cp'_2Zr(NNPh_2)(DMAP)$ (**29**) has a slightly different spectrum due to the presence of a methyl substituent on the cyclopentadienyl ring. At room temperature four broad resonances exist in the ^{1}H NMR spectrum which are attributable to the diastereotopic cyclopentadienyl protons. At low temperatures these sharpen to become four multiplets, and on warming coalesce to two resonances as the rate of exchange increases, each corresponding to a pair of diastereotopic protons. This point is elaborated on in a discussion of the mechanism in Section 4.7. The same behaviour is observed in the $^{13}C\{^1H\}$ NMR spectra. Resonances attributable to the hydrazido(2-) ligand are fully consistent with those in compounds **1.151** and **28**.

Diffraction-quality crystals of $Cp_2Hf(NNPh_2)(DMAP)$ (**28**) and $Cp'_2Zr(NNPh_2)(DMAP)$ (**29**) were grown by slow cooling of saturated benzene solutions from 60 °C to room temperature. For comparison with the hafnium and zirconium analogues, the structure of the previously synthesised compound $Cp_2Ti(NNPh_2)(DMAP)$ (**4.2**) was also elucidated, the pyridine stabilised analogue having been obtained earlier.[68,123] The molecular structures of **28**, **4.2** and **29** are presented in Figure 4.3. Selected distances and angles for **1.151** (for comparison), **28**, **4.2** and **29** are listed in Table 4.3.

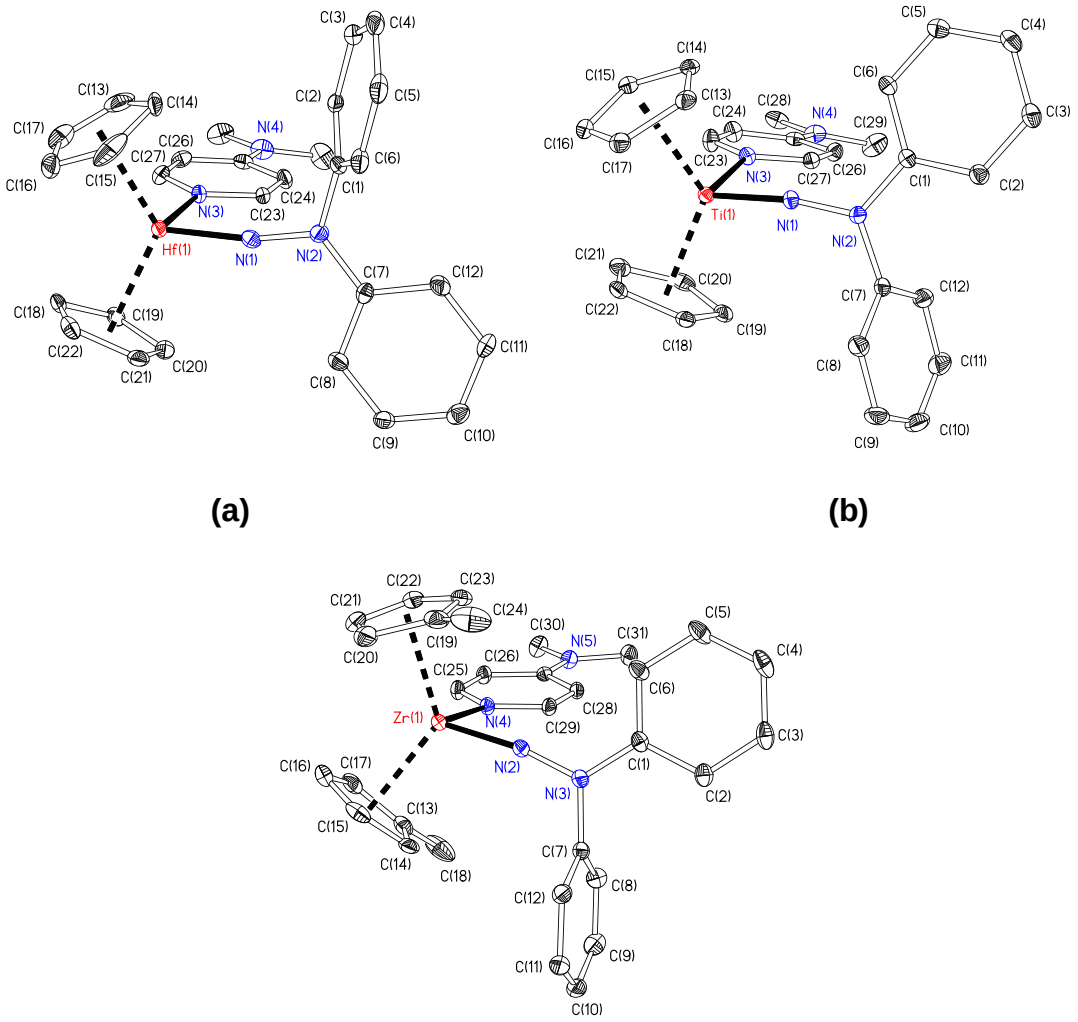

Figure 4.3. Displacement ellipsoid plots (20 % probability) of (a) $Cp_2Hf(NNPh_2)(DMAP)$ (**28**), (b) $Cp_2Ti(NNPh_2)(DMAP)$ (**4.2**) and (c) $Cp'_2Zr(NNPh_2)(DMAP)$ (**29**). H atoms omitted for clarity.

$Cp_2Zr(NNPh_2)(DMAP)$ (**1.151**), $Cp_2Hf(NNPh_2)(DMAP)$ (**28**) and $Cp_2Ti(NNPh_2)(DMAP)$ (**4.2**) constitute the first strucutrally characterised homologous series of any metal hydrazido(2-) compounds. In addition, **28** is the first example of a structurally characterised hafnium hydrazide with a neutral N_β (the other example contains a 1-pyridinio N_β group).[37,38] The structures presented in Figures 4.3 are fully consistent with NMR spectroscopy and other data. In all four compounds the metal centre has a pseudo tetrahedral environment, with two sites occupied by the cyclopentadienyl rings and the other two by the hydrazido(2-) and DMAP ligands. In **4.2** the metal-ligand distances are systematically shorter than those in **1.151**, **28** and

29, as expected by the smaller covalent radius of titanium, and it will be considered first. The cyclopentadienyl rings are staggered in all cases.

Table 4.3. Selected distances (Å) and angles (°) for $Cp_2Zr(NNPh_2)(DMAP)$ (**1.151**),[25] $Cp_2Hf(NNPh_2)(DMAP)$ (**28**), $Cp_2Ti(NNPh_2)(DMAP)$ (**4.2**) and $Cp'_2Zr(NNPh_2)(DMAP)$ (**29**).

Parameter	**1.151**	**28**	**4.2**	**29**
M(1)–N(1)	1.878(7)	1.874(5)	1.7455(19)	1.875(3)
M(1)–N(3)	2.310(8)	2.290(4)	2.226(2)	2.331(3)
$M(1)–Cp_{cent(1)}$[a]	2.295	2.245	2.215	2.300
$M(1)–Cp_{cent(2)}$[a]	2.303	2.268	2.163	2.302
N(1)–N(2)	1.351(10)	1.372(6)	1.351(3)	1.367(4)
N(2)–C(1)	1.409(11)	1.427(6)	1.401(3)	1.387(4)
N(2)–C(7)	1.418(13)	1.392(7)	1.435(3)	1.427(4)
$Cp_{cent(1)}–M(1)–Cp_{cent(2)}$	125.5	125.8	125.8	125.5
$Cp_{cent(1)}–M(1)–N(1)$	114.0	111.2	111.5	113.2
$Cp_{cent(1)}–M(1)–N(3)$	103.4	106.8	105.0	101.9
$Cp_{cent(2)}–M(1)–N(1)$	112.3	113.3	113.0	112.8
$Cp_{cent(2)}–M(1)–N(2)$	103.0	101.9	103.1	105.3
N(1)–M(1)–N(3)	90.90	91.36(18)	91.74(8)	90.73(10)
M(1)–N(1)–N(2)	169.91	168.7(4)	171.18(18)	170.0(2)

[a] Cp_{cent} is the computed Cp/Cp′ ring carbon centroid.

The Ti(1)–N(1) bond length in **4.2** (1.7455(19) Å) is the same within error as that seen in $Cp_2Ti(NNPh_2)(py)$ (**1.103**, $Ti=N_\alpha$ = 1.757(2) Å).[68,69,123] This is also the case for the M(1)–Cp_{cent} distances (**4.2**, Ti(1)–$Cp_{cent(1)}$ = 2.215 Å, Ti(1)–$Cp_{cent(2)}$ = 2.163 Å; **1.103**, Ti–Cp_{cent} = 2.21 and 2.15 Å) with one being significantly longer than the other. The $N_\alpha–N_\beta$ bond length in **4.2** is identical to that in **1.103** (1.351(3) Å in both complexes) and the Ti–N_{py} length in **1.103** is longer than the Ti(1)–N(3) distance in **4.2** as expected by the stronger donating properties of DMAP (**1.103**, Ti–N_{py} =

2.266(2) Å; **4.2**, Ti(1)–N(3) = 2.226(2) Å). In compound **4.2**, as in **1.103**, the phenyl rings of the hydrazido(2-) ligand are found to be perpendicular to the approximate plane deriving from N(3)–Ti(1)–N(1) so as to maximise the π-bonding interaction between the hydrazide and Cp_2Ti–L fragments.[68] The $Cp_{cent(1)}$–Ti(1)–$Cp_{cent(2)}$ angle in **4.2** (125.75 º) is slightly wider than in **1.103** (123.8 º), but in general, somewhat more acute than in other bis(cyclopentadienyl) titanium complexes (e.g. 130.9 º in Cp_2TiCl_2). The Ti(1)–N(1)–N(2) angle is marginally less than in $Cp_2Ti(NNPh_2)(py)$ (**1.103**) (171.18(18) º *vs.* 175.93(19) º), but within the values expected for Ti hydrazides (range, 180(2) - 156.56(13) º, 20 examples). All distances and angles in **4.2** are similar to those in the related hydrazide $Cp^{Ad}{}_2Ti(NNPh_2)(py)$ (**4.1**), although in this case both Ti–Cp_{cent} distances are equal.[70]

In $Cp_2Zr(NNPh_2)(DMAP)$ (**1.151**), $Cp_2Hf(NNPh_2)(DMAP)$ (**28**) and $Cp'_2Zr(NNPh_2)(DMAP)$ (**29**), the M=N_α bond lengths are all the same within error (**1.151**, 1.878(7) Å; **28**, 1.874(5) Å; **29**, 1.875(3) Å) and also equal to that of $Cp_2Zr(NAr')(THF)$ (**1.48**, Ar′ = 2,6-$C_6H_3{}^iPr_2$, Zr=N_{imido} = 1.888(2) Å). They are, however, significantly longer than that found in the alkyl imide $Cp_2Zr(N^tBu)(THF)$ (**1.45**, Zr=N_{imido} = 1.826(4) Å), a trend mirroring that seen in titanium hydrazide and imide chemistry.[64] The M=N_α distances are at the shorter end of the range found for other heavy Group 4 metal hydrazides (2 examples, 1.899(2) and 1.885(3) Å, those with the pyridinium hydrazide moiety NNC_5H_5 have been excluded due to the formal positive charge on N_β).[24,29,30,36] However, when compared with a range of zirconium and hafnium aryl imides (excluding **1.48**) the M=N_α distances appear marginally longer, although the same within error (M = Zr, range 1.844(9) – 1.868(3) Å, 4 examples; M = Hf, range 1.822 – 1.859(2) Å, 4 examples).[92,99-101] Other distances to hafnium are slightly shorter than to zirconium due to the lanthanoid contraction (e.g. **28**, M(1)–N(3) = 2.290(4) Å, avg. M(1)–Cp_{cent} = 2.257 Å; **1.151**, M(1)–N(3) = 2.310(8) Å, avg. M(1)–Cp_{cent} = 2.299 Å; **29**, M(1)–N(3) = 2.331(3) Å, avg. M(1)–Cp_{cent} = 2.301 Å).

The Zr–Cp_{cent} distances in **1.151** and **29** are similar to the average of those in **1.48** (avg Zr–Cp_{cent} = 2.295 Å). However, it is interesting to note that, unlike in **4.2** and **1.48** (**1.48**, Zr–Cp_{cent} = 2.312(1) and 2.277(1) Å), where one Cp ring is markedly further from the metal centre, both M–Cp_{cent} distances in **1.151**, **28** and **29** are nearly identical. The M–Cp_{cent} lengths are slightly longer than in other examples with these

metals, (e.g Cp_2MCl_2 avg. M–Cp_{cent} = 2.194 Å (M = Zr), 2.182 Å (M = Hf)) due to the π-loaded nature of the imido and hydrazido compounds (as discussed in Chapter One).[124,125]

In compounds **1.151**, **28** and **29**, the N_α–N_β bond lengths are the same within error, lying in the middle of the range seen for other Group 4 hydrazides (lit. range 1.329(2) – 1.403(4) Å, 22 examples). The M(1)–N(1)–N(2) angles (**1.151**, 169.91 º; **28**, 168.7(4) º; **4.2**, 171.18(18) º; **29**, 170.0(2) º) are indicative of an *sp* hybridised N_α and again within the expected range for other Group 4 hydrazides (lit. range, 180 - 156.56(13) º, 22 examples). In the same way as $Cp_2Ti(NNPh_2)(DMAP)$ (**4.2**), $Cp_2Zr(NNPh_2)(DMAP)$ (**1.151**), $Cp_2Hf(NNPh_2)(DMAP)$ (**28**) and $Cp'_2Zr(NNPh_2)(DMAP)$ (**29**) all have the phenyl rings of the hydrazide group perpendicular to the plane of N(3)–M(1)–N(1). Cp_{cent}–M–Cp_{cent} angles for all the structures are nearly identical, being slightly more acute than those reported elsewhere (e.g. Cp_2MCl_2; Cp_{cent}–M–Cp_{cent} = 129.03 º (M = Zr), 129.14 º (M = Hf)).

Given the different products accessible from the reactions between alkynes and Group 4 hydrazides it was also of interest to to prepare the dimethyl hydrazide compound $Cp_2Zr(NNMe_2)(DMAP)$. In this instance N_α–N_β cleavage is possible, however, it can clearly not be followed by the C–H activation seen with **1.151**. This means formation of vinyl imide products, of the type seen by the reaction between $Ti(N_2N^{Me})(NNPh_2)(py)$ (**1.93**) and ArCCMe (Ar = electron donating or withdrawing aryl group) as outlined in Equation 4.1, may occur instead. The synthesis of $Cp_2Zr(NNMe_2)(DMAP)$ was attempted using the same methodology as that used in the syntheses of **1.151**, **28** and **29** (Equation 4.4). Unfortunately, despite the use of a wide range of conditions, isolation of $Cp_2Zr(NNMe_2)(DMAP)$ was unsuccessful. Synthesis of $Cp_2Zr(NNMe_2)(DMAP)$ *via* the literature method first employed by Bergman was more promising (Scheme 4.3).

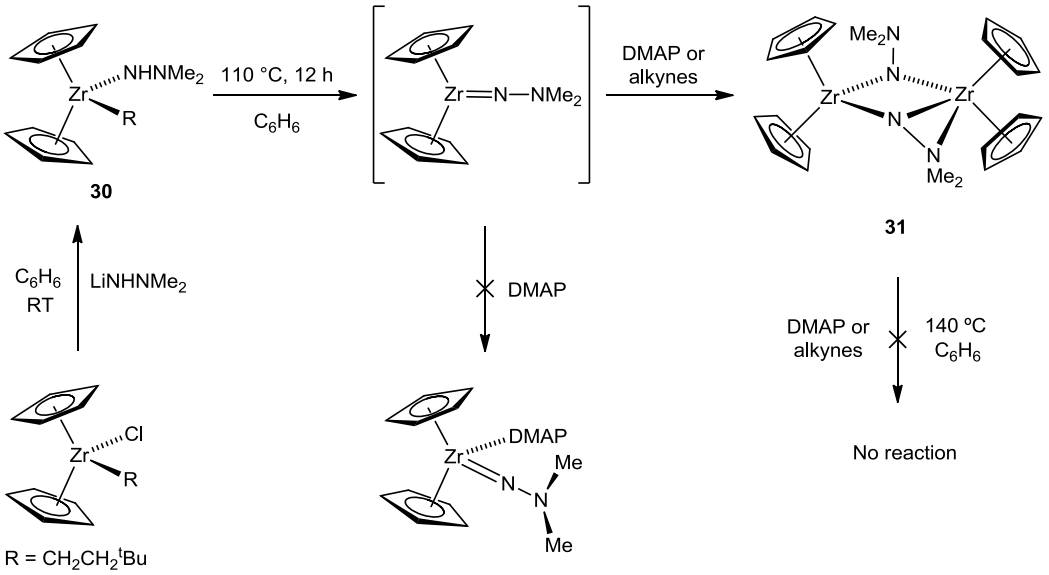

Scheme 4.3. Attempted synthesis of $Cp_2Zr(NNMe_2)(DMAP)$.

Compound $Cp_2Zr(CH_2CH_2{}^tBu)(NHNMe_2)$ (**30**) was synthesised in 87 % yield from the alkyl chloride $Cp_2Zr(CH_2CH_2{}^tBu)Cl$ and $LiNHNMe_2$ (Scheme 4.3). Upon heating to 110 ºC for 48 h this eliminated $MeCH_2{}^tBu$ forming the proposed transient species $Cp_2Zr(NNMe_2)$. This quickly dimerised to form the unsymmetrical dimer $Cp_4Zr_2(\mu\text{-}\eta^1\text{:}\eta^1\text{-}NNMe_2)(\mu\text{-}\eta^2\text{:}\eta^1\text{-}NNMe_2)$ (**31**), typical of other dimeric hydrazide compounds,[68,126,127] even in the presence of 5 equivalents of DMAP. Isolated $Cp_4Zr_2(\mu\text{-}\eta^1\text{:}\eta^1\text{-}NNMe_2)(\mu\text{-}\eta^2\text{:}\eta^1\text{-}NNMe_2)$ (**31**) did not react with DMAP, PhCCPh, $Me_3SiCCMe$, ^{t}BuCCMe or EtCCEt even at 140 ºC (Scheme 4.3). Despite this lack of reactivity, it was anticipated that the transient species $Cp_2Zr(NNMe_2)$ might react with alkynes when it was generated *in situ*, as seen by Bergman for $Cp_2Zr(NNPh_2)$ (**1.153**). However, despite using a range of alkynes, temperatures and reaction times the only isolable product was **31**.

The ^1H and $^{13}C\{^1H\}$ NMR data for $Cp_2Zr(CH_2CH_2{}^tBu)(NHNMe_2)$ (**30**) are similar to those for $Cp_2Zr(CH_2CH_2{}^tBu)(NHNPh_2)$ (**1.152**). The resonances relating to the alkyl group consist of two multiplets at 0.68 and 1.53 ppm with the ^{t}Bu resonance found at 1.09 ppm. The cyclopentadienyl resonance occurs at 5.71 ppm, with the hydrazido(1-) resonances at 5.15 and 2.12 ppm for NH and NMe_2, respectively. The NMe_2 shift of 52.3 ppm in the $^{13}C\{^1H\}$ spectrum is similar to that seen in other 1,1-dimethylhydrazido(1-) ligands.[20,128]

Unfortunately due to its extremely insoluble nature, NMR data of **31** could only be obtained in pyridine-d_5 making direct comparisons with other dimeric 1,1-dimethylhydrazido(2-) compounds impossible. Diffraction-quality crystals of $Cp_4Zr_2(\mu\text{-}\eta^1\text{:}\eta^1\text{-}NNMe_2)(\mu\text{-}\eta^2\text{:}\eta^1\text{-}NNMe_2)$ (**31**) were grown by slow cooling of a saturated benzene solution, from 60 °C to room temperature, but found to be poor diffractors. A solution, confirming the connectivity outlined in Scheme 4.3 could nonetheless be found and is presented in Appendix C. However, a full refinement could not be carried out.

4.4. Concurrent N_α–N_β cleavage and C–H activation reactivity between bis(cyclopentadienyl) supported Group 4 hydrazides and symmetrical alkynes

Following the previously reported reactivity of $Cp_2Zr(NHNPh_2)(CH_2CH_2{}^tBu)$ (**1.152**) with RCCR (R = Et, Ph or Tol)[25] and successful syntheses of compounds **1.151** and **28**, it was decided to investigate their reactivity with 2-butyne, in order to gain information about the minimum temperature for which the N_α–N_β cleavage, C–H activation reaction can occur. Structural elucidation of the products $Cp_2M\{N(H)C(Me)C(Me)\text{-}1,2\text{-}C_6H_4N(Ph)\}$ (M = Zr (**32**) or Hf (**33**)) would also be useful in providing ground state geometries for DFT calculations which would initially be performed using the most simple compounds (i.e the products with 2-butyne).

When heated to 50 ºC with a 50 fold excess of 2-butyne in benzene, $Cp_2Zr(NNPh_2)(DMAP)$ (**1.151**) was quantitatively converted to $Cp_2Zr\{N(H)C(Me)C(Me)\text{-}1,2\text{-}C_6H_4N(Ph)\}$ (**32**) over the course of 16 h. In contrast, $Cp_2Hf(NNPh_2)(DMAP)$ (**28**) did not react appreciably under identical conditions, but at 60 ºC did react to form $Cp_2Hf\{N(H)C(Me)C(Me)\text{-}1,2\text{-}C_6H_4N(Ph)\}$ (**33**) over 16 h (Equation 4.5). The reactivity of $Cp_2Zr(NNPh_2)(DMAP)$ (**1.151**) with the electron-donating and -withdrawing bis(aryl) *para*-substituted alkynes ArCCAr (Ar = $4\text{-}C_6H_4X$, X = OMe or CF_3) was also investigated forming $Cp_2Zr\{N(H)C(Ar)C(Ar)\text{-}1,2\text{-}C_6H_4N(Ph)\}$ (Ar = $4\text{-}C_6H_4X$, X = OMe (**34**) or CF_3 (**35**)). In addition, $Cp_2Hf(NNPh_2)(DMAP)$ (**28**) and $Cp'_2Zr(NNPh_2)(DMAP)$ (**29**) were reacted with PhCCPh yielding $Cp_2Hf\{N(H)C(Ph)C(Ph)\text{-}1,2\text{-}C_6H_4N(Ph)\}$ (**36**) and $Cp'_2Zr\{N(H)C(Ph)C(Ph)\text{-}1,2\text{-}C_6H_4N(Ph)\}$ (**37**) in modest isolated yields (Equation 4.5).

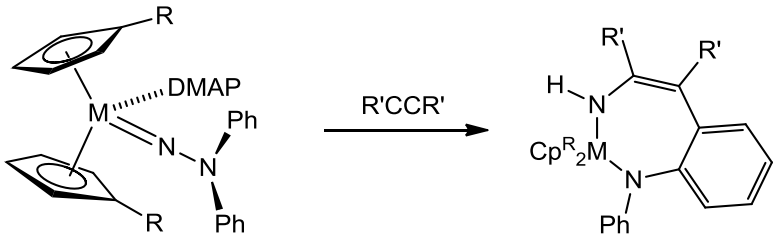

R = H, M = Zr (**1.151**), Hf (**28**);
R = Me, M = Zr (**29**)

M = Zr, R = H, R' = Me (**32**), Ph (**1.156**),
4-C_6H_4OMe (**34**), 4-$C_6H_4CF_3$ (**35**);
M = Hf, R = H, R' = Me (**33**), Ph (**36**);
M = Zr, R = Me, R' = Ph (**37**)

Equation 4.5

Diffraction-quality crystals of $Cp_2Zr\{N(H)C(Me)C(Me)$-1,2-$C_6H_4N(Ph)\}$ (**32**), $Cp_2Hf\{N(H)C(Me)C(Me)$-1,2-$C_6H_4N(Ph)\}$ (**33**) and $Cp_2Hf\{N(H)C(Ph)C(Ph)$-1,2-$C_6H_4N(Ph)\}$ (**36**) were grown from saturated benzene solutions at room temperature. The molecular structures of **32**, **33** and **36** as determined by X-ray crystallography, are illustrated in Figures 4.4 and 4.5 with selected distances and angles presented in Table 4.4.

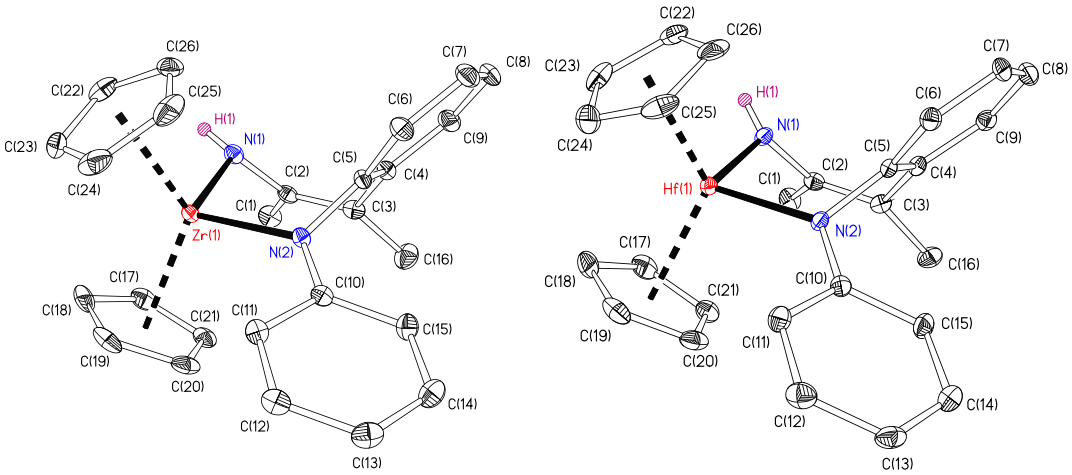

(a) **(b)**

Figure 4.4. Displacement ellipsoid plots (25 % probability) of (a) $Cp_2Zr\{N(H)C(Me)C(Me)$-1,2-$C_6H_4N(Ph)\}$ (**32**) and (b) $Cp_2Hf\{N(H)C(Me)C(Me)$-1,2-$C_6H_4N(Ph)\}$ (**33**). C bound H atoms omitted for clarity. H(1) is drawn as a sphere of arbitrary radius.

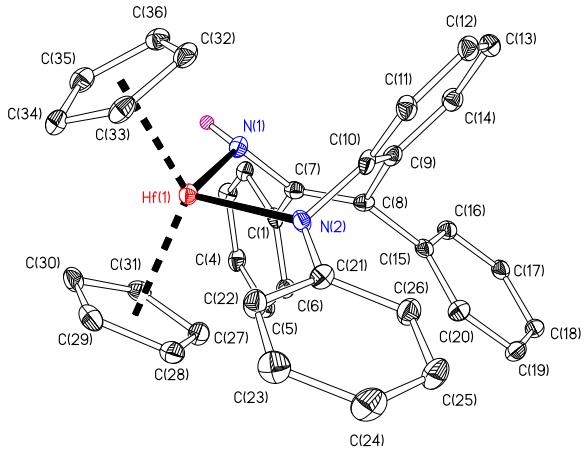

Figure 4.5. Displacement ellipsoid plot (20 % probability) of $Cp_2Hf\{N(H)C(Ph)C(Ph)\text{-}1,2\text{-}C_6H_4N(Ph)\}$ (**36**). C bound H atoms omitted for clarity. H(1) is drawn as a sphere of arbitrary radius.

Compounds $Cp_2Zr\{N(H)C(Me)C(Me)\text{-}1,2\text{-}C_6H_4N(Ph)\}$ (**32**), $Cp_2Hf\{N(H)C(Me)C(Me)\text{-}1,2\text{-}C_6H_4N(Ph)\}$ (**33**) and $Cp_2Hf\{N(H)C(Ph)C(Ph)\text{-}1,2\text{-}C_6H_4N(Ph)\}$ (**36**) are directly related to $Cp_2Zr\{N(H)C(Tol)C(Tol)\text{-}1,2\text{-}C_6H_4N(Ph)\}$ (**1.157**) synthesised by Bergman and $Zr(N_2{*}N^{py})\{N(H)C(R)C(R)\text{-}1,2\text{-}C_6H_4N(Ph)\}$ (R = Et (**4.3**), Ph (**4.4**)) and $Zr(N_2{}^{Mes}N^{py})\{N(H)C(R)C(R)\text{-}1,2\text{-}C_6H_4N(Ph)\}$ (R = Me (**4.5**), Et (**4.6**)) recently reported by Gade.[25,36,39] They all clearly contain the 7-membered metallacycles formed from N_α–N_β bond cleavage and C–H activation, with **33** and **36** being the first examples of this type of reactivity with a hafnium hydrazide. The solid state structures are fully consistent with NMR spectroscopy and other data.

The coordination geometries are pseudo tetrahedral in each case, two positions occupied by amide donors and two by cyclopentadienyl rings. The M(1)–N(1) and M(1)–N(2) bond lengths (**32**, 2.0972(18) and 2.1527(16) Å; **33**, 2.056(4) and 2.119(3) Å; **36**, 2.084(6) and 2.134(5) Å, resectively) lie within the expected range for monoanionic nitrogen ligands bound to a heavy Group 4 metal (lit. range 1.877 – 2.404 Å),[36] with the distances to zirconium systematically longer than in the hafnium examples.[118]

The Zr(1)–N(1) distance in **32** (2.0972(18) Å) is slightly shorter than that seen in Bergman's $Cp_2Zr\{N(H)C(Tol)C(Tol)\text{-}1,2\text{-}C_6H_4N(Ph)\}$ (**1.157**, 2.120(4) Å), presumably due to both the lesser bulk of the alkyne methyl substituents in **32** and the enhanced delocalisation of the nitrogen lone pair into the 7-membered ring aromatic system for aryl substituted alkynes. The same trend is observed when progressing

from **33** to **36** (Hf(1)–N(1) = 2.056(4) Å (**33**), 2.084(6) Å (**36**)), in this case the phenyl substituents causing the slight lengthening of the Hf(1)–N(1) bond.

The M(1)–N(2) bond lengths in **33** and **36** are the same within error (**33**, 2.119(3) Å; **36**, 2.134(5) Å) but in **32** it is marginally longer than in **1.157** (**32**, 2.1527(16) Å; **1.157**, 2.131(3) Å). The C(1)–C(2) distances in **32** and **33** and C(7)–C(8) distance in **36** are consistent with C=C double bonds, as depicted in the structures drawn in Equation 4.5. The M–Cp_{cent} lengths are shorter when compared to those in the starting hydrazides (**1.151**/**29** avg. Zr(1)–Cp_{cent} = 2.300 Å; **28**, avg. Hf(1)–Cp_{cent} = 2.257 Å; **32**, avg. Zr(1)–Cp_{cent} = 2.254 Å; **33**/**36**, avg. Hf(1)–Cp_{cent} = 2.229 Å). This is indicative of reduced competition between the amide 2pπ and the Cp π orbitals and makes them a similar length to those seen in other bis(cyclopentadienyl) compounds (e.g. Cp_2MCl_2 avg. M–Cp_{cent} = 2.194 Å (M = Zr), 2.182 Å (M = Hf)). The average Cp_{cent}–M–Cp_{cent} angles in **32**, **33** and **36** are very similar (126.84 – 127.62 º) and slightly larger than in $Cp_2M(NNPh_2)$(DMAP) (Cp_{cent}–M–Cp_{cent} = 125.52 º (M = Zr); 125.75 º (M = Hf)). This brings them closer to the values seen in other bis(cyclopentadienyl) complexes (e.g. Cp_2MCl_2 Cp_{cent}–M–Cp_{cent} = 129.0 º (M = Zr), 129.1 º (M = Hf)).

The NMR spectra of compounds **32** - **37** exhibit the same characteristics as described by Bergman.[25] The most notable features are the presence of two cyclopentadienyl resonances (or resonances indicating two distinct cyclopentadienyl rings in the case of **37**) which coalesce at *ca*. 75 ºC, varying slightly depending on the alkyne used, and the N(H)C(R)C(R) and N(H)C(R)C(R) shifts which range between 156 – 143 ppm and 126 – 113 ppm, respectively.

Table 4.4. Selected distances (Å) and angles (°) for $Cp_2Zr\{N(H)C(Me)C(Me)\text{-}1,2\text{-}C_6H_4N(Ph)\}$ (**32**), $Cp_2Hf\{N(H)C(Me)C(Me)\text{-}1,2\text{-}C_6H_4N(Ph)\}$ (**33**) and $Cp_2Hf\{N(H)C(Ph)C(Ph)\text{-}1,2\text{-}C_6H_4N(Ph)\}$ (**36**).

Parameter	**32**	**33**	**36**[b]
M(1)–N(1)	2.0972(18)	2.056(4)	2.084(6)
M(1)–N(2)	2.1527(16)	2.119(3)	2.134(5)
$M(1)–Cp_{cent(1)}$[a]	2.254	2.219	2.222
$M(1)–Cp_{cent(2)}$[a]	2.254	2.249	2.225
N(1)–C(2)	1.401(3)	1.410(6)	1.395(8)
N(2)–C(5)	1.422(3)	1.431(6)	1.428(8)
C(2)–C(3)	1.356(3)	1.346(7)	1.358(9)
C(3)–C(4)	1.483(3)	1.491(6)	1.492(8)
C(4)–C(5)	1.405(3)	1.412(6)	1.422(9)
$Cp_{cent(1)}–M(1)–Cp_{cent(2)}$	127.1	126.8	127.6
$Cp_{cent(1)}–M(1)–N(1)$	101.8	103.3	100.7
$Cp_{cent(1)}–M(1)–N(2)$	107.7	110.2	110.8
$Cp_{cent(2)}–M(1)–N(1)$	109.1	109.2	108.6
$Cp_{cent(2)}–M(1)–N(2)$	107.4	106.8	105.8
N(1)–M(1)–N(2)	100.62(7)	96.10(15)	99.8(2)
M(1)–N(1)–C(2)	111.84(13)	117.4(3)	116.8(4)
M(1)–N(2)–C(5)	113.35(12)	114.5(3)	112.4(4)
N(1)–C(2)–C(3)	120.55(19)	120.7(4)	119.2(6)
N(2)–C(5)–C(4)	121.86(18)	121.9(4)	121.6(6)
C(2)–C(3)–C(4)	123.2(2)	120.7(4)	121.2(5)
C(3)–C(4)–C(5)	126.14(19)	125.9(4)	127.4(6)

[a] Cp_{cent} is the computed Cp ring carbon centroid.

[b] For **36**: C(2) = C(7), C(3) = C(8), C(4) = C(9), C(5) = C(10)

4.5. Evidence for [2+2] cycloaddition intermediates along the reaction coordinate

The experimental, mechanistic and computational studies performed on the N_α–N_β insertion reaction, described in Chapter Two, indicate that the mechanism proceeds through a [2+2] cycloaddition intermediate.[63] This implies that the N_α–N_β cleavage C–H activation reaction, introduced earlier in this Chapter, might also proceed *via* azametallacycles of the type $Cp^R{}_2M\{N(NPh_2)C(R')C(R')\}$ (Cp^R = Cp or Cp′, M = Zr or Hf, R′ = alkyl or aryl group).

In his initial communication, Bergman did not identify any cycloaddition compounds formed between **1.151** and alkynes. However, the reactivity of the related imido compound $Cp_2Zr(NXyl)(NC_5H_4{}^tBu)$ (**1.47**) with alkynes forming a range of azametallacyclobutenes has been thoroughly investigated.[25,86] Gade, in his recent study of the same reaction, using diamide-amine supporting ligand sets, proposes a mechanism proceeding through an azametallacyclobutene intermediate. As part of this he has reported and structurally characterised the [2+2] cycloaddition between $Zr(N_2{*}N^{py})(NNPh_2)(py)$ (**1.159**) and phenylallene.[36,39] Upon heating this compound loses pyridine and forms the 7-membered metallacycle $Zr(N_2{*}N^{py})\{N(H)C(Me)C(Ph)\text{-}1,2\text{-}C_6H_4N(Ph)\}$ (**1.163**) analogous to compounds **32** - **37**. Previous work by Mountford has also reported cycloadditions between $Cp_2Ti(NNPh_2)(py)$ (**1.103**) and PhCCPh and the phosphaalkyne ^{t}BuCP, forming $Cp_2Ti\{N(NPh_2)C(Ph)C(Ph)\}$ (**1.111**) and $Cp_2Ti\{N(NPh_2)C(^tBu)P\}$ (**1.110**, Figure 4.6), respectively.[68,69] The latter has been structurally characterised. There are currently no instances of cycloadditions involving alkynes or polar substrates and bis(cyclopentadienyl) zirconium or hafnium hydrazides. Attempts to form cycloadditions between **1.151** or **28** and a range of alkynes of the type RCCR (R = alkyl, silyl, electron-donating or -withdrawing aryl group) under varying conditions, were unsuccessful, forming either the N_α–N_β cleaved, C–H activated products (*vide supra*) or mixtures of products.

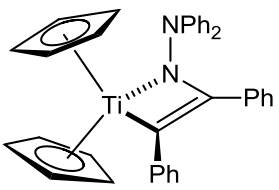

1.111

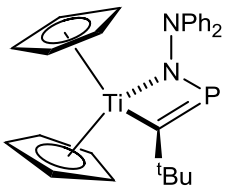

1.110

Figure 4.6. $Cp_2Ti\{N(NPh_2)C(Ph)C(Ph)\}$ (**1.111**) and $Cp_2Ti\{N(NPh_2)C(^tBu)P\}$ (**1.110**).

In order to gain more evidence for a cycloaddition intermediate, attempts were made to synthesise the hydrazides $Cp^R{}_2Zr(NNPh_2)(py)$ (Cp^R = Cp* or Cp^{Me4}, Cp^{Me4} = C_5HMe_4) reasoning that the increased steric bulk should stabilise the azametallacycles. In addition, the volatility of pyridine as the stabilising donor, in place of DMAP, allows it to be removed under reduced pressure in order to shift any equilibrium in favour of a cycloaddition product, as demonstrated by the reactions of $Cp_2Ti(NNPh_2)(py)$ (**1.103**) with PhCCPh and that of $Ti(N_2N^{py})(NNPh_2)(py)$ (**1.97**) with PhCCMe.[68,69]

A range of methods were employed to synthesise $Cp^*{}_2Zr(NNPh_2)(py)$ and $Cp^{Me4}{}_2Zr(NNPh_2)(py)$. However, isolation was only successful in quantities < 10 mg and yields < 3 %. These syntheses are discussed in detail in Appendix D. The failure to find a suitable synthesis meant that the reactions of these hydrazides with alkynes could not be studied.

It was also of interest to structurally characterise a cycloaddition between $Cp_2Ti(NNPh_2)(py)$ (**1.103**) and an alkyne. Taking into account the previous observation that electron withdrawing alkynes stabilise [2+2] cycloaddition products of Group 4 hydrazides, $Cp_2Ti(NNPh_2)(py)$ (**1.103**) was reacted with a range of electron-withdrawing alkynes. As expected, in contrast to the reaction reported with PhCCPh, which formed an equilibrium mixture at room temperature, when $Cp_2Ti(NNPh_2)(py)$ (**1.103**) was reacted with one equivalent of RCCR′ (R = Me, R′ = C_6F_5; R = R′ = 4-$C_6H_4CF_3$; R = R′ = C_6F_5) at room temperature, it was quantitatively converted into the expected azametallacycles, $Cp_2Ti\{N(NPh_2)C(R)C(R')\}$ (R = Me, R′ = C_6F_5 (**38**); R = R′ = 4-$C_6H_4CF_3$ (**39**); R = R′ = C_6F_5 (**40**); Scheme 4.4). The ^1H NMR and an expansion of the $^{13}C\{^1H\}$ NMR

spectra between 205 and 145 ppm of $Cp_2Ti\{N(NPh_2)C(R)C(R')\}$ (R = R′ = 4-$C_6H_4CF_3$ (**39**)), representative for the entire series, are presented in Figure 4.7.

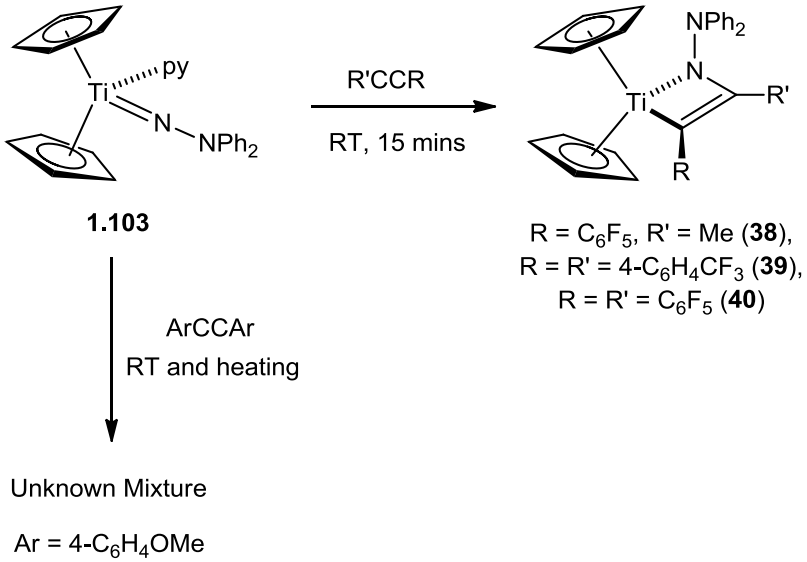

Scheme 4.4. Reactions of $Cp_2Ti(NNPh_2)(py)$ (**1.103**) with alkynes.

The mass spec., elemental analyses and NMR spectra of compounds **38** – **40** are fully consistent with the expected azametallacyclobutenes. The pyridine, present in the starting material has been displaced, and as illustrated for **39**, (Figure 4.7) the carbon resonances at 196.7 and 154.1 ppm corresponding to Ti<u>C</u>(Ar)C(Ar) and TiC(Ar)<u>C</u>(Ar), respectively, are very similar to those seen in the previously reported cycloaddition products $Cp_2Ti\{N(NPh_2)C(Ph)C(Ph)\}$ (**1.111**) and $Ti(N_2N^{py})\{N(NPh_2)C(Me)C(4\text{-}C_6H_4CF_3)\}$ (**4.7**).

The stability of the azametallacyclobutenes was found to follow the sequence **38** < **39** < **40**, increasing as the alkyne becomes more electron-deficient and as the steric bulk increases ($t_{1/2}$ for decomposition in a C_6D_6 solution at room temperature and identical concentrations ~ 12 h (**38**), 24 h (**39**) and 48 h (**40**)). The decomposition products are ^{1}H NMR silent species, possibly formed by reduction of Ti(IV) to Ti(III). Compound **38** is only formed in the isomer shown in Scheme 4.4, the same orientation as that seen between $Ti(N_2N^{py})(NNPh_2)(py)$ (**1.97**) and ArCCMe (See Chapter Two). This was confirmed using HMQC and HMBC correlation exeriments. Despite repeated attempts, diffraction-quality crystals of these compounds could not be obtained.

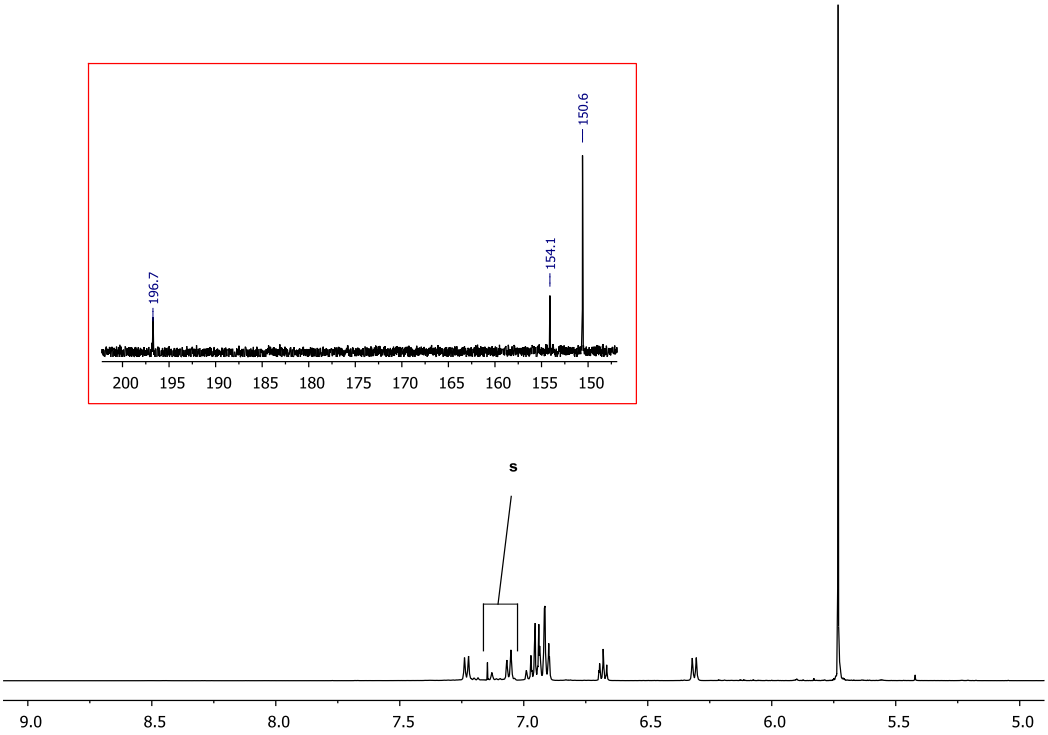

Figure 4.7. ^{1}H NMR spectrum (499.9 MHz, 293 K) of $Cp_2Ti\{N(NPh_2)C(R)C(R')\}$ (R = R′ = 4-$C_6H_4CF_3$ (**39**)) in toluene-d_8. The inset illustrates the $^{13}C\{^{1}H\}$ spectrum (125.7 MHz) between 145 and 205 ppm.

The cycloaddition compounds **38** - **40** do not undergo controlled reactivity, yielding only decomposition products upon heating. In an effort to promote the same reactivity seen with zirconium and hafnium, the reaction with an excess of the electron rich alkyne ArCCAr (Ar = 4-C_6H_4OMe) was performed. It is known from the N_α–N_β insertion reaction presented in Chapter Two that electron rich alkynes promote N_α–N_β cleavage. However, there was no reaction, consistent with electron-rich alkynes forming less stable cycloaddition products (see Chapter Two), and ^{1}H NMR silent species were formed upon heating suggesting further, unknown, reactivity forming Ti(III) species (Scheme 4.4).

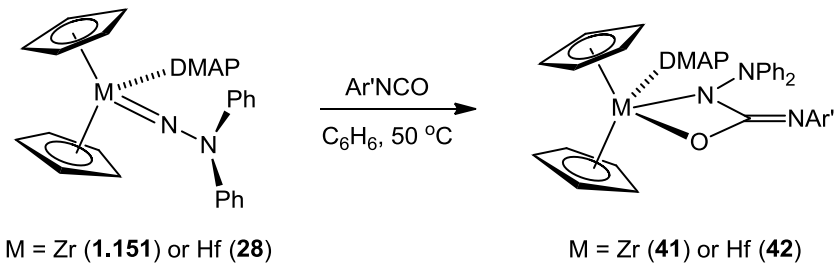

M = Zr (**1.151**) or Hf (**28**) M = Zr (**41**) or Hf (**42**)

Equation 4.6

As shown in Chapter Three, isocyanates can be used to stabilise cycloaddition products as they cannot reductively cleave the N_α–N_β bond. Therefore the reactions of $Cp_2M(NNPh_2)(DMAP)$ (M = Zr (**1.151**) or Hf (**28**)) with isocyanates was investigated. As with alkynes, when **1.151** or **28** were reacted with Ar′NCO (Ar′ = 2,6-$C_6H_4{}^iPr_2$) at room temperature there was no reaction. However, when heated to 50 ºC they formed the highly insoluble cycloaddition compounds $Cp_2M\{N(NPh_2)C(NAr')O\}(DMAP)$ (M = Zr (**41**) or Hf (**42**)) in modest isolated yields (Equation 4.6). Diffraction-quality crystals of $Cp_2M\{N(NPh_2)C(NAr')O\}(DMAP)$ (M = Zr (**41**) or Hf (**42**)) were grown by slow cooling of saturated benzene solutions from 50 °C to room temperature. The molecular structures as determined by X-ray crystallography are presented in Figure 4.8 with selected distances and angles in Table 4.5. These constitute the first examples of cycloadditions between second and third row Group 4 hydrazides and an isocyanate. However, the related compound $Zr(N_2{*}N^{py})\{(NPh_2)C(NPh)S\}(py)$ (**1.172**) and compounds of the type $Zr(N_2{*}N^{py})\{(NPh_2)CM(CO)_xO\}$ (**1.171**, M = Cr, Mo, W, x = 5; M = Fe, x = 4) have been prepared previously by the reaction of $Zr(N_2{*}N^{py})(NNPh_2)(py)$ (**1.159**) with PhNCS and a range of metal carbonyls.[40,129]

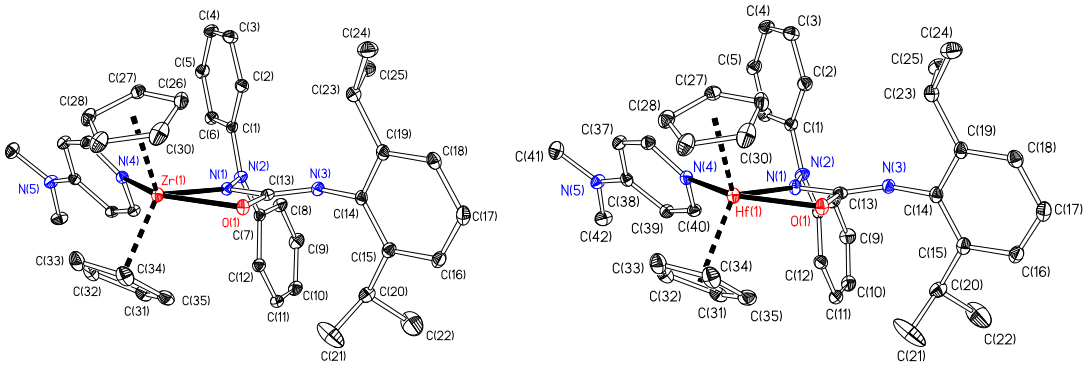

Figure 4.8. Displacement ellipsoid plot (20 % probability) of (a) $Cp_2Zr\{N(NPh_2)C(NAr')O\}(DMAP)$ (**41**) and (b) $Cp_2Hf\{N(NPh_2)C(NAr')O\}(DMAP)$ (**42**). H atoms omitted for clarity.

Table 4.5. Selected distances (Å) and angles (^{o}) for $Cp_2Zr\{N(NPh_2)C(NAr')O\}(DMAP)$ (**41**) and $Cp_2Hf\{N(NPh_2)C(NAr')O\}(DMAP)$ (**42**).

Parameter	**41**	**42**
M(1)–O(1)	2.1997(15)	2.183(3)
M(1)–N(1)	2.1709(17)	2.163(4)
M(1)–N(4)	2.3960(19)	2.367(4)
$M(1)–Cp_{cent(1)}$[a]	2.248	2.230
$M(1)–Cp_{cent(2)}$[a]	2.255	2.232
N(1)–N(2)	1.403(2)	1.391(5)
O(1)–C(13)	1.332(3)	1.334(5)
N(1)–C(13)	1.384(3)	1.382(6)
N(3)–C(13)	1.280(3)	1.280(6)
O(1)–M(1)–N(1)	59.42(6)	59.76(13)
O(1)–M(1)–N(4)	135.92(6)	136.37(12)
$O(1)–M(1)–Cp_{cent(1)}$	98.2	98.1
$O(1)–M(1)–Cp_{cent(2)}$	100.6	100.4
N(1)–M(1)–N(4)	76.51(7)	76.62(14)
$N(1)–M(1)–Cp_{cent(1)}$	117.1	117.0
$N(1)–M(1)–Cp_{cent(2)}$	118.0	118.1
$N(4)–M(1)–Cp_{cent(1)}$	102.8	102.9
$N(4)–M(1)–Cp_{cent(2)}$	99.0	98.8
$Cp_{cent(1)}–M(1)–Cp_{cent(2)}$	123.9	123.9
M(1)–O(1)–C(13)	97.31(12)	97.3(3)
M(1)–N(1)–C(13)	96.99(13)	96.7(3)
O(1)–C(13)–N(1)	105.78(18)	105.7(4)

[a] Cp_{cent} is the computed Cp ring carbon centroid.

Both $Cp_2Zr\{N(NPh_2)C(NAr')O\}(DMAP)$ (**41**) and $Cp_2Hf\{N(NPh_2)C(NAr')O\}(DMAP)$ (**42**) contain a κ^2-*N,O* bound $\{N(NPh_2)C(NAr')O\}$ ligand formed by the [2+2] cycloaddition of Ar′NCO to the $NNPh_2$ functional group. They also contain DMAP, with the cyclopentadienyl ligands taking the remaining two coordination sites of the distorted trigonal bipyramidal metal centre.

The M–Cp_{cent} distances are slightly reduced compared to that of the starting hydrazides. (**41**, avg. Zr–Cp_{cent} = 2.252 Å; **42**, avg. Hf–Cp_{cent} = 2.231 Å; **1.151**, avg. Zr–Cp_{cent} = 2.299 Å; **28**, avg. Hf–Cp_{cent} = 2.257 Å). In addition the Cp_{cent}–M–Cp_{cent} angles are slightly more acute (**41**, Cp_{cent}–Zr–Cp_{cent} = 123.9 º; **42**, Cp_{cent}–Hf–Cp_{cent} = 123.9 º; **1.151**, Cp_{cent}–Zr–Cp_{cent} = 125.5 º; **28**, Cp_{cent}–Hf–Cp_{cent} = 125.8 º). The M–Cp_{cent} distances for **41** and **42** are slightly larger than those seen in other bis(cyclopentadienyl) complexes while the Cp_{cent}–M–Cp_{cent} angles are more acute (e.g. Cp_2MCl_2 avg. M–Cp_{cent} = 2.194 Å (M = Zr), 2.182 Å (M = Hf); Cp_{cent}–M–Cp_{cent} = 129.0 º (M = Zr), 129.1 º (M = Hf)).

The M(1)–O(1) and M(1)–N(1) bond distances are in the usual ranges for single bonds and comparable with the other metallacycles described below. The M(1)–N(1) distances are lengthened when compared to the starting hydrazides **1.151** and **28**, consistent with the decrease in bond order. There is also a slight lengthening of the N_α–N_β bonds (N(1)–N(2) = 1.403(2) Å (**41**), 1.391(5) Å (**42**); N_α–N_β = 1.351(10) Å (**1.151**), 1.372(6) Å (**28**)) as expected from other cycloaddition products and the DMAP distances increase by *ca*. 0.08 Å. Note that while DMAP remains bound in **41** and **42**, with bis(cyclopentadienyl) zirconium imido complexes, the donor present in the starting materials is displaced on forming the cycloaddition products with alkynes.[86] This is also true for the products with diamide-amine supported titanium hydrazides. [2+2] cycloadditions with alkynes lead to pyridine displacement, but with Ar′NCO it remains bound (Chapters Two and Three).

The main point of interest in **41** and **42** are the four-membered metalla-ureate moieties $M\{N(NPh_2)C(NAr')O\}$. The steric influence of the bulky Ar′ group causes both to form as the *N,O*- bound isomer, despite calculations on other systems (see Chapter Three) indicating that this is, electronically, the least stable isomer. An *N,N*′- bound [2+2] cycloaddition, $Zr(Me_4taa)\{N(Ar')C(N^tBu)O\}$(**4.8**, Ar′ = 2,6-$C_6H_3{}^iPr_2$) between a zirconium imide and ^{t}BuNCO has been observed by Mountford.[130] While there are

no examples of reactions between $Cp_2Zr(NAr)(THF)$ (Ar = aryl) and isocyanates, the reactivity of $Cp_2Zr(N^tBu)(THF)$ (**1.45**) has been studied. Compounds **41** and **42** are stable cycloadditions with no elimination of the carbodiimide fragment occurring, in contrast $Cp_2Zr\{N(^tBu)C(N^tBu)O\}$ rapidly extrudes $^tBuNCN^tBu$, leading to the formation of $[Cp_2Zr(\mu\text{-}O)]_2$.[64] This is part of a more general trend in early metal chemistry that sees imido/hydrazido cycloadditions of the type $(L)M\{N(Ar)C(NR)O\}$ (M = Group 4 metal, Ar = aryl or NAr_2, R = alkyl or aryl) less likely to eliminate the carbodiimide fragment while those of the type $(L)M\{N(R')C(NR)O\}$ (M = Group 4 metal, R′ = alkyl or NR_2, R = alkyl or aryl) show a higher propensity to. In concordance with this trend and in addition to the stable cycloadditions above, Woo has reported stable zirconium and hafnium cycloadditions between porphyrin supported aryl imides and *tert*-butylisocyanate.[92] While there is no extrusion of the carbodiimide, isomerisation of the (Ar)*N*,*O*- bound metallacycle to form the (^{t}Bu)*N*,*O*- bound occurs for both Zr and Hf. The contrast between stable cycloadditions and elimination has been studied in more depth by Mountford using compounds of the type $Cp^*Ti\{MeC(N^iPr)_2\}(NNR_2)$ (R = Ph (**1.104**) or Me (**1.106**)).[131]

Despite examples of [2+2] cycloadditions between bis(cyclopentadienyl) supported zirconium or hafnium hydrazides and alkynes remaining elusive, the above results, when combined with the literature examples of cycloadditions with related substrates and the studies on similar imido systems, provide clear evidence that azametallacyclobutenes can be implicated as intermediates in the formation of the 7-membered metallacycles from Group 4 hydrazides and alkynes.

4.6. Selectivity of the combined N_α–N_β cleavage, C–H activation reaction of bis(cyclopentadienyl) Group 4 hydrazides with unsymmetrical alkynes

The reaction between $Ti(N_2N^{Me})(NNPh_2)(py)$ (**1.93**) and ArCCMe proceeds in a regiospecific manner, only the isomer with Ar<u>C</u> bound to N_α and the alkyne substituents arranged *cis* to each other is observed (Equation 4.1). Previous studies of the reactions of $Cp_2Zr(NNPh_2)(DMAP)$ (**1.151**) with alkynes[25] and the experiments described so far in this Chapter all involve symmetrical alkynes. As such they give no information on the selectivity of the N_α–N_β cleavage, C–H activation reaction. $Ti(HN_2N^{Me})\{N(SiMe_3)C(Me)C(Fc)\text{-}1,2\text{-}C_6H_4N(Ph)\}$ (**24**) was formed exclusively as the isomer shown (Equation 4.2, Figure 4.1). However, this was isolated from a

mixture of products, therefore the presence of small amounts of other isomers cannot be ruled out. In his study of the reaction, Gade observed high selectivity in favour of the isomer with the aryl group bound to the activated phenyl ring when terminal alkynes were used. With internal alkynes there was rather less selectivity (Figure 4.9, Table 4.6). The compounds shown in Figure 4.9 were not isolated, the selectivity being assigned by analogy from the indoles produced following protonation and NH_3 elimination. The origins of this selectivity have not been addressed in his study of the mechanism.[36,39]

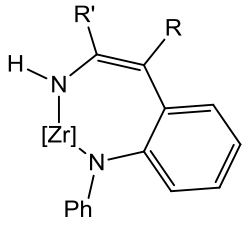

4.9a

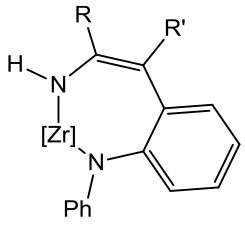

4.9b

Figure 4.9. 7-membered metallacyclic intermediates (inferred from the phenyl indole products) formed between RCCR′ and H_2NNPh_2 with 10 mol % $Zr(N_2^{Xyl}N^{py})(NMe_2)_2$. [Zr] = $Zr(N_2^{Xyl}N^{py})$.

Table 4.6. Ratios of the 7-membered metallacyclic intermediates (derived from the phenyl indole products) formed between RCCR′ and H_2NNPh_2 with 10 mol % $Zr(N_2^{Xyl}N^{py})(NMe_2)_2$.[36,39]

R	R′	**4.9a**	**4.9b**
Ph	H	>90	<10
4-C_6H_4Br	H	>90	<10
4-C_6H_4OMe	H	83	17
Ph	Me	67	33
Et	Me	67	33

The steric and electronic influences of alkynes involved in [2+2] cycloadditions with bis(cyclopentadienyl) zirconium imido compounds are well documented,[86] the favoured metallacycles placing the bulkier alkyne substituent α to the zirconium centre (Table 4.7). This has been attributed to steric repulsion between the alkyne and N_{imide} substituent (in the case of **1.151** this would be NPh_2). This effect increases with increasing steric bulk, and for ^{t}BuCCMe is the only regioisomer observed (Figure 4.10, Table 4.7). Under thermodynamic control there is a tendency to favour the regioisomer which positions the aryl group α to the metal centre. This effect increases as the aryl ring becomes more electron deficient (Figure 4.10, Table 4.7). No [2+2] cycloadditions between Group 4 imides or hydrazides and silyl-substituted alkynes have been reported.[80,86,132]

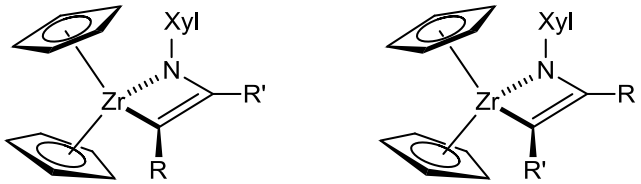

1.51a **1.51b**

Figure 4.10. Possible cycloaddition products formed between $Cp_2Zr(NXyl)(4\text{-}NC_5H_4{}^{t}Bu)$ (**1.47**) and a range of asymmetric alkynes.[86]

Table 4.7. Ratios of cycloaddition products formed between $Cp_2Zr(NXyl)(4\text{-}NC_5H_4{}^{t}Bu)$ (**1.47**) and a range of asymmetric alkynes.[86]

Temperature (ºC)	R	R′	**1.51a**	**1.51b**
25	^{t}Bu	Me	> 98	< 2
25	Ph	Me	82	18
110	Ph	Me	> 99	< 1
25	4-$C_6H_4CF_3$	4-C_6H_4Me	35	65
68.5	4-$C_6H_4CF_3$	4-C_6H_4Me	82	18

Initially, to provide a comparison with the reactivity seen in Chapter Two, $Cp_2Zr(NNPh_2)(DMAP)$ (**1.151**) was reacted with one equivalent of PhCCMe at 60 ºC. The two possible isomers, $Cp_2Zr\{N(H)C(Ph)C(Me)\text{-}1,2\text{-}C_6H_4N(Ph)\}$ (**43a**) and $Cp_2Zr\{N(H)C(Me)C(Ph)\text{-}1,2\text{-}C_6H_4N(Ph)\}$ (**43b**), were formed in a 38:62 ratio (Equation 4.7). The reaction was then carried out using $Cp_2Zr(CH_2CH_2{}^tBu)(NHNPh_2)$ (**1.152**) *in lieu* of **1.151** and at a higher temperature (110 ºC). The products **43a** and **43b** were found to form in the same ratio within experimental error.

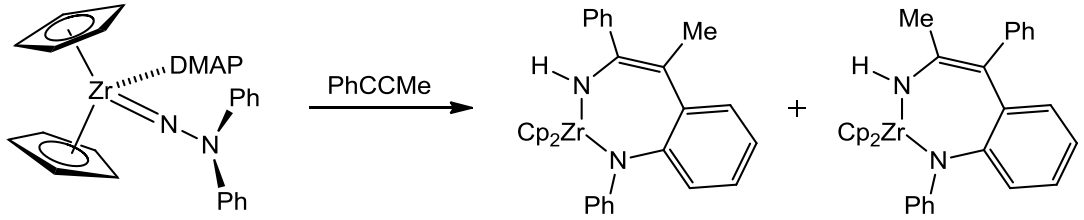

1.151 **43a** **43b**

Equation 4.7

In order to further probe the selectivity of the reaction, **1.151** was then reacted with the more sterically differentiated alkynes RCCR′ (R = ^{t}Bu or $SiMe_3$, R′ = Me; R = $SiMe_3$, R′ = Ph). In these instances the reactions were slow below 90 ºC, with ^{t}BuCCMe reacting significantly faster than either of the silyl substituted alkynes and only one isomer being formed in each case (^{t}BuCCMe, $t_{1/2}$ = 4,650 s; $Me_3SiCCMe$, $t_{1/2}$ = 17,360 s; PhCCPh, $t_{1/2}$ = 1,670 s; MeCCMe, $t_{1/2}$ = 750 s, 74 °C, 20 equivalents alkyne, 10.2 equivalents DMAP).

The regiochemistry of the product obtained from the reaction between $Cp_2Zr(NNPh_2)(DMAP)$ (**1.151**) and $Me_3SiCCMe$ was determined by X-ray analysis (Figure 4.13) and shown to be $Cp_2Zr\{N(H)C(Me)C(SiMe_3)\text{-}1,2\text{-}C_6H_4N(Ph)\}$ (**44**, Scheme 4.5). In this isomer the Me<u>C</u> carbon is adjacent to the nitrogen apparently derived from N_α in the starting hydrazide, the Me_3Si<u>C</u> bound to the activated phenyl ring.

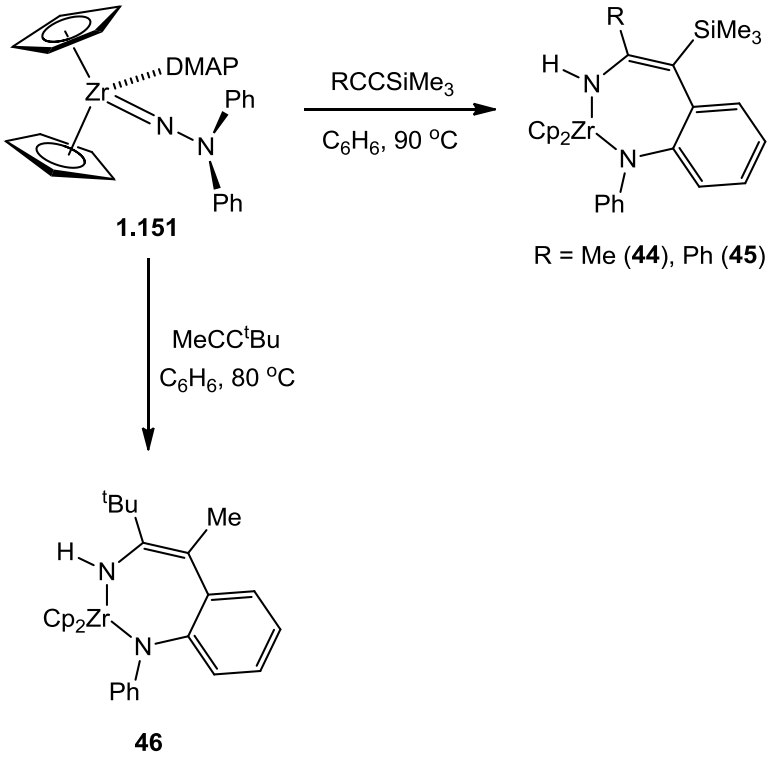

Scheme 4.5. Reactions of $Cp_2Zr(NNPh_2)(DMAP)$ (**1.151**) with Me_3SiCCR (R = Me or Ph) and ^tBuCCMe.

Wary that this could be a crystal of a minor product, not seen by ^1H NMR spectroscopy, this selectivity was confirmed to be identical in the bulk material using a 1D nOe difference experiment (Figure 4.11). Irradiation of the methyl group augments the NH resonance indicating they are close in space. When irradiated, the $SiMe_3$ group was also shown to be close to several of the phenyl resonances, but not the NH. Analogous experiments showed that $Me_3SiCCPh$ formed the same isomer, namely $Cp_2Zr\{N(H)C(Ph)C(SiMe_3)\text{-}1,2\text{-}C_6H_4N(Ph)\}$ (**45**, Scheme 4.5). The molecular structure of $Cp_2Zr\{N(H)C(Me)C(SiMe_3)\text{-}1,2\text{-}C_6H_4N(Ph)\}$ (**44**) as determined by X-ray crystallography is presented in Figure 4.13 with selected distances and angles in Table 4.8.

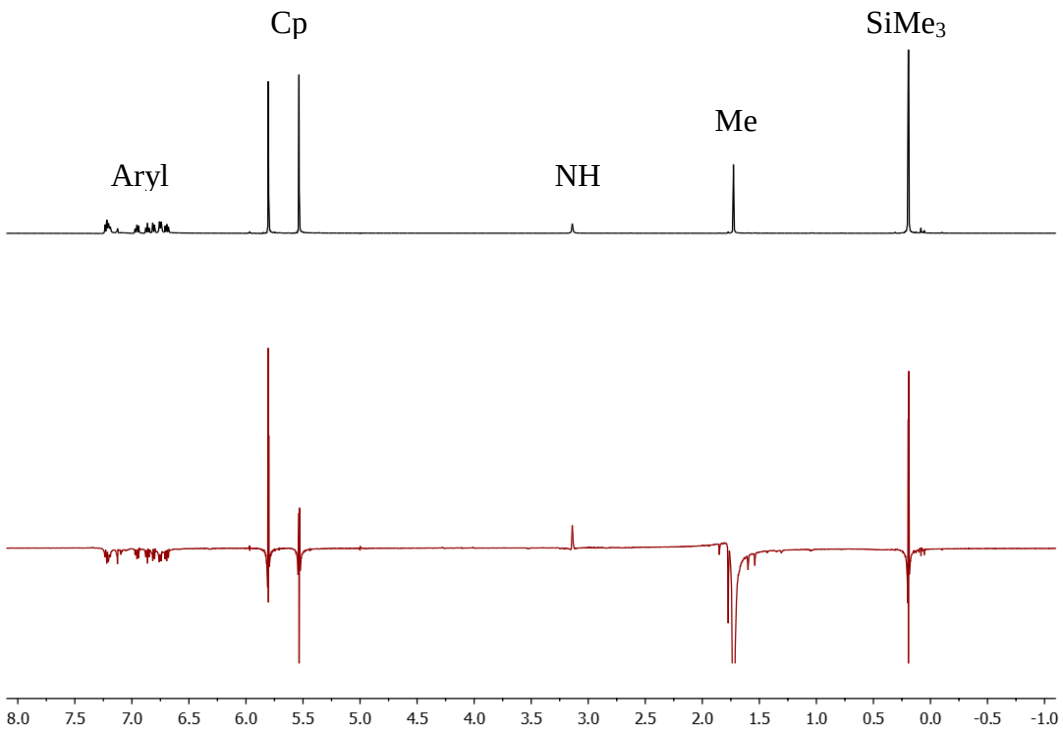

Figure 4.11. Top: ^{1}H NMR spectrum (499.9 MHz, 298 K) of $Cp_2Zr\{N(H)C(Me)C(SiMe_3)$-1,2-$C_6H_4N(Ph)\}$ (**44**) in C_6D_6. Bottom: nOe difference spectrum with Me resonance irradiated, indicating enhancement of the NH resonance.

In contrast to **44** and **45**, nOe experiments on the product obtained with ^{t}BuCCMe indicated that the sole isomer obtained in this instance, $Cp_2Zr\{N(H)C(^{t}Bu)C(Me)$-1,2-$C_6H_4N(Ph)\}$ (**46**, Scheme 4.5), has the alkyne inserted with the opposite orientation (Figure 4.12). This can be seen by the nOe between the ^{t}Bu resonance and NH proton. This complete (and opposite) selectivity for ^{t}Bu and $SiMe_3$ groups is very interesting and is discussed in more detail in the computational section. It is important to note that the same products were formed at 120 ºC and with $Cp_2Zr(NHNPh_2)(CH_2CH_2{}^{t}Bu)$ (**1.152**) *in lieu* of **1.151**. This indicates that DMAP has no effect on the selectivity and that in each case the reaction proceeds *via* base-free $Cp_2Zr(NNPh_2)$ (**1.153**).

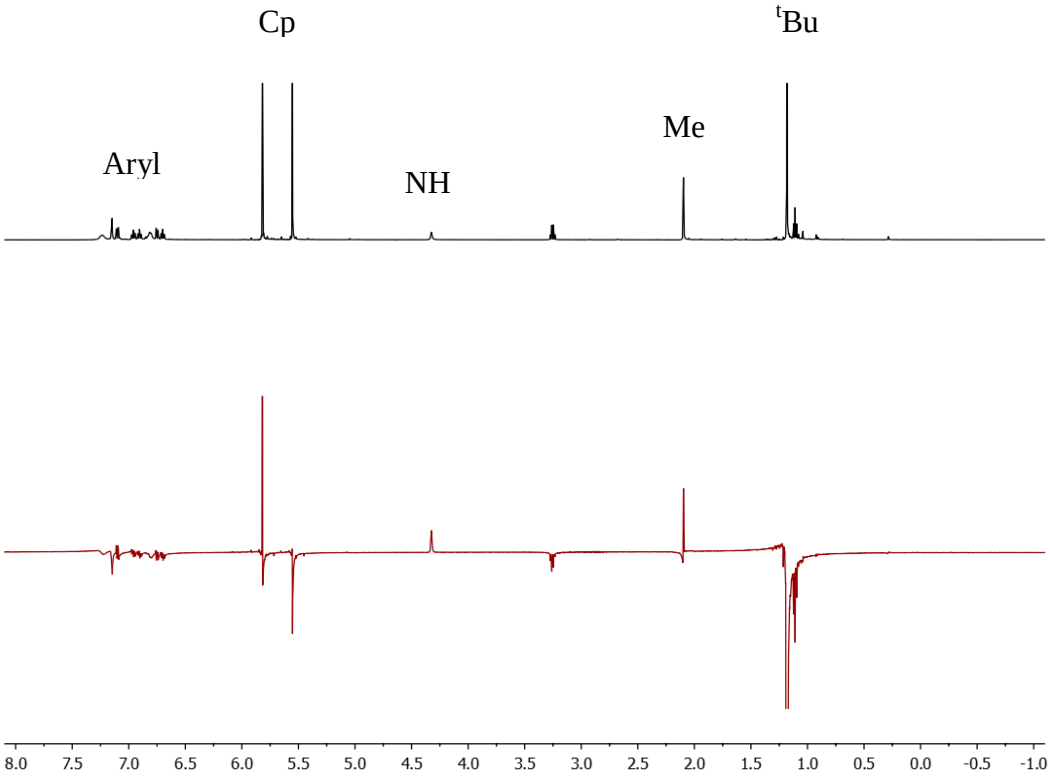

Figure 4.12. Top: ^{1}H NMR spectrum (499.9 MHz, 298 K) of $Cp_2Zr\{N(H)C(^tBu)C(Me)$-1,2-$C_6H_4N(Ph)\}$ (**46**) in C_6D_6. Bottom: nOe difference spectrum with ^{t}Bu resonance irradiated, indicating enhancement of the NH resonance.

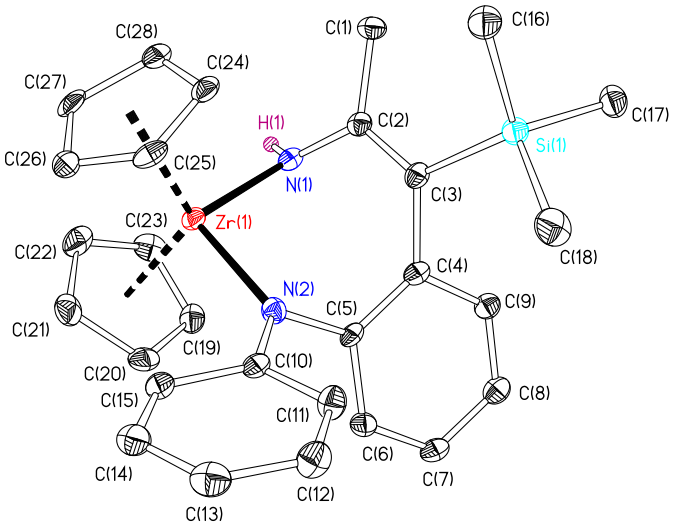

Figure 4.13. Displacement ellipsoid plot (20 % probability) of $Cp_2Zr\{N(H)C(Me)C(SiMe_3)$-1,2-$C_6H_4N(Ph)\}$ (**44**). C bound H atoms omitted for clarity. H(1) drawn as a sphere of arbitrary radius.

Table 4.8. Selected distances (Å) and angles (°) for $Cp_2Zr\{N(H)C(Me)C(SiMe_3)$-1,2-$C_6H_4N(Ph)\}$ (**44**).

Zr(1)−N(1)	2.110(5)	N(1)−Zr(1)−N(2)	100.28(19)
Zr(1)−N(2)	2.140(5)	N(1)−Zr(1)−$C_{cent(1)}$	108.3
Zr(1)−$C_{cent(1)}$[a]	2.248	N(1)−Zr(1)−$C_{cent(2)}$	102.6
Zr(1)−$C_{cent(2)}$[a]	2.255	N(2)−Zr(1)−$C_{cent(1)}$	107.6
N(1)−C(2)	1.386(8)	N(2)−Zr(1)−$C_{cent(2)}$	108.0
N(2)−C(5)	1.416(8)	$C_{cent(1)}$−Zr(1)−$C_{cent(2)}$	126.9
C(1)−C(2)	1.506(8)	Zr(1)−N(1)−C(2)	114.3(4)
C(2)−C(3)	1.376(8)	Zr(1)−N(2)−C(5)	112.5(4)
C(3)−C(4)	1.502(8)	N(1)−C(2)−C(3)	121.6(5)
C(4)−C(5)	1.413(9)	C(2)−C(3)−C(4)	119.9(5)
		C(3)−C(4)−C(5)	125.5(5)
		N(2)−C(5)−C(4)	122.9(5)

[a] Cp_{cent} is the computed Cp ring carbon centroid.

The solid state structure of $Cp_2Zr\{N(H)C(Me)C(SiMe_3)$-1,2-$C_6H_4N(Ph)\}$ (**44**) is fully consistent with the NMR data and the structure drawn in Scheme 4.5. Compound **44** is very similar to $Cp_2Zr\{N(H)C(Me)C(Me)$-1,2-$C_6H_4N(Ph)\}$ (**32**), $Cp_2Hf\{N(H)C(Me)C(Me)$-1,2-$C_6H_4N(Ph)\}$ (**33**) and $Cp_2Hf\{N(H)C(Ph)C(Ph)$-1,2-$C_6H_4N(Ph)\}$ (**36**, *vide supra*). It contains the same type of 7-membered metallacycle formed by N_α–N_β bond cleavage and C–H activation of the hydrazide moiety of $Cp_2Zr(NNPh_2)(DMAP)$ (**1.151**), with the zirconium in an approximate tetrahedral environment. The main point of interest is the presence of only one isomer despite $Me_3SiCCMe$ being an unsymmetrical alkyne, as discussed above.

The distances to the metal centre are all the same within error as those in **32**, although there is a slight lenthening of one of the Zr(1)–Cp_{cent} distances relative to the other, as seen in **33** (**44**, Zr(1)–$Cp_{cent(1)}$ = 2.248 Å, Zr(1)–$Cp_{cent(2)}$ = 2.255 Å; **33**, Hf(1)–$Cp_{cent(1)}$ = 2.219 Å, Hf(1)–$Cp_{cent(2)}$ = 2.249 Å). The C(2)–C(3) bond length (1.376(8) Å) is

indicative of a C=C double bond and the angle between cyclopentadienyl rings is 126.9 º, very similar to that in **32** (127.1 º).

Using the nOe spectrum it is possible to differentiate between the two cyclopentadienyl rings. There are close contacts between one of the hydrogens bound to both C(1) and C(16) with one bound to C(24) (2.700 and 2.528 Å, respectively). This implies that the resonance at 5.83 ppm corresponds to the 'up' ring (C(24)–C(28)) as there is a clear enhancement of this resonance in the methyl irradiated spectrum (Figure 4.11), while that at 5.57 ppm corresponds to the 'down' ring (C(19)–C(23)).

4.7. Mechanistic investigations of the combined N_α–N_β cleavage, C–H activation reaction

In order to further probe the mechanism leading to the formation of the 7-membered metallacycles of the type $Cp_2Zr\{N(H)C(R)C(R')$-1,2-$C_6H_4N(Ph)\}$ a range of mechanistic studies were carried out. The energetics of DMAP loss (k_1, Scheme 4.7, *vide infra*) proved to be important in understanding the mechanism, as such they are described first.

The rate of ligand exchange from $Cp_2Zr(NNPh_2)$(DMAP) (**1.151**) can be explicitly measured by looking at the line broadening of a mixture of **1.151** and DMAP. However, this proved impossible due to the low temperatures required to freeze out the exchange and the sparing solubility of **1.151** in toluene at these temperatures. In order to overcome this problem $Cp'_2Zr(NNPh_2)$(DMAP) (**29**) was synthesised (Equation 4.5). The methyl group reduces the symmetry of the cyclopentadienyl ring and ensures that, instead of all being equivalent, the four cyclopentadienyl protons are diastereotopic.

The DMAP ligand in **29** exchanges readily at room temperature, as demonstrated by the four broad resonances attributable to the cyclopentadienyl ring protons. On warming to 35 ºC these coalesced to become two resonances, while cooling led to sharpening and the observation of ^{1}H-^{1}H coupling below -5 ºC. Analogous features were seen in the $^{13}C\{^1H\}$ NMR spectrum. It is immediately clear from these observations that the exchange process is dissociative rather than associative.

In a dissociative process, such as that outlined in Scheme 4.6, DMAP loss from **29a** forms base-free **29′**. It can then either bind in the same position, reforming **29a**, or on

the opposite side leading to **29b**. In the latter the diastereotopic ring protons and carbons of Cp′ have undergone pairwise exchange. As the rate of DMAP exchange increases, the four proton resonances broaden and/or coalesce. From this broadening, the rate (k_1) of DMAP dissociation at different temperatures can be calculated.[133]

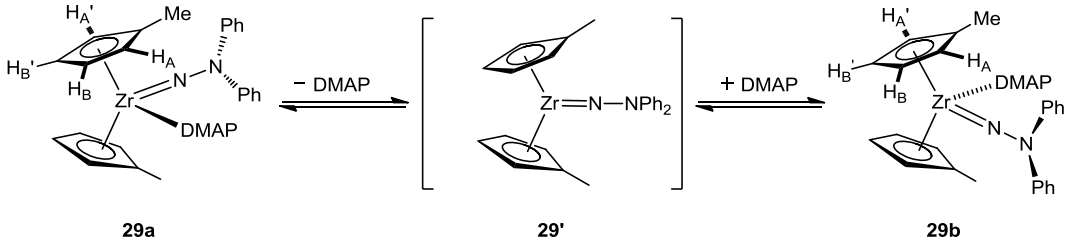

Scheme 4.6. Interchanging of H_A and H_A' *via* DMAP exchange in $Cp'_2Zr(NNPh_2)(DMAP)$ (**29**).

Unfortunately the exchange of H_A/H_A' and H_B/H_B' cound not be modelled due to temperature dependant shifts and overlapping resonances, so the broadening of the $^{13}C\{^1H\}$ resonances was measured instead.[134] The Eyring plot for the process is shown in Figure 4.14 and gives activation parameters of $\Delta H^{\ddagger}$ = 22.6(16) kcal mol^{-1} and $\Delta S^{\ddagger}$ = 25(5) cal mol^{-1} K^{-1}, comparable to those obtained for pyridine loss in other early second row transition metal compounds.[135-137] The free energy of activation at 347 K is 14(3) kcal mol^{-1}. Note that the observed rate of reaction for formation of the N_α–N_β bond cleaved C–H activated product is comparable for both $Cp_2Zr(NNPh_2)(DMAP)$ (**1.151**) and $Cp'_2Zr(NNPh_2)(DMAP)$ (**29**, k_{obs} = 0.416(3) × 10^{-3} s^{-1} (**1.151**) and 0.294(1) × 10^{-3} s^{-1} (**29**), 74 ºC, 20 equivalents PhCCPh, 10.2 equivalents DMAP). This indicates that both **1.151** and **29** are chemically similar and it is fair to estimate k_1 for **1.151** from **29**.

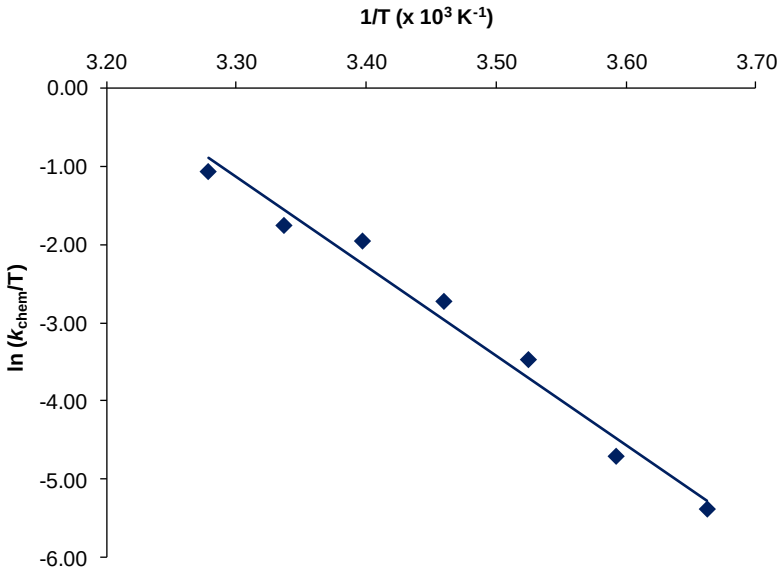

Figure 4.14. Plot of ln(k_1/T) *vs.* 1/T. Activation parameters derived from the line broadening of $^{13}C\{^1H\}$ resonances (r^2 = 0.978): $\Delta H^{\ddagger}$ = 22.6(16) kcal mol^{-1}, $\Delta S^{\ddagger}$ = 25(5) cal mol^{-1} K^{-1}; $\Delta G_{347}^{\ddagger}$ = 14(3) kcal mol^{-1}.

The reaction between $Cp_2Zr(NNPh_2)(DMAP)$ (**1.151**) and PhCCPh in toluene-d_8 was monitored by ^1H NMR spectroscopy between 30 and 90 °C in the presence of 1,4-dimethoxybenzene as an internal standard. Between 30 and 50 ^oC there was no reaction between **1.151** and the alkyne, while between 55 and 60 ^oC the starting materials were slowly but quantitatively converted to $Cp_2Zr\{N(H)C(Ph)C(Ph)$-1,2-$C_6H_4N(Ph)\}$ (**1.156**). No intermediates or other products were observed, and the reaction was complete after 16 h at 60 ^oC. When the reaction between **1.151** and an excess of PhCCPh (10 – 40 equivalents) in the presence of DMAP (10.2 equivalents) was followed at 74 °C in toluene-d_8, the decay of the hydrazide starting material followed well-behaved pseudo first order kinetics as illustrated in Figure 4.15. The evolution of **1.156** could not be followed due to the fluxional nature of the cyclopentadienyl rings at this temperature preventing accurate intensity or integration measurements. Other resonances were obscured by the excess DMAP and alkyne.[138]

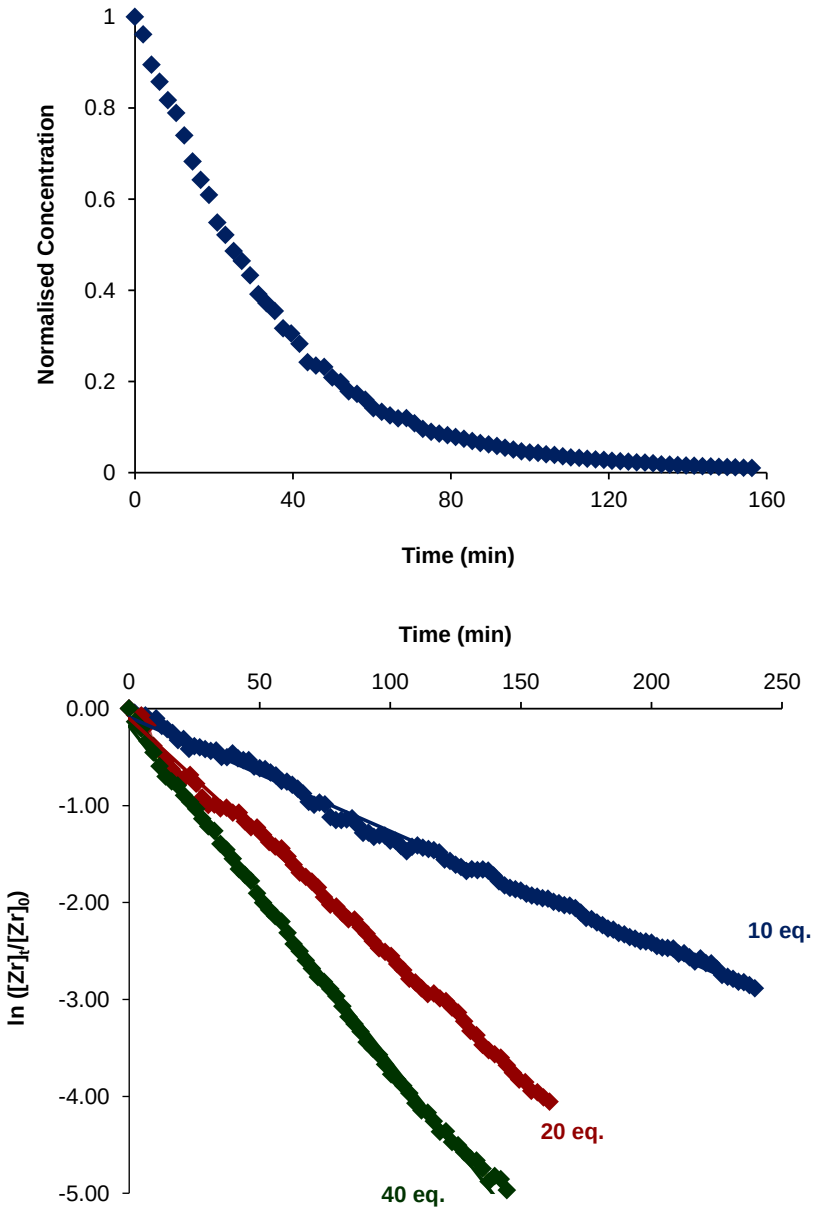

Figure 4.15. Top: decay of $Cp_2Zr(NNPh_2)(DMAP)$ (**1.151**) with time for the reaction between **1.151** and PhCCPh (30 equivalents) at 74 ^{o}C. Bottom: pseudo first order ln plots for the reaction of $Cp_2Zr(NNPh_2)(DMAP)$ (**1.151**) with PhCCPh (10, 20, 40 equivalents) at 74 ^{o}C. The best-fit lines shown had avg. r^2 = 0.996, range 0.994 – 0.999.

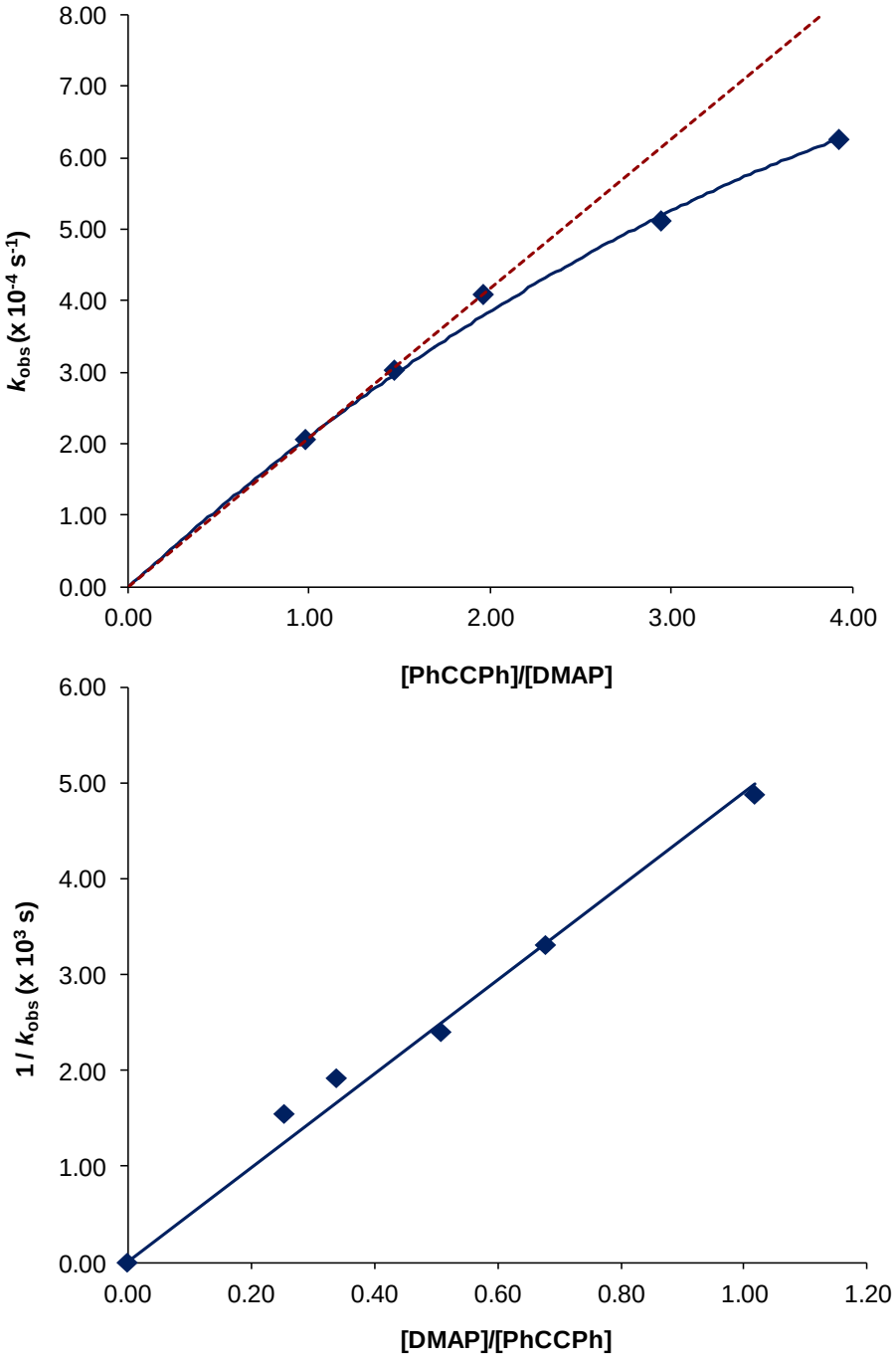

Figure 4.16. Top: plot of k_{obs} *vs.* equivalents of alkyne for the reaction of $Cp_2Zr(NNPh_2)(DMAP)$ (**1.151**) with PhCCPh; the dotted line is that expected for a linear relationship between k_{obs} and equivalents based on extrapolation from the first data point ([PhCCPh]/[DMAP] = 0.98). Bottom: the corresponding double-reciprocal plot. The linear fit (r^2 = 0.991) gives a gradient of 4.9(2) × 10^3 s.

As in Chapter Two and the N_α–N_β insertion reaction, the observed rate constants (k_{obs}) obtained from the linear ln plots do not scale linearly as the ratio of

[PhCCPh]/[DMAP] increases (Figure 4.16, top). At high values of [PhCCPh]/[DMAP]:[**1.151**] the onset of saturation kinetics is very evident. In contrast, the corresponding double-reciprocal plot (Figure 4.16, bottom) is linear over the range of PhCCPh equivalents used.[63,86] The inverse of the rate of DMAP dissociation from **1.151** ($1/k_1$, Equation 4.10) corresponds to the intercept at the vertical axis (*vide infra*) and, as discussed above, is similar for both **1.151** and **29**. This allows the inverse rate of DMAP loss from **29** (8.0×10^{-5} s, *vide supra*) to be used as a data point in the double-reciprocal plots described below.[139]

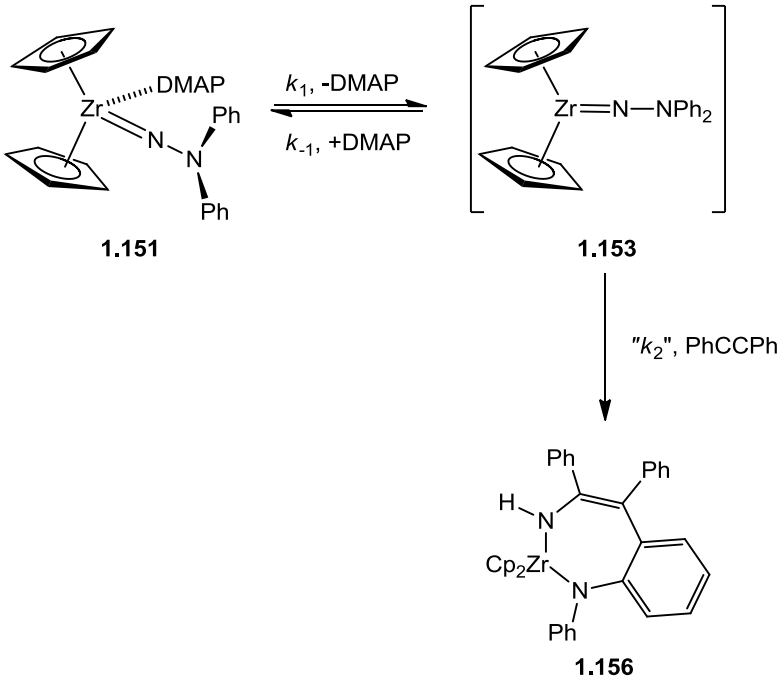

Scheme 4.7. Experimentally implicated steps in the formation of **1.156** from **1.151** and PhCCPh.

$$\text{Rate} = k_{obs}[\mathbf{1.151}] \qquad \text{(Equation 4.8)}$$

$$k_{obs} = \frac{k_1 k_2[\text{PhCCPh}]}{k_2[\text{PhCCPh}] + k_{-1}[\text{DMAP}]} \qquad \text{(Equation 4.9)}$$

$$\frac{1}{k_{obs}} = \frac{1}{k_1} + \frac{k_{-1}}{k_1 k_2} \times \frac{[\text{DMAP}]}{[\text{PhCCPh}]} \qquad \text{(Equation 4.10)}$$

At first sight, the data in Figures 4.15 and 4.16 are consistent with the general process outlined in Scheme 4.7, in which dissociation of DMAP from **1.151** forms the reactive base-free intermediate **1.153** prior to the rate limiting step (or steps), the rate constant

for which is denoted as "k_2". Scheme 4.7 is analogous to that described in Chapter Two and other, previously established, mechanisms[86,137] for the cycloaddition reactions of the base-stabilised imides $Cp_2Zr(NXyl)(L)$ (**1.47**, L = THF, $NC_5H_4{}^tBu$ or $OPPh_3$) or $Ti(N_2N^R)(N^tBu)(py)$ (N_2N^R = N_2N^{py} (**1.71**) or $N_2{}^{Xyl}N^{py}$) with alkynes. Scheme 4.7 predicts that, in the presence of an excess of alkyne, the rates of reaction should follow pseudo first order kinetics according to Equation 4.8 where k_{obs} is given by Equation 4.9, with the onset of saturation kinetics occurring at high alkyne concentrations. The linear double-reciprocal plot is consistent with Equation 4.10 and is found to have a gradient of 4.9(2) × 10^3 s. Using the value of k_1 calculated for **29** (*vide supra*) this gives a ratio of k_{-1}/k_2 = 61(3) × 10^6 (Equation 4.10).

According to Equations 4.9 and 4.10, varying the equivalents of DMAP while keeping the equivalents of PhCCPh constant should also produce plots analogous to those in Figures 4.15 and 4.16. When the reaction between $Cp_2Zr(NNPh_2)(DMAP)$ (**1.151**) and an excess of PhCCPh (20 equivalents) in toluene-d_8 was followed at 74 ºC in the presence of varying amounts of DMAP (10 – 20 equivalents) it again followed well-behaved pseudo first order kinetics. In agreement with the observations from varying the alkyne concentration, the observed rate constants, obtained from the linear ln plots, do not scale linearly with the inverse of the equivalents of DMAP added (Figure 4.17, top), although the deviation is not large as the range of DMAP concentrations which could be used was limited by its solubility. Again, using $1/k_1$ obtained explicitly from **29** as the intercept of the vertical axis, the plot of $1/k_{obs}$ against equivalents of DMAP is linear over the range studied and has a gradient of 4.19(12) × 10^3 s (Figure 4.17, bottom). This gives a k_{-1}/k_2 ratio of 52.4(15) × 10^6, as expected, very similar to that obtained by varying the alkyne concentration. The ratios of k_{-1}/k_2 indicate that $Cp_2Zr(NNPh_2)$ (**1.153**) reacts with DMAP between 52.4(15) and 61(3) × 10^6 times faster than with PhCCPh. Therefore the barrier to formation of **1.156** is 12.32(16) kcal mol^{-1} higher than re-formation of **1.151**.

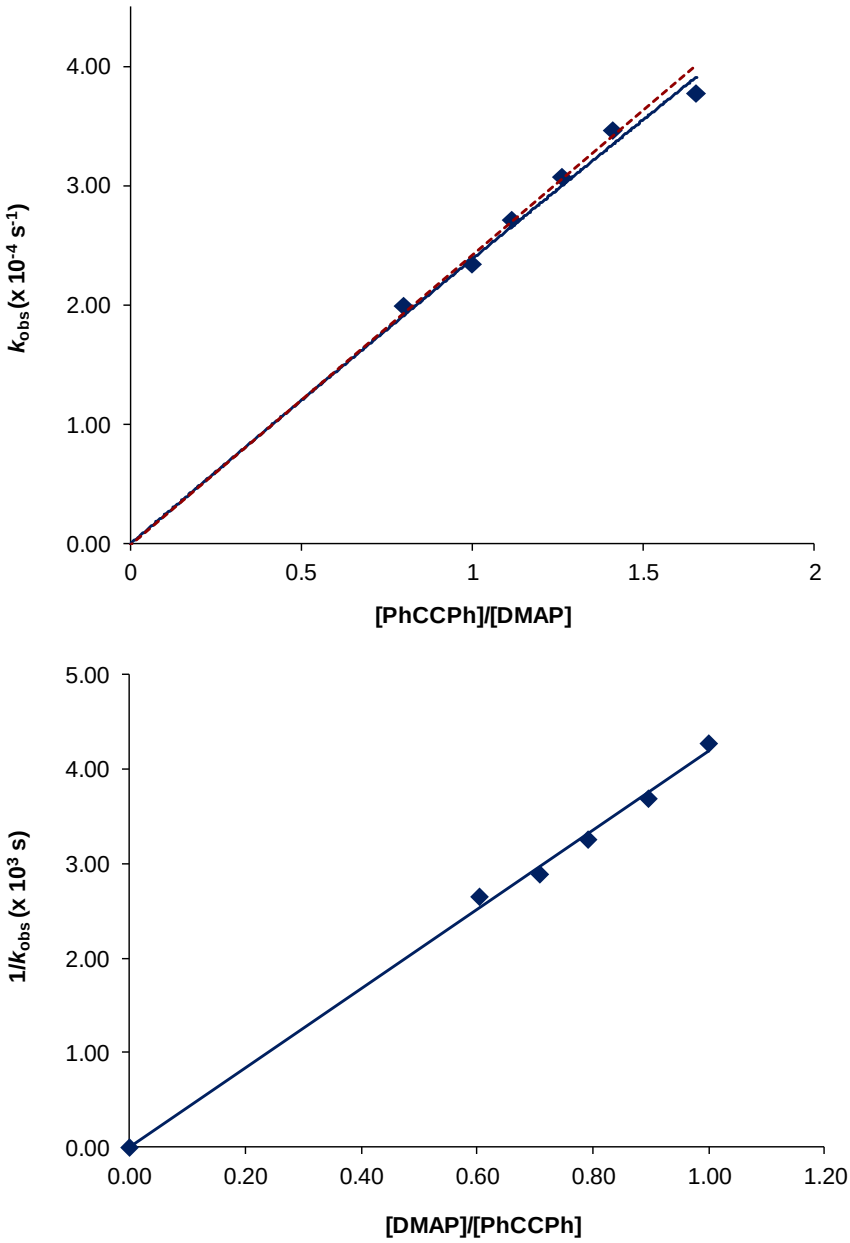

Figure 4.17. Top: plot of k_{obs} *vs*. [PhCCPh]/[DMAP] for the reaction of $Cp_2Zr(NNPh_2)(DMAP)$ (**1.151**) with PhCCPh; the dotted line is that expected for a linear relationship between k_{obs} and [PhCCPh]/[DMAP] based on extrapolation from the first three data points. Bottom: the corresponding plot of $1/k_{obs}$ against [DMAP]/[PhCCPh]. The linear fit ($r^2 = 0.996$) gives a gradient of $4.19(12) \times 10^3$ s.[140]

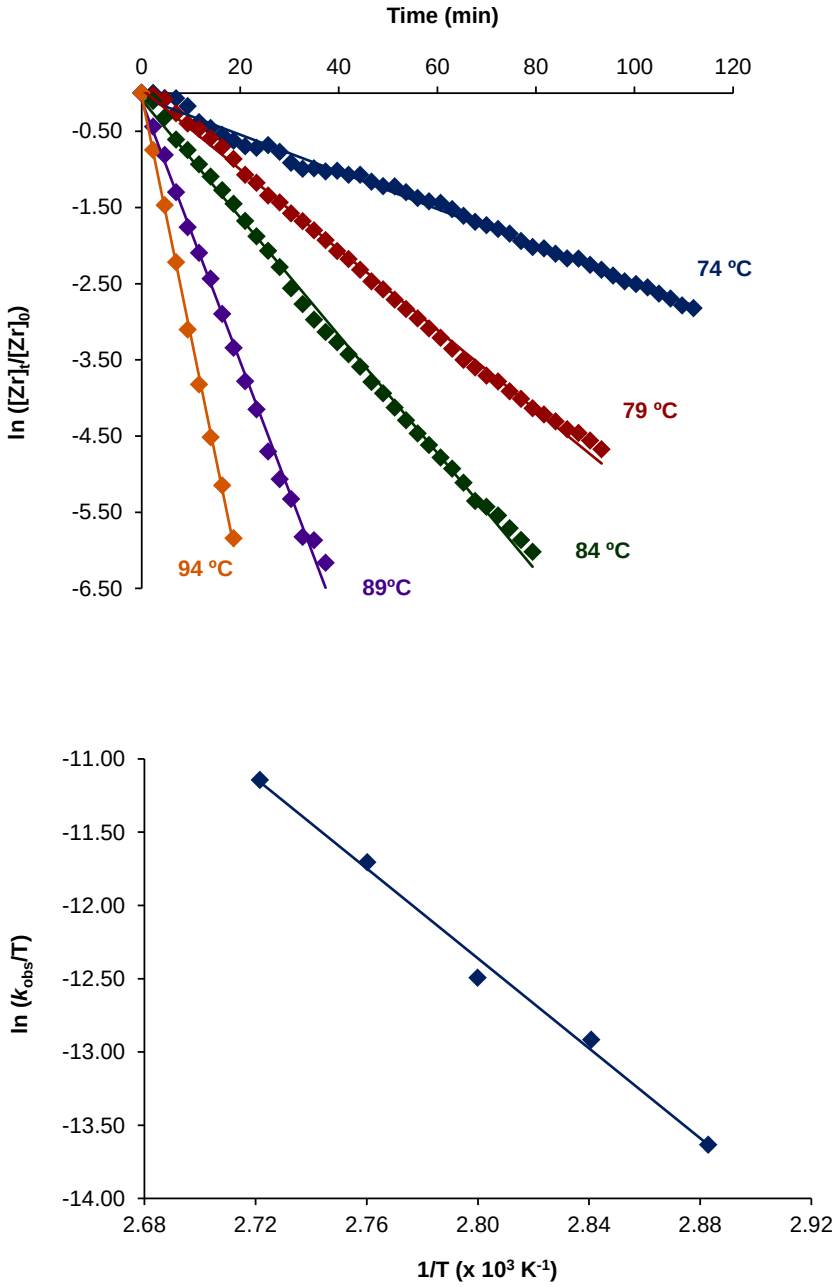

Figure 4.18. Top: pseudo first order ln plots for the reaction of $Cp_2Zr(NNPh_2)(DMAP)$ (**1.151**) with PhCCPh (20 equivalents) at the temperatures indicated (avg. r^2 = 0.996, range 0.993 – 0.999). Bottom: corresponding plot of $\ln(k_{obs}/T)$ *vs.* 1/T. Activation parameters derived from linear regression analysis (r^2 = 0.994): $\Delta H^{\ddagger}$ = 30.5(14) kcal mol^{-1}, $\Delta S^{\ddagger}$ = 13(4) cal mol^{-1} K^{-1}; $\Delta G_{347}{}^{\ddagger}$ = 26(3) kcal mol^{-1}.

These observations provide strong evidence that the reaction proceeds *via* a base free intermediate. However, they do not provide much information about the subsequent

steps ("k_2" in Scheme 4.7). In order to gain further insight into this system an Eyring analysis was carried out. The reaction between **1.151** and PhCCPh (20 equivalents) was followed at five different temperatures between 74 and 94 ^{o}C. The linear pseudo first order ln plots and corresponding Eyring analysis ($\ln(k_{obs}/T)$ *vs*. 1/T) are shown in Figure 4.18. The derived activation enthalpy and entropy values for the rate-limiting barrier on the reaction coordinate **1.151** + PhCCPh → **1.156** are $\Delta H^{\ddagger}$ = 30.5(14) kcal mol^{-1} and $\Delta S^{\ddagger}$ = 13.6(4) cal mol^{-1} K^{-1} giving $\Delta G_{347}{}^{\ddagger}$ = 26(3) kcal mol^{-1}, significantly larger than that found for DMAP loss from **1.151** (derived from k_1). The process appears to have a moderate positive enthalpy of activation. The difference in energy between the highest barrier calculated from the Eyring plot (26(3) kcal mol^{-1}) and that of DMAP loss from $Cp'_2Zr(NNPh_2)$(DMAP) (**29**, 14(3) kcal mol^{-1}) is 12(3) kcal mol^{-1}, identical to that calculated from the double reciprocal plot gradients (*vide supra*), showing good agreement between the Eyring and saturation kinetics experiments.

As shown in Equation 4.5, compound **1.151** also reacted with *p*-substituted alkynes ArCCAr (Ar = 4-C_6H_4X, X = OMe and CF_3) to form **34** and **35**. To glean more information about the rate-limiting "k_2" step, the reactions were followed at 74 ^{o}C in toluene-d_8 with 20 equivalents of alkyne in the presence of DMAP (10.2 equivalents). The reactions showed the same behaviour as for PhCCPh (i.e. X = H, Figure 4.15, top) and the pseudo first order rate constants (k_{obs}) for X = H, OMe and CF_3 are listed in Table 4.9 along with the corresponding Hammett substituent constants, σ_p.[141]

Table 4.9. Rate constants (k_{obs}) for reactions of $Cp_2Zr(NNPh_2)$(DMAP) (**1.151**) with ArCCAr (20 equivalents, Ar = 4-C_6H_4X, X = H, OMe and CF_3) at 74 ^{o}C in toluene-d_8. σ_p is the Hammett substituent constant.

X	k_{obs} ($\times 10^{-4}$ s^{-1})	σ_p
H	4.16(2)	0.00
OMe	5.54(6)	-0.27
CF_3	3.067(14)	0.54

The k_{obs} data show that the rate of reaction increases slightly as the *para*-X substituent becomes more electron releasing. The conclusion is that less electron-deficient alkynes lead to an increased rate of reaction, as seen in the N_α–N_β insertion reaction discussed in Chapter Two, with a near doubling of the rate when changing from CF_3 to OMe substituted alkynes. However, as the effect is not particularly large a full Hammett analysis was not completed. It does, however, indicate that the electronic nature of the reacting alkyne has an effect on the highest energy barrier.

The reaction of $Cp_2Hf(NNPh_2)(DMAP)$ (**28**) with 20 quivalents of PhCCPh, in the presence of 10.2 equivalents of DMAP was followed at 84 ºC, in order to probe the effect of changing the metal centre on the rate of reaction. The reaction was found to be significantly slower with k_{obs} = 0.577(2) × 10^{-4} s^{-1} (for **1.151**, k_{obs} = 12.91(12) × 10^{-4} s^{-1} under otherwise identical conditions, Figure 4.19). This implies that the rate-limiting step involves some degree of metal-ligand bond breaking. To gain further insight into the mechanism and selectivity a computational study was carried out by Dr E. Clot and Dr A. Nova.

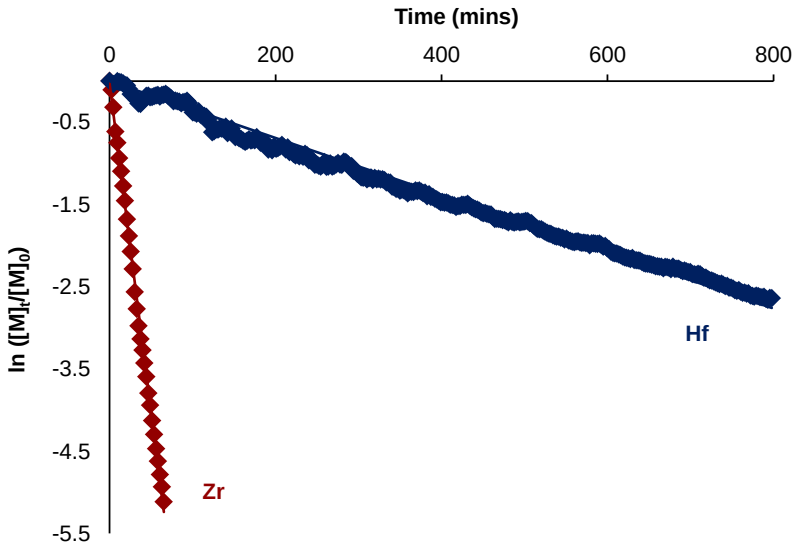

Figure 4.19. Pseudo first order ln plots for the reactions of $Cp_2Zr(NNPh_2)(DMAP)$ (**1.151**) and $Cp_2Hf(NNPh_2)(DMAP)$ (**28**) with PhCCPh (20 equivalents) in the presence of DMAP (10.2 equivalents) at 84 ºC (r^2 = 0.991 and 0.994, respectively).

4.8. Computational investigation of the combined N_α–N_β cleavage, C–H activation reaction

4.8.1. Mechanism of the combined N_α–N_β cleavage, C–H activation reaction

Calculations were carried out using the model $Cp_2Zr(NNPh_2)(DMAP)$ (**E1**) identical to **1.151**. Initially 2-butyne was considered as the reacting alkyne for computational efficiency. Following the mechanism of the N_α–N_β insertion reaction discussed in Chapter Two, Gade's recently proposed mechanism of the analogous reactivity seen between $Zr(N_2{*}N^{py})(NNPh_2)(py)$ (**1.159**) and alkynes and the extensive evidence for [2+2] cycloaddition compounds, as mentioned earlier in this Chapter, it has been assumed that azametallacyclobutenes of the type $Cp_2Zr\{N(NPh_2)C(R)C(R)\}$ play an active role in the reaction. The Gibbs free energy profile of the calculated mechanism is outlined in Scheme 4.8. It is similar to that proposed by Gade but is described in order to explain the experimental observations discussed previously.[36,39]

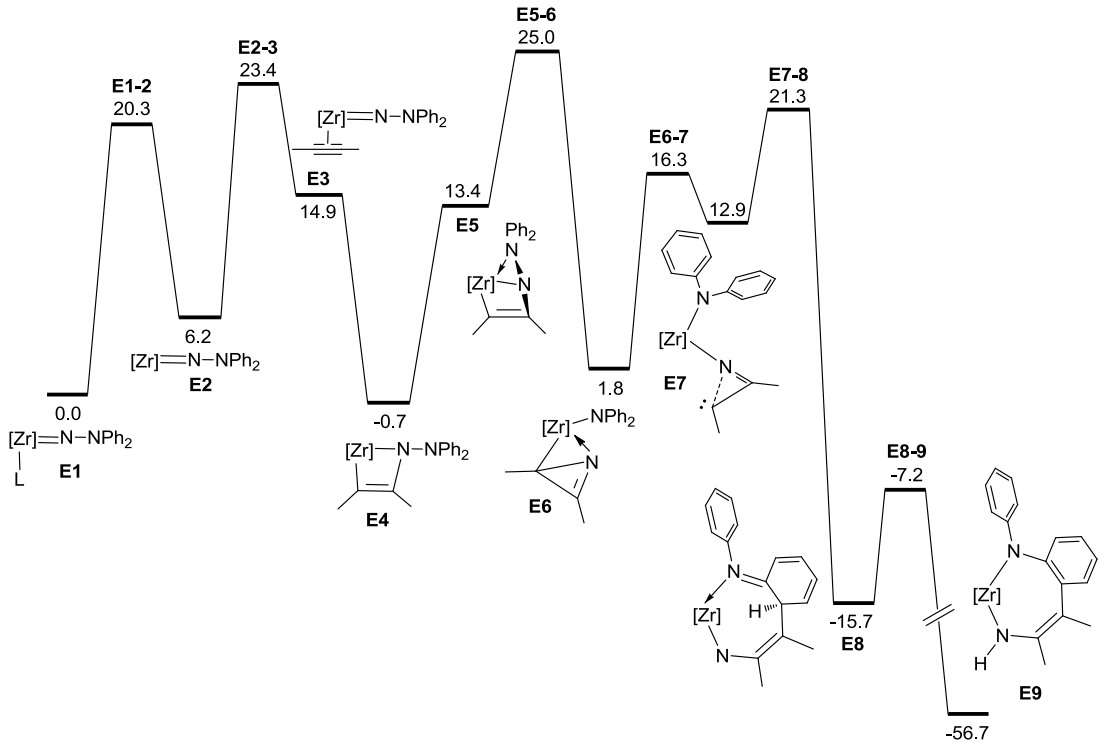

Scheme 4.8. Gibbs free energy (kcal mol^{-1}) profile for N_α–N_β cleavage and C–H activation of $Cp_2Zr(NNPh_2)(DMAP)$ (**E1**) when reacted with MeCCMe at 347 K. L = DMAP, [Zr] = Cp_2Zr.

The vacant site in **E2**, created by DMAP decoordination, is a potential site for alkyne binding, forming **E3**. Assuming that $\Delta G^{\ddagger} = \Delta H$, giving an upper limit for the Gibb's

free energy of activation,[142] the barrier to formation of the base free intermediate is 20.3 kcal mol^{-1}, with **E2** lying 6.2 kcal mol^{-1} above **E1** and 2-butyne. This shows strong agreement with the experimentally determined enthalpy of activation for DMAP loss from Cp′$_2$Zr(NNPh$_2$)(DMAP) (**29**, $\Delta H^{\ddagger}$ = 22.6(16) kcal mol^{-1}). Utilising the same assumption, TS **E2-3** is slightly higher in energy lying at 23.4 kcal mol^{-1} and leads to formation of the alkyne adduct **E3** (ΔG = 14.9 kcal mol^{-1}).

Subsequent [2+2] cycloaddition from **E3** allows formation of the azametallacyclobutene (**E4**) which is approximately isoenergetic with **E1** and the free alkyne (ΔG = -0.7 kcal mol^{-1}). From **E4**, intramolecular coordination of $N_\beta Ph_2$ yields the key intermediate **E5**, which enables N_α–N_β bond scisson and lies 13.4 kcal mol^{-1} above the separated reactants. N_α–N_β cleavage can then occur *via* exergonic nucleophilic attack by C_α on N_α, through **E5-6**, yielding the C,N-metallated azirine **E6** lying just 1.8 kcal mol^{-1} above the starting materials. The barrier to N_α–N_β cleavage is 25.0 kcal mol^{-1}, 1.6 kcal mol^{-1} higher than the next highest TS (**E2-3**, $\Delta G^{\ddagger}$ = 23.4 kcal mol^{-1}), although no entropy considerations have been taken into account for TS **E2-3**, which would be likely to increase its free energy. The TS to N_α–N_β bond cleavage was found to be the highest barrier in both the diamination reaction described in Chapter Two and the mechanism proposed by Gade in his study of the same reaction.[36,39,63]

In the mechanism described by Gade, the C,N-metallated azirine formed is in equilibruim with its N-metallated equivalent. An N-metallated azirine in the system described here (**E10**, not shown) was located and calculated to have a free energy of -1.3 kcal mol^{-1}. In the case of asymmetric alkynes, the presence of the N-metallated azirine is proposed to allow rapid interconversion between the two different isomers.[36,39] This point is elaborated on in a discussion of the regioselectivity with certain alkynes.

From **E6**, the key intermediate for C–H activation, **E7**, is thermally accesible (**E6-7** $\Delta G^{\ddagger}$ = 16.3 kcal mol^{-1}) where C_α is now an N-stabilised carbene. This lies 11.1 kcal mol^{-1} above **E6** and offers a site for nucleophilic attack by an *ortho*-carbon on one of the amide phenyl rings *via* **E7-8** ($\Delta G^{\ddagger}$ = 21.3 kcal mol^{-1}). This process is strongly exergonic with **E8** lying 15.7 kcal mol^{-1} below **E1** and butyne, and is the initiation of the C–H activation, which continues by H atom transfer from the now *sp*^{3} hybridised *ortho*-carbon to N_α forming **E9**, identical to the product Cp$_2$Zr{N(H)C(Me)C(Me)-1,2-C$_6$H$_4$N(Ph)} (**32**). The transition state for the rearrangement (**E8-9**) is calculated

to have an energy of -7.2 kcal mol^{-1}, only 8.5 kcal mol^{-1} above **E8** and the final product **E9** is 56.7 kcal mol^{-1} more stable than the starting materials.

4.8.2. Effect of alkyne substituents on the reaction pathway

In order to probe whether the nature of the alkyne has any effect on the various intermediates and transition states, calculations were also performed using PhCCPh, ^{t}BuCCMe and $Me_3SiCCMe$. For the asymmetrical alkynes both possible regioisomers were considered. The free energy profile for PhCCPh is outlined in Scheme 4.9, those of ^{t}BuCCMe and $Me_3SiCCMe$ are included in Appendix E.

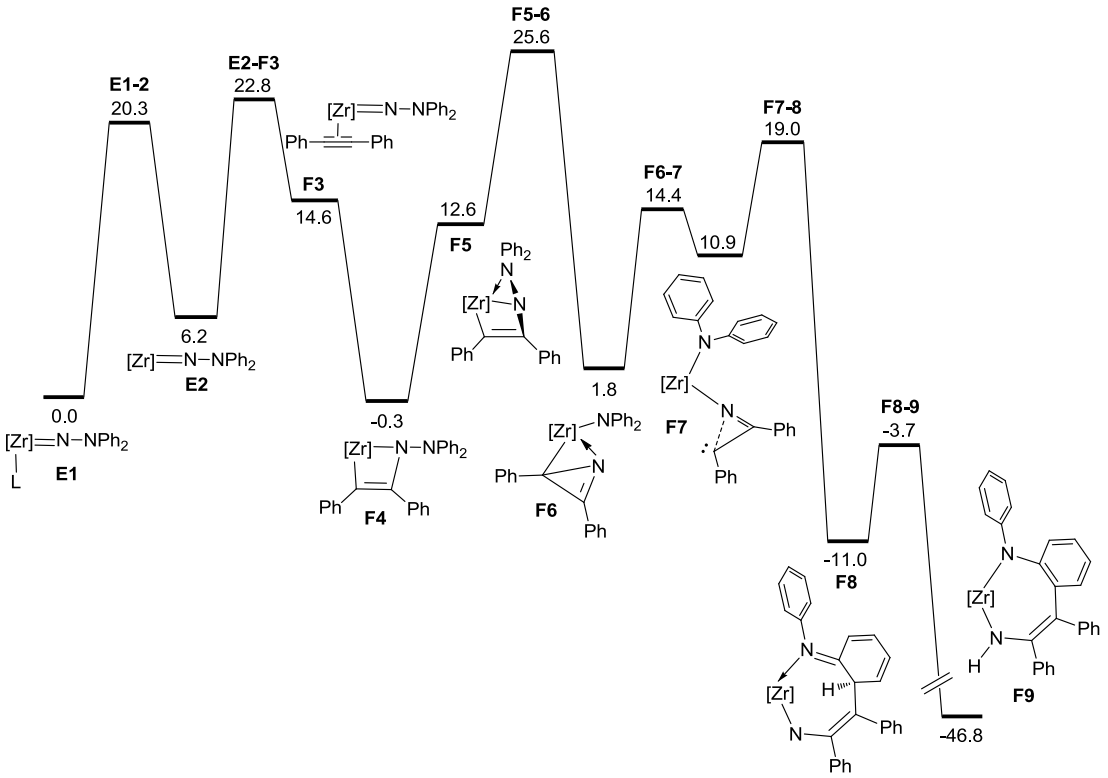

Scheme 4.9. Gibbs free energy (kcal mol^{-1}) profile for N_α–N_β cleavage and C–H activation of $Cp_2Zr(NNPh_2)(DMAP)$ (**E1**) when reacted with PhCCPh at 347 K. L = DMAP, [Zr] = Cp_2Zr.

The free energy profile for ^{t}BuCCMe is broadly similar to that of MeCCMe, with the highest energy barriers again being N_α–N_β cleavage ($\Delta G^{\ddagger}$ = 31.2 and 30.3 kcal mol^{-1} for the two isomers) with all other barriers significantly lower (the next highest **E2-G/H3** are both 22.6 kcal mol^{-1}). The N-metallated azirines (ΔG = 1.4 kcal mol^{-1} for both **G10** and **H10**) are, unlike **E10** (*vide supra*), less stable than the starting materials but stable with respect to their C,N-metallated analogues. For the reaction with $Me_3SiCCMe$ the barrier to N_α–N_β cleavage is calculated to be slightly higher

(ΔG = 31.0 and 35.7 kcal mol^{-1} for the two isomers) than that of ^{t}BuCCMe, in agreement with the experimental evidence. Again the N-metallated azirines are unstable with respect to **E1** and free alkyne (**I10**, ΔG = 1.7 kcal mol^{-1}; **J10**, ΔG = 1.8 kcal mol^{-1}) and **E2-I/J3** are calculated to be substantially less than the barriers to N_α–N_β cleavage ($\Delta G^{\ddagger}$ = 22.7 and 22.1 kcal mol^{-1} for **E2-I3** and **E2-J3**, respectively).

When PhCCPh is used as the reacting alkyne the reaction steps are identical and N_α–N_β cleavage remains the greatest barrier, raised slightly with respect to that for butyne (**E5-6**, $\Delta G^{\ddagger}$ = 25.0 kcal mol^{-1}, **F5-6**, $\Delta G^{\ddagger}$ = 25.6 kcal mol^{-1}), the next highest being **E2-F3** ($\Delta G^{\ddagger}$ = 22.8 kcal mol^{-1}). It can be concluded, therefore, that while the nature of the alkyne does have a small effect on the energy profile, N_α–N_β cleavage remains, arguably, the highest barrier on the potential energy surface with the previous and subsequent reaction steps all proceeding *via* lower energies. However, with 2-butyne and PhCCPh the barriers to alkyne aduct formation are competitive. The experimental trend in the observed rate constants (MeCCMe, k_{obs} = 0.928(7) × 10^{-3} s^{-1}, $\Delta G_{obs}^{\ddagger}$ = 25.26(1) kcal mol^{-1}; PhCCPh, k_{obs} = 0.416(3) × 10^{-3} s^{-1}, $\Delta G_{obs}^{\ddagger}$ = 25.81(1) kcal mol^{-1}; ^{t}BuCCMe, k_{obs} = 0.149(1) × 10^{-3} s^{-1}, $\Delta G_{obs}^{\ddagger}$ = 26.52(1) kcal mol^{-1}, $Me_3SiCCMe$, $\Delta G_{obs}^{\ddagger}$ = 27.4 kcal mol^{-1})[143] agrees with that seen in the calculations (MeCCMe, $\Delta G_{calc}^{\ddagger}$ = 25.0 kcal mol^{-1}, PhCCPh, $\Delta G_{calc}^{\ddagger}$ = 25.6 kcal mol^{-1}, ^{t}BuCCMe, $\Delta G_{calc}^{\ddagger}$ = 30.3 kcal mol^{-1}, $Me_3SiCCMe$, $\Delta G_{calc}^{\ddagger}$ = 31.0 kcal mol^{-1}). Note that **F10**, the N-metallated azirine is calculated to be unstable with respect to the starting materials (ΔG = 2.4 kcal mol^{-1}).

4.8.3. Analysis of the highest energy transition states

As described previously, the energies of the [2+2] cycloaddition intermediates and highest barrier on the energy surface corresponding to N_α–N_β cleavage (**E5-6**, $\Delta G^{\ddagger}$ = 26.2 kcal mol^{-1}) agree with a mechanism of the kind shown in Scheme 4.7. A pre-equilibrium between the base stabilised and free hydrazide is followed by reaction with the alkyne. There is no build up of metallacyclic intermediates as they are not sufficiently stable with respect to the hydrazide and free alkyne. The free energy barriers compare favourably with the activation parameters derived from the Eyring analysis ($\Delta H^{\ddagger}$ = 30.5(14) kcal mol^{-1}, $\Delta S^{\ddagger}$ = 13(4) cal K^{-1} mol^{-1}, $\Delta G_{347}^{\ddagger}$ = 26(3) kcal mol^{-1}) and the observed rate constants (*vide supra*). Despite being moderate and positive, the entropy term does not rule out a unimolecular step being rate determining as in complicated, multi-step reactions, such as the one described here, many

individual parts may contribute to the measured value. The free energy is within 1 kcal mol^{-1} of that calculated using the same alkyne ($\Delta G_{calc}^{\ddagger}$ = 25.6 kcal mol^{-1}).

Another check on the accuracies of the calculated energies is by comparison with the experimentally determined k_{-1}/k_2 ratio. In Scheme 4.9, this corresponds to the difference in energy between **F5-6** and **E1-2** ($\Delta\Delta G_{calc}^{\ddagger}$ = 5.3 kcal mol^{-1}). While this is significantly lower than that calculated from experiment ($\Delta\Delta G_{exp}^{\ddagger}$ = 12.32(16) kcal mol^{-1}, *vide supra*), the assumption used to calculate DMAP loss from **E1** is an upper estimate of the actual value of TS **E1-2** as it assumes no contribution from the entropy term in the transition state.[142] The true value will be lower (as seen for that explicitly determined using **29**, $\Delta G^{\ddagger}$ = 14(3) kcal mol^{-1}) causing $\Delta\Delta G_{calc}^{\ddagger}$ to agree more closely with $\Delta\Delta G_{exp}^{\ddagger}$.

For butyne and PhCCPh the barrier to alkyne adduct formation (**E2-3** and **E2-F3**) is comparable to that of N_α–N_β bond cleavage ($\Delta\Delta G^{\ddagger}$ = 1.6 and 2.8 kcal mol^{-1}, respectively). These energies do not include any entropy terms and would be expected to increase if they were included. As such it is not clear whether the barrier to alkyne adduct formation or N_α–N_β bond cleavage is the highest point on the potential energy surface. However, the fact that the related imido system $Cp_2Zr(NXyl)(NC_5H_4{}^tBu)$ (**1.47**) also requires temperatures of 50 ºC to react with alkynes (as does **1.151** to react with isocyanates) implies that it could be the former. In contrast, for ^{t}BuCCMe and $Me_3SiCCMe$, the difference between the two barriers is larger (range $\Delta\Delta G^{\ddagger}$ = 13.7 – 7.7 kcal mol^{-1}) implying that in these cases the highest barrier could be that of N_α–N_β bond cleavage. In his recent paper Gade reports that N_α–N_β cleavage is the highest barrier ($\Delta G^{\ddagger}$ = 22.9 kcal mol^{-1}) with that for C–H activation (equivalent to **E7-9**) the next highest ($\Delta G^{\ddagger}$ = 18.2 kcal mol^{-1}). The experimentally determined activation parameters are reported as $\Delta H^{\ddagger}$ = 11.5(7) kcal mol^{-1}, $\Delta S^{\ddagger}$ = -45(10) cal K^{-1} mol^{-1}, $\Delta G_{275}^{\ddagger}$ = 24(2) kcal mol^{-1}. In the system studied in this Chapter, it is not possible to state conclusively whether N_α–N_β cleavage or alkyne adduct formation is the highest barrier on the reaction coordinate.

4.8.4. Product Selectivity: N_α–N_β insertion vs. combined N_α–N_β cleavage and C–H activation

The way subtle factors affect the reactivity of Group 4 hydrazides is very interesting. In the case of $Ti(N_2N^{Me})(NNPh_2)(py)$ (**1.93**) N_α–N_β insertion is seen with methyl

substituted alkynes of the type RCCMe (R = Me, aryl) and ArCCAr (Ar = electron withdrawing substituent). With ArCCAr (Ar = electron releasing aryl group) mixtures of N_α–N_β insertion and N_α–N_β cleavage, C–H activation products are produced, and with $Cp_2M(NNPh_2)(DMAP)$ (M = Zr (**1.151**), M = Hf (**28**)) no N_α–N_β insertion compounds are formed. Varied reactivity is also seen by Gade using the zirconium hydrazide $Zr(N_2{*}N^{py})(NNPh_2)(py)$ (**1.159**), which predominantly forms 7-membered metallacycles analogous to **32** – **37**. However, exclusively with butyne, **1.159** gives an equal mixture of $Zr(N_2{*}N^{py})\{NC(Me)C(Me)NPh_2\}(py)$ (**1.164**) and $Zr(N_2{*}N^{py})\{N(H)C(Me)C(Me)\text{-}1,2\text{-}C_6H_4NPh\}$ (**1.163**) (Equation 4.11).[36]

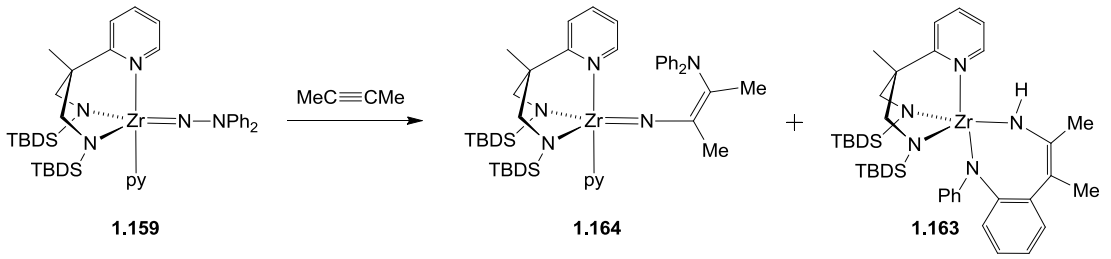

Equation 4.11

It would be difficult to accurately attempt a computational study on the product selectivity of $Ti(N_2N^{Me})(NNPh_2)(py)$ (**1.93**) or $Zr(N_2{*}N^{py})(NNPh_2)(py)$ (**1.159**) with different alkynes. The limited number of reactions producing multiple products. However, it is clear that for **1.93**, nucleophilic attack at the C_β of the C,N-metallated azirine by N_β is favoured by electron-withdrawing groups, explaining the observation that only the vinyl imide product is obtained with ArCCAr (Ar = 4-$C_6H_4CF_3$). Presumably the barrier to attack by N_β increases as the electron density on the aryl ring (and therefore C_β) is increased, as illustrated by the change in product distribution going from Ar = Ph to Ar = 4-C_6H_4OMe (Equation 4.3).

The reasons behind the selectivity of $Cp_2M(NNPh_2)(DMAP)$ (M = Zr (**1.151**), M = Hf (**28**)) to only form 7-membered ring products of the type $Cp_2M\{N(H)C(R)C(R')\text{-}1,2\text{-}C_6H_4N(Ph)\}$ is more easily explained with reference to the orbital constraints caused by the bis(cyclopentadienyl) ligand set. As illustrated in Figure 4.20, the N_2N^{Me} ligand allows the *fac*-arrangement of the C–N–NR_2 bonds, enabling N_β to act as a nucleophile, donating into the C=N π^* orbital. In contrast, the Cp_2 ligand set confines the C–N–NR_2 bonds in the equatorial plane. This prevents nucleophilic attack by N_β group causing the different reactivity observed experimentally.[144]

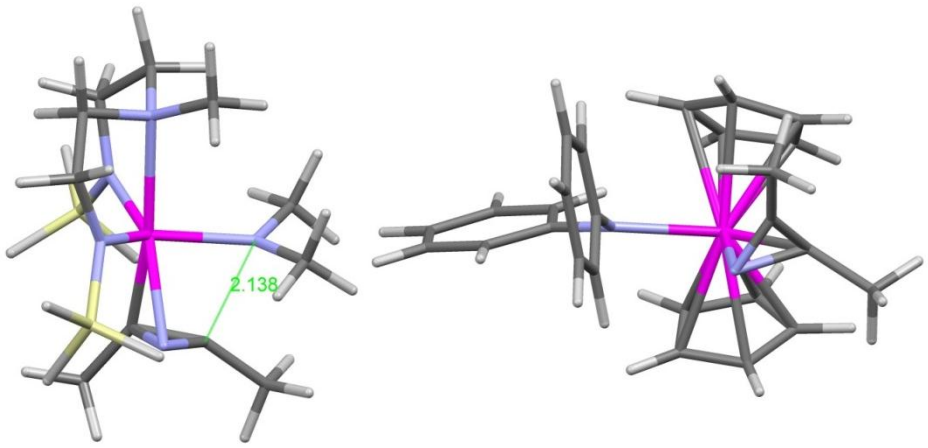

Figure 4.20. (a) The N_2N^{Me} ligand allows the *fac*-C–N–NR_2 arrangement. (b) The Cp_2M frontier MOs force the three M–L bonds to be in the equatorial plane so the *fac* arrangement required for N_β attack is not possible.

4.8.5. Product Selectivity: Regioselectivity

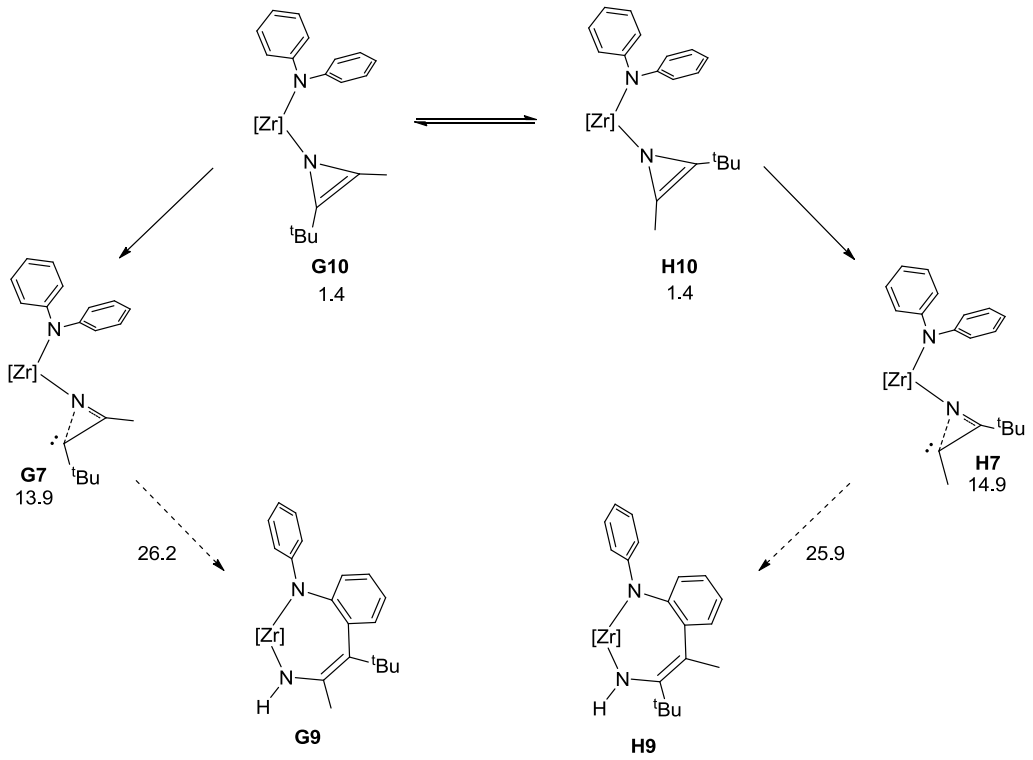

Scheme 4.10. Formation of $Cp_2Zr\{N(H)C(Me)C(^tBu)$-1,2-$C_6H_4N(Ph)\}$ (**G9**) and $Cp_2Zr\{N(H)C(^tBu)C(Me)$-1,2-$C_6H_4N(Ph)\}$ (**H9**) starting from interchangeable N-metallated azirine intermediates.

While orbital considerations of the Cp_2 ligand set can explain the different reactivity between $Ti(N_2N^{Me})(NNPh_2)(py)$ (**1.93**) and $Cp_2Zr(NNPh_2)(DMAP)$ (**1.151**) they do not explain the different isomers obtained by the reaction with ^{t}BuCCMe and $Me_3SiCCMe$.

There are two possible steps where the preference for one isomer can be introduced. If the N-metallated azirine is accessed as an intermediate and both isomers can exchange rapidly, as suggested by Gade,[36,39] then any selectivity introduced from the [2+2] cycloaddition would be scrambled (Scheme 4.10). This would imply that the alkyne substituents act as directing groups for nucleophilic attack by the phenyl ring. This would agree for the reaction with ^{t}BuCCMe, the nucleophile attacking the least sterically bulky carbon (Pathway H, Scheme 4.10). Looking at other alkynes, however, if the selectivity was indeed introduced by attack at the N-metallated azirine, the reactivity observed with $Me_3SiCCMe$ appears to be the incorrect isomer. The nucleophilic phenyl ring would be required to attack exclusively at the carbon bound to the bulkier $SiMe_3$ substituent. In addition, it is well documented that silyl groups stabilise α-anions and β-cations, indicating that nucleophilic attack at the methyl substituted carbon would be preferred on both steric and electronic grounds. Indeed, calculations predict the barrier to formation of $Cp_2Zr\{N(H)C(SiMe_3)C(Me)$-1,2-$C_6H_4N(Ph)\}$ (**J9**) to be 6.1 kcal mol^{-1} *lower* than that of the observed isomer when starting from the N-metallated azirine. In the results reported by Gade, attack at a phenyl substituted carbon appears to be favoured over a proton bound carbon, and attack at an ethyl preferred to a methyl substituted carbon (Figure 4.9 and Table 4.6, *vide supra*), again not agreeing with attack at the least sterically bulky carbon of a symmetrical N-metallated azirine.

If the regioselectivity is not introduced by attack at the azirine, it may instead stem from the orientation of the [2+2] cycloaddition intermediate in the transition state for N_α–N_β bond cleavage, as in the related diamination mechanism outlined in Chapter Two.[63] This would require that C_α and C_β are not able to interchange *via* an N-metallated azirine intermediate, enabling the alkyne orientation introduced in the metallacycle to be maintained throughout the reaction.

Looking again at $Cp_2Zr\{N(H)C(Me)C(SiMe_3)$-1,2-$C_6H_4N(Ph)\}$ (**44**) and $Cp_2Zr\{N(H)C(^tBu)C(Me)$-1,2-$C_6H_4N(Ph)\}$ (**46**), both would be expected to form the same [2+2] cycloaddition regioisomers with the bulky substituent bound to the carbon

adjacent to the metal centre (C_α) and the less bulky methyl group bound to the carbon adjacent to the NPh_2 group (C_β) (*vide supra*).[86] DFT calculations confirm this, the expected isomers $Cp_2Zr\{N(NPh_2)C(Me)C(^tBu)\}$ (**G4**) and $Cp_2Zr\{N(NPh_2)C(Me)C(SiMe_3)\}$ (**I4**) are calculated as being 10.0 and 12.6 kcal mol^{-1} more stable than the disfavoured isomers $Cp_2Zr\{N(NPh_2)C(^tBu)C(Me)\}$ (**H4**) and $Cp_2Zr\{N(NPh_2)C(SiMe_3)C(Me)\}$ (**J4**), respectively. Interestingly, while the barrier to N_α–N_β bond cleavage for $Me_3SiCCMe$ (analogous to **E5-6**) is explicitly calculated to be *lower* for the favoured metallacycle (**G4**/**I4**) than from the disfavoured one (**H4**/**J4**) ($\Delta\Delta G^\ddagger$ = 4.7 kcal mol^{-1}), for ^tBuCCMe it is 0.9 kcal mol^{-1} *higher* (Schemes 1 and 2, Appendix E) This inversion of transition state energies predicts products with the correct regioselectivity as that observed by experiment (Scheme 4.5).

This hypothesis also satisfactorily accounts for the results of Gade. Terminal alkynes of the type ArCCH (Ar = Ph or electron withdrawing group) have been shown to form [2+2] cycloadditions with diamide-amine supported Group 4 hydrazides. The sole isomer formed has the aryl group bound to C_α, the orientation which would produce the observed indole products. For more electron donating aryl groups (e.g. *para*-methoxy substituted) this isomer is calculated to be less stable than in the case for phenyl or electron withdrawing aryl substituents, agreeing with the change in the ratios C_α(Ar):C_β(Ar) from 9:1 for Ar = Ph to 5:1 for Ar = 4-C_6H_4OMe.[63,69] Unfortunately it is not possible to rule either of these possibilities out. Indeed, it may even be that the selectivity is introduced from the N-metallated azirine for some alkynes while for others it stems from the cycloaddition intermediate.

4.9. Conclusion

The transformations of the hydrazide group outlined in Chapters Two and Three were limited to reactivity of the M=N_α and N_α–N_β bonds. In contrast, the reactivity studied in this Chapter incoorporates M=N_α and N_α–N_β reactivity in conjunction with C–H activation. This further illustrates the importance of N_β functionalisation of the hydrazide ligand and the wide scope of organo-nitrogen products accessible *via* direct coupling of Group 4 hydrazides with alkynes and other small unsaturated molecules.

This Chapter has shown that C–H activation of hydrazide phenyl rings can occur using a titanium or hafnium metal centre, as well as the previously reported zirconium.[25,36,39] A new and more facile route for the synthesis of

bis(cyclopentadienyl) supported zirconium and hafnium hydrazides has beeen presented along with structural studies for $Cp_2M(NNPh_2)$(DMAP (M = Hf (**28**) or Ti(**4.2**)). When combined with the data for $Cp_2Zr(NNPh_2)$(DMAP) (**1.151**), these constitute the first series of hydrazides spanning all the Group 4 metals. The synthesis of tetra- and penta-methyl substituted derivatives were unsuccessful but led to the isolation of several compounds, as outlined in Appendix D, including the *ortho*-metallated compound $Cp^*_2Zr\{N(H)N(Ph)\text{-}1,2\text{-}C_6H_4\}$ (**52**), formed by concerted metathesis of $Cp^*_2Zr(NHNPh_2)(Me)$ (**51**).

The reactivity of $Cp_2Zr(NNPh_2)$(DMAP) (**1.151**) with alkynes, first discovered by Bergman, has been extended to unsymmetrical alkynes and the mechanism studied. Through a series of kinetic, mechanistic and computational work the mechanism for the transformation has been elucidated and the highest barriers to the reaction probed. This was found to be very similar to that proposed recently by Gade,[36,39] with the highest barrier to the reaction for the bis(cyclopentadienyl) supported system either N_α–N_β cleavage, as in the diamide-amine supported system or alkyne adduct formation. The parameters elucidated from the Eyring analysis were $\Delta H^\ddagger$ = 30.5(14) kcal mol^{-1}, $\Delta S^\ddagger$ = 13(4) cal mol^{-1} K^{-1}; $\Delta G_{347}^\ddagger$ = 26(3) kcal mol^{-1}. *Tert*-butyl and trimethylsilyl groups were found to promote total and opposite regioselectivity in the products, while less sterically bulky alkynes gave mixtures. This selectivity appears to be introduced by the sense of alkyne cycloaddition and N_α–N_β cleavage step, although selectivity from an N-metallated azirine cannot be explicitly ruled out.

Other work by Gade and in this group has shown that, in addition to the alkyne being able to act as a directing group, para-substituted hydrazides of the type $Cp_2Zr(NN(Ph)Ar)$(DMAP) (Ar = 4-C_6H_4OMe) can also direct attack towards the unsubstituted phenyl ring.[36,39,145] This opens the possibilities of targeting specific phenylindoles using different combinations of hydrazides and alkynes. In more general terms, it is clear that Group 4 hydrazides offer a realistic route to the catalytic and selective syntheses of a wide range of organo-nitrogen products from readily available starting materials. In probing the limitations and mechanisms of some of these transformations, this Thesis has attempted to increase our understanding of early transition metal hydrazide chemistry to allow improvements in catalyst design and reaction scope.

4.10. References

1. Johnson, B. F. G.; Haymore, B. L.; Dilworth, J. D.: Comprehensive Coordination Chemistry. Wilkinson, G., Gillard, R. D., McCleverty, J. A., Eds.; Pergamon Press: Oxford, 1987; Vol. 2; pp 100.
2. Nugent, W. A.; Mayer, J. M.; *Metal-Ligand Multiple Bonds*; Wiley-Interscience: New York, 1988.
3. Mindiola, D. J.; *Angew. Chem. Int. Ed.* **2008**, *47*, 1557.
4. Fryzuk, M. D.; *Chem. Rec.* **2003**, *3*, 2.
5. MacKay, B. A.; Fryzuk, M. D.; *Chem. Rev.* **2004**, *104*, 385.
6. Kozak, C. M.; Mountford, P.; *Angew. Chem. Int. Ed.* **2004**, *43*, 1186
7. Chatt, J.; Pearman, A. J.; Richards, R. L.; *Nature* **1975**, *253*, 39.
8. Pickett, C. J.; Leigh, G. J.; *J. Chem. Soc., Chem. Commun.* **1981**, 1033.
9. Hussain, W.; Leigh, G. J.; Pickett, C. J.; *J. Chem. Soc., Chem. Commun.* **1982**, 747.
10. Pickett, C. J.; Talamarin, J.; *Nature* **1985**, *317*, 652.
11. Yandulov, D. V.; Schrock, R. R.; *Science* **2003**, 76.
12. Schrock, R. R.; *Acc. Chem. Res.* **2005**, *38*, 955.
13. Stephan, G. C.; Sivasankar, C.; Studt, F.; Tuczek, F.; *Chem. Eur. J.* **2008**, *14*, 644.
14. Studt, F.; Tuczek, F.; *Angew. Chem. Int. Ed.* **2005**, *44*, 5639.
15. Schrock, R. R.; *Angew. Chem. Int. Ed.* **2008**, *47*, 5512.
16. Schenk, S.; Kirchner, B.; Reiher, M.; *Chem. Eur. J.* **2009**, *15*, 5073.
17. Schenk, S.; Le Guennic, B.; Kirchner, B.; Reiher, M.; *Inorg. Chem.* **2008**, *47*, 3634.
18. Hidai, M.; *Coord. Chem. Rev.* **1999**, *185-186*, 99.
19. Ohki, Y.; Fryzuk, M. D.; *Angew. Chem. Int. Ed.* **2007**, *46*, 3180.
20. Clulow, A. J.; Selby, J. D.; Cushion, M. G.; Schwarz, A. D.; Mountford, P.; *Inorg. Chem.* **2008**, *47*, 12049.
21. Selby, J. D.; Manley, C. D.; Feliz, M.; Schwarz, A. D.; Clot, E.; Mountford, P.; *Chem. Commun.* **2007**, 4937.
22. Blake, A. J.; McInnes, J. M.; Mountford, P.; Nikonov, G. I.; Swallow, D.; Watkin, D. J.; *J. Chem. Soc., Dalton Trans.* **1999**, 379.
23. Weitershaus, K.; Wadepohl, H.; Gade, L. H.; *Organometallics* **2009**, *28*, 3381.

24. Herrmann, H.; Fillol, J. L.; Wadepohl, H.; Gade, L. H.; *Angew. Chem. Int. Ed.* **2007**, *46*, 8426.
25. Walsh, P. J.; Carney, M. J.; Bergman, R. G.; *J. Am. Chem. Soc.* **1991**, *113*, 6343.
26. Wiberg, N.; Haring, H.-W.; Huttner, G.; Friedrich, P.; *Chem. Ber.* **1978**, *111*, 2708.
27. Selby, J. D.; Manley, C. D.; Schwarz, A. D.; Clot, E.; Mountford, P.; *Organometallics* **2008**, *27*, 6479.
28. Parsons, T. B.; Hazari, N.; Cowley, A. R.; Green, J. C.; Mountford, P.; *Inorg. Chem.* **2005**, *44*, 8442.
29. Herrmann, H.; Wadepohl, H.; Gade, L. H.; *Dalton Trans.* **2008**, 2111.
30. Herrmann, H.; Fillol, J. L.; Gehrmann, T.; Enders, M.; Wadepohl, H.; Gade, L. H.; *Chem. Eur. J.* **2008**, *14*, 8131.
31. Patel, S.; Li, Y.; Odom, A. L.; *Inorg. Chem.* **2007**, *46*, 6373.
32. Banerjee, S.; Odom, A. L.; *Organometallics* **2006**, *25*, 3099.
33. Li, Y.; Shi, Y.; Odom, A. L.; *J. Am. Chem. Soc.* **2004**, *126*, 1794.
34. Thorman, J. L.; Woo, L. K.; *Inorg. Chem.* **2000**, *39*, 1301.
35. Schrock, R. R.; *J. Chem. Soc., Dalton Trans.* **2001**, 2541.
36. Gehrmann, T.; Scholl, S. A.; Fillol, J. L.; Wadepohl, H.; Gade, L. H.; *Chem. Eur. J.* **2012**, *18*, 3925.
37. Herrmann, H.; Gehrmann, T.; Wadepohl, H.; Gade, L. H.; *Dalton Trans.* **2008**, 6231.
38. Herrmann, H.; Fillol, J. L.; Wadepohl, H.; Gade, L. H.; *Organometallics* **2008**, *27*, 172.
39. Gehrmann, T.; Fillol, J. L.; Scholl, S. A.; Wadepohl, H.; Gade, L. H.; *Angew. Chem. Int. Ed.* **2011**, *50*, 5757.
40. Gehrmann, T.; Fillol, J. L.; Wadepohl, H.; Gade, L. H.; *Organometallics* **2010**, *29*, 28.
41. Gehrmann, T.; Fillol, J. L.; Wadepohl, H.; Gade, L. H.; *Angew. Chem. Int. Ed.* **2009**, *48*, 2152.
42. Doye, S.; *Synlett* **2004**, 1653.
43. Bytschkov, I.; Doye, S.; *Eur. J. Org. Chem.* **2003**, 935.
44. Hultzsch, K. C.; *Adv. Synth. Catal.* **2005**, *347*, 367.
45. Odom, A. L.; *Dalton Trans.* **2005**, 225.

46. Johnson, J. S.; Bergman, R. G.; *J. Am. Chem. Soc.* **2001**, *123*, 2923.
47. Ackermann, L.; Born, R.; *Tetrahedron. Lett.* **2004**, *45*, 9541.
48. Tillack, A.; Jiao, H.; Garcia Castro, I.; Hartung, C. G.; Beller, M.; *Chem. Eur. J.* **2004**, *10*, 2410.
49. Cao, C.; Shi, Y.; Odom, A. L.; *Org. Lett.* **2002**, *4*, 2853.
50. Banerjee, S.; Barnea, E.; Odom, A. L.; *Organometallics* **2008**, *27*, 1005.
51. Schwarz, N.; Alex, K.; Sayyed, I. A.; Khedkar, V.; Tillack, A.; Beller, M.; *Synlett* **2007**, 1091.
52. Sayyed, I. A.; Alex, K.; Tillack, A.; Schwarz, N.; Michalik, D.; Beller, M.; *Eur. J. Org. Chem.* **2007**, 4525.
53. Krüger, K.; Tillack, A.; Beller, M.; *Adv. Synth. Catal.* **2008**, *350*, 2153.
54. Alex, K.; Tillack, A.; Schwarz, N.; Beller, M.; *Angew. Chem. Int. Ed.* **2008**, *47*, 2304.
55. Alex, K.; Tillack, A.; Schwarz, N.; Beller, M.; *Org. Lett.* **2008**, *10*, 2377.
56. Alex, K.; Tillack, A.; Schwarz, N.; Beller, M.; *Tetrahedron Lett.* **2008**, *49*, 4607.
57. Khedkar, V.; Tillack, A.; Michalik, M.; Beller, M.; *Tetrahedron Lett.* **2004**, *45*, 3123.
58. Dissanayake, A. A.; Odom, A. L.; *Chem. Commun.* **2012**, *48, 440*.
59. Banerjee, S.; Shi, Y.; Cao, C.; Odom, A. L.; *J. Organomet. Chem.* **2005**, *690*, 5066.
60. Majumder, S.; Gipson, K. R.; Staples, R. J.; Odom, A. L.; *Adv. Synth. Catal.* **2009**, *351*, 2013.
61. Majumder, S.; Gipson, K. R.; Odom, A. L.; *Org. Lett.* **2009**, *11*, 4720.
62. Majumder, S.; Odom, A. L.; *Tetrahedron* **2010**, *66*, 3152.
63. Schofield, A. D.; Nova, A.; Selby, J. D.; Manley, C. D.; Schwarz, A. D.; Clot, E.; Mountford, P.; *J. Am. Chem. Soc.* **2010**, *132*, 10484.
64. Duncan, A. P.; Bergman, R. G.; *Chem. Rec.* **2002**, *2*, 431.
65. Green, M. L. H.; James, J. T.; Chernega, A. N.; *J. Chem. Soc., Dalton Trans.* **1997**, 1719.
66. Wiberg, N.; Häring, H. W.; Schieda, O.; *Angew. Chem.* **1976**, *88*, 383.
67. Tonks, I. A.; Bercaw, J. E.; *Inorg. Chem.* **2010**, *49*, 4648.
68. Selby, J. D.; Feliz, M.; Schwarz, A. D.; Clot, E.; Mountford, P.; *Organometallics* **2011**, *30*, 2295.

69. Selby, J. D.; Schulten, C.; Schwarz, A. D.; Stasch, A.; Clot, E.; Jones, C.; Mountford, P.; *Chem.Commun.* **2008**, 5101.
70. Janssen, T.; Severin, R.; Diekmann, M.; Friedemann, M.; Haase, D.; Saak, W.; Doye, S.; Beckhaus, R.; *Organometallics* **2010**, *29*, 1806.
71. Cai, S. a.; Schrock, R. R.; Kempe, R. R.; Davis, W. M.; *Polyhedron* **1998**, *17*, 749.
72. Green, M. L. H.; James, J. T.; Saunders, J. F.; Souter, J.; *J. Chem. Soc., Dalton Trans.* **1997**, 1281.
73. Vale, M. G.; Schrock, R. R.; *Inorg. Chem.* **1993**, *32*, 2767.
74. Schrock, R. R.; Glassman, T. E.; Vale, M. G.; Kol, M.; *J. Am. Chem. Soc.* **1993**, *115*, 1760.
75. Glassman, T. E.; Vale, M. G.; Schrock, R. R.; *J. Am. Chem. Soc.* **1992**, *114*, 8098.
76. Weitershaus, K.; Fillol, J. L.; Wadepohl, H.; Gade, L. H.; *Organometallics* **2009**, *28*, 4747.
77. Manzur, C.; Carrillo, D.; Robert, F.; Gouzerh, P.; Hamon, J.-R.; *Organometallics* **1998**, *17*, 3728.
78. Barrientos-Penna, C. F.; Einstein, F. W. B.; Jones, T.; Sutton, D.; *Inorg. Chem.* **1982**, *21*, 2578.
79. Redshaw, C.; Gibson, V. C.; Clegg, W.; Edwards, A. J.; Miles, B.; *J. Chem. Soc., Dalton Trans.* **1997**, 3343.
80. Walsh, P. J.; Hollander, F. J.; Bergman, R. G.; *Organometallics* **1993**, *12*, 3705.
81. Walsh, P. J.; Hollander, F. J.; Bergman, R. G.; *J. Am. Chem. Soc.* **1988**, *110*, 8729.
82. Cummins, C. C.; Baxter, S. M.; Wolczanski, P. T.; *J. Am. Chem. Soc.* **1988**, *110*, 8731.
83. Zuckerman, R. L.; Bergman, R. G.; *Organometallics* **2000**, *19*, 4795.
84. Sweeney, Z. K.; Salsman, J. L.; Andersen, R. A.; Bergman, R. G.; *Angew. Chem. Int. Ed.* **2000**, 2339.
85. Lee, S. Y.; Bergman, R. G.; *J. Am. Chem. Soc.* **1995**, *117*, 5877.
86. Lee, S. Y.; Bergman, R. G.; *Tetrahedron* **1995**, *51*, 4255.
87. Baranger, A. M.; Walsh, P. J.; Bergman, R. G.; *J. Am. Chem. Soc.* **1993**, *115*, 2753.

88. Harlan, C. J.; Tunge, J. A.; Bridgewater, B. M.; Norton, J. R.; *Organometallics* **2000**, *19*, 2365.
89. Hanna, T. A.; Baranger, A. M.; Walsh, P. J.; Bergman, R. G.; *J. Am. Chem. Soc.* **1995**, *117*, 3292.
90. Lee, S. Y.; Bergman, R. G.; *J. Am. Chem. Soc.* **1996**, *118*, 6396.
91. Thorman, J. L.; Guzei, I. A.; Young, V. G.; Woo, L. K.; *Inorg. Chem.* **2000**, *39*, 2344.
92. Thorman, J. L.; Guzei, I. A.; Young, V. G.; Woo, L. K.; *Inorg. Chem.* **1999**, *38*, 3814.
93. Meyer, K. E.; Walsh, P. J.; Bergman, R. G.; *J. Am. Chem. Soc.* **1995**, *117*, 974.
94. Zuckerman, R. L.; Bergman, R. G.; *Organometallics* **2001**, *20*, 1792.
95. Meyer, K. E.; Walsh, P. J.; Bergman, R. G.; *J. Am. Chem. Soc.* **1994**, *116*, 2669.
96. Krska, S. W.; Zuckerman, R. L.; Bergman, R. G.; *J. Am. Chem. Soc.* **1998**, *120*, 11828.
97. Gade, L. H.; Mountford, P.; *Coord. Chem. Rev.* **2001**, *216-217*, 65.
98. Cundari, T. R.; *J. Am. Chem. Soc.* **1992**, *114*, 7879.
99. Hamaki, H.; Takeda, N.; Tokitoh, N.; *Organometallics* **2006**, *25*, 2457.
100. Zambrano, C. H.; Profilet, R. D.; Hill, J. E.; Fanwick, P. E.; Rothwell, I. P.; *Polyhedron* **1993**, *12*, 689.
101. Castillo, I.; Don Tilley, T.; *J. Organomet. Chem.* **2002**, *643–644*, 431.
102. Hamaki, H.; Takeda, N.; Nabika, M.; Tokitoh, N.; *Macromolecules* **2012**, *45*, 1758.
103. Munha, R. F.; Veiros, L. F.; Duarte, M. T.; Fryzuk, M. D.; Martins, A. M.; *Dalton Trans.* **2009**, 7494.
104. Otero, A.; Fernández-Baeza, J.; Antiñolo, A.; Tejeda, J.; Lara-Sánchez, A.; Sánchez-Barba, L. F.; Sánchez-Molina, M.; Bo, C.; Urbano-Cuadrado, M.; *Inorg. Chim. Acta* **2009**, *362*, 2909.
105. Chen, F.; Kapon, M.; Woollins, J. D.; Eisen, M. S.; *Organometallics* **2009**, *28*, 2391.
106. Gott, A. L.; Clarke, A. J.; Clarkson, G. J.; Scott, P.; *Chem. Commun.* **2008,** *12*, 1422.
107. Chiu, M.; Hoyt, H. M.; Michael, F. E.; Bergman, R. G.; van Halbeek, H.; *Angew. Chem. Int. Ed.* **2008**, *47*, 6073.

108. Thomson, R. K.; Bexrud, J. A.; Schafer, L. L.; *Organometallics* **2006**, *25*, 4069.
109. Hoyt, H. M.; Bergman, R. G.; *Angew. Chem. Int. Ed.* **2007**, *46*, 5580.
110. Skinner, M. E. G.; Toupance, T.; Cowhig, D. A.; Tyrrell, B. R.; Mountford, P.; *Organometallics* **2005**, *24*, 5586.
111. Li, Y.; Banerjee, S.; Odom, A. L.; *Organometallics* **2005**, *24*, 3272.
112. Baunemann, A.; Kim, Y.; Winter, M.; Fischer, R. A.; *Dalton Trans.* **2006,** 121.
113. Dubberley, S. R.; Evans, S. E.; Boyd, C. L.; Mountford, P.; *Dalton Trans.* **2005**, 1448.
114. Gomes, P. T.; Green, M. L. H.; Martins, A. M.; Mountford, P.; *J. Organomet. Chem.* **1997**, *541*, 121.
115. Dubberley, S. R.; Friedrich, A.; Willman, D. A.; Mountford, P.; Radius, U.; *Chem. Eur. J.* **2003**, *9*, 3634.
116. Profilet, R. D.; Zambrano, C. H.; Fanwick, P. E.; Nash, J. J.; Rothwell, I. P.; *Inorg. Chem.* **1990**, *29*, 4362.
117. Arney, D. J.; Bruck, M. A.; Huber, S. R.; Wigley, D. E.; *Inorg. Chem.* **1992**, *31*, 3749.
118. Fletcher, D. A.; McMeeking, R. F.; Parkin, D.; *J. Chem. Inf. Comput. Sci.* **1996**, *36*, 746 (The UK Chemical Database Service: CSD version 5.33 updated February 2012).
119. In addition the solid state structure of $Ti(N_2N^{Me})\{N(H)C(Ph)C(Ph)NPh_2\}_2$ (**25a′**), the hydrolysis product of $Ti(N_2N^{Me})\{NC(Ph)C(Ph)NPh_2\}(py)$ (**25a**) was elucidated and clearly shows the presence of the $NC(Ph)C(Ph)NPh_2$ fragment with the same regioselectivity as compounds **2 - 8**, Chapter Two.
120. Buchwald, S. L.; LaMaire, S. J.; Nielsen, R. B.; Watson, B. T.; King, S. M.; *Org. Synth.* **1993**, *71*, 77.
121. Buchwald, S. L.; LaMaire, S. J.; Nielsen, R. B.; Watson, B. T.; King, S. M.; *Tetrahedron Lett.* **1987**, *28*, 3895.
122. Carr, D. B.; Schwartz, J.; *J. Am. Chem. Soc.* **1979**, *101*, 3521.
123. Selby, J. D., D.Phil Thesis, University of Oxford, 2009.
124. Prout, K.; Cameron, T. S.; Forder, R. A.; Critchley, S. R.; Denton, B.; Rees, G. V.; *Acta Crystallogr.* **1974**, *B30*, 2290.

125. Soloveichik, G. L.; Arkhireeva, T. M.; Bel'skii, V. K.; Bulychev, B. M.; *Metalloorg. Khim.* **1988**, *1*, 226.
126. Arvanitis, G. M.; Smegal, J.; Meier, I.; Wong, A. C. C.; Schwartz, J.; Van Engen, D.; *Organometallics* **1989**, *8*, 2717.
127. Arvanitis, G. M.; Schwartz, J.; Van Engen, D.; *Organometallics* **1986**, *5*, 2157.
128. Toomey, H. E.; Pun, D.; Veiros, L. F.; Chirik, P. J.; *Organometallics* **2008**, *27*, 872.
129. Gehrmann, T.; Plundrich, G. T.; Wadepohl, H.; Gade, L. H.; *Organometallics* **2012**, *31*, 3346.
130. Blake, A. J.; Mountford, P.; Nikonov, G. I.; Swallow, D.; *Chem. Commun.* **1996**, 1835.
131. Tiong, P. J.; Nova, A.; Groom, L. R.; Schwarz, A. D.; Selby, J. D.; Schofield, A. D.; Clot, E.; Mountford, P.; *Organometallics* **2011**, *30*, 1182.
132. Walsh, P. J.; Baranger, A. M.; Bergman, R. G.; *J. Am. Chem. Soc.* **1992**, *114*, 1708.
133. In this instance the rate of DMAP loss (k_1) is equal to twice the rate of observed broadening as each time DMAP leaves **29a** it is equally likely to form **29a** or **29b**. As such the diastereotopic protons and carbons only exchange once for every two times DMAP decoordinates.
134. No line-broadening was used in processing the FID.
135. Pugh, S. M.; Blake, A. J.; Gade, L. H.; Mountford, P.; *Inorg. Chem.* **2001**, *40*, 3992.
136. Stewart, P. J.; Blake, A. J.; Mountford, P.; *Inorg. Chem.* **1997**, *36*, 3616.
137. Vujkovic, N.; Ward, B. D.; Maisse-Francois, A.; Wadepohl, H.; Mountford, P.; Gade, L. H.; *Organometallics* **2007**, *26*, 5522.
138. Excess DMAP is required to prevent the net release of DMAP during the reaction affecting the kinetic regine.
139. Despite the large error on k_1, there is no experimentally significant effect on the gradient.
140. Despite the large error on k_1, there is no experimentally significant effect on the gradient.
141. Hansch, C.; Leo, A.; Taft, R. W.; *Chem. Rev.* **1991**, *91*, 165.

142. Hartwig, J. F.; Cook, K. S.; Hapke, M.; Incarvito, C. D.; Fan, Y.; Webster, C. E.; Hall, M. B.; *J. Am. Chem. Soc.* **2005**, *127*, 2538.

143. $\Delta G_{obs}^{\ddagger}$ for $Me_3SiCCMe$ was calculated from the half-life, as such no errors are available.

144. Lauher, J. W.; Hoffmann, R.; *J. Am. Chem. Soc.* **1976**, *98*, 1729.

145. Schwarz, A. D.; Mountford, P.; *Unpublished Work.* **2012**.

Chapter Five

Experimental details and characterising data

5.1 General methods and instrumentation

All manipulations were carried out under an inert atmosphere of argon or dinitrogen using standard Schlenk line or dry-box procedures. Solvents were predried over activated 4 Å molecular sieves and refluxed over sodium (toluene, xylene), sodium/potassium (pentane, diethyl ether), or calcium hydride (dichloromethane) under a dinitrogen atmosphere and collected by distillation. Alternatively, solvents were degassed by sparging with dinitrogen and dried by passing through a column of activated alumina.[1] Deuterated solvents were dried over potassium (C_6D_6, toluene-d_8 or pyridine-d_5) or P_2O_5 (CD_2Cl_2), distilled under reduced pressure, and stored under dinitrogen in Young's Teflon valve ampoules.

Solution NMR samples were prepared under a dinitrogen atmosphere in a dry-box, in 5 mm Wilmad NMR tubes possessing Young's Teflon valves. ^{1}H, ^{19}F and ^{13}C{^{1}H} NMR spectra were recorded on Varian Mercury 300 or Unity Plus 500 spectrometers or a Bruker AVII 500 spectrometer with a ^{13}C cryoprobe. ^{1}H and ^{13}C{^{1}H} spectra were referenced internally to residual protio-solvent (^{1}H) or solvent (^{13}C) resonances, and are reported relative to tetramethylsilane (δ = 0 ppm). ^{19}F spectra were referenced externally to $CFCl_3$. Chemical shifts are quoted in δ (ppm) and coupling constants in Hz. Where necessary, ^{1}H and ^{13}C assignments were assisted by the use of one and two-dimensional ^{1}H–^{1}H and ^{1}H–^{13}C correlation experiments. IR spectra were recorded on a Perkin-Elmer 1710 or Nicolet Magna 560 FTIR spectrometer. Samples were prepared in a dry-box as Nujol mulls between NaCl plates. IR data are quoted as wavenumbers (cm^{-1}) within the range 4000−400 cm^{-1}. Mass spectra were recorded by the departmental service, and elemental analyses were carried out by the Elemental Analysis Service at the London Metropolitan University or by Elemental Microanalysis Ltd, Devon.

5.2 Literature preparations

$Li_2N_2N^{py}$,[2] $Li_2N_2N^{Me}$,[3] $Ti(N_2N^{Me})(NNPh_2)(py)$ (**1.93**),[4,5] $Ti(N_2N^{py})(NNPh_2)(py)$ (**1.97**),[4,6] $Cp_2Ti(NNPh_2)(DMAP)$ (**4.2**),[6,7] C_6F_5CCMe,[8] 4-C_6H_4XCCMe (X = CF_3, OMe, ^{t}Bu, Me, Cl or F),[9] ArCCAr (Ar = C_6F_5[10,11] or 4-C_6H_4X, X = CF_3[12] or OMe[13]), FcCCMe,[14-16] LiCp,[17] LiCp′,[17,18] $LiCp^{Me_4}$,[19] LiCp*,[20,21] Cp'_2ZrCl_2,[22] Cp_2HfCl_2,[22] $Cp^*_2ZrCl_2$,[23] $Cp^{Me_4}{}_2ZrCl_2$,[24,25] $Cp^*_2Zr(Me)Cl$,[26,27] $Cp_2Zr(CH_2CH_2{}^tBu)Cl$,[28,29] $Cp_2Zr(NHNPh_2)(CH_2CH_2{}^tBu)$ (**1.152**)[30] and *N*-(2,6-di*iso*propylphenyl)formamide[31]

were prepared according to literature methods. 1,1-diphenylhydrazine was obtained from Sigma-Aldrich as the hydrogen chloride salt, from which the free hydrazine was obtained by basification, drying and removal of residual solvent, followed by distillation under inert atmospheric conditions. 1,1-dimethylhydrazine and pyridine were dried over freshly ground CaH_2 and distilled before use. Lithiated hydrazines were obtained by reaction of the appropriate hydrazine and *n*-butyl lithium. Other reagents were obtained commercially and used directly, degassed or dried over CaH_2, as appropriate, before use.

5.3 Experimental details and characterising data for Chapter Two

5.3.1 Kinetic measurements. A standard solution of 1,4-dimethoxybenzene in toluene-d_8 was used for all kinetic experiments (0.09 M). The general procedure is as follows. In a dry-box, compound **1.93** (15.1 mg, 26.6 μmol) was weighed into a vial, dissolved in the standard solution (0.35 mL) and cooled to -45 °C. In a separate vial, RCCMe was dissolved in the standard solution (0.30 mL) and also cooled to -45 °C. The two vials were placed on a pre-cooled tile and the solutions combined using a pre-cooled pipette, agitated quickly and transferred to a pre-cooled J. Young NMR tube. The NMR tube was taken out of the glovebox and placed in a dry ice/isopropanol cold bath. The NMR probe was cooled to -35 °C and the sample added before being locked and shimmed. It was then warmed to -26 °C (other reaction temperatures were also used as appropriate as noted in the main text), allowed to thermally equilibrate, the shimming checked and an array set up recording a spectrum of 4 scans every 140 s. The ratios of the species were calculated by measuring the integrals of the trimethylsilyl groups relative to the internal standard. Pseudo first order rate constants were obtained from linear plots of $\ln([Ti]/[Ti]_0)$ *vs.* time.

5.3.2 Ti(N_2N^{py}){N(NPh_2)C(Me)C(C_6F_5)} (**1**). To a stirred brown solution of Ti(N_2N^{py})($NNPh_2$)(py) (**1.97**, 0.310 g, 0.503 mmol) in C_6H_6 (10 mL), was added C_6F_5CCMe (0.104 g, 0.503 mmol). The solution immediately turned red and was stirred for a further 2 h. Volatiles were removed under reduced pressure and the solid recrystallised from hot hexanes (5 mL, 60 °C to RT) affording dark red diffraction-quality crystals of **1**. Yield = 0.243 g (66 %). Diffraction-quality crystals were also grown from a saturated pentane solution at RT.

^{1}H NMR (C_6D_6, 499.9 MHz, 293 K): δ 8.93 (1 H, d, ^{3}J = 6.6 Hz, py-H^{6}), 7.41 (4 H, d, ^{3}J = 8.0 Hz, *o*-NC_6H_5), 7.15 (4 H, app. t, app. ^{3}J = 8.0 Hz, *m*-NC_6H_5), 6.79 – 6.73 (3 H, overlapping py-H^{4} and *p*-NC_6H_5), 6.65 (1 H, d, ^{3}J = 6.6 Hz, py-H^{3}), 6.26 (1 H, app. t, app. ^{3}J = 6.6 Hz, py-H^{5}), 3.98 (2 H, d, ^{2}J = 12.7 Hz, C$\underline{H}_a$H$_b$NSiMe$_3$), 3.15 (2 H, d, ^{2}J = 12.7 Hz, CH$_a$$\underline{H}_b$NSiMe$_3$), 2.14 (3 H, s, TiC=CMe), 1.05 (3 H, s, CH$_2$C$\underline{Me}$), 0.02 (18 H, s, SiMe$_3$). ^{13}C{^{1}H} NMR (C_6D_6, 125.7 MHz, 293 K): δ 183.8 (Ti$\underline{C}$=CMe), 179.7 (TiC=$\underline{C}$Me), 160.1 (py-C^{2}), 148.3 (*i*-NC_6H_5), 146.8 (py-C^{6}), 139.2 (py-C^{4}), 129.4 (*m*-NC_6H_5), 122.3 (py-C^{5}), 121.4 (*p*-NC_6H_5), 119.7 (py-C^{3}), 119.4 (*o*-NC_6H_5), 63.1 ($\underline{C}$H$_2$NSiMe$_3$), 50.5 (CH$_2$$\underline{C}$Me), 23.1 (CH$_2C\underline{Me}$), 17.9 (TiC=C$\underline{Me}$), 0.5 (SiMe$_3$). Resonances attributable to carbons directly bound to ^{19}F atoms were not observed. ^{19}F NMR (C_6D_6, 470.4 MHz, 293 K): δ -141.6 (d, $^{3}J_{FF}$ = 21 Hz, *o*-C_6F_5), -166.8 (dt, $^{3}J_{FF}$ = 21 Hz, $^{4}J_{FF}$ = 11 Hz, *p*-C_6F_5), -168.5 (app. t, app. $^{3}J_{FF}$ = 21 Hz, *m*-C_6F_5). IR (NaCl plates, Nujol mull, cm^{-1}): 1639 (w), 1599 (m), 1587 (s), 1524 (m), 1502 (m), 1491 (m), 1468 (m, br.), 1386 (m), 1366 (w), 1359 (m), 1296 (m), 1270 (w), 1245 (m), 1224 (m), 1167 (m), 1141 (m), 1089 (w), 1063 (m), 1056 (w), 1030 (m), 1014 (w), 993 (w), 978 (m), 952 (w), 923 (s), 896 (m), 860 (s, br.), 837 (s), 800 (w), 779 (m), 760 (w), 746 (s), 730 (w), 694 (s), 662 (w), 648 (w), 633 (w), 620 (w), 604 (w). EI-MS: *m/z* = 743 [*M*]$^{+}$ (70 %), 575 [*M* – NPh$_2$]$^{+}$ (20 %), 374 [*M* – NPh$_2$ – (CH$_2$NSiMe$_3$)$_2$]$^{+}$ (80 %), 168 [NPh$_2$]$^{+}$ (100 %). Anal. found (calcd. for $C_{36}H_{42}F_5N_5Si_2Ti$): C, 58.2 (58.1); H, 5.7 (5.7); N, 9.3 (9.4) %.

5.3.3 Ti(N$_2$N^{Me}){NC(4-C$_6$H$_4$OMe)C(Me)NPh$_2$}(py) (**2**). To a solution of Ti(N$_2$N^{Me})(NNPh$_2$)(py) (**1.93**, 0.414 g, 0.729 mmol) in Et$_2$O (10 mL) was added (4-C$_6$H$_4$OMe)CCMe (0.107 g, 0.729 mmol) at RT. An immediate colour change from green to dark red was observed and the solution left for a further 2 h. Volatiles were removed under reduced pressure affording **2** as a red powder which was washed with pentane (3 × 5 mL) and dried *in vacuo*. Yield: 0.326 g (62 %).

^{1}H NMR (C_6D_6, 499.9 MHz, 293 K): δ 8.12 (2 H, d, ^{3}J = 7.5 Hz, *o*-NC_5H_5), 7.70 (4 H, d, ^{3}J = 8.0 Hz, *o*-NC_6H_5), 7.62 (2 H, d, ^{3}J = 6.5 Hz, *o*-CC_6H_4OMe), 7.33 (4 H, app. t, app. ^{3}J = 8.0 Hz, *m*-NC_6H_5), 6.93 (4 H, overlapping *m*-CC_6H_4OMe and *p*-NC_6H_5), 6.69 (1 H, t, ^{3}J = 7.5 Hz, *p*-NC_5H_5), 6.39 (2 H, app. t, app. ^{3}J = 7.5 Hz, *m*-NC_5H_5), 3.42 and 3.21 (2 × 2 H, 2 × m, C$\underline{H}_2$NSiMe$_3$), 3.35 (3 H, s, CC$_6$H$_4$O$\underline{Me}$), 2.63 and 2.14 (2 × 2 H, 2 × m, C$\underline{H}_2$NMe), 2.13 (3 H, s, NMe), 1.70 (3 H, s, NC=CMe), 0.03 (18 H, s, SiMe$_3$). ^{13}C{^{1}H} NMR (C_6D_6, 125.7 MHz, 293 K): δ 158.4 (*i*-CC_6H_4OMe), 157.4

(N<u>C</u>=CMe), 153.0 (*o*-NC_5H_5), 147.6 (*i*-NC_6H_5), 137.7 (*p*-NC_5H_5), 137.0 (*p*-CC_6H_4OMe), 130.8 (*o*-CC_6H_4OMe), 129.1 (*m*-NC_6H_5), 123.0 (*m*-NC_5H_5), 121.1 (*o*-NC_6H_5), 120.5 (*m*-CC_6H_4OMe), 113.3 (*p*-NC_6H_5), 112.1 (NC=<u>C</u>Me), 61.0 (<u>C</u>H_2NMe), 54.7 (CC_6H_4O<u>Me</u>), 48.1 (<u>C</u>H_2NSiMe_3), 46.2 (NMe), 15.8 (NC=C<u>Me</u>), 1.9 ($SiMe_3$). IR (NaCl plates, Nujol mull, cm^{-1}): 1603 (s, br.), 1506 (s), 1326 (m, br.), 1249 (m, br.), 1205 (m), 1169 (w), 1137 (m), 1101 (m), 1083 (m), 1067 (m), 1039 (m, br.), 1013 (m), 992 (m), 968 (m), 918 (m, br.), 858 (m, br.), 769 (m), 750 (w, br.), 717 (w), 693 (m), 672 (m), 637 (m), 629 (m), 607 (w). EI-MS: *m/z* = 635 $[M - py]^+$ (30 %), 401 $[M - (NSiMe_3)_2 - py - OMe - NMe]^+$ (100 %), 307 $[M - NC(C_6H_4OMe)C(Me)NPh_2]^+$ (60 %), 283 $[C(C_6H_4OMe)C(Me)NPh_2]^+$ (50 %), 168 $[NPh_2]^+$ (70 %). Anal. found (calcd. for $C_{38}H_{54}N_6OSi_2Ti$): C, 63.8 (63.8); H, 7.7 (7.6); N, 11.7 (11.8) %.

5.3.4 Ti(N_2N^{Me}){NC(4-$C_6H_4{}^tBu$)C(Me)NPh_2}(py) (**3**). To a solution of Ti(N_2N^{Me})($NNPh_2$)(py) (**1.93**, 0.393 g, 0.691 mmol) in Et_2O (10 mL) was added (4-$C_6H_4{}^tBu$)CCMe (0.119 g, 0.691 mmol) in Et_2O (10 mL) at RT. An immediate colour change from green to dark red was observed and the solution left for a further 2 h. Volatiles were removed under reduced pressure giving a red powder which was extracted into pentane (5 mL). The dark red solution was cooled to -80 °C and the precipitate filtered and washed with cold pentane (2 × 5 mL, -78 °C) affording **4** as a red powder which was dried *in vacuo*. Yield: 0.231 g (46 %).

^{1}H NMR (C_6D_6, 499.9 MHz, 293 K): δ 8.13 (2 H, d, ^3J = 6.5 Hz, *o*-NC_5H_5), 7.72 (4 H, d, ^3J = 8.5 Hz, *o*-NC_6H_5), 7.65 (2 H, d, ^3J = 8.0 Hz, *o*-$CC_6H_4{}^tBu$), 7.37 (2 H, d, ^3J = 8.0 Hz, *m*-$CC_6H_4{}^tBu$), 7.32 (4 H, app. t, app. ^3J = 8.5 Hz, *m*-NC_6H_5), 6.92 (2 H, t, ^3J = 8.5 Hz, *p*-NC_6H_5), 6.72 (1 H, t, ^3J = 6.5 Hz, *p*-NC_5H_5), 6.44 (2 H, app. t, app. ^3J = 6.5 Hz, *m*-NC_5H_5), 3.42 and 3.22 (2 × 2 H, 2 × m, C<u>H</u>$_2NSiMe_3$), 2.65 and 2.16 (2 × 2 H, 2 × m, C<u>H</u>$_2$NMe), 2.10 (3 H, s, NMe), 1.69 (3 H, s, NC=CMe), 1.26 (9 H, s, CC_6H_4C<u>Me</u>$_3$), 0.03 (18 H, s, $SiMe_3$). $^{13}C\{^1H\}$ NMR (C_6D_6, 125.7 MHz, 293 K): δ 157.8 (N<u>C</u>=CMe), 153.0 (*o*-NC_5H_5), 148.6 (*i*-$CC_6H_4{}^tBu$), 147.6 (*i*-NC_6H_5), 141.6 (*p*-$CC_6H_4{}^tBu$), 137.7 (*p*-NC_5H_5), 129.5 (*o*-$CC_6H_4{}^tBu$), 129.1 (*m*-NC_6H_5), 124.6 (*m*-$CC_6H_4{}^tBu$), 123.0 (*m*-NC_5H_5), 121.1 (*o*-NC_6H_5), 120.5 (*p*-NC_6H_5), 111.9 (NC=<u>C</u>Me), 63.2 (CC_6H_4<u>C</u>Me_3), 61.0 (<u>C</u>H_2NMe), 48.1 (<u>C</u>H_2NSiMe_3), 46.1 (NMe), 31.5 (CC_6H_4C<u>Me</u>$_3$), 15.8 (NC=C<u>Me</u>), 1.6 ($SiMe_3$). IR (NaCl plates, Nujol mull, cm^{-1}): 1603 (m), 1586 (s), 1490 (s), 1304 (m, br.), 1237 (m), 1205 (m), 1180 (w), 1136 (w),

1107 (w), 1087 (m), 1067 (m), 1040 (m), 1014 (w), 994 (m), 971 (w), 943 (m), 928 (s), 859 (s), 831 (s), 797 (m), 750 (m), 696 (m), 682 (w), 665 (w), 638 (w), 623 (w). EI-MS: *m/z* = 661 $[M - py]^+$ (90 %), 354 $[NC(C_6H_4{}^tBu)C(Me)NPh_2]^+$ (100 %), 307 $[M - NC(C_6H_4{}^tBu)C(Me)NPh_2]^+$ (100 %), 168 $[NPh_2]^+$ (70 %). Anal. found (calcd. for $C_{41}H_{60}N_6Si_2Ti$): C, 66.4 (66.5); H, 8.2 (8.2); N, 11.2 (11.3) %.

5.3.5 Ti(N_2N^{Me}){NC(Tol)C(Me)NPh_2}(py) (**4**). To a solution of Ti(N_2N^{Me})($NNPh_2$)(py) (**1.93**, 0.407 g, 0.716 mmol) in Et_2O (10 mL) was added TolCCMe (0.0934 g, 0.716 mmol) in Et_2O (10 mL) at RT. An immediate colour change from green to dark red was observed and the solution left for a further 2 h. Volatiles were removed under reduced pressure affording **4** as a beige powder which was washed with pentane (3 × 5 mL) and dried *in vacuo*. Yield: 0.314 g (62 %).

^{1}H NMR (C_6D_6, 499.9 MHz, 293 K): δ 8.10 (2 H, d, ^{3}J = 6.0 Hz, *o*-NC_5H_5), 7.69 (4 H, d, ^{3}J = 8.5 Hz, *o*-NC_6H_5), 7.62 (2 H, d, ^{3}J = 6.0 Hz, *o*-CC_6H_4Me), 7.32 (4 H, app. t, app. ^{3}J = 8.5 Hz, *m*-NC_6H_5), 7.12 (2 H, d, ^{3}J = 6.0 Hz, *m*-CC_6H_4Me), 6.92 (2 H, t, ^{3}J = 8.5 Hz, *p*-NC_6H_5), 6.70 (1 H, t, ^{3}J = 6.0 Hz, *p*-NC_5H_5), 6.39 (2 H, app. t, app. ^{3}J = 6.0 Hz, *m*-NC_5H_5), 3.44 and 3.23 (2 × 2 H, 2 × m, C$\underline{H}_2$NSiMe_3), 2.65 and 2.17 (2 × 2 H, 2 × m, C$\underline{H}_2$NMe), 2.20 (3 H, s, $CC_6H_4\underline{Me}$), 2.13 (3 H, s, NMe), 1.72 (3 H, s, NC=CMe), 0.08 (18 H, s, $SiMe_3$). ^{13}C{^{1}H} NMR (C_6D_6, 125.7 MHz, 293 K): δ 157.8 (N$\underline{C}$=CMe), 153.0 (*o*-NC_5H_5), 147.6 (*i*-NC_6H_5), 141.6 (*p*-CC_6H_4Me), 137.7 (*p*-NC_5H_5), 135.2 (*i*-CC_6H_4Me), 129.7 (*o*-CC_6H_4Me), 129.1 (*m*-NC_6H_5), 128.5 (*m*-CC_6H_4Me), 123.0 (*m*-NC_5H_5), 121.1 (*o*-NC_6H_5), 120.5 (*p*-NC_6H_5), 111.9 (NC=$\underline{C}$Me), 61.0 ($\underline{C}H_2$NMe), 48.1 ($\underline{C}H_2$NSiMe_3), 46.2 (NMe), 21.2 ($CC_6H_4\underline{Me}$), 15.8 (NC=C$\underline{Me}$), 1.7 ($SiMe_3$). IR (NaCl plates, Nujol mull, cm^{-1}): 1603 (m), 1585 (s), 1488 (s), 1311 (s), 1238 (m), 1213 (w), 1195 (m), 1135 (w), 1086 (m), 1067 (m), 1038 (m), 1013 (m), 994 (w), 943 (m), 928 (s), 854 (s), 831 (s, br.), 798 (m), 751 (m), 696 (m), 684 (w), 665 (w), 638 (m). EI-MS: *m/z* = 670 $[M - NMe]^+$ (10 %), 312 $[NC(C_6H_4Me)C(Me)NPh_2]^+$ (100 %), 168 $[NPh_2]^+$ (90 %). Anal. found (calcd. for $C_{38}H_{54}N_6Si_2Ti$): C, 65.2 (65.3); H, 7.9 (7.8); N, 12.1 (12.0) %.

5.3.6 Ti(N_2N^{Me}){NC(4-C_6H_4F)C(Me)NPh_2}(py) (**5**). To a solution of Ti(N_2N^{Me})($NNPh_2$)(py) (**1.93**, 0.551 g, 0.971 mmol) in Et_2O (10 mL) was added (4-C_6H_4F)CCMe (0.130 g, 0.971 mmol) in Et_2O (10 mL) at RT. An immediate colour change from green to dark red was observed and the solution left for a further 90 min. Volatiles were removed under reduced pressure and the resulting red powder was

washed with pentane (3 × 5 mL) and dried *in vacuo* affording **5** as a beige powder. Yield: 0.316 g (46 %). Diffraction-quality crystals were grown from a saturated pentane solution at -30 ºC.

^{1}H NMR (C_6D_6, 499.9 MHz, 293 K): δ 8.03 (2 H, d, ^{3}J = 5.0 Hz, *o*-NC_5H_5), 7.62 (4 H, d, ^{3}J = 8.5 Hz, *o*-NC_6H_5), 7.47 (2 H, dd, $^{3}J_{HH}$ = 5.5 Hz and $^{4}J_{HF}$ = 6.5 Hz, *o*-CC_6H_4F), 7.30 (4 H, app. t, app. ^{3}J = 8.5 Hz, *m*-NC_6H_5), 6.94 (2 H, dd, $^{3}J_{HH}$ = 5.5 Hz and $^{3}J_{HF}$ = 10.0 Hz, *m*-CC_6H_4F), 6.91 (2 H, t, ^{3}J = 8.5 Hz, *p*-NC_6H_5), 6.66 (1 H, t, ^{3}J = 5.0 Hz, *p*-NC_5H_5), 6.34 (2 H, app. t, app. ^{3}J = 5.0 Hz, *m*-NC_5H_5), 3.37 and 3.16 (2 × 2 H, 2 × m, C$\underline{H}_2$NSiMe$_3$), 2.57 and 2.05 (2 × 2 H, 2 × m, C$\underline{H}_2$NMe), 2.00 (3 H, s, NMe), 1.57 (3 H, s, NC=CMe), 0.04 (18 H, s, SiMe$_3$). ^{13}C{^{1}H} NMR (C_6D_6, 125.7 MHz, 293 K): δ 161.6 (d, $^{1}J_{CF}$ = 238.8 Hz, *p*-CC_6H_4F), 156.6 (N$\underline{C}$=CMe), 152.8 (*o*-NC_5H_5), 147.5 (*i*-NC_6H_5), 140.5 (d, $^{4}J_{CF}$ = 2.5 Hz, *i*-CC_6H_4F), 137.8 (*p*-NC_5H_5), 131.2 (d, $^{3}J_{CF}$ = 7.5 Hz, *o*-CC_6H_4F), 129.1 (*m*-NC_6H_5), 123.1 (*m*-NC_5H_5), 121.1 (*o*-NC_6H_5), 120.6 (*p*-NC_6H_5), 114.5 (d, $^{2}J_{CF}$ = 21.0 Hz, *m*-CC_6H_4F), 112.2 (NC=$\underline{C}$Me), 60.9 ($\underline{C}H_2$NMe), 48.1 ($\underline{C}H_2$NSiMe$_3$), 46.0 (NMe), 15.7 (NC=C$\underline{Me}$), 1.6 (SiMe$_3$). ^{19}F (C_6D_6, 470.4 MHz, 293 K): δ -177.9 (1 F, m). IR (NaCl plates, Nujol mull, cm^{-1}): 1603 (m), 1592 (m), 1584 (s), 1500 (m), 1488 (s), 1307 (m), 1277 (w), 1250 (w), 1237 (m), 1215 (w), 1196 (m), 1136 (w), 1084 (m), 1067 (m), 1042 (m), 1037 (m), 1014 (w), 994 (w), 944 (m), 928 (s), 920 (m), 857 (s), 833 (s), 800 (m), 750 (m), 695 (m), 682 (m), 639 (w). EI-MS: *m/z* = 623 [*M* – py]$^{+}$ (5 %), 344 [TiNC(C_6H_4)C(Me)NPh$_2$]$^{+}$ (10 %), 318 [NC(C_6H_4F)C(Me)NPh$_2$]$^{+}$ (10 %), 307 [*M* – py – NC(C_6H_4F)C(Me)NPh$_2$] (5 %), 168 [NPh$_2$]$^{+}$ (20 %). Anal. found (calcd. for $C_{37}H_{51}FN_6Si_2Ti$): C, 63.2 (63.2); H, 7.2 (7.3); N, 11.9 (12.0) %.

5.3.7 Ti(N$_2$N^{Me}){NC(4-C$_6$H$_4$Cl)C(Me)NPh$_2$}(py) (**6**). To a solution of Ti(N$_2$N^{Me})(NNPh$_2$)(py) (**1.93**, 0.387 g, 0.681 mmol) in Et$_2$O (10 mL) was added (4-C_6H_4Cl)CCMe (0.103 g, 0.681 mmol) in Et$_2$O (10 mL) at RT. An immediate colour change from green to dark red was observed and the solution left for a further 90 min. Volatiles were removed under reduced pressure and the resulting red powder was washed with pentane (3 × 5 mL) and dried *in vacuo* affording **6** as a beige powder. Yield: 0.367 g (75 %).

^{1}H NMR (C_6D_6, 499.9 MHz, 293 K): δ 8.02 (2 H, d, ^{3}J = 5.0 Hz, *o*-NC_5H_5), 7.63 (4 H, d, ^{3}J = 7.5 Hz, *o*-NC_6H_5), 7.46 (2 H, d, ^{3}J = 8.5 Hz, *o*-CC_6H_4Cl), 7.31 (4 H, app. t, app. ^{3}J = 7.5 Hz, *m*-NC_6H_5), 7.27 (2 H, d, ^{3}J = 8.5 Hz *m*-CC_6H_4Cl), 6.92 (2 H, t, ^{3}J =

7.5 Hz, *p*-NC_6H_5), 6.69 (1 H, t, ^3J = 5.0 Hz, *p*-NC_5H_5), 6.38 (2 H, app. t, app. ^3J = 5.0 Hz, *m*-NC_5H_5), 3.40 and 3.17 (2 × 2 H, 2 × m, C$\underline{H}_2$NSiMe$_3$), 2.62 and 2.10 (2 × 2 H, 2 × m, C$\underline{H}_2$NMe), 2.04 (3 H, s, NMe), 1.61 (3 H, s, NC=CMe), 0.02 (18 H, s, SiMe$_3$). $^{13}C\{^1H\}$ NMR (C_6D_6, 125.7 MHz, 293 K): δ 156.4 (N$\underline{C}$=CMe), 152.8 (*o*-NC_5H_5), 147.4 (*i*-NC_6H_5), 142.9 (*p*-CC_6H_4Cl), 137.9 (*p*-NC_5H_5), 131.7 (*i*-CC_6H_4Cl), 131.2 (*o*-CC_6H_4Cl), 129.1 (*m*-NC_6H_5), 128.0 (*m*-CC_6H_4Cl), 123.1 (*m*-NC_5H_5), 121.1 (*o*-NC_6H_5), 121.0 (*p*-NC_6H_5), 112.2 (NC=$\underline{C}$Me), 61.0 ($\underline{C}H_2$NMe), 48.1 ($\underline{C}H_2$NSiMe$_3$), 46.1 (NMe), 15.7 (NC=C$\underline{Me}$), 1.6 (SiMe$_3$). IR (NaCl plates, Nujol mull, cm^{-1}): 1603 (m), 1585 (s), 1489 (s), 1308 (m), 1294 (m), 1237 (m), 1197 (m), 1088 (m), 1067 (m), 1037 (w), 1013 (w), 994 (w), 943 (m), 928 (s), 854 (s), 843 (m), 799 (m), 750 (m), 695 (m). EI-MS: *m/z* = 639 $[M - py]^+$ (30 %), 345 $[TiNC(C_6H_4)C(Me)NPh_2]^+$ (30 %), 307 [*M* – py – $NC(C_6H_4Cl)C(Me)NPh_2$] (80 %), 168 $[NPh_2]^+$ (20 %). An accurate elemental analysis could not be obtained.

5.3.8 Ti(N$_2$N^{Me}){NC(4-C$_6$H$_4$CF$_3$)C(Me)NPh$_2$}(py) (**7**). To a solution of Ti(N$_2$N^{Me})(NNPh$_2$)(py) (**1.93**, 0.399 g, 0.703 mmol) in Et_2O (10 mL) was added (4-$C_6H_4CF_3$)CCMe (0.129 g, 0.703 mmol) in Et_2O (10 mL) at RT. An immediate colour change from green to dark red was observed and the solution left for a further 90 min. Volatiles were removed under reduced pressure and the resulting red powder was extracted into pentane (3 × 5 mL) and crystallised at -80 °C affording **7** as a red powder which was dried *in vacuo*. Yield: 0.363 g (69 %).

^1H NMR (C_6D_6, 499.9 MHz, 293 K): δ 7.99 (2 H, d, ^3J = 6.0 Hz, *o*-NC_5H_5), 7.63 (4 H, d, ^3J = 7.5 Hz, *o*-NC_6H_5), 7.60 (2 H, d, ^3J = 8.0 Hz, *o*-$CC_6H_4CF_3$), 7.54 (2 H, d, ^3J = 8.0 Hz, *m*-$CC_6H_4CF_3$), 7.32 (4 H, app. t, app. ^3J = 7.5 Hz, *m*-NC_6H_5), 6.93 (2 H, t, ^3J = 7.5 Hz, *p*-NC_6H_5), 6.67 (1 H, t, ^3J = 6.0 Hz, *p*-NC_5H_5), 6.37 (2 H, app. t, app. ^3J = 6.0 Hz, *m*-NC_5H_5), 3.39 and 3.16 (2 × 2 H, 2 × m, C$\underline{H}_2$NSiMe$_3$), 2.60 and 2.07 (2 × 2 H, 2 × m, C$\underline{H}_2$NMe), 1.99 (3 H, s, NMe), 1.58 (3 H, s, NC=CMe), 0.01 (18 H, s, SiMe$_3$). $^{13}C\{^1H\}$ NMR (C_6D_6, 125.7 MHz, 293 K): δ 156.4 (*p*-$CC_6H_4CF_3$), 152.9 (N$\underline{C}$=CMe), 152.8 (*o*-NC_5H_5), 148.2 (*i*-$CC_6H_4CF_3$), 147.5 (*i*-NC_6H_5), 138.0 (*p*-NC_5H_5), 130.2 (*o*-$CC_6H_4CF_3$), 129.3 (*m*-NC_6H_5), 125.0 (*m*-$CC_6H_4CF_3$), 123.2 (*m*-NC_5H_5), 121.2 (*o*-NC_6H_5), 120.8 (*p*-NC_6H_5), 112.6 (NC=$\underline{C}$Me), 61.1 ($\underline{C}H_2$NMe), 48.2 ($\underline{C}H_2$NSiMe$_3$), 46.2 (NMe), 15.8 (NC=C$\underline{Me}$), 1.7 (SiMe$_3$). The resonance attributable to CF_3 was not observed. ^{19}F NMR (C_6D_6, 282.5 MHz, 293 K): δ -61.7 (3 F, s). IR (NaCl plates, Nujol mull, cm^{-1}): 1603 (s), 1587 (s, br.), 1490 (s, br.), 1465 (s, br.), 1402 (m), 1327

(m, br.), 1239 (m), 1201 (m), 1184 (w), 1124 (m, br.), 1103 (m), 1082 (m), 1065 (m), 1039 (m), 1014 (m), 994 (m), 970 (m), 927 (s, br.), 859 (m), 839 (s, br.), 800 (s), 747 (m), 695 (m), 685 (m), 638 (m), 621 (w). EI-MS: *m/z* = 366 $[NC(C_6H_4CF_3)C(Me)NPh_2]^+$ (100 %), 307 [*M* – py – $NC(C_6H_4CF_3)C(Me)NPh_2$] (20 %), 168 $[NPh_2]^+$ (90 %). Anal. found (calcd. for $C_{38}H_{51}F_3N_6Si_2Ti$): C, 60.6 (60.6); H, 6.8 (6.8); N, 11.1 (11.2) %.

5.3.9 Ti(N_2N^{Me}){$NC(C_6F_5)C(Me)NPh_2$}(py) (**8**). To a solution of Ti(N_2N^{Me})($NNPh_2$)(py) (**1.93**, 0.273 g, 0.480 mmol) in Et_2O (10 mL) was added C_6F_5CCMe (0.0991 g, 0.480 mmol) in Et_2O (10 mL) at RT. An immediate colour change from green to dark red was observed and the solution left for a further 16 h. Volatiles were removed under reduced pressure affording **8** as a red powder which was washed with pentane (3 × 5 mL) and dried *in vacuo*. Yield: 0.308 g (81 %). Diffraction-quality crytals were grown from a saturated pentane solution at -30 ºC.

^{1}H NMR (C_6D_6, 499.9 MHz, 293 K): δ 8.43 (2 H, d, ^{3}J = 6.0 Hz, *o*-NC_5H_5), 7.61 (4 H, d, ^{3}J = 9.0 Hz, *o*-NC_6H_5), 7.27 (4 H, app. t, app. ^{3}J = 9.0 Hz, *m*-NC_6H_5), 6.89 (2 H, t, ^{3}J = 9.0 Hz, *p*-NC_6H_5), 6.72 (1 H, t, ^{3}J = 6.0 Hz, *p*-NC_5H_5), 6.47 (2 H, app. t, app. ^{3}J = 6.0 Hz, *m*-NC_5H_5), 3.39 and 3.08 (2 × 2 H, 2 × m, C$\underline{H}_2$NSiMe_3), 2.56 and 2.13 (2 × 2 H, 2 × m, C$\underline{H}_2$NMe), 2.20 (3 H, s, NMe), 1.56 (3 H, s, NC=CMe), 0.23 (18 H, s, SiMe_3). ^{13}C{^{1}H} NMR (C_6D_6, 125.7 MHz, 293 K): δ 152.9 (*o*-NC_5H_5), 150.2 (m, *i*-CC_6F_5), 147.1 (*i*-NC_6H_5), 142.1 (N$\underline{C}$=CMe), 138.3 (*p*-NC_5H_5), 129.1 (*m*-NC_6H_5), 123.3 (*m*-NC_5H_5), 121.1 (*o*-NC_6H_5), 120.9 (*p*-NC_6H_5), 118.9 (NC=$\underline{C}$Me), 62.2 ($\underline{C}H_2$NMe), 48.0 ($\underline{C}H_2$NSiMe_3), 47.6 (NMe), 16.1 (NC=C$\underline{Me}$), 1.0 (SiMe_3). Resonances attributable to carbons directly bound to ^{19}F atoms were not observed. ^{19}F NMR (C_6D_6, 470.4 MHz, 293 K): δ -141.6 (2 F, d, $^3J_{FF}$ = 25 Hz, *o*-CC_6F_5), -159.8 (1 F, t, $^3J_{FF}$ = 21.0 Hz, *p*-CC_6F_5), -163.2 (2 F, dd, $^3J_{FF}$ = 21.0 and 25.0 Hz, *m*-CC_6F_5). IR (NaCl plates, Nujol mull, cm^{-1}): 1602 (s), 1586 (s, br.), 1516 (s), 1491 (s, br.), 1463 (s, br.), 1411 (w), 1319 (m), 1287 (m), 1240 (m), 1213 (m), 1191 (m), 1150 (m), 1139 (m, br.), 1127 (s), 1068 (m), 1060 (m), 1041 (m), 1028 (m), 1013 (m, br.), 980 (s, br.), 929 (s, br.), 901 (w), 889 (w), 838 (s, br.), 793 (m), 749 (m), 733 (w), 710 (w), 702 (m), 693 (m), 672 (w), 665 (w), 650 (w), 638 (w). EI-MS: *m/z* = 695 [*M* – py]$^+$ (80 %), 168 $[NPh_2]^+$ (60 %), 167 $[C_6F_5]^+$ (50 %). Anal. found (calcd. for $C_{37}H_{47}F_5N_6Si_2Ti$): C, 57.3 (57.4); H, 6.1 (6.1); N, 10.8 (10.9) %.

5.3.10 MeCC(2,3,5,6-C_6F_4)CCMe (9). The method used was a modification of a literature procedure.[8] Propyne (*ca.* 60 mmol) was condensed *in vacuo* in THF (80 mL) at -196 °C. The schlenk was brought under an argon atmosphere and allowed to warm slowly to -80 °C. BuLi (32.8 mL, 52.5 mmol, 1.6 M in hexanes) was added dropwise under vigorous stirring and after addition was complete the white suspension was allowed to warm to -30 °C and react for 1 h. The suspension was cooled to -60 °C and a solution of hexafluorobenzene (8.74 g, 47.0 mmol) in THF (50 mL) was slowly added. After addition was complete the reaction was left to warm to RT and react for 16 h during which time it turned dark green. The reaction was quenched with H_2O (100 mL), the product extracted into Et_2O (3 × 100 mL) and dried over $MgSO_4$. The volatiles were removed on a rotary evaporator (40 °C, 300 mbar) giving a green oil. This was sublimed onto a cold finger (0 °C) at ~ 10^{-1} mbar giving **9** as a white crystalline solid. Yield: 1.79 g (30 %). Diffraction-quality crystals were grown from a saturated chloroform solution at RT.

^{1}H NMR (C_6D_6, 300.3 MHz, 293 K): δ 1.47 (6 H, s, Me). ^{19}F NMR (C_6D_6, 282.5 MHz, 293 K): -139.0 (4 F, s). ^{13}C{^{1}H} NMR (C_6D_6, 75.5 MHz, 293 K): 149.3 (m, *i*-C_6F_4), 146.0 (m, *o*-C_6F_4), 101.3 (MeC<u>C</u>), 66.1 (Me<u>C</u>C), 4.5 (<u>Me</u>CC). IR (NaCl plates, Nujol mull, cm^{-1}): 2286 (w), 2226 (m, br.), 1547 (w), 1325 (s, br.), 1262 (w), 1111 (w), 1085 (w), 1077 (m), 1064 (m), 978 (s, br.), 813 (m, br.), 791 (s). FI-MS: *m/z* = 226 [*M*]$^+$ (100 %). Anal. found (calc. for $C_{12}H_6F_4$): C, 63.8 (63.7); H, 2.6 (2.7) %.

5.3.11 [Ti(N_2N^{Me}){NCC(Me)NPh$_2$}(py)]$_2$(μ-2,3,5,6-C_6F_4) (10). To a solution of Ti(N_2N^{Me})(NNPh$_2$)(py) (**1.93**, 0.470 g, 0.827 mmol) in toluene (10 mL) was added MeCC(2,3,5,6-C_6F_4)CCMe (0.0943 g, 0.414 mmol) in toluene (10 mL) at RT. An immediate colour change from green to dark red was observed and the solution left for a further 16 h. Pentane (40 mL) was added and upon standing **10** formed as orange diffraction-quality crystals The supernatant was decanted, the crystals washed with pentane (3 × 5 mL) and dried *in vacuo*. Yield: 0.210 g (36 %).

^{1}H NMR (C_6D_6, 499.9 MHz, 293 K): δ 8.41 (2 H, d, ^{3}J = 4.5 Hz, *o*-NC_5H_5), 7.60 (4 H, d, ^{3}J = 7.5 Hz, *o*-NC_6H_5), 7.29 (4 H, app. t, app. ^{3}J = 7.5 Hz, *m*-NC_6H_5), 6.89 (2 H, t, ^{3}J = 7.5 Hz, *p*-NC_6H_5), 6.69 (1 H, t, ^{3}J = 4.5 Hz, *p*-NC_5H_5), 6.46 (2 H, app. t, app. ^{3}J = 4.5 Hz, *m*-NC_5H_5), 3.40 and 3.14 (2 × 2 H, 2 × m, C<u>H$_2$</u>NSiMe$_3$), 2.63 and 2.17 (2 × 2 H, 2 × m, C<u>H$_2$</u>NMe), 2.31 (3 H, s, NMe), 1.79 (3 H, s, NC=CMe), 0.10 (18 H, s, SiMe$_3$). ^{13}C{^{1}H} NMR (C_6D_6, 125.7 MHz, 293 K): δ 153.0 (*o*-NC_5H_5), 147.3

(*i*-NC_6H_5), 145.0 (m, *o*-CC_6F_4), 143.9 (N<u>C</u>=CMe), 143.1 (m, *i*-CC_6F_4), 138.2 (*p*-NC_5H_5), 129.3 (*m*-NC_6H_5), 123.3 (*m*-NC_5H_5), 121.2 (*o*-NC_6H_5), 120.9 (*p*-NC_6H_5), 116.8 (NC=<u>C</u>Me), 61.5 (<u>C</u>H_2NMe), 48.2 (<u>C</u>H_2N$SiMe_3$), 47.0 (NMe), 16.3 (NC=C<u>Me</u>), 1.4 ($SiMe_3$). ^{19}F NMR (C_6D_6, 282.5 MHz, 293 K): δ -141.7 (4 F, s). IR (NaCl plates, Nujol mull, cm^{-1}): 1587 (s, br.), 1492 (s), 1327 (m, br.), 1296 (m, br.), 1273 (m), 1240 (m), 1212 (m), 1182 (m), 1150 (w), 1136 (m, br.), 1081 (m), 1067 (m), 1039 (m), 1014 (w), 993 (w), 972 (m), 940 (m), 921 (s, br.), 885 (w), 833 (s, br.), 782 (w), 753 (m, br.), 714 (m), 694 (m), 676 (m), 659 (w), 637 (w). EI-MS: *m/z* = 1036 [*M* – 2py – NPh_2]$^+$ (70 %), 528 [Ti(N_2N^{Me})NCC(Me)NPh_2]$^+$ (10 %), 508 [Ti(N_2N^{Me})NC(C_6F_4)C(Me)]$^+$ (70 %), 168 [NPh_2]$^+$ (90 %). Anal. found (calcd. for $C_{68}H_{94}F_4N_{12}Si_4Ti_2$): C, 59.6 (59.9); H, 7.3 (7.0); N, 12.4 (12.3) %.

5.3.12 Ti(N_2N^{Me})($NNPh_2$)(DMAP) (**11**). To a mixture of Ti(N_2N^{Me})($NNPh_2$)(py) (**1.93**, 0.864 g, 1.52 mmol) and DMAP (0.163 g, 1.52 mmol) was added Et_2O (20 mL) at RT. The green solution was left for 4 h, during which time there was a colour change to dark brown. Volatiles were removed under reduced pressure affording **11** as a green solid which was washed with pentane (3 × 5 mL) and dried *in vacuo*. Yield: 0.934 g (79 %).

^{1}H NMR (C_6D_6, 499.9 MHz, 293 K): δ 8.48 (2 H, d, ^{3}J = 7.5 Hz, *o*-$NC_5H_4NMe_2$), 7.99 (4 H, d, ^{3}J = 8.0 Hz, *o*-NC_6H_5), 7.34 (4 H, app. t, app. ^{3}J = 8.0 Hz, *m*-NC_6H_5), 6.91 (2 H, t, ^{3}J = 8.0 Hz *p*-NC_6H_5), 5.73 (2 H, d, ^{3}J = 7.5 Hz, *m*-$NC_5H_4NMe_2$), 3.61 and 3.51 (2 × 2 H, 2 × m, C<u>H</u>$_2$N$SiMe_3$), 2.81 and 2.57 (2 × 2 H, 2 × m, C<u>H</u>$_2$NMe), 2.65 (3 H, s, NMe), 1.84 (6 H, s, NC_5H_4N<u>Me</u>$_2$), 0.11 (18 H, s, $SiMe_3$). ^{13}C{^{1}H} NMR (C_6D_6, 125.7 MHz, 293 K): δ 154.4 (*p*-$NC_5H_4NMe_2$), 153.4 (*o*-$NC_5H_4NMe_2$), 147.7 (*i*-NC_6H_5), 128.9 (*m*-NC_6H_5), 127.8 (*p*-NC_6H_5), 118.6 (*o*-NC_6H_5), 105.1 (*m*-$NC_5H_4NMe_2$), 62.5 (<u>C</u>H_2NMe), 49.5 (NMe), 48.1 (<u>C</u>H_2N$SiMe_3$), 37.9 (NC_5H_4N<u>Me</u>$_2$), 1.9 ($SiMe_3$). IR (NaCl plates, Nujol mull, cm^{-1}): 1616 (m), 1576 (w), 1559 (m), 1540 (m), 1534 (m), 1507 (m), 1497 (w), 1437 (w), 1419 (w), 1016 (s), 929 (w), 668 (w). EI-MS: *m/z* = 389 [*M* – 2($SiMe_3$) – Ph]$^+$ (90 %), 373 [*M* – 2($SiMe_3$) – Ph – Me]$^+$ (90 %), 357 [*M* – $SiMe_3$ – $NNPh_2$]$^+$ (100 %), 341 [*M* – $SiMe_3$ – $NNPh_2$ – Me]$^+$ (100 %). Anal. found (calcd. for $C_{30}H_{49}N_7Si_2Ti$): C, 58.8 (58.9); H, 8.2 (8.1); N, 15.9 (16.0) %.

5.3.13 Ti(N_2N^{Me}){NC(Ph)C(Me)NPh_2}(DMAP) (**12**). To a solution of Ti(N_2N^{Me})($NNPh_2$)(py) (**1.93**, 0.387 g, 0.681 mmol) in Et_2O (10 mL) was added

PhCCMe (85.4 μL, 0.681 mmol) at RT. An immediate colour change from green to dark red was observed and the solution left for 3 h. DMAP (0.0832 g, 0.681 mmol) in Et_2O (10 mL) was added and the red solution left for a further 1 h. Volatiles were removed under reduced pressure affording **12** as a red powder which was dried *in vacuo*. Yield: 0.307 g (61 %).

^{1}H NMR (C_6D_6, 499.9 MHz, 293 K): δ 7.98 (2 H, d, ^{3}J = 6.0 Hz, *o*-$NC_5H_4NMe_2$), 7.77 (4 H, d, ^{3}J = 8.0 Hz, *o*-NC_6H_5), 7.75 (2 H, d, ^{3}J = 7.5 Hz, *o*-CC_6H_5), 7.35 (4 H, app. t, app. ^{3}J = 8.0 Hz, *m*-NC_6H_5), 7.31 (2 H, app. t, app. ^{3}J = 7.5 Hz, *m*-CC_6H_5), 7.15 (1 H, t, ^{3}J = 7.5 Hz, *p*-CC_6H_5), 6.93 (2 H, t, ^{3}J = 8.0 Hz, *p*-NC_6H_5), 5.71 (2 H, d, ^{3}J = 6.0 Hz, *m*-$NC_5H_4NMe_2$), 3.51 and 3.32 (2 × 2 H, 2 × m, C$\underline{H}_2$NSiMe$_3$), 2.71 and 2.16 (2 × 2 H, 2 × m, C$\underline{H}_2$NMe), 2.16 (3 H, s, NMe), 1.89 (6 H, s, $NC_5H_4N\underline{Me}_2$), 1.70 (3 H, s, NC=CMe), 0.16 (18 H, s, $SiMe_3$). ^{13}C{^{1}H} NMR (C_6D_6, 125.7 MHz, 293 K): δ 157.9 (N$\underline{C}$=CMe), 154.1 (*p*-$NC_5H_4NMe_2$), 153.1 (*o*-$NC_5H_4NMe_2$), 147.9 (*i*-NC_6H_5), 145.0 (*i*-CC_6H_5), 129.9 (*o*-CC_6H_5), 129.2 (*m*-NC_6H_5), 127.8 (*m*-CC_6H_5), 126.0 (*p*-CC_6H_5), 121.3 (*o*-NC_6H_5), 120.4 (*p*-NC_6H_5), 111.7 (NC=$\underline{C}$Me), 104.6 (*m*-$NC_5H_4NMe_2$), 60.8 ($\underline{C}H_2$NMe), 48.5 ($\underline{C}H_2$NSiMe$_3$), 46.2 (NMe), 37.8 ($NC_5H_4N\underline{Me}_2$), 15.8 (NCC$\underline{Me}$), 2.0 ($SiMe_3$). IR (NaCl plates, Nujol mull, cm^{-1}): 1613 (s), 1586 (s), 1534 (m), 1490 (m), 1347 (w), 1324 (m), 1244 (m), 1203 (m), 1181 (w), 1081 (w), 1066 (m), 1040 (w), 1014 (m), 990 (m), 971 (w), 942 (m), 921 (s), 866 (m), 840 (s), 743 (m), 702 (m), 691 (m). EI-MS: *m/z* = 605 [*M* – DMAP]$^+$ (10 %), 412 [*M* – DMAP – $CMeNPh_2$]$^+$ (10 %), 168 [NPh_2]$^+$ (90 %). Anal. found (calcd. for $C_{39}H_{57}N_7Si_2Ti$): C, 64.4 (64.4); H, 7.9 (7.9); N, 13.5 (13.5) %.

Alternative NMR tube scale synthesis of Ti(N_2N^{Me}){NC(Ph)C(Me)NPh_2}(DMAP) (**12**). To a green solution of Ti(N_2N^{Me})($NNPh_2$)(DMAP) (**11**, 27.9 mg, 45.7 μmol) in C_6D_6 was added PhCCMe (5.7 μL, 45.7 μmol). An immediate colour change from brown to red was observed. After 18 h at RT the ^{1}H NMR spectrum showed quantitative conversion to **12**.

5.3.14 Ti(N_2N^{Me})($NNPh_2$)(bipy) (**14**). To a solution of Ti(N_2N^{Me})($NNPh_2$)(py) (**1.93**, 0.347 g, 0.611 mmol) in C_6H_6 (10 mL) was added 2,2′-bipyridine (0.0953 g, 0.611 mmol) in C_6H_6 (10 mL) at RT and the solution left for 4 h. Volatiles were removed under reduced pressure and the resulting green powder washed with pentane (3 × 5 mL) and dried *in vacuo* affording **14** as a green crystalline powder. Yield: 0.244 g (62 %). Diffraction-quality crytals were grown from a saturated benzene solution at RT.

^{1}H NMR (C_6D_6, 499.9 MHz, 293 K): δ 9.89 (2 H, d, ^{3}J = 5.0 Hz, 6-NC_5H_4), 7.02 (4 H, d, ^{3}J = 8.5 Hz, *o*-NC_6H_5), 6.94 (4 H, app. t, app. ^{3}J = 8.5 Hz, *m*-NC_6H_5), 6.87 (2 H, app. t, app. ^{3}J = 5.0 Hz, 4-NC_5H_4), 6.79 (2 H, d, ^{3}J = 5.0 Hz, 3-NC_5H_4), 6.72 (4 H, overlapping 5-NC_5H_4 and *p*-NC_6H_5), 3.62 and 3.46 (2 × 2 H, 2 × m, C$\underline{H}_2$NSiMe$_3$), 2.43 and 1.98 (2 × 2 H, 2 × m, C$\underline{H}_2$NMe), 0.91 (3 H, s, NMe), 0.64 (18 H, s, SiMe$_3$). ^{13}C{^{1}H} NMR (C_6D_6, 125.7 MHz, 293 K): δ 154.1 (6-NC_5H_4), 152.2 (2-NC_5H_4), 147.7 (*i*-NC_6H_5), 137.1 (5-NC_5H_4), 128.0 (*m*-NC_6H_5), 123.7 and 121.0 (4-NC_5H_4 and *p*-NC_6H_5), 120.1 (*o*-NC_6H_5), 120.0 (3-NC_5H_4), 59.6 (C$\underline{H}_2$NMe), 47.1 (C$\underline{H}_2$NSiMe$_3$), 42.7 (NMe), 1.3 (SiMe$_3$). IR (NaCl plates, Nujol mull, cm^{-1}): 1596 (s), 1582 (s), 1556 (w), 1479 (s, br.), 1468 (s, br.), 1416 (m), 1353 (m), 1310 (w), 1303 (w), 1291 (w), 1291 (m), 1275 (m), 1232 (m, br.), 1179 (w), 1160 (m), 1140 (w), 1080 (m), 1064 (s), 1054 (m), 1028 (s), 1018 (m), 1005 (m, br.), 992 (m), 938 (s, br.), 902 (w), 864 (m, br.), 828 (m, br.), 789 (w), 772 (m), 750 (s), 739 (m, br.), 697 (m). EI-MS: *m/z* = 645 $[M]^+$ (5 %), 390 $[M - SiMe_3 - NNPh_2]^+$ (5 %), 168 $[NPh_2]^+$ (100 %), 156 $[bipy]^+$ (100 %). Anal. found (calc. for $C_{33}H_{47}N_7Si_2Ti$): C, 61.1 (61.4); H, 7.4 (7.3); N, 14.9 (15.2) %.

5.3.15 Low temperature NMR tube scale synthesis of Ti(N$_2$N^{Me}){N(NPh$_2$)C(Me)C(4-C$_6$H$_4$CF$_3$)} (**15**). To a solution of Ti(N$_2$N^{Me})(NNPh$_2$)(py) (**1.93**, 15.1 mg, 26.6 μmol) in toluene-d_8 was added (4-$C_6H_4CF_3$)CCMe (97.8 mg, 0.532 mmol) in toluene-d_8, all at -40 °C in a dry-box. The green solution was agitated quickly and a colour change from green to dark red was observed. The solution was transferred to a pre-cooled J. Young NMR tube. This was removed from the dry-box and transferred to a pre-cooled NMR probe at -30 °C. The ^{1}H NMR spectrum showed a mixture of **1.93**, (4-$C_6H_4CF_3$)CCMe, free pyridine and **15** in a 3:2 (**1.93**:**15**) ratio. The following resonances were assigned to the product.

^{1}H NMR (C_6D_6, 499.9 MHz, 243 K): δ 7.51 (4 H, d, ^{3}J = 7.5 Hz, *o*-NC_6H_5), 6.83 (4 H, app. t, app. ^{3}J = 7.5 Hz, *m*-NC_6H_5), 6.64 (2 H, t, ^{3}J = 7.5 Hz, *p*-NC_6H_5), 3.21 and 3.11 (2 × 2 H, 2 × m, C$\underline{H}_2$NSiMe$_3$), 2.45 and 1.87 (2 × 2 H, 2 × m, C$\underline{H}_2$NMe), 2.19 (3 H, s, TiC=CMe), 1.91 (3 H, s, NMe), 0.25 (18 H, s, SiMe$_3$). ^{13}C{^{1}H} NMR (C_6D_6, 125.7 MHz, 243 K): δ 200.9 (Ti$\underline{C}$=CMe), 173.0 (TiC=$\underline{C}$Me), 156.2 (*p*-$CC_6H_4CF_3$), 146.8 (*i*-NC_6H_5), 130.2 (*o*-$CC_6H_4CF_3$), 123.5 (*m*-NC_6H_5), 121.4 (*m*-$CC_6H_4CF_3$), 121.0 (*o*-NC_6H_5), 120.7 (*p*-NC_6H_5), 58.4 (C$\underline{H}_2$NMe), 45.2 (C$\underline{H}_2$NSiMe$_3$), 43.2 (NMe), 15.8

(TiC=C<u>Me</u>), 3.8 ($SiMe_3$). Remaining resonances could not be assigned due to overlap with those belonging to other species.

5.3.16 Low temperature NMR tube scale synthesis of Ti(N_2N^{Me}){N(NPh_2)C(Me)C(C_6F_5)} (**16**). To a solution of Ti(N_2N^{Me})($NNPh_2$)(py) (**1.93**, 28.1 mg, 49.5 μmol) in toluene-d_8 was added C_6F_5CCMe (10.2 mg, 49.5 μmol) in toluene-d_8, all at -40 °C in a glovebox. The green solution was agitated quickly and a colour change from green to dark red was observed. The solution was transferred to a pre-cooled J. Young NMR tube. This was removed from the glove box and transferred to a pre-cooled NMR probe at -30 °C. The ^{1}H NMR spectrum showed a mixture **1.93**, C_6F_5CCMe, free pyridine and **16** in a 11:1 (**1.93**:**16**) ratio with the following peaks assigned to the product.

^{1}H NMR (C_6D_6, 499.9 MHz, 243 K): δ 7.31 (4 H, d, ^3J = 5.0 Hz, *o*-NC_6H_5), 7.15 (4 H, dd, ^3J = 5.0 and 8.0 Hz, *m*-NC_6H_5), 6.81 (2 H, t, ^3J = 8.0 Hz, *p*-NC_6H_5), 3.19 and 3.12 (2 × 2 H, 2 × m, C<u>H</u>$_2$NSiMe_3), 2.46 and 1.92 (2 × 2 H, 2 × m, C<u>H</u>$_2$NMe), 2.22 (3 H, s, TiC=CMe), 1.92 (3 H, s, NMe), 0.29 (18 H, s, $SiMe_3$). ^{13}C{^{1}H} NMR (C_6D_6, 125.7 MHz, 243 K): δ 200.9 (Ti<u>C</u>=CMe), 199.5 (m, *i*-CC_6F_5), 174.9 (TiC=<u>C</u>Me), 150.2 (m, *o*-CC_6F_5), 148.6 (m, *m*-CC_6F_5), 146.8 (*i*-NC_6H_5), 146.6 (m, *p*-CC_6F_5), 138.4 (*m*-NC_6H_5), 121.4 (*o*-NC_6H_5), 117.7 (*p*-NC_6H_5), 64.3 (<u>C</u>H_2NMe), 59.0 (<u>C</u>H_2NSiMe_3), 43.5 (NMe), 16.9 (TiC=C<u>Me</u>), 4.0 ($SiMe_3$). ^{19}F NMR (C_6D_6, 470.4 MHz, 243 K): -133.9 (2 F, br., s, *o*-CC_6F_5), -158.0 (1 F, t, $^3J_{FF}$ = 22.0 Hz, *p*-CC_6F_5), -160.3 (2 F, app. t, app. $^3J_{FF}$ = 22.0 Hz, *m*-CC_6F_5). Remaining resonances could not be assigned due to overlap with those belonging to other species.

5.4 Experimental details and characterising data for Chapter Three

5.4.1 Ti(N_2N^{Me}){NC(Ar^{F_2})$NNPh_2$}(py) (**17**, Ar^{F_2} = 2,6-$C_6H_3F_2$). To a solution of Ti(N_2N^{Me})($NNPh_2$)(py) (**1.93**, 0.235 g, 0.414 mmol) in Et_2O (10 mL) was added $Ar^{F_2}CN$ (0.173 g, 0.414 mmol) in Et_2O (10 mL) at RT. An immediate colour change from green to dark red was observed and over the course of 3 h an orange precipitate formed. The supernatent was decanted and the orange powder dried *in vacuo* affording **17**. Yield: 0.146 g (50 %). Diffraction-quality crystals were grown from a saturated diethyl ether solution at RT.

^{1}H NMR (C_6D_6, 499.9 MHz, 293 K): δ 9.45 (2 H, d, ^3J = 5.0 Hz, *o*-NC_5H_5), 7.43 (4 H, d, ^3J = 7.5 Hz, *o*-NC_6H_5), 7.19 (4 H, app. t, app. ^3J = 7.5 Hz, *m*-NC_6H_5), 6.85 (2 H, t,

^{3}J = 7.5 Hz, *p*-NC_6H_5), 6.80 (1 H, t, ^{3}J = 5.0 Hz, *p*-NC_5H_5), 6.55 (2 H, app. t, app. ^{3}J = 5.0 Hz, *m*-NC_5H_5), 6.52 (1 H, app. quintet, $^{3}J_{HH}$ and $^{4}J_{HF}$ = 7.0 Hz, *p*-$C_6H_3F_2$), 6.40 (2 H, app. t, $^{3}J_{HH}$ and $^{3}J_{HF}$ = 7.0 Hz, *m*-$C_6H_3F_2$), 3.68 and 3.13 (2 × 2 H, 2 × m, C$\underline{H}_2$NSiMe$_3$), 2.74 and 2.22 (2 × 2 H, 2 × m, C$\underline{H}_2$NMe), 2.09 (3 H, s, NMe), 0.22 (18 H, s, SiMe$_3$). $^{13}C\{^{1}H\}$ NMR (aided by a $^{13}C\{^{19}F\}$ HMQC spectrum, C_6D_6, 125.7 MHz, 293 K): δ 164.5 (*i*-$C_6H_3F_2$), 159.9 (dd, $^{1}J_{CF}$ = 249 Hz, $^{3}J_{CF}$ = 9 Hz, *o*-$C_6H_3F_2$), 153.8 (*o*-NC_5H_5), 150.3 (*i*-NC_6H_5), 138.6 (*p*-NC_5H_5), 128.6 (*o*-NC_6H_5), 123.6 (*m*-NC_5H_5), 121.5 (*p*-NC_6H_5), 121.3 (*m*-NC_6H_5), 110.6 (dd, $^{2}J_{CF}$ = 21 Hz, $^{4}J_{CF}$ = 5 Hz, *m*-$C_6H_3F_2$), 109.1 (NC=N), 92.8 (t, $^{3}J_{CF}$ = 19 Hz, *p*-$C_6F_2H_3$), 63.2 ($\underline{C}H_2$NMe), 48.9 ($\underline{C}H_2$SiMe$_3$), 47.6 (NMe), 1.3 (SiMe$_3$). ^{19}F NMR (C_6D_6, 470.4 MHz, 293 K): δ -148.1 (app. t, $^{3}J_{HF}$ and $^{4}J_{FF}$ = 6.6 Hz, $C_6H_3F_2$). IR (NaCl plates, Nujol mull, cm^{-1}): 1618 (w), 1585 (s), 1487 (s), 1380 (s), 1350 (m), 1306 (w), 1289 (w), 1272 (m), 1238 (m), 1174 (w), 1115 (w, br.), 1079 (s), 1041 (m), 1000 (s), 939 (s), 917 (s), 899 (m), 880 (w), 859 (m), 834 (s), 799 (m), 789 (m), 753 (m), 739 (m), 719 (m), 699 (m), 672 (w). EI-MS: *m/z* = 628 $[M - py]^+$ (100 %), 168 $[NPh_2]^+$ (100 %). Anal. found (calcd for $C_{35}H_{47}F_2N_7Si_2Ti$): C, 59.3 (59.4); H, 6.7 (6.7); N, 13.8 (13.9) %.

5.4.2 Ti(N$_2$N^{Me}){NC(Ar^{F5})NNPh$_2$}(py) (18, Ar^{F5} = C_6F_5). To a solution of Ti(N$_2$N^{Me})(NNPh$_2$)(py) (**1.93**, 0.213 g, 0.380 mmol) in toluene (5 mL) was added Ar^{F5}CN (47.3 μL, 0.380 mmol) at RT. An immediate colour change from green to dark red was observed and the solution left to react for a further 4 h. Solvent was removed under reduced pressure and the resulting solid washed with pentane (3 × 5 mL) affording **18** as an orange powder which was dried *in vacuo*. Yield: 0.116 g (40 %). Diffraction-quality crystals were grown from a saturated pentane solution at -30 °C.

^{1}H NMR (C_6D_6, 499.9 MHz, 293 K): δ 9.36 (2 H, d, ^{3}J = 7.5 Hz, *o*-NC_5H_5), 7.33 (4 H, d, ^{3}J = 9.0 Hz, *o*-NC_6H_5), 7.15 (4 H, app. t, app. ^{3}J = 9.0 Hz, *m*-NC_6H_5), 6.85 (2 H, t, ^{3}J = 9.0 Hz *p*-NC_6H_5), 6.74 (1 H, t, ^{3}J = 7.5 Hz, *p*-NC_5H_5), 6.50 (2 H, app. t, app. ^{3}J = 7.5 Hz, *m*-NC_5H_5), 3.61 and 3.05 (2 × 2 H, 2 × m, C$\underline{H}_2$NSiMe$_3$), 2.65 and 2.14 (2 × 2 H, 2 × m, C$\underline{H}_2$NMe), 1.98 (3 H, s, NMe), 0.16 (18 H, s, SiMe$_3$). $^{13}C\{^{1}H\}$ NMR (aided by a $^{13}C\{^{19}F\}$ HMQC spectrum, C_6D_6, 125.7 MHz, 293 K): δ 159.9 (*i*-C_6F_5), 153.5 (*o*-NC_5H_5), 153.1 (*i*-NC_6H_5), 150.0 (N$\underline{C}$=N), 143.2 (*o*-C_6F_5), 139.9 (*p*-C_6F_5), 138.7 (*p*-NC_5H_5), 137.5 (*m*-C_6F_5), 128.8 (*o*-NC_6H_5), 123.7 (*m*-NC_5H_5), 121.9 (*p*-NC_6H_5), 121.4 (*m*-NC_6H_5), 63.1 ($\underline{C}H_2$NMe), 49.0 ($\underline{C}H_2$NSiMe$_3$), 47.4 (NMe), 1.2 (SiMe$_3$). ^{19}F

NMR (C_6D_6, 470.4 MHz, 293 K): δ -140.0 (2 F, d, $^3J_{FF}$ = 23.5 Hz, *o*-C_6F_5), -159.1 (1 F, t, $^3J_{FF}$ = 23.5 Hz, *p*-C_6F_5), -164.3 (2 F, app. t, app. $^3J_{FF}$ = 23.5 Hz, *m*-C_6F_5). IR (NaCl plates, Nujol mull, cm^{-1}): 1590 (m), 1587 (m), 1519 (m), 1492 (s), 1406 (w), 1351 (m), 1292 (m), 1275 (w), 1241 (m, br.), 1210 (m), 1108 (m), 1080 (m, br.), 1039 (w), 987 (m), 950 (m), 933 (m), 915 (m), 837 (s, br.), 802 (m), 756 (m), 712 (m), 700 (m), 674 (w). EI-MS: *m/z* = 682 $[M - py]^+$ (100 %), 168 $[NPh_2]^+$ (100 %). Anal. found (calcd for $C_{35}H_{44}F_5N_7Si_2Ti$): C, 55.1 (55.2); H, 5.7 (5.8); N, 12.8 (12.9).

5.4.3 Ti(N_2N^{Me}){NC(Me)NNPh$_2$}(MeCN) (**19**). MeCN (7 mL) was added to Ti(N_2N^{Me})($NNPh_2$)(py) (**1.93**, 0.246 g, 0.434 mmol) and the mixture heated to 50 ºC and sonicated until all the solid had dissolved, forming a dark red solution. It was slowly cooled to -30 ºC and left for 16 h, during which time a solid precipitated. The supernatant was decanted and the solid washed with pentane (3 × 5 mL), before being dried *in vacuo* to afford **19** as a dark red powder. Yield: 0.173 g (70 %).

^{1}H NMR (C_6D_6, 499.9 MHz, 293 K): δ 7.30 (4 H, d, ^3J = 7.5 Hz, *o*-NC_6H_5), 7.08 (4 H, app. t, app. ^3J = 7.5 Hz, *m*-NC_6H_5), 6.74 (2 H, t, ^3J = 7.5 Hz, *p*-NC_6H_5), 3.29 and 3.18 (2 × 2 H, 2 × m, C$\underline{H}_2$NSiMe$_3$), 2.48 and 1.63 (2 × 2 H, 2 × m, C$\underline{H}_2$NMe), 2.26 (3 H, s, NMe), 2.05 and 2.03 (2 × 3 H, 2 × s, 2 × NCMe), 0.36 (18 H, s, $SiMe_3$). $^{13}C\{^1H\}$ NMR (C_6D_6, 125.7 MHz, 293 K): δ 178.5 and 173.0 (2 × N$\underline{C}$Me), 144.4 (*i*-NC_6H_5), 128.9 (*o*-NC_6H_5), 121.2 (*p*-NC_6H_5), 118.4 (*m*-NC_6H_5), 58.8 ($\underline{C}H_2$NMe), 50.7 ($\underline{C}H_2$NSiMe$_3$), 43.8 (NMe), 23.2 and 22.6 (2 × NC$\underline{Me}$), 3.1 ($SiMe_3$). IR (NaCl plates, Nujol mull, cm^{-1}): 1589 (s), 1564 (s), 1494 (s, br.), 1240 (s), 1218 (m), 1065 (m), 1041 (m), 1022 (m, br.), 990 (m), 939 (s), 913 (m), 858 (s, br.), 744 (m). EI-MS: *m/z* = 557 [*M*-Me]$^+$ (20 %), 530 [*M*-MeCN]$^+$ (80 %), 168 $[NPh_2]^+$ (100 %). Anal. found (calcd. for $C_{27}H_{45}N_7Si_2Ti$): C, 56.7 (56.7); H, 8.0 (7.9); N, 17.1 (17.2) %.

5.4.4 Ti(N_2N^{Me})(NCNXyl)(NPh_2) (**20**). To a stirred mixture of Ti(N_2N^{Me})($NNPh_2$)(py) (**1.93**, 0.259 g, 0.456 mmol) and XylNC (0.0602 g, 0.456 mmol) was added toluene (10 mL), all at -78 °C. The green suspension was allowed to warm to RT and stirred for a further 1 h, during which time it turned dark red. Volatiles were removed under reduced pressure and the resulting red oil triturated with pentane (10 mL). Volatiles were removed under reduced pressure and the resulting red powder dried *in vacuo* to afford **20**. Yield: 0.167 g (59 %). Diffraction-quality crystals were grown from a saturated hexanes solution at -30 °C.

^{1}H NMR (C_6D_6, 499.9 MHz, 293 K): δ 7.15 – 7.10 (2 × 4 H, overlapping *o*- and *m*-NC_6H_5), 6.92 (2 H, d, ^{3}J = 7.5 Hz, *m*-$C_6H_3Me_2$), 6.88 (2 H, t, ^{3}J = 6.5 Hz, *p*-NC_6H_5), 6.80 (1 H, t, ^{3}J = 7.5 Hz, *p*-$C_6H_3Me_2$), 3.33 and 3.17 (2 × 2 H, 2 × m, C$\underline{H}_2$NSiMe_3), 2.51 and 2.16 (2 × 2 H, 2 × m, C$\underline{H}_2$NMe), 2.45 (6 H, s, $C_6H_3\underline{Me}_2$), 2.13 (3 H, s, NMe), 0.35 (18 H, s, SiMe_3). ^{13}C{^{1}H} NMR (C_6D_6, 125.7 MHz, 293 K): δ 152.6 (*i*-NC_6H_5), 138.6 (*o*-$C_6H_3Me_2$), 132.8 (*m*-$C_6H_3Me_2$), 129.5 (*i*-$C_6H_3Me_2$), 129.1 (*o*-NC_6H_5), 123.3 (*m*-NC_6H_5), 122.9 (*p*-NC_6H_5), 122.6 (*p*-$C_6H_3Me_2$), 118.1 (NCN), 59.1 (C$\underline{H}_2$NMe), 51.9 (C$\underline{H}_2$NSiMe_3), 45.0 (NMe), 19.9 ($C_6H_3\underline{Me}_2$), 2.3 (SiMe_3). IR (NaCl plates, Nujol mull, cm^{-1}): 2183 (m), 2110 (s, br.), 1589 (s), 1576 (w), 1569 (w), 1559 (w), 1540 (w), 1522 (w), 1506 (w), 1497 (w), 1190 (w), 1147 (w), 1033 (w), 912 (w), 844 (w), 656 (w). EI-MS: *m/z* = 620 [*M*]$^{+}$ (20 %), 452 [*M* – NPh_2]$^{+}$ (100 %). Anal. found (calcd. for $C_{32}H_{48}N_6Si_2Ti$): C, 61.8 (61.9); H. 7.8 (7.8); N, 13.5 (13.5) %.

5.4.5 Ti(N_2N^{Me}){N(NPh_2)C(NAr′)O}(py) (**21**, Ar′ = 2,6-$C_6H_3{}^{i}Pr_2$). To a solution of Ti(N_2N^{Me})($NNPh_2$)(py) (**1.93**, 0.280 g, 0.490 mmol) in Et_2O (10 mL) was added Ar′NCO (0.105 mL, 0.490 mmol) at RT. There was an immediate colour change from green to red and the solution was left to react for a further 1 h, during which time an orange precipitate formed. Volatiles were removed under reduced pressure affording **21** as an orange powder which was dried *in vacuo*. Yield: 0.247 g (65 %). Diffraction-quality crystals were grown from a saturated pentane solution at -80 °C.

^{1}H NMR (C_6D_6, 499.9 MHz, 333 K): δ 8.52 (2 H, d, ^{3}J = 4.5 Hz, *o*-NC_5H_5), 7.57 (4 H, d, ^{3}J = 7.0 Hz, *o*-NC_6H_5), 7.21 (4 H, app. t, app. ^{3}J = 7.0 Hz, *m*-NC_6H_5), 7.17 (1 H, t, ^{3}J = 7.5 Hz, *p*-$C_6H_3{}^{i}Pr_2$ and 1 H, app. t, app. ^{3}J = 4.5 Hz, *p*-NC_5H_5), 7.01 (2 H, d, ^{3}J = 7.5 Hz, *m*-$C_6H_3{}^{i}Pr_2$), 6.86 (2 H, t, ^{3}J = 7.0 Hz, *p*-NC_6H_5), 6.68 (2 H, t, ^{3}J = 4.5 Hz, *m*-NC_5H_5), 3.27 (2 H, m, C$\underline{H}Me_2$), 3.18 and 3.09 (2 × 2 H, 2 × m, C$\underline{H}_2$NSiMe_3), 2.70 and 2.26 (2 × 2 H, 2 × m, C$\underline{H}_2$NMe), 2.28 (3 H, s, NMe), 1.23 (12 H, d, ^{3}J = 6.5 Hz, CH$\underline{Me}_2$), 0.14 (18 H, s, SiMe_3). ^{13}C{^{1}H} NMR (C_6D_6, 125.7 MHz, 333 K): δ 150.3 (*o*-NC_5H_5), 148.4 (OCN), 147.5 (*i*-NC_6H_5), 143.7 (*o*-$C_6H_3{}^{i}Pr_2$), 140.2 (*p*-$C_6H_3{}^{i}Pr_2$), 138.2 (*i*-$C_6H_3{}^{i}Pr_2$), 135.2 (*m*-NC_5H_5), 128.8 (*o*-NC_6H_5), 123.4 (*p*-NC_5H_5), 122.1 (*m*-$C_6H_3{}^{i}Pr_2$), 121.0 (*m*-NC_6H_5), 119.0 (*p*-NC_6H_5), 59.1 (C$\underline{H}_2$NMe), 48.7 (C$\underline{H}_2$NSiMe_3), 43.4 (NMe), 29.1 (C$\underline{H}Me_2$), 23.5 (CH$\underline{Me}_2$), 0.10 (SiMe_3). IR (NaCl plates, Nujol mull, cm^{-1}): 1638 (m, br.), 1583 (m, br.), 1487 (m), 1328 (w), 1311 (w), 1243 (w), 1217 (w), 1071 (w, br.), 1071 (w), 1040 (w), 989 (m), 932 (w), 906 (m), 867 (w), 840 (s, br.), 746 (m), 693 (w). EI-MS: *m/z* = 610 [*M* – Ar′]$^{+}$ (10 %), 442 [*M* –

Ar′ – NPh_2]$^+$ (20 %), 387 [*M* – {N(NPh_2)C(NAr´)O}]$^+$ (60 %), 259 [TiN(NPh_2)C(O)]$^+$ (100 %). Anal. found (calcd for $C_{41}H_{61}N_7OSi_2Ti$): C, 63.9 (63.8); H, 8.1 (8.0); N, 12.6 (12.7) %.

5.4.6 Ti(N_2N^{Me}){N(NPh_2)C(NAr′)S} (**22**, Ar′ = 2,6-$C_6H_3{}^iPr_2$). To a solution of Ti(N_2N^{Me})($NNPh_2$)(py) (**1.93**, 0.263 g, 0.460 mmol) in Et_2O (10 mL) was added Ar′NCS (0.103 mL, 0.460 mmol) at RT. There was an immediate colour change from green to red and the solution was left to react for a further 1 h during which time a red precipitate formed. The supernatant was decanted affording **22** as a red powder which was dried *in vacuo*. Yield: 0.166 g (51 %). Diffraction-quality crystals were grown from a saturated diethyl ether solution at RT.

^{1}H NMR (C_6D_6, 499.9 MHz, 298 K): δ 7.66 (4 H, d, ^3J = 10.0 Hz, *o*-NC_6H_5), 7.22 – 7.19 (6 H, overlapping *m*-NC_6H_5 and *m*-$C_6H_3{}^iPr_2$), 7.10 (1 H, t, ^3J = 7.5 Hz, *p*-$C_6H_3{}^iPr_2$), 6.85 (2 H, t, ^3J = 7.5 Hz, *p*-NC_6H_5), 3.22 (4 H, overlapping m, C<u>H</u>Me_2 and C<u>H</u>$_2$N$SiMe_3$), 3.08 (2 H, m, C<u>H</u>$_2$N$SiMe_3$), 2.52 and 2.09 (2 × 2 H, 2 × m, C<u>H</u>$_2$NMe), 2.21 (3 H, s, NMe), 1.46 and 1.04 (2 × 6 H, 2 × d, ^3J = 7.0 Hz, CH<u>Me</u>$_2$), 0.32 (18 H, s, $SiMe_3$). ^{13}C{^{1}H} NMR (C_6D_6, 125.7 MHz, 298 K): δ 147.3, (*i*-NC_6H_5), 145.2 (SCN), 144.1 (*i*-$C_6H_3{}^iPr_2$), 140.4 (*o*-$C_6H_3{}^iPr_2$), 128.8 (*m*-NC_6H_5), 123.1 (*p*-$C_6H_3{}^iPr_2$), 122.7 (*m*-$C_6H_3{}^iPr_2$), 121.2 (*p*-NC_6H_5), 118.9 (*o*-NC_6H_5), 58.7 (<u>C</u>H_2NMe), 50.5 (<u>C</u>H_2N$SiMe_3$), 42.8 (NMe), 28.5 (<u>C</u>HMe_2), 24.1 and 23.9 (CH<u>Me</u>$_2$), 1.5 ($SiMe_3$). IR (NaCl plates, Nujol mull, cm^{-1}): 1612 (s, br.), 1581 (s, br.), 1491 (s), 1414 (w), 1402 (w), 1358 (w), 1344 (w), 1309 (w), 1290 (w), 1269 (m), 1241 (s), 1187 (m), 1175 (m), 1145 (s, br.), 1107 (w), 1085 (s), 1074 (m), 1059 (s), 1053 (s, br.), 992 (m, br.), 934 (m), 916 (m), 887 (m), 862 (m), 839 (m, br.), 802 (m), 787 (m), 757 (m), 747 (m), 690 (m), 665 (w), 645 (m), 608 (m). EI-MS: *m/z* = 274 [*M* – N_2N^{Me} – $NC_6H_3{}^iPr_2$]$^+$ (100 %), 233 [SC(N)$NC_6H_3{}^iPr_2$]$^+$ (100 %), 168 [NPh_2]$^+$ (100 %). Anal. found (calcd for $C_{36}H_{56}N_6SSi_2Ti$): C, 61.1 (61.0); H, 8.1 (8.0); N, 11.9 (11.9) %.

5.4.7 Ar′NCSe (Ar′ = 2,6-$C_6H_3{}^iPr_2$). The following is a modification of a literature procedure.[32] *N*-(2,6-di*iso*propylphenyl)formamide (4.10 g, 0.020 mols), black selenium powder (2.37 g, 0.030 mols) and triethylamine (11.1 mL, 0.080 mols) were dissolved in toluene (50 mL) and cooled to 0 °C in a Teflon valve ampoule. Phosgene (15 mL, 0.030 mols, 2 M in toluene) was added dropwise *via* a cannula while keeping the temperature at 0 °C. After the addition was complete, the suspension was left to warm to RT and react for 3 h before being heated to 110 °C and left to react for a

further 48 h. The solvent was removed under reduced pressure giving a red oil, which was passed through a silica plug using hexanes as elutant. This afforded Ar′NCSe as a colourless oil, which was dissolved in pentane, dried over CaH_2 and filtered twice before use. Yield 3.72 g (70 %).

^{1}H NMR (CD_2Cl_2, 300 MHz, 298 K): δ 7.29 (1 H, t, ^{3}J = 8.0 Hz, *p*-$C_6H_3{}^iPr_2$), 7.17 (2 H, d, ^{3}J = 8.0 Hz, *m*-$C_6H_3{}^iPr_2$), 3.26 (2 H, sept, ^{3}J = 6.5 Hz, C<u>H</u>Me_2), 1.28 (12 H, d, ^{3}J = 6.5 Hz, CH<u>Me</u>$_2$). ^{13}C{^{1}H} NMR (CD_2Cl_2, 75.4 Hz, 298 K): δ 146.0 (*o*-$C_6H_3{}^iPr_2$), 128.7 (*p*-$C_6H_3{}^iPr_2$), 123.9 (*m*-$C_6H_3{}^iPr_2$), 30.3 (<u>C</u>HMe_2), 22.9 (CH<u>Me</u>$_2$). Resonances attributable to NCSe and *i*-$C_6H_3{}^iPr_2$ were not observed. IR (NaCl plates, cm^{-1}): 3067 (m), 2964 (s, br.), 2928 (s, br.), 2871 (s), 2289 (s, br.), 2070 (s, br.), 1586 (m), 1475 (s), 1462 (s), 1434 (s), 1386 (m), 1365 (m), 1349 (w), 1334 (m), 1259 (s), 1182 (m), 1164 (w), 1109 (m), 1062 (m), 935 (m), 795 (s), 746 (s), 692 (s), 626 (s). FI-MS: *m/z* = 267 [*M*]$^+$ (100 %). Anal. found (calcd. for $C_{13}H_{17}NSe$): C, 58.7 (58.4); H, 6.4 (6.3); N, 5.3 (5.3) %.

5.4.8 Ti(N_2N^{Me}){N(NPh_2)C(NAr′)Se} (**23**, Ar′ = 2,6-$C_6H_3{}^iPr_2$). To a solution of Ti(N_2N^{Me})($NNPh_2$)(py) (**1.93**, 0.314 g, 0.553 mmol) in Et_2O (15 mL) was added Ar′NCSe (0.147 g, 0.553 mmol) at RT. There was an immediate colour change from green to red and the solution was left to react for a further 1 h, during which time a dark red precipitate formed. The supernatant was decanted affording **23** as a red powder which was dried *in vacuo*. Yield: 0.216 g (51 %). Diffraction-quality crystals were grown from a saturated diethyl ether solution at RT.

^{1}H NMR (C_6D_6, 299.9 MHz, 298 K): δ 7.67 (4 H, d, ^{3}J = 6 Hz, *o*-NC_6H_5), 7.24 – 7.17 (7 H, overlapping *m*-NC_6H_5, *m*-$C_6H_3{}^iPr_2$ and *p*-$C_6H_3{}^iPr_2$), 6.86 (2 H, t, ^{3}J = 6 Hz, *p*-NC_6H_5), 3.25 (2 H, m, C<u>H</u>Me_2), 3.14 and 2.47 (2 × 2 H, 2 × m, C<u>H$_2$</u>N$SiMe_3$), 2.05 and 1.30 (2 × 2 H, 2 × m, C<u>H$_2$</u>NMe), 2.17 (3 H, s, NMe), 1.45 and 1.02 (2 × 6 H, 2 × d, ^{3}J = 6 Hz, CH<u>Me</u>$_2$), 0.37 (18 H, s, $SiMe_3$). Due to the low solubility and stability of **23** it was not possible to obtain a suitable ^{13}C{^{1}H} NMR spectrum. IR (NaCl plates, Nujol mull, cm^{-1}): 1615 (s, br.), 1580 (s, br.), 1491 (s), 1467 (s, br.), 1378 (m), 1358 (w), 1269 (m), 1254 (m), 1248 (m), 1241 (m), 1215 (w), 1186 (w), 1177 (w), 1155 (w), 1129 (m), 1108 (w), 1083 (m), 1072 (m), 1059 (m), 1035 (m), 1021 (m), 999 (w), 993 (w), 987 (w), 935 (m), 925 (m), 914 (m), 886 (m), 860 (m), 838 (m, br.), 800 (m), 786 (m), 757 (m), 747 (m), 699 (m), 690 (s), 665 (m), 637 (m), 608 (m). EI-MS: *m/z* =

387 $[(N_2N^{Me})TiSe]^+$ (100 %), 168 $[NPh_2]^+$ (100 %), 167 $[TiNSeCN]^+$ (100 %). Anal. found (calcd for $C_{56}H_{39}N_6SeSi_2Ti$): C, 57.6 (57.2); H, 7.5 (7.5); N, 10.8 (11.2) %.

5.5 Experimental details and characterising data for Chapter Four

5.5.1 Kinetic measurements. A standard solution of 1,4-dimethoxybenzene in toluene-d_8 was used for all kinetic experiments (0.09 M). The general procedure is as follows. In a dry-box, compound **1.151** (9.9 mg, 18.9 μmol) was weighed into a vial and dissolved in the standard solution (0.35 mL). In a separate vial, the alkyne was dissolved in the standard solution (0.30 mL). The two vials were then combined, agitated quickly and transferred to a J. Young NMR tube. The NMR tube was taken out of the dry-box and placed in the NMR probe at RT before being locked and shimmed. The probe was heated to 50 °C, allowed to thermally equilibriate and the sample shimmed again. The probe was then heated to 74 ºC (other reaction temperatures were also used as noted in the main text), allowed to thermally equilibrate, the shimming checked and an array set up recording a spectrum of 4 scans every 140 s. The ratios of the species were calculated by measuring the intensity of the cyclopentadienyl groups in **1.151** relative to the internal standard. Pseudo first order rate constants were obtained from linear plots of $\ln([Zr]/[Zr]_0)$ *vs.* time.

5.5.2 Ti(HN_2N^{Me}){N($SiMe_3$)C(Me)C(Fc)-1,2-C_6H_4N(Ph)} (**24**). To a mixture of $Ti(N_2N^{Me})(NNPh_2)(py)$ (**1.93**, 0.217 g, 0.382 mmol) and FcCCMe (0.0856 g, 0.382 mmol) at RT was added Et_2O (10 mL). The resultant dark red solution was stirred for 16 h before the volatiles were removed under reduced pressure. The resulting dark red solid was extracted into pentane (3 × 5 mL), dried under reduced pressure and crystallised by slow cooling of a hot hexanes solution (5 mL, 60 ºC to RT). The supernatant was decanted and the dark red crystals washed with pentane (2 mL) before being dried *in vacuo* to yield **24** as a dark red powder. Yield: 0.0818 g (30 %). Diffraction-quality crystals were grown by slow cooling of a saturated hexanes solution from 60 ºC to RT.

^{1}H NMR (C_6D_6, 499.9 MHz, 293 K): δ 8.06 (2 H, d, ^3J = 7.0 Hz, *o*-NC_6H_5), 7.39 (1 H, d, ^3J = 5.5 Hz, 3-$NC_6H_4CR_2$), 7.15 (1 H, app. t, app. ^3J = 5.5 Hz, 4-$NC_6H_4CR_2$), 7.06 (2 × 1 H, overlapping *p*-NC_6H_5 and 6-$NC_6H_4CR_2$), 6.96 (2 H, app. t, app. ^3J = 7.0 Hz, *m*-NC_6H_5), 6.78 (1 H, app. t, app. ^3J = 5.5 Hz, 5-$NC_6H_4CR_2$), 6.68 (1 H, s, NH), 4.57, 4.15, 4.11 and 4.05 (4 × 1 H, 4 × m, $FeC_5\underline{H}_4CCMe$), 4.23 (5 H, s, C_5H_5), 3.65 and

3.03 (2 × 1 H, m, HNC$\underline{H}_2$CH$_2$), 3.32 and 3.24 (2 × 1 H, m, Me$_3$SiNC$\underline{H}_2$CH$_2$), 3.32 and 1.82 (2 × 1 H, m, Me$_3$SiNCH$_2$C$\underline{H}_2$), 3.03 and 2.21 (2 × 1 H, m, HNCH$_2$C$\underline{H}_2$), 2.36 (3 H, s, CCMe), 2.22 (3 H, s, NMe), -0.06 and -0.15 (2 × 9 H, 2 × s, 2 × SiMe$_3$). ^{13}C{^{1}H} NMR (C$_6$D$_6$, 125.7 MHz, 293 K): δ 156.0 (2-NC$_6$H$_4$R), 154.2 (*i*-NC$_6$H$_5$), 139.6 (MeC$\underline{C}$), 134.7 (1-NC$_6$H$_4$R), 132.0 (*o*-NC$_6$H$_5$), 129.3 (4-NC$_6$H$_4$CR$_2$), 127.3 (6-NC$_6$H$_4$CR$_2$), 123.6 (*p*-NC$_6$H$_5$), 120.8 (3-NC$_6$H$_4$CR$_2$), 120.4 (*m*-NC$_6$H$_5$), 120.3 (5-NC$_6$H$_4$CR$_2$), 89.1 (MeC$\underline{C}$), 73.1, 68.8, 68.6 and 68.2 (2-, 3-, 4- and 5-Fe$\underline{C}_5$H$_4$CCMe), 69.4 (C$_5$H$_5$), 69.0 (1-Fe$\underline{C}_5$H$_4$CCMe), 59.3 (HNCH$_2\underline{C}$H$_2$), 56.7 (Me$_3$SiNCH$_2\underline{C}$H$_2$), 50.6 (Me$_3$SiN$\underline{C}$H$_2$CH$_2$), 50.5 (HN$\underline{C}$H$_2$CH$_2$), 44.3 (NMe), 27.5 ($\underline{Me}$CC), 2.9 and 1.4 (2 × SiMe$_3$). IR (NaCl plates, Nujol mull, cm^{-1}): 3331 (s, NH), 1587 (m), 1483 (m), 1429 (w), 1292 (m), 1275 (m), 1261 (m), 1242 (m, br.), 1194 (m), 1173 (m), 1106 (s), 1100 (s), 1072 (m), 1062 (m), 1035 (m), 983 (m), 969 (m), 945 (w), 922 (s), 913 (m), 891 (s), 842 (s, br.), 691 (m). EI-MS: *m/z* = 713 [*M*]$^+$ (2 %), 391 [N(Ph)C$_6$H$_4$C(Fc)CMe]$^+$ (100 %). Anal. found (calcd. for C$_{36}$H$_{51}$FeN$_5$Si$_2$Ti): C, 60.6 (60.6); H, 7.1 (7.2); N, 9.7 (9.8) %.

5.5.3 Ti(N$_2$N^{Me}){NC(Ph)C(Ph)NPh$_2$}(py) (25a) and Ti(HN$_2$N^{Me}){N(SiMe$_3$)C(Ph)C(Ph)-1,2-C$_6$H$_4$N(Ph)} (25b). To a mixture of Ti(N$_2$N^{Me})(NNPh$_2$)(py) (**1.93**, 0.286 g, 0.503 mmol) and PhCCPh (0.0895 g, 0.503 mmol) at RT was added toluene (5 mL). The dark green solution turned dark red after several minutes and was left stirring at RT for 72 h. Volatiles were removed under reduced pressure and the resulting oily solid was triturated with Et$_2$O (5 mL). Volatiles were removed under reduced pressure and the resulting red powder dried *in vacuo* to yield **25a** and **25b** in the ratio 44:56. Yield: 0.296 g (82 %).

Resonances for each compound were assigned using COSY, HMQC and HMBC NMR and by comparison with related compounds.

Common data: EI-MS: *m/z* = 667 [*M* (**25b**) and/or *M* – py (**25a**)]$^+$ (30 %), 499 [*M* (**25b**) – NPh$_2$ and/or *M* (**25a**) – py – NPh$_2$]$^+$ (100 %), 393 [C(Ph)C(Ph)C$_6$H$_4$N(Ph)]$^+$ (5 %), 168 [NPh$_2$]$^+$ (5 %), 167 [N(Ph)C$_6$H$_5$]$^+$ (5 %). IR (NaCl plates, Nujol mull, cm^{-1}): 1591 (s, br.), 1483 (s, br.), 1314 (s, br.), 1242 (s, br.), 1183 (m), 1152 (m), 1068 (s, br.), 1028 (s), 956 (s), 933 (s, br.), 857 (w, br.), 754 (w), 699 (w). Anal. found (calcd. for C$_{42}$H$_{54}$N$_6$Si$_2$Ti and C$_{37}$H$_{49}$N$_5$Si$_2$Ti (44:56)): C, 67.3 (66.9); H, 7.3 (7.4); N, 10.4 (10.8) %.

Data for 25a: ^{1}H NMR (C_6D_6, 499.9 MHz, 293 K): δ 8.42 (2 H, d, ^{3}J = 5.0 Hz, *o*-NC_5H_5), 7.84 (8 H, overlapping *o*-NC_6H_5, *o*-$NC(C_6\underline{H}_5)C(C_6H_5)$ and *o*-$NC(C_6H_5)C(C_6\underline{H}_5)$), 7.25 (4 H, overlapping peaks, *m*-NC_6H_5), 7.04 – 6.98 (4 H, overlapping *m*-$NC(C_6\underline{H}_5)C(C_6H_5)$ and *m*-$NC(C_6H_5)C(C_6\underline{H}_5)$), 6.84 (2 H, t, ^{3}J = 10.0 Hz, *p*-NC_6H_5), 6.82 and 6.63 (1 H, overlapping peaks and 1 H, t, ^{3}J = 10.0 Hz, *p*-$NC(C_6\underline{H}_5)C(C_6H_5)$ and *p*-$NC(C_6H_5)C(C_6\underline{H}_5)$), 6.71 (1 H, t, ^{3}J = 5.0 Hz, *p*-NC_5H_5), 6.42 (2 H, app. t, app. ^{3}J = 5.0 Hz, *m*-NC_5H_5), 3.39 and 3.24 (2 × 2 H, 2 × m, $C\underline{H}_2NSiMe_3$), 2.59 and 2.20 (2 × 2 H, 2 × m, $C\underline{H}_2NMe$), 2.05 (3 H, s, NMe), 0.01 (18 H, s, $SiMe_3$). $^{13}C\{^{1}H\}$ NMR (C_6D_6, 125.7 MHz, 293 K): δ 159.6 (*i*-NC_6H_5), 153.5 (*o*-NC_5H_5), 150.3 (*i*-$NC(C_6H_5)C(\underline{C}_6H_5)$), 147.9 ($N\underline{C}(C_6H_5)C(C_6H_5)$), 145.0 (*i*-$NC(\underline{C}_6H_5)C(C_6H_5)$), 138.2 (*p*-$NC_5H_5$), 133.6 (overlapping *o*-$NC(\underline{C}_6H_5)C(C_6H_5)$ and *o*-$NC(C_6H_5)C(\underline{C}_6H_5)$), 129.1 (overlapping *m*-NC_6H_5, *m*-$NC(\underline{C}_6H_5)C(C_6H_5)$ and *m*-$NC(C_6H_5)C(\underline{C}_6H_5)$), 127.1 (overlapping *p*-$NC(\underline{C}_6H_5)C(C_6H_5)$ and *p*-$NC(C_6H_5)C(\underline{C}_6H_5)$), 123.5 (*m*-$NC_5H_5$), 120.9 (*o*-$NC_6H_5$), 120.5 (*p*-$NC_6H_5$), 117.9 ($NC(C_6H_5)\underline{C}(C_6H_5)$), 62.2 ($\underline{C}H_2NMe$), 48.0 ($\underline{C}H_2NSiMe_3$), 47.1 (NMe), 1.8 ($SiMe_3$).

Data for 25b: ^{1}H NMR (C_6D_6, 499.9 MHz, 293 K): δ 7.29 (1 H, d, ^{3}J = 5.0 Hz, 3-$NC_6H_4CR_2$), 7.25 (4 H, overlapping *o*-$NC(C_6\underline{H}_5)C(C_6H_5)$ and *o*-$NC(C_6H_5)C(C_6\underline{H}_5)$), 7.14 (2 H, app. t, app. ^{3}J = 10.0 Hz, *m*-NC_6H_5), 7.04 – 6.94 (7 H, overlapping 5-$NC_6H_4CR_2$, *m*-$NC(C_6\underline{H}_5)C(C_6H_5)$ and *m*-$NC(C_6H_5)C(C_6\underline{H}_5)$, *p*-$NC(C_6\underline{H}_5)C(C_6H_5)$ and *p*-$NC(C_6H_5)C(C_6\underline{H}_5)$), 6.89 (1 H, t, ^{3}J = 10.0 Hz, *p*-NC_6H_5), 6.83 (4 H, overlapping 6-$NC_6H_4CR_2$, 4-$NC_6H_4CR_2$ and *o*-NC_6H_5), 6.67 (1 H, br. s, NH), 3.48 and 3.24 (2 × 1 H, 2 × m, $HNC\underline{H}_2CH_2$), 3.29 and 2.89 (2 × 1 H, 2 × m, $Me_3SiNC\underline{H}_2CH_2$), 2.20 and 2.13 (2 × 1 H, 2 × m, $HNCH_2C\underline{H}_2$), 2.11 (3 H, s, NMe), 1.92 and 1.51 (2 × 1 H, 2 × m, $Me_3SiNCH_2C\underline{H}_2$), 0.45 and 0.10 (2 × 9 H, 2 × s, 2 × $SiMe_3$). $^{13}C\{^{1}H\}$ NMR (C_6D_6, 125.7 MHz, 293 K): δ 159.6 (*i*-NC_6H_5), 153.5 (2-$NC_6H_4CR_2$), 147.9 ($N\underline{C}(C_6H_5)C(C_6H_5)$), 141.1 and 140.5 (overlapping *i*-$NC(\underline{C}_6H_5)C(C_6H_5)$ and *i*-$NC(C_6H_5)C(\underline{C}_6H_5)$), 137.9 (1-$NC_6H_4CR_2$), 132.1 (4-$NC_6H_4CR_2$), 131.1 (*o*-$NC(C_6H_5)C(\underline{C}_6H_5)$), 130.3 (*o*-$NC(\underline{C}_6H_5)C(C_6H_5)$), 128.9 (overlapping *m*-NC_6H_5, *m*-$NC(\underline{C}_6H_5)C(C_6H_5)$ and *m*-$NC(C_6H_5)C(\underline{C}_6H_5)$), 128.6 (6-$NC_6H_4CR_2$), 127.5 (3-$NC_6H_4CR_2$), 126.8 and 126.3 (overlapping *p*-$NC(\underline{C}_6H_5)C(C_6H_5)$ and *p*-$NC(C_6H_5)C(\underline{C}_6H_5)$), 126.5 (*o*-$NC_6H_5$), 124.3 ($NC(C_6H_5)\underline{C}(C_6H_5)$), 121.9 (*p*-$NC_6H_5$), 120.5 (5-$NC_6H_4CR_2$), 58.4 and 56.7

($HNCH_2\underline{C}H_2$ and $Me_3SiNCH_2\underline{C}H_2$), 52.0 and 48.7 ($HN\underline{C}H_2CH_2$ and $Me_3SiN\underline{C}H_2CH_2$), 42.6 (NMe), 3.7 and 1.6 (2 × $SiMe_3$).

5.5.4 $Ti(N_2N^{Me})\{NC(Ar)C(Ar)NPh_2\}(py)$ (**26a**) and $Ti(HN_2N^{Me})\{N(SiMe_3)C(Ar)C(Ar)\text{-}1,2\text{-}C_6H_4N(Ph)\}$ (**26b**, Ar = 4-C_6H_4OMe).

To a mixture of $Ti(N_2N^{Me})(NNPh_2)(py)$ (**1.93**, 0.287 g, 0.505 mmol) and ArCCAr (0.120 g, 0.505 mmol) at RT was added toluene (5 mL). The dark green solution turned dark red after several minutes and was left stirring at RT for 72 h. Volatiles were removed under reduced pressure and the resulting red, oily solid was triturated with Et_2O (5 mL). Volatiles were removed under reduced pressure and the resulting red powder dried *in vacuo* to yield **26a** and **26b** in the ratio 32:68. Yield: 0.325 g (85 %).

Resonances for each compound were assigned using COSY, HMQC and HMBC NMR and by comparison with related compounds.

Common data: EI-MS: *m/z* = 727 [*M* (**26b**) and/or *M* – py (**26a**)]$^+$ (10 %), 558 [*M* (**426b**) – NPh_2 and/or *M* (**26a**) – py – NPh_2]$^+$ (50 %). IR (NaCl plates, Nujol mull, cm^{-1}): 1592 (s, br.), 1564 (m), 1462 (s, br.), 1419 (m), 1405 (m), 1399 (w), 1377 (m), 1319 (m), 1291 (m), 1172 (s), 1152 (w), 1106 (m), 1082 (s), 1031 (s), 994 (m), 955 (m), 921 (s), 838 (s, br.), 748 (s), 697 (s), 638 (w), 588 (w). Anal. found (calcd. for $C_{44}H_{58}N_6O_2Si_2Ti$ and $C_{39}H_{53}N_5O_2Si_2Ti$ (32:68)): C, 64.7 (64.6); H, 7.2 (7.3); N, 9.9 (9.3) %.

Data for 26a: ^{1}H NMR (C_6D_6, 499.9 MHz, 293 K): δ 8.48 (2 H, d, ^3J = 5.0 Hz, *o*-NC_5H_5), 7.86 and 7.57 (4 H, d, ^3J = 10 Hz, overlapping *o*-NC(4-$C_6\underline{H}_4OMe$)C(4-C_6H_4OMe) and *o*-NC(4-C_6H_4OMe)C(4-$C_6\underline{H}_4OMe$)), 7.26 (12 H, overlapping *o*-NC_6H_5, *m*-NC_6H_5, *m*-NC(4-$C_6\underline{H}_4OMe$)C(4-C_6H_4OMe) and *m*-NC(4-C_6H_4OMe)C(4-$C_6\underline{H}_4OMe$)), 6.86 (2 H, t, ^3J = 10.0 Hz, *p*-NC_6H_5), 6.72 (1 H, t, ^3J = 5.0 Hz, *p*-NC_5H_5), 6.45 (2 H, app. t, app. ^3J = 5.0 Hz, *m*-NC_5H_5), 3.37 and 3.24 (2 × 2 H, 2 × m, $C\underline{H}_2NSiMe_3$), 3.18 and 3.28 (2 × 3 H, 2 × s, 2 × OMe), 2.61 and 2.24 (2 × 2 H, 2 × m, $C\underline{H}_2NMe$), 2.08 (3 H, s, NMe), 0.03 (18 H, s, $SiMe_3$). $^{13}C\{^1H\}$ NMR (C_6D_6, 125.7 MHz, 293 K): δ 159.9 (*i*-NC_6H_5), 153.5 (*o*-NC_5H_5), 158.5 and 158.3 (*p*-NC(4-$C_6\underline{H}_4OMe$)C(4-C_6H_4OMe) and *p*-NC(4-C_6H_4OMe)C(4-$C_6\underline{H}_4OMe$)), 148.0 (N$\underline{C}$(4-C_6H_4OMe)C(4-C_6H_4OMe)), 138.2 and 135.2 (*i*-NC(4-$C_6\underline{H}_4OMe$)C(4-C_6H_4OMe) and

i-NC(4-C_6H_4OMe)C(4-$\underline{C}_6H_4OMe$)), 134.7 (overlapping *o*-NC(4-$\underline{C}_6H_4OMe$)C(4-C_6H_4OMe) and *o*-NC(4-C_6H_4OMe)C(4-$\underline{C}_6H_4OMe$)), 133.3 (*p*-NC_5H_5), 129.1 (overlapping *m*-NC_6H_5, *m*-NC(4-$\underline{C}_6H_4OMe$)C(4-C_6H_4OMe) and *m*-NC(4-C_6H_4OMe)C(4-$\underline{C}_6H_4OMe$)), 123.5 (*m*-NC_5H_5), 121.0 (*o*-NC_6H_5), 120.5 (*p*-NC_6H_5), 117.7 (NC(4-C_6H_4OMe)$\underline{C}$(4-C_6H_4OMe)), 62.3 ($\underline{C}H_2NMe$), 58.6 and 56.4 (2 × OMe), 47.9 ($\underline{C}H_2NSiMe_3$), 47.3 (NMe), 1.8 ($SiMe_3$).

Data for 26b: ^{1}H NMR (C_6D_6, 499.9 MHz, 293 K): δ 7.83 and 7.51 (4 H, d, ^3J = 10 Hz, overlapping *o*-NC(4-$C_6\underline{H}_4OMe$)C(4-C_6H_4OMe) and *o*-NC(4-C_6H_4OMe)C(4-$C_6\underline{H}_4OMe$)), 7.26 (5 H, overlapping 3-$NC_6H_4CR_2$, *m*-NC(4-$C_6\underline{H}_4OMe$)C(4-C_6H_4OMe) and *m*-NC(4-C_6H_4OMe)C(4-$C_6\underline{H}_4OMe$)), 7.11 (2 H, app. t, app. ^3J = 10.0 Hz, *m*-NC_6H_5), 6.96 (1 H, overlapping peaks, 5-$NC_6H_4CR_2$), 6.86 (1 H, t, ^3J = 10.0 Hz, *p*-NC_6H_5), 6.81 (4 H, overlapping 6-$NC_6H_4CR_2$, 4-$NC_6H_4CR_2$ and *o*-NC_6H_5), 6.73 (1 H, br. s, NH), 3.55 and 3.25 (2 × 1 H, 2 × m, HNC$\underline{H}_2CH_2$), 3.14 and 3.05 (2 × 3 H, 2 × s, 2 × OMe), 3.34 and 2.89 (2 × 1 H, 2 × m, $Me_3SiNC\underline{H}_2CH_2$), 2.25 and 2.09 (2 × 1 H, 2 × m, $HNCH_2C\underline{H}_2$), 2.15 (3 H, s, NMe), 2.09 and 1.53 (2 × 1 H, 2 × m, $Me_3SiNCH_2C\underline{H}_2$), 0.46 and 0.17 (2 × 9 H, 2 × s, 2 × $SiMe_3$). $^{13}C\{^1H\}$ NMR (C_6D_6, 125.7 MHz, 293 K): δ 159.9 (*i*-NC_6H_5), 158.8 and 158.7 (overlapping *p*-NC(4-$\underline{C}_6H_4OMe$)C(4-C_6H_4OMe) and *p*-NC(4-C_6H_4OMe)C(4-$\underline{C}_6H_4OMe$)), 153.5 (2-$NC_6H_4CR_2$), 150.3 (N$\underline{C}$(4-C_6H_4OMe)C(4-C_6H_4OMe)), 138.2 and 135.2 (*i*-NC(4-$\underline{C}_6H_4OMe$)C(4-C_6H_4OMe) and *i*-NC(4-C_6H_4OMe)C(4-$\underline{C}_6H_4OMe$)), 137.7 (1-$NC_6H_4CR_2$), 132.2 (4-$NC_6H_4CR_2$), 131.4 and 130.2 (*o*-NC(4-$\underline{C}_6H_4OMe$)C(4-C_6H_4OMe) and *o*-NC(4-C_6H_4OMe)C(4-$\underline{C}_6H_4OMe$)), 129.5 (*m*-NC_6H_5), 129.1 (overlapping *m*-NC(4-$\underline{C}_6H_4OMe$)C(4-C_6H_4OMe) and *m*-NC(4-C_6H_4OMe)C(4-$\underline{C}_6H_4OMe$)), 129.1 (6-$NC_6H_4CR_2$), 128.8 (3-$NC_6H_4CR_2$), 124.7 (*o*-NC_6H_5), 123.5 (NC(4-C_6H_4OMe)$\underline{C}$(4-C_6H_4OMe)), 121.7 (*p*-NC_6H_5), 120.5 (5-$NC_6H_4CR_2$), 58.6 and 56.4 ($HNCH_2\underline{C}H_2$ and $Me_3SiNCH_2\underline{C}H_2$), 54.5 and 54.4 (2 × OMe), 52.0 and 48.8 ($HN\underline{C}H_2CH_2$ and $Me_3SiN\underline{C}H_2CH_2$), 42.6 (NMe), 3.6 and 1.6 (2 × $SiMe_3$).

5.5.5 Ti(N_2N^{Me}){NC(Ar)C(Ar)NPh_2}(py) (**27**, Ar = 4-$C_6H_4CF_3$). To a mixture of Ti(N_2N^{Me})($NNPh_2$)(py) (**1.93**, 0.284 g, 0.499 mmol) and ArCCAr (0.157 g, 0.499 mmol) at RT was added Et_2O (5 mL). The green solution turned dark red and was left stirring for 48 h. Volatiles were removed under reduced pressure and the resulting dark red powder dried *in vacuo* to yield **27**. Yield: 0.319 g (78 %).

^{1}H NMR (C_6D_6, 499.9 MHz, 293 K): δ 8.18 (2 H, d, ^{3}J = 5 Hz, *o*-NC_5H_5), 7.72 (6 H, overlapping *o*-NC_6H_5 and *o*-NC(4-$C_6H_4CF_3$)C(4-$C_6\underline{H}_4CF_3$)), 7.39 (2 H, d, ^{3}J = 10 Hz, *m*-NC(4-$C_6H_4CF_3$)C(4-$C_6\underline{H}_4CF_3$)), 7.23 (4 H, app. t, app. ^{3}J = 5 Hz, *m*-NC_6H_5), 7.10 (2 H, d, ^{3}J = 10 Hz, *o*-NC(4-$C_6\underline{H}_4CF_3$)C(4-$C_6H_4CF_3$)), 6.98 (2 H, d, ^{3}J = 10 Hz, *m*-NC(4-$C_6\underline{H}_4CF_3$)C(4-$C_6H_4CF_3$)), 6.85 (2 H, d, ^{3}J = 5 Hz, *p*-NC_6H_5), 6.68 (1 H, t, ^{3}J = 5 Hz, *p*-NC_5H_5), 6.39 (2 H, app. t, app. ^{3}J = 5 Hz, *m*-NC_5H_5), 3.34 and 3.15 (2 × 2 H, 2 × m, C$\underline{H}_2$NSiMe$_3$), 2.56 and 2.10 (2 × 2 H, 2 × m, C$\underline{H}_2$NMe), 1.94 (3 H, s, NMe), 0.06 (18 H, s, SiMe$_3$). ^{13}C{^{1}H} NMR (C_6D_6, 125.7 MHz, 293 K): δ 159.6 (*i*-NC_6H_5), 152.9 (*o*-NC_5H_5), 148.2 (*i*-NC(4-$C_6H_4CF_3$)C(4-$\underline{C}_6H_4CF_3$)), 147.4 (NC(4-$C_6H_4CF_3$)$\underline{C}$(4-$C_6H_4CF_3$)), 144.7 (*i*-NC(4-$\underline{C}_6H_4CF_3$)C(4-$C_6H_4CF_3$)), 138.6 (*p*-NC_5H_5), 131.2 (*o*-NC(4-$C_6H_4CF_3$)C(4-$\underline{C}_6H_4CF_3$)), 129.6 (*o*-NC(4-$\underline{C}_6H_4CF_3$)C(4-$C_6H_4CF_3$)), 129.3 (*m*-NC_6H_5), 125.6 (m, overlapping *p*-NC(4-$C_6H_4CF_3$)C(4-$\underline{C}_6H_4CF_3$) and *p*-NC(4-$\underline{C}_6H_4CF_3$)C(4-$C_6H_4CF_3$)), 125.2 (q, $^{3}J_{CF}$ = 3.8 Hz, *m*-NC(4-$\underline{C}_6H_4CF_3$)C(4-$C_6H_4CF_3$)), 124.4 (q, $^{3}J_{CF}$ = 3.8 Hz, *m*-NC(4-$C_6H_4CF_3$)C(4-$\underline{C}_6H_4CF_3$)), 123.5 (*m*-NC_5H_5), 121.1 (*p*-NC_6H_5), 120.7 (*o*-NC_6H_5), 117.3 (N$\underline{C}$(4-$C_6H_4CF_3$)C(4-$C_6H_4CF_3$)), 61.9 ($\underline{C}H_2$NMe), 48.3 ($\underline{C}H_2$NSiMe$_3$), 46.8 (NMe), 1.7 (SiMe$_3$). Resonances attributable to carbons bound directly to ^{19}F atoms were not observed. ^{19}F NMR (C_6D_6, 282.2 MHz, 293 K): δ -61.8 and -61.9 (2 × 3 F, 2 × s, 2 × CF_3). IR (NaCl plates, Nujol mull, cm^{-1}): 1604 (s), 1595 (s), 1591 (s), 1560 (m), 1539 (w), 1514 (m), 1492 (s), 1444 (s), 1437 (m), 1419 (w), 1402 (s), 1323 (s, br.), 1293 (m), 1276 (w), 1234 (m), 1202 (m), 1164 (s), 1126 (m), 1088 (m), 1065 (m), 1041 (w), 1029 (m), 1017 (m), 1013 (w), 997 (m), 946 (m), 929 (m), 919 (m), 864 (m), 834 (s, br.), 802 (m), 753 (m), 696 (m). EI-MS: *m/z* = 498 [NC($C_6H_4CF_3$)C($C_6H_4CF_3$)NPh$_2$]$^{+}$ (80 %), 168 [NPh$_2$]$^{+}$ (100 %), 147 [$C_6H_4CF_3$]$^{+}$ (100 %). Anal. found (calcd. for $C_{44}H_{52}F_6N_6Si_2Ti$): C, 59.8 (59.9); H, 6.1 (5.9); N, 9.3 (9.5) %.

5.5.6 Cp$_2$Zr(NNPh$_2$)(DMAP) (**1.151**). This is a new synthesis for a literature compound.[30] To a solution of Cp_2ZrCl_2 (3.510 g, 0.0120 mol) and DMAP (1.465 g, 0.0120 mol) in THF (15 mL) at RT was added dropwise, over the course of 30 mins, a solution of LiNHNPh$_2$ (2.269 g, 0.0120 mol) in THF (10 mL). The solution was stirred for 2 h before a solution of LiN(SiMe$_3$)$_2$ (1.993 g, 0.0120 mol) in THF (5 mL) was added and the reaction left at RT for 16 h. Volatiles were removed under reduced pressure and the resulting solid extracted into refluxing C_6H_6 (3 × 5 mL) which, upon slow cooling to RT, yielded dark red crystals. The supernatant was decanted and the

crystals washed with C_6H_6 (3 mL) before being dried *in vacuo* to afford **1.151**. Yield: 3.402 g (54 %).

5.5.7 $Cp_2Hf(NNPh_2)(DMAP)$ (**28**). To a solution of Cp_2HfCl_2 (2.528 g, 6.66 mmol) and DMAP (0.813 g, 6.66 mmol) in THF (15 mL) at RT was added dropwise, over the course of 30 mins, a solution of $LiNHNPh_2$ (1.259 g, 6.66 mmol) in THF (10 mL). The solution was stirred for 2 h before a solution of $LiN(SiMe_3)_2$ (1.106 g, 6.66 mmol) in THF (5 mL) was added and the reaction left at RT for 16 h. Volatiles were removed under reduced pressure and the resulting solid extracted into refluxing C_6H_6 (3 × 5 mL) which, upon slow cooling to RT, yielded dark red crystals. The supernatant was decanted and the crystals washed with C_6H_6 (3 mL) before being dried *in vacuo* to afford **28**. Yield: 2.373 g (59 %). Diffraction-quality crystals were grown by slow cooling of a benzene solution from 60 ºC to RT.

^{1}H NMR (C_6D_6, 499.9 MHz, 293 K): δ 8.31 (2 H, br. s, *o*-$NC_5H_4NMe_2$), 7.56 (4 H, d, ^3J = 5 Hz, *o*-NC_6H_5), 7.31 (4 H, app. t, app. ^3J = 5 Hz, *m*-NC_6H_5), 6.88 (2 H, t, ^3J = 5 Hz, *p*-NC_6H_5), 6.02 (10 H, s, C_5H_5), 5.48 (2 H, br. s, *m*-$NC_5H_4NMe_2$), 2.03 (6 H, br. s, NMe_2). $^{13}C\{^1H\}$ NMR (C_6D_6, 125.7 MHz, 293 K): δ 154.9 (*p*-$NC_5H_4NMe_2$), 153.8 (*o*-$NC_5H_4NMe_2$), 149.0 (*i*-NC_6H_5), 129.2 (*m*-NC_6H_5), 120.4 (*p*-NC_6H_5), 120.2 (*o*-NC_6H_5), 107.5 (C_5H_5), 106.1 (*m*-$NC_5H_4NMe_2$), 38.2 (NMe_2). IR (NaCl plates, Nujol mull, cm^{-1}): 1631 (s, br.), 1457 (m, br.), 1385 (m), 1338 (m), 1301 (m), 1272 (m), 1227 (m, br.), 1178 (m), 1164 (m), 1149 (m, br.), 1123 (w), 1112 (m), 1063 (s), 1018 (s), 986 (m), 950 (m), 924 (m), 913 (w), 895 (m), 879 (w), 859 (m), 848 (m), 816 (s, br.), 692 (s), 668 (w), 659 (m), 626 (m), 612 (m). EI-MS: *m/z* = 492 [*M* – DMAP]$^+$ (20 %), 168 [NPh_2]$^+$ (100 %). Anal. found (calcd. for $C_{29}H_{30}HfN_4$): C, 56.4 (56.8); H, 4.9 (4.9); N, 8.9 (9.1) %.

5.5.8 $Cp'_2Zr(NNPh_2)(DMAP)$ (**29**). To a solution of Cp'_2ZrCl_2 (0.850 g, 2.66 mmol) and DMAP (0.324 g, 2.66 mmol) in THF (20 mL) at RT was added dropwise, over the course of 30 mins, a solution of $LiNHNPh_2$ (0.502 g, 2.66 mmol) in THF (10 mL). The solution was stirred for 2 h before a solution of $LiN(SiMe_3)_2$ (0.441 g, 2.66 mmol) in THF (5 mL) was added and the reaction left at RT for 16 h. Volatiles were removed under reduced pressure and the resulting solid extracted into refluxing C_6H_6 (3 × 5 mL) which, upon slow cooling to RT, yielded dark red crystals. The supernatant was decanted and the crystals washed with Et_2O (3 mL) before being

dried *in vacuo* to afford **29**. Yield: 0.761 g (52 %). Diffraction-quality crystals were grown by slow cooling of a benzene solution from 60 ºC to RT.

^{1}H NMR (toluene-d_8, 499.9 MHz, 298 K): δ 8.27 (2 H, br. s, *o*-$NC_5H_4NMe_2$), 7.46 (4 H, d, ^{3}J = 5 Hz, *o*-NC_6H_5), 7.26 (4 H, app. t, app. ^{3}J = 5 Hz, *m*-NC_6H_5), 6.86 (2 H, t, ^{3}J = 5 Hz, *p*-NC_6H_5), 5.95 (4 H, overlapping 2- and 5-$C_5\underline{H}_4Me$), 5.92 and 5.80 (4 H, br. s, 3- and 4-$C_5\underline{H}_4Me$), 5.61 (2 H, br. s, *m*-$NC_5H_4NMe_2$), 2.05 (6 H, br. s, NMe_2), 2.00 (6 H, s, $C_5H_4\underline{Me}$). ^{13}C{^{1}H} NMR (toluene-d_8, 125.7 MHz, 298 K): δ 154.5 (*o*-$NC_5H_4NMe_2$), 153.9 (*p*-$NC_5H_4NMe_2$), 148.7 (*i*-NC_6H_5), 129.1 (*m*-NC_6H_5), 120.7 (*p*-NC_6H_5), 120.2 (*o*-NC_6H_5), 119.5 (1-$\underline{C}_5H_4Me$), 111.7 and 109.8 (3- and 4-$\underline{C}_5H_4Me$), 109.3 and 105.3 (2- and 5-$\underline{C}_5H_4Me$), 105.9 (*m*-$NC_5H_4NMe_2$), 38.1 (NMe_2), 15.5 ($C_5H_4\underline{Me}$). IR (NaCl plates, Nujol mull, cm^{-1}): 1639 (m), 1622 (s, br.), 1459 (m, br.), 1419 (w), 1379 (m, br.), 1325 (m, br.), 1301 (m), 1222 (m, br.), 1166 (m), 1152 (m), 1144 (m), 1112 (m), 1062 (m), 1046 (w), 1031 (m), 1010 (m), 986 (m), 964 (w), 951 (m), 934 (m), 923 (m), 902 (m), 859 (m), 852 (m), 830 (m), 819 (s), 791 (s, br.), 699 (m), 659 (m), 619 (m). EI-MS: *m/z* = 431 [*M* – DMAP]$^{+}$ (20 %), 168 [NPh_2]$^{+}$ (100 %). Anal. found (calcd. for $C_{31}H_{34}N_4Zr$): C, 67.3 (67.2); H, 6.3 (6.2); N, 9.9 (10.1) %.

5.5.9 $Cp_2Zr(NHNMe_2)(CH_2CH_2{}^tBu)$ (**30**). To a solution of $Cp_2Zr(CH_2CH_2{}^tBu)Cl$ (2.055 g, 6.02 mmol) in THF (10 mL), was added a solution of $LiNHNMe_2$ (0.391 g, 6.02 mmol) in THF (5 mL) and the resulting yellow solution was left stirring at RT for 16 h. Volatiles were removed under reduced pressure and the resulting solid extracted into hexanes (3 × 5 mL) and dried *in vacuo* to yield **30** as a beige solid. Yield: 1.91 g (87 %).

^{1}H NMR (C_6D_6, 499.9 MHz, 293 K): δ 5.71 (10 H, s, C_5H_5), 5.15 (1 H, s, NH), 2.12 (6 H, s, NMe_2), 1.53 (2 H, m, $CH_2C\underline{H}_2{}^tBu$), 1.09 (9 H, s, $CH_2CH_2C\underline{Me}_3$), 0.68 (2 H, m, $C\underline{H}_2CH_2{}^tBu$). ^{13}C{^{1}H} NMR ($C_6D_6$, 125.7 MHz, 293 K): δ 109.1 (C_5H_5), 52.3 (NMe_2), 49.1 ($CH_2\underline{C}H_2{}^tBu$), 33.1 ($CH_2CH_2\underline{C}Me_3$), 31.3 ($\underline{C}H_2CH_2{}^tBu$), 29.5 ($CH_2CH_2C\underline{Me}_3$). IR (NaCl plates, Nujol mull, cm^{-1}): 3442 (m, NH), 1589 (m), 1550 (m, br.), 1437 (s), 1422 (m), 1390 (w), 1306 (s), 1260 (m), 1230 (m), 1156 (w), 992 (w), 860 (w), 781 (m, br.), 761 (m), 746 (m), 705 (m, br.), 694 (m). EI-MS: *m/z* = 321 [*M* – NMe_2]$^{+}$ (5 %), 293 [*M* – $CH_2{}^tBu$]$^{+}$ (10 %), 279 [*M* – $CH_2CH_2{}^tBu$]$^{+}$ (10 %), 220 [Cp_2Zr]$^{+}$ (100 %). Anal. found (calcd. for $C_{18}H_{30}N_2Zr$): C, 58.9 (59.1); H, 8.3 (8.1); N, 7.6 (7.7) %.

5.5.10 $[Cp_2Zr(\mu\text{-}NNMe_2)]_2$ (31). $Cp_2Zr(NHNMe_2)(CH_2CH_2{}^tBu)$ (**30**, 0.546 g, 1.50 mmol) and C_6H_6 (3 mL) were added to a Teflon valve ampoule, which was partially evacuated and sealed before being heated to 110 °C for 48 h. Upon cooling to RT, dark brown crystals formed from the dark brown mother liquor. The supernatant was decanted and the crystals dried *in vacuo* to yield **31** as a dark brown powder. Yield: 0.307 g (72 %). Diffraction-quality crystals were grown by slow cooling of a saturated benzene solution from 110 ºC to RT.

^{1}H NMR (pyridine-d_5, 499.9 MHz, 293 K): δ 6.08 (20 H, s, C_5H_5), 2.84 (12 H, s, Me). $^{13}C\{^1H\}$ NMR (pyridine-d_5, 125.7 MHz, 293 K): δ 109.1 (C_5H_5), 53.9 (Me). IR (NaCl plates, Nujol mull, cm^{-1}): 1562 (m, br.), 1459 (s), 1437 (m), 1419 (m), 1409 (w), 1399 (w), 1394 (m), 1263 (m), 1231 (s), 1202 (m), 1179 (m), 1161 (s), 1144 (m), 1129 (s), 1098 (s), 1077 (s), 973 (m), 890 (m), 867 (s), 853 (s), 801 (s, br.), 611 (m, br.). EI-MS: *m/z* = 556 $[M]^+$ (15 %), 491 $[M - Cp]^+$ (10 %). Anal. found (calcd. for $C_{24}H_{32}N_4Zr_2$): C, 51.7 (51.6); H, 5.6 (5.8); N, 9.9 (10.0) %.

5.5.11 $Cp_2Zr\{N(H)C(Me)C(Me)\text{-}1,2\text{-}C_6H_4N(Ph)\}$ (32). In a Teflon valve ampoule, to a solution of $Cp_2Zr(NNPh_2)(DMAP)$ (**1.151**, 0.516 g, 9.83 mmol) in C_6H_6 (3 mL) was added MeCCMe (0.5 mL) and the ampoule sealed and heated to 60 °C for 16 h. The volume was reduced by approximately three quarters and left for 16 h at RT. A powder separated from the dark red solution, the supernatant was decanted and the powder washed with Et_2O (3 × 2 mL) and dried *in vacuo* affording **32** as a yellow powder. Yield: 0.282 g (63 %). Diffraction-quality crystals were grown from a saturated benzene solution at RT.

^{1}H NMR (C_6D_6, 499.9 MHz, 293 K): δ 7.27 (1 H, dd, ^3J = 5 Hz, ^4J = 2 Hz, 3-$NC_6H_4CR_2$), 7.01 (1 H, app. dt, app. ^3J = 6 Hz, ^4J = 2 Hz, 5-$NC_6H_4CR_2$), 6.87 (1 H, tt, ^3J = 5 Hz, ^4J = 2 Hz, *p*-NC_6H_5), 6.80 (3 H, overlapping *m*-NC_6H_5 and 4-$NC_6H_4CR_2$), 6.78 (1 H, dd, ^3J = 5 Hz, ^4J = 2 Hz, 6-$NC_6H_4CR_2$), 6.71 (2 H, br. d, ^3J = 5 Hz, *o*-NC_6H_5), 5.73 and 5.62 (2 × 5 H, 2 × s, 2 × C_5H_5), 3.47 (1 H, br. s, NH), 3.31 (3 H, s, NC(Me)C(<u>Me</u>)), 1.62 (3 H, s, NC(<u>Me</u>)C(Me)). $^{13}C\{^1H\}$ NMR (C_6D_6, 125.7 MHz, 293 K): δ 160.1 (*i*-NC_6H_5), 152.9 (N<u>C</u>(Me)C(Me)), 150.6 (2-$NC_6H_4CR_2$), 141.4 (5-$NC_6H_4CR_2$), 139.4 (1-$NC_6H_4CR_2$), 129.2 (3-$NC_6H_4CR_2$), 126.8 (overlapping 4-$NC_6H_4CR_2$ and *m*-NC_6H_5), 123.5 (*o*-NC_6H_5), 121.0 (6-$NC_6H_4CR_2$), 119.4 (*p*-NC_6H_5), 118.0 (NC(Me)<u>C</u>(Me)), 110.7 and 109.4 (2 × C_5H_5), 22.2 (NC(Me)C(<u>Me</u>)),

21.4 (NC(Me)C(Me)). IR (NaCl plates, Nujol mull, cm^{-1}): 3337 (s, NH), 1591 (m, br.), 1553 (m), 1458 (s, br.), 1318 (w), 1272 (m, br.), 1194 (w), 1176 (w), 1155 (w), 1116 (w), 1078 (m, br.), 1038 (w), 1028 (m), 1015 (s), 989 (s), 965 (m), 954 (m), 936 (m), 893 (s), 886 (s), 872 (m), 846 (m), 838 (s), 830 (s, br.), 808 (s), 748 (m), 700 (m), 694 (s), 675 (m), 660 (m), 640 (m), 603 (w), 587 (w), 542 (m), 525 (m). EI-MS: *m/z* = 456 $[M]^+$ (5 %), 221 $[Cp_2Zr]^+$ (10 %). Anal. found (calcd. for $C_{26}H_{26}N_2Zr$): C, 67.8 (68.2); H, 5.7 (5.7); N, 6.4 (6.1) %.

5.5.12 $Cp_2Hf\{N(H)C(Me)C(Me)$-1,2-$C_6H_4N(Ph)\}$ (**33**). In a Teflon valve ampoule, to a solution of $Cp_2Hf(NNPh_2)(DMAP)$ (**28**, 0.451 g, 0.736 mmol) in C_6H_6 (3 mL) was added MeCCMe (0.5 mL) and the ampoule sealed before being heated to 60 °C for 16 h. The volume was reduced by approximately three quarters and left for 16 h at RT. A precipitate separated from the dark red solution, the supernatant was decanted and the solid washed with Et_2O (3 × 2 mL) and dried *in vacuo* affording **33** as a yellow powder. Yield: 0.274 g (69 %). Diffraction-quality crystals were grown from a saturated benzene solution at RT.

^1H NMR (C_6D_6, 499.9 MHz, 293 K): δ 7.35 (1 H, dd, ^3J = 5 Hz, ^4J = 2 Hz, 3-$NC_6H_4CR_2$), 7.04 (1 H, app. dt, app. ^3J = 5 Hz, ^4J = 2 Hz, 5-$NC_6H_4CR_2$), 6.88 (2 H, overlapping *p*-NC_6H_5 and 4-$NC_6H_4CR_2$), 6.84 (3 H, overlapping *m*-NC_6H_5 and 6-$NC_6H_4CR_2$), 6.64 (2 H, br. s, *o*-NC_6H_5), 5.73 and 5.61 (2 × 5 H, 2 × s, 2 × C_5H_5), 3.28 (1 H, br. s, NH), 2.14 (3 H, s, NC(Me)C(Me)), 1.72 (3 H, s, NC(Me)C(Me)). $^{13}C\{^1H\}$ NMR (C_6D_6, 125.7 MHz, 293 K): δ 161.0 (*i*-NC_6H_5), 154.0 (NC(Me)C(Me)), 153.9 (2-$NC_6H_4CR_2$), 140.2 (5-$NC_6H_4CR_2$), 139.9 (1-$NC_6H_4CR_2$), 129.1 (3-$NC_6H_4CR_2$), 128.7 (*m*-NC_6H_5), 128.4 (4-$NC_6H_4CR_2$), 125.2 (br., *o*-NC_6H_5), 121.5 (*p*-NC_6H_5), 119.9 (6-$NC_6H_4CR_2$), 119.3 (NC(Me)C(Me)), 109.7 and 108.9 (2 × C_5H_5), 21.6 (NC(Me)C(Me)), 21.3 (NC(Me)C(Me)). IR (NaCl plates, Nujol mull, cm^{-1}): 3328 (m, NH), 1591 (s, br.), 1514 (w), 1270 (m, br.), 1255 (m), 1191 (w), 1172 (w), 1149 (w), 1076 (m, br.), 1014 (m), 989 (m), 945 (w), 900 (m), 884 (w), 856 (w), 800 (s, br.), 750 (s), 695 (m). EI-MS: *m/z* = 546 $[M]^+$ (80 %), 481 $[M - Cp]^+$ (60 %). Anal. found (calcd. for $C_{26}H_{26}HfN_2$): C, 57.2 (57.3); H, 4.7 (4.8); N, 5.0 (5.1) %.

5.5.13 $Cp_2Zr\{N(H)C(Ar)C(Ar)$-1,2-$C_6H_4N(Ph)\}$ (**34**, Ar = 4-C_6H_4OMe). In a Teflon valve ampoule, to a mixture of $Cp_2Zr(NHNPh_2)(CH_2CH_2{}^tBu)$ (**1.152**, 0.356 g, 0.727 mmol) and ArCCAr (0.173 g, 0.727 mmol) was added C_6H_6 (2 mL). The ampoule

was partially evacuated, sealed and heated to 110 °C for 16 h forming a dark brown solution. After cooling to RT, volatiles were removed under reduced pressure and the resulting oil triturated with Et_2O (5 mL). Volatiles were removed under reduced pressure and the resulting solid dried *in vacuo* to yield **34** as a yellow powder. Yield: 0.239 g (50 %).

^{1}H NMR (C_6D_6, 499.9 MHz, 293 K): δ 7.49 (1 H, d, ^{3}J = 5 Hz, 3-$NC_6H_4CR_2$), 7.44 (2 H, d, ^{3}J = 10 Hz, *m*-NC(4-C_6H_4OMe)C(4-$C_6\underline{H}_4$OMe)), 7.24 (2 H, d, ^{3}J = 10 Hz, *m*-NC(4-$C_6\underline{H}_4$OMe)C(4-C_6H_4OMe)), 7.17 (2 H, br. app. t, app. ^{3}J = 10 Hz, *m*-NC_6H_5), 7.08 (1 H, app. t, app. ^{3}J = 5 Hz, 5-$NC_6H_4CR_2$), 6.86 (1 H, t, ^{3}J = 10 Hz, *p*-NC_6H_5), 6.82 (2 H, overlapping 6- and 4-$NC_6H_4CR_2$), 6.76 (2 H, br. d, ^{3}J = 10 Hz, *o*-NC_6H_5), 6.71 (2 H, d, ^{3}J = 10 Hz, *o*-NC(4-C_6H_4OMe)C(4-$C_6\underline{H}_4$OMe)), 6.60 (2 H, d, ^{3}J = 10 Hz, *o*-NC(4-$C_6\underline{H}_4$OMe)C(4-C_6H_4OMe)), 5.96 and 5.65 (2 × 5 H, 2 × s, 2 × C_5H_5), 4.32 (1 H, br. s, NH), 3.28 and 3.22 (2 × OMe). ^{13}C{^{1}H} NMR (C_6D_6, 125.7 MHz, 293 K): δ 159.7 (*p*-NC(4-C_6H_4OMe)C(4-$\underline{C}_6H_4$OMe)), 159.6 (*i*-NC_6H_5), 157.4 (*p*-NC(4-$\underline{C}_6H_4$OMe)C(4-C_6H_4OMe)), 154.5 (2-$NC_6H_4CR_2$), 149.5 (N$\underline{C}$(Ar)C(Ar)), 139.7 (1-$NC_6H_4CR_2$), 136.1 (*i*-NC(4-C_6H_4OMe)C(4-$\underline{C}_6H_4$OMe)), 133.9 (*i*-NC(4-$\underline{C}_6H_4$OMe)C(4-C_6H_4OMe)), 131.7 (3-$NC_6H_4CR_2$), 131.2 (*m*-NC(4-C_6H_4OMe)C(4-$\underline{C}_6H_4$OMe)), 130.9 (*m*-NC(4-$\underline{C}_6H_4$OMe)C(4-C_6H_4OMe)), 128.7 (*m*-NC_6H_5), 128.5 (5-$NC_6H_4CR_2$), 127.1 (6-$NC_6H_4CR_2$), 125.1 (*o*-NC_6H_5), 120.7 (4-$NC_6H_4CR_2$), 120.4 (*p*-NC_6H_5), 119.8 (NC(Ar)$\underline{C}$(Ar)), 113.8 (*o*-NC(4-$\underline{C}_6H_4$OMe)C(4-C_6H_4OMe)), 113.7 (*o*-NC(4-C_6H_4OMe)C(4-$\underline{C}_6H_4$OMe)), 111.2 and 110.9 (2 × C_5H_5), 54.8 and 54.6 (2 × OMe). IR (NaCl plates, Nujol mull, cm^{-1}): 3346 (s, NH), 1602 (s), 1558 (m), 1502 (s), 1469 (s, br.), 1327 (m), 1287 (m, br.), 1169 (m), 1107 (m), 1074 (m), 1011 (s, br.), 995 (m), 932 (m), 901 (m), 898 (m), 884 (m), 834 (s, br.), 755 (s), 698 (m), 682 (m), 660 (w), 599 (w). EI-MS: *m/z* = 640 $[M]^+$ (5 %), 510 $[M - Cp_2]^+$ (90 %), 468 $[M - C_6H_4OMe - Cp]^+$ (100 %). Anal. found (calcd. for $C_{38}H_{34}N_2O_2Zr$): C, 70.9 (71.1); H, 5.3 (3.3); N, 4.6 (4.4) %.

Alternative NMR tube scale synthesis of Cp_2Zr{N(H)C(Ar)C(Ar)-1,2-$C_6H_4N(Ph)$} (**34**). $Cp_2Zr(NNPh_2)$(DMAP) (**1.151**, 13.7 mg, 26.1 μmol) was dissolved in C_6D_6 (0.5 mL). ArCCAr (6.2 mg, 26.1 μmol) was added and the sealed NMR tube heated to 90 °C for 48 h. ^{1}H NMR spectroscopy showed quantitative conversion to **34**.

5.5.14 $Cp_2Zr\{N(H)C(Ar)C(Ar)\text{-}1,2\text{-}C_6H_4N(Ph)\}$ (**35**, Ar = 4-$C_6H_4CF_3$). To a mixture of $Cp_2Zr(NNPh_2)(DMAP)$ (**1.151**, 0.333 g, 0.634 mmol) and ArCCAr (0.199 g, 0.634 mmol) in a Teflon valve ampoule was added C_6H_6 (3 mL). The ampoule was sealed and heated to 70 °C for 16 h. After cooling to RT the volatiles were removed under reduced pressure. The resulting orange oily residue was triturated with Et_2O (5 mL) and volatiles removed under reduced pressure leaving an orange powder. This was washed with pentane (3 × 5 mL) and dried *in vacuo* affording **35** as an orange powder. Yield: 0.202 g (44 %).

^{1}H NMR (C_6D_6, 499.9 MHz, 293 K): δ 7.24 (3 H, overlapping 3-$NC_6H_4CR_2$ and *m*-NC(4-$C_6H_4CF_3$)C(4-$C_6\underline{H}_4CF_3$)), 7.16 (2 H, overlapping with solvent peak, *m*-NC_6H_5), 7.06 (2 H, d, ^{3}J = 10 Hz, *m*-NC(4-$C_6\underline{H}_4CF_3$)C(4-$C_6H_4CF_3$)), 7.03 (1 H, app. t, app. ^{3}J = 5 Hz, 5-$NC_6H_4CR_2$), 6.99 (2 H, d, ^{3}J = 10 Hz, *o*-NC(4-$C_6\underline{H}_4CF_3$)C(4-$C_6H_4CF_3$)), 6.90 (1 H, t, ^{3}J = 8 Hz, *p*-NC_6H_5), 6.80 – 6.75 (4 H, overlapping *o*-NC(4-$C_6H_4CF_3$)C(4-$C_6\underline{H}_4CF_3$), 6- and 4-$NC_6H_4CR_2$), 6.60 (2 H, d, ^{3}J = 8 Hz, *o*-NC_6H_5), 5.80 and 5.59 (2 × 5 H, 2 × s, C_5H_5), 3.96 (1 H, br. s, NH). ^{13}C{^{1}H} NMR (C_6D_6, 125.7 MHz, 293 K): δ 159.1 (*i*-NC_6H_5), 154.0 (2-$NC_6H_4CR_2$), 153.7 (N$\underline{C}$(4-$C_6H_4CF_3$)C(4-$C_6H_4CF_3$)), 152.3 (1-$NC_6H_4CR_2$), 146.4 (*i*-NC(4-$C_6H_4CF_3$)C(4-$\underline{C}_6H_4CF_3$)), 144.9 (*i*-NC(4-$\underline{C}_6H_4CF_3$)C(4-$C_6H_4CF_3$)), 131.5 (3-$NC_6H_4CR_2$), 130.0 (*o*-NC(4-$C_6H_4CF_3$)C(4-$\underline{C}_6H_4CF_3$)), 129.8 (*o*-NC(4-$\underline{C}_6H_4CF_3$)C(4-$C_6H_4CF_3$)), 129.0 (5-$NC_6H_4CR_2$), 128.9 (*m*-NC_6H_5), 128.3 (6-$NC_6H_4CR_2$), 125.6 and 125.0 (2 × q, 2 × $^3J_{CF}$ = 3.8 Hz, *m*-NC(4-$\underline{C}_6H_4CF_3$)C(4-$C_6H_4CF_3$) and *m*-NC(4-$C_6H_4CF_3$)C(4-$\underline{C}_6H_4CF_3$)), 125.2 (*o*-NC_6H_5), 121.4 (*p*-NC_6H_5), 118.9 (NC(4-$C_6H_4CF_3$)$\underline{C}$(4-$C_6H_4CF_3$)), 112.5 (4-$NC_6H_4CR_2$), 111.6 and 111.2 (2 × C_5H_5). Resonances attributable to *p*-NC(4-$\underline{C}_6H_4CF_3$)C(4-$C_6H_4CF_3$), *p*-NC(4-$C_6H_4CF_3$)C(4-$\underline{C}_6H_4CF_3$), NC(4-$C_6H_4\underline{C}F_3$)C(4-$C_6H_4CF_3$) and NC(4-$C_6H_4CF_3$)C(4-$C_6H_4\underline{C}F_3$) were not observed. ^{19}F NMR (C_6D_6, 282.1 MHz, 293 K): δ -61.8 and -62.2 (2 × 3 F, 2 × s, 2 × CF_3). IR (NaCl plates, Nujol mull, cm^{-1}): 3244 (s, NH), 1598 (s), 1538 (m), 1459 (s, br.), 1399 (w), 1322 (s, br.), 1261 (s), 1228 (m), 1164 (m), 1105 (s), 1065 (s), 1015 (s), 998 (m), 827 (m), 803 (s, br.), 748 (m), 694 (m). EI-MS: *m/z* = 716 $[M]^+$ (5 %), 651 $[M - Cp]^+$ (10 %). An accurate elemental analysis could not be obtained.

5.5.15 $Cp_2Hf\{N(H)C(Ph)C(Ph)\text{-}1,2\text{-}C_6H_4N(Ph)\}$ (**36**). To a mixture of $Cp_2Hf(NNPh_2)(DMAP)$ (**28**, 0.443 g, 0.724 mmol) and PhCCPh (0.129 g, 0.724 mmol) in a Teflon valve ampoule was added C_6H_6 (3 mL). The ampoule was sealed

and heated to 80 °C for 48 h. After cooling to RT, volatiles were removed under reduced pressure and the resulting orange oily residue was triturated with Et_2O (5 mL). Volatiles were removed under reduced pressure, leaving a powder which was washed with pentane (3 × 5 mL) and dried *in vacuo* affording **36** as an orange powder. Yield: 0.250 g (51 %). Diffraction-quality crystals were grown from a saturated benzene solution at RT.

^{1}H NMR (C_6D_6, 499.9 MHz, 293 K): δ 7.37 (2 H, dd, ^{3}J = 7.0 Hz, ^{4}J = 1.5 Hz, *o*-NC($C_6\underline{H}_5$)C(C_6H_5)), 7.35 (2 H, dd, ^{3}J = 7.0 Hz, ^{4}J = 1.5 Hz, *o*-NC(C_6H_5)C($C_6\underline{H}_5$)), 7.32 (1 H, dd, ^{3}J = 6.5 Hz, ^{4}J = 1.5 Hz, 3-$NC_6H_4CR_2$), 7.19 (2 H, br. app. t, app. ^{3}J = 8.0 Hz, *m*-NC_6H_5), 7.06 – 7.01 (5 H, overlapping *m*-NC($C_6\underline{H}_5$)C(C_6H_5), *m*-NC(C_6H_5)C($C_6\underline{H}_5$) and 5-$NC_6H_4CR_2$), 6.99 and 6.92 (2 × 1 H, 2 × t, ^{3}J = 7.0 Hz, *p*-NC($C_6\underline{H}_5$)C(C_6H_5) and *p*-NC(C_6H_5)C($C_6\underline{H}_5$)), 6.90 – 6.87 (2 H, overlapping *p*-NC_6H_5 and 6-$NC_6H_4CR_2$), 6.80 (2 H, br. d, ^{3}J = 8.0 Hz, *o*-NC_6H_5), 6.77 (1 H, app. dt, app. ^{3}J = 6.5 Hz, ^{4}J = 1.5 Hz, 4-$NC_6H_4CR_2$), 5.75 and 5.63 (2 × 5 H, 2 × s, 2 × C_5H_5), 4.20 (1 H, br. s, NH). ^{13}C{^{1}H} NMR (C_6D_6, 125.7 MHz, 293 K): δ 160.7 (*i*-NC_6H_5), 155.4 (2-$NC_6H_4CR_2$), 147.4 (N$\underline{C}$(Ph)C(Ph)), 143.8 and 143.0 (*i*-NC($\underline{C}_6H_5$)C(C_6H_5) and *i*-NC(C_6H_5)C($\underline{C}_6H_5$)), 139.8 (1-$NC_6H_4CR_2$), 131.3 (*o*-NC(C_6H_5)C($\underline{C}_6H_5$)), 129.6 (*o*-NC($\underline{C}_6H_5$)C(C_6H_5)), 129.2 (3-$NC_6H_4CR_2$), 128.8 (6-$NC_6H_4CR_2$), 128.5 (br. overlapping *m*-NC($\underline{C}_6H_5$)C(C_6H_5) and *m*-NC($\underline{C}_6H_5$)C(C_6H_5)), 128.3 (*m*-NC_6H_5), 127.6 (5-$NC_6H_4CR_2$), 127.2 and 125.7 (*p*-NC($\underline{C}_6H_5$)C(C_6H_5) and *p*-NC(C_6H_5)C($\underline{C}_6H_5$)), 126.3 (NC(Ph)$\underline{C}$(Ph)), 126.2 (*o*-NC_6H_5), 121.4 (4-$NC_6H_4CR_2$), 120.9 (*p*-NC_6H_5), 110.2 and 109.9 (2 × C_5H_5). IR (NaCl plates, Nujol mull, cm^{-1}): 3357 (s, NH), 1666 (m), 1588 (s, br.), 1550 (m), 1420 (m), 1323 (m), 1294 (m), 1261 (m), 1229 (s), 1196 (m), 1171 (m), 1129 (w), 1108 (m), 1070 (s), 1043 (m), 1011 (s), 997 (s), 988 (m), 948 (w), 937 (w), 905 (s), 880 (m), 870 (s), 847 (m), 833 (s), 811 (s), 776 (m), 759 (m), 749 (m), 712 (m), 696 (s), 659 (w), 639 (m), 615 (w), 595 (w), 530 (w, br.). EI-MS: *m/z* = 670 $[M]^+$ (60 %), 605 $[M - Cp]^+$ (100 %). A successful elemental analysis could not be obtained.

5.5.16 Cp′$_2$Zr{N(H)C(Ph)C(Ph)-1,2-C_6H_4N(Ph)} (**37**). To a mixture of Cp′$_2$Zr(NNPh$_2$)(DMAP) (**29**, 0.0910 g, 0.165 mmol) and PhCCPh (0.0294 g, 0.165 mmol) in a Teflon valve ampoule was added C_6H_6 (3 mL). The ampoule was sealed and heated to 80 °C for 48 h. After cooling to RT, volatiles were removed under reduced pressure and the resulting orange oily residue triturated with Et_2O (2 mL).

Volatiles were removed under reduced pressure leaving a powder which was washed with pentane (3 × 2 mL) and dried *in vacuo* affording **37** as an orange powder. Yield: 0.0454 g (42 %).

^{1}H NMR (C_6D_6, 499.9 MHz, 293 K): δ 7.51 and 7.29 (2 × 2 H, 2 × d, ^{3}J = 6.5 and 7.0 Hz, *o*-NC($C_6\underline{H}_5$)C(C_6H_5) and *o*-NC(C_6H_5)C($C_6\underline{H}_5$)), 7.43 (1 H, dd, ^{3}J = 7.5 Hz, ^{4}J = 1.5 Hz, 3-$NC_6H_4CR_2$), 7.10 – 6.98 (6 H, overlapping 5-$NC_6H_4CR_2$, *p*-NC_6H_5, *m*-NC($C_6\underline{H}_5$)C(C_6H_5) and *m*-NC(C_6H_5)C($C_6\underline{H}_5$)), 6.95 and 6.88 (1 × 1 H and 1 × 2 H, 1 × t and overlapping, ^{3}J = 6.5 Hz, *p*-NC($C_6\underline{H}_5$)C(C_6H_5), *p*-NC(C_6H_5)C($C_6\underline{H}_5$) and 6-$NC_6H_4CR_2$), 6.84 (2 H, app. t, app. ^{3}J = 7.0 Hz, *m*-NC_6H_5), 6.79 (2 H, br. d, ^{3}J = 7.0 Hz, *o*-NC_6H_5), 6.75 (1 H, t, ^{3}J = 7.5 Hz, 4-$NC_6H_4CR_2$), 5.92 and 5.65 (2 × 1 H, 2 × m, 3- and 4-$C_5\underline{H}_4Me^{a}$), 5.87 and 5.74 (2 × 1 H, 2 × m, 2- and 5-$C_5\underline{H}_4Me^{a}$), 5.79 and 5.69 (2 × 1 H, 2 × m, 3- and 4-$C_5\underline{H}_4Me^{b}$), 5.53 and 5.19 (2 × 1 H, 2 × m, 2- and 5-$C_5\underline{H}_4Me^{b}$), 3.15 (1 H, s, NH), 1.74 (3 H, s, $C_5H_4\underline{Me}^{a}$), 1.54 (3 H, s, $C_5H_4\underline{Me}^{b}$). $^{13}C\{^{1}H\}$ NMR (C_6D_6, 125.7 MHz, 293 K): δ 159.2 (i-NC_6H_5), 154.7 (2-$NC_6H_4CR_2$), 151.1 (N$\underline{C}$(C_6H_5)C(C_6H_5)), 143.6 and 142.5 (*i*-NC($\underline{C}_6H_5$)C(C_6H_5) and *i*-NC(C_6H_5)C($\underline{C}_6H_5$)), 138.6 (1-$NC_6H_4CR_2$), 133.1 (3-$NC_6H_4CR_2$), 130.5 and 129.8 (*o*-NC($\underline{C}_6H_5$)C(C_6H_5) and *o*-NC(C_6H_5)C($\underline{C}_6H_5$)), 128.6 and 124.9 (*p*-NC($\underline{C}_6H_5$)C(C_6H_5) and *p*-NC(C_6H_5)C($\underline{C}_6H_5$)), 128.5 (6-$NC_6H_4CR_2$), 128.4 (5-$NC_6H_4CR_2$), 126.4 (1-$\underline{C}_5H_4Me^{b}$), 125.7 (br., *o*-NC_6H_5), 125.1 (1-$\underline{C}_5H_4Me^{a}$), 121.4 (*m*-NC_6H_5), 121.3 (4-$NC_6H_4CR_2$), 118.8 (*p*-NC_6H_5), 117.2 (NC(C_6H_5)$\underline{C}$(C_6H_5)), 114.7 and 110.8 (2- and 5-$\underline{C}_5H_4Me^{b}$), 113.3 and 105.9 (3- and 4-$\underline{C}_5H_4Me^{a}$), 113.3 and 109.5 (2- and 5-$\underline{C}_5H_4Me^{a}$), 108.9 and 108.7 (3- and 4-$\underline{C}_5H_4Me^{b}$), 14.9 ($C_5H_4\underline{Me}^{a}$), 14.1 ($C_5H_4\underline{Me}^{b}$). IR (NaCl plates, Nujol mull, cm^{-1}): 3378 (s, NH), 1595 (s), 1468 (s, br.), 1306 (s, br.), 1261 (m), 1229 (m), 1193 (m), 1155 (m), 1111 (m), 1071 (s), 1027 (m), 988 (m), 951 (w), 935 (w), 907 (w), 848 (w), 801 (m, br.). EI-MS: *m/z* = 608 $[M]^{+}$ (5 %), 362 $[HNC(Ph)C(Ph)C_6H_4N(Ph)]^{+}$ (100 %), 345 $[C(Ph)C(Ph)C_6H_4N(Ph)]^{+}$ (100 %). Anal. found (calcd. for $C_{38}H_{34}N_2Zr$): C, 74.7 (74.8); H, 5.5 (5.6); N, 4.8 (4.6) %. Note: [a] and [b] refer to the two distinct Cp′ rings.

5.5.17 $Cp_2Ti\{N(NPh_2)C(Me)C(C_6F_5)\}$ (**38**). To a mixture of $Cp_2Ti(NNPh_2)(py)$ (**1.103**, 0.217 g, 0.494 mmol) and C_6F_5CCMe (0.102 g, 0.494 mmol) was added C_6H_6 (10 mL) at RT. The solution immediately turned dark red and was stirred for a further 2 h. Volatiles were removed under reduced pressure affording **38** as a dark red

powder. Yield: 0.196 g (69 %). Compound **38** decomposes over 12 h in a benzene solution at RT, or 3 days in the solid state.

^{1}H NMR (C_6D_6, 499.9 MHz, 293 K): δ 7.10 (4 H, app. t, app. ^{3}J = 5 Hz, *m*-NC_6H_5), 6.91 (4 H, d, ^{3}J = 5 Hz, *o*-NC_6H_5), 6.85 (2 H, t, ^{3}J = 5 Hz, *p*-NC_6H_5), 5.72 (10 H, s, C_5H_5), 1.63 (3 H, s, Me). $^{13}C\{^{1}H\}$ NMR (C_6D_6, 125.7 MHz, 293 K): δ 171.8 (Ti<u>C</u>CMe), 158.2 (TiC<u>C</u>Me), 148.7 (*i*-NC_6H_5), 141.9 (dd, $^{1}J_{CF}$ = 240 Hz, $^{2}J_{CF}$ = 7.5 Hz, *o*-C_6F_5), 138.2 (dm, $^{1}J_{CF}$ = 244 Hz, *m*-C_6F_5), 136.9 (dm, $^{1}J_{CF}$ = 243 Hz, *p*-C_6F_5), 129.5 (*m*-NC_6H_5), 122.6 (*p*-NC_6H_5), 121.6 (*o*-NC_6H_5), 114.0 (C_5H_5), 13.5 (Me). The resonance corresponding to *i*-C_6F_5 was not observed. ^{19}F NMR (C_6D_6, 470.4 MHz, 293 K): δ -142.5 (2 F, d, $^{3}J_{FF}$ = 33 Hz, *o*-C_6F_5), -164.6 (1 F, t, $^{3}J_{FF}$ = 33 Hz, *p*-C_6F_5), -165.0 (2 F, app. t, app. $^{3}J_{FF}$ = 33 Hz, *m*-C_6F_5). IR (NaCl plates, Nujol mull, cm^{-1}): 1589 (m), 1559 (w), 1554 (m), 1539 (m), 1533 (w), 1517 (m), 1491 (m), 1419 (w), 1394 (s), 1307 (w, br.), 1272 (w, br.), 1170 (w), 1017 (m, br.), 978 (s, br.), 807 (m, br.), 747 (m), 722 (m), 696 (m). EI-MS: *m/z* = 390 $[M - Cp_2Ti]^+$ (70 %), 168 $[NPh_2]^+$ (100 %). Anal. found (calcd. for $C_{31}H_{23}F_5N_2Ti$): C, 65.8 (65.7); H, 4.1 (4.1); N, 5.0 (5.0) %.

5.5.18 $Cp_2Ti\{N(NPh_2)C(Ar)C(Ar\}$ (**39**, Ar = 4-$C_6H_4CF_3$). To a mixture of $Cp_2Ti(NNPh_2)(py)$ (**1.103**, 0.356 g, 0.811 mmol) and ArCCAr (0.255 g, 0.811 mmol) was added C_6H_6 (10 mL) at RT. The solution immediately turned dark red and was stirred for a further 2 h. Volatiles were removed under reduced pressure affording **39** as a dark red powder. Yield: 0.473 g (87 %). Compound **39** decomposes over 24 h in a benzene solution at RT, or 1 week in the solid state.

^{1}H NMR (toluene-d_8, 499.9 MHz, 248 K): δ 7.23 (2 H, d, ^{3}J = 8.5 Hz, *m*-TiC(4-$C_6\underline{H}_4CF_3$)C(4-$C_6H_4CF_3$)), 7.06 (2 H, d, ^{3}J = 8.0 Hz, *m*-TiC(4-$C_6H_4CF_3$)C(4-$C_6\underline{H}_4CF_3$)), 6.96 – 6.90 (10 H, overlapping *o*-, *m*-NC_6H_5 and *o*-TiC(4-$C_6H_4CF_3$)C(4-$C_6\underline{H}_4CF_3$)), 6.68 (2 H, tt, ^{3}J = 7.5 Hz, ^{4}J = 1.5 Hz, *p*-NC_6H_5), 6.31 (2 H, d, ^{3}J = 8.5 Hz, *o*-TiC(4-$C_6\underline{H}_4CF_3$)C(4-$C_6H_4CF_3$)), 5.73 (10 H, s, C_5H_5). $^{13}C\{^{1}H\}$ NMR (toluene-d_8, 125.7 MHz, 248 K): δ 196.7 (Ti<u>C</u>(4-$C_6H_4CF_3$)C(4-$C_6H_4CF_3$)), 154.1 (*i*-TiC(4-<u>C</u>$_6H_4CF_3$)C(4-$C_6H_4CF_3$)), 150.6 (*i*-NC_6H_5), 137.6 (*i*-TiC(4-$C_6H_4CF_3$)C(4-<u>C</u>$_6H_4CF_3$)), 134.2 (TiC(4-$C_6H_4CF_3$)<u>C</u>(4-$C_6H_4CF_3$)), 131.0 (*p*-TiC(4-$C_6H_4CF_3$)C(4-<u>C</u>$_6H_4CF_3$)), 130.2 (overlapping *o*-TiC(4-$C_6H_4CF_3$)C(4-<u>C</u>$_6H_4CF_3$) and *m*-NC_6H_5), 129.4 (*p*-TiC(4-<u>C</u>$_6H_4CF_3$)C(4-$C_6H_4CF_3$)), 128.7 (*o*-TiC(4-<u>C</u>$_6H_4CF_3$)C(4-$C_6H_4CF_3$)), 127.1

(overlapping *m*-TiC(4-$\underline{C}_6H_4CF_3$)C(4-$C_6H_4CF_3$) and *m*-TiC(4-$C_6H_4CF_3$)C(4-$\underline{C}_6H_4CF_3$)), 123.9 (*p*-NC_6H_5), 123.6 (*o*-NC_6H_5), 114.8 (C_5H_5). Resonances attributable to carbon atoms bound directly to ^{19}F atoms were not observed. ^{19}F NMR (C_6D_6, 470.4 MHz, 293 K): δ -56.3 and -57.2 (2 x 3 F, 2 x s, 2 x CF_3). IR (NaCl plates, Nujol mull, cm^{-1}): 1601 (s, br.), 1539 (w), 1521 (m), 1507 (m), 1492 (s), 1467 (s, br.), 1405 (m), 1329 (s, br.), 1270 (m), 1205 (m), 1166 (s, br.), 1107 (s, br.), 1066 (s), 1017 (s), 923 (m), 887 (m), 842 (m), 810 (m), 746 (m), 698 (m). EI-MS: *m/z* = 656 $[M - F]^+$ (5 %), 168 $[NPh_2]^+$ (100 %), 65 $[Cp]^+$ (100 %). Anal. found (calcd. for $C_{38}H_{28}F_6N_2Ti$): C, 67.9 (67.7); H, 4.4 (4.2); N, 4.0 (4.2) %.

5.5.19 $Cp_2Ti\{N(NPh_2)C(C_6F_5)C(C_6F_5)\}$ (**40**). To a mixture of $Cp_2Ti(NNPh_2)(py)$ (**1.103**, 0.323 g, 0.736 mmol) and $C_6F_5CCC_6F_5$ (0.264 g, 0.736 mmol) was added C_6H_6 (10 mL) at RT. The solution immediately turned dark red and was stirred for a further 2 h. Volatiles were removed under reduced pressure and the oily solid triturated with Et_2O (5 mL). Volatiles were removed under reduced pressure and the resulting solid dried *in vacuo* to yield **40** as a dark red powder. Yield: 0.419 g (79 %). Compound **40** decomposes over 48 h in a benzene solution at RT, or 2 weeks in the solid state.

^1H NMR (C_6D_6, 299.9 MHz, 293 K): δ 7.05 (4 H, d, ^3J = 9.0 Hz, *o*-NC_6H_5), 6.92 (4 H, app. t, app. ^3J = 9.0 Hz, *m*-NC_6H_5), 6.64 (2 H, t, ^3J = 9.0 Hz, *p*-NC_6H_5), 5.86 (10 H, s, C_5H_5). $^{13}C\{^1H\}$ NMR (C_6D_6, 125.7 MHz, 293 K): δ 179.4 (Ti$\underline{C}(C_6F_5)C(C_6F_5)$), 154.7 ($TiC(C_6F_5)\underline{C}(C_6F_5)$), 148.8 (*i*-$NC_6H_5$), 144.4 (dm, $^1J_{CF}$ = 246 Hz, *o*-$TiC(C_6F_5)C(\underline{C}_6F_5)$), 141.7 (dm, $^1J_{CF}$ = 245 Hz, *o*-$TiC(\underline{C}_6F_5)C(C_6F_5)$), 140.7 (dm, $^1J_{CF}$ = 254 Hz, *p*-$TiC(C_6F_5)C(\underline{C}_6F_5)$), 138.0 (dm, $^1J_{CF}$ = 253 Hz, *p*-$TiC(\underline{C}_6F_5)C(C_6F_5)$), 137.9 (dm, $^1J_{CF}$ = 245 Hz, *m*-$TiC(C_6F_5)C(\underline{C}_6F_5)$), 137.6 (dm, $^1J_{CF}$ = 250 Hz, *m*-$TiC(\underline{C}_6F_5)C(C_6F_5)$), 129.0 (*m*-$NC_6H_5$), 122.6 (*p*-$NC_6H_5$), 122.1 (*o*-$NC_6H_5$), 114.3 ($C_5H_5$). Resonances corresponding to *i*-C_6F_5 were not observed. ^{19}F NMR (C_6D_6, 282.2 MHz, 293 K): δ -141.8 (2 F, dd, $^3J_{FF}$ = 25.4 Hz, $^4J_{FF}$ = 8.5 Hz, *o*-$TiC(C_6F_5)C(C_6\underline{F}_5)$), -142.37 (2 F, dd, $^3J_{FF}$ = 25.4 Hz, $^4J_{FF}$ = 8.5 Hz, *o*-$TiC(C_6\underline{F}_5)C(C_6F_5)$), -154.46 (1 F, tt, $^3J_{FF}$ = 22.6 Hz, $^4J_{FF}$ = 8.5 Hz, *p*-$TiC(C_6F_5)C(C_6\underline{F}_5)$), -160.38 (1 F, tt, $^3J_{FF}$ = 22.6 Hz, $^4J_{FF}$ = 8.5 Hz, *p*-$TiC(C_6\underline{F}_5)C(C_6F_5)$), -162.4 (2 F, ddm, $^3J_{FF}$ = 25.4 Hz and 22.6 Hz, *m*-$TiC(C_6F_5)C(C_6\underline{F}_5)$), -163.65 (2 F, ddm, $^3J_{FF}$ = 25.4 Hz and 22.6 Hz, *m*-$TiC(C_6\underline{F}_5)C(C_6F_5)$). IR (NaCl plates, Nujol mull, cm^{-1}): 1650 (s), 1623 (m), 1617

(m), 1597 (s), 1560 (m), 1530 (s, br.), 1315 (s), 1269 (m), 1210 (s), 1181 (m), 1172 (m), 1154 (m), 1100 (m, br.), 1064 (m), 1019 (m), 970 (m, br.), 926 (m), 882 (s), 819 (m, br.), 747 (m), 701 (m), 631 (w), 543 (w). EI-MS: *m/z* = 718 $[M]^+$ (5 %), 653 $[M - Cp]^+$ (5 %), 550 $[M - NPh_2]^+$ (30 %), 168 $[NPh_2]^+$ (100 %). Anal. found (calcd. for $C_{36}H_{20}F_{10}N_2Ti$): C, 60.0 (60.2); H, 2.7 (2.8); N, 3.8 (3.9) %.

5.5.20 $Cp_2Zr\{N(NPh_2)C(NAr')O\}(DMAP)$ (**41**, Ar′ = 2,6-$C_6H_3{}^iPr_2$). In a Teflon valve ampoule, to an orange suspension of $Cp_2Zr(NNPh_2)(DMAP)$ (**1.151**, 0.551 g, 1.05 mmol) in C_6H_6 (2 mL) was added Ar′NCO (224 µL, 1.05 mmol). The ampoule was sealed and heated to 50 °C for 16 h during which time a yellow precipitate formed below a dark brown solution. The supernatant was decanted and the precipitate washed with pentane (2 × 2 mL) and dried *in vacuo* to yield **41** as a pale yellow powder. Yield: 0.336 g (44 %). Diffraction-quality crystals were grown by slow cooling of a freshly prepared sample in benzene from 50 ºC to RT.

Due to the insolubility of **41** in polar and non-polar solvents NMR spectroscopic data could not be obtained. IR (NaCl plates, Nujol mull, cm^{-1}): 1627 (s, br.), 1480 (m, br.), 1215 (w, br.), 1059 (m), 1032 (m), 991 (s, br.), 991 (m, br.), 988 (m), 985 (m), 978 (m), 829 (s), 818 (s), 756 (m), 694 (m), 687 (m), 620 (m), 538 (m). EI-MS: *m/z* = 662 $[M\text{-}Cp]^+$ (30 %), 606 $[M - DMAP]^+$ (60 %), 422 $[M - Cp_2 - NAr']^+$ (100 %), 168 $[NPh_2]^+$ (70 %). Anal. found (calcd. for $C_{42}H_{47}N_5OZr$): C, 68.9 (69.2); H, 6.7 (6.5); N, 9.5 (9.2) %.

5.5.21 $Cp_2Hf\{N(NPh_2)C(NAr')O\}(DMAP)$ (**42**, Ar′ = 2,6-$C_6H_3{}^iPr_2$). In a Teflon valve ampoule, to an orange suspension of $Cp_2Hf(NNPh_2)(DMAP)$ (**28**, 0.376 g, 0.613 mmol) in C_6H_6 (2 mL) was added Ar′NCO (131 µL, 0.613 mmol). The ampoule was sealed and heated to 50 °C for 16 h during which time a yellow precipitate formed below a dark brown solution. The supernatant was decanted and the precipitate washed with pentane (2 × 2 mL) and dried *in vacuo* to yield **42** as a pale yellow powder. Yield: 0.188 g (37 %). Diffraction-quality crystals were grown by slow cooling of a freshly prepared sample in benzene from 50 ºC to RT.

Due to the insolubility of **42** in polar and non-polar solvents NMR spectroscopic data could not be obtained. IR (NaCl plates, Nujol mull, cm^{-1}): 1622 (s, br.), 1582 (m, br.), 1462 (m, br.), 1325 (m, br.), 1279 (m, br.), 1257 (m), 1228 (m, br.), 1170 (m), 1059 (m), 1032 (m), 1007 (m), 991 (m), 952 (m), 936 (m), 897 (m, br.), 831 (m), 807 (s,

br.), 756 (m), 744 (m), 739 (m), 694 (m), 539 (s, br.). EI-MS: *m/z* = 695 [*M* – *DMAP*]$^+$ (20 %), 308 [Cp_2Hf]$^+$ (20 %), 168 [NPh_2]$^+$ (100 %). Anal. found (calcd. for $C_{42}H_{47}HfN_5O$): C, 61.8 (61.8); H, 5.9 (5.8); N, 8.7 (8.6) %.

5.5.22 $Cp_2Zr\{N(H)C(Ph)C(Me)$-1,2-$C_6H_4N(Ph)\}$ (43a) and $Cp_2Zr\{N(H)C(Me)C(Ph)$-1,2-$C_6H_4N(Ph)\}$ (43b). In a Teflon valve ampoule, to a yellow suspension of $Cp_2Zr(NHNPh_2)(CH_2CH_2{}^tBu)$ (**1.152**, 0.372 g, 0.760 mmol) in C_6H_6 (2 mL) was added PhCCMe (95 µL, 0.760 mmol). The ampoule was partially evacuated, sealed and heated to 110 °C for 16 h. After cooling to RT, volatiles were removed under reduced pressure and the resulting oil triturated with Et_2O (5 mL). Volatiles were removed under reduced pressure and the resulting yellow powder dried *in vacuo* to yield a mixture of **43a** and **43b** in the ratio 38:62. Yield: 0.190 g (48 %).

Common data: IR (NaCl plates, Nujol mull, cm^{-1}): 3351 (s, br., NH), 1591 (s), 1556 (m), 1509 (m), 1468 (s, br.), 1394 (w), 1262 (m, br.), 1192 (w), 1172 (w), 1154 (w), 1101 (w), 1074 (w, br.), 1015 (m), 994 (w), 953 (m), 939 (m), 892 (m), 877 (m), 860 (m), 844 (m), 800 (s), 751 (m), 699 (m), 534 (w, br.). EI-MS: *m/z* = 300 [*M* – Cp_2Zr]$^+$ (50 %), 283 [*M* – Cp_2ZrMe]$^+$ (70 %), 167 [$PhNC_6H_4$]$^+$ (100 %). Anal. found (calcd. for $C_{31}H_{28}N_2Zr$): C, 71.5 (71.6); H, 5.5 (5.4); N, 5.3 (5.4) %.

A small amount of pure **43b** was separated and characterised by ^{1}H and $^{13}C\{^1H\}$ NMR. **43a** was assigned from the mixture and the known peaks for **43b**.

Data for 43a: ^{1}H NMR (C_6D_6, 499.9 MHz, 293 K): δ 7.48 (2 H, d, ^3J = 10 Hz, *o*-NC(C_6H_5)C(Me)), 7.35 (1 H, d, ^3J = 10 Hz, 3-$NC_6H_4CR_2$), 7.24 (4 H, br. t, app. ^3J = 10 Hz, overlapping *m*-NC_6H_5 and *m*-NC(C_6H_5)C(Me)), 7.09 (1 H, t, ^3J = 10 Hz, *p*-NC(C_6H_5)C(Me)), 7.04 (1 H, app. t, app. ^3J = 10 Hz, 5-$NC_6H_4CR_2$), 6.91 (1 H, t, ^3J = 10 Hz, *p*-NC_6H_5), 6.85 (1 H, d, ^3J = 10 Hz, 6-$NC_6H_4CR_2$), 6.83 (3 H, overlapping *o*-NC_6H_5 and 4-$NC_6H_4CR_2$), 5.80 and 5.62 (2 × 5 H, 2 × s, 2 × C_5H_5), 4.21 (1 H, br. s, NH), 2.25 (3 H, s, Me). $^{13}C\{^1H\}$ NMR (C_6D_6, 125.7 MHz, 293 K): δ 160.2 (*i*-NC_6H_5), 153.7 (2-$NC_6H_4CR_2$), 146.2 (N<u>C</u>(Ph)C(Me)), 141.9 (*i*-NC(C_6H_5)C(Me)), 140.4 (1-$NC_6H_4CR_2$), 129.5 (*o*-NC(C_6H_5)C(Me)), 129.1 (3-$NC_6H_4CR_2$), 128.6 (br. overlapping *m*-NC_6H_5 and *m*-NC(C_6H_5)C(Me)), 128.4 (6-$NC_6H_4CR_2$), 127.5 (5-$NC_6H_4CR_2$), 125.0 (*p*-NC(C_6H_5)C(Me)), 121.2 (*o*-NC_6H_5), 120.4 (4-$NC_6H_4CR_2$), 118.7 (NC(Ph)<u>C</u>(Me)), 118.1 (*p*-NC_6H_5), 110.9 and 110.2 (2 × C_5H_5), 24.1 (Me).

Data for 43b: ^{1}H NMR (C_6D_6, 499.9 MHz, 293 K): δ 7.41 (1 H, d, ^{3}J = 10 Hz, 3-$NC_6H_4CR_2$), 7.38 (2 H, d, ^{3}J = 10 Hz, *o*-NC(Me)C(C_6H_5)), 7.20 (4 H, br. t, app. ^{3}J = 10 Hz, overlapping *m*-NC_6H_5 and *m*-NC(Me)C(C_6H_5)), 7.03 (1 H, t, ^{3}J = 10 Hz, *p*-NC(Me)C(C_6H_5)), 6.96 (1 H, app. t, app. ^{3}J = 10 Hz, 5-$NC_6H_4CR_2$), 6.88 (1 H, t, ^{3}J = 10 Hz, *p*-NC_6H_5), 6.83 (1 H, d, ^{3}J = 10 Hz, 6-$NC_6H_4CR_2$), 6.74 (2 H, br. d, ^{3}J = 10 Hz, *o*-NC_6H_5), 6.69 (1 H, app. t, app. ^{3}J = 10 Hz, 4-$NC_6H_4CR_2$), 5.82 and 5.64 (2 × 5 H, 2 × s, 2 × C_5H_5), 3.43 (1 H, br. s, NH), 1.73 (3 H, s, Me). ^{13}C{^{1}H} NMR (C_6D_6, 125.7 MHz, 293 K): δ 160.0 (*i*-NC_6H_5), 152.3 (2-$NC_6H_4CR_2$), 145.0 (N<u>C</u>(Me)C(Ph)), 144.4 (*i*-NC(Me)C(C_6H_5)), 138.1 (1-$NC_6H_4CR_2$), 131.1 (3-$NC_6H_4CR_2$), 129.5 (*o*-NC(Me)C(C_6H_5)), 128.8 (br. overlapping *m*-NC_6H_5 and *m*-NC(Me)C(C_6H_5)), 128.4 (5-$NC_6H_4CR_2$), 128.3 (6-$NC_6H_4CR_2$), 125.9 (*p*-NC(Me)C(C_6H_5)), 123.5 (*o*-NC_6H_5), 122.8 (NC(Me)<u>C</u>(Ph)), 121.2 (4-$NC_6H_4CR_2$), 119.7 (*p*-NC_6H_5), 111.0 and 109.8 (2 × C_5H_5), 22.4 (Me).

Alternative NMR tube scale synthesis of $Cp_2Zr\{N(H)C(Ph)C(Me)$-1,2-$C_6H_4N(Ph)\}$ (43a) and $Cp_2Zr\{N(H)C(Me)C(Ph)$-1,2-$C_6H_4N(Ph)\}$ (43b). To a solution of $Cp_2Zr(NNPh_2)$(DMAP) (**1.151**, 15.4 mg, 29.3 μmol) in C_6D_6 (0.5 mL) was added PhCCMe (3.7 μL, 29.3 μmol). The NMR tube was sealed and heated to 60 °C for 18 h. ^{1}H NMR spectroscopy showed quantitative conversion to **43a** and **43b** in the ratio 38:62.

5.5.23 $Cp_2Zr\{N(H)C(Me)C(SiMe_3)$-1,2-$C_6H_4N(Ph)\}$ (44). In a Teflon valve ampoule, to an orange suspension of $Cp_2Zr(NHNPh_2)(CH_2CH_2{}^{t}Bu)$ (**1.152**, 0.331 g, 0.678 mmol) in C_6H_6 (2 mL) was added $Me_3SiCCMe$ (100 μL, 0.678 mmol). The ampoule was partially evacuated, sealed and heated to 110 °C for 16 h. Upon cooling to RT a yellow solid precipitated, the supernatent was decanted and the solid washed with pentane (2 mL) and dried *in vacuo* to yield **44**. Yield: 0.184 g (53 %). Diffraction-quality crystals were grown by slow cooling of a saturated benzene solution from 110 ºC to RT.

^{1}H NMR (C_6D_6, 499.9 MHz, 293 K): δ 7.25 (1 H, dd, ^{3}J = 5 Hz, ^{4}J = 2 Hz, 3-$NC_6H_4CR_2$), 7.22 (2 H, br. app. t, app. ^{3}J = 5 Hz, *m*-NC_6H_5), 6.98 (1 H, app. dt, app. ^{3}J = 5 Hz, ^{4}J = 2 Hz, 5-$NC_6H_4CR_2$), 6.88 (1 H, tt, ^{3}J = 5 Hz, ^{4}J = 2 Hz, *p*-NC_6H_5), 6.83 (1 H, dd, ^{3}J = 5 Hz, ^{4}J = 2 Hz, 6-$NC_6H_4CR_2$), 6.78 (2 H, br. d, ^{3}J = 5 Hz, *o*-NC_6H_5), 6.72 (1 H, app. dt, app. ^{3}J = 5 Hz, ^{4}J = 2 Hz, 4-$NC_6H_4CR_2$), 5.83 and 5.57 (2 × 5 H, 2

× s, 2 × C_5H_5), 3.19 (1 H, br. s, NH), 1.78 (3 H, s, Me), 0.26 (9 H, s, $SiMe_3$). $^{13}C\{^1H\}$ NMR (C_6D_6, 125.7 MHz, 293 K): δ 159.6 (*i*-NC_6H_5), 155.9 (N<u>C</u>(Me)C($SiMe_3$)), 150.8 (2-$NC_6H_4CR_2$), 140.7 (1-$NC_6H_4CR_2$), 130.0 (3-$NC_6H_4CR_2$), 128.7 (6-$NC_6H_4CR_2$), 128.4 (*m*-NC_6H_5), 127.4 (5-$NC_6H_4CR_2$), 123.4 (*o*-NC_6H_5), 120.8 (4-$NC_6H_4CR_2$), 119.9 (*p*-NC_6H_5), 116.5 (NC(Me)<u>C</u>($SiMe_3$)), 111.1 and 109.7 (2 × C_5H_5), 25.2 (Me), 1.7 ($SiMe_3$). IR (NaCl plates, Nujol mull, cm^{-1}): 3321 (m, NH), 1576 (m), 1570 (m), 1554 (m), 1540 (m), 1490 (s), 1275 (s), 1260 (s), 1245 (s), 1188 (m), 1171 (s, br.), 1149 (m), 1102 (s), 1075 (s), 1043 (s), 1015 (s, br.), 938 (m), 897 (m), 878 (m), 804 (s, br.), 749 (m, br.), 697 (m). EI-MS: *m/z* = 516 $[M]^+$ (10 %), 451 $[M - Cp]^+$ (10 %). Anal. found (calcd. for $C_{28}H_{32}N_2SiZr$): C, 65.1 (65.2); H, 6.3 (6.3); N, 5.3 (5.4) %.

Alternative NMR tube synthesis of $Cp_2Zr\{N(H)C(Me)C(SiMe_3)$-1,2-$C_6H_4N(Ph)\}$ (**44**). To a solution of $Cp_2Zr(NNPh_2)$(DMAP) (**1.151**, 16.1 mg, 31.0 μmol) in C_6D_6 (0.5 mL) was added $Me_3SiCCMe$ (4.5 μL, 31.0 μmol). The NMR tube was sealed and heated to 90 °C for 48 h. ^1H NMR spectroscopy showed quantitative conversion to **44**.

5.5.24 $Cp_2Zr\{NHC(Ph)C(SiMe_3)$-1,2-$C_6H_4N(Ph)\}$ (**45**). In a Teflon valve ampoule, to a yellow suspension of $Cp_2Zr(NHNPh_2)(CH_2CH_2{}^tBu)$ (**1.152**, 0.305 g, 0.624 mmol) in C_6H_6 (2 mL) was added $Me_3SiCCPh$ (123 μL, 0.624 mmol). The ampoule was partially evacuated, sealed and heated to 110 °C for 16 h. Upon cooling to RT volatiles were removed under reduced pressure and the resulting oil triturated with Et_2O (5 mL). Volatiles were removed under reduced pressure and the resulting yellow powder dried *in vacuo* to yield **45**. Yield: 0.213 g (58 %).

^1H NMR (C_6D_6, 499.9 MHz, 293 K): δ 7.65 (2 H, d, ^3J = 5 Hz, *o*-$NC(C_6H_5)C(SiMe_3)$), 7.49 (1 H, d, ^3J = 5 Hz, 3-$NC_6H_4CR_2$), 7.25 – 7.18 (5 H, overlapping *m*-NC_6H_5, *m*- and *p*-$NC(C_6H_5)C(SiMe_3)$), 7.03 (1 H, app. t, app. ^3J = 10 Hz, 5-$NC_6H_4CR_2$), 6.92 (1 H, t, ^3J = 10 Hz, *p*-NC_6H_5), 6.87 (3 H, br. d, ^3J = 10 Hz, overlapping *o*-NC_6H_5 and 6-$NC_6H_4CR_2$), 6.81 (1 H, app. t, app. ^3J = 10 Hz, 4-$NC_6H_4CR_2$), 5.99 and 5.53 (2 × 5 H, 2 × s, 2 × C_5H_5), 3.94 (1 H, br. s, NH), 0.06 (9 H, s, $SiMe_3$). $^{13}C\{^1H\}$ NMR (C_6D_6, 125.7 MHz, 293 K): δ 162.5 (*i*-$NC(C_6H_5)C(SiMe_3)$), 159.3 (*i*-NC_6H_5), 151.5 (2-$NC_6H_4CR_2$), 144.3 (N<u>C</u>(Ph)C($SiMe_3$)), 140.9 (1-$NC_6H_4CR_2$), 130.5 (3-$NC_6H_4CR_2$), 129.8 (*o*-$NC(C_6H_5)C(SiMe_3)$), 128.8 (*p*-$NC(C_6H_5)C(SiMe_3)$), 128.5 (6-$NC_6H_4CR_2$), 128.3

(*m*-NC_6H_5), 128.2 (5-$NC_6H_4CR_2$), 127.4 (*m*-$NC(C_6H_5)C(SiMe_3)$), 124.1 (*o*-NC_6H_5), 120.6 (4-$NC_6H_4CR_2$), 120.4 (*p*-NC_6H_5), 116.4 (NC(Ph)C(SiMe$_3$)), 111.4 and 110.7 (2 × C_5H_5), 2.0 ($SiMe_3$). IR (NaCl plates, Nujol mull, cm^{-1}): 3356 (s, NH), 1589 (s), 1554 (m), 1511 (m), 1504 (m), 1482 (s), 1468 (s), 1420 (m), 1314 (m), 1246 (s), 1192 (m), 1175 (m), 1154 (w), 1111 (w), 1076 (m), 1047 (w), 1021 (m), 1015 (m), 993 (w), 965 (m), 895 (w), 883 (m), 867 (w), 837 (m, br.), 813 (m, br.), 775 (w), 754 (m), 704 (m). EI-MS: *m/z* = 578 $[M]^+$ (10 %), 252 $[PhNC_6H_4CSiMe_3]^+$ (25 %), 234 $[Cp_2ZrN]^+$ (40 %), 165 $[PhNC_6H_4]^+$ (90 %). Anal. found (calcd. for $C_{33}H_{34}N_2SiZr$): C, 68.6 (68.6); H, 5.9 (5.9); N, 4.7 (4.9) %.

Alternative NMR tube scale synthesis of $Cp_2Zr\{N(H)C(Ph)C(SiMe_3)$-1,2-$C_6H_4N(Ph)\}$ (**45**). To a solution of $Cp_2Zr(NNPh_2)$(DMAP) (**1.151**, 14.2 mg, 27.0 µmol) in C_6D_6 (0.5 mL) was added $Me_3SiCCPh$ (5.3 µL, 27.0 µmol). The NMR tube was sealed and heated to 90 °C for 48 h. ^{1}H NMR spectroscopy showed quantitative conversion to **45**.

5.5.25 $Cp_2Zr\{N(H)C(^tBu)C(Me)$-1,2-$C_6H_4N(Ph)\}$ (**46**). In a Teflon valve ampoule, to a suspension of $Cp_2Zr(NHNPh_2)(CH_2CH_2{}^tBu)$ (**1.152**, 0.309 g, 0.632 mmol) in C_6H_6 (2 mL) was added ^{t}BuCCMe (85 µL, 0.632 mmol). The ampoule was partially evacuated, sealed and heated to 110 °C for 16 h. Upon cooling to RT volatiles were removed under reduced pressure and the resulting oil triturated with Et_2O (5 mL). Volatiles were removed under reduced pressure and the resulting yellow powder dried *in vacuo* to afford **46**. Yield: 0.199 g (61 %).

^{1}H NMR (C_6D_6, 499.9 MHz, 293 K): δ 7.24 (2 H, br. s, *m*-NC_6H_5), 7.10 (1 H, d, ^3J = 10 Hz, 3-$NC_6H_4CR_2$), 6.96 (1 H, app. t, app. ^3J = 10 Hz, 5-$NC_6H_4CR_2$), 6.90 (1 H, t, ^3J = 10 Hz, *p*-NC_6H_5), 6.81 (2 H, br. d, ^3J = 10 Hz, *o*-NC_6H_5), 6.75 (1 H, d, ^3J = 10 Hz, 6-$NC_6H_4CR_2$), 6.70 (1 H, app. t, app. ^3J = 10 Hz, 4-$NC_6H_4CR_2$), 5.82 and 5.55 (2 × 5 H, 2 × s, 2 × C_5H_5), 4.33 (1 H, br. s, NH), 2.10 (3 H, s, Me), 1.18 (9 H, s, CMe_3). $^{13}C\{^1H\}$ NMR (C_6D_6, 125.7 MHz, 293 K): δ 159.4 (*i*-NC_6H_5), 155.8 (NC(^{t}Bu)C(Me)), 153.1 (2-$NC_6H_4CR_2$), 143.0 (1-$NC_6H_4CR_2$), 129.8 (3-$NC_6H_4CR_2$), 128.8 (*m*-NC_6H_5), 128.5 (5-$NC_6H_4CR_2$), 125.3 (6-$NC_6H_4CR_2$), 123.9 (*o*-NC_6H_5), 120.4 (4-$NC_6H_4CR_2$), 119.6 (*p*-NC_6H_5), 112.5 (NC(^{t}Bu)C(Me)), 110.8 and 110.2 (2 × C_5H_5), 35.9 (CMe_3), 29.7 (CMe_3), 23.7 (Me). IR (NaCl plates, Nujol mull, cm^{-1}): 3394 (m, NH), 1591 (s), 1556 (m), 1539 (w), 1521 (w), 1507 (w), 1467 (s, br.), 1419

(m), 1395 (m), 1284 (s, br.), 1223 (m), 1194 (m), 1171 (m), 1152 (m), 1112 (w), 1075 (m), 1016 (s), 995 (m), 896 (m), 864 (w), 848 (m), 806 (s, br.), 751 (m), 696 (m), 675 (w), 592 (w). EI-MS: *m/z* = 498 $[M]^+$ (70 %), 439 $[M - {}^t\text{Bu}]^+$ (20 %), 433 $[M - \text{Cp}]^+$ (40 %). Anal. found (calcd. for $C_{29}H_{32}N_2Zr$): C, 69.5 (69.7); H, 6.3 (6.5); N, 5.5 (5.6) %.

Alternative NMR tube scale synthesis of $Cp_2Zr\{N(H)C(^tBu)C(Me)\text{-}1,2\text{-}C_6H_4N(Ph)\}$ (**46**). To a solution of $Cp_2Zr(NNPh_2)(DMAP)$ (**1.151**, 15.1 mg, 28.8 µmol) in C_6D_6 (0.5 mL) was added ^{t}BuCCMe (3.9 µL, 28.8 µmol). The NMR tube was sealed and heated to 90 °C for 48 h. ^{1}H NMR spectroscopy showed quantitative conversion to **46**.

5.6 Experimental details and characterising data for Appendix B

5.6.1 $Ti(N_2N^{Me})(N^tBu)(py)$ (**47**). To a stirred mixture of $Ti(N^tBu)Cl_2(py)_3$ (2.464 g, 5.78 mmol) and $Li_2N_2N^{Me}$ (1.568 g, 5.78 mmol) was added toluene (20 mL), at -78 °C. The orange suspension was allowed to warm to RT and stirred for a further 2 h during which time a darkening of colour was observed. Volatiles were removed under reduced pressure and the orange solid extracted into Et_2O (3 × 15 mL). Volatiles were removed under reduced pressure to yield an orange powder, which was triturated with pentane (2 × 5 mL). Volatiles were removed under reduced pressure and the resulting orange powder dried *in vacuo* to give $Ti(N_2N^{Me})(N^tBu)(py)$ (**47**). Yield: 2.266 g (86 %). Diffraction-quality crystals were grown from a saturated pentane solution at -30 °C.

^{1}H NMR (C_6D_6, 299.9 MHz, 293 K): δ 8.75 (2 H, d, ^3J = 7.0 Hz, *o*-NC_5H_5), 6.77 (1 H, t, ^3J = 7.0 Hz, *p*-NC_5H_5), 6.47 (2 H, app. t, app. ^3J = 7.0, *m*-NC_5H_5), 3.52 and 3.33 (2 × 2 H, 2 × m, $C\underline{H}_2NSiMe_3$), 2.72 and 2.38 (2 × 2 H, 2 × m, $C\underline{H}_2NMe$), 2.60 (3 H, s, NMe), 1.41 (9 H, s, CMe_3), 0.19 (18 H, s, $SiMe_3$). $^{13}C\{^1H\}$ NMR (C_6D_6, 75.4 MHz, 293 K): δ 153.2 (*o*-NC_5H_5), 138.1 (*p*-NC_5H_5), 123.3 (*m*-NC_5H_5), 67.7 ($\underline{C}Me_3$), 62.9 ($\underline{C}H_2NMe$), 48.8 (NMe), 47.7 ($\underline{C}H_2NSiMe_3$), 34.3 ($C\underline{Me}_3$), 2.15 ($SiMe_3$). IR (NaCl plates, Nujol mull, cm^{-1}): 1603 (m), 1576 (w), 1559 (m), 1540 (m), 1507 (w), 1457 (s), 1447 (s), 1419 (w), 1346 (m), 1238 (s), 1213 (m), 1204 (m), 1121 (m), 1084 (m), 1071 (m), 1040 (m), 994 (w), 928 (s), 865 (m), 832 (s, br.), 797 (m), 783 (w), 752 (m), 742 (m), 696 (m), 679 (w), 668 (m). EI-MS: *m/z* = 378 $[M - \text{py}]^+$ (80 %), 363 [*M*

– py – Me]$^+$ (30 %), 307 [*M* – py – N^{t}Bu]$^+$ 90 %. Anal. found (calcd. for $C_{20}H_{43}N_5Si_2Ti$): C, 52.4 (52.5); H, 9.4 (9.5); N, 15.2 (15.3).

5.7 Experimental details and characterising data for Appendix D

5.7.1 Cp*$_2$Zr(NHNPh$_2$)$_2$ (50). To a solution of Cp*$_2$ZrCl$_2$ (0.945 g, 2.19 mmol) in THF (10 mL) was added a solution of LiNHNPh$_2$ (0.827 g, 4.38 mmol) in THF (10 mL). After 16 h the volatiles were removed under reduced pressure and the resulting yellow solid extracted into hot hexanes (3 × 3 mL, 70 ºC) which, upon cooling to -30 °C, afforded pale yellow crystals. The supernatant was decanted and the crystals washed with pentane (5 mL) before being dried *in vacuo* to yield **50** as a yellow powder. Yield: 1.373 g (87 %). Diffraction-quality crystals were grown by slow cooling of a saturated hexanes solution from 70 ºC to RT.

^{1}H NMR (C_6D_6, 499.9 MHz, 293 K): δ 7.14 (16 H, br. s, overlapping *o*- and *m*-NC$_6$H$_5$), 6.88 (4 H, tt, ^{3}J = 10 Hz, ^{4}J = 5 Hz, *p*-NC$_6$H$_5$), 4.95 (2 H, s, NH), 1.77 (30 H, s, C$_5$Me$_5$). ^{13}C{^{1}H} NMR (C_6D_6, 125.7 MHz, 293 K): δ 153.7 (*i*-NC$_6$H$_5$), 129.0 (*o*-NC$_6$H$_5$), 122.1 (*m*-NC$_6$H$_5$), 121.8 (*p*-NC$_6$H$_5$), 119.9 (C$_5$Me$_5$), 11.9 (C$_5$Me$_5$). IR (NaCl plates, Nujol mull, cm^{-1}): 3246 (s, NH), 1586 (s, br.), 1560 (m), 1521 (m), 1506 (w), 1490 (s, br.), 1306 (m), 1292 (m), 1261 (s), 1208 (m), 1170 (s), 1150 (m), 1089 (w), 1075 (m), 1054 (m), 1021 (s), 995 (s), 970 (w), 959 (w), 906 (w), 895 (m), 884 (m), 828 (m), 801 (m, br.), 766 (s), 752 (s), 731 (s), 695 (s), 620 (m), 614 (m). EI-MS: *m/z* = 648 [*M* – Ph]$^+$ (20 %), 542 [*M* – NHNPh$_2$]$^+$ (60 %), 359 [Cp*$_2$Zr]$^+$ (80 %). Anal. found (calcd. for $C_{44}H_{52}N_4Zr$): C, 72.5 (72.6); H, 7.4 (7.2); N, 7.9 (7.5) %.

5.7.2 Cp*$_2$Zr(NHNPh$_2$)(Me) (51). To a solution of Cp*$_2$Zr(Me)Cl (2.479 g, 6.02 mmol) in THF (10 mL) was added a solution of LiNHNPh$_2$ (1.366 g, 7.23 mmol) in THF (10 mL). After 16 h the volatiles were removed under reduced pressure and the resulting solid extracted into hot hexanes (3 × 5 mL, 70 ºC) which, upon cooling to 4 °C, afforded dark red/brown crystals. The supernatant was decanted and the crystals washed with pentane (3 mL) before being dried *in vacuo* to yield **51** as a brown powder. Yield: 2.090 g (62 %). Diffraction-quality crystals were grown by slow cooling of a saturated hexanes solution from 70 ºC to RT.

^{1}H NMR (C_6D_6, 499.9 MHz, 293 K): δ 7.22 (8 H, br. s, overlapping *o*- and *m*-NC$_6$H$_5$), 6.84 (2 H, br. s, *p*-NC$_6$H$_5$), 5.99 (1 H, s, NH), 1.75 (30 H, s, C$_5$Me$_5$), -0.48 (3 H, s,

Me). $^{13}C\{^{1}H\}$ NMR (C_6D_6, 125.7 MHz, 293 K): δ 152.3 (*i*-NC_6H_5), 123.0 (*o*-NC_6H_5), 121.8 (*m*-NC_6H_5), 119.7 (*p*-NC_6H_5), 117.3 ($\underline{C}_5Me_5$), 11.9 ($C_5\underline{Me}_5$), 11.3 (Me). IR (NaCl plates, Nujol mull, cm^{-1}): 3241 (s, NH), 1586 (s, br.), 1489 (s, br.), 1296 (m), 1271 (m, br.), 1167 (w), 1149 (w), 1128 (w), 1091 (w), 1063 (m), 1024 (m, br.), 993 (m), 957 (w), 912 (m), 883 (m), 834 (w), 822 (w), 801 (w), 772 (s), 751 (s), 733 (s), 695 (s), 665 (m), 636 (s), 619 (m), 608 (m), 533 (m, br.). EI-MS: *m/z* = 542 [*M* – Me]$^+$ (80 %), 359 [Cp*$_2$Zr]$^+$ (100 %). Anal. found (calcd. for $C_{33}H_{44}N_2Zr$): C, 70.7 (70.8); H, 7.7 (7.9); N, 4.9 (5.0) %.

5.7.3 Cp*$_2$Zr{N(H)N(Ph)-1,2-C_6H_4} (**52**). A Teflon valve ampoule containing a solution of Cp*$_2$Zr(NHNPh$_2$)(Me) (**51**, 0.338 g, 0.605 mmol) in C_6H_6 (2 mL) was partially evacuated and heated to 110 °C for 5 d. During this time the dark red/brown solution lightened slightly. After cooling to RT, volatiles were removed under reduced pressure, the resulting brick red solid washed with pentane (3 × 3 mL) and dried *in vacuo* to yield **52**. Yield: 0.278 g (73 %). Diffraction-quality crystals were grown by slow cooling of a saturated benzene solution from 60 ºC to RT.

^{1}H NMR (C_6D_6, 499.9 MHz, 293 K): δ 7.55 (2 H, d, ^{3}J = 5 Hz, *o*-NC_6H_5), 7.40 (1 H, d, ^{3}J = 5 Hz, 3- or 6-NC_6H_4), 7.26 (2 H, app. t, app. ^{3}J = 5 Hz, *m*-NC_6H_5), 6.99 and 6.89 (2 × 1 H, 2 × app. t, app. ^{3}J = 5 Hz, 4- and 5-NC_6H_4), 6.85 (2 H, overlapping *p*-NC_6H_5 and 3- or 6-NC_6H_4), 4.49 (1 H, br. s, NH), 1.70 (30 H, C_5Me_5). $^{13}C\{^{1}H\}$ NMR (C_6D_6, 125.7 MHz, 293 K): δ 176.6 and 167.1 (1- and 2-NC_6H_4), 148.3 (*i*-NC_6H_5), 136.6 and 124.8 (4- and 5-NC_6H_4), 128.8 (*m*-NC_6H_5), 119.6 and 112.3 (3- and 6-NC_6H_4), 119.1 ($\underline{C}_5Me_5$), 119.0 (*p*-NC_6H_5), 118.1 (*o*-NC_6H_5), 11.4 ($C_5\underline{Me}_5$). IR (NaCl plates, Nujol mull, cm^{-1}): 3440 (m, NH), 1589 (m), 1573 (m), 1556 (m, br.), 1437 (s), 1419 (m), 1399 (w), 1395 (w), 1306 (s), 1262 (m), 1246 (m), 1197 (w), 1156 (w), 1080 (w, br.), 992 (w), 879 (w), 800 (m, br.), 761 (m), 746 (m), 718 (m, br.), 694 (m), 636 (w). EI-MS: *m/z* = 542 [*M*]$^+$ (2 %), 359 [Cp*$_2$Zr]$^+$ (10 %), 169 [PhNC$_6$H$_4$]$^+$ (15 %). Anal. found (calcd. for $C_{32}H_{40}N_2Zr$): C, 70.6 (70.7); H, 7.6 (7.4); N, 5.0 (5.2) %.

5.7.4 Cp$^{Me_4}{}_2$Zr(Np)Cl (**53**). This is a modification of the synthesis of Cp*$_2$Zr(Np)Cl.[33,34] To a suspension of Cp$^{Me_4}{}_2$ZrCl$_2$ (2.471 g, 6.12 mmol) in a 1:1 mixture of Et$_2$O and toluene (20 mL) was added slowly, at RT, LiNp (11.7 mL, 7.02 mmol, 0.6 M in toluene/cyclohexane) with vigorous stirring. The milky suspension

was left stirring for 16 h during which time it became a bright yellow suspension. Volatiles were removed under reduced pressure and the resulting solid extracted into hexanes (3 × 10 mL) and dried *in vacuo* to yield **53** as a yellow powder. Yield: 2.041 g (76 %). Diffraction-quality crystals were grown from a saturated hexanes solution at RT.

^{1}H NMR (C_6D_6, 499.9 MHz, 293 K): δ 5.43 (2 H, s, $C_5Me_4\underline{H}$), 1.95, 1.89, 1.71 and 1.69 (4 × 6 H, 4 × s, 1-, 2-, 3- and 4-$C_5\underline{Me}_4H$), 1.23 (9 H, s, $CH_2C\underline{Me}_3$), 0.65 (2 H, s, $C\underline{H}_2CMe_3$). ^{13}C{^{1}H} NMR (C_6D_6, 125.7 MHz, 293 K): δ 125.1, 124.5, 119.7 and 117.4 (1-, 2-, 3- and 4-$\underline{C}_5Me_4H$), 110.6 (5-$\underline{C}_5Me_4H$), 62.0 ($\underline{C}H_2CMe_3$), 36.0 ($CH_2\underline{C}Me_3$), 35.4 ($CH_2C\underline{Me}_3$), 13.4, 12.6 and 12.4 (1-, 2-, 3- and 4-$C_5\underline{Me}_4H$). IR (NaCl plates, Nujol mull, cm^{-1}): 1596 (w), 1462 (s, br.), 1419 (m), 1399 (m), 1357 (s), 1331 (m), 1262 (m), 1225 (m), 1204 (m), 1148 (m), 1093 (m, br.), 1021 (s), 1002 (m), 975 (m), 921 (m), 899 (m), 859 (m), 833 (s), 736 (m), 699 (w). EI-MS: *m/z* = 367 [*M* – $CH_2{}^{t}Bu$]$^{+}$ (100 %). A satisfactory elemental analysis could not be obtained.

5.7.5 $Cp^{Me4}{}_2Zr(Np)(Me)$ (**54**). To a yellow solution of $Cp^{Me4}{}_2Zr(Np)Cl$ (**53**, 1.186 g, 2.70 mmol) in THF (10 mL) was added MeMgCl (5.1 mL, 8.10 mmol, 1.6 M in Et_2O) dropwise over 10 mins with vigorous stirring and the resulting suspension left at RT for 16 h. Volatiles were removed under reduced pressure and the residue extracted into hexanes (3 × 5 mL) and dried under reduced pressure. The resulting yellow solid was extracted into cold pentane (2 × 5 mL, -40 °C) and dried *in vacuo* to yield **54** as a yellow powder. Yield: 0.734 g (66 %).

^{1}H NMR (C_6D_6, 499.9 MHz, 293 K): δ 5.27 (2 H, s, $C_5Me_4\underline{H}$), 1.86, 1.81 and 1.61 (12 H and 2 × 6 H, 3 × s, 1-, 2-, 3- and 4-$C_5\underline{Me}_4H$), 1.12 (9 H, s, $CH_2C\underline{Me}_3$), 0.15 (2 H, s, $C\underline{H}_2CMe_3$), -0.42 (3 H, s, Me). ^{13}C{^{1}H} NMR (C_6D_6, 125.7 MHz, 293 K): δ 121.4, 121.1, 117.7 and 115.7 (1-, 2-, 3- and 4-$\underline{C}_5Me_4H$), 107.7 (5-$\underline{C}_5Me_4H$), 64.6 ($\underline{C}H_2CMe_3$), 40.5 (Me), 35.9 ($CH_2C\underline{Me}_3$), 35.5 ($CH_2\underline{C}Me_3$), 13.2, 13.0 and 12.1 (1-, 2-, 3- and 4-$C_5\underline{Me}_4H$). IR (NaCl plates, Nujol mull, cm^{-1}): 1640 (m), 1624 (w), 1595 (m), 1559 (m), 1554 (m), 1503 (m), 1469 (s, br.), 1380 (s, br.), 1355 (s), 1333 (s), 1263 (m), 1250 (m), 1226 (s), 1204 (s), 1177 (m), 1149 (m), 1118 (s), 1024 (s, br.), 976 (m), 935 (m), 922 (m), 900 (m), 826 (s, br.), 738 (m, br.), 617 (m, br.). EI-MS: *m/z* = 419 [*M*]$^{+}$ (20 %), 348 [*M* – Np]$^{+}$ (100 %). A satisfactory elemental analysis could not be obtained.

5.7.6 $Cp^{Me4}{}_2Zr(NHNPh_2)Cl$ (**55**). In a Teflon valve ampoule, to a mixture of $Cp^{Me4}{}_2Zr(Np)Cl$ (**51**, 0.890 g, 2.03 mmol) and H_2NNPh_2 (0.373 g, 2.03 mmol) was added toluene (10 mL). The ampoule was partially evacuated, sealed and the yellow solution heated to 140 °C for 48 h. After cooling to RT volatiles were removed under reduced pressure leaving a dark brown oily residue. The residues were extracted into hexanes (3 × 5 mL) and the solvent removed under reduced pressure leaving a brown powder, which was dissolved in pentane (3 × 5 mL). The volume was reduced by half and after 3 h yellow crystals formed below the brown solution. The supernatant was decanted and the crystals dried *in vacuo* affording **55** as an orange powder. Yield: 0.439 g (39 %). Diffraction-quality crystals were grown by slow cooling of a saturated toluene solution from 140 ºC to RT.

^{1}H NMR (C_6D_6, 499.9 MHz, 293 K): δ 7.35 (4 H, d, ^{3}J = 5 Hz, *o*-NC_6H_5), 7.23 (4 H, app. t, app. ^{3}J = 5 Hz, *m*-NC_6H_5), 6.86 (2 H, t, ^{3}J = 5 Hz, *p*-NC_6H_5), 6.41 (2 H, s, $C_5Me_4\underline{H}$), 5.56 (1 H, br. s, NH), 1.86 (12 H, s, 2- and 3-$C_5\underline{Me}_4H$), 1.78 and 1.61 (2 × 6 H, 2 × br. s, 1- and 4-$C_5\underline{Me}_4H$). $^{13}C\{^1H\}$ NMR (C_6D_6, 125.7 MHz, 293 K): δ 152.9 (*i*-NC_6H_5), 128.9 (*o*-NC_6H_5), 128.4 (*m*-NC_6H_5), 121.6 (*p*-NC_6H_5), 120.4 (br. 1-, 2-, 3- and 4-$\underline{C}_5Me_4H$), 115.1 (br. 5-$\underline{C}_5Me_4H$), 13.1 (2- and 3- $C_5\underline{Me}_4H$), 12.9 and 11.0 (1- and 4-$C_5\underline{Me}_4H$). IR (NaCl plates, Nujol mull, cm^{-1}): 3275 (s, NH), 1600 (s), 1586 (s), 1540 (w), 1485 (s, br.), 1295 (m, br.), 1273 (m, br.), 1172 (m), 1153 (m), 1113 (w), 1093 (m), 1076 (m), 1063 (m), 1024 (s), 990 (m), 964 (m), 938 (w), 913 (m), 879 (s), 840 (s, br.), 762 (s), 749 (s), 733 (s), 702 (m), 693 (m), 639 (m), 618 (m), 611 (m). EI-MS: *m/z* = 550 $[M]^+$ (5 %), 367 $[M - NHNPh_2]^+$ (100 %). Anal. found (calcd. for $C_{30}H_{37}ClN_2Zr$): C, 65.0 (65.2); H, 6.7 (6.8); N, 5.1 (5.0) %.

5.8 X-ray data collection and processing parameters

Crystal data collection and processing parameters are given in Tables 5.1 to 5.5. Crystals were mounted on glass fibres using perfluoropolyether oil and cooled rapidly in a stream of cold N_2 using an Oxford Cryosystems Cryostream unit. Diffraction data were measured using an Enraf-Nonius KappaCCD diffractometer. As appropriate, absorption and decay corrections were applied to the data and equivalent reflections merged.[35] The structures were solved by direct methods (SIR92[36]) and further refinements and all other crystallographic calculations were performed using the CRYSTALS program suite.[37] Other details of the structure solution and refinements

are given in the Supporting Information (CIF data – see CD Appendix). A full listing of atomic coordinates, bond lengths and angles and displacement parameters for all the structures have been deposited at the Cambridge Crystallographic Data Centre. See Notice to Authors, Issue No. 1.

Table 5.1. X-Ray data collection and processing parameters for Chapter Two: $Ti(N_2N^{py})\{N(NPh_2)C(Me)C(C_6F_5)\}$ (**1**), $[Ti(N_2N^{Me})\{NCC(Me)NPh_2\}(py)]_2(\mu\text{-}2,3,5,6\text{-}C_6F_4)$ (**10**) and $Ti(N_2N^{Me})(NNPh_2)(bipy)$ (**14**).

compound	**1**	**10•2(C_6H_6)**	**14**
empirical formula	$C_{36}H_{42}F_5N_5Si_2Ti$	$C_{78}H_{100}F_4N_{14}Si_4Ti_2 \cdot 2(C_6H_6)$	$C_{33}H_{47}N_7Si_2Ti$
fw	743.83	1674.11	645.86
temp / K	150	150	150
wavelength / Å	0.71073	0.71073	0.71073
space group	$P\ \bar{1}$	$P\ 2_1/c$	$P\ 2_1/c$
a / Å	14.7234(2)	10.76610(10)	10.9272(2)
b / Å	16.5773(2)	25.1842(3)	18.3875(4)
c / Å	20.6285(3)	16.8160(3)	17.9123(4)
α / deg	103.8462(4)	90	90
β / deg	94.6175(5)	98.4518(6)	92.9509(11)
γ / deg	115.8704(5)	90	90
V / $Å^3$	4298.99(10)	4509.90(11)	3594.24(13)
Z	4	2	4
d (calcd) / $Mg \cdot m^{-3}$	1.149	1.233	1.193
abs coeff / mm^{-1}	0.305	0.290	0.337
R indices:[a] R_1 =	0.0449	0.0497	0.0538
R_w =	0.0460	0.0559	0.0551

[a] $R_1 = \Sigma||F_o|-|F_c|| / \Sigma|F_o|$; $R_w = \sqrt{\{\Sigma w(|F_o|-|F_c|)^2 / \Sigma w|F_o|^2\}}$ for data with $I > 3\sigma(I)$.

Table 5.2. X-Ray data collection and processing parameters for Chapter Three: Ti(N_2N^{Me}){NC(Ar^{F_2})$NNPh_2$}(py) (**17**), Ti(N_2N^{Me}){NC(Ar^{F_5})$NNPh_2$)}(py) (**18**), *trans*-Ti(N_2N^{Me})(NCNXyl)(NPh_2) (**20**), Ti(N_2N^{Me}){N(NPh_2)C(NAr′)O}(py) (**21**), Ti(N_2N^{Me}){N(NPh_2)C(NAr′)S} (**22**) and Ti(N_2N^{Me}){N(NPh_2)C(NAr′)Se} (**23**).

compound	**17**	**18**	**20**	**21**
empirical formula	$C_{35}H_{47}F_2N_7Si_2Ti$	$C_{35}H_{44}F_5N_7Si_2Ti$	$C_{32}H_{48}N_6Si_2Ti$	$C_{48}H_{69}N_7OSi_2Ti$
fw	707.87	761.84	620.85	864.19
temp / K	150	150	150	150
wavelength / Å	0.71073	0.71073	0.71073	0.71073
space group	*P* $2_1/n$	*P* $2_1/n$	*P* $2_1/c$	*P* $2_1/c$
a / Å	13.22900(10)	13.7067(2)	10.38770(10)	21.0764(2)
b / Å	18.1467(2)	18.2074(2)	21.6084(3)	11.44970(10)
c / Å	15.1822(2)	15.3084(2)	15.2834(2)	21.4804(2)
α / deg	90	90	90	90
β / deg	94.3665(4)	93.8645(6)	95.2404(5)	109.4941(4)
γ / deg	90	90	90	90
V / $Å^3$	3634.10(7)	3811.73(9)	3416.20(7)	4886.47(8)
Z	4	4	4	4
d (calcd) / $Mg·m^{-3}$	1.294	1.327	1.207	1.175
abs coeff / mm^{-1}	0.347	0.347	0.351	0.266
R indices:[a] R_1 =	0.0308	0.0329	0.0736	0.0539
R_w =	0.0312	0.0355	0.0782	0.0573

[a] $R_1 = \Sigma||F_o|-|F_c|| / \Sigma|F_o|$; $R_w = \sqrt{\{\Sigma w(|F_o|-|F_c|)^2 / \Sigma w|F_o|^2\}}$ for data with $I > 3\sigma(I)$.

Table 5.2. (Contd.)

compound		**22**	**23**
empirical formula		$C_{36}H_{56}N_6SSi_2Ti$	$C_{36}H_{56}N_6SeSi_2Ti$
fw		709.02	755.91
temp / K		150	150
wavelength / Å		0.71073	0.71073
space group		$P\ \bar{1}$	$P\ \bar{1}$
a / Å		11.1521(3)	11.1457(2)
b / Å		12.4944(4)	12.5497(2)
c / Å		15.0464(5)	15.1306(3)
α / deg		97.9703(12)	98.1633(8)
β / deg		101.4914(13)	101.7160(9)
γ / deg		107.1657(15)	107.5843(9)
V / Å^3		1918.85(11)	1928.03(6)
Z		2	2
d (calcd) / Mg·m^{-3}		1.227	1.302
abs coeff / mm^{-1}		0.373	1.261
R indices:[a]	R_1 =	0.0446	0.0321
	R_w =	0.0334	0.0390

[a] $R_1 = \Sigma||F_o|-|F_c|| / \Sigma|F_o|$; $R_w = \sqrt{\{\Sigma w(|F_o|-|F_c|)^2 / \Sigma w|F_o|^2\}}$ for data with I > 3σ(I).

Table 5.3. X-Ray data collection and processing parameters for Chapter Four: Ti(HN_2N^{Me}){N($SiMe_3$)C(Me)C(Fc)-1,2-C_6H_4N(Ph)} (**24**), $Cp_2Hf(NNPh_2)$(DMAP) (**28**), $Cp_2Ti(NNPh_2)$(DMAP) (**4.2**), $Cp^{Me}{}_2Zr(NNPh_2)$(DMAP) (**29**), Cp_2Zr{N(H)C(Me)C(Me)-1,2-C_6H_4N(Ph)} (**32**), Cp_2Hf{N(H)C(Me)C(Me)-1,2-C_6H_4N(Ph)} (**33**), Cp_2Hf{N(H)C(Ph)C(Ph)-1,2-C_6H_4N(Ph)} (**36**), Cp_2Zr{N(NPh_2)C(NAr′)O}(DMAP) (**41**), Cp_2Hf{N(NPh_2)C(NAr′)O}(DMAP) (**42**) and Cp_2Zr{NHC(Me)C($SiMe_3$)-1,2-C_6H_4N(Ph)} (**44**).

compound	**24**	**28•3(C_6H_6)**	**4.2•0.5(C_6H_6)**	**29**
empirical formula	$C_{36}H_{51}FeN_5Si_2Ti$	$C_{29}H_{30}HfN_4 \cdot 3(C_6H_6)$	$C_{29}H_{30}N_4Ti \cdot 0.5(C_6H_6)$	$C_{31}H_{34}N_4Zr$
fw	713.75	847.41	521.54	553.86
temp / K	150	150	150	230
wavelength / Å	0.71073	0.71073	0.71073	0.71073
space group	$P\ \bar{1}$	$P\ 2_1$	$C\ 2/c$	$P\ 2_1/n$
a / Å	10.28040(10)	10.20000(10)	31.5314(3)	14.17720(10)
b / Å	10.75170(10)	34.0677(3)	10.6174(2)	12.12100(10)
c / Å	18.0571(2)	11.66010(10)	20.2357(3)	16.1618(2)
α / deg	83.1330(4)	90	90	90
β / deg	73.7263(4)	99.5562(4)	127.2564(5)	101.2968(5)
γ / deg	70.2973(6)	90	90	90
V / $Å^3$	1803.05(3)	3995.55(6)	5392.09(14)	2723.47(5)
Z	2	4	8	4
d (calcd) / $Mg \cdot m^{-3}$	1.315	1.409	1.285	1.351
abs coeff / mm^{-1}	0.723	2.648	0.345	0.430
R indices:[a] R_1 =	0.0310	0.0324	0.0398	0.0394
R_w =	0.0413	0.0298	0.0453	0.0469

[a] $R_1 = \Sigma||F_o|-|F_c|| / \Sigma|F_o|$; $R_w = \sqrt{\{\Sigma w(|F_o|-|F_c|)^2 / \Sigma w|F_o|^2\}}$ for data with $I > 3\sigma(I)$.

Table 5.3. (Contd.)

compound	**32**	**33**	**36**	**41•0.5(C_6H_6)**
empirical formula	$C_{26}H_{26}N_2Zr$	$C_{26}H_{26}HfN_2$	$C_{36}H_{30}HfN_2$	$C_{42}H_{47}N_5OZr\cdot0.5(C_6H_6)$
fw	457.73	545.00	669.14	768.15
temp / K	150	150	150	150
wavelength / Å	0.71073	0.71073	0.71073	0.71073
space group	*P* $2_1/n$	*P* $2_1/n$	*R* $\bar{3}$	*C* 2/*c*
a / Å	11.8798(2)	10.81030(10)	39.640(6)	15.29560(10)
b / Å	10.5544(2)	9.79430(10)	39.640(6)	19.2103(2)
c / Å	16.7884(3)	20.6205(3)	9.5400(19)	26.6498(3)
α / deg	90	90	90	90
β / deg	95.1915(7)	104.7493(6)	90	100.1055(5)
γ / deg	90	90	120	90
V / $Å^3$	2096.36(7)	2111.34(4)	12982(4)	7709.11(13)
Z	4	4	18	8
d (calcd) / $Mg\cdot m^{-3}$	1.450	1.714	1.541	1.324
abs coeff / mm^{-1}	0.539	4.955	3.643	0.327
R indices:[a] R_1 =	0.0307	0.0313	0.0466	0.0390
R_w =	0.0376	0.0291	0.0468	0.0455

[a] $R_1 = \Sigma||F_o|-|F_c|| / \Sigma|F_o|$; $R_w = \sqrt{\{\Sigma w(|F_o|-|F_c|)^2 / \Sigma w|F_o|^2\}}$ for data with $I > 3\sigma(I)$.

Table 5.3. (Contd.)

compound	**42•0.5(C_6H_6)**	**44**
empirical formula	$C_{42}H_{47}HfN_5O{\cdot}0.5(C_6H_6)$	$C_{28}H_{32}N_2SiZr$
fw	855.41	515.88
temp / K	150	150
wavelength / Å	0.71073	0.71073
space group	*C* 2/*c*	*P* 2_1
a / Å	15.25730(10)	11.3604(3)
b / Å	19.1917(2)	10.5147(4)
c / Å	26.6090(3)	11.7902(4)
α / deg	90	90
β / deg	100.0001(5)	118.007(2)
γ / deg	90	90
V / $Å^3$	7673.10(13)	1243.42(8)
Z	8	2
d (calcd) / $Mg{\cdot}m^{-3}$	1.481	1.378
abs coeff / mm^{-1}	2.761	0.508
R indices:[a] R_1 =	0.0376	0.0694
R_w =	0.0384	0.0731

[a] $R_1 = \Sigma||F_o|-|F_c|| / \Sigma|F_o|$; $R_w = \sqrt{\{\Sigma w(|F_o|-|F_c|)^2 / \Sigma w|F_o|^2\}}$ for data with $I > 3\sigma(I)$.

Table 5.4. X-Ray data collection and processing parameters for Appendices A, B and C: Ti(N_2N^{Me}){NC(4-C_6H_4F)C(Me)NPh_2}(py) (**5**), Ti(N_2N^{Me}){NC(C_6F_5)C(Me)NPh_2}(py) (**8**), MeCC(1,4-C_6F_4)CCMe (**9**), Ti(N_2N^{Me})(N^tBu)(py) (**47**), Ti(N_2N^{Me}){N(H)C(Ph)C(Ph)NPh_2}$_2$ (**25a′**) and $Cp_2Zr\{NNMe_2\}_2$ (**31**).

compound	**5**	**8**	**9**	**47**
empirical formula	$C_{37}H_{51}FN_6Si_2Ti$	$C_{37}H_{47}F_5N_6Si_2Ti$	$C_{12}H_6F_4$	$C_{20}H_{43}N_5Si_2Ti$
fw	651.52	645.86	226.17	457.67
temp / K	150	150	150	150
wavelength / Å	0.71073	0.71073	0.71073	0.71073
space group	$P\ \bar{1}$	$P\ 2_1\ 2_1\ 2_1$	$P\ \bar{1}$	$P\ 2_1/c$
a / Å	9.9426(3)	9.9603(10)	5.0929(2)	9.91240(10)
b / Å	19.9970(6)	19.677(2)	7.3053(3)	20.6288(3)
c / Å	19.8514(7)	40.600(5)	7.6069(4)	13.6419(2)
α / deg	75.4937(13)	90	108.7974(19)	90
β / deg	89.3550(14)	90	98.662(2)	101.9308(6)
γ / deg	89.6810(14)	90	108.823(2)	90
V / $Å^3$	3820.8(2)	7957.3(15)	243.14(2)	2729.25(6)
Z	2	4	1	4
d (calcd) / $Mg\cdot m^{-3}$	1.133	1.214	1.545	1.114
abs coeff / mm^{-1}	0.322	0.330	0.143	0.415
R indices:[a] R_1 =	0.1290	0.1393	0.0519	0.0441
R_w =	0.1605	0.1574	0.0609	0.0448

[a] $R_1 = \Sigma||F_o|-|F_c|| / \Sigma|F_o|$; $R_w = \sqrt{\{\Sigma w(|F_o|-|F_c|)^2 / \Sigma w|F_o|^2\}}$ for data with $I > 3\sigma(I)$.

Table 5.4. (Contd.)

compound		**25a′**	**31**
empirical formula		$C_{63}H_{71}N_7Si_2Ti$	$C_{24}H_{32}N_4Zr_2$
fw		1030.38	558.98
temp / K		150	150
wavelength / Å		0.71073	0.71073
space group		*P* 2_1	*P n*
a / Å		15.308(3)	8.6813(17)
b / Å		20.095(4)	16.742(3)
c / Å		18.485(4)	15.710(3)
α / deg		90	90
β / deg		90.14(3)	104.40(3)
γ / deg		90	90
V / $Å^3$		5686.2(20)	2211.6(8)
Z		8	8
d (calcd) / $Mg \cdot m^{-3}$		1.204	1.679
abs coeff / mm^{-1}		0.238	0.961
R indices:[a]	R_1 =	0.0632	0.1253
	R_w =	0.0716	0.1240

[a] $R_1 = \Sigma||F_o|-|F_c|| / \Sigma|F_o|$; $R_w = \sqrt{\{\Sigma w(|F_o|-|F_c|)^2 / \Sigma w|F_o|^2\}}$ for data with $I > 3\sigma(I)$.

Table 5.5. X-Ray data collection and processing parameters for Appendix D: $Cp^*_2Zr(NNPh_2)(DMAP)$ (**48**), $Cp^*_2Zr(NNPh_2)(py)$ (**49**), $Cp^*_2Zr(NHNPh_2)_2$ (**50**), $Cp^*_2Zr(NHNPh_2)(Me)$ (**51**), $Cp^*_2Zr\{N(H)N(Ph)\text{-}1,2\text{-}C_6H_4\}$ (**52**), $Cp^{Me_4}{}_2Zr(Np)Cl$ (**53**) and $Cp^{Me_4}{}_2Zr(NHNPh_2)Cl$ (**55**).

compound		**48**	**49**	**50**	**51**
empirical formula		$C_{39}H_{50}N_4Zr$	$C_{37}H_{45}N_3Zr$	$C_{44}H_{52}N_4Zr$	$C_{33}H_{44}N_2Zr$
fw		666.07	623.00	728.14	559.95
temp / K		150	150	150	150
wavelength / Å		0.71073	0.71073	0.71073	0.71073
space group		*P* $2_1/n$	*P* $2_1/c$	*P* $2_1/c$	*P* $2_1/c$
a / Å		10.0801(10)	9.75920(10)	11.98760(10)	15.6350(2)
b / Å		40.857(3)	16.7984(2)	16.7815(2)	11.2674(1)
c / Å		17.1623(9)	19.5356(2)	18.5396(2)	16.7339(2)
α / deg		90	90	90	90
β / deg		99.739(7)	93.6713(4)	100.6515(6)	101.468(1)
γ / deg		90	90	90	90
V / $Å^3$		6966.2(10)	3196.07(6)	3665.35(7)	2889.09(6)
Z		8	4	4	4
d (calcd) / $Mg \cdot m^{-3}$		1.270	1.295	1.319	1.287
abs coeff / mm^{-1}		2.817	0.373	0.337	0. 404
R indices:[a]	R_1 =	0.0791	0.0343	0.0425	0.0492
	R_w =	0.0110	0.0387	0.0393	0.0595

[a] $R_1 = \Sigma||F_o|-|F_c|| / \Sigma|F_o|$; $R_w = \sqrt{\{\Sigma w(|F_o|-|F_c|)^2 / \Sigma w|F_o|^2\}}$ for data with $I > 3\sigma(I)$.

Table 5.5. (Contd.)

compound	**52**	**53**	**55**
empirical formula	$C_{32}H_{40}N_2Zr$	$C_{23}H_{37}ClZr$	$C_{30}H_{37}N_2ClZr$
fw	543.90	440.22	552.31
temp / K	150	150	150
wavelength / Å	0.71073	0.71073	.71073
space group	$P\,2_1\,2_1\,2_1$	$P\,\bar{1}$	$P\,2_1/n$
a / Å	9.0133(2)	9.2762(2)	12.1698(2)
b / Å	16.8977(5)	16.3800(3)	17.0010(3)
c / Å	17.3808(5)	16.7411(3)	12.9710(3)
α / deg	90	63.2818(10)	90
β / deg	90	77.7229(8)	95.4810(8)
γ / deg	90	85.6135(7)	90
V / Å^3	2647.17(12)	2219.62(8)	2671.41(9)
Z	4	4	4
d (calcd) / Mg·m^{-3}	1.365	1.317	1.373
abs coeff / mm^{-1}	0.439	0.619	0.532
R indices:[a] R_1 =	0.0444	0.0478	0.0623
R_w =	0.041	0.0556	0.0721

[a] $R_1 = \Sigma||F_o|-|F_c|| / \Sigma|F_o|$; $R_w = \sqrt{\{\Sigma w(|F_o|-|F_c|)^2 / \Sigma w|F_o|^2\}}$ for data with $I > 3\sigma(I)$.

5.9 References

1. Pangborn, A. B.; Giardello, M. A.; Grubbs, R. H.; Rosen, R. K.; Timmers, F. J.; *Organometallics* **1996**, *15*, 1518.
2. Galka, C. H.; Trösch, D. J. M.; Schubart, M.; Gade, L. H.; Radojevic, S.; Scowen, I. J.; McPartlin, M.; *Eur. J. Inorg. Chem.* **2000**, 2577.
3. Whannel, R. A.; *D. Phil. Thesis* **2006**, *University of Oxford*
4. Selby, J. D.; Manley, C. D.; Schwarz, A. D.; Clot, E.; Mountford, P.; *Organometallics* **2008**, *27*, 6479.
5. Selby, J. D.; Manley, C. D.; Feliz, M.; Schwarz, A. D.; Clot, E.; Mountford, P.; *Chem. Commun.* **2007**, 4937.
6. Selby, J. D.; Schulten, C.; Schwarz, A. D.; Stasch, A.; Clot, E.; Jones, C.; Mountford, P.; *Chem.Commun.* **2008**, 5101.
7. Selby, J. D.; Feliz, M.; Schwarz, A. D.; Clot, E.; Mountford, P.; *Organometallics* **2011**, *30*, 2295.
8. Quiroga Norambuena, V. F.; Heeres, A.; Heeres, H. J.; Meetsma, A.; Teuben, J. H.; Hessen, B.; *Organometallics* **2008**, *27*, 5672.
9. Weiss, H. M.; Touchette, K. M.; Angell, S.; Khan, J.; *Org. Bio. Chem.* **2003**, *1*, 2152.
10. Bayatyan, R.; Bayatyan, B.; Saakyan, L.; *Russ. J. Appl. Chem.* **2006**, *79*, 1849.
11. Gastinger, R. G.; Tokas, E. F.; Rausch, M. D.; *J. Org. Chem.* **1978**, *43*, 159.
12. Thomas, R. L.; Souza, F. E. S.; Marder, T. B.; *J. Chem. Soc., Dalton Trans.* **2001**, 1650.
13. Mio, M. J.; Kopel, L. C.; Braun, J. B.; Gadzikwa, T. L.; Hull, K. L.; Brisbois, R. G.; Markworth, C. J.; Grieco, P. A.; *Org. Lett.* **2002**, *4*, 3199.
14. Zora, M.; Acikgoz, C.; Tumay, T. A.; Odabasoglu, M.; Buyukgungor, O.; *Acta Crystallogr., Sect. C: Cryst. Struct. Commun.* **2006**, *62*, m327.
15. Doisneau, G.; Balavoine, G.; Fillebeen-Khan, T.; *J. Organomet. Chem.* **1992**, *425*, 113.
16. Polin, J.; Schottenberger, H.; *Org. Synth.* **1996**, *73*, 262.
17. Panda, T. K.; Gamer, M. T.; Roesky, P. W.; *Organometallics* **2003**, *22*, 877.
18. Jana, R.; Kumar, M. S.; Singh, N.; Elias, A. J.; *J. Organomet. Chem.* **2008**, *693*, 3780.

19. Fendrick, C. M.; Schertz, L. D.; Day, V. W.; Marks, T. J.; *Organometallics* **1988**, *8*, 1828.
20. Robbins, J. L.; Edelstein, N. M.; Cooper, S. R.; Smart, J. C.; *J. Am. Chem. Soc.* **1979**, *101*, 3853.
21. Fendrick, C. M.; Schertz, L. D.; Mintz, E. A.; Marks, T. J.; Bitterwolf, T. E.; Horine, P. A.; Hubler, T. L.; Sheldon, J. A.; Belin, D. D.; *Inorg. Synth.* **1992**, *29*, 193.
22. Stone, F. G. A.; *Rev. Pure Appl. Chem.* **1967**, *17*, 41.
23. Manriquez, J. M.; McAlister, D. R.; Rosenberg, E.; Shiller, A. M.; Williamson, K. L.; Chan, S. I.; Bercaw, J. E.; *J. Am. Chem. Soc.* **1978**, *100*, 3078.
24. Hiller, J.; Thewalt, U.; Polášek, M.; Petrusová, L.; Varga, V.; Sedmera, P.; Mach, K.; *Organometallics* **1996**, *15*, 3752.
25. Courtot, P.; Pichon, R.; Salaun, J. Y.; Toupet, L.; *Can. J. Chem.* **1991**, *69*, 661.
26. Miller, F. D.; Sanner, R. D.; *Organometallics* **1988**, *7*, 818.
27. Chiu, M.; Hoyt, H. M.; Michael, F. E.; Bergman, R. G.; van Halbeek, H.; *Angew. Chem. Int. Ed.* **2008**, *47*, 6073.
28. Carr, D. B.; Schwartz, J.; *J. Am. Chem. Soc.* **1979**, *101*, 3521.
29. Buchwald, S. L.; LaMaire, S. J.; Nielsen, R. B.; Watson, B. T.; King, S. M.; *Tet. Letts.* **1987**, *28*, 3895.
30. Walsh, P. J.; Carney, M. J.; Bergman, R. G.; *J. Am. Chem. Soc.* **1991**, *113*, 6343.
31. Krishnamurthy, S.; *Tetrahedron* **1982**, *23*, 3315.
32. Barton, D. H. R.; Parekh, S. I.; Tajbakhsh, M.; Theodorakis, E. A.; Tse, C.-L.; *Tetrahedron* **1994**, *50*, 639.
33. Moore, E. J.; Straus, D. A.; Armantrout, J.; Santarsiero, B. D.; Grubbs, R. H.; Bercaw, J. E.; *J. Am. Chem. Soc.* **1983**, *105*, 2068.
34. Fandos, R.; Meetsma, A.; Teuben, J. H.; *Organometallics* **1991**, *10*, 59.
35. Otwinowski, Z.; Minor, W.; *Processing of X-ray Diffraction Data Collected in Oscillation Mode*; Academic press: New York, 1997.
36. Altomare, A.; Cascarano, G.; Giacovazzo, G.; Guagliardi, A.; Burla, M. C.; Polidori, G.; Camalli, M.; *J. Appl. Crystallogr.* **1994**, *27*, 435.
37. Betteridge, P. W.; Cooper, J. R.; Cooper, R. I.; Prout, K.; Watkin, D. J.; *J. Appl. Cryst.* **2003**, *36*, 1487.

Appendices

Appendix A - Crystal structures of Ti(N_2N^{Me}){NC(4-C_6H_4F)C(Me)NPh_2}(py) (5), Ti(N_2N^{Me}){NC(C_6F_5)C(Me)NPh_2}(py) (8) and MeCC(1,4-C_6F_4)CCMe (9)

Ti(N_2N^{Me}){NC(4-C_6H_4F)C(Me)NPh_2}(py) (**5**) and Ti(N_2N^{Me}){NC(C_6F_5)C(Me)NPh_2}(py) (**8**) were synthesised as described in Chapter Two. Diffraction-quality crystals were grown from saturated pentane solutions at -30 ºC. However, in both cases they were found to be poor diffractors. The connectivity of the structures could still be ascertained and both compounds were refined isotropically. The structure of Ti(N_2N^{Me}){NC(4-C_6H_4F)C(Me)NPh_2}(py) (**5**) is presented in Figure 1 and Ti(N_2N^{Me}){NC(C_6F_5)C(Me)NPh_2}(py) (**8**) in Figure 2.

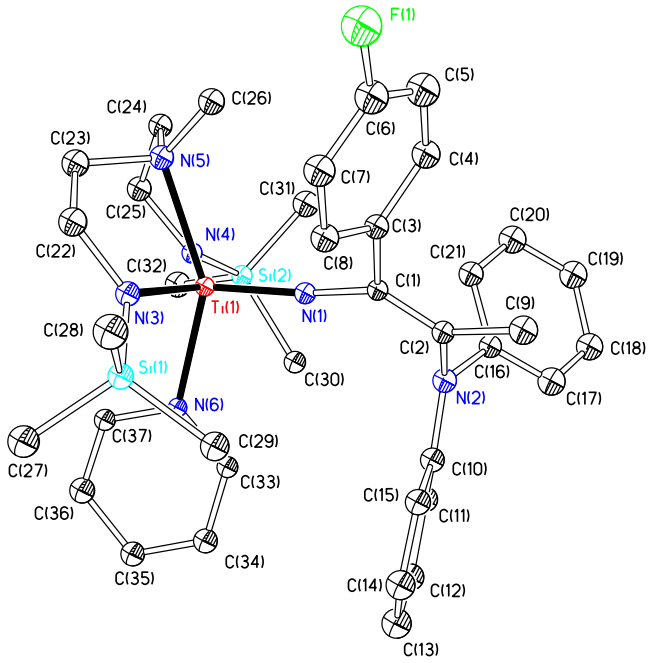

Figure 1. Displacement ellipsoid plot (20 % probability) of Ti(N_2N^{Me}){NC(4-C_6H_4F)C(Me)NPh_2}(py) (**5**) establishing overall connectivity. H atoms were not refined.

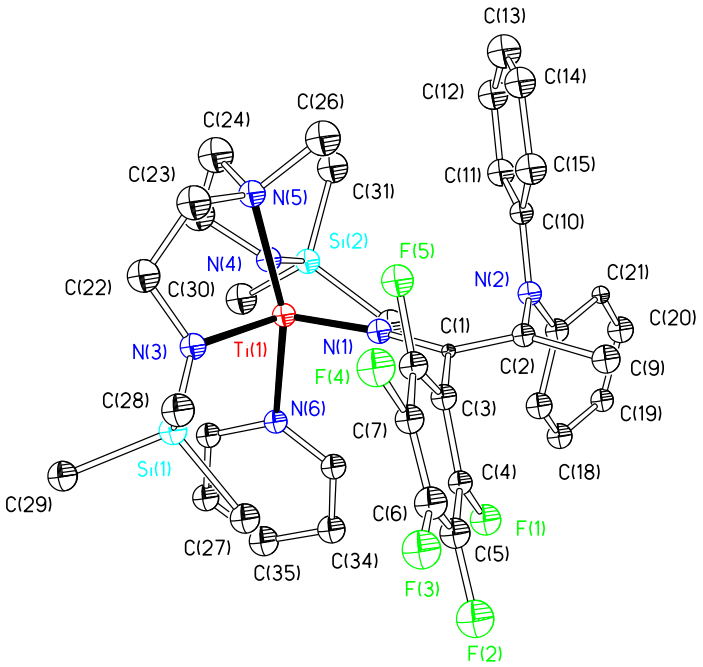

Figure 2. Displacement ellipsoid plot (20 % probability) of $Ti(N_2N^{Me})\{NC(C_6F_5)C(Me)NPh_2\}(py)$ (**8**) establishing overall connectivity. H atoms omitted for clarity.

The new alkyne $MeCC(1,4\text{-}C_6F_4)CCMe$ (**9**) was synthesised during the course of these studies according to Equation 1.

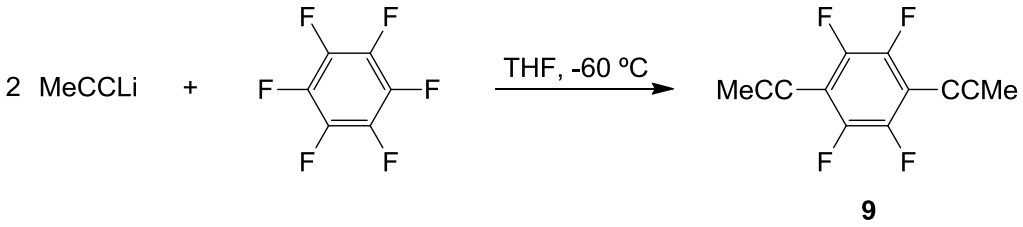

9

Equation 1

Diffraction-quality crystals were grown from a saturated chloroform solution at room temperature. The solid state structure is presented in Figure 3 and is nearly planar with typical bond lengths and angles. The π-stacking interactions between the electron rich alkyne groups and electron deficient tetraflurobenzene units are illustrated in Figure 4. The closest $C_{alkyne}\cdots C_{arene}$ distances are found to be 3.408 and 3.378 Å close to the sum of the van der Waal's radii (3.40 Å)[1]. Similar alkynes have also been made *via* Sonogashira cross coupling reactions[2]

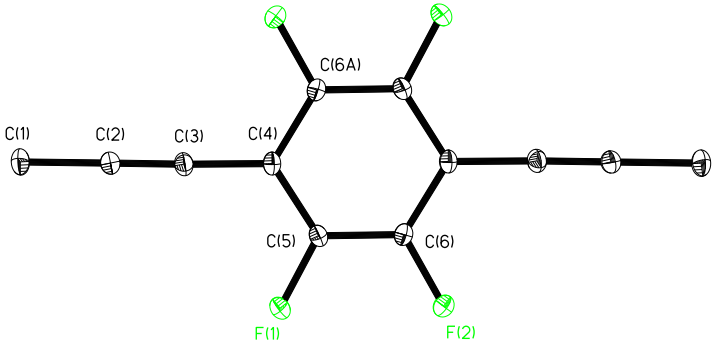

Figure 3. Displacement ellipsoid plot (25 % probability) of MeCC(1,4-C_6F_4)CCMe (**9**). H atoms omitted for clarity.

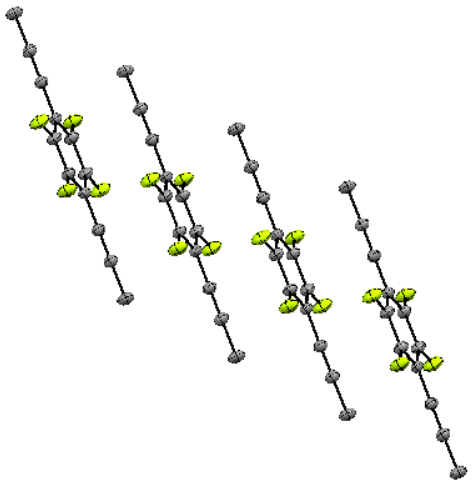

Figure 4. Illustration of the π-stacking interactions between the electron rich alkne groups and electron deficient tetraflurobenzene units in MeCC(1,4-C_6F_4)CCMe (**9**).

References

1. Bondi, A.; *J. Phys. Chem.* **1964**, *68*, 441.
2. Kane, C. M.; Meyers, T. B.; Yu, X.; Gerken, M.; Etzkorn, M.; *Eur. J. Org. Chem.* **2011**, *2011*, 2969.

Appendix B - Synthesis and crystal structure of $Ti(N_2N^{Me})(N^tBu)(py)$ (47)

$Ti(N_2N^{Me})(N^tBu)(py)$ (**47**) was obtained as an orange powder in 86 % yield by reacting $Li_2N_2N^{Me}$ with $Ti(N^tBu)Cl_2(py)_3$ (Equation 1) in toluene. Diffraction-quality crystals were grown from a saturated Et_2O solution at room temperature.

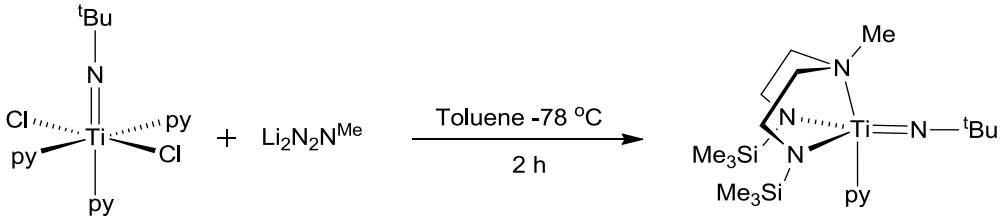

47

Equation 1

The solid state structure of $Ti(N_2N^{Me})(N^tBu)(py)$ (**47**) is fully consistent with its solution NMR data and is presented in Figure 1. Selected distances and angles are given in Table 1. The five-coordinate titanium metal centre has an approximate trigonal bipyramidal environment with the ligand bound in a *fac* manner. The equatorial positions are occupied by the *tert*-butylimido and the two amide nitrogens, with the axial sites taken by the ligand amine nitrogen and coordinated pyridine.

The Ti(1)-N(1) length of 1.712(2) Å, is the same within error to that of the starting material $Ti(N^tBu)Cl_2(py)_3$,[1] the related compound $Ti(N_2N^{SiMe_3})(N^tBu)(py)$ (**1.65**; $H_2N_2N^{SiMe_3}$ = $Me_3SiN(CH_2CH_2N(H)SiMe_3)_2$)[2] and is very similar to that found in $Ti(N_2N^{py})(N^tBu)(py)$ (**1.71**).[3,4] The near-linear Ti(1)-N(1)-C(1) angle of 172.6(2) º indicates that the *tert*-butylimido group is acting as a four-electron donor to the metal centre as seen in **1.65**, **1.71** and related compounds.[5,6] The Ti–N_{amide} bond lengths (Ti(1)-N(2) = 2.037(2), Ti(1)-N(3) = 2.023(2) Å) and sum of the angles subtended at the nitrogen atoms (N(2) = 357.7, N(3) = 358.1 º) are indicative of π-donation from the amide nitrogen lone pairs to the metal centre and again very similar to the aforementioned examples.

As in $Ti(N_2N^{SiMe_3})(N^tBu)(py)$ (Ti-N_{py} = 2.228(3) Å, N_{amine}-Ti-N_{py} = 148.3(1) º), due to the nature of the chelating ligand, the amine donor in **47** cannot attain a position strictly *trans* to the bound pyridine (Ti(1)-N(5) = 2.221(2) Å, N(4)-Ti(1)-N(5) = 150.15(9) º) and the pyridine molecule is therefore more tightly bound than in $Ti(N_2N^{py})(N^tBu)(py)$ (**1.71**) where the stronger pyridyl donor can position itself closer

to an exact *trans* orientation (Ti-N_{py} = 2.278(2) Å, $N_{pyridyl}$-Ti-N_{py} = 175.10(17) º). Reactivity studies were not performed on this compound.

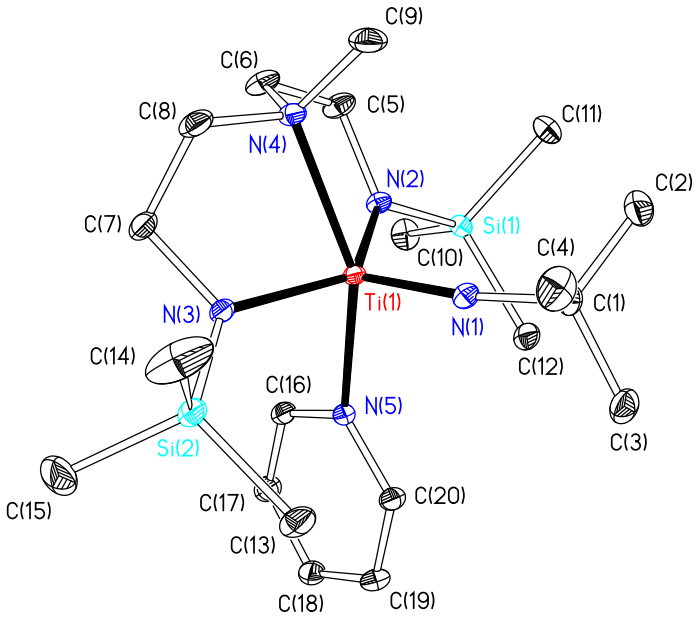

Figure 1. Displacement ellipsoid plot (15% probability) of Ti(N_2N^{Me})(N^tBu)(py) (**47**). H atoms omitted for clarity.

Table 1. Selected distances (Å) and angles (º) for Ti(N_2N^{Me})(N^tBu)(py) (**47**).

Ti(1)-N(1)	1.712(2)	N(4)-Ti(1)-N(5)	150.15(9)
Ti(1)-N(2)	2.037(2)	Si(2)-N(3)-C(7)	113.44(18)
Ti(1)-N(3)	2.023(2)	N(1)-Ti(1)-N(2)	113.38(10)
Ti(1)-N(4)	2.275(2)	N(1)-Ti(1)-N(3)	112.15(10)
Ti(1)-N(5)	2.221(2)	N(1)-Ti(1)-N(4)	108.54(10)
N(1)-C(1)	1.465(3)	N(1)-Ti(1)-N(5)	101.31(10)
Ti(1)-N(1)-C(1)	172.6(2)	N(2)-Ti(1)-N(3)	133.33(9)
Ti(1)-N(2)-Si(1)	128.89(12)	N(2)-Ti(1)-N(4)	77.96(8)
Ti(1)-N(2)-C(5)	117.57(17)	N(2)-Ti(1)-N(5)	89.88(9)
Si(1)-N(2)-C(5)	111.22(17)	N(3)-Ti(1)-N(4)	78.56(8)
Ti(1)-N(3)-Si(2)	130.75(12)	N(3)-Ti(1)-N(5)	90.97(9)
Ti(1)-N(3)-C(7)	113.88(17)	N(4)-Ti(1)-N(5)	150.15(9)

References

1. Collier, P. E.; Dunn, S. C.; Mountford, P.; Shishkin, O. V.; Swallow, D.; *J. Chem. Soc., Dalton Trans.* **1995**, *22*, 3743.
2. Collier, P. E.; Pugh, S. M.; Clark, H. S. C.; Love, J. B.; Blake, A. J.; Cloke, F. G. N.; Mountford, P.; *Inorg. Chem.* **2000**, *39*, 2001.
3. Blake, A. J.; Collier, P. E.; Gade, L. H.; Mountford, P.; Lloyd, J.; Pugh, S. M.; Schubart, M.; Skinner, M. E. G.; Trösch, J. M.; *Inorg. Chem.* **2001**, *40*, 870.
4. Blake, A. J.; Collier, P. E.; Gade, L. H.; McPartlin, M.; Mountford, P.; Schubart, M.; Scowen, I. J.; *Chem. Commun.* **1997**, 1555.
5. Wigley, D. E.; *Prog. Inorg. Chem.* **1994**, *42*, 239.
6. Mountford, P.; *Chem. Commun.* **1997**, 2127.

Appendix C - Crystal structures of $Ti(N_2N^{Me})\{N(H)C(Ph)C(Ph)NPh_2\}_2$ (25a′) and $Cp_4Zr_2(\mu\text{-}\eta^1\text{:}\eta^1\text{-}NNMe_2)(\mu\text{-}\eta^2\text{:}\eta^1\text{-}NNMe_2)$ (31)

The molecular structure of $Ti(N_2N^{Me})\{N(H)C(Ph)C(Ph)NPh_2\}_2$ (**25a′**), the hydrolysis product of $Ti(N_2N^{Me})\{NC(Ph)C(Ph)NPh_2\}(py)$ (**25a**) is presented in Figure 1. It clearly shows the $NC(Ph)C(Ph)NPh_2$ moieity formed by insertion of an alkyne molecule into the N_α–N_β bond.

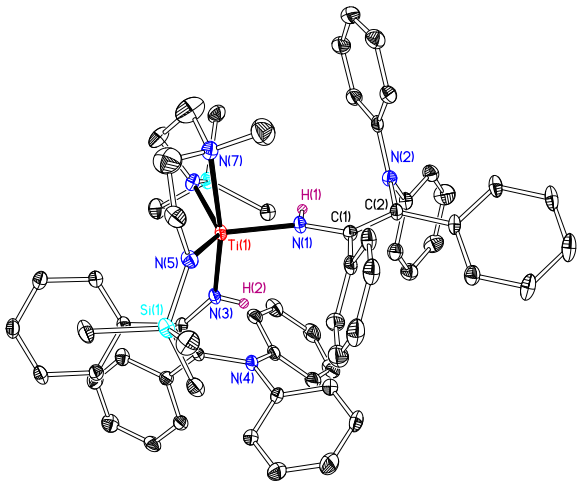

Figure 1. Displacement ellipsoid plot (20 % probability) of $Ti(N_2N^{Me})\{N(H)C(Ph)C(Ph)NPh_2\}_2$ (**25a′**) establishing insertion of PhCCPh into the N_α–N_β bond. H atoms omitted for clarity.

X-ray diffraction quality crystals of $Cp_4Zr_2(\mu\text{-}\eta^1\text{:}\eta^1\text{-}NNMe_2)(\mu\text{-}\eta^2\text{:}\eta^1\text{-}NNMe_2)$ (**31**) were grown from a saturated benzene solution but found to be poor diffractors. The connectivity could still be ascertained indicating an unsymmetrical dimer and is presented in Figure 2.

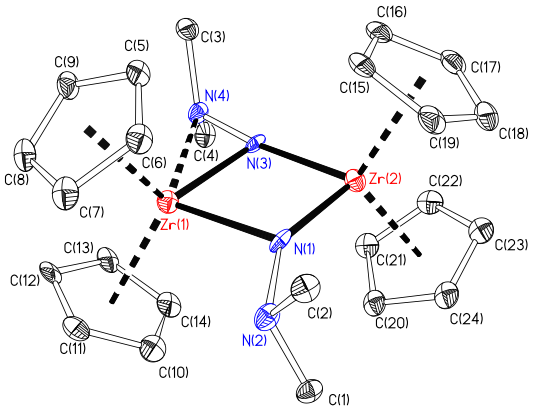

Figure 2. Displacement ellipsoid plot (20 % probability) of $Cp_4Zr_2(\mu\text{-}\eta^1\text{:}\eta^1\text{-}NNMe_2)(\mu\text{-}\eta^2\text{:}\eta^1\text{-}NNMe_2)$ (**31**). H atoms were not refined.

Appendix D – Attempted syntheses of permethylated-bis(cyclopentadienyl) zirconium hydrazides

As mentioned in Chapter Four, in order to isolate a [2+2] cycloaddition product between an alkyne and a zirconium hydrazide supported by a bis(cyclopentadienyl) derived ligand set the syntheses of $Cp^R{}_2Zr(NNPh_2)(L)$ (Cp^R = C_5Me_4H or C_5Me_5, L = py or DMAP) were attempted. While these were unsuccessful on scales larger than 10 mg, several new compounds were formed and their syntheses are discussed below.

When $Cp^*{}_2ZrCl_2$ in the presence of one equivalent of DMAP, was reacted with $LiNHNPh_2$, followed by $LiN(SiMe_3)_2$, in an analogous method to the synthesis of $Cp^R{}_2Zr(NNPh_2)(DMAP)$ (Cp^R = Cp (**1.151**) or Cp′ (**29**)), trace amounts of $Cp^*{}_2Zr(NNPh_2)(DMAP)$ (**48**) were formed, as characterised by X-ray diffraction spectroscopy (Scheme 1). The molecular structure has some interesting characteristics and is discussed below. Unfortunately the nature of the bulk of the material could not be elucidated, but significant quantities of unreacted starting materials were recovered.

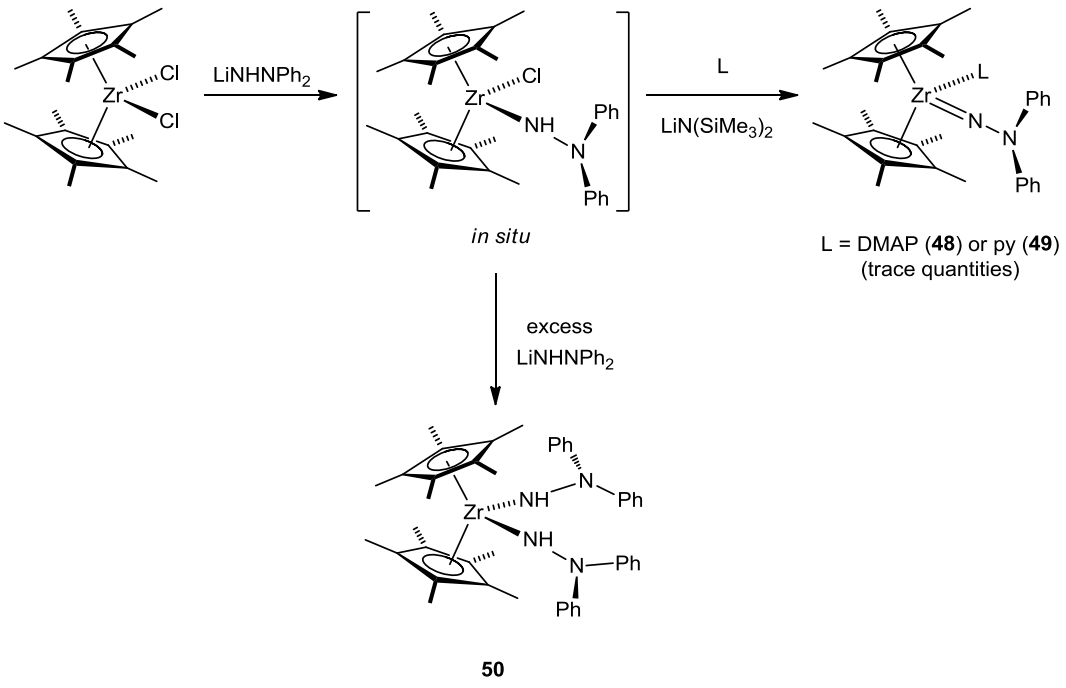

Scheme 1. Attempted synthesis of $Cp^*{}_2Zr(NNPh_2)(L)$ (L = DMAP (**48**) or py (**49**)).

Attempts to drive the substitution of the chloride with the hydrazide(1-) anion by increasing the concentration of $LiNHNPh_2$, this time in the presence of an excess of pyridine, again led to trace quantities (< 3 % yield) of the hydrazide(2-) compound

$Cp^*_2Zr(NNPh_2)(py)$ (**49**), as characterised by X-ray diffraction, with the major product, formed in 86 % yield, being the bis(hydrazido(1-)) $Cp^*_2Zr(NHNPh_2)_2$ (**50**, Scheme 1). Formation of bis(hydrazido(1-)) species instead of the desired terminal hydrazido(2-) is well documented for the larger Group 4 metals.[1,2]

Diffraction-quality crystals of $Cp^*_2Zr(NHNPh_2)_2$ (**50**) were grown from a saturated hexanes solution at 4 ºC. The molecular structures of $Cp^*_2Zr(NNPh_2)(DMAP)$ (**48**, both molecules in the asymmetric unit) and $Cp^*_2Zr(NNPh_2)(py)$ (**49**) as elucidated by X-ray diffraction are presented in Figure 1 with selected distances and angles listed in Table 1. The molecular structure of $Cp^*_2Zr(NHNPh_2)_2$ (**50**) is given in Figure 2 with selected bond lengths and angles in Table 2.

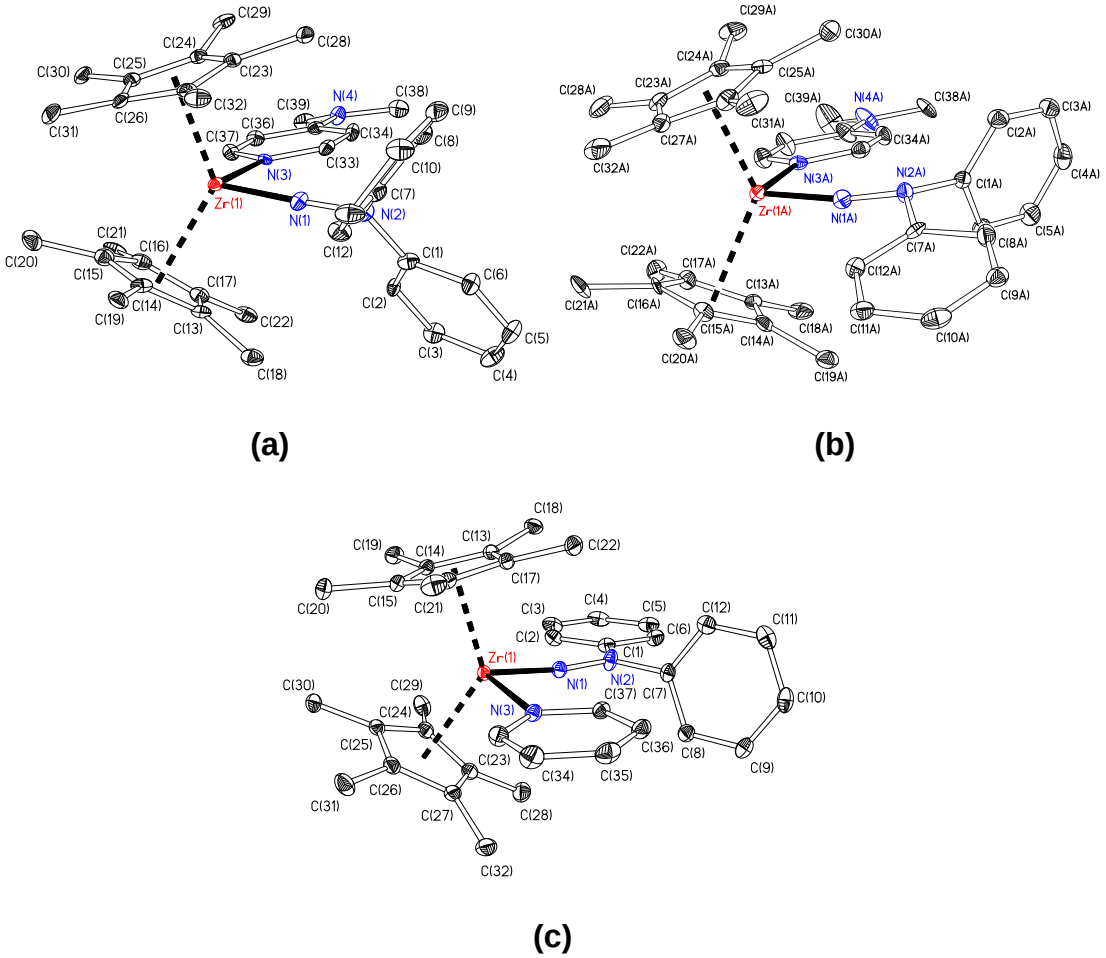

Figure 1. Displacement ellipsoid plot (20 % probability) of (a) $Cp^*_2Zr(NNPh_2)(DMAP)$ (**48a**), (b) $Cp^*_2Zr(NNPh_2)(DMAP)$ (**48b**) and (c) $Cp^*_2Zr(NNPh_2)(py)$ (**49**). H atoms omitted for clarity.

Table 1. Selected distances (Å) and angles (^{o}) for $Cp^*_2Zr(NNPh_2)(DMAP)$ (**48a** and **48b**) and $Cp^*_2Zr(NNPh_2)(py)$ (**49**).

Parameter	**48a**	**48b**	**49**
Zr(1)–N(1)	1.853(5)	1.847(5)	1.871(2)
Zr(1)–N(3)	2.339(4)	2.322(4)	2.362(2)
$Zr(1)–Cp_{cent(1)}$[a]	2.343	2.310	2.365
$Zr(1)–Cp_{cent(2)}$[a]	2.361	2.385	2.339
N(1)–N(2)	1.381(7)	1.418(6)	1.386(3)
N(2)–C(1)	1.398(6)	1.416(7)	1.376(3)
N(2)–C(7)	1.433(7)	1.398(6)	1.425(3)
Zr(1)–C(13)	2.570(4)	2.610(6)	2.574(2)
Zr(1)–C(14)	2.577(6)	2.604(6)	2.595(2)
Zr(1)–C(15)	2.723(6)	2.646(6)	2.698(2)
Zr(1)–C(16)	2.714(6)	2.743(5)	2.683(2)
Zr(1)–C(17)	2.658(5)	2.746(6)	2.602(2)
Zr(1)–C(23)	2.588(5)	2.680(6)	2.575(2)
Zr(1)–C(24)	2.635(5)	2.643(6)	2.583(2)
Zr(1)–C(25)	2.713(6)	2.571(6)	2.731(2)
Zr(1)–C(26)	2.688(5)	2.530(7)	2.745(2)
Zr(1)–C(27)	2.555(5)	2.592(7)	2.632(2)
N(1)–Zr(1)–N(3)	91.09(18)	94.86(17)	93.59(7)
$N(1)–Zr(1)–Cp_{cent(1)}$	110.7	108.7	111.2
$N(1)–Zr(1)–Cp_{cent(2)}$	111.7	110.9	109.7
$N(3)–Zr(1)–Cp_{cent(1)}$	100.7	100.0	103.7
$N(3)–Zr(1)–Cp_{cent(2)}$	105.1	103.2	100.2
$Cp_{cent(1)}–Zr(1)–Cp_{cent(2)}$	129.2	131.7	130.7
Zr(1)–N(1)–N(2)	178.0(3)	167.5(5)	173.16(17)

[a]Cp_{cent} is the computed Cp* ring carbon centroid.

While data on compounds **48** and **49** could not be obtained the ^{1}H and $^{13}C\{^{1}H\}$ NMR data of $Cp^*_2Zr(NHNPh_2)_2$ (**50**) are in full agreement with the structure drawn in Scheme 1, with ^{13}C peaks between 154 and 121 ppm corresponding to the hydrazido(1-) resonances, in keeping with those seen in related compounds (*vide infra*). There is a sharp singlet at 4.95 ppm in the ^{1}H spectrum attributable to the NH protons and the Cp* and phenyl resonances are within the expected shifts.

The molecular structures of $Cp^*_2Zr(NNPh_2)(DMAP)$ (**48**) and $Cp^*_2Zr(NNPh_2)(DMAP)$ (**49**) clearly indicate the presence of a 1,1-diphenyl hydrazido(2-) ligand. All contain a zirconium atom with pseudo tetrahedral geometry, the other coordination sites occupied by DMAP and the pentamethylcyclopentadienyl ligands. The most interestingly feature of **48** is the presence of two distinct molecules in the asymmetric unit. In the majority of cases the two independent molecules are nearly identical, however in this instance one (designated **48a**) has the hydrazide phenyl rings orientated 'up' and 'down' relative to the equatorial plane that contains Zr, N_α and N_{DMAP} (C(1)–N(2)–Zr(1)–N(3) = 60.61 º) while the other (**48b**) has them situated horizontally (C(1)–N(2)–Zr(1)–N(3) = 4.53 º). In the case of **49** only one orientation is observed with the phenyl rings arranged horizontally (C(1)–N(2)–Zr(1)–N(3) = 3.54 º), analogous to **48b** and diamide-amine supported titanium hydrazides such as $Ti(N_2N^{Me})(NNPh_2)(py)$ (**1.93**).[3] In contrast, other cyclopentadienyl supported hydrazides (e.g. $Cp_2M(NNPh_2)(L)$ L = DMAP, M = Ti (**4.2**), Zr (**1.151**) or Hf (**28**), L = py, M = Ti (**1.103**)) exclusively have the phenyl rings orientated vertically as in **48a** (avg. C–N–M–N = *ca*. 90 º).[4]

The bonding in $Cp_2Ti(NNPh_2)(py)$ (**1.103**) has been studied by Mountford who found that the isomer with the phenyl rings orientated vertically was calculated to be 3.0 kcal mol^{-1} more stable than that with them horizontal.[4] However, on moving to the bulkier $SiMe_3$ substituted hydrazide the optimum geometry had the substituents placed 62 º out of the equatorial plane (i.e. in between a horizontal and vertical alignment). This is attributed to the competition between the vertical, electronically preferred, isomer and unfavourable steric interaction between the $SiMe_3$ groups and the cyclopentadienyl rings, which is reduced in the horizontal isomer. It is not difficult to imagine that in **48** and **49**, the significantly bulkier pentamethyl(cyclopentadienyl) groups destabilise the electronically preferred hydrazide orientation forcing it to become horizontal. Even in the case of **48a** the

phenyl rings are ″less vertical″ (indicated by the lower torsion angles listed above) than in the cyclopentadienyl supported hydrazides, being closer to the calculated optimal geometry of $Cp_2Ti(NN(SiMe_3)_2)$ (**1.29**).

The calculations predict that, when compared to a hydrazide with the phenyl rings placed vertically (e.g. **48a**), a hydrazide with the phenyl rings placed horizontally (e.g. **48b**) will see a decrease in the M=N_α distance and an increase in the N_α–N_β bond length, as well as a change from η^5- to η^3- coordination for one cyclopentadienyl ring. These are borne out in a comparison of **48a** and **48b**. While being the same within error, the Zr(1)=N(1) distance may show a slight decrease (**48a**, Zr(1)=N(1) = 1.853(5) Å; **48b**, Zr(1)=N(1) = 1.847(5) Å). The N(1)–N(2) bond length increase is larger but again within error (**48a**, N(1)–N(2) = 1.381(7) Å; **48b**, N(1)–N(2) = 1.418(6) Å). However, the general trends agree with the computational predictions. The Zr–Cp_{cent} trends also agree, in **48b** Zr(1)–$Cp_{cent(2)}$ (2.385 Å) is significantly lengthened compared to Zr(1)–$Cp_{cent(1)}$ (2.310 Å), consistent with η^5/η^3- coordinated cyclopentadienyl rings, while in **48a** they are more similar (Zr(1)–$Cp_{cent(1)}$ = 2.343 and Zr(2)–$Cp_{cent(2)}$ = 2.361 Å) consistent with η^5/η^5- coordinated cyclopentadienyl rings.

Despite having a horizontal orientation of the hydrazide phenyl rings, **49** has Zr(1)–Cp_{cent} distances similar to **48a** (avg. for both = 2.352 Å). This is presumable due to the fact that pyridine is a worse donor than DMAP, allowing the Cp* rings to bind more strongly, in turn lengthening the Zr(1)=N(1) distance (**49**, 1.871(2) Å; **48a**, 1.853(5) Å) and preventing the expected increase in N(1)–N(2) bond length (N(1)–N(2) = 1.386(3) Å (**49**), 1.381(7) Å (**48a**)).

In all cases (**48a**, **48b** and **49**) the Zr=N_α distances are the same within error to that of the related compound $Cp_2Zr(NNPh_2)$(DMAP) (Zr=N_α = 1.878(7) Å (**1.151**), 1.853(5) Å (**48a**), 1.847(5) Å (**48b**), 1.871(2) Å (**49**)) as are the N_α–N_β bond lengths in **48a** and **49**, that of **48b** being slightly longer as discussed above (N_α–N_β = 1.351(10) Å (**1.151**), 1.381(7) Å (**48a**), 1.386(3) Å (**49**)). The Zr(1)–N(1)–N(2) angles (178.0(3) º (**48a**), 167.5(5) º (**48b**), 173.16(17) º (**49**)) are indicative of *sp* hybridised N_α atoms and within the ranges found in Group 4 hydrazides. The Zr(1)–N(3) distances are within the expected values for Zr–N_{DMAP} and N_{py} bonds.

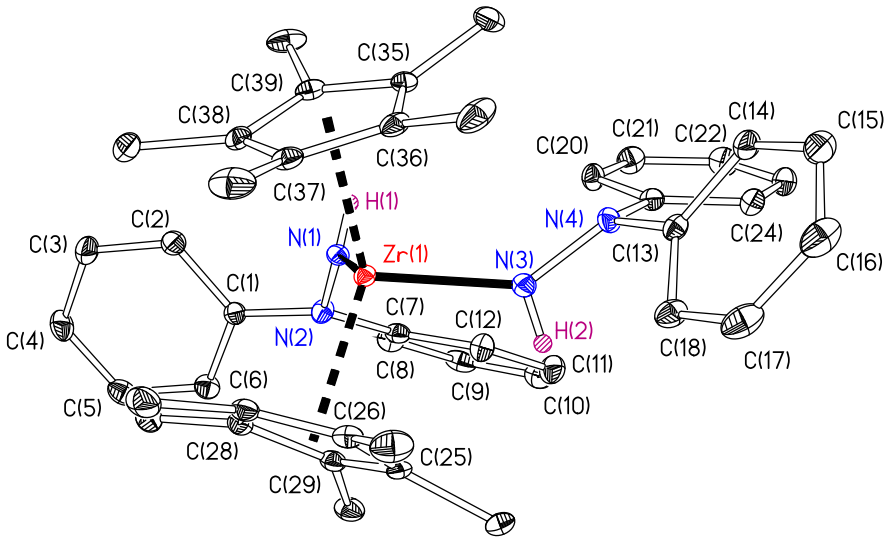

Figure 2. Displacement ellipsoid plot (20 % probability) of $Cp^*_2Zr(NHNPh_2)_2$ (**50**). C bound H atoms omitted for clarity.

Table 2. Selected distances (Å) and angles (°) for $Cp^*_2Zr(NHNPh_2)_2$ (**50**).

Zr(1)–N(1)	2.135(3)	N(1)–Zr(1)–N(3)	101.03(11)
Zr(1)–N(3)	2.121(3)	N(1)–Zr(1)–$Cp_{cent(1)}$	103.7
Zr(1)–$Cp_{cent(1)}$[a]	2.299	N(1)–Zr(1)–$Cp_{cent(2)}$	105.6
Zr(1)–$Cp_{cent(2)}$[a]	2.314	N(3)–Zr(1)–$Cp_{cent(1)}$	105.5
N(1)–N(2)	1.432(4)	N(3)–Zr(1)–$Cp_{cent(2)}$	103.8
N(3)–N(4)	1.426(4)	$Cp_{cent(1)}$–Zr(1)–$Cp_{cent(2)}$	133.2
N(2)–C(1)	1.412(4)	Zr(1)–N(1)–N(2)	137.1(2)
N(2)–C(7)	1.415(4)	Zr(1)–N(3)–N(4)	138.5(2)
N(4)–C(13)	1.420(4)		
N(4)–C(19)	1.426(4)		

[a]Cp_{cent} is the computed Cp* ring carbon centroid.

The molecular structure of $Cp^*_2Zr(NHNPh_2)_2$ (**50**) is fully consistent with the solution ^{1}H NMR spectrum. The zirconium possesses tetrahedral geometry, two coordination sites being occupied by the pentamethyl(cyclopentadienyl) ligands and the reminaing two by the hydrazido(1-) groups. While there are no structurally authenticated N_α(H)

substituted bis(hydrazido(1-)) zirconium complexes there are several examples with $N_\alpha(R)$ (R = alkyl).[5-7] There are also several bis(pentamethylcyclopentadienyl) supported bis(amide) compounds[8,9] with $Cp^*_2Zr(NHPh)_2$ (**4.10**) being the most similar to **50**.[10]

The Zr–N bond lengths are typical of zirconium bonds to an anionic nitrogen (Zr(1)–N(1) = 2.135(3) Å, Zr(1)–N(3) = 2.121(3) Å; lit. range = 1.877 – 2.404 Å)[11] as are the Zr–Cp_{cent} distances (avg. 2.302 Å) with both similar to those in **4.10** (avg. Zr–N = 2.121(3) Å, Zr–Cp_{cent} = 2.289 Å). The N_α–N_β lengths (N(1)–N(2) = 1.432(4) Å, N(3)–N(4) = 1.426(4) Å) are typical of single bonds between nitrogen atoms and nearly identical to that found in $Cp^*_2Zr(NHNPh_2)(Me)$ (**51**, *vide infra*). The N(1)–Zr(1)–N(3) angle of 101.13(11) º is broadly the same as that of **4.10** (98.4(1) º). The N–Zr–Cp_{cent} angles range from 103.7 – 105.6 º and the Cp_{cent}–Zr–Cp_{cent} angle is 133.2 º. These are again typical for bis(pentamethylcyclopentadienyl) compounds and very similar to those in **4.10** (N–Zr–Cp_{cent} range = 100.1 – 109.3 º, Cp_{cent}–Zr–Cp_{cent} = 134.3 º). The Zr(1)–N(1)–N(2) and Zr(1)–N(3)–N(4) angles of 137.1(2) and 138.5(2) º are indicative of an sp^2 hybridised nitrogen, as in $Cp^*_2Zr(NHNPh_2)(Me)$ (**51**, *vide infra*).

The unsuccessful nature of the route outlined in Scheme 1 meant a different method was required. Bergman's success in forming $Cp_2Zr(NNPh_2)(DMAP)$ (**1.151**) *via* alkane elimination (as discussed in Chapter Four) and more recently $Cp^R_2Zr(N^tBu)(THF)$ (Cp^R = bulky substituted cyclopentadienyl) from compounds of the type $Cp^R_2Zr(NH^tBu)(Me)$ indicated that isolation of $Cp^*_2Zr(NNPh_2)(L)$ might be possible *via* thermolysis of $Cp^*_2Zr(NHNPh_2)(Me)$ (**51**).

$Cp^*_2Zr(Me)Cl$ was reacted with $LiNHNPh_2$ forming $Cp^*_2Zr(NHNPh_2)(Me)$ (**51**) in 62 % yield. In contrast to the related *tert*-butyl imdo chemistry explored by Bergman,[12] there was no deprotonation of the hydrazido(1-) ligand, as such only a small excess of the lithiated hydrazide was necessary instead of the two-fold required with $LiNH^tBu$ (Scheme 2). The ^1H and $^{13}C\{^1H\}$ NMR data are fully consistent with the structure proposed in Scheme 2. The hydrazido(1-) resonances are broad, possibly due to hindered rotation about the N_α–N_β and/or N_β–C_{ipso} bonds caused by the bulky Cp* ligands. There is a sharp singlet at 5.99 ppm arising from the NH with the Cp* and methyl resonances found in the expected regions. The $^{13}C\{^1H\}$ NMR spectrum

shows peaks corresponding to the resonances of the 1,1-diphenylhydrazido(1-) ligand between 153 and 120 ppm, similar to those observed in **50**.

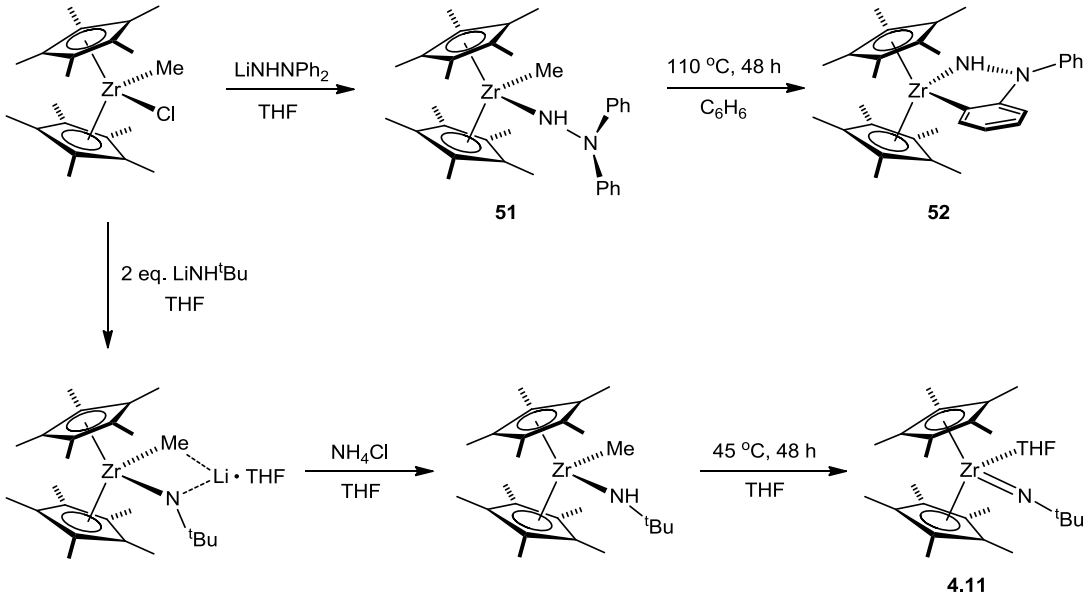

Scheme 2. Syntheses of $Cp^*_2Zr\{N(H)N(Ph)\text{-}1,2\text{-}C_6H_4\}$ (**52**) and $Cp^*_2Zr(N^tBu)(THF)$ (**4.11**).[13]

X-ray diffraction-quality crystals of $Cp^*_2Zr(NHNPh_2)(Me)$ (**51**) were grown by slow cooling of a saturated hexanes solution from 70 °C to room temperature. The molecular structure is presented in Figure 3 with selected distances and angles listed in Table 3.

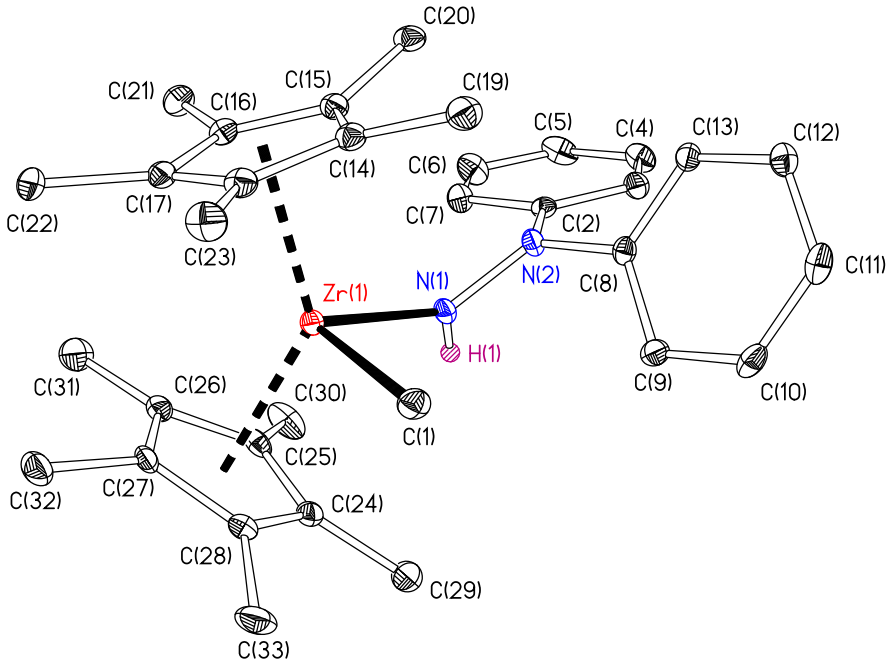

Figure 3. Displacement ellipsoid plot (20 % probability) of $Cp^*_2Zr(NHNPh_2)(Me)$ (**51**). C bound H atoms omitted for clarity.

Table 3. Selected distances (Å) and angles (°) for $Cp^*_2Zr(NHNPh_2)(Me)$ (**51**).

Zr(1)–N(1)	2.101(3)	N(1)–Zr(1)–C(1)	95.68(13)
Zr(1)–C(1)	2.287(4)	N(1)–Zr(1)–$Cp_{cent(1)}$	110.7
Zr(1)–$Cp_{cent(1)}$[a]	2.280	N(1)–Zr(1)–$Cp_{cent(2)}$	102.1
Zr(1)–$Cp_{cent(2)}$[a]	2.274	C(1)–Zr(1)–$Cp_{cent(1)}$	102.5
N(1)–N(2)	1.426(4)	C(1)–Zr(1)–$Cp_{cent(2)}$	101.7
N(2)–C(2)	1.404(4)	$Cp_{cent(1)}$–Zr(1)–$Cp_{cent(2)}$	138.6
N(2)–C(8)	1.414(4)	Zr(1)–N(1)–N(2)	136.1(2)

[a]Cp_{cent} is the computed Cp* ring carbon centroid.

The solid state structure of $Cp^*_2Zr(NHNPh_2)(Me)$ (**51**) confirms the presence of methyl and hydrazido(1-) ligands bound to a zirconium atom with tetrahedral geometry, the other two coordination sites being occupied by the pentamethylcyclopentadienyl ligands. It is fully consistent with the solution ^{1}H NMR data.

$Cp^*_2Zr(NHNPh_2)(Me)$ (**51**) is only the second structurally authenticated N_α(H) mixed hydrazido(1-)-alkyl zirconium compound, the other being $Zr(N_2{*}N^{py})(NHNMe_2)(CH_2SiMe_3)$ (**4.12**) although in this example N_β is coordinated to the metal centre.[14] There are more examples with an alkyl/aryl substituted N_α.[15-18] There is only one reported crystallographically characterised bis(pentamethylcyclopentadienyl) supported non-chelating mixed amide-alkyl, $Cp^*_2Zr(Me)(NEt_2)$ (**4.13**).[19]

The Zr(1)–N(1) and Zr(1)–C(1) distances are within the expected ranges for the respective bond type (Zr(1)–N(1) = 2.101(3) Å, Zr(1)–C(1) = 2.287(4) Å, lit. range Zr–N = 2.003 – 2.272 Å, Zr–C = 2.046 – 2.480 Å) and within error to those in **4.13** (Zr–N = 2.099(2) Å, Zr–C = 2.296(3) Å). The Zr–Cp_{cent} distances are also within the expected ranges (avg. Zr–Cp_{cent} = 2.287 Å (**51**), 2.194 Å ($Cp^*_2ZrCl_2$)), slightly less

than in **4.13** (avg. Zr–Cp_{cent} = 2.306 Å) due to the steric bulk being further removed from the metal centre. The N(1)–N(2) bond length of 1.426(4) Å is typical of a hydrazido(1-) ligand bound to a Group 4 metal and the same within error as those seen in $Cp^*_2Zr(NHNPh_2)_2$ (**50**, avg. N_α–N_β = 1.429(4) Å, *vide supra*).

The N(1)–Zr(1)–C(1) angle (95.68(13) º) is similar to that seen between two non-chelating anionic ligands in other bis(pentamethylcyclopentadienyl) supported systems. Angles to the pentamethylcyclopentadienyl rings range between 101.7 and 110.7 º with the angle between the centroids 138.6 º. In the related compounds **50**, **52** and **4.13** these measurements are all comparable (**50**, X–Zr–Cp_{cent} range = 103.7 – 105.6 º, Cp_{cent}–Zr–Cp_{cent} = 133.2 º; **52**, X–Zr–Cp_{cent} range = 103.2 – 110.0 º, Cp_{cent}–Zr–Cp_{cent} = 138.1 º; **4.13**, X–Zr–Cp_{cent} range = 102.2 – 110.8 º, Cp_{cent}–Zr–Cp_{cent} = 132.8 º). The Zr(1)–N(1)–N(2) angle (136.1(2) º) is indicative of an sp^2 hybridised nitrogen, as observed in **50**.

When $Cp^*_2Zr(NHNPh_2)(Me)$ (**51**) was heated in a sealed vessel, no reaction was observed below 110 ºC. At this temperature a slow reaction proceeded, with loss of methane and formation of the new compound $Cp^*_2Zr\{N(H)N(Ph)\text{-}1,2\text{-}C_6H_4\}$ (**52**) containing two *ortho*-phenyl resonances in a 2:1 ratio (Scheme 2). The transformation is quantitative on the NMR tube scale. The ^1H NMR spectrum is presented in Figure 4, showing a broad singlet at 4.5 ppm (marked *) corresponding to an NH resonance and two *ortho*-phenyl peaks (doublets at 7.54 and 7.40 ppm). In addition, despite the reaction being carried out both in the presence and absence of added pyridine, none is incorporated in the final product, which remains unchanged. The $^{13}C\{^1H\}$ NMR spectrum (inset Figure 4) also indicates that the product is not the expected terminal hydrazide but a different species. The single hydrazide(2-) *ipso*-phenyl shift in $Cp_2M(NNPh_2)(DMAP)$ (M = Zr (**1.151**) or Hf (**28**)) can be found at *ca*. 150 ppm. However, in this instance there are three *ipso*-phenyl resonances at 176.6, 167.1 and 148.3 ppm, the two former significantly shifted downfield from that of the terminal hydrazide compounds.

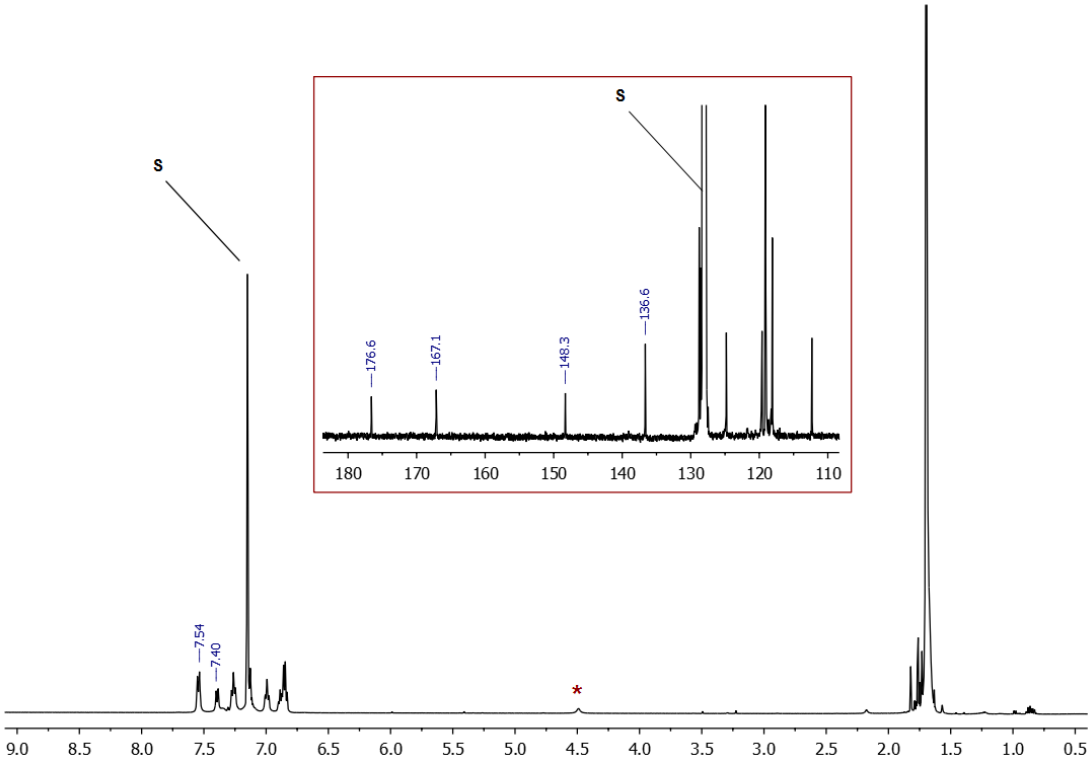

Figure 4. ^{1}H NMR spectrum (499.9 MHz, 293 K) of Cp*$_2$Zr{N(H)N(Ph)-1,2-C$_6$H$_4$} (**52**) in C$_6$D$_6$. The inset illustrates the ^{13}C{^{1}H} spectrum (125.7 MHz) between 105 and 185 ppm. ('**s**' denotes residual protio solvent).

X-ray diffraction-quality crystals of Cp*$_2$Zr{N(H)N(Ph)-1,2-C$_6$H$_4$} (**52**) were grown by slow cooling of a saturated toluene solution from 140 °C to room temperature. The molecular structure as determined by X-ray diffraction is presented in Figure 5 with selected distances and angles in Table 4.

The most interesting feature of Cp*$_2$Zr{N(H)N(Ph)-1,2-C$_6$H$_4$} (**52**) is the presence of the hydrazido(1-)-alkyl chelating ligand formed by *ortho*-metallation of one of the phenyl rings bound to N$_\beta$ in Cp*$_2$Zr(NHNPh$_2$)(Me) (**51**). This is the first crystallographically characterised example of a hydrazido-alkyl ligand bound to a Group 4 metal, however similar ligands have been used with other metals.[20-24] The most closely related, structurally characterised Group 4 compound, is Cp*$_2$Zr{NC(Me)-1,2-C$_6$H$_4$} (**4.14**) where N$_\beta$(Ph) has been replaced by C(Me) and N$_\alpha$ is now doubly bonded to the carbon and has no proton attached.[25]

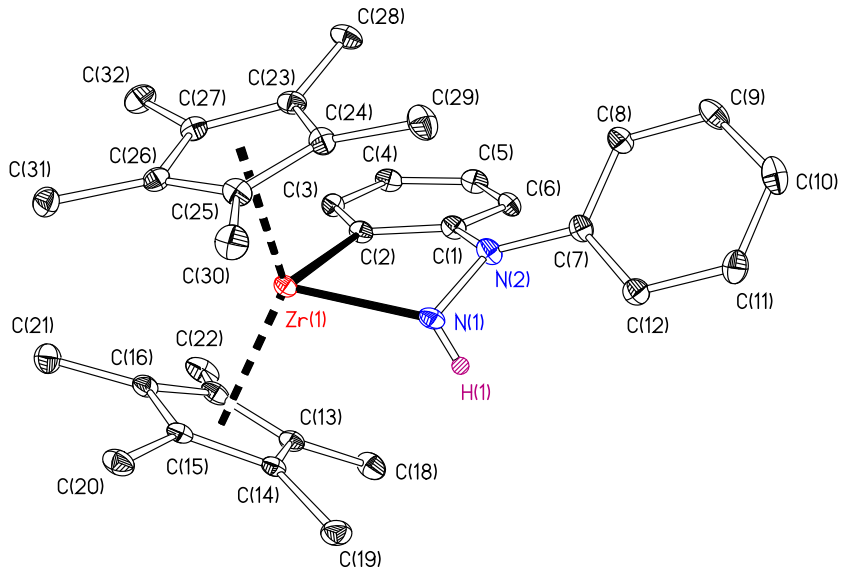

Figure 5. Displacement ellipsoid plot (20 % probability) of $Cp^*_2Zr\{N(H)N(Ph)\text{-}1,2\text{-}C_6H_4\}$ (**52**). C bound H atoms omitted for clarity.

Table 4. Selected distances (Å) and angles (°) for $Cp^*_2Zr\{N(H)N(Ph)\text{-}1,2\text{-}C_6H_4\}$ (**52**).

Zr(1)–N(1)	2.117(3)	N(1)–Zr(1)–C(2)	75.70(15)
Zr(1)–C(2)	2.290(3)	N(1)–Zr(1)–$Cp_{cent(1)}$	110.0
Zr(1)–$Cp_{cent(1)}$[a]	2.253	N(1)–Zr(1)–$Cp_{cent(2)}$	104.8
Zr(1)–$Cp_{cent(2)}$[a]	2.252	C(2)–Zr(1)–$Cp_{cent(1)}$	103.2
N(1)–N(2)	1.424(5)	C(2)–Zr(1)–$Cp_{cent(2)}$	107.6
N(2)–C(1)	1.431(5)	$Cp_{cent(1)}$–Zr(1)–$Cp_{cent(2)}$	138.1
N(2)–C(7)	1.402(5)	Zr(1)–N(1)–N(2)	111.2(3)
C(1)–C(2)	1.396(6)	N(1)–N(2)–C(1)	114.0(3)
		N(2)–C(1)–C(2)	116.6(3)
		Zr(1)–C(2)–C(1)	109.8(2)

[a]Cp_{cent} is the computed Cp* ring carbon centroid.

The central zirconium atom has an approximate tetrahedral geometry, two coordination sites are occupied by the pentamethylcyclopentadienyl ligands with the

others filled by the chelating hydrazido-alkyl donor. The Zr(1)–N(1) bond length is 2.117(3) Å, within the ranges for Zr–N single bonds (lit. range 1.877 – 2.404 Å)[11] and comparable to that in **4.14** (2.079(3) Å). The Zr(1)–C(2) distance of 2.290(3) Å is also similar to that found in **4.14** (2.298(3) Å) and typical of a Zr–C single bond. The N(1)–N(2) length remains unchanged, within error, to that of the starting material $Cp^*_2Zr(NHNPh_2)(Me)$ (**51**) (**51**, 1.426(4) Å; **52,** 1.424(5) Å). However, due to the constraints of the hydrazido ligand in **52** the N_β–C distances are no longer equal (**52**, N(2)–C(1) = 1.431(5) Å, N(2)–C(7) = 1.402(5) Å; **51**, N(2)–C(2) = 1.404(4) Å, N(2)–C(8) = 1.414(4) Å). In addition there is a shortening of the Zr–Cp_{cent} distances, which are in good agreement with those of **4.14** (**52**, avg. Zr–Cp_{cent} = 2.253 Å; **51**, avg. Zr–Cp_{cent} = 2.277 Å; **4.14**, avg. Zr–Cp_{cent} = 2.248 Å).

As expected for a five membered chelating ligand such as {(H)NN(Ph)-1,2-C_6H_4}, the angle between the two anionic atoms is significantly reduced relative to those seen in non-chelating examples (**52**, N(1)–Zr(1)–C(1) = 75.70(15) º; **51**, N–Zr–C = 95.68(13) º), but is similar to that found in **4.14** (75.99(12) º). Other angles in the chelating ring also deviate from their ideal values (e.g. Zr(1)–N(1)–N(2) = 111.2(3) º). The angle between the pentamethylcyclopentadienyl rings is slightly larger than that of the dichloride (**52**, Cp_{cent}–Zr–Cp_{cent} = 138.1 º; $Cp^*_2ZrCl_2$, Cp_{cent}–Zr–Cp_{cent} = 129.1 º). Note that the unsubstituted phenyl ring is twisted out of the plane containing the N_β lone pair implying that conjugation with the aromatic system only occurs within the metallated ring.

Following the formation of Cp^*_2Zr{N(H)N(Ph)-1,2-C_6H_4} (**52**) instead of the expected $Cp^*_2Zr(NNPh_2)(py)$ (**49**), DFT calculations were carried out on the relative stability of compounds **49** and **52** to determine if the reaction proceeds under kinetic or thermodynamic control. It was also of interest to elucidate if the reaction proceeds in a concerted manner or *via* the fulvene complex (**Int**). To this end the free energies of the two pathways, using $Cp^*_2Zr(NHNPh_2)(Me)$ (**K1**) as the model system, identical to the experimental compound **51**, were calculated and are presented in Scheme 3.

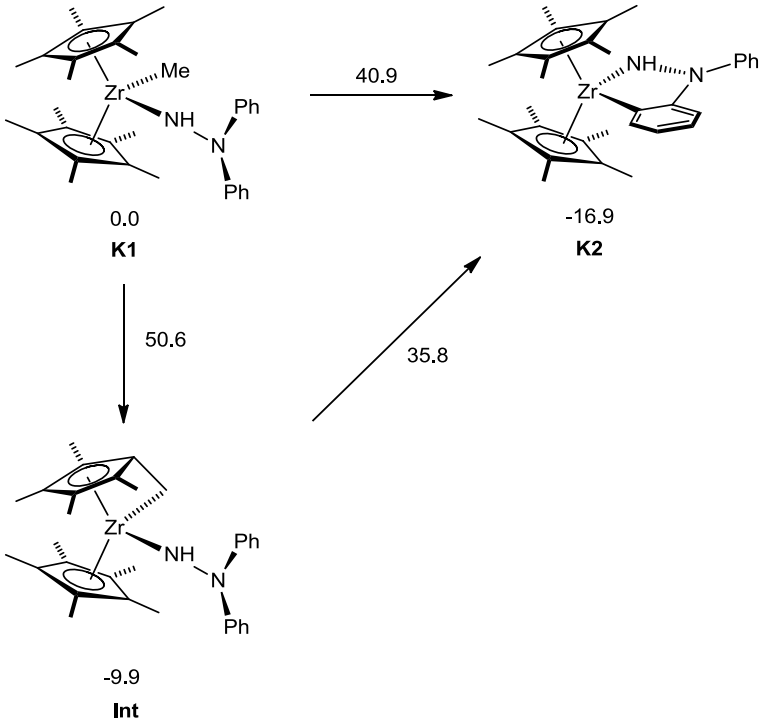

Scheme 3. Calculated Gibbs free energies (kcal mol^{-1}) and energies of activation for the formation of $Cp^*_2Zr\{N(H)N(Ph)\text{-}1,2\text{-}C_6H_4\}$ (**K2**) from $Cp^*_2Zr(NHNPh_2)(Me)$ (**K1**) by either direct metathesis or *via* the fulvene intermediate (**Int**).

The activation barrier to direct metathesis is calculated to be 40.9 kcal mol^{-1}, while that to form the fulvene intermediate is nearly 10 kcal mol^{-1} higher ($\Delta G^{\ddagger}$ = 50.6 kcal mol^{-1}) indicating that the reaction proceeds *via* the concerted pathway (Scheme 3).

Calculations on the relative stabilities of the hydrazido(2-) compound $Cp^*_2Zr(NNPh_2)$ and the *ortho*-metallated isomer $Cp^*_2Zr\{N(H)N(Ph)\text{-}1,2\text{-}C_6H_4\}$ (**52**) indicate that the latter is 14.5 kcal mol^{-1} more stable. In addition, calculations on the stabilities of the analogous cyclopentadienyl complexes $Cp_2Zr(NNPh_2)$ and $Cp_2Zr\{N(H)N(Ph)\text{-}1,2\text{-}C_6H_4\}$ show that in this instance the *ortho*-metallated isomer is, again, more stable ($\Delta\Delta G$ = 13.8 kcal mol^{-1}, -4.1 kcal mol^{-1} relative to $Cp_2Zr(NNPh_2)(py)$). These calculations imply that while the reactivity observed in Scheme 2 is under thermodynamic control, that seen by Bergman in the synthesis of $Cp_2Zr(NNPh_2)(DMAP)$ (**1.151**) is instead under kinetic control. This could concievably be due to a combination of the bulkier nature of the alkyl group ($CH_2CH_2{}^tBu$ *vs.* Me) raising the energy of the transition state to *ortho*-metallation and

the less bulky cyclopentadienyl ligands lowering the transition state to NH bond activation.

Mindful of the above results, and previous literature successes[26] on moving to the less sterically crowded tetramethylcyclopentadienyl ligands the synthesis of $Cp^{Me4}{}_2Zr(NNPh_2)(py)$ was attempted. As expected, substitution of a chloride anion in $Cp^{Me4}{}_2ZrCl_2$ by $LiNHNPh_2$ was unsuccessful with multiple products forming and significant quantities of starting material being recovered.

A thermolysis route as attempted with pentamethylcyclopentadienyl, was tried next. Wary that the steric bulk of the alkyl group may prove important in preventing o*rtho*-metallation, $Cp^{Me4}{}_2Zr(NHNPh_2)(Np)$ (Np = $CH_2{}^tBu$) was identified as the target molecule instead of $Cp^{Me4}{}_2Zr(NHNPh_2)(Me)$. The lower steric bulk of the cyclopentadienyl ligand set and larger size of the alkyl group were anticipated to favour formation of $Cp^{Me4}{}_2Zr(NNPh_2)(py)$ over $Cp^{Me4}{}_2Zr\{N(H)N(Ph)\text{-}1,2\text{-}C_6H_4\}$.

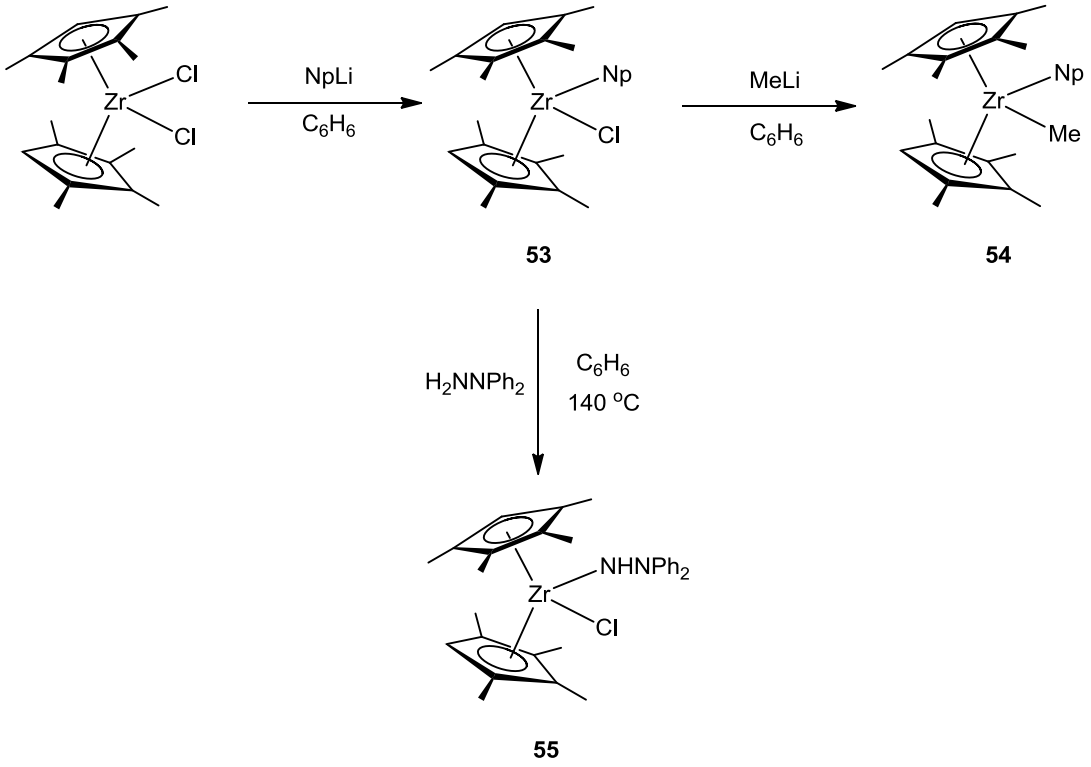

Scheme 4. Syntheses of $Cp^{Me4}{}_2Zr(Np)(Me)$ (**54**) and $Cp^{Me4}{}_2Zr(NHNPh_2)(Np)$ (**55**).

$Cp^{Me4}{}_2Zr(Np)Cl$ (**53**) was successful synthesised in 76 % yield from the dichloride and neopentyl lithium solution (Scheme 4). However, the subsequent reaction with $LiNHNPh_2$ did not occur, even under forcing conditions, the only isolable compounds

being starting materials. In addition to the neopentyl and cyclopentadienyl-H resonances (found at 1.23, 0.65 and 5.43 ppm, respectively) the compound contains four sharp cyclopentadienyl-methyl resonances at 1.95, 1.89, 1.71 and 1.69 ppm. This is due to the absence of neopentyl-chloride exchange, with the result that the two methyl groups adjacent, and two removed from the proton on the cyclopentadienyl ring cannot exchange.

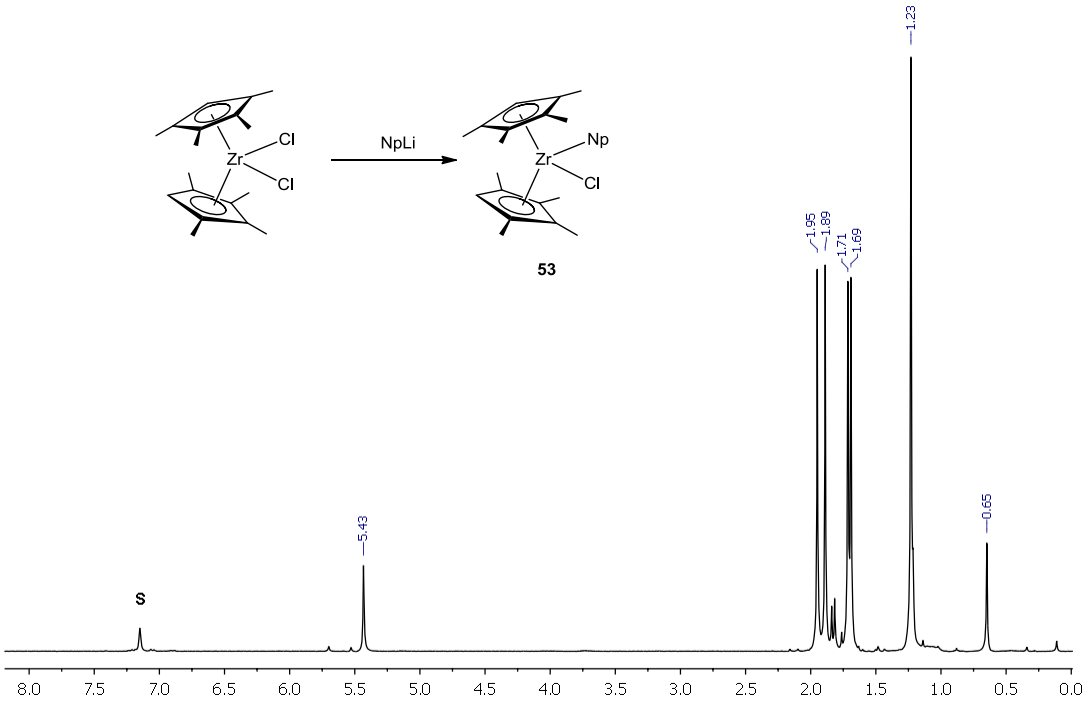

Figure 6. ^{1}H NMR spectrum (299.9 MHz, 293 K) of $Cp^{Me4}{}_2Zr(Np)Cl$ (**53**) in C_6D_6. ('s' denotes residual protio solvent).

Diffraction quality crystals of $Cp^{Me4}{}_2Zr(Np)Cl$ (**53**) were grown from a saturated pentane solution at -30 ºC. The molecular structure as determined by X-ray diffraction is presented in Figure 7 with selected distances and angles listed in Table 5.

The molecular structure of $Cp^{Me4}{}_2Zr(Np)Cl$ (**53**) is comparable to that of the related compound $Cp^{Me4}{}_2Zr(Ph)Cl$ (**4.15**). The metal chloride distances are 2.450(1) and 2.442(3) Å, respectively, the same within error. The Zr–C_{alkyl} bond in **4.15** (2.291(2) Å) is slightly shorter than the Zr(1)–C(1) distance in **53** (2.338(4) Å) in keeping with the sp^2 character of C_α and lower steric bulk of the phenyl group compared to the neopentyl. The Zr(1)–C(1) bond (2.450(1) Å) is slightly longer than other zirconium bound neopentyl groups (range 2.084 – 2.352 Å, 38 examples), due to the steric bulk of the two tetramethylcyclopentadienyl ligands.

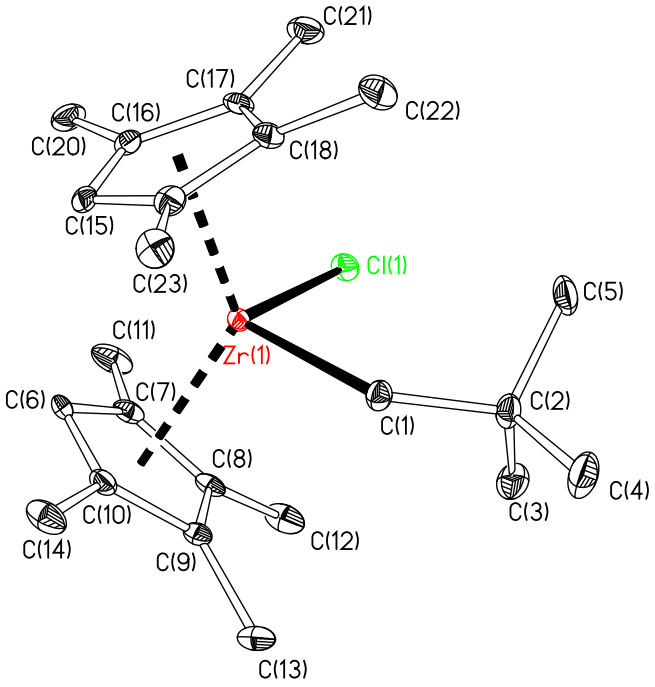

Figure 7. Displacement ellipsoid plot (20 % probability) of $Cp^{Me_4}{}_2Zr(Np)Cl$ (**53**). H atoms omitted for clarity.

Table 5. Selected distances (Å) and angles (°) for $Cp^{Me_4}{}_2Zr(Np)Cl$ (**53**).

Zr(1)–Cl(1)	2.450(1)	Cl(1)–Zr(1)–C(1)	102.85(11)
Zr(1)–C(1)	2.338(4)	Cl(1)–Zr(1)–$Cp_{cent(1)}$	107.1
Zr(1)–$Cp_{cent(1)}$[a]	2.252	Cl(1)–Zr(1)–$Cp_{cent(2)}$	103.8
Zr(1)–$Cp_{cent(2)}$[a]	2.271	C(1)–Zr(1)–$Cp_{cent(1)}$	103.6
C(1)–C(2)	1.553(6)	C(1)–Zr(1)–$Cp_{cent(2)}$	106.9
		$Cp_{cent(1)}$–Zr(1)–$Cp_{cent(2)}$	129.7
		Zr(1)–C(1)–C(2)	125.0(3)

[a]Cp_{cent} is the computed Cp^{Me_4} ring carbon centroid.

A large difference between **53** and **4.15** is the relative orientation of the tetramethylcyclopentadienyl rings. While they are staggered in both cases, the position of the carbon not possessing a methyl group varies. In **53** both are positioned away from the neopentyl and chloride groups, allowing the rings to deviate

significantly from being parallel ($Cp_{cent(1)}$–Zr(1)–$Cp_{cent(2)}$ = 129.7 º) and, in doing so, reduce the unfavourable interaction between the methyl substituents and neopentyl group. In **4.15**, while one is also positioned directly away from the phenyl and chloride groups, the other is rotated by *ca*. 72 º. This means the rings cannot deviate to such an extent and leads to a larger Cp_{cent}–Zr–Cp_{cent} angle (133.2 º). This rotation also causes one of the Zr–Cp_{cent} distances to be elongated compared to the other (2.240 *vs*. 2.347 Å) whereas in **53** both are similar (Zr(1)–Cp_{cent}(1) = 2.252 Å, Zr(1)–Cp_{cent}(2) = 2.271 Å). Other angles between the ligands are broadly similar and in the range spanned by other bis(tetramethylcyclopentadienyl) supported compounds. (e.g. for $Cp^{Me4}_2ZrCl_2$; avg. Cp_{cent}–Zr–Cl = 105.1 º, Cl–Zr–Cl = 97.6 º).

Previous work in this research group has shown metathesis, between lithium reagents and cations with non-coordinating anions, to be a viable route in the synthesis of metal-heteroatom bonds.[27] With this in mind, the mixed alkyl compound $Cp^{Me4}_2Zr(Np)(Me)$ (**54**) was synthesised in 65 % yield from **53** and MeLi (Scheme 4). The ^1H and $^{13}C\{^1H\}$ NMR data for $Cp^{Me4}_2Zr(Np)(Me)$ (**54**) are as expected, very similar to those of $Cp^{Me4}_2Zr(Np)Cl$ (**53**). The ^1H NMR spectrum exhibits the same peaks for the tetramethylcyclopentadienyl and neopentyl ligands, but shifted upfield slightly due to the presence of an electron donating methyl group in place of the chloride in **53**. The methyl resonance is found at -0.42 ppm, typical for Group 4 (IV) metal bound methyl groups. In the $^{13}C\{^1H\}$ NMR spectrum there is a very small upfield shift of the tetramethylcyclopentadienyl resonances.

Unfortunately, subsequent methyl abstraction by $[Ph_3C][B(Ar^F)_4]$ (Ar^F = C_6F_5), followed by addition of $LiNHNPh_2$ did not yield the desired compound. Internal β-methyl elimination of the transient $[Cp^{Me4}_2Zr(Np)][B(Ar^F)_4]$ species was significantly faster than the metathesis reaction, even at temperatures as low as -60 ºC and in the presence of up to 5 equivalents of THF.[28]

Following the lack of success proceeding *via* metathesis reactions, a protonolysis route was attempted. Separately, $Cp^{Me4}_2Zr(Np)Cl$ (**53**) and $Cp^{Me4}_2Zr(Np)(Me)$ (**54**) were mixed with H_2NNPh_2 and heated in sealed NMR tubes. While **54** produced a mixture of products, **53** underwent clean protonolysis at 140 ºC over the course of 48 h, yielding $Cp^{Me4}_2Zr(NHNPh_2)Cl$ (**55**) in 38 % yield (quantitative by NMR spectroscopy, Scheme 4).

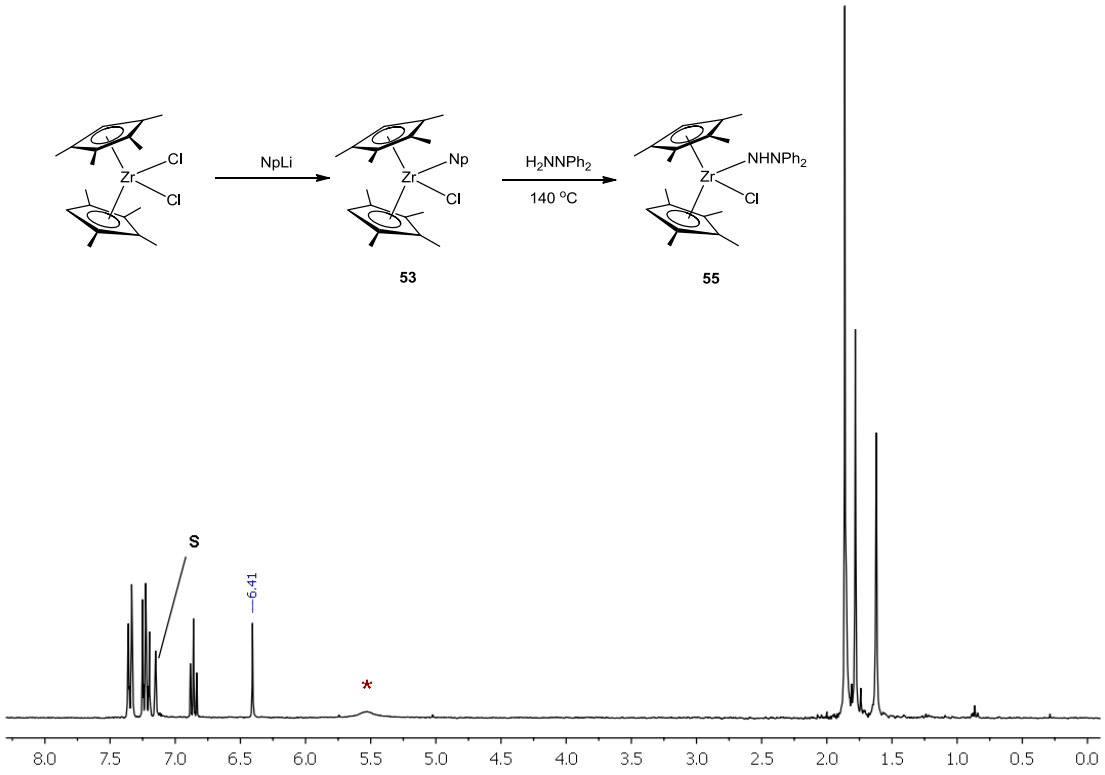

Figure 8. ^{1}H NMR spectrum (299.9 MHz, 293 K) of $Cp^{Me4}{}_2Zr(NHNPh_2)Cl$ (**55**) in C_6D_6. ('s' denotes residual protio solvent).

As in $Cp^{Me4}{}_2Zr(Np)Cl$ (**53**) and $Cp^{Me4}{}_2Zr(Np)(Me)$ (**54**), $Cp^{Me4}{}_2Zr(NHNPh_2)Cl$ (**55**) exhibits four sharp cyclopentadienyl-methyl resonances between 1.5 and 2.0 ppm (two are overlapping) and a sharp peak at 6.41 ppm corresponding to the cyclopentadienyl-H resonance (Figure 8). It is clear that the neopentyl group has been protonated by the hydrazine, as indicated by the replacement of the neopentyl resonances by aromatic ones and the broad peak (marked *) denoting the presence of an NH bond. The $^{13}C\{^{1}H\}$ phenyl resonances range between 153 and 121 ppm, characteristic of 1,1-diphenylhydrazide(1-) ligands (e.g. $Cp^*{}_2Zr(NHNPh_2)(Me)$ (**51**) and $Cp^*{}_2Zr(NHNPh_2)_2$ (**50**), range 154 – 120 ppm).

X-ray diffraction quality crystals were grown from a saturated pentane solution at room temperature. The molecular structure as determined by X-ray diffraction is shown in Figure 9 with selected distances and angles in Table 6.

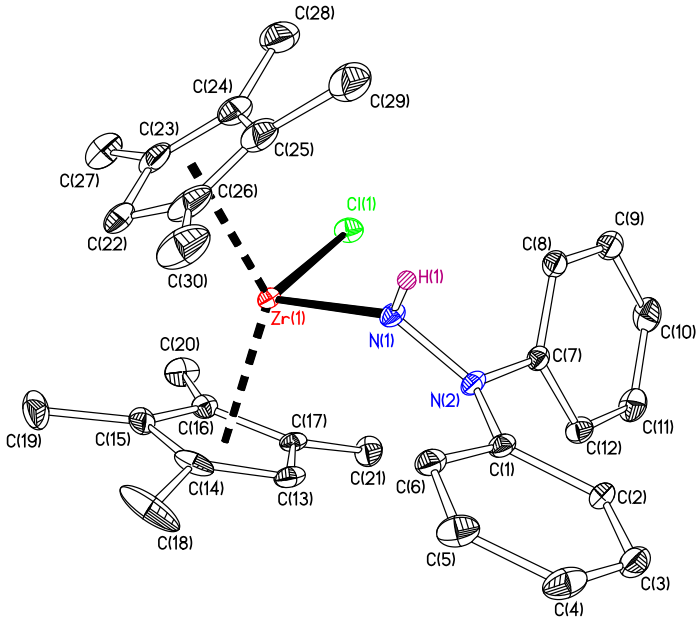

Figure 9. Displacement ellipsoid plot (20 % probability) of $Cp^{Me_4}{}_2Zr(NHNPh_2)Cl$ (**55**). C bound H atoms omitted for clarity.

Table 6. Selected distances (Å) and angles (°) for $Cp^{Me_4}{}_2Zr(NHNPh_2)Cl$ (**55**).

Zr(1)–N(1)	2.097(4)	N(1)–Zr(1)–Cl(1)	98.41(12)
Zr(1)–Cl(1)	2.452(1)	N(1)–Zr(1)–$Cp_{cent(1)}$	101.6
Zr(1)–$Cp_{cent(1)}$[a]	2.257	N(1)–Zr(1)–$Cp_{cent(2)}$	108.8
Zr(1)–$Cp_{cent(2)}$[a]	2.244	Cl(1)–Zr(1)–$Cp_{cent(1)}$	101.7
N(1)–N(2)	1.416(5)	Cl(1)–Zr(1)–$Cp_{cent(2)}$	104.6
N(2)–C(1)	1.396(6)	$Cp_{cent(1)}$–Zr(1)–$Cp_{cent(2)}$	135.8
N(2)–C(7)	1.421(6)	Zr(1)–N(1)–N(2)	129.5(3)

[a]Cp_{cent} is the computed Cp^{Me_4} ring carbon centroid.

The molecular structure of $Cp^{Me_4}{}_2Zr(NHNPh_2)Cl$ (**55**) is fully consistent with the solution ^1H NMR spectrum. It is immediately clear that the neopentyl group in $Cp^{Me_4}{}_2Zr(Np)Cl$ (**53**) has been replaced by the 1,1-diphenylhydrazido(1-) ligand, with the tetramethylcyclopentadienyl rings and chloride occupying the other coordination sites around the tetrahedral zirconium. There are several other mixed hydrazido(1-)-

chloride zirconium compounds, mostly involving N_β coordination to the metal centre,[14,29-31] but only one example utilising a bis(tetramethylcyclopentadienyl) supporting ligand set, although this is a dimer.[32]

The Zr(1)–Cl(1) distance of 2.452(1) Å is the same within error to that in **53** (*ut supra*) while the Zr(1)–N(1) bond length (2.097(4) Å) is comparable to that seen in Gade's related structure $Zr(N_2{*}N^{py})(NHNPh_2)Cl$ (**4.16**, Zr-N_α = 2.080(6) Å). Both are well within the expected range for zirconium-amide bonds (lit. range 1.877 – 2.404 Å).[11] The Zr–Cp_{cent} distances in **55** (avg. 2.251 Å) are slightly shorter than those of **53** (avg. Zr–Cp_{cent} = 2.262 Å) as the hydrazide ligand is less sterically bulky than the neopentyl. This slight shortening of the Zr–Cp_{cent} distances can also be attributed to the fact that in **53** the carbons bound to hydrogen in the cyclopentadienyl rings are aligned. In **55**, one is pointed directly away from the hydrazide and chloride groups with the other rotated by *ca*. 140 º (as observed to a lesser extent for **4.15**). As explained for **53** and **4.15** this produces a larger $Cp_{cent(1)}$–Zr(1)–$Cp_{cent(2)}$ angle in **54** (135.8 º) relative to that found for **53** (129.7 º), where the alignment of the proton bound carbon enables a compression of the Cp_{cent}–Zr–Cp_{cent} angle. Angles between other ligands are as expected. The Zr(1)–N(1)–N(2) angle (129.5(3) º) is indicative of an sp^2 hybridised nitrogen and the N(1)–N(2) distance (1.416(5) Å) is similar to that of other zirconium bound hydrazide(1-) ligands (*vide supra*) and **4.16** (1.427(8) Å).

It was envisaged that in the presence of a suitable base, dehydrohalogenation would occur relatively easily from $Cp^{Me4}{}_2Zr(NHNPh_2)Cl$ (**55**), producing $Cp^{Me4}{}_2Zr(NNPh_2)(L)$ (L = donor). Unfortunately there was no reaction with an excess of $LiN(SiMe_3)_2$ and pyridine, even upon heating. Reactivity with DMAP present was more promising, agreeing with previous studies that DMAP can act as a proton shuttle.[33] However the terminal hydrazide was only ever produced in trace amounts, presumably in order to form such a π-loaded, electron rich complex, a significantly stronger base would be required.

References

1. Clulow, A. J.; Selby, J. D.; Cushion, M. G.; Schwarz, A. D.; Mountford, P.; *Inorg. Chem.* **2008**, *47*, 12049.
2. Munha, R. F.; Veiros, L. F.; Duarte, M. T.; Fryzuk, M. D.; Martins, A. M.; *Dalton Trans.* **2009**, *36*, 7494.

3. Selby, J. D.; Manley, C. D.; Schwarz, A. D.; Clot, E.; Mountford, P.; *Organometallics* **2008**, *27*, 6479.
4. Selby, J. D.; Feliz, M.; Schwarz, A. D.; Clot, E.; Mountford, P.; *Organometallics* **2011**, *30*, 2295.
5. Lehn, J.-S. M.; Hoffman, D. M.; *Inorg. Chim. Acta* **2003**, *345*, 327.
6. Lehn, J.-S. M.; Javed, S.; Hoffman, D. M.; *Inorg. Chem.* **2007**, *46*, 993.
7. Baunemann, A.; Kim, Y.; Winter, M.; Fischer, R. A.; *Dalton Trans.* **2006**, 121.
8. Hou, Z.; Stephan, D. W.; *J. Am. Chem. Soc.* **1992**, *114*, 10088.
9. Berg, F. J.; Petersen, J. L.; *Tetrahedron* **1992**, *48*, 4749.
10. Hoskin, A. J.; Stephan, D. W.; *Organometallics* **2000**, *19*, 2621.
11. Gehrmann, T.; Scholl, S. A.; Fillol, J. L.; Wadepohl, H.; Gade, L. H.; *Chem. Eur. J.* **2012**, *18*, 3925.
12. Duncan, A. P.; Bergman, R. G.; *Chem. Rec.* **2002**, *2*, 431.
13. Chiu, M.; Hoyt, H. M.; Michael, F. E.; Bergman, R. G.; van Halbeek, H.; *Angew. Chem. Int. Ed.* **2008**, *47*, 6073.
14. Herrmann, H.; Wadepohl, H.; Gade, L. H.; *Dalton Trans.* **2008**, 2111.
15. Gambarotta, S.; Basso-Bert, M.; Floriani, C.; Guastini, C.; *J. Chem. Soc., Chem. Commun.* **1982**, 374.
16. Gambarotta, S.; Floriani, C.; Chiesi-Villa, A.; Guastini, C.; *Inorg. Chem.* **1983**, *22*, 2029.
17. Zambrano, C. H.; Fanwick, P. E.; Rothwell, I. P.; *Organometallics* **1994**, *13*, 1174.
18. Walsh, P. J.; Hollander, F. J.; Bergman, R. G.; *J. Organomet. Chem.* **1992**, *428*, 13.
19. Novarino, E.; Guerrero Rios, I.; van der Veer, S.; Meetsma, A.; Hessen, B.; Bouwkamp, M. W.; *Organometallics* **2010**, *30*, 92.
20. Zambrano, C. H.; Sharp, P. R.; Barnes, C. L.; *Organometallics* **1995**, *14*, 3607.
21. García-Herbosa, G.; Connelly, N. G.; Muñoz, A.; Cuevas, J. V.; Orpen, A. G.; Politzer, S. D.; *Organometallics* **2001**, *20*, 3223.
22. Nöth, H.; Seifert, T.; *Eur. J. Inorg. Chem.* **2002**, *2002*, 602.
23. Padělková, Z.; Nechaev, M. S.; Lyčka, A.; Holubová, J.; Zevaco, T. A.; Růžička, A.; *Eur. J. Inorg. Chem.* **2009**, *2009*, 2058.

24. Carroll, J. A.; Cobbledick, R. E.; Einstein, F. W. B.; Farrell, N.; Sutton, D.; Vogel, P. L.; *Inorg. Chem.* **1977**, *16*, 2462.
25. Lee, H.; Bridgewater, B. M.; Parkin, G.; *J. Chem. Soc., Dalton Trans.* **2000**, 4490.
26. Chirik, P. J.; *Organometallics* **2010**, *29*, 1500.
27. Saleh, L. M. A.; Birjkumar, K. H.; Protchenko, A. V.; Schwarz, A. D.; Aldridge, S.; Jones, C.; Kaltsoyannis, N.; Mountford, P.; *J. Am. Chem. Soc.* **2011**, *133*, 3836.
28. Horton, A. D.; *Organometallics* **1996**, *15*, 2675.
29. Herrmann, H.; Fillol, J. L.; Gehrmann, T.; Enders, M.; Wadepohl, H.; Gade, L. H.; *Chem. Eur. J.* **2008**, *14*, 8131.
30. Herrmann, W. A.; Menjon, B.; Herdtweck, E.; *Organometallics* **1991**, *10*, 2134.
31. Bai, G.; Roesky, H. W.; Hao, H.; Noltemeyer, M.; Schmidt, H.-G.; *Inorg. Chem.* **2001**, *40*, 2424.
32. Bernskoetter, W. H.; Pool, J. A.; Lobkovsky, E.; Chirik, P. J.; *J. Am. Chem. Soc.* **2005**, *127*, 7901.
33. Höfle, G.; Steglich, W.; Vorbrüggen, H.; *Angew. Chem. Int. Ed* **1978**, *17*, 569.

Appendix E – Gibbs free energy profiles for the reaction of $Cp_2Zr(NNPh_2)(DMAP)$ (E1) with ^tBuCCMe and $Me_3SiCCMe$.

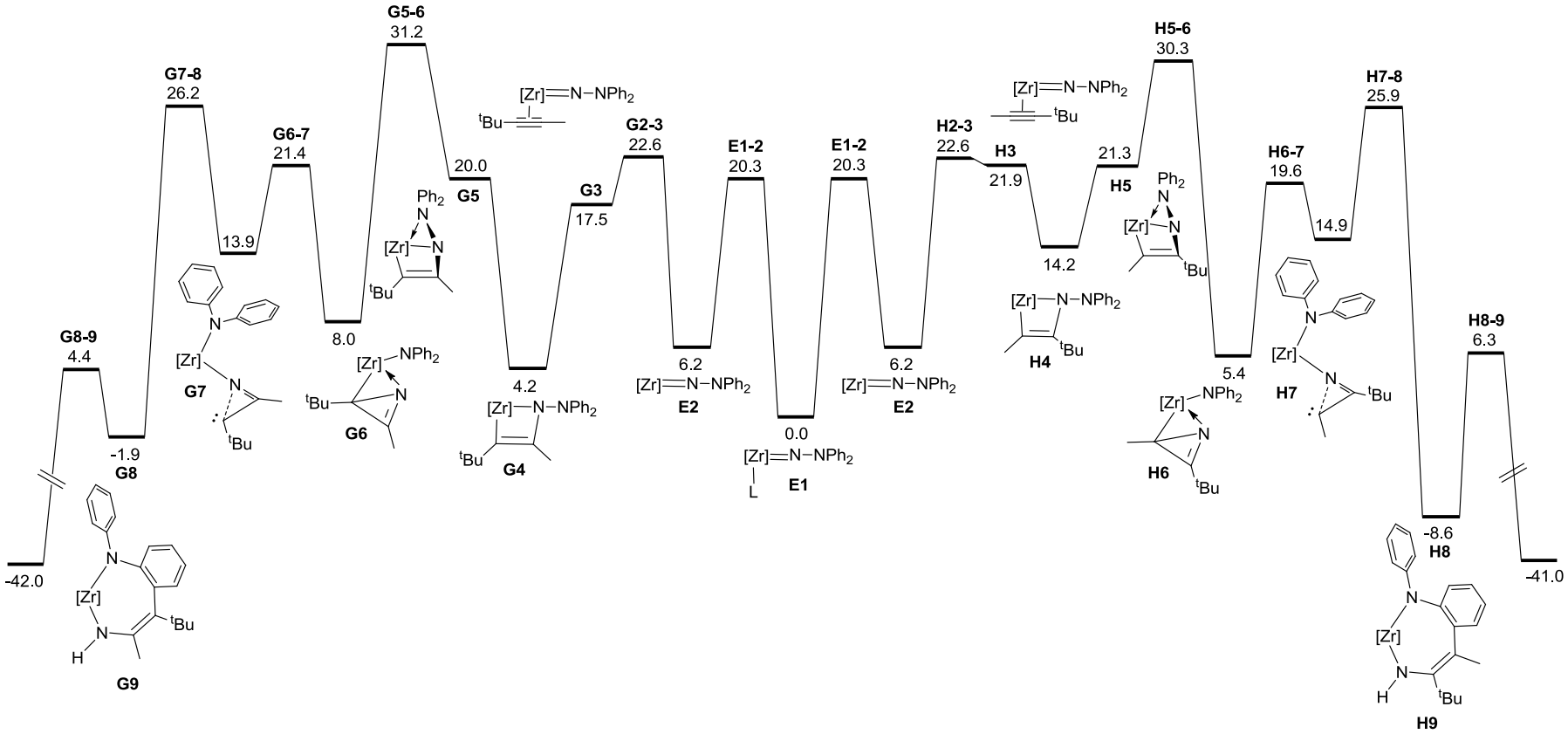

Scheme 1. Gibbs free energy (kcal mol^{-1}) profile for N_α–N_β cleavage and C–H activation of $Cp_2Zr(NNPh_2)(DMAP)$ (**E1**) when reacted with ^tBuCCMe at 347 K. L = DMAP.

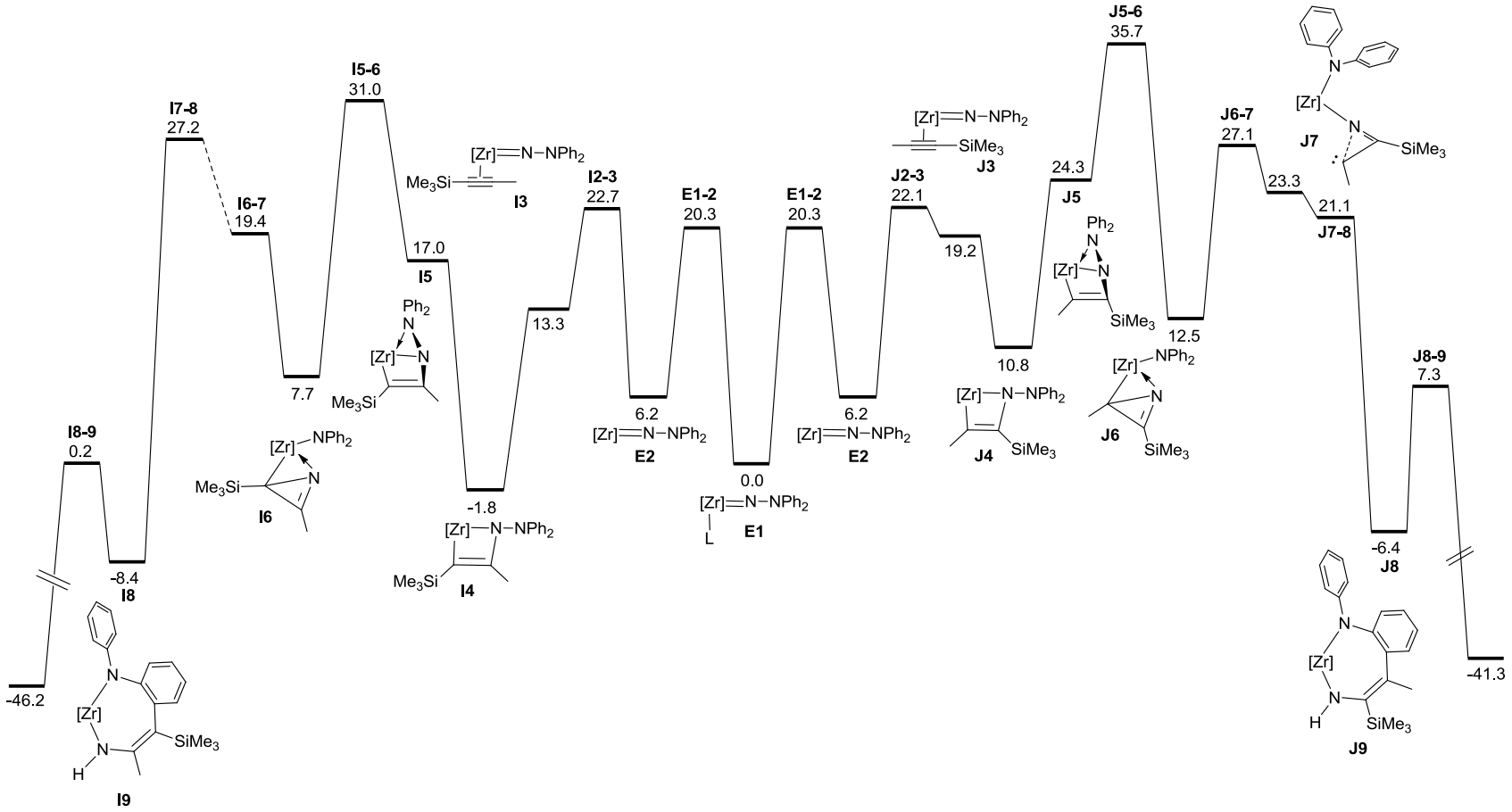

Scheme 2. Gibbs free energy (kcal mol^{-1}) profile for N_α–N_β cleavage and C–H activation of $Cp_2Zr(NNPh_2)$(DMAP) (**E1**) when reacted with $Me_3SiCCMe$ at 347 K. L = DMAP. Intermediate **I7** could not be located.